ISSN 1738-1142

Volume 15(1) **2017**

KOREAN RADIOACTIVE WASTE SOCIETY

2017
춘계학술논문요약집

| 일시 |

2017. 5. 24(수) ~ 5. 26(금)

| 장소 |

부산 해운대 그랜드 호텔

Abstracts of Proceedings of the
Korean Radioactive Waste Society
SPRING 2017

사단법인 한국방사성폐기물학회
Korean Radioactive Waste Society

2017 춘계학술발표회

이 발표논문집은 2017년도 정부재원(과학기술진흥기금 및 복권기금)으로
한국과학기술단체총연합회의 지원을 받아 발간되었음

ISSN 1738-1142

Volume 15(1) **2017**

KOREAN RADIOACTIVE WASTE SOCIETY

2017
춘계학술논문요약집

| 일시 |

2017. 5. 24(수) ~ 5. 26(금)

| 장소 |

부산 해운대 그랜드 호텔

Abstracts of Proceedings of the
Korean Radioactive Waste Society
SPRING 2017

사단법인 한국방사성폐기물학회
Korean Radioactive Waste Society

Contents

KOREAN
RADIOACTIVE WASTE
SOCIETY

1분과 핵주기정책 (Oral)

초청발표

09:00~09:40 The Role of IAEA in Developing a Safeguards System for Fuel Cycle Facilities in Korea
June Ho Ahn[Former IAEA Inspector]

09:40~10:00 Safeguards System Development Status and Future Prospects of Fuel Cycle Facilities at KAERI ····· 19
Ho-Dong Kim, Hee Seo, Se-Hwan Park, Hee-Sung Shin, Dae-Yong Song, Jong-Myeong Oh, Jeong-Hoe Ku, and Seong-Kyu Ahn[KAERI]

10:00~10:20 Consideration of Hold-up for Material Accountancy in Pyroprocessing Plant ····· 21
Seong-Kyu Ahn, Byung-Hee Won, Bong-Young Kim, and Jeong-Hoe Ku[KAERI]

10:40~11:00 Effects of One-sided Weights on Multi-criteria Decision Making for Promising Nuclear Fuel Cycle Options in Korea ····· 23
Hong Jang, Hyo On Nam, Chul Min Kim, and Won il Ko[KAERI]

11:00~11:20 A Study on the Implementation of Export Controls for Spent Nuclear Fuel ····· 25
Chansuh Lee, Jinho Chung, and Donghoon Shin[KINAC]

11:20~11:40 Case and Trends Study for Establishing Cyber Security Information Sharing System ····· 27
Soo Min Lim and Chae Chang Lee[KINAC]

11:40~12:00 Establishment of Vital Digital Asset Verification Environment Design Base ···· 29
Yeeun Byun, Hyundoo Kim, and Kookhei Kwon[KINAC]

1분과 핵주기정책 (Poster)

P0101 Proliferation Resistance Analysis of Autonomous Small Modular Reactor Design Optimization ····· 33
Chul Min Kim, Man-Sung Yim, Philseo Kim, and Sobin Cho[KAIST],
Sung Ki Kim, Kwang-Rag Kim, Hong Jang, Won Il Ko, Chung-Seok Seo, and Hyo On Nam[KAERI]

P0102 Input Material Accounting Method With Homogenization Mixers for an Engineering Scale Pyroprocessing Facility ····· 35
Chaehun Lee, Bong Young Kim, SangHo Na, Hee Seo, Byung-Hee Won, Se-Hwan Park, Hee-Sung Shin, Ho-Dong Kim, Jong-Myeong Oh, Ha-Jin Song, Junghoe Ku, and Seong-Kyu Ahn[KAERI]

P0103 Measurement of Detector Parameters of Neutron Coincidence Counter for Nuclear Material Accountancy ····· 37
Hee Seo, Chaehun Lee, Jong-Myeong Oh, Seong-Kyu Ahn, Jeong-Hoe Ku, and Ho-Dong Kim[KAERI], Seonkwang Yoon[UST]

P0104 Investigation of Design Requirements and Potential Sampling Methods for Engineering-scale Pyroprocessing Safeguards ····· 39
Bong Young Kim, Chaehun Lee, Seong-Kyu Ahn, Hee Seo, Byung-Hee Won, Se-Hwan Park, and Jeong Hoe Ku[KAERI]

P0105 The Exploration of Machine Learning Based Process Monitoring for Pyroprocessing Safeguards ····· 41
Young-Eun Jung, Chul-Min Kim, and Man-Sung Yim[KAIST], Bong-Young Kim[KAERI]

P0106 Study on Improvement of Licensing Requirements of Fuel Cycle Facilities ···· 43
Hyeong Ki Shin, Seung-Jae Han, Byoung-Jik Kim, Ara Go, and Jae-Yeong Park[KINS], Sang Hoon Park[RadWorks]

P0107 Development of a Guideline for the Preparation of SAR on Spent Nuclear Fuel Recycling Facilities ····· 45
Jihyun Kim, Hyunseok Seo, Kyongwon Ham, and Sang Hoon Park[RadWorks Corp.], Hyeong Ki Shin[KINS]

P0108 How to Control the Intangible Transfer of Technology Related to the Trigger List Items ····· 47
Jinho Chung[KINAC]

P0109 Conflicts and Proposals on Physical Protection Related Law of Intermediate and low-level Radioactive Waste Disposal Facilities ····· 49
Yeon Uk Kang, Min Ho Kang, and Sung Soon Jang[KINAC]

P0110 A Study on the Recent Tendency of Cyber Security Regulation for the Nuclear Fuel Cycle Facilities ····· 51
Siwon Kim[KINAC]

P0111 Study on the Position Enhancement for Cyber Security Organization of the Nuclear Facilities ····· 53
Hyundoo Kim[KINAC]

P0112 Applied Parallel Coordinates for ICS Network Traffic in Simulated Nuclear Power Plant Environments ····· 55
Chaechang Lee and Soomin Kim[KINAC]

2분과 사용후핵연료관리 (Oral)

09:00~09:20 Porous Media Modelling for Thermal Analysis of Storage Cask With Bird Screen Meshes ····· 59
Ju-Chan Lee, Kyoung-Sik Bang, Seung-Hwan Yu, Ki-Seog Seo, and Woo-Seok Choi[KAERI]

09:20~09:40 A PSA Framework for Interim Storage Facility Subject to Aircraft Engine Crash ····· 61
Sanghoon Lee [KeiMyung Univ.], Belal Almomani and Dongchan Jang[KAIST], Hyun-Gook Kang[RPI]

09:40~10:00 Structural Evaluation Under Off-normal Condition for Concrete Storage Cask of Spent Fuels ····· 63
Tae-Chul Moon, Chang-Yeal Baeg, and Chun-Hyung Cho[KORAD]

10:00~10:20 A New Perspective of Hydride Re-orientation in SNF ····· 65
J.S. Noh[ACT], Y.K. Kim[KEPCO NF], M. Tayal[Expert in CANDU Fuel]

10:40~11:00 Determination of Uranium, Plutonium, Neodymium, Cesium, Cerium and Europium Isotopes in Irradiated Dual-cooled Annular Fuel by Isotope Dilution Mass Spectrometry and γ -Ray Spectrometry ····· 67
Jung Suk Kim, Byungman Kang, Yang-Soon Park, Young Bok Kim, Jai Il Park, and Yeong Keong Ha[KAERI]

11:00~11:20 Passivation of Al_2O_3-based Refractories by Air Plasma Spray Coatings of Y_2O_3 ····· 69
Sang-Chae Jeon, Jae-Won Lee, Joo-Young Yoon, and Yung-Zun Cho[KAERI]

11:20~11:40 Spectroscopic and Electrochemical Investigation of Reactions of Oxide Ions With U^{3+} and Ln^{3+} (Ln=Nd, Ce, and La) in LiCl-KCl Melts ····· 71
Suhee Choi, Sang-Eun Bae, and Tae-Hong Park[KAERI]

11:40~12:00 Re-fabrication of U-Zr Alloy System Fuel Slugs Recycling Metallic Fuel Scraps ····· 73
Ki-Hwan Kim, Young-Mo Ko, Seok-Jin Oh, and Jeong Yong Park[KAERI], Seong-Jun Ha[Chungnam Natl. Univ.]

2분과 사용후핵연료관리 (Poster)

P0201 An Analysis on Applicability of Temporary Onsite Storage Facilities of Spent Fuel From PWRs in Korea ····· 77
Hakyun Lee and Jongsoon Song[Chosun Univ.]

P0202 Estimation Radioactivity of Reference Spent Fuel With Time and Total Radioactivity of All Spent Fuel at 2035 ····· 79
Ara Go, Daesik Yook, and Kyuhwan Jeong[KINS]

P0203 Kr Capture in Head-End Process of Pyroprocess ····· 81
Seok-Min Hong, Ahreum Han, Jae Hwan Yang, and Yung-Zun Cho[KAERI]

P0204 Salt Distiller With Mesh-covered Crucible for Electrorefiner Uranium Deposits ····· 83
S.W. Kwon, Y.S. Lee, H.B. Kang, J.H. Jung, J.H. Chang, S.H. Kim, and S.J. Lee[KAERI]

P0205 Viscosities of UCl_3-LiCl-KCl Molten Salts ····· 84
Sang-Heon Lee, Jong-Yun Kim, Sang-Eun Bae, and Tae-Hong Park[KAERI]

P0206 Development of a Methodology for the Determination of Metal Reduction Yields of Highly Radioactive Nuclear Fuel ····· 86
Young-Hwan Cho, Ji-Hye Kim, Byung-Man Kang, Jung-Suk Kim, and Tae-Hong Park[KAERI]

P0207 Lessons Learned From the Use of Metal Halide Lamp in the ACPF Argon Cell ····· 88
Byungsuk Park, Yunmok Jung, Jongkwang Lee, Kiho Kim, Ilje Cho, and Eunyoung Choi[KAERI]

P0208 Electrolytic Behaviors in Large-scale LCC Electrowinning System ····· 90
Si Hyung Kim, Jun-Bo Sim, Han Byeol Kang, Young Sang Lee, Sungbin Park, Sang-Woon Kwon, Moon-Sik Woo, Jae-Hoo Jung, and Sung-Jai Lee[KAERI]

P0209 Cyclic Voltammetry Depending on the Electrode Connection Mode in Small-scale LCC Electrowinning System ····· 92
Si Hyung Kim, Taek-Jin Kim, Gha-Young Kim, Seul Gi Lee, Junhyuk Jang, Seungwoo Paek, Hansoo Lee, Hee-Chul Eun, Sung-Jai Lee, and Do-Hee Ahn[KAERI]

P0210 Effect of Electrolyte Agitation on an Electrolytic Reduction Process ····· 94
Sang-Kwon Lee, Sung-Wook Kim, Eun-Young Choi, Sun-Seok Hong, Seung-Chul Oh, and Jin-Mok Hur[KAERI]

P0211 Electrolytic Reduction of 1 kg-UO_2 Using a Graphite Anode ····· 96
Sung-Wook Kim, Dong Hyun Heo, Sang-Kwon Lee, Jin-Mok Hur, and Eun-Young Choi[KAERI]

P0212 Change of Oxygen Concentration Accoring to Argon Purging of Storage Vault in ACPF ····· 98
Yunmock Jung, Byungsuk Park, Jongkwang Lee, Sunseok Hong, and Eunyoung Choi[KAERI]

P0213 The Oxidation Effect on the Reinforcement Particles of Al / B_4C Metal Matrix Composite ····· 100
Tae Gyu Lee and Ho Jin Ryu[KAIST]

P0214 Cesium Diffusion Tests in Graphite With Optimized ICP-MS Measurement Conditions ····· 102
Je-Kyun Baek and Ho Jin Ryu[KAIST], Sunghwan Yeo, Young Woo Lee, and Jeongmook Lee[KAERI]

P0215 Spray Coatings of Al_2O_3 Layer for Passivation of Al_2O_3-SiO_2-based Refractory ····· 104
Joo-Young Yoon, Jae-Won Lee, Sang-Chae Jeon, Yung-Zun Cho, Ju-Ho Lee, Kweon-Ho Kang, Do-Youn Lee, Jang-Jin Park, and Kwang-Hoon Cho[KAERI]

P0216 Development of Graphene Reinforced Calcium Hydroxyaptite Matrices for the Immobilization of Radioiodine ····· 106
Muhmood ul Hassan and Ho Jin Ryu[KAIST]

P0217 A Quantification Approach to Pyro-electrochemical Performance for Scale-up Design ····· 108
K.R. Kim, C.M. Kim, H. Jang, S.K. Kim, J.G. Kim, C.S. Seo, H.O. Nam, and W.I. Goh[KAERI]

P0218 The Temperature Distribution of a Fuel Rod With the Presence of a Thermocouple Using COMSOL MULTIPHYSICS ····· 110
Sunwoo Park and Kwangheon Park[Kyunghee Univ.]

P0219 Example Operating Procedure for an Automation Concept of Electrochemical Process ····· 112
Dongseok Ryu, Jonghui Han, Jongkwang Lee, Kiho Kim, and Seunghyun Kim[KAERI]

P0220 Chemical Process Safety at a Pyroprocess Facility ····· 114
Seok-Jun Seo, Hongrae Jeon, Woojin Jo, Siwan Noh, Jeong-Hoe Ku, and Hyojik Lee[KAERI]

P0221 A Study on Characteristics of Airborne Materials for Pyroprocess Using MELCOR ····· 116
Siwan Noh, Jaehoon Lim, Hongrae Jeon, Seok-Jun Seo, Woo jin Jo, Gil Sung You, and Hyo Jik Lee[KAERI], Jae-Uk Shin[ARITEC]

P0222 Thermal Analysis for Spent Nuclear Fuel Temporary Storage System in Pyroprocessing Facility ····· 118
Jaehoon Lim, Seung Nam Yu, Seok-Jun Seo, Ho Hee Lee, Won Myung Choung, Woo Jin Jo, Hongrae Jeon, and Hyo Jik Lee[KAERI]

P0223 Preliminary Safety Evaluation of Nuclear Criticality in a Large-scale Pyroprocess Facility ····· 120
Woo Jin Jo, Seok-Jun Seo, Hun Suk Im, Hongrae Jeon, Siwan Noh, and Hyo Jik Lee[KAERI]

P0224 Wall-tube Flange Refurbishment for Securing Gas-tightness of Telemanipulators in the ACPF Hot-cell ····· 122
Kiho Kim[KAERI]

P0225 Development of a Virtual 3D Simulator Working With an Actual Hardware Testbed to Verify Element Technologies for Pyroprocessing Automation ····· 123
Doyeon Kim, Dongseok Ryu, Jongkwang Lee, Kiho Kim, and Jonghui Han[KAERI]

P0226 Adaptability Study of Hybrid ISA-PSA Method on Safety of Pyroprocess Facilities ····· 125
Gilsung You, Seokjun Seo, Siwan Noh, Hongrae Jeon, Hyojik Lee, Woojin Jo, Hyunsook Im, Hohee Lee, Wonmyung Choung, Seungnam Yu, Jaehoon Lim, and Jeonghoe Ku[KAERI]

P0227 Review of Spent Nuclear Fuel Dry Storage Demonstration Programs in US ····· 127
Sanghoon Lee[Keimyung Univ.], Daesik Yook[KINS]

P0228 Safety Strengthening for On-Site Spent Nuclear Fuel Dry Storage Facilities ··· 129
Sunghwan Chung and Jwayoung Kim[KHNP-CRI]

P0229 Stepwise Approach on Spent Nuclear Fuel Integrity Evaluation R&D Work in Korea ····· 131
Donghak Kook, Jaeyong Kim, Yongsik Yang, and ChangHwan Shin[KAERI]

P0230 Methodology of Delayed Hydride Cracking Assessment of Spent Fuel Cladding ····· 133
Jong-Dae Hong, Euijung Kim, Yong-Sik Yang, and Dong-Hak Kook[KAERI]

P0231 Sensitivity Analysis of COBRA-SFS for Dry Storage of Spent Fuel ····· 135
ChangHwan Shin, Kyong-won Seo, and Dong-hak Kook[KAERI]

P0232 Assessment of COBRA-SFS Cycle-4 With Various Single Phase Flow Tests ··· 137
Kyong-Won Seo, Chang-Hwan Shin, and Dong-Hak Kook[KAERI]

P0233 Preliminary Approach of Impact Simulation for the Simplified Unit Grid ····· 139
Sunguk Lee, Jaeyong Kim, Sooho Kim, Yongsik Yang, Hyochan Kim, and Donghak Kook[KAERI]

P0234 Correlation Between Hydrogen Contents and Stiffness of Oxidized Spacer Grid for Calculating Spent Fuel Rod Response to Impacting Force ····· 141
Young-Ho Lee, Hyun Gil Kim, and Donghak Kook[KAERI]

P0235 Confirmatory Procedure of Spent Fuel Information for Spent Fuel Transport to the Interim Storage Facility ····· 143
Daesik Yook, Ara Go, Gyeong-uk Kang, and Kyuhwan Jeong[KINS]

P0236 Preliminary Numerical Simulation and Test Plan for Actual Drop Accident Condition ····· 145
Woo-seok Choi, Sangsoon Cho, Ki-Seog Seo, Yun-young Yang, and Yong-hui Park[KAERI], Sanghyeok Han[Sungshin ENG]

P0237 Comparison of Permeability Calculation Inside a Spent Nuclear Fuel in a Dry Storage ····· 147
Seung-Hwan Yu, Kyung-Sik Bang, Ju-Chan Lee, and Woo-Seok Choi[KAERI]

P0238 Measurement Plan of Residual Moisture ····· 149
K.S. Bang, S.H. Yu, J.C. Lee, K.S. Seo, and W.S. Choi[KAERI]

P0239 Structure Integrity Evaluation of Fresh Nuclear Fuel ····· 151
Yun-Young Yang, Sang Soon Cho, Ki-seog Seo, and Woo-seok Choi[KAERI]

P0240 Thermal Analysis of Transportation and Storage Cask of Spent Nuclear Fuel for Forced Gas Drying Condition ····· 153
Suk-Nam Lim, Gyung-Sun Chae, Jae-Hyun Han, and Jae-Seok Park[SAE-AN Eng.], Dong-Gyu Lee[KONEC]

P0241 Structural Integrity Evaluation of Spent Nuclear Fuel Assembly Under Normal Transportation Drop Conditions ····· 155
Sang Soon Cho, Woo Seok Choi, Ki-Seog Seo, and Yun-Young Yang[KAERI]

P0242 Remote Operation and Maintenance of Crane System for Use in ACPF Argon Cell ····· 157
Jong Kwang Lee, Byungsuk Park, Sunghyun Kim, Kiho Kim, Il-Je Cho, and Eun-Young Choi [KAERI]

3분과 고준위폐기물처분 (Oral)

09:00~09:20 Vitrification of Radioactive Waste Salt Using Modified Si-Al-P Composites ·· 161
Ki Rak Lee, Hwan-Seo Park, Ahreum Han, Jung-Hoon Choi, and Seung Youb Han[KAERI]

09:20~09:40 Review of Anion Diffusion in Highly Compacted Montmorillonite for Copper Corrosion Modeling ····· 163
Heui-Joo Choi, In-Young Kim, Minsoo Lee, and Dong-Keun Cho[KAERI]

09:40~10:00 Complex Behavior of Radionuclides in a Disposal Environment ····· 165
Jae-Kwang Lee, Seung-Yeop Lee, and Min-Hoon Baik[KAERI]

10:00~10:20 Investigation of Dry Unit Weight for Bentonite Buffer Block ····· 167
Seok Yoon, Jinseop Kim, and Geonyoung Kim[KAERI],
Seungrae Lee, Donghwa Noh, and Minjun Kim[KAIST]

10:40~11:00 Prediction of Inflow and Wetting Behaviors of Bentonite in Deposition Hole Under In-situ Geological Features ····· 169
Jin-Seop Kim, Chang-Soo Lee, Jae-Won Lee, and Geon-Young Kim[KAERI]

11:00~11:20 Numerical Analysis of Thermo-Hydro-Mechanical Coupled Behavior in Multi-level HLW Repository Concept ····· 171
Changsoo Lee, Won-Jin Cho, Jaewon Lee, and Geon-Young Kim[KAERI]

11:20~11:40 Earthquake Modelling and Application to Long-term Safety Analysis of a Final Repository of Spent Nuclear Fuels in Forsmark Sweden ····· 173
Jeoung Seok Yoon, Arno Zang, Ove Stephansson, Fabrice Cotton[Helmhotz Centre],
Ki-Bok Min[Seoul Natl. Univ.], Flavio Lanaro[SSM]

11:40~12:00 Study on the 3D Site-descriptive Model for the HLW Disposal Site Characteristics Evaluation ····· 175
Soo-Gin Kim, Jae-Yeol Cheong, Jeong-Hwan Lee, and Jeong-Hyoun Yoon[KORAD]

3분과 고준위폐기물처분 (Poster)

P0301 Dissolution Characteristics of Uranium From the KURT Granite in Various Geochemical Conditions ····· 179
Wan Hyoung Cho, Min Hoon Baik, and Jae Kwang Lee[KAERI]

P0302 Analyses of Double Layered Disposal System for the Spent Nuclear Fuels Considering the Deposition of Time Difference ····· 181
Jongyoul Lee, Hyeona Kim, Minsoo Lee, Heuijoo Choi, and Kyungsu Kim[KAERI]

P0303 Review on the Foreign Uncertainty Management Programs on the Safety Case for a HLW Repository ····· 183
Jongtae Jeong, Dong-Keun Cho, and Min Hoon Baik[KAERI]

P0304 A Review of Process-based Total System Performance Assessment Model for A Geological Disposal System ····· 185
Jung-Woo Kim, Jaewon Lee, and Dong-Keun Cho[KAERI]

P0305 Conceptual Study on Thermal Analysis for Disposal System of Spent Nuclear Fuel ····· 187
Seunghyun Kim, Jeonghwan Lee, and Jeonghyoun Yoon[KORAD]

P0306 Correlation Study Between Fracture Zone and Geophysical Logging Data in Crystalline Rock ····· 189
Kyung-Woo Park, Dae-Hee Kim, and Hong-Yung Jung[KAERI]

P0307 Microstructure and Corrosion Properties Zr-Cr-Si-NM Alloy Metallic Waste Form for Long-term Disposal ····· 191
Seung-Youb Han, Seon-Ah Jang, and Hwan-Seo Park[KAERI]

P0308 Microstructure and Corrosion Properties of Zirlo-Inconel718-SS304-NM Metal Waste Form Alloys for Improving Stability of Metal Waste Generated by Pyro-Process and Long-term Disposal Stability ····· 193
Seon-Ah Jang, Seung-Youb Han, and Hwan-Seo Park[KAERI]

P0309 Estimating Arrival Time of Crack Wave by Using Moving Window ····· 195
Young-Chul Choi, Jin-Seop Kim, and Tae-Jin Park[KAERI]

P0310 Implementation of Damage Model to TOUGH2-MP/FLAC3D Coupled Code ··· 197
Jaewon Lee, Changsoo Lee, and Geon Young Kim[KAERI]

P0311 High Speed Boreshear Tests of an Engineered Barrier System for High Level Waste Disposal ····· 199
Minsoo Lee, Heui-Joo Choi, Jongyoul Lee, and Sung-Hoon Ji[KAERI]

P0312 Evidence From Fracture Filling Minerals for the Interpretation of Uranium Isotopes in Investigating Ancient Redox in Granitic Rock in KURT Site ····· 201
Ji-Hun Ryu and Hong-Yun Jeong[KAERI]

P0313 Thermal Design Concept of Gap Between Canister and Buffer in an HLW Repository ····· 203
Jae Owan Lee and Geon Young Kim[KAERI]

P0314 Preliminary Study on Optimization of Disposal Facilities Against Human Intrusion ····· 205
Dong-Keun Cho, Jung-Woo Kim, Jongtae Jeong, and Min-Hoon Baik[KAERI]

P0315 Spectroscopic Characterizations of Aqueous Am(III) Species ····· 207
Hee-Kyung Kim, Euo Chang Jung, Hye-Ryun Cho, and Wansik Cha[KAERI]

P0316 Coffinite in the KURT Environments and in Natural Analogue Sites ····· 209
Tae-Jin Park, Wan Hyoung Cho, and Jae-Kwang Lee[KAERI]

P0317 Basic Research to Reconstruct Paleo-geological Evolution Model Around KURT Area ····· 211
Soolim Jung, Yong-Kwon Koh, and Sung-Hoon Ji[KAERI],
Chang-Whan Oh and K. S. Yengkhom[Chonbuk Natl. Univ.]

P0318 Numerical Analysis of Thermo-Hydro-Mechanical Coupled Behavior in Korean Reference HLW Disposal System (KRS) ····· 213
Changsoo Lee, Won-Jin Cho, Jaewon Lee and Geon-Young Kim[KAERI]

4분과 방사성폐기물관리 (Oral)

09:00~09:20 Site Selection Process in Germany for Radioactive Waste Disposal ····· 217
Jeoung Seok Yoon, Arno Zang, Ove Stephansson, and Fabrice Cotton[Helmholtz Centre]

09:20~09:40 Glass-Ceramic Waste Forms for Immobilization of Cs Trapping Filters ····· 219
Jae Hwan Yang, Ahreum Han, Joo Young Yoon, Hwan-Seo Park, and Yung-Zun Cho[KAERI]

09:40~10:00 Hydrogeochemical Changes in the Groundwater System at the Gyeongju LILW Disposal Site After Construction ····· 221
Nam C. Woo, Eunhye Kwon, Jae-Min Lee, and Youn-Tae Kim[Yonsei Univ.],
Sang Min Ryu[Hyundai Eng.], Soon-Il Ok[KORAD]

10:00~10:20 Management Plan for the Intermediate Level Liquid Waste From the Fission ^{99}Mo Production Process in the KIJANG Research Reactor ····· 223
Chul Gyo Seo, Seung-Kon Lee, and Jong-Sik Shon[KAERI]

10:40~11:00 Numerical Simulation on the Diffusion and Sorption of Radionuclides Along the Heterogeneous Microstructures in Rock Matrix ····· 225
Dongkyu Park and Sung-Hoon Ji[KAERI]

11:00~11:20 Electrochemical Behavior of Ce Ion and Bi Ion in LiCl-KCl Molten Salt ····· 227
Beom-Kyu Kim, Hwa-Jeong Han, Ji-Hye Park, Won-Ki Kim, and Byung Gi Park [Soonchunhyang Univ.]

11:20~11:40 Uranium Removal by Tributyl Phosphate-Coated Hydroxyapatite ····· 229
HyunJu Kim and Wooyong Um[POSTECH]

11:40~12:00 Development of Treatment Equipment for Spent Resin Mixture in Heavy Water Reactors(HWR) ····· 231
Kyu-Tae Park, Jung-Min Yoo, and Young-Ku Choi[Sunkwang T&S]

4분과 방사성폐기물관리 (Poster)

P0401 The Study of an Additional Liquid Waste Collection Tank Arrangement on the GA Drawings ····· 235
Keun-Pack Chang, Mu-Gap Shin, Gi-Won Hwang, and Dong-Jae Lee[KEPCO E&C]

P0402 Analysis of Inlet Air Characteristics of Air Cleaning Unit in Nuclear Power Plants ····· 237
Hak-Soo Kim and Cho-Rong Kim[KHNP-CRI]

P0403 Development of Silver-Graphene Fiber Composites as Sorbents for Radioactive Iodine Gas ····· 239
Minseok Lee and Ho Jin Ryu[KAIST]

P0404 Preliminary Test of ^{3}H and ^{14}C Analysis Methods in Radioactive Waste ····· 241
Kahee Jeong, Eun Kyung Jung, Kyu-Min Song, and Seung Chul Park[KHNP-CRI]

P0405 Comparative Study on Electrothermal Radioactive Waste Dryer & Non-Electronic Power Source Radioactive Waste Dryer Utilizing Air Circulation of Ventilation /Exhaust System in NPP ····· 243
Kwang-sik Seo, Hyo-cheol Kim, Dong-hyun Park, Sang-tae Lee, Soon-hwan Yang, and Sang-uk Lim[Hana Nuclear Power Eng.]

P0406 The Effect of Fractured Rock to Radionuclides Transport through Unsaturated Zone ····· 245
Won-Seok Kim, Sangsoo Han, and Wooyong Um[POSTECH]

P0407 Preliminary Analysis on Radionuclides Transport in the Unsaturated Environment ····· 247
Jaechul Ha, Jeonghwan Lee, and Jeonghyoun Yoon[KORAD]

P0408 Basic Study on Development of Solidification Agent for Disposal Container Recycled From Paste Powder at Concrete in Decommissioning Nuclear Power Plant ····· 249
Youngbum Mun, Jaehyung Lee, Hyunkook Choi, and Jaeyung Kim[Sung Shin Cement]
Chulwoo Chung[Pukyung Natl. Univ.]

P0409 Modelling of the Spent Nuclear Fuel Assembly Using the Monte Carlo Method ····· 251
Hwa Jeong Han, Beom Kyu Kim, Ji Hye Park, Won Ki Kim, and Byung Gi Park [Soonchunhyang Univ.]

P0410 Decontamination Technology of Spent Resin From PHWR ····· 253
Young-Soo Jo and Jin-Hyun Sung[Huvis Water]

P0411 A Feasibility Study of the Quantification of C-14 by Photocatalytic Oxidation ····· 255
Byungman Kang, Jung Suk Kim, Jai Il Park, Hong-Joo Ahn, and Yeong-Keong Ha[KAERI]

P0412 Reaction Characteristics of $CsNO_3$ by Different Adsorbents ····· 257
Dasom Yang, Jinmyeong Shin, and Sangho Na[KAERI]

P0413 Study on Vitrification of Slag From Metal Melting Process ····· 259
Mi-hyun Lee, Young Hwan Hwang, Seok Ju Hwang, and Cheon-Woo Kim[KHNP-CRI]

P0414 Study on Long-term Performance of Reinforcing Concrete Structures in Subsurface Environment ····· 261
Ki-jung Kwon, Hyun-jin Cho, and Jung-hyun Yoon[KORAD]

P0415 Estimation of Centerline Temperature of the Rare Earth Glass Waste Form ··· 263
Jung-Hoon Choi, Tae-Kyo Lee, Ki-Rak Lee, Seung-Youb Han, Na-Young Kim, Seon-Ah Jang, and Hwan-Seo Park[KAERI]

P0416 Thermogravimetric Analysis on External Wall Coating Material of Cold Crucible Induction Melter ····· 265
Young Hwan Hwang, Seokju Hwang, Mi-Hyun Lee, and Cheon-Woo Kim[KHNP-CRI]

P0417 Study on Thermal-Flow Analysis of the Cold Crucible Induction Melter ····· 267
Seokju Hwang, Young Hwan Hwang, Mihyun Lee, and Cheon-Woo Kim[KHNP-CRI]

P0418 Leaching Characteristics of Intermediate Level Liquid Radwastes ····· 269
Jong Sik Shon, Won Hyuk Jang, Dong Ju Lee, and Dae Seok Hong[KAERI]

P0419 Treatment and Disposability of Intermediate Level Liquid Radwastes Generated by Fission Moly Production ····· 271
Jong Sik Shon, Jongjin Kim, Dae Seok Hong, and Chul Gyo Seo[KAERI]

P0420 Safety Analysis of Cementation Including Deliquescent Na Compound for Final Disposal ····· 273
Jong Sik Shon, Ki Baek Shin, Jongjin Kim, Dae Seok Hong, and Gi Yong Kim[KAERI]

P0421 Recovery of the Magnetic Adsorbent for Cs Separation From Liquid Waste by Using the Magnetic Liquid-Solid Separation Method ····· 275
Hyo-Jeong Lee, Jung-Weon Choi, Seung-Yeon Cho, Won-Zin Oh, and Sang-June Choi [Kyungpook Natl. Univ.]

P0422 Recovery Tests for Analysis of Radionuclides in Spent Resin Using Elution and Microwave Digestion Method ····· 277
Simon Oh, Jaesik Hwang, Kwang-Soon Choi, and Hong Joo Ahn[KAERI]

P0423 Recovery Rate of Fe, Nb, Ni, Re, Sr According to Elution Speeds in the Column Examination for the Pretreatment of Spent Resin ····· 279
Jaesik Hwang, Simon Oh, Kwang-Soon Choi, and Hong-Joo Ahn[KAERI]

P0424 Dissolution of Large Amount of Ash Produced From Radioactive Waste Using High-Performance Microwave Digestion Systems ····· 281
Kwang-Soon Choi, Jaesik Hwang, Simon Oh, Young-Bok Kim, and Hong Joo Ahn[KAERI]

P0425 Development of Nuclear Waste Filter Sampling Device and Process ····· 283
Kyung-Ho Kim, Hyeon-Oh Park, and Young-Ku Choi[Sunkwang T&S], Mi-Rang Lee[KHNP]

P0426 CaO Absorbent Development for ^{14}C Immobilization Generated From Waste Resin of Heavy-Water Reactor and Mechanism Study ····· 285
Hyeon-Oh Park, Kyu-Tae Park, Jung-Min Yoo, and Young-Ku Choi[Sunkwang T&S], Hwan-Seo Park and Ki-Rak Lee[KAERI]

P0427 Separation Characteristics of Fission Products in LiCl-KCl Waste Salt by Layer-melt Crystallization ····· 287
Tae-Kyo Lee, Jung-Hoon Choi, Ki-Rak Lee, Seung-Youb Han, and Hwan-Seo Park[KAERI]

5분과 제염해체 (Oral)

초청발표

09:00~09:40 ASDOC_D-mod, FSD Decontamination Process Successful Executed 2016 in NPP Biblis Unit A
Laura Schneider and Detlef Queiß er[Siempelkamp NIS]

09:40~10:00 Development of Level 1 Schedule for Nuclear Power Plant Decommissioning Project in Korea ····· 291
Wanil Jung, Hae Jeong Lee, Myung Duck Yang, and Yong Beom Kwon[KEPCO E&C]

10:00~10:20 Fabrication and Cs Removal Performance of Various Metal-Ferrocyanide Functionalized Magnetic Adsorbents ····· 293
Kyu Sun Hwang, Chan Woo Park, In-Ho Yoon, Kune-Woo Lee, and Hee-Man Yang[KAERI]

10:40~11:00 Effects of Site Characteristics on Dose Assessment in NPP Decommissioning ····· 295
Sanghyun Hong, Woongik Hwang, and Jong Seh Lee[Hanyang Univ.], Yongmin Kim [Catholic Univ.], Seokyoung Ahn[Pusan Natl. Univ.]

11:00~11:20 Integration of the Unit Modules of the Nuclear Facility Dismantle Simulation System ····· 297
Ikjune Kim, ByungSeon Choi, Dongjun Hyun, JeiKwon Moon, Jonghwan Lee, KwanSeong Jeong, and Shinyoung Kang[KAERI]

11:20~11:40 Estimation of Waste Volume for Kori # 1 Decontamination Using SP-HyBRID Process ····· 299
Sang Yoon Park, Wang Kyu Choi, Seon Byeong Kim, Hui Jun Won, and Man Soo Choi[KAERI]

11:40~12:00 Studies on the Behavior of Spontaneous Reductive Decomposition of Hydrogen Permanganate in Water for HP/CORD Process ····· 301
Hyun-Kyu Lee, June-Hyun Kim, Won-Zin Oh, and Sang-June Choi[Kyungpook Natl. Univ.]

5분과 제염해체 (Poster)

P0501 Fluidity of Cement Solidification of Residual Radioactive Waste ····· 305
Daeseo Koo, Hyun-Hee Sung, Seung-Soo Kim, Sang Bum Hong, Bum Kyoung Seo, and Jong-Won Choi[KAERI]

P0502 Feasibility Study on the Laser Cutting of Stainless Steel Pipes for Dismantling of Nuclear Power Plants ····· 307
Sangwoo Seon, Jae Sung Shin, Seong Yong Oh, Hyunmin Park, Taek-Soo Kim, Lim Lee, Chin-Man Chung, and Jonghwan Lee[KAERI]

P0503 Dismantling Process Development of the General Equipment / System of Nuclear Power Plant ····· 309
Myungduck Yang, Wanil Jung, Jaihoon Jung, and Yongbeom Kwon[KEPCO E&C]

P0504 Thermal Decomposition of Chabazite-Cs and Chabazite-PCFC-Cs Zeolite ··· 311
Eil-Hee Lee, Ji-Min Kim, Maeng-Kyo Oh, Min-Jeong Kim, Keun-Young Lee, Kwang-Wook Kim, Hyung-Ju Kim, Ik-Soo Kim, Dong-Yong Chung, Jei-Kwon Moon, and Jong-Won Choi[KAERI]

P0505 Spent Fuel Pool Island System Configuration Concept-Comparison of German and the US Regulatory Standards ····· 313
Kwangsoon Choi, Dongjin Lee, and Jaihoon Jung[KEPCO E&C]

P0506 Development of Decontamination Guidelines for the Management of Contaminated Areas as an Emergency Preparedness ····· 315
Jin O Lee, Tae Gwan Do, Ji Young Song, and Kwang Pyo Kim[Kyung Hee Univ.]

P0507 Decommissioning Strategy and Method for Preparation of Preliminary Decommissioning Plan for Research Nuclear Facilities ····· 317
Seung-Kook Park, Kook-Nam Park, Yun-Dong Choi, and Young-San Choe[KAERI], Jin-Ho Park[New Decom]

P0508 Pressure Water Jet Cleaning of Residue Inside Tank in Foam Decontamination ····· 319
Han Beom Yang, In Ho Yoon, Seung Eun Kim, Chong Hun Jung, Wang Kyu Choi, and Seon Byeong Kim[KAERI]

P0509 Specification Requirement and Considerations Based on Operation Experiences of Spent Fuel Pool Island ····· 321
Dongjin Lee and Jaihoon Jung[KEPCO E&C]

P0510 Simulation-Based Evaluation for the Dismantling Scenario of the Reactor Vessel at Kori Unit 1 ····· 323
Dongjun Hyun, Ikjune Kim, Jonghwan Lee, Kwan-Seong Jeong, Byung-Seon Choi, and Shin Young Kang[KAERI]

P0511 Solid Liquid Separation for the Foam Decontamination Waste Treatment Using Candle Filter ····· 325
Seung-Eun Kim, In-Ho Yoon, Wang-Kyu Choi, Seon-Byeong Kim, and Chong-Hun Jung[KAERI]

P0512 Cesium Removal From Aqueous Solution by Bioaccumulation of Microalgae ·· 327
Ilgook Kim, Bum-Kyoung Seo, and Jong-Won Choi [KAERI], Byung-Gon Ryu[NNIBR]

P0513 Electrochemical Behavior of Uranium(VI) in Ionic Liquid ····· 329
Iksoo Kim, Sumin Kwon, Dongyong Chung, Keunyoung Lee, and Jongwon Choi[KAERI]

P0514 The Study of Radiation Safety Treatment for Dismantling Contaminated Piping in NPP ····· 331
Cheol-Young Jeong, Min-Soo Kim, Dong-Kyu Jang, Dunk-Chul Hwang, and Hee-Kyoung Kim[ACT-RMT]

P0515 Removal of Sodium Dodecyl Benzene Sulfonate (SDBS) From Radioactive Liquid Wastes by Adsorption of Porous Polymer Resins ····· 333
Jongho Kim, Young-Jin Gwon, Hyungchul Kim, and Taek Seung Lee[Chungnam Natl. Univ.] Kune-Woo Lee[KAERI]

P0516 Stoichiometry of Palladium Extraction in Ionic Liquid ····· 334
Sumin Kwon, Ik-Soo Kim, and Dong-Yong Chung[KAERI]

P0517 Effect of the Addition of Oxalic Acid to the Phosphoric Acid Electrolyte on the Electro-decontamination Behavior of the SUS Metal Surface ····· 336
Dong-Yeon Kim, Hyun-Kyu Lee, Won-Zin Oh, and Sang-Jun Choi[Kyungpook Natl. Univ.]

P0518 Effect of the Temperature and UV Reflector on the AOP Decomposition Behavior of the Oxalates From the Chemical Decontamination Waste ····· 338
Jin-Hee Kim, Hyun-Kyu Lee, Won-Zin Oh, and Sang-June Choi[Kyungpook Natl. Univ.]

P0519 Innovative Biological Method to Remove Cesium-137 ····· 340
Seung Yeop Lee, Jae Kwang Lee, Min Hoon Baik, and Bum Kyoung Seo[KAERI]

P0520 Temperature Sensitive Strippable Coating for the Removal of Radioactive Cesium From Contaminated Surface ····· 342
Hee-Man Yang, Kyu Sun Hwang, Chan Woo Park, Kune-Woo Lee, Ilgook Kim, and In-Ho Yoon[KAERI]

P0521 Experimental Results of Oxidation / Reduction Process Based on Permanganic-Oxalic Acid ····· 344
Chorong Kim and Hak-Soo Kim[KHNP-CRI]

P0522 Estimation of Mixed Nuclide Inventory Using MicroShield Computer Program ···· 346
Jonghoa Kim, Homin Jeon, Yongsik Kim, Kyeongho Han, and Jangsoo Seo[Sae-An Eng.]

P0523 Derivation of Surface Soil $DCGL_w$ for Kori-1 NPP Reuse Scenario ····· 348
Ji Hyang Byon, Sang June Park, and Seokyoung Ahn[Pusan Natl. Univ.]

P0524 Requirement of Conceptual Design for Decommissioning Information Integration Management System ····· 350
Yunjeong Hong, Seungkook Park and Heeseong Park[KAERI]

P0525 Characterization of Clay Minerals in Soil Near Nuclear Facilities in Korea ···352
Chan Woo Park, Bo Hyun Kim, Hee-Man Yang, Kune-Woo Lee, and In-Ho Yoon[KAERI]

P0526 Efficiency of Decontamination Foam With Silica Nanoparticles and Chemical Reagent for Radionuclide Contaminated Surface ·····354
In-Ho Yoon, Chong-Hun Jung, Seung Eun Kim, So Hyeon Lee, Seon Byeong Kim, and Wang-Kyu Choi[KAERI]

P0527 Parameters and Procedures of Electro-kinetic Decontamination Experiments for Radioactive Concrete ·····356
Chanyoung Kim, Sungyeol Choi, and Myoungsu Shin[UNIST]

P0528 Application Review of Clearance for Metallic Waste After Decommissioning ····358
Sang-Ho Lee, Hyung-Woo Seo, and Chang-Lak Kim[KINGS]

P0529 Assessment of Radiation Dose by Applying Cover Depth for the Site Reuse After NPP Decommissioning ·····360
Hyung-Woo Seo, Sang-Ho Lee, and Chang-Lak Kim[KINGS]

P0530 Analysis on Disassembling Methods of Nozzle for PWR Spent Fuel ·····362
Younghwan Kim, Yungzon Cho, and Youngsoon Lee[KAERI]

P0531 Discussion on Non-fuel Waste Treatment in Connection With Dismantlement of Kori Unit 1 ·····364
Ju-Young Yoon and Cheon-Woo Kim[KHNP-CRI]

P0532 Desorption of Cesium From Montmorillonite and Hydrobiotite by Cationic Detergent ·····366
Bo Hyun Kim, Chan Woo Park, Hee-Man Yang, and Kune-Woo Lee[KAERI],
So Jin Park[Chungnam Natl. Univ.]

P0533 Study on Adsorption of Sodium Dodecylbenzenesulfonate by Using Amino Group-substituted Mesoporous Silica Nanoparticles ·····368
Daewon Kim, Jongho Kim, and Taek Seung Lee[Chungnam Natl. Univ.]

P0534 A Scheme to Develop a Decommissioning Safety Case ·····369
Byung-Sik Lee[Dankook Univ.]

6분과 방사선환경 및 안전 (Oral)

09:00~09:20 Environmental Gamma Distribution of Ulsan City With the Highest Nuclear Power Plant Density in Korea ·····373
Ukjae Lee, Jun Woo Bae, and Hee Reyoung Kim[UNIST]

09:20~09:40 Dose Assessment of the Public in Ulsan Under Normal Operation of Nuclear Power Plants Using FLEXPART ·····375
Jaeseong Min, Ukjae Lee, and Heereyoung Kim[UNIST]

09:40~10:00 Analysis of Inhalation Dose Rate to Workers in NORM Industries : Packing Area ·····377
Seung Woo Ji, Jung Hwan Jang, Il Park, and Kwang Pyo Kim[KyungHee Univ.],
Jae Kook Lee[KINS]

10:00~10:20 Asia-Pacific ALMERA Group Proficiency Test and Intercomparison Exercise on the Determination of Gross-Alpha and -Beta and Gamma Radionuclides ····· 379
C.S. Kim, J.Y. Yun, and M.H. Song[KINS]

10:40~11:00 Preliminary Studies on Reuse of Particle Accelerator Rooms After Decommissioning ····· 381
Jae Min Lee, Na Yoon Choi, and Jae Hak Cheong[Kyunghee Univ.]

11:00~11:20 Synthesis of Graphene Oxide Based Material for Removing Radioactive Iodine ····· 383
Sangsoo Han, Won-Seok Kim, and Wooyong Um[POSTECH]

11:20~11:40 Leak Path Factor Calculation of RIPF Hot-cell During an Accident ····· 385
Goanyup Lee, Bongseok Kim, Hyunki Kim, Haecho Lee, Jongsoo Kim, and Munja Kang[KAERI]

11:40~12:00 A Study on the Correlation Between Earthquakes and Nuclear Power Plants Analyzed Using SNS Big Data ····· 387
Seungkook Roh and Ik Jeong[KAERI], Yongjun Kim and Kibo Sim[KNEA], Jaesung Lee[GoGreat]

6분과 방사선환경 및 안전 (Poster)

P0601 Development of Radiation Emergency Movable Access Control System ····· 391
Cheol Hyun Kang, Jang-Lyul Kim, and Jong Il Lee[KAERI], Jung Bok Lee[UST]

P0602 Gap Analysis Between the National Arrangements on Emergency Preparedness and Response and IAEA GSR Part 7 ····· 393
Youngmin Lee, Seung-Young Jung, and Namyoung Kim[KINS]

P0603 The Evaluation of Radiation to Zinc Injection of Pressurized Water Reactor(PWR) ····· 395
Hee-Gyeong Kim, Min-Soo Kim, Dong-Kyu Jang, and Cheol-Young Jeong[ACT-RMT]

P0604 A Study on Applicability of Evaluation Code for Calculation of Exposure Dose of Workers for NPPs Decommissioning ····· 397
Seungsu Shin and Jongsoon Song[Chosun Univ.]

P0605 The Improvement Method of Oxidation Furnace of Chemical Cleaning Liquid Waste Treatment System ····· 399
Kyung-Wook Shin, Gyung-Sun Chae, Byeong-Mok Park, Jae-Young Hong, Yun-Soon Jeong, and Hee-Kon Jang[SAE-AN Eng.]

P0606 Impact Analysis on the Uranium Evaluation Related to the Collecting Location of the Environmental Sample ····· 401
Ju Young Jeon, Ji-Yeon Song, Sung-Hwan Kim, Jong-Ho Yoon, Seungho Jeong, and Hana Seo[KINAC]

P0607 A comparison Between Alpha-emitting Calibration Source and Electro-deposited Plate of KINAC ····· 403
Jong-Ho Yoon, Ju Young Jeon, JiYeon Song, and Hana Seo[KINAC]

P0608 Research of Self-disposal Evaluation for Domestic Hard-to-treat Radioactive Waste ····· 405
Yongho Hong, Hyoungmin Park, Eunsuk Choi, and Wonjin Jeong[ACT]

P0609 The Performance Test of Induction Type Furnace for the Design of Tritium Desorption System ····· 407
Eunkyung Jung, Kyu Min Song, Byunwook Ko, Kahee Jeong, and Seungchul Park[KHNP-CRI]

P0610 Introduction of the Environmental Sampling Network for the Safeguards in KINAC ····· 409
Ju Young Jeon, Jong-Ho Yoon, and Hana Seo[KINAC]

P0611 Development of Emergency Plan for Permanently Defueled Condition of Kori Unit 1 ····· 411
Jeongmi Kim[KHNP-CRI]

P0612 Thousand-fold Sensitivity Enhancement of Lanthanide by Capillary Electrophoresis ····· 413
Jihye Kim and Tae-Hong Park [KAERI], Kihwan Choi[KRISS]

P0613 Mock-up Training Effects for Steam Generator Lancing & FOSAR ····· 415
Byeong-Mok Park, Kyung-Wook Shin, Cheol-Wan Park, Ah-Ran Cha, Dong-Hyun Yoo, Min-Gyu Kim, and Do-Yeong Jung[SAE-AN Eng.]

P0614 Quality Management for Steam Generator Lancing & FOSAR ····· 417
Byeong-Mok Park, Jae-Hyun Han, Kwan-Seok Choi, Young-Kug Kim, Sam-Hyun Kim, Chang-Yul Lee, and Hee-Kon Jang[SAE-AN Eng.]

P0615 Compression Behavior Studies on Ammonium Molybdophosphate (AMP) ··· 419
Junhyuck Im and Yongjae Lee[Yonsei Univ.]

1분과

핵주기정책 (Oral)

Safeguards System Development Status and Future Prospects of Fuel Cycle Facilities at KAERI

Ho-Dong Kim*, Hee Seo, Se-Hwan Park, Hee-Sung Shin, Dae-Yong Song, Jong-Myung Oh,
Jeong-Hoe Ku, and Seong-Kyu Ahn
Korea Atomic Energy Research Institute, 111, Daedeok-daero 989beon-gil, Yuseong-gu, Daejeon, Republic of Korea
*khd@kaeri.re.kr

1. Introduction

Since the early 1990s, KAERI has developed safeguards systems of several nuclear fuel cycle facilities for research activities on spent fuel treatment. Such facilities include the DUPIC Fuel Development Facility (DFDF), the Advanced spent fuel Conditioning Process Facility (ACPF), and the Pyroprocessing Integrated inactive DEmonstration facility (PRIDE). As part of a cooperative effort with the IAEA to find a safeguards approach for the pyroprocessing facility, the ROK designed a Reference Engineering-scale Pyroprocessing Facility (REPF) and developed a safeguards system for the REPF that was reviewed by the IAEA. An advanced safeguards system, including nuclear material accounting technologies and new safeguards approaches for pyroprocessing facilities, has been under development at KAERI.

2. Safeguards Systems of Nuclear Fuel Cycle Facilities at KAERI

According to the "Agreement for Cooperation between the Government of the Republic of Korea and the Government of the United States of America Concerning Peaceful Uses of Nuclear Energy" revised in 2015, KAERI has been using DFDF for preparing the feed material (porous pellet or fragment) from the used PWR fuel generated in domestic nuclear power plants for the ACPF electrolytic reduction process. The ACPF at KAERI has been refurbished for the test of an electrolytic oxide reduction process using spent fuels.

The safeguards approaches for the DFDF and ACPF have been developed, that include neutron counters and containment and surveillance equipment with a process and radiation monitoring system.

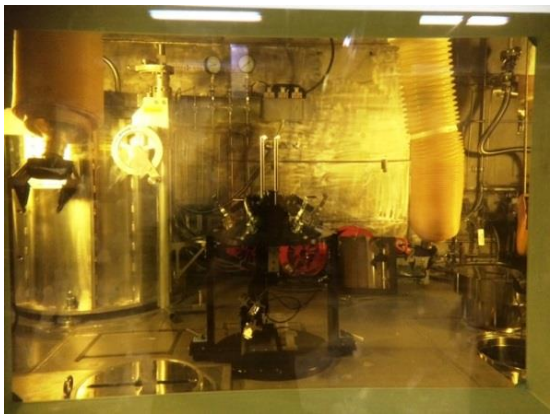


Fig. 1. ASNC and ALIM.

The ACPF can provide a valuable opportunity to test various types of safeguards equipment for nuclear material accountancy, containment and surveillance, as well as process monitoring. At the moment, there are two types of safeguards equipment at the ACPF, i.e., ASNC (ACP Safeguards Neutron Counter) and ALIM (ACP LIBS Monitoring system) [1].

PRIDE is an engineering-scale R&D facility, handling non-irradiated depleted uranium (DU) and

surrogates to develop and test key technologies for pyroprocessing prior to the development and construction of an engineering-scale facility.

The demands for robust safeguards applied to pyroprocessing facilities require the IAEA to develop new measures and techniques to complement the more traditional safeguards systems. The bus bar system, together with portal radiation monitors, were selected and installed in the PRIDE facility to support IAEA safeguards implementation in this facility [2].

Process monitoring data such as voltage, current, temperature, and humidity are collected from the process equipment. Most of parameters relevant to the PRIDE safeguards are collected, and they are displayed and provided to the IAEA.

3. Safeguards System of Reference Engineering-scale Pyroprocessing Facility

The ROK was working closely with the IAEA under the ROK's Member State Support Program to develop a model SG approach for a REPF. REPF design is part of the IAEA's effort to develop an effective SG approach for pyroprocessing facilities. As a result of the project, a model DIQ (Design Information Questionnaire), a model FA (Facility Attachment) and a model SG approach were prepared [3].

Based on the experience with the ROK MSSP, the IAEA is well on the way to establish effective safeguards for future engineering/commercial scale facilities.

4. Conclusion

KAERI has developed several nuclear fuel cycle facilities (DFDF, ACPF and PRIDE) for research activities on spent fuel treatment. The ROK designed the REPF through IAEA MSSP and developed a safeguards system for the REPF that was reviewed by the IAEA.

The application of Safeguards by Design (SBD) to these efforts will contribute to improving nonproliferation and safeguards technology so that pyroprocessing technology can be realized in the future. It is expected that the deployment of these safeguards technologies would be useful for the advanced nuclear fuel cycle.

REFERENCES

[1] H. Seo et al., "Development of ACP Safeguards Neutron Counter (ASNC)," KAERI/TR-6594/2016, pp.1-29 (2016).

[2] W. Bekiert et al., "Safeguarding Pyro. Related Facilities in the ROK', Proceedings of IAEA Safeguards Symposium (2014).

[3] H.D. Kim, H.S. Lee, D.Y. Song, T.H. Lee, B.Y. Han, S.K. Ahn, and S.H. Park, "Application of safeguards-by-design for the pyroprocessing facilities in the ROK', JNMM, Vol. XL(4), 24 (2012).

Consideration of Hold-up for Material Accountancy in Pyroprocessing Plant

Seong-Kyu Ahn*, Byung-Hee Won, Bong-Young Kim, and Jeong-Hoe Ku
Korea Atomic Energy Research Institute, 111, Daedeok-daero 989beon-gil, Yuseong-gu, Daejeon, Republic of Korea
*skahn76@kaeri.re.kr

1. Introduction

A safeguards material accountancy usually relies on the accounting analysis of physical inventories at the time of annual physical inventory taking. During that period, the operation process is stopped and cleaned-out to minimize the amount of materials impossible to measure, so called residual hold-up. The way to clean-out the process as well as the material hold-up amount have not yet been investigated in detail, mostly due to the lack of integrated operation schemes and dedicated experimental data. Therefore, the clean-out and hold-up issue tends to be regarded one of the major challenges in safeguarding a pyro-processing plant. The purpose of this study is to analyze the material hold-up effect on material accountancy and suggest possible clean-out approaches for safeguarding a pyro-process.

2. Hold-up in Material Accountancy

Hold-up in the field of safeguards defined as nuclear material deposits remaining after shutdown of a plant in and about process equipment, interconnecting piping, filters and adjacent work area [1]. For plants in operation, the hold-up is the amount of nuclear material contained in the process. It is also referred to as in-process inventory. Because the hold-up is un-measureable inventory, it is usually treated as hidden inventories, which means a part of materials unaccounted for (MUF) in materials accounting terminology.

In general, hold-up amount does saturate in steady-state conditions after a certain period of initial operation. The data set from the calciner of the ammonium diuranate (ADU) experiment is a good example of the steady-state behavior of hold-up with time [2].

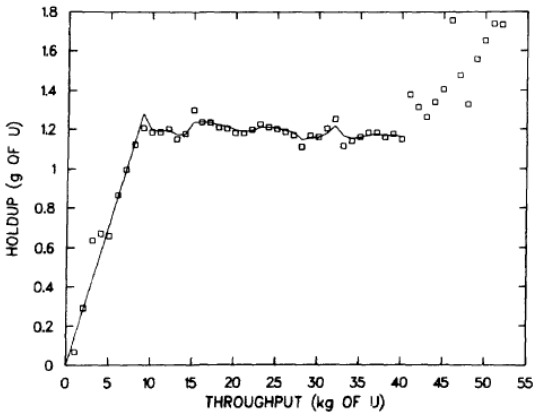


Fig. 1. Uranium holdup data and model for the calciner (from Ref [2]).

Hold-up data from mixed oxide fuel (MOX) fabrication plant shows 0.1 ~ 0.4% of batch size in the 200 kg-batch capacity blender [3]. Another example of powder material hold-up in MOX plant shows 5 g/meter of ceramic power hold-up observed in the transfer pipes [4]. With the assumption of 20 cm of pipe diameter, it refers to 5 g/m^2 hold-up on a surface

3. Hold-up in Pyroprocessing

The major anticipated mechanisms of material accumulation in pyroprocess are (1) the accumulation

of fine particles of spent fuel on the surfaces or in the gaps of process equipment in a region of head-end process, and (2) the condensation of salt phase process materials on the surface of process equipment in the main pyroprocessing area.

The hold-up amount of powder mixing equipment for head-end pyroprocess was estimated by the weight difference between before and after the 50 kg-batch mixing experiments. Measured hold-up was about 30 g, which is equivalent to 0.06% of batch size.

In case of detection of an abrupt diversion under a near real-time accountancy, the hold-up of about 1.8 kg of plutonium-equivalent materials over the entire processes can falls in the acceptable range.

There can be several ways to minimize or recover hold-up materials in a design concept or fabrication technique, such as special surface treatment, knocker or scrapper with recovery mechanism, or encapsulation to minimize powder scattering or salt evaporation area, etc [6].

4. Conclusion

The amount of material hold-up in the process directly affects the requirements of accounting measurement uncertainties to satisfy allowed MUF evaluation. The hold-up does not continuously increase but fluctuation under steady-state operation conditions. Experiences from other similar facilities and our own experimental results with estimated accounting uncertainty estimation seems like the practically achievable range of hold-up and MUF evaluation results. It should be, however, noticed that the margin of accounting measurement uncertainty does not always allow as much residual material. In case of protracted diversion cases, however, the effect by hold-up material worsens the accountancy performance. Therefore, process equipment design and operation scheme should carefully take into account the way how to minimize hold-up materials.

REFERENCES

[1] IAEA, “IAEA Safeguards Glossary 2001 Edition”, International Nuclear Verification Series NO.3, 2001.

[2] K. Pillay and R. Picard, “Fundamentals of Materials Accounting for Nuclear Safeguards”, Ch.6, p.152, LA-11569-1, LANL, 1989.

[3] ESARDA MOX Working Group, “Control of nuclear material hold-up: the key factors for design and operation of MOX fuel fabrication plants in Europe”, IAEA-SM-367/8/04, 2004

[4] E. Haas, “Description and Safeguards Concept for the former Siemens MOX Fuel Fabrication Plant (MOX II) Siemens Brennelementewerk Hanau, Germany”, and personal communications.

[5] T. Iwamoto, “Hold-up Measurement in a Reprocessing Facility”, JNFL.

Effects of One-sided Weights on Multi-criteria Decision Making for Promising Nuclear Fuel Cycle Options in Korea

Hong Jang*, Hyo On Nam, Chul Min Kim, and Won Il Ko
Korea Atomic Energy Research Institute, 111, Daedeok-daero 989beon-gil, Yuseong-gu, Daejeon, Republic of Korea
*janghong@kaeri.re.kr

1. Introduction

Most countries adopting the nuclear energy have cast a doubt on the nuclear sustainability and postponed making the decision on policies aimed at managing spent fuel. One reason is that, the nuclear sustainability is significantly interconnected with the multiple controversial issues. In this point, the integrated evaluation method, such as multi-criteria decision making (MCDM) methods, can help decision makers to assess the nuclear fuel cycle (NFC) options quantitatively and systematically.

2. Nuclear Fuel Cycle Evaluation

Based on the current situation in Korea, two NFC options are promising; once-through (OT) cycle, and pyroprocessing and sodium-cooled fast reactor (pyro-SFR) cycle. To evaluate them, five evaluation criteria related with key issues were selected; natural U requirement, waste management, NFC cost, proliferation resistance, technical readiness. And the waste management were further divided into three sub-criteria; disposal area for the high level waste (HLW), disposal area for the low and intermediate level waste (LILW), storage area for Cs/Sr.

The first three criteria were quantified based on the dynamic mass flow calculated from the NFC model [1] and an assumed growth scenario of nuclear electricity demand. The scenario follows the 7th Basic Plan on Electricity Demand and Supply until 2029, and then fixes the power capacity at 2029 from 2030 to 2100. The mass flow was converted to the disposal and storage area, and the NFC cost through additional analysis. The proliferation resistance was quantified based on the previous KAERI report [2]. And the technical readiness was quantified based on the engineering sense. As a result, pyro-SFR has higher scores for the natural U requirement and waste management, and OT has higher scores for the rest.

3. Multi-criteria Decision Making

For fair evaluation of the NFC options, two different MCDM methods were used; technique for order of preference by similarity to ideal solution (TOPSIS) and preference ranking organization method for enrichment evaluation (PROMETHEE) [3]. A prior step for the integrated evaluation using MCDM is determining the weights for the criteria. In this study, various decision making groups were assumed to see the effect of their biased characteristics. And the characteristics were reflected in the weights. For example, a group against nuclear weapons might give a higher (doubled) weight on the proliferation resistance than others. Like this way, 6 groups were assumed; G1) neutral, G2) conservationist, G3) local resident, G4) economic realist, G5) anti-nuclear, G6) technician. Table 1 shows the weights for all groups. Weights for sub-criteria are same for all groups. The weight of the HLW disposal area is two times higher than that of the Cs/Sr storage area and four times higher than that of the LILW disposal area.

Table 1. Weights for the different decision making groups

Criteria	G1	G2	G3	G4	G5	G6
Natural U requirement	1/5	1/3	1/6	1/6	1/6	1/6
Waste Management	1/5	1/6	1/3	1/6	1/6	1/6
NFC cost	1/5	1/6	1/6	1/3	1/6	1/6
Proliferation Resistance	1/5	1/6	1/6	1/6	1/3	1/6
Technical Readiness	1/5	1/6	1/6	1/6	1/6	1/3

4. Results and Discussions

Fig. 1 ~ 6 show evaluation results from TOPSIS and PROMETHEE with same weights in Table 1. TOPSIS gives a higher priority on pyro-SFR except on G6 (Fig. 6). PROMETHEE gives a higher priority on OT except on G3 (Fig. 3).

TOPSIS is based on the multidimensional distance (root of squares) from the best and worst options [3] so that the priority is largely dominated by the highest score among all criteria. For G1~G5, pyro-SFR gets a higher priority because its score for the waste management is dominant regardless of their weights. In case of G6, however, the dominant score moves to the technical readiness of OT so that the priorities are reversed.

On the other hand, PROMETHEE is based on the degree of outranking for one option over another [3], which is usually estimated by using linear or stepwise functions. For the groups except on G3, OT having more outranking criteria than pyro-SFR gets a higher priority regardless of their weights. But in case of G3, the degree of outranking of the waste management of pyro-SFR becomes higher than the sum of others of OT. Therefore, the priorities are changed.

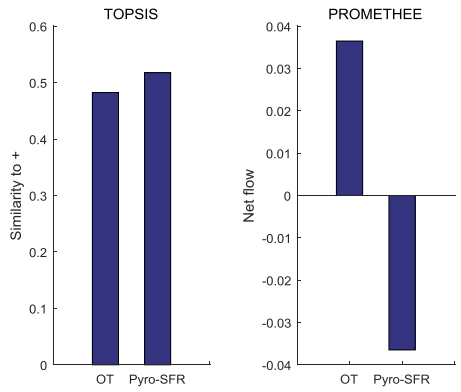


Fig. 1. Integrated evaluation results for G1.

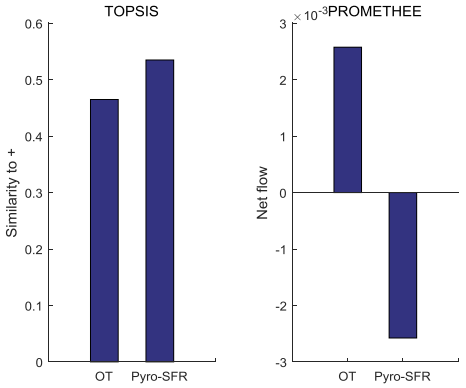


Fig. 2. Integrated evaluation results for G2.

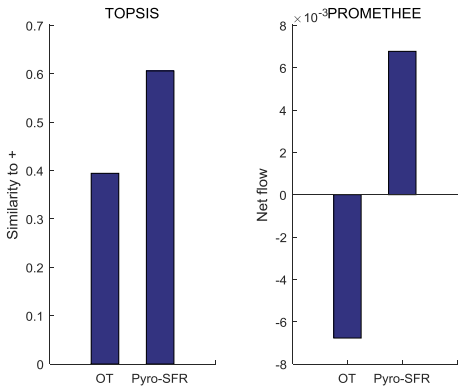


Fig. 3. Integrated evaluation results for G3.

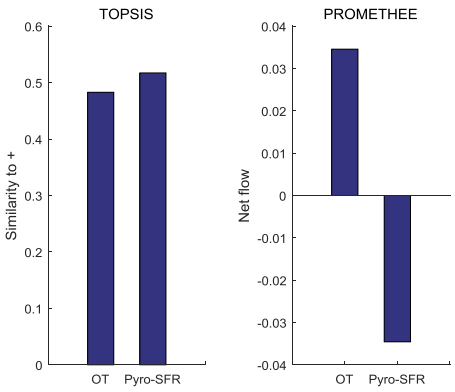


Fig. 4. Integrated evaluation results for G4.

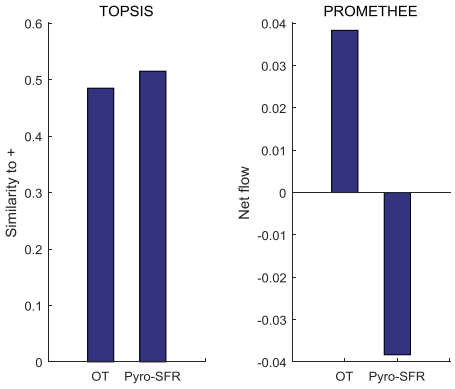


Fig. 5. Integrated evaluation results for G5.

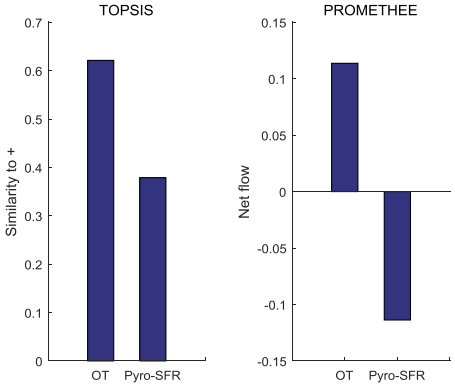


Fig. 6. Integrated evaluation results for G6.

5. Conclusions

Based on the evaluation results for two NFC options considered in Korea, one-sided weights (doubled weight) for TOPSIS and PROMETHEE seems not to affect their priorities significantly. TOPSIS can be recommended for decision makers who want to give higher priorities to the option getting a few but dominant scores among the criteria. And PROMETHEE can be recommended for decision makers who want to give higher priorities to the option having many favorable criteria.

In the future, the sensitivity analysis for the degree of bias of weights will be performed.

REFERENCES

[1] S. Choi, H.J. Lee, and W.I. Ko, “Dynamic analysis of once-through and closed fuel cycle economics using Monte Carlo Simulation”, Nuclear Engineering and Design, 277, 234-247 (2014).

[2] KAERI, “Analysis of Proliferation Resistance of Nuclear Fuel Cycle Systems”, Korea Atomic Energy Research Institute, Deajeon, Korea (2009).

[3] V. Belton, and T.J. Stewart, “Multiple criteria decision analysis: an integrated approach”, Boston: Kluwer Academic Publication (2002).

A Study on the Implementation of Export Controls for Spent Nuclear Fuel

Chansuh LEE*, Jinho CHUNG, and Donghoon SHIN

Korea Institute of Nuclear Nonproliferation and Control, 1534 Yuseong-daero, Yuseong-gu, Daejeon, Republic of Korea

*chans@kinac.re.kr

1. Introduction

Recently, various studies related to the storage, management and treatment of spent nuclear fuel have been actively conducted in domestic and abroad. However, there are not many studies on export control of spent fuel. South Korea is implementing export control of nuclear items and technology in accordance with the NSG Guidelines, Nuclear Safety Act and the Foreign Trade Act. If the spent fuel is to be exported or imported as needed, or if exporting spent fuel reprocessing technology, a government ex/import license is required.

In this paper, characteristics of reprocessing of spent fuel were analyzed and items for ex/import licenses were reviewed. On the basis on there, it intends to draw some points to be used for improvement of nuclear export control system in ROK.

2. Reprocessing of spent nuclear fuel

2.1 Process and status of spent fuel processing

The spent fuel treatment method is largely a wet and dry method. According to NSG guidelines, Reprocessing irradiated nuclear fuel separates plutonium and uranium from intensely radioactive fission products and other transuranic elements. That is, the method of physically separating Pu and U corresponds to reprocessing. Currently, in the case of pyro-processing under development in Korea, Pu and U are not separated and thus do not fall into the category of reprocessing. In the case of enriched U or Pu, which is the core material of nuclear weapons, it is a controlled item. In recent years, several countries are studying ways to make Pu separation difficult in reprocessing in order to improve nuclear nonproliferation. US UREX + (Uranium Extraction), UK GANEX (Group ActiNides Extraction) and Japan's NEXT (New Extraction System for TRU Recovery) are under development.

2.2 Export control related to reprocessing of spent nuclear fuel

According to the NSG Guidelines and the Public Notice on trade of strategic goods and technologies, the export of sensitive items or technology is controlled strictly. Facilities, equipment and technology related to concentrate reprocessing are sensitive items or technology. These sensitive exports to countries covered by the NSG denial notification are limited.

Suppliers should not authorize the transfer of enrichment and reprocessing facilities, and equipment and technology therefore if the recipient does not meet, at least, all of the following criteria: NPT Party, comply with the obligations of the IAEA safeguards agreement, adhere to NSG guidelines, comply with UNSCR 1540, comply with inter-governmental nuclear cooperation agreements, apply physical protection, and comply with IAEA safety standards. Prior to beginning transfers of reprocessing facilities, equipment, or technology, suppliers should consult with NSG Participating Governments regarding the non-proliferation-related terms and conditions applicable to the transfer.

3. Export control implementation of spent nuclear fuel

Nuclear fuel assemblies are subject to control items in accordance with the Public Notice on trade of strategic goods and technologies Annex 2 0A001.f, 0C002 before and after use. There are two cases where export control related to spent fuel is required. First, reprocessing of spent nuclear fuel to overseas consignment, and second, export of items or technology related to spent fuel reprocessing. In both cases the export control procedure will be very similar.

3.1 Export control procedures for reprocessing of spent nuclear fuel

Japan has reprocessed approx. 7,000 tons in the UK and France. If Korea is reprocessed abroad, it will be possible in the UK and France as well as in Japan. Licensing is required from the Nuclear Safety and Security Commission (NSSC) before import and export, and a government to government assurances (GTGA) are required in advance. When exporting trigger list items, it is necessary to receive the GTGA from the recipient country and it takes several months to exchange through diplomatic channels of the Ministry of Foreign Affairs.

In addition, because nuclear fuel assemblies contain more than 1 effective kg of nuclear material, suppliers should report them at the time of importation and exportation according to the provisions of the IAEA Comprehensive Safeguards Agreement. Based on this, The NSSC conducts an advance notification to the IAEA.

3.2 Expected Control Items

According to the Public Notice on trade of strategic goods and technologies, plants for the reprocessing of irradiated fuel elements, and equipment specially designed or prepared therefor are controlled as 0B006. Detailed control items are as follows; irradiated fuel element chopping machines (0B006.b), dissolvers(0B006.c), solvent extractors and solvent extraction equipment(0B006.d), chemical holding or storage vessels(0B006.e), neutron measurement systems for process control(0B006.f), The complete system (0B006.f) is composed of a neutron generator, a neutron detector, amplifiers, and signal processing electronics. Most of the detailed items are related to wet reprocessing. The only overlap in the wet and dry processes is the process of peeling and chopping the fuel cladding. In the case of wet reprocessing, the process proceeds to dissolution in a nitric acid solution after cutting, whereas in the case of dry process, the porous pellet is produced through powder production or high temperature heat treatment for the next step of electrolytic reduction. Therefore, items that are highly likely to be controlled in Korea are 0B006.b and 0B006.f.

3.3 Other considerations

If the spent fuel contains US or Canadian nuclear material, it is necessary to further review the bilateral nuclear cooperation agreement and observe its obligations.

In addition, transportation of nuclear fuel assemblies must be reported in accordance with the Nuclear Safety Act. In the case of international transport, it must be guaranteed from the countries concerned that the nuclear material under international carriage will be protected and shall comply with the physical protection rating standards and requirements in accordance with INFCIRC/225 rev5. The fuel after irradiation is Category 2. Further research is needed on these areas.

4. Conclusion

Domestic and overseas interest in the processing of spent nuclear fuel is increasing. Several countries are actively conducting research on nuclear nonproliferation related to spent nuclear fuel. In this article, we examined the implementation of export control related to spent fuel.

Technology related to the reprocessing of spent nuclear fuel is sensitive technology, and there are many requirements for import and export as follows; Export control of INFCIRC/254, physical protection of INFCIRC/225, safeguards and additional protocol obligations of the IAEA, obligations for nuclear cooperation agreements, and public safety requirements.

It is expected that Korea will continue to be interested and researches such as improving the related laws on nuclear nonproliferation related to processing of spent nuclear fuel and developing related systems.

REFERENCES

[1] IAEA INFCIRC/254/Part1/Rev13 (2016).

[2] IAEA INFCIRC/225/Rev5 (2011).

[3] Nuclear Safety Act (2015).

[4] The Public Notice on Trade of Strategic Goods and Technologies (2017).

[5] Gil-Sung You, “A Status of Technology and Policy of Nuclear Spent Fuel Treatment in Advanced Nuclear Program Countries”, Journal of Nuclear Fuel Cycle and Waste Technology, 5(4), 330-350 (2007).

Case and Trends Study for Establishing Cyber Security Information Sharing System

Soo Min Lim* and Chae Chang Lee

Korea Institute of Nuclear Non-proliferation and Control, 1534 Yuseong-daero, Yuseong-gu, Daejeon, Republic of Korea

*s2min@kinac.re.kr, chiching@kinac.re.kr

1. Introduction

Cyber threats that occur worldwide are becoming more diverse in their threat forms and attack targets. In recent years, the demand and necessity of research for timely response has been increasing due to the increase of cyber attacks targeting the infrastructure in overseas. However, it is not easy to take various evolving attacks and to formulate countermeasures against which infrastructure are quite differentiated from the general IT infrastructure. For this reason, the importance of sharing information related to past incidents including cyber incidents and recovery processes is emerging. The purpose of this paper is to review the requirements of the European institutions and the United States that have established an information sharing system preemptively and to utilize them to build cyber threat information sharing system in domestic nuclear facilities.

2. Precedent Case and Trends Study for Information Sharing System

2.1 General information

In nuclear facilities, timely response to safety is important. In particular, Korea's nuclear facilities have been strengthened in response to the cyber incident in 2014, when KHNP data were leaked as an example of cyber security infringement. In order to cope with an effective cyber-infringement incident, a corresponding system should be established through a series of processes, such as preparation-detection-initial response-recovery. This series of process requires knowledge of threat attributes and actual attack cases, but due to the nature of the nuclear industry, it is difficult to collect such information easily. Therefore, this paper overlook at the status of sharing information gathered by other international organizations including cyber events and IAEA member countries in the world, and establish information sharing system of domestic nuclear facilities and other infrastructure.

2.2 IAEA

The IAEA is developing a draft recommendation to establish cyber incident information sharing system related to nuclear security for cyber incident information sharing. The detailed information of the sharing information system would refer from the IAEA Computer Security Plan (2016-2018) [1], Computer Security Implementation Plan (2016-2018) for cyber security implementation plans.

2.3 EU Research Activities for Information Sharing System

According to the ENISA annual report 2016 [2], information sharing research for cyber security incidents are progressed in various EU nations, such as Netherlands (NCSC, National Cyber Security Centrum) [3], Germany (UP KRITIS) [4], Finland (FICORA, Finnish Communications Regulatory Authority) [5], Belgium (CTRISRP, Cyber Threat Intelligence Research Project) [6], and the Czech Republic (CZ NSA) [7].

2.3.1 UP KRITIS (Germany). Various countries around world, such as Canada, Australia, South Africa, Finland, France, Japan, India and the Netherlands has established a national security strategy through cyber security private-public partnership (PPP). As part of the European SCADA and Control System Information Sharing (E-SCSIE), Germany adopted a more specific approach to the partnership mechanism and submitted a recommendation to the National Cyber Security Council with a clear charter. UP KRITIS is developing a strategic cyber security solution by a specialist in order to avoid overlooking new security threats with a mature civil-public partnership space.

2.3.2 EU DENSEK Project (EU ISAC). The Information Sharing Platform will form a trusted network to liaise between the ISAC and its members. It will facilitate the distribution of information, newsletters, alerts etc. It provides the members of the Energy ISAC possibilities to stay informed regarding cyber security news and events in an efficient and effective way[8].

2.4 US NIST SP800-150

NIST SP 800-150 [9], "Guide to Cyber Threat Information Sharing", encourages greater sharing of cyber threat information among organizations, both in acquiring threat information from other organizations and in providing internally-generated threat information to other organizations. Recommendations described in this paper enables organizations to make more efficient and effective use of information sharing capabilities.

3. Experience and Plan for Computer Security Incident Response in ROK

Legal basis of incident response in ROK are following Act on Physical Protection and Radiological Emergency (APPRE).

3.1 Incident Experience

By a group calling itself “Who am I” who seems rebel to the nuclear power plant operation, releasing KHNP information to public in 2014. The incidents breaks irregularly 10 times more until the august of 2015. The cooperative government investigation team stating that ongoing leaks of NPP information were the work of a North Korean hacker’s organization.

3.2 KINAC/RS-015

As part of operational security measures in 2.5.6 of KINAC/RS015 [10], nuclear power operators should work with cyber security related organizations to share information on the latest cyber security threats, vulnerabilities, accidents, technologies, techniques, and countermeasures.

4. Conclusion

According to Cisco's white paper on how to respond to security threats to public utilities and energy industries, infrastructure that has undergone a security breach is likely to apply security measures, including application whitelisting, security solutions, and process safety reviews[11].

In general, the facility are opposed to considering an information sharing. Especially, for sharing cyber security issues between different institutes are sensitive information that the vulnerability of facility may expose classified information to the public and the information abasement.

For this purpose, it is recommended to establish a trusted channel and interagency body and to share information among different institutions.

REFERENCES

[1] Computer Security at Nuclear facilities, IAEA Nuclear Security Series No. 17.

[2] "ENISA Annual Report 2016", September 09, 2016.

[3] NCSC, https://www.ncsc.nl/english (last access date: 31 March 2017).

[4] http://www.kritis.bund.de/SubSites/Kritis/EN/publications/Fortschreibungsdokument_engl..html (last access date: 31 March 2017).

[5] https://www.viestintavirasto.fi/en/cybersecurity/ficorasinformationsecurityservices/cert-fi/rfc2350.html (last access date: 31 March 2017).

[6] http://www.politiestudies.be/userfiles/20141202%20BISC%20Luc%20Beirens%20voor%20verspreiding.pdf (last access date: 31 March 2017).

[7] http://www.nbu.cz/en/ (last access date: 31 March 2017).

[8] "Security Information Sharing for Smart Grids developing the Right Data Model", the 9th International Conference for Internet Technology and Secured Transactions (ICITST-2014), 2014.

[9] "Guide to Cyber Threat Information Sharing", NIST Special Publication 800-150, October 2016.

[10] Regulatory Standard for Security for Computer and Information System of Nuclear Facility, KINAC/RS015, October 2014.

[11] Utility and Energy Security: Responding to Evolving Threats, 2016.

Establishment of Vital Digital Assets Verification Environment Design Base

Yeeun Byun, Hyundoo Kim, and Kookhei Kwon
Korea Institute of Nuclear Nonproliferation and Control, 1534 Yuseong-daero, Yuseong-gu, Daejeon, Republic of Korea
hibye@kinac.re.kr

1. Introduction

As cyber-attacks continue to occur at nuclear facilities, the importance of cyber security to nuclear facilities is getting higher. In this situation, there is also a growing need to establish cyber security measures against electronic infringement and establish a fundamental defense system for the nuclear facilities. Therefore, it is possible to establish a verification environment for vital digital assets (VDA) that are directly related to the nuclear accidents including fuel damage among the critical digital assets (CDA). In this paper, we discuss what to consider when designing the VDA verification environment.

2. Test Requirements of VDA Verification Environment

2.1 General Requirements

To be used as VDA verification environment, the requirements of ANSI/ANS 3.5(2009) "Nuclear power plant simulators for use in operator training and examination" must be satisfied. After establishing the VDA verification environment, we should test the items required for comprehensive operating status, abnormal operation, safety status, and transient status according to ANSI/ANS 3.5 in order to verify that the analysis environment operates correctly.

2.2 Comprehensive Operating Status

3.1.3.2 Normal Evolutions of ANSI/ANS 3.5 requires testing to include at least the following in order to test the overall operating condition.

- Power plant startup from cold shutdown to rated power conditions
- Power shutdown from rated power to cold shutdown conditions
- Power operation and load changes
- Surveillance testing performed by the driver on safety-related equipment or systems.

2.3 Abnormal Operation

3.1.4 Malfunctions of ANSI/ANS 3.5 require testing to include 24 malfunction points to test for abnormal operating conditions.

2.4 Safety Status

ANSI / ANS 3.5 Appendix B B.1.1 The Steady-State Test requires the following to test the steady state: In this test, an acceptable steady-state response is tested by comparing the parameters between the simulator and the existing plant. The thermal balance data should be compared against three distinct output levels over at least 50% of the available operating range. Therefore, it may be considered to perform the following test in such a state.

- 100% output steady state
- 75% output steady state
- 50% output steady state
- 25% output steady state

2.5 Transient Status

ANSI/ANS 3.5 Appendix B B.3.2 the Transient Performance Test requires tests to include 11 malfunction statements to test transient conditions.

3. Details on Test of VDA Verification Environments

In order to construct the VDA verification environment, the following data and environment should be prepared.

Table 1. Data List for VDA Verification Environments

Data for Development of Process Model	P&ID (Piping and Instrument Diagram), System Operation Diagram ,Control & Instrument Diagram, Control Logic Diagram, General Arrangement Drawing, Single Line Diagram, Schematic Diagram, Component List, Component Technical Specification & Component Data, Board Elevation Drawing, Data from Turbine, S/G, PZR, RCP, RX, Condenser, MSR etc. ,Core Input Deck, Fuel Assembly Map, Neutron Instrument Locations, Fuel Geometry, Reactor Vessel Geometry, Primary Loop Piping, Pressurizer Geometry, Steam Generator Geometry, Reactor Coolant Pump Parameters, Detail Drawing of Reactor Vessel Internals,
Data for Development of Plant Process Computer	Turbine Control System Control Logic & HMI, CPC/ENFMS algorithm and HMI Design Report, PAS algorithm and HMI Design Report, PMS algorithm and HMI Design Report. etc.
Data for Detail Environments	System Function Description, Set-Point List, Controller Gain & Constant, Instrument Range
Data for Development for self-test and test procedure	FSAR, Operating Procedure, Operation Data by Output

In order to construct the VDA analysis environment, the following equipment should be prepared.

Table 2. Hardware and Software for establishing VDA Verification Environments

Hardware	Main Server, Computer for Instructor, Engineering Work Station, Plant Process Computer, Network Equipment
Software	Simulation Environment, Core Program, Development tool

4. Conclusion

We have discussed what needs to be considered to design the VDA verification environment and what materials need to be prepared. Each data for the VDA verification environment could be produced by a variety of organizations such as system designers, software designers, manufacturers, licensees and operators. Further research on VDA verification environment should be studied for effective regulation and in-depth cyber security and it is expected that cyber security for nuclear facilities will be strengthened by developing regulatory technology.

ACKNOWLEDGEMENTS

This work was supported by the Nuclear Safety Research Program through the Korea Foundation Of Nuclear Safety (KoFONS), granted financial resource from the Nuclear Safety and Security Commission (NSSC), Republic of Korea (No. 1605007).

REFERENCES

[1] American Nuclear Society, “Nuclear Power Plant Simulators For Use In Operator Training And Examination”, 3.5 (2009).

[2] KINAC, “Regulatory Standard – Security for Computer and Information System of Nuclear Facilities” (2015).

1분과

핵주기정책 (Poster)

Proliferation Resistance Analysis of Autonomous Small Modular Reactor Design Optimization

Chul Min Kim[1,2], Man-Sung Yim[1], Philseo Kim[1], Sobin Cho[1], Sung Ki Kim[2], Kwang-Rag Kim[2], Hong Jang[2], Won Il Ko[2], Chung-Seok Seo[2], and Hyo On Nam[2]

[1]Korea Advanced Institute of Science and Technology, 291 Daehak-ro, Yuseong-gu, Daejeon, Republic of Korea

[2]Korea Atomic Energy Research Institute, 111, Daedeok-daero 989beon-gil, Yuseong-gu, Daejeon, Republic of Korea

usekim00@kaist.ac.kr

1. Introduction

ATOM (Autonomous, Transportable, On-demand, Modular) reactor is a conceptual Small Modular Reactor (SMR), based on the Pressurized Water Reactor (PWR), which is currently advocated for further development by Korea Advanced Institute of Science and Technology (KAIST). When developing the design requirements of ATOM, Security/ Safeguards-by-design (SSBD) should be considered at the earliest stage of the design process to optimize the system. This paper evaluates the characteristics of various design options, in terms of cost, proliferation resistance and safeguardability. This paper evaluates the cost and proliferation resistance for selected scenarios for core design options.

2. Top-tier Core Requirements Development

Various core performance scenario were assumed to analyze the proliferation resistance and estimated cost for ATOM reactor. Table 1 shows the basic core performance of ATOM, which is based on Pressurized Water Reactor (PWR).

Table 1. Assumed Core Performance of ATOM for Calculation

Enrichment	4.95%
Capacity factor	85%
Power conversion rate	35.15%
Reactor life	60

Table 2 shows the core performance scenario for optimizing proliferation resistance and cost of ATOM.

Table 2. Core Performance Scenario of ATOM

Power (MWe)	100,150,200,250,300
Power density (KW/l)	60, 70, 80
Burnup (GWd/MTU)	33(1batch), 44(2batch), 49.5(3batch)
Cycle length (yr)	Dependent

3. Proliferation Resistance Evaluation based on TOPS Method

TOPS task force suggested the framework for evaluating proliferation resistance of various fuel cycle systems [2]. The evaluation criteria consist of 3 main categories (material barriers, technical barriers, institutional barriers) and 15 subcategories. Table 3 summarizes the difference of proliferation resistance by evaluating each subcategory.

Table 3. Proliferation Resistance Evaluation Results based on Core Design Scenario

Barriers	Evaluation Result
Radiological	Self-protection characteristics is maintained when core characteristics changes, since the spent fuel has similar constituent compared to PWR SF.
Mass and Bulk	The attractiveness of SF decreases when burnup increases. However, no significant change occurs in 5% enrichment/33~49.5 GWd/MTU range.
Isotopic	Pu-239 fraction decreases when burnup increases.

Facility Access	Proliferation resistance increases when autonomous level and cycle length increases.
Available Mass	The amount of nuclear material increases when power increases. However, the amount per unit electricity will remain same. If burnup increases, PR increases since the amount of nuclear material decreases.

For different core characteristics, mass and bulk and isotopic barrier changed significantly. Table 4 summarizes the value of mass and bulk barrier and isotopic barrier for different burnup scenarios.

Table 4. The Difference of Isotopic Barrier Value based on Burnup

Average Burnup	Isotopic Barrier			
	Critical Mass	Isotope Enrichment	Neutron Emission	Heat
MWd/MTU	Pu	Pu-239/Pu	(Pu-240+ Pu-242) / Pu	Pu-238/Pu
33000	Same	56.6	27.9	1.3
43000		52.5	30.3	2.0
53000		50.4	31.2	2.7

4. Conclusion

For SMRs, modular design concept is widely considered as viable option. However, security and safeguards aspects should be carefully considered for modular design concept. Fuel burnup and cycle length should be maximized to reduce cost and achieve high proliferation resistance. Cycle length is dependent to fuel burnup, and no trade-off has been found in terms of cost and proliferation resistance. Finally, when autonomous operation level is increased, the facility access level is decreased so that the proliferation resistance is increased and security cost (which is included in O&M cost) can be decreased. During the design process of ATOM reactor, refueling method of modular reactors and spent fuel monitoring should be deeply considered to achieve security/safeguards-by-design, while the rest of requirements are similar with other PWRs.

Acknowledgments

This research was supported by Basic Science Research Program through the National Research Foundation of Korea (NRF) funded by the Ministry of Science, ICT & Future Planning (No. NRF-2016R1A5A1013919).

REFERENCES

[1] Bari, R. a. (2015). Proliferation resistance and physical protection (PR&PP) in small modular reactors (SMRs). Chap. 9 in Handbook of Small Modular Nuclear Reactors. Woodhead Publishing Limited.

[2] A. Hassberger (2001), Application of Proliferation Resistance Barriers to Various Existing and Proposed Nuclear Fuel Cycles, Lawrence Livermore National Laboratory, UCRL-ID-147001.

[3] H. L. Chang et al. (2009), Analysis of Proliferation Resistance of Nuclear Fuel Cycle Systems, Korea Atomic Energy Research Institute, KAERI/TR-3928/2009.

Input Material Accounting Method With Homogenization Mixers for an Engineering Scale Pyroprocessing Facility

Chaehun Lee*, Bong Young Kim, SangHo Na, Hee Seo, Byung-Hee Won, Se-Hwan Park, Hee-Sung Shin, Ho-Dong Kim, Jong-Myeong Oh, Ha-Jin Song, Junghoe Ku, and Seong-Kyu Ahn

Korea Atomic Energy Research Institute, 111, Daedeok-daero 989beon-gil, Yuseong-gu, Daejeon, Republic of Korea

*chlee80@kaeri.re.kr

1. Introduction

Pyroprocessing is a promising technology to recycle spent fuel, and to reduce the volume and toxicity as well as an advantage on proliferation resistance compared to Plutonium and Uranium Extraction (PUREX) reprocessing [1]. To secure proliferation resistance, Nuclear Material Accountancy (NMA), especially input material accountancy, is the most difficult in an engineering scale facility because the solid form of input material is different from aqueous processing, PUREX in which an Input Accountability Tank (IAT) is used for input material accountancy.

In this study, two homogenization mixers were tested with surrogate powder materials, and powder and Pu heterogeneity were estimated using the test results. Additionally, the Pu accounting uncertainty was calculated with respect to the number of Destructive Analysis (DA) samples in the double stage homogenization process.

2. Double Stage Homogenization Process

2.1 Concept of the Double Stage Homogenization

The homogenization method for input accountancy was proposed in the REPF model [2] in which a 500 kg large homogenization mixer was adapted to process a spent fuel assembly per operation. However, Equipment operated in hot-cell should be remotely controlled and maintainable. Thus, homogenization mixers should be relatively small and the operation mechanism should be simple for maintenance. Two types of homogenization mixers were used for the double stage homogenization. The first mixer is three tumbler mixers of 75 kg which 75 kg spent fuel powder is charged into, and the second one is a 10 kg Nauta or tumbler mixer as shown in Fig. 1. After mixing spent fuel powder in each 75 kg tumbler mixer, kg scale samples are taken from three tumbler mixers to represent the whole population, and three samples are charged into a 10 kg mixer. After mixing in the 10 kg mixer, DA samples of 1 g are taken. The Pu accounting uncertainty is not affected only by the mixing performance, but also by the distribution of Pu concentrations in spent fuel powder, the mass uncertainty charged into the first mixer (75 kg tumbler), and the first sampling mass uncertainty in double stage homogenization process. Thus all parameters should be considered to estimate the Pu accounting uncertainty.

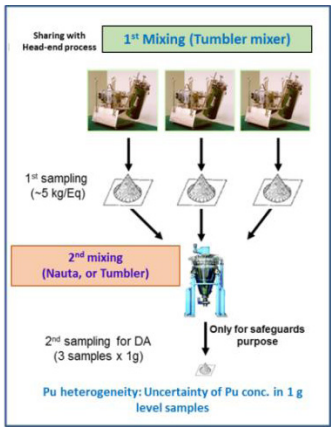


Fig. 1. Concept of the double stage homogenization process.

2.2 Performance evaluation of mixers

As shown in fig. 2, a 10 kg Nauta and tumbler mixer were designed and fabricated to evaluate the mixing performance. 10 kg and 50 kg containers for the tumbler mixer were tested to check the scale-up effect. 45 *u*m CuO and NiO were prepared and charged into each container at a mass ratio of 3:7, nine DA samples of 1 g were taken from various positions of the container, and analyzed by

Inductively Coupled Plasma Optical Emission Spectrometry (ICP-OES, Thermo Scientific iCAP 6300). Relative Standard Deviations (RSD) of the mass ratio with respect to the mixing time are shown in Fig. 3 in which RSDs from the Nauta mixer is smaller than 0.3% at an arm speed of 0.7, and all RSD values are lower than 0.8% after 3 hours of mixing.

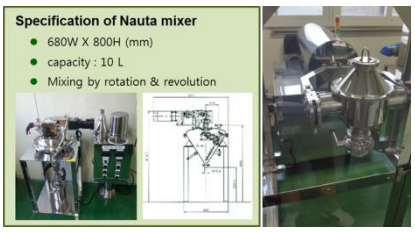


Fig. 2. Nauta mixer (left) and tumbler mixer (right).

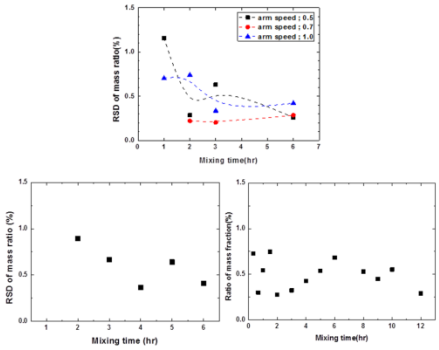


Fig. 3. Measured RSD of the mass ratio (10 kg Nauta: top, 10 kg tumbler: bottom left, 50 kg tumbler: bottom right).

2.3 Powder heterogeneity

Mixing two types of powder (binary mixture) is a general method to evaluate the powder heterogeneity and determine the variance of the composition. However, spent fuel powder has many different types (multi-component mixture) of powder containing various Pu concentrations rather than a binary mixture. Thus, the uncertainty (RSD) of each powder component having different mass fractions was calculated as explained by R. Hogg [3]. Based on the RSD of mass ratio from the test, the powder heterogeneity was plotted as a function of mass fraction in Fig. 4. The powder with the lower mass fraction is more heterogeneous because the number of powder particles in the DA samples is smaller than the higher mass fraction.

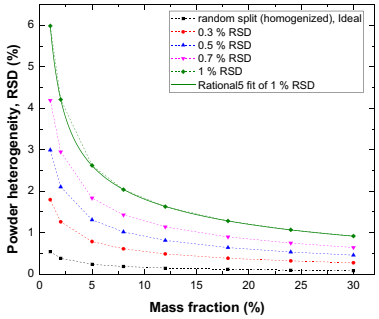


Fig. 4. Powder heterogeneity as a function of mass fractions.

3. Discussion

In the previous section, the powder heterogeneity based on the performance test result was calculated. The Pu heterogeneity is affected by the distribution of Pu concentration as well as the powder heterogeneity. The Pu heterogeneity will be calculated with the calculated powder heterogeneity using the existing gamma scan profile of a spent fuel rod. The result will be presented including estimate of the Pu accounting uncertainty at the conference.

4. Conclusion

The double stage homogenization was proposed for input accountancy in an engineering scale pyroprocessing facility, and the candidates of homogenization mixers were tested and analyzed. To minimize the Pu accounting uncertainty, the method to charge the spent fuel powder into the first mixer, and the first sampling method should be carefully designed. The estimate of the Pu accounting uncertainty in this study will help in conceptual design of devices used in the double stage homogenization process.

REFERENCES

[1] T. Inoue, et al., “Development of pyroprocessing and its future direction”, Nucl. Eng. Tech. 40(3), 183-190 (2008).

[2] H. Shin, et al., “Analysis of the present status of conceptually designed pyroprocessing facilities for determining a reference pyroprocessing facility”, KAERI/TR-398; 2009.

[3] R. Hogg, “Characterization of relative homogeneity in particulate mixtures”, Int. J. Miner. Process. 72, 477-487 (2003).

Measurement of Detector Parameters of Neutron Coincidence Counter for Nuclear Material Accountancy

Hee Seo[1*], Chaehun Lee[1], Jong-Myeong Oh[1], Seong-Kyu Ahn[1], Jeong-Hoe Ku[1],
Ho-Dong Kim[1], and Seonkwang Yoon[1,2]
[1]Korea Atomic Energy Research Institute, 111, Daedeok-daero 989beon-gil, Yuseong-gu, Daejeon, Republic of Korea
[2]University of Science & Technology, 217 Gajeong-ro, Yuseong, Daejeon 34113, Republic of Korea
[*]hseo@kaeri.re.kr

1. Introduction

The Advanced spent fuel Conditioning Process Facility (ACPF) in KAERI has been refurbished for the demonstration of the technologies related to the oxide reduction process of pyroprocessing [1]. The ACPF can provide good opportunities not only for process purposes but also for safeguards technologies. In this study, a well-type passive neutron coincidence counter, called ASNC (ACP safeguards neutron counter), was developed and its detector parameters were measured.

2. ACP safeguards neutron counter (ASNC)

The ASNC, based on the passive neutron coincidence measurement technique, measures the amount of 244Cm. Based on that measurement, the amount of nuclear material subsequently can be determined by using the Cm balance technique, which multiplies the measured 244Cm amount by the Pu/244Cm or 235U/244Cm ratio to calculate the amount of nuclear material of interest (Pu or 235U). This ratio can be obtained by a destructive analysis, gamma-ray spectroscopy, or burnup-code calculation. In a previous study [2], the ASNC was installed in a hot cell of the ACPF and tested successfully with spent fuel rod cuts. However, its inner structure, with a horizontally-laid geometry, becomes deformed over the course of many years due to the weight and the ductility of the leaden gamma-ray shield. To address this problem, the ASNC was to be redesigned for a vertically-standing geometry based on the MCNP simulation and irradiation test results. Fig. 1 shows the modified ASNC.



Fig. 1. Modified ACP Safeguards Neutron Counter.

3. Detector parameters

Various detector parameters are needed to be determined in order to characterize the measurement system and to correct the measured data. The parameters determined in this study were operating voltage, dead-time correction factors, and efficiency profile.

Fig. 2 shows the high-voltage plateaus for 24 ^{3}He detectors installed in the ASNC. The gains of detectors with associated electronics were matched to each other and showed good agreement between the

detectors. The operating voltage was determined as 1720 V from the measured high-voltage plateau.

The dead-time corrected singles (S_c) and doubles (D_c) can be expressed as follows:

$$S_c = S_m \times e^{\frac{1}{4}\delta S_m}, D_c = D_m \times e^{\delta S_m} \qquad (1)$$

where S_m and D_m is the measured singles and doubles count rate, respectively. δ is the dead-time coefficient and given by $\delta=A+B\times S_m\times 10^{-6}$ where A and B are constant. The A and B were determined to be 2.1286×10^{-6} and 1.1328×10^{-12}, respectively, by using a two source method.

The detection efficiency profile in the axial and radial directions was measured for a ^{252}Cf standard source in order to characterize the system and verify the MCNP model. Ideally, a good system shows the same efficiency regardless source locations, resulting in low measurement error. The system showed flat response in terms of the measured efficiency, as shown in Fig. 3. In addition, the simulated results showed excellent agreement with the measured data, which confirmed the accuracy of the MCNP model for the measurement system.

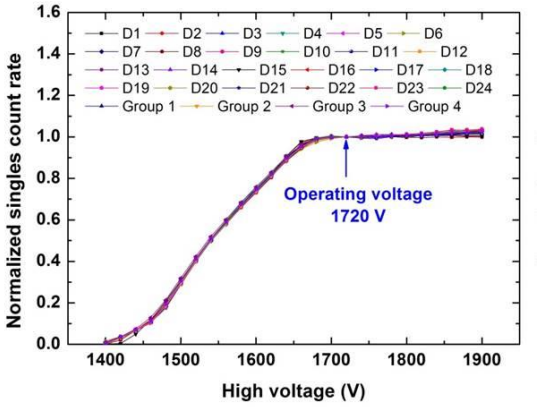


Fig. 2. Modified ACP Safeguards Neutron Counter.

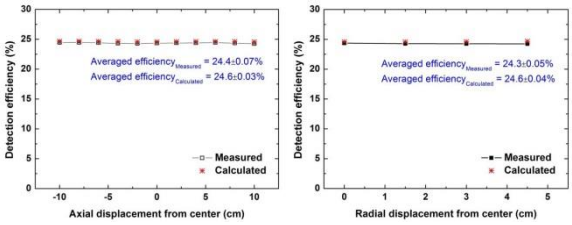


Fig. 3. Modified ACP Safeguards Neutron Counter.

4. Conclusion

The modified ASNC will be tested with the spent fuel rod cuts for calibration and with the input and output materials of oxide reduction process for evaluation of the performance.

REFERENCES

[1] S. N. Yu *et al.*, "Hot cell renovation in the spent fuel conditioning process facility at the Korea Atomic Energy Research Institute," Nucl. Eng. Technol. 47(6), 776-790 (2015).

[2] T. H. Lee *et al.*, "Hot-test Results of the Advanced Spent Fuel Conditioning Process Safeguards Neutron Counter for PWR Spent Fuel Rods," Nucl. Technol. 176, 147-154 (2011).

Investigation of Design Requirements and Potential Sampling Methods for Engineering-scale Pyroprocessing Safeguards

Bong Young Kim*, Chaehun Lee, Seong-Kyu Ahn, Hee Seo, Byung-Hee Won, Se-Hwan Park, and Jeong Hoe Ku

Korea Atomic Energy Research Institute, 111, Daedeok-daero 989beon-gil, Yuseong-gu, Daejeon, Republic of Korea

*bykim@kaeri.re.kr

1. Introduction

For safeguards of pyroprocessing, destructive analysis (DA) is required for nuclear material accountancy (NMA) and sampling is essential for DA measurement. However, study of sampling approach has not been performed and there are several technical issues due to the high radiation and temperature of pyroprocessing. In this study, design requirements of sampling system and potential sampling methods for various types if sample were investigated.

2. Design requirements of sampling system

The sampling system is covered from a taking a sample to transfer the sample to the analytical laboratory (AL). The design requirements of a sampling system for NMA, such as sampling positions, uncertainty, sample amount and sampling period, are developed based on the conceptual safeguards system of an engineering-scale pyroprocess facility [1]. In other words, sampling uncertainty and sample amount were decided through the feedback with MUF evaluation results. Moreover, sampling position and step were decided by considering representativeness. After taking a sample, it is transferred from the main process cell to the AL through a pneumatic transfer tube. Moreover, all the process is required to be an automated system.

3. Sampling methods

3.1 Input material

The form of input material is SF oxide powder and samples are taken from homogenization mixer during the pre-treatment process. KAERI developed the double stage homogenization concept and the tests were performed with metal oxide powders [2].

Table 1. Design requirements of sampling system

Type		Requirements
SF oxide powder [Input material]	Positions	2nd homogenization mixer
	Uncertainty & amount	2%, 1g/ea.
	Period	twice /SF assembly
	Weight	Powder inserted into 1st mixer, powder inserted into 2nd mixer, DA sample
Electro-recovery (ER[4] & EW[5]) molten salt [In-process material]	Positions	Electro-recovery vessels (sample: molten phase)
	Uncertainty & amount	1.4%, 1g/ea.
	Period	once/NRTA[1] & RE DD[2] period, twice/WIP[3]& distillation
	Weight	DA sample, total salt weight in vessel (volume x density)
U&U/TRU ingot [Products]	Positions	Ingot manufacture equipment (sample: molten phase)
	Uncertainty & amount	1.4%, 1g/ea.
	Period	U product: 3 times/ three months, 1ea/ingot U/TRU product: 1ea/ingot
	Weight	Ingot, DA sample

[1]NRTA: Near-Real Time Accountancy, [2]RE DD: Rare Earth Drawdown, [3]WIP: Work In Process, [4]ER: Electro-Refining, [5]EW: Electro-Winning

For the double stage homogenization, two types of mixer are needed. The concept of double stage homogenization is shown in Fig. 1. The oxidized SF powder from an assembly was charged and homogenized by 3 of 1st mixers with 75 kg/mixer capacity. After mixing, several kg of powder is taken from each 1st mixer and charged into the 2nd mixer. The 2nd mixer has higher performance than 1st mixer

and 1 g of DA samples are taken from 2nd mixer after mixing. By this concept, sampling uncertainty and number of DA sample can be reduced. However, specific sampling method is not fully developed yet. The MOX fuel fabrication facility has an automated powder sampling system and KAERI will develop sampling techniques for input accountancy based on the precedent experience in detail.

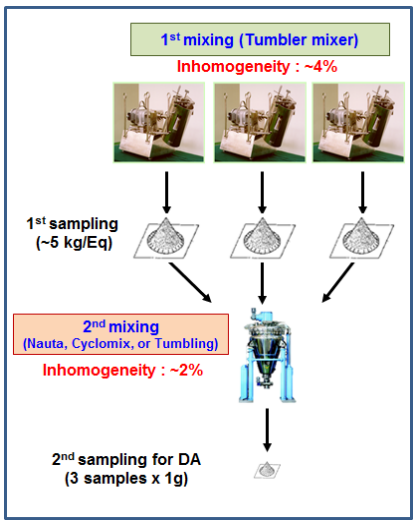


Fig. 1. Concept of double stage homogenization process [2].

3.2 In-process material

The operating temperature of ER/EW process is 500°C. For that reason, temperature is main issue of molten salt sampling. The micro-fluidic and dipstick methods are considered as a salt sampling under the high temperature condition. The microfluidic techniques enable production of uniform micro-samples of molten salt automatically by utilizing sampling line, pump, and droplet generator [3]. For the dipstick method, molten salt is taken by inserting the STS or Ta rod into the electro-recovery vessel and take it out. According to this procedure, molten salt is covered the rod surface and the salt sample can be obtained. This method has been applied at PRIDE and INL. The microfluidic method is valuable but technology readiness level is low and more feasibility study is needed in the future. Therefore, dipstick is considered as a primary salt sampling method for the pyroprocessing.

3.3 Products

The final form of product is U and U/TRU metal ingot. To manufacture the ingot, U and U/TRU metal, recovered by ER and EW process, are melted. Molten phase is proper to take a sample due to the representativeness. According to the melting point of U and U/TRU metal, the temperature is the most difficult obstacle as like salt sampling. The counter-gravity casting process is one of the potential sampling methods. This approach is utilized to cast components of machine and fabricate metal fuel of fast reactor. The counter-gravity casting is that the molten metal is forced to fill mold cavity against gravity under the pressure difference and solidified [4]. This method is expected to be applied for molten metal sampling by optimizing the operation conditions and quartz tube is considered as a mold.

4. Conclusion

The design requirements of the sampling system and potential sampling methods were investigated. However, this study is a fundamental research and further research on developing the sampling methods for various forms of waste and specific conceptual design of automated sampling devices will be performed.

REFERENCES

[1] S.K. Ahn et al., “Development of safeguards requirements for preliminary conceptual design of pyroprocessing facility”, KRS spring meeting (2015).

[2] C.H. Lee et al., “A study on input nuclear material accountancy methods for pyroprocessing”, KRS autumn meeting (2015).

[3] C. Pereira et al., “Application of microfluidic techniques to pyrochemical salt sampling and analysis:, IAEA-CN-220-199.

[4] Z. Jianmin et al., “A new counter-gravity casting process, mold filing dynamics, convective heat transfer and influence on mechanical properties”, Asian Pacific Conference for Materials and Mechanics, November 12-16, 2009, Japan.

The Exploration of Machine Learning Based Process Monitoring for Pyroprocessing Safeguards

Young-Eun Jung[1,2], Chul-Min Kim[1,2], Bong-Young Kim[2], and Man-Sung Yim[1*]

[1]Korea Advanced Institute of Science and Technology, 291 Daehak-ro, Yuseong-gu, Daejeon, Republic of Korea

[2]Korea Atomic Energy Research Institute, 111, Daedeok-daero 989beon-gil, Yuseong-gu, Daejeon, Republic of Korea

*msyim@kaist.ac.kr

1. Introduction

Pyroprocessing has been considered as an important part of spent fuel management in the Republic of Korea. One of the major challenges in the development of pyroprocessing technology is nuclear safeguards. To augment the capability for pyroprocessing safeguards, use of Process Monitoring (PM) has been suggested [1,2]. The PM-based approach takes advantage of various process data produced during operation to detect anomalies which may be related to safeguards-significant events.

In this study, use of PM for pyroprocessing safeguards through the machine learning-based approach was investigated.

2. Process Monitoring

PM has been used to monitor the operational state and operating conditions in a variety of commercial plants. By installing different sensors in proper locations at the facility, during the operation, various signals can be produced including physical, electrochemical [3], and spectroscopic analytical signal in a pyroprocessing facility. Fig. 1 shows an example of the concept using the electrorefining (ER) process, which is one of the major unit processes in pyroprocessing. Therefore, the first step is listing available sensors and their corresponding signals.

Prior to obtaining information about process operation from signal, normal and off-normal operating conditions should be defined. In off-normal operation, diversion would be suspected through an inductive method. As a next step, process applicable signals need to be selected from among the available signals. This can be done by investigating the function and performance of each signal. As a result, the off-normal operation can be distinguished in real time, based on signal data.

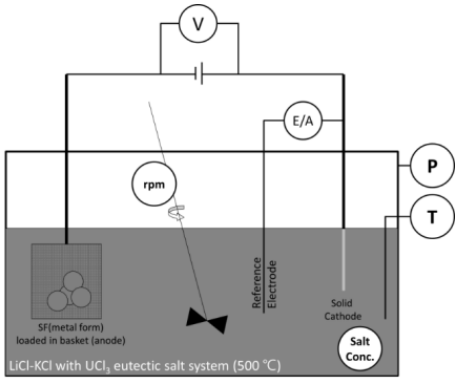


Fig. 1. Application of applicable sensors to electro-refiner.

For example, in case of ER process where uranium is selectively separated from spent fuel and deposits on a cathode, detection of an off-normal operation based on PM is describe in the following. In normal operation, the density of electrolyte, which includes special nuclear material, maintains a certain range. However, regardless of the intention, if the operating condition is shifted to a certain way, plutonium could co-deposits on a cathode with uranium. As a results, the density would be slightly decreased because of the weight difference. For the same reason, a cathode density is increased. Therefore, if the density is measured correctly and its information is provided in a timely manner, the off-normal operation would be detected [4].

3. Machine Learning

Machine Learning (ML) is an application of artificial intelligence. Using statistical inference, the computer learns without explicit programing. Based on existing data, ML can predict unseen data. Therefore, to employ this approach, sufficient quantities of data should be acquired.

3.1 Data development

ML requires extensive data, from which statistical inference can be drawn. The collected data should be produced in various operating conditions including both normal and off-normal operations. Considering efficiency and practicality, data development will be achieved through both experiments and model simulations. For these reasons, the target is limited to the ER process.

In ML, the obtained data should be categorized into three data sets: training data, validation data, and test data. In the training stage, to reduce decision error, a variety of data should be used including the data that represent normal and off-normal conditions. Data available for each of the three stages above must match the objectives. Training will use a majority of the data while rational validation requires about 20% of data. Finally, in the testing stage, the performance of the machine is examined using 20% of available data.

3.2 Algorithm study

To develop a system using provided data properly, the appropriate type of algorithm should be studied. Based on a purpose of ML, there are various applicable algorithms. Considering that the purpose of this study is predicting/estimating the operation state or operating condition of the process from data, the algorithm function is to classify anomalous data.

There are several algorithms for the classification. Depending on the characters of selected signal(s), adequate algorithm(s) will be attempted.

4. Conclusion

In this study, an approach to develop a machine learning based process monitoring method was discussed to support pyroprocessing safeguards. Necessary data development will be an important part of this effort and further research will be conducted to examine the feasibility of the proposed work.

REFERENCES

[1] Metcalf, R., Bevill, A., Charlton, W., and Bean, R. “Safeguards Envelope: Previous Work and Examples”, No. INL/CON--08-14405, Idaho National Laboratory (United States)(2008).

[2] Henkel, J. J. "Development of a Safeguards Monitoring System for Special Nuclear Facilities"(2011).

[3] Samaneh R. P., Dumidu W., Milos M., and Supathorn. P. “Electrochemical Data Analysis and Simulation via Artificial Neural Intelligence for Pyroprocessing Safeguards Application”, Proc. of the 2016 INMM 57th Annual Meeting, Atlanta, Georgia.

[4] Garcia H. E., Simpson M. F. Lin W. C., Carlson R. B., and Yoo T. S. “Application of process monitoring to anomaly detection in nuclear material processing systems via system-centric event interpretation of data from multiple sensors of varying reliability”, Annals of Nuclear Energy 103(2017).

Study on Improvement of Licensing Requirements of Fuel Cycle Facilities

Hyeong Ki Shin[1*], Seung-Jae Han[1], Byoung-Jik Kim[1], Ara Go[1], Jae-Yeong Park[1], and Sang Hoon Park[2]

[1]Korea Institute of Nuclear Safety, 62 Gwahak-ro Yuseong-gu, Daejeon, Republic of Korea

[2]RadWorks®, Cheomdan Store Da-308, Doryong-dong, Yuseong-gu, Daejeon, Republic of Korea

[*]hkshin@kins.re.kr

1. Introduction

As the cumulative amount of spent fuel generated from 24 nuclear reactors operating in Korea is expected to become gradually saturated in near future, Public Engagement Commission on Spent Nuclear Fuel Management, through the final report published in 2015, recommended that the spent fuel stored in NPPs be transferred to an interim storage facility before the on-site storage capacity is exceeded and that a waste disposal facility be constructed and operated.

While there is an aspect of difficulty in securing the budget and the site when directly disposing of the spent fuel generated from the light water reactor, there are also discussions on how to use the spent fuel as a useful resource by recycling it, as an alternative to the direct disposal of spent fuel. For this purpose, pyro-processing, one of the dry processing methods of spent nuclear fuel, has been studied for years by Korea Atomic Energy Research Institute (KAERI). However, there is no experience of safety review to license the spent fuel recycling facility in Korea yet and its safety evaluation methods have not yet been established. Therefore, it would be necessary to review and prepare a licensing system for spent fuel processing facilities in the current Nuclear Safety Act in Korea.

In 2014, IAEA Integrated Regulatory Review Service (IRRS) of the nuclear fuel cycle facilities in Korea demanded that legal bases for the periodic safety review (PSR) and for the safety assessment report by an integrated safety assessment (ISA), including chemical and radiological hazards, should be provided to improve the safety regulatory framework of nuclear fuel cycle facilities.

This study will review on the licensing system in Nuclear Safety Act for the fuel cycle facilities and discuss what needs to be improved in the future.

2. Legal basis for fuel cycle facilities

In order to carry forward a project of spent fuel recycling facilities in the future, the legal basis for this sort of facility should be specified in Nuclear Safety Law beforehand. So, it would be necessary to first consider whether legal terms are well defined in nuclear safety act and regulations. The legal basis for fuel cycle facilities in Nuclear Safety Act were reviewed whether the pyro-processing facility can be classified as a spent fuel processing facility and whether transuranic fuel manufacturing facility, which handles transuranic elements extracted from pyro-processing, can be classified as a manufacturing facility.

In addition, the relevance of licensing procedure for the spent fuel processing facility was examined through the review of the Article 35 in the Nuclear Safety Act. In fact, the revised bill on the second clause of the article that applicants for the spent fuel processing facility are required to be designated by the competent Minster according to the enforcement decree, has already been laid before the National Assembly in 2016. This clause was modified to strengthen the safety on the spent fuel processing facility by Nuclear Safety and Security Commission as well as to separate the utilization of nuclear power and its regulations.

3. Documents to be submitted for license application related to fuel cycle facilities

The documents to be submitted for license application such as refining, processing and conversion facilities of nuclear fuel materials or nuclear raw materials shall be prepared in accordance with the third clause of Article 35 of the Nuclear Safety Act. The documents involve reports on radiological environmental impact assessment, safety

management regulations, quality assurance plan, decommissioning plan and other documents prescribed by the enforcement regulations. When compared to the cases of power reactors and radioactive waste management facilities, the most significant difference in license application of the spent fuel recycling facilities is that documents to be submitted as a license application do not currently require a safety analysis report and that the documents required by the enforcement regulations of the Nuclear Safety Act are more complex than the other two cases.

Documents required by the second clause of Article 31, Article 40 and Article 44 of the enforcement regulations for the license of spent fuel related facilities, already include site characteristics, design, radiation protection and accident analysis, which are described in the safety analysis report of the other facilities. However, it would be desirable to submit a safety analysis report to simplify the document submission for authorization and of increasing efficiency for safety evaluation. It would be desirable that facility location and structure, radiation exposure management, radioactive waste management, design and construction manuals, etc. be all integrated into the safety analysis report in order to simplify the document submission.

4. Licensing step for fuel cycle facilities

Another aspect of discussion involves licensing step. Licensing the power reactor requires usually two steps, i.e. a construction permit followed by an operating license. Radiological risk for the materials handled by spent fuel recycling facilities are relatively high compared to other nuclear fuel cycle facilities, such as low enrichment uranium fuel fabrication facility, currently in operation. Actually, one-step licensing may not be appropriate to a technology where there has been essentially no experience and when it isn't even known how to assess the risk of this technology yet. No data other than laboratory data is available with almost no idea of operational problems and frequencies of failure. Therefore, one-step licensing system could be a burden not only to both the regulatory bodies and the utilities but also to the acquirement of public acceptance.

On the other hand, two-step licensing system similar to the case of power reactor, would have demerits that it require more cost and time to be consumed for the legal improvements. In addition, prolonged time for licenses can result in the delay of project launching. IAEA safety document requires that every project for a new fuel cycle facility shall follow an authorization process that comprehensively addresses all safety aspects, so that two-step licensing process would be desirable to cover sufficiently safety features of facilities with relatively high risk of radiological hazard. Further discussion would be required on formulating the rulemaking to allow either one-step or two-step licensing.

5. Conclusion

The review on the licensing system of the spent fuel recycling facilities in Nuclear Safety Act was carried out in comparison with those of other nuclear facilities, referring to IAEA Safety Standards and US regulatory documents. Some improvements on legal basis, license application documents to be submitted and licensing steps were proposed for the licensing system of the nuclear fuel cycle facilities in Nuclear Safety Act. It is expected that proposed improvements will be effectively utilized to revise the licensing system of the fuel cycle facilities in the future.

REFERENCES

[1] IAEA Safety Standards, "Safety of Nuclear Fuel Cycle Facilities", No. NS-R-5 (rev. 1), 2014.

[2] U.S.NRC, "Draft Regulatory Basis for Licensing and Regulating Reprocessing Facilities", SECY-11-0163, 2011.

Development of a Guideline for the Preparation of SAR on Spent Nuclear Fuel Recycling Facilities

Jihyun Kim[1*], Hyunseok Seo[1], Kyongwon Han[1], Sang Hoon Park[1], and Hyeong Ki Shin[2]

[1]RadWorks Corp., 530 Daeduckdae-ro, Yuseong-gu Daejeon, Republic of Korea

[2]Korea Institute of Nuclear Safety, 62 Gwahak-ro, Yuseong-gu, Daejeon, Republic of Korea

[*]jhkim9775@gmail.com

1. Introduction

The development of a spent nuclear fuel recycling process in Korea necessitates revision and supplement of current nuclear safety regulations including the establishment of a guideline for the preparation of a Safety Analysis Report (SAR) on spent nuclear fuel recycling facilities. The revision tends to integrate various documents to be submitted for a nuclear fuel cycle facility license application into a SAR [1]. For this, a previous study reviewed the conventional and current approaches for the format and contents of SAR on spent nuclear fuel recycling facilities in the United States [2]. The study also investigated on the Integrated Safety Analysis (ISA) [2]. These studies expected the utilization of current ISA based approach as a reference to the development of our SAR preparation guideline. Actually, NUREG-1520 [3] was considered to be a relevant representative document for the referencing.

This paper presents a guideline that has been developed in terms of SAR framework for licensing spent nuclear fuel recycling facilities.

2. Method and Results

2.1 Identification of key references

Reviews have been made to IAEA recommendations and regulations of the United States and Korea with regard to the SAR framework as shown in Fig. 1. These have led to the identification of key aspects worth for being referenced in the formulation of the intended SAR framework, as follows:

2.1.1 IAEA NS-R-5 recommends basic concepts of As Low as Reasonably Achievable (ALARA) and defense in depth [4].

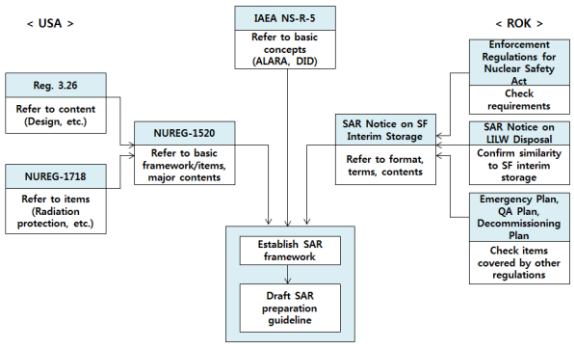


Fig. 1. Development approach for SAR framework.

2.1.2 US NUREG-1520 is, as mentioned earlier, a representative reference of current approach for SAR preparation, providing a framework, items to be covered and major contents. NUREG-1718, "Standard Review Plan for the Review of an Application for a Mixed Oxide Fuel Fabrication Facility" is similar to NUREG-1520 and provides additional information on radiation protection, etc. Regulatory Guide 3.26, "Standard Format and Content of Safety Analysis Reports for Fuel Reprocessing Plants" is conventional guide, but still useful partly in particular for building and process design, etc.

2.1.3 The Korean Nuclear Safety and Security Commission (NSSC) Notice 2015-020 [5] is another principal reference providing a type of framework, items to be covered, technical terms, and contents that are being used for nuclear fuel cycle facilities under Korean nuclear safety regulatory system. NSSC Notice 2015-018 on "Standard Format and Contents of SAR for Low and Intermediate Level Radioactive Waste Repository" is similar to the notice for the storage facilities except for items dealing with systems related to long term safety. SAR contents on nuclear power plants in the Enforcement Regulations of the Nuclear Safety Act

are also similar to the notice for the storage facilities, but focusing on specific reactor systems. On the other hand, it is confirmed that documents on emergency preparedness, decommissioning, and quality assurance have to be submitted for licensing application separately in accordance with “The Act on Measures for the Protection of Nuclear Facilities, etc. and Prevention of Radiation Disaster” and “The Nuclear Safety Act”, respectively.

2.2 Review of major components of SAR

2.2.1 Site characteristics and process. Items for site characteristics and building/process design which are included in “General Information” of NUREG-1520, are taken out to become independent major items. The reason is as follows. Site characteristics is one of the major components related to the facility safety and actually deals with a large amount of information in SAR. The same is true with building/process design. Even though building/process design can be dealt dispersedly as part of major items for ISA and safety provisions following the NUREG-1520 approach, it is thought there should be a place where all of the design information is described in an integrated way.

2.2.2 ISA. The item of ISA from NUREG-1520 is introduced with a modification of its sub-items on “Site” and “Facility” to that of “Safety Information”.

2.2.3 Items for safety provision. Items for safety provision from NUREG-1520 are introduced excluding that of emergency preparedness, decommissioning, and quality assurance which are to be dealt in other licensing documents. While, waste management is added as part of environmental protection. With the introduced items, their individual ways of description approach are rearranged to come consistently under sub-items of safety consideration, design features, operational program, and assurance of items relied on for safety (IROFS).

2.3 Establishment of framework

Based on the aforementioned review, the SAR framework is formulated in four parts as shown in Fig. 2. They are facility information (general information, site characteristics, building/process design), ISA, safety provisions (radiation protection, criticality safety, chemical process safety, fire safety, waste management and environmental protection), and management measures.

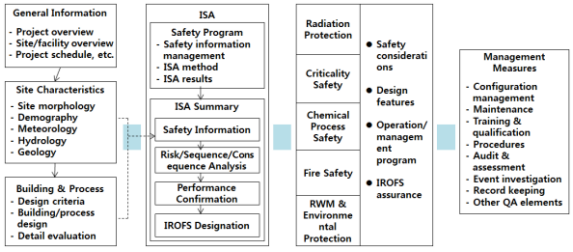


Fig. 2. The developed SAR framework.

3. Conclusions

A framework of guideline on format and contents of SAR for license application of spent nuclear fuel recycling facilities has been developed by the need for integrating various documents into a SAR, which is referring to current approaches in USA and to Korean nuclear safety regulations related to format and content of SAR, as well as taking account of specific nature of the facility. The study results are expected to serve as a useful input to the planned revision and supplement of the current Korean nuclear safety regulations for licensing spent nuclear fuel recycling facilities.

REFERENCES

[1] KINS/RR-1474, Development of Licensing Requirements for the Spent Fuel Recycling Facility (2016).
[2] KINS/HR-1490, Investigation and Analysis on the Safety Regulation of Spent Nuclear Fuel Recycling Facility (2016).
[3] NUREG-1520, Standard Review Plan for the Review of a License Application for a Fuel Cycle Facility (2015).
[4] IAEA NS-R-5, Safety of Nuclear Fuel Cycle Facilities (2008).
[5] NSSC Notice 2015-020, Standard Format and contents of SAR for Spent Fuel Interim Storage Facilities (2015).

How to Control the Intangible Transfer of Technology Related to the Trigger List Items

Jinho Chung

Korea Institute of Nuclear Nonproliferation and Control, 1534 Yuseong-daero, Yuseong-gu, Daejeon, Republic of Korea

jinho@kinac.re.kr

1. Introduction

The advent of new technology has expanded the range of possible technology transfers through various electronic devices, including telephone and internet. As technology related to the Trigger List items defined by the Nuclear Suppliers Group (NSG) Guideline proliferates verbally or by means of electronics, the international community is paying more attention to combat the Intangible Transfer of Technology (ITT) to countries of concern. According to the recommendations of the Wassenaar Arrangement (WA), each nuclear supplier carries the full responsibility for establishing an effective measures to control the ITT. This paper is designed to explore how to control the ITT by utilizing various measures such as adopting a step-by-step approach, implementing Export License of Technology for Nuclear Project, and making a list of reliable countries. In addition, taking a mandatory education course on export control is explored as a way of complementing the existing control mechanism and raising awareness of the ITT.

2. Intangible Transfer of Technology

2.1 Current Status

According to a survey on fifteen organizations dealing with technology related to nuclear energy, about 67% of respondents stated that they have experiences in transferring nuclear-related technology to a foreign country. In addition, about 20% of those that replied have recruited foreigners, and approximately 50% of respondents answered that they have concluded a Memorandum of Understandings (MOU) with organizations overseas. Even though this survey was carried out targeting practitioners in field, only 60% of respondents are aware of the ITT. Based on these findings, it can be incurred that an effective control mechanisms are needed to prevent unintended transfer of nuclear-related technology.

2.2 Definition of ITT

The ITT has been controlled under the legal framework of the Foreign Trade Act and the Minister's Regulations on Export and Import of Strategic Items in the Republic of Korea. According to these regulations, the ITT occurring from a local resident to a foreign national and from the territory of the ROK to a foreign country is regarded as against the law. However, these Act and Minister's Regulations rather focused on dual-use items and has a limit to fully distinguish and cover the unique feature of controlling the Trigger List (TL) items, such as GTGA mandatory for TL exporting. Hence, it is requisite to devise effective and comprehensive measures tailored for the ITT for uses regarding TL.

3. How to Control the ITT

There are several factors that ITT control measures should take into account. First, the control of non-sensitive technology with relatively low propensity for proliferation could be eased in order to prevent excessive regulations. Second, export control procedures can be differentiated and subdivided by target countries. Third, the additional administrative onerousness generated by implementing the new regulation should be minimized. Lastly, raising awareness of personnel who is handling the ITT is also emphasized. These new control measures are expected to embrace all these aspects and maintain balance between easing regulatory burdens and strengthening the international nonproliferation regime.

3.1 Step-by-step Approach

The new ways to control the ITT should take a step-by-step approach. By identifying and clarifying the targets for the ITT, the process for issuing an export license could avoid unnecessary implementation. In addition, by differentiating the process of applying the license by the characteristics

of technology to be transferred or types of project or contract, this stepwise approach could reduce the administrative burden for both applicants and administrators. For instance, if an ITT is a part of a commercial contract, which is considered non-sensitive information, the licensing process could be simplified. Also, to clearly define each specific case that require a Governmental Assurance in advance could help applicants presume to estimate time for the whole application process.

3.2 Export License of Technology for Nuclear Project

The conditions mentioned above could be applied in more practical ways. For instance, if a transfer of technology is approved as an umbrella framework, the subordinated ITTs could be exempt from obligations to apply for additional licenses for each case. Second, if a large scale of project is planned and conducted, a comprehensive license for the entire project is issued once. Then the each technology transfer is identified by the government before the transfer actually occurs. This concept is so-called "Export License of Technology for Nuclear Project." According to this idea, a comprehensive license covering both tangible and intangible transfer of technology of an entire project is issued once. Then subordinated cases of the ITT under the issued license are considered being part of the authorized project.

3.3 List of Reliable Countries

Even though an identical technology is transferred in a same way, the possible consequences varies depending on the technology capabilities and the level of willingness to support the nonproliferation regime of the recipient country. For instance, transfers with destination to the Nuclear Weapons States by the Treaty on the Nuclear Nonproliferation (NPT) has exempted from obligation of requiring the Governmental Assurance. Other countries such as Sweden and Iran are treated in a same way despite of the stark contrast of their nonproliferation efforts. In this sense, it would make sense to categorize the recipient countries by their institutional, technical, and political attitude towards nonproliferation. By doing so, limited resources could be managed and distributed in a more effective and efficient way.

4. Complement measures

Minimizing the administrative burdens does not mean weakening the effectiveness of export controls. The new controls measures of the ITT could adopt education requirements and penalty clauses to complement the suggested control mechanism. First, the exemption of license application and the Export License of Technology for Nuclear Project can be complemented by setting up a mandatory education sessions to attend before applying the export license. Moreover, the penalty clauses applied to the violator for the ITT regulations could play a significant role as a deterrent against the illegal transfers. The implementation of these educational measures is inevitable in order to protect exporters from suffering any possible disadvantages caused by illegal transfers of technology in the international community.

5. Conclusion

The intangible technology controls has become an emerging issue in the area of export controls. This paper sought ways to control ITT by easing administrative burdens through a step-by-step approach, adopting a concept of Export License of Technology for Nuclear Project, establishing a list of reliable recipient countries. To this end, issuing a license and a governmental assurance and exemption of unnecessary documents were considered the best possible means to be implemented for the ITT controls. In addition, education was also highlighted so as to complement the control systems. At the moment, all these measures are supposed to be implemented in a mandatory manner. To develop more advanced control mechanism in the future, further research on ITT control measures on a voluntary basis should take into consideration.

REFERENCES

[1] Ian J. Stewart, "The Contribution of Intangible Technology Controls in Controlling the Spread of Strategic Technologies", Strategic Trade Review, Vol. 1, Issue 1, Autumn (2015).

[2] Vincente Garrido Rebolledo, "Intangible Transfers of Technology and Visa Screening in the European Union", EU Non-Proliferation Consortium Papers, No.13, march (2012).

[3] Lisa Thiele, "Regulatory Considerations: Nuclear Technology, Prescribed Information and Export Controls", Canadian Nuclear Safety Commission, Presented November 13, 2015.

Conflicts and Proposals on Physical Protection Related Law of Intermediate and Low-level Radioactive Waste Disposal Facilities

Yeon Uk Kang*, Min Ho Kang, and Sung Soon Jang

Korea Institute of Nuclear Nonproliferation and Control, 1534 Yuseong-daero, Yuseong-gu, Daejeon, Republic of Korea

*yeonuk@kinac.re.kr

1. Introduction

Radioactive waste is generated in the process of generating electricity using nuclear power or in using radioactive materials in various fields. In order to protect such radioactive waste, radioactive waste disposal facility is defined as a nuclear facility in the Act on Physical Protection and Radiological Emergency (hereinafter refer to as "APPRE"). In this paper, we analyze related laws and regulations affecting physical protection of intermediate and low-level disposal facilities (hereinafter refer to as "ILDF") and propose a plan for strengthening the physical protection level of ILDF.

2. Radioactive waste disposal facilities

Currently, the cave disposal facility is operating in the first stage in Korea, and the surface disposal facility is being prepared through the second stage project. In Korea, the type of disposal is limited by the level of radioactive waste by law. The table below summarizes these.

Table 1. Restriction on the disposal of radioactive waste

Disposal method		Target waste
Shallow Disposal	Embedded	Ultra-low(UL)
	Surface	Low, UL
	Cave	Intermediate, Low, UL
Deep Disposal		High, Intermediate, Low, UL

According to the regulation on the classification of radioactive waste and its own disposal standards, it is divided into intermediate level, low-level and ultra-low-level radioactive waste. When the second stage project is completed, wastes below intermediate level will be operated in surface form. Disposal in embedded type is limited to ultra-low level radioactive materials in domestic law and is limited to less than 100 times concentration of its own disposal.

3. Physical protection of disposal facilities

As mentioned in the introduction, disposal facilities should be classified as a nuclear facility in accordance with APPRE. In addition, domestic technical standard on management of ILDF describes physical protection standards. Disposal facilities have many obligations under APPRE, but most of the content is in order to comply with physical protection requirements.

In general, nuclear facilities have requirements for physical protection against unauthorized removal and sabotage in use and storage, both at fixed sites and during transport. However, in ILDF, unlike nuclear power plants, there are protection requirement exemptions. Intermediate and low-level radioactive wastes are generally classified as out-of-class nuclear material according to APPRE's classification. Therefore, it does not fall under unauthorized removal and sabotage requirements of nuclear materials in transit, and there is no protection requirement against unauthorized removal of nuclear materials in use. In conclusion, ILDF must satisfy the protection requirements for sabotage of nuclear facilities that do not use or store nuclear material. The main contents of the protection requirements are access control, detection of illegal intrusion, planning and training, education, evaluation of physical protection regulation, and cyber security response. Since the protection requirements are described simply and minimum requirements are strong, nuclear facility licensee establishes and operates the facility physical protection regulations in detail.

4. Conflict with relevant law and regulation

4.1 Disaster and safety management basic law

According to this law, the head of relevant central administrative agency can designate the national infrastructure as needed. Currently, ILDF is

designated as the national infrastructure. However, the national infrastructure is not closely linked to the military and police because to the focus on disaster such as earthquake, tsunami, ship sinking.

4.2 Integrated defense law

In this law, national important facilities are designated and managed in three stage in consideration of importance and value. If we look at the meaning of the military and police in terms of domestic protection, you can see how important it is to protect the facility by being classified as national important facilities.

Unfortunately, ILDF is not included national important facilities under this law and is not included in the national security target facility designated by NIS.

4.3 Security business law

Although a facility is equipped with physical protection systems, security guards are a key issue that is to protection of facilities. According to current definition of security business law, special security guards can be operated in case of national important facilities, and therefore it is decided whether they are general security guards or special security guards according to integrated defense law. Therefore, ILDF is a nuclear facility based on APPRE, but operates a general security guard in accordance with security business law.

5. Suggestion

The basic idea is that APPRE is the most specific description of physical protection for nuclear facility, so we believe that physical protection level of facility should not be restricted according to other relevant laws. I would like to suggest various suggestions to solve this problem. First is a method of requesting minister of national defense through head of administrative agency or commander of regional army in accordance with procedure for designating national important facilities. Although there is an advantage to be able to carry out without changing procedure, it is difficult to participate in NSSC because national important facilities deliberation committee decide and members concerned with military are determined. Second is to add nuclear facility defined in APPRE to definition of special security services in article 2 of security business law. In this case, although it is not a national important facility, special security guard can be operated and strict requirements and duties of special guard defined in security business law can be applied to ILDF. Good results can be obtained from point of physical protection, for example, possession of weapons, strict qualification, and strike prevention. These measures increase level of protection of facility sufficiently, but there is a limit to support of military and police due to absence of national important facilities. The last way is to reflect on current APPRE in consultation with relevant agencies and government departments, including MOU with military and police, and definition of a nuclear facility guard similar to a special security guard. Advantages include ability to control all aspects of APPRE itself and to be able to replace it flexibly, which ultimately is direction to go. However, there may be confusion in other facilities, such as nuclear power plants, which are currently operating well, and there are many related organizations, and time is needed and initial confusion is expected.

6. Conclusion

Domestic ILDF are operated in accordance with the protection requirements according to APPRE. In Korea, national facilities are classified and managed in order to respond to disasters and threats. The basic idea is that the most specific law on physical protection of nuclear facility is APPRE, and many of measures necessary to implement this law should not be restricted by other relevant laws. It is necessary to discuss whether the relevant laws are intended because ILDF based on APPRE are not important facilities in the country, and it is difficult to conclude an MOU with the military and police and operation of special security guards.

REFERENCES

[1] “APPRE”, NSSC, 2016.6.2.
[2] “Security business law”, Police, 2016.1.26.
[3] “Integrate defense law”, DOD, 2016.11.30.
[4] “Disaster safety law”, NSA, 2017.1.17.

A Study on the Recent Tendency of Cyber Security Regulation for the Nuclear Fuel Cycle Facilities

Siwon Kim

Korea Institute of Nuclear Nonproliferation and Control, 1534 Yuseong-daero, Yuseong-gu, Daejeon, Republic of Korea

swkim@kinac.re.kr

1. Introduction

The cyber security regulations for nuclear facility in Unites States are based on the federal regulation 10 CFR 73.54[1] issued in 2009. The 10 CFR 73.54 requires licensee to protect their computers and information systems from cyber attacks that could lead to the theft or diversion of nuclear materials and the radiological sabotage. The NRC provides an acceptable approach and methodology for meeting the requirements for satisfying these demands through RG 5.71[2]. Also, NEI issued the NEI 08-09 to inform the licensee of the details necessary to satisfy 10 CFR 73.54 and RG 5.71.

The above-mentioned laws and guides have been applied to Nuclear Power Plants (NPPs) and it is difficult to apply them fitly to nuclear facilities other than NPPs. So, the regulations appropriate to the characteristics of each facility are needed. The purpose of this paper is to review the regulatory trends in US nuclear Fuel Cycle Facilities (FCFs) and provide the information on the differences from existing regulatory requirements for NPPs.

2. Cyber Security Regulation for the FCFs

As mentioned in the introduction, regulatory measures are being developed for nuclear FCFs in the United States. The draft federal regulation 10 CFR 73.53 [3] was proposed in March 2016, and will be finally issued in the first half of 2017 after several public meetings [4]. In addition, draft regulatory guides document DG-5062 [5] was developed as a detailed guide to support 10 CFR 73.53, and is undergoing formal comment period for rulemaking. When 10 CFR 73.53 is finally issued, the licensee submits the CSP within six months and will implement the CSP to satisfy the rule for 18 months.

This section provides the information about how the cyber security regulatory requirements for the nuclear FCFs are structured and how they differ from existing regulatory requirements of the NPPs.

2.1 Cyber Security Regulation Trends in FCFs

The draft regulatory guide for FCFs, which has been developed to date, requires details such as organization, asset identification, defense in depth, security controls, periodic review, and event reporting and records in the same manner as the regulatory guide for nuclear power plants. The draft guide states that the target assets for applying regulatory requirements are not Critical Digital Assets (CDAs) but Vital Digital Assets (VDAs). It also required that assets are protected from cyber attacks that could cause a consequence of concern on FCFs. These consequences of concern are classified into the four types in the table below [5].

Table 1. Consequences of Concern[5]

Type	Type Name
1	Latent - Design-Basis Threat
2	Latent - Safeguards
3	Active - Safety
4	Latent - Safety and Security

In the US, Special Nuclear Materials (SNMs) are classified into three main category [6] according to the risk as shown in the table 2. The consequences of concern are different for each category. Types 3 and 4 can occur commonly to all categories. Type 1 can occur only in Category I FCF, and Type 2 can occur only in Category II FCF.

Security controls should be applied to identified VDAs. At this time, different security controls are applied depending on what type of consequence of concern on the FCF when the asset is compromised,

Table 2. Safeguard Categories of SNM[6]

Category	Category Name
I	Strategic SNM
II	SNM of moderate strategic significance
III	SNM of low strategic significance

as a result of a cyber attack. Above all, 48 security controls are commonly applied irrespective of the consequences of concern. Thereafter, 79, 85, and 105 security controls are additionally applied depending on the consequence of concern type. If two or more consequences of concern can be occurred, apply all security controls for each type. Subsequent fulfillment of requirements such as periodic review, incident reporting, and records will satisfy all CSPs. After that, if all of the requirements for periodic review, incident reporting, and records are satisfied, all CSPs are completed [5].

2.2 Differences from Regulation for NPPs

The cyber security regulations for FCFs are similar to those currently applied in NPPs, but they differ in several points. This section describes these major differences.

First of all, the assets that could adversely affect the safety, security, or Emergency Preparedness (EP) function were selected for protection in NPP [2], but EP function were excluded and safeguard function was added in consideration of facility characteristics that FCFs treats large quantities of nuclear materials and there is no fission reaction in the FCFs. In addition, the name of the assets to be protected is named as VDA instead of CDA.

Secondly, in RG 5.71, the principle was to apply all applicable security controls for each CDA, and to apply alternative controls instead of unavailable security controls. However, after the CDA identification, the licensee applied a graded approach that grouped the CDAs according to the characteristics and consequences of each asset and applied the security controls differentially through NEI 13-10. Reflecting this experience, in the regulatory guide for FCF, the possible consequences of concern for each facility have been predetermined and security controls to be applied for each consequence of concern are assigned. There are also common security controls, and it is allowed that a way to group the VDAs by their characteristics and apply the same set of security controls [5].

Finally, the concept of Temporary Compensatory Measures (TCMs) was introduced. After completing the implementation of the security controls, if the intended method does not meet the performance specification of the security control, the licensee may instead implement the TCM. The TCM is an interim solution to allow the operation of the VDA while performing long-term measures required to adequately implement and validate the security controls [5].

3. Conclusion

So far, this paper has reviewed the cyber security regulatory trends of US nuclear FCFs and provided information on how they differ from regulations on NPPs. Follow-up study is to analyze in detail the differences between security control groups that apply to the four consequence of concern types and to identify which security controls are applied differently in Category I, II, and III facilities. Through this, the key elements, which convert deterministic approach into a consequence-based approach in NRC's existing regulation, can be analyzed.

REFERENCES

[1] U.S. Nuclear Regulatory Commission, "Protection of Digital Computer and Communication Systems and Networks," Title 10, Code of Federal Regulations, Part 73, Section 54, Dec. 2015.

[2] U.S. Nuclear Regulatory Commission, "Cyber Security Programs for Nuclear Facilities," Regulatory Guide 5.71, Jan. 2010.

[3] U.S. Nuclear Regulatory Commission, "Require-ments for Cyber Security at Nuclear Fuel Cycle Facilities," Draft Title 10, Code of Federal Regulations, Part 73, Section 53, Oct. 2016.

[4] U.S. Nuclear Regulatory Commission, Public Meeting Presentation Material, "Discussion of Draft Proposed Rule Text for Fuel Cycle Cyber Security," May 2016.

[5] U.S. Nuclear Regulatory Commission, "Cyber Security Programs for Nuclear Fuel Cycle Facilities," Draft Regulatory Guide DG-5062, Jan. 2017.

[6] U.S. Nuclear Regulatory Commission, "Safeguard Categories of SNM," https://www.nrc.gov/security/domestic/mca/snm.html Feb. 2017.

Study on the Position Enhancement for Cyber Security Organization of the Nuclear Facilities

Hyundoo Kim*

Korea Institute of Nuclear Nonproliferation and Control, 1534 Yuseong-daero, Yuseong-gu, Daejeon, Republic of Korea

*hdkim@kinac.re.kr

1. Introduction

The digital I&C systems and commercial programs adopted for the nuclear facilities are getting to be increased, compared with analog I&C systems and specifically private programs. Moreover, the trend of cyber threat is toward from individual attack to national scale attack by using special malware which is developed to attack the particular targeted system such as 'Stuxnet' in Iran, 'Energetic Bear' in U.S. and 'Black Energy' in Ukraine. In consequence of the trends, cyber threats and attacks can occur anywhere and at the any time.

2. Background of Cyber Security Organization

The Act on Physical Protection and Radiological Emergency, its enforcement decree and enforcement regulation were added or revised to enhance cyber security. Based on the laws, the Notice for details of Cyber Security Plan (CSP) was issued and KINAC's regulation standard, KINAC/RS-015 was developed to establish cyber security framework for the nuclear facilities against cyber threats and attacks.

Licensees planed 7 phases for the cyber security program to meet the Notice and KINAC's regulation standard and implement CSP. The 1st phase from among this plan is composition of cyber security organization and licensees have composited their cyber security organization since 2015.

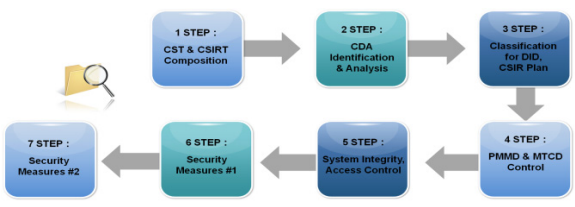


Fig. 1. Seven (7) Phases of the CSP.

3. Requirements for the QA organization

The cyber security organization for the nuclear facilities has been composited in accordance with CSP since 2015. But the requirements for the Quality Assurance (QA) organization have been studied and established for a long time and a lot of companies adopted and organized their QA team as one of Quality Assurance Programs, Plans or Activities.

3.1 Regulatory Guide 5.71

The Regulatory Guide 5.71, "Cyber Security Programs for Nuclear Facilities" in U.S. requires that licensees form a cyber security team (CST) including sponsor, manager and specialists by defining and documenting roles, responsibilities, authorities and functional relationships, which are detailed in the RG 5.71. The licensees' CST are required to have the authority to conduct an objective assessment, make determinations that are not constrained by operational goals, implement the defense-n-depth protective strategies and ensure the implementation of the security controls of the cyber security program [1].

3.2 KINAC/RS-015

The Regulation Standard KINAC/RS-015, "Security for Computer and Information of Nuclear Facilities" in ROK requires licensees to compose a CST with the sponsor, manager and specialists which is independent and separated from the system operation parties and define and document roles, responsibilities and authorities which are in KINAC/RS-015 [2].

3.3 ISO 9001

The International Standard ISO 9001, "Quality Management Systems – Requirements" requires that

the QA organization determine external and internal issues that are relevant to its purpose and its strategic direction and that affect its ability to achieve the intended result(s) of its quality management system. The organization also is required to determine the interested parties and the requirements of these interested parties that are relevant to the quality management system [3].

3.4 10 CFR 50 Appendix B

Appendix B, "Quality Assurance Criteria for Nuclear Power Plants and Fuel Reprocessing Plants" in Title 10, Code of Federal Regulations (CFR) Part 50, "Domestic Licensing of Production and Utilization Facilities" requires that the persons and organizations performing QA functions have sufficient authority and organizational freedom including sufficient independence from cost and schedule to identify quality problems, to verify implementation of solutions and to report to a management level. Irrespective of the organizational structure, the individual assigned the responsibility for assuring effective execution of any portion of the QA program is required to have direct access to the levels of management necessary to perform QA function [4].

3.5 ASME NQA-1-1994

The American Society of Mechanical Engineers (ASME) committee on Nuclear Quality Assurance (NQA) through Basic Requirement 1, ASME NQA-1-1994 requires that the persons or organizations responsible for assuring that an appropriate QA program has been established and verifying that activities affecting quality have been correctly performed have sufficient authority, access to work areas, organizational freedom and direct access to responsible management at a level where appropriate action can be effected [5].

3.6 NUREG-0800

The Standard Review Plan (SRP) for the Review of Safety Analysis Reports for Nuclear Power Plants: Edition – Quality Assurance, NUREG-0800 Chapter 17 requires that licensees identify a management position that retains overall authority and responsibility for the QA program and this position has the following characteristics:

a. Is at the same or higher organization level as the highest line manager directly responsible for performing activities affecting quality such as engineering, procurement construction and operation and is sufficiently independent from cost and schedule.

b. Has effective communication channels with other senior management positions.

c. Has no other duties or responsibilities unrelated to QA that would prevent his full attention to QA matters [6].

4. Conclusion

The regulation requirements for the quality assurance organization of nuclear facility are more detailed, stronger and stricter than those for the cyber security organization. The Korea Institute of Nuclear Safety (KINS) applies, reviews and regulates above mentioned QA standards for the nuclear facilities to the Design and Construction Phases as well as the Operations Phase.

The regulation requirements for composing cyber security organization which is one of the security assurance activities should be further developed and strengthened.

REFERENCES

[1] U.S.NRC, Regulatory Guide 5.71, "Cyber Security Programs for Nuclear Facilities", January 2010.

[2] KINAC, Regulatory Standard KINAC/RS-015, Security for Computer and Information of Nuclear Facilities, October 2014.

[3] ISO, International Standard ISO 9001, "Quality Management Systems – Requirements", September 2015.

[4] U.S.NRC, https://www.nrc.gov/reading-rm/doc-collections/cfr/part050/part050-appb.html

[5] ASME, ASME NQA-1-1994 edition and 1995 addenda, "Quality Assurance Manual".

[6] U.S.NRC, NUREG-0800, "Standard Review Plan for the Review of Safety Analysis Reports on for Nuclear Power Plants: LWR Edition).

Applied Parallel Coordinates for ICS Network Traffic in Simulated Nuclear Power Plant Environments

Chaechang Lee* and Soomin Lim

Korea Institute of Nuclear Nonproliferation and Control, 1534 Yuseong-daero, Yuseong-gu, Daejeon, Republic of Korea

*chiching@kinac.re.kr, s2min@kinac.re.kr

1. Introduction

A visualization is an important approach to helping understand what data means and discover data values. Parallel coordinates are a useful method to visualize high-dimensional geometry and analyzing multivariate data. For those inherent characteristics, they were already studied well to apply in IT environment in order to detect unknown large-scale Internet attacks including Internet worms, DDoS attacks, and network scanning activities [1]. This article presents differences of the application of parallel coordinates between IT environment and Instrument and Control System (ICS) network, especially nuclear facilities, effectivenesses of this method, and practical consideration to apply them to a real site.

2. Visualization Description

2.1 Materials

A main material used in this study is a Distributed Control System(DCS), OPERASYSTEM-1400, developed by Woori technology Inc. The DCS localized digital I&C system in Korea is used as a platform for non-safety control systems of Advanced Power Reactor 1400 (APR-1400) in nuclear power plants [2].

In this study, it receives digital input signals and sends digital output signals from and to a simulator which plays a role as controllers and actuators in nuclear facilities. It is also connected to other two systems via a local-area network (LAN): One is a Human-Machine Interface (HMI) PC for controlling and monitoring DCS, the other is workbench PC for building and uploading a program logic to DCS. Fig. 1 shows the LAN structure used in this study.

For an example of the data capture of the network traffics we used Wireshark with a promiscuous mode at the HMI PC. R, a free software environment for statistical computing and graphics, was used to visualize to parallel coordinate plots from the captured traffics with its associated libraries such as MASS.



Fig. 1. LAN structure used in this study.

2.2 Method

To draw parallel coordinates in this study we used 5 parallel lines to represent captured traffics source and destination IP address, destination port, a length of a packet, and its protocol. A set of the above five features extracted from the captured traffic is represented as a polyline with vertices on the parallel axes. Two sets which have same features from the traffic data was not drawn as one polyline but two lines distinguishable from each other. It helps to find out its scales and patterns with frequencies of the packets. In addition, we assign a different color to each source IP address to find out the relationship with two axes even if they are not adjacent.

3. Result and Discussion

Fig. 2 shows the parallel coordinates with the method mentioned above.

3.1 Effectiveness of this Method

The effectiveness of this method is to make easy to analyze the network traffic patterns even if it uses proprietary protocols. A lot of systems in the industry sites, including the DCS we used in this study, uses proprietary protocols. Since they are unknown to publics, it is difficult to understand what values in a payload mean though all packets are deeply captured. Most proprietary protocols, however, use Ethernet network based on TCP/IP like IT protocols. By plotting parallel coordinates with 3rd layer's information, the traffic patterns of them can be

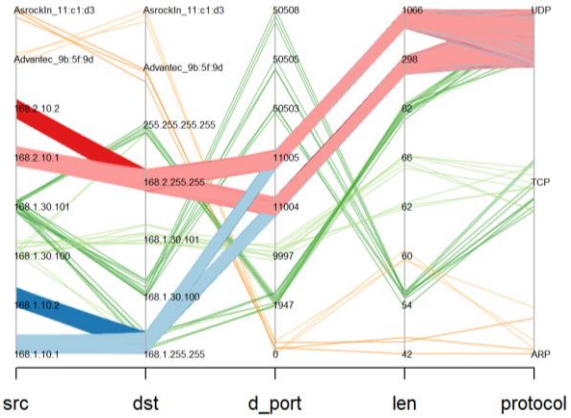


Fig. 2. The applied parallel coordinates on simulated ICS network traffic.

revealed as for where they are going from and to, and how much their amounts are.

Assigning different colors to each source IP addresses helps to find out the relationship between two traffic features even not adjacency axes. In a case of plotting with one color, the parallel coordinate should be analyzed with whole shapes, since it shows the relationship only between adjacent axes.

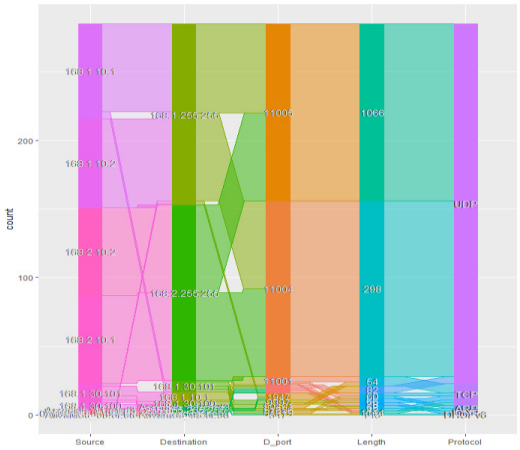


Fig. 3. An example of ambiguous parallel coordinates.

Parallel coordinates with this method reveal the main stream of the ICS traffic in its network. A thick line represents a large amount of the traffic with the same pattern. A thin line means that the traffic pattern is an uncommon occurrence. With the results, the specific traffic patterns can be used as a whitelist for outlier detections in the ICS network that its network traffic patterns are somewhat static.

To use this method, network traffics occurred in an ICS network should be visualized to identify its scale and one packet should be represented as a polyline. Besides, any two packets which have same traffic features should not be overlapped into a polyline when plotted. If scales in a parallel coordinate are visually ambiguous, it is not useful to get any information from the plot. Fig. 3 shows an example of ambiguous parallel coordinates.

3.2 Differences IT and ICS

In a case of a network with IT systems, especially connected to the internet network, there are too many hosts that represent source and destination IP addresses to assign colors that are distinguishable. In other words, parallel coordinates plotted on IT networks do not tell us what a destination port is, what a protocol service is, and what a length is a packet from one source IP address. They only show us the whole shapes in order to detect an outline of network compromises with a broad view.

On the other hand, parallel coordinates plotted on ICS networks have relatively small number of hosts. They can reveal which features are related to a source IP address with a colored line. It also helps to find out an overview of the whole network situation without detail specifications of proprietary protocols.

4. Conclusion

In this study, we visualize network traffics in a DCS network, simulated nuclear power plant environments with the parallel coordinate method. The network traffics have proprietary protocols and we can get some intuitive information with this method. As a next work, we plan to collect characteristics on parallel coordinates when there is any kind of abnormal behavior in the network and develop visualized signatures to detect the network compromise.

REFERENCES

[1] Choi, Hyunsang, Heejo Lee, and Hyogon Kim. “Fast detection and visualization of network attacks on parallel coordinates.” computers & security 28.5 (2009): 276-288.

[2] Kwon, Kee-Choon, and Myeong-Soo Lee. “Technical review on the localized digital instrumentation and control systems.” Nuclear engineering and technology 41.4 (2009): 447-454.

2분과

사용후핵연료관리 (Oral)

Porous Media Modelling for Thermal Analysis of Storage Cask with Bird Screen Meshes

Ju-Chan Lee*, Kyoung-Sik Bang, Seung-Hwan Yu, Ki-Seog Seo, and Woo-Seok Choi
Korea Atomic Energy Research Institute, 111, Daedeok-daero 989beon-gil, Yuseong-gu, Daejeon, Republic of Korea
*sjclee@kaeri.re.kr

1. Introduction

A concrete storage cask has been developed for dry storage of 21 spent PWR fuel assemblies [1]. The cask consists of a concrete overpack, which has an air cooling system and a sealed canister including the fuel baskets as shown in Fig. 1. Air inlet and outlet ducts are installed at the bottom and top of the concrete overpack. Bird screen meshes are installed at the air inlet and outlet ducts to prevent the intrusion of debris from the external environment.

The presence of this screens introduce an additional resistance to air flow through the ducts. Porous media model can be used to simulate the flow effects in the bird screen meshes. The purpose of this study is to develop the porous media model for the simulation of bird screen meshes and to prove the validation of the porous media model.

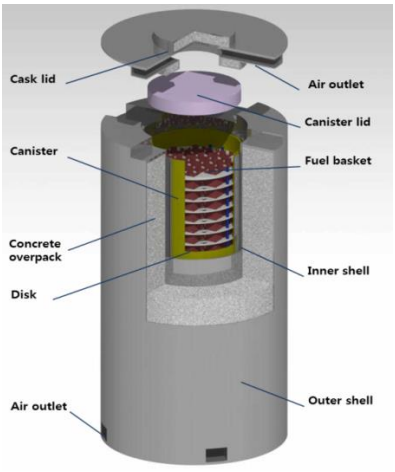


Fig. 1. Overview of concrete storage cask.

2. Porous Media Modelling

The theoretical pressure drop between the inside and the outside of a bird screen mesh can be predicted using following relation [2].

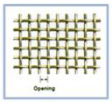
$$\frac{\Delta P}{t} = \frac{\mu_f}{\alpha} v + C\left(\frac{1}{2}\rho v^2\right) \qquad (1)$$

Where,

ΔP : pressure drop [Pa],
t : thickness of bird screen mesh [m]
μ : viscosity of air [kg/m-s]
α : permeability [㎡] (1/α : viscous resist. coeff.)
C : inertial resistance coefficient [m^{-1}]
ρ : density of air [kg/㎥]
v : superficial velocity [m/s]

In this study, pressure drops through the bird screen meshes were calculated by CFD analysis. Inertial resistance factor (C) and a viscous resistance factor (1/α) were predicted by pressure drop correlation. Five types of the meshes were considered in this study. Table 1 shows the specifications of bird screen meshes. Fig. 2 shows the flow analysis model for calculation of pressure drop, and the result of velocity vector for the bird screen mesh.

Table 1. Specifications of bird screen meshes

Mesh no.	Wire dia. (mm)	Opening (mm)	Open area (%)	Mesh Shape
#4	0.71	5.64	78.9	
#6	0.71	3.53	69.6	
#8	0.71	2.46	60.2	
#10	0.71	1.83	51.8	
#12	0.71	1.40	43.6	

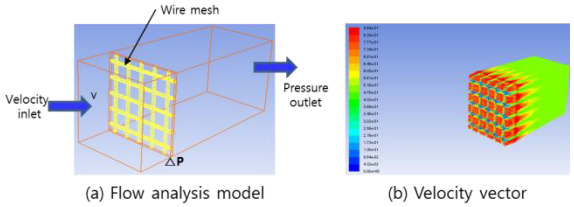


Fig. 2. Flow analysis model and velocity vector.

Table 2 and Fig. 3 show the fluid flow analysis results for bird screen meshes. The velocities at the inlet of bird screens were considered with 0.4 m/s ~ 0.8 m/s. Pressure drops were calculated as a variation of the velocities for each screen mesh. Viscosity and inertial resistance factors were calculated from the polynomial curve of the second order and Equation (1). Table 3 shows the flow resistance coefficients for porous media models of bird screen meshes.

Table 2. Fluid flow analysis results for bird screen meshes

Velocity [m/s]	Pressure drop [Pa]		
	Mesh #4	Mesh #8	Mesh #12
0.4	0.0509	0.1543	0.3948
0.5	0.0730	0.2213	0.5700
0.6	0.0981	0.2991	0.7761
0.7	0.1265	0.3877	1.0126
0.8	0.1581	0.4871	1.2795

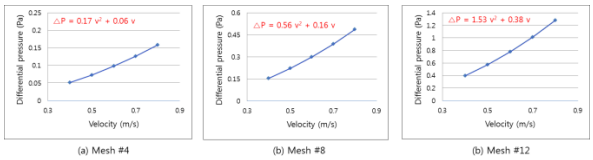


Fig. 3. Pressure drop - velocity and approximation formula.

Table 3. Flow resistance coefficients for porous media model of bird screen meshes

Mesh size	Permeability (α), [㎡]		Inertial res. factor (C), [1/m]	
	Inlet	Outlet	Inlet	Outlet
#4	2.20E-7	2.66E-7	406	468
#8	7.90E-8	9.56E-8	1,299	1,494
#12	3.46E-8	4.18E-8	3,576	4,115

3. Verification of Porous Media Model

Thermal tests have been carried out for the concrete cask with bird screen meshes. Also, thermal analyses have been carried out for the concrete cask using a porous media model to prove the validation of the analysis model. Decay heat from the 21 fuel assemblies was considered as 16.8 kW. Ambient temperature was assumed as 20°C.

Fig. 4 shows the comparison of the thermal analysis and test results for the mesh #4 and mesh #12. The analysis results agreed well with the test results. The analysis temperatures were slightly higher than the test temperatures. Therefore, the reliability and conservatism of the analysis results for porous model have been demonstrated. The temperatures for mesh #12 are slightly higher than the temperatures for mesh #4. It was shown that the screen mesh sizes don't significantly affect the cask temperatures.

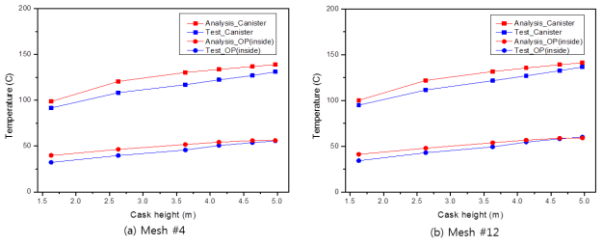


Fig. 4. Comparison of thermal analysis and test results.

4. Conclusions

Porous media model was developed to simplify the bird screen meshes. Flow resistance coefficients for porous media model were derived from the fluid flow analysis. The analysis temperatures for the storage cask were slightly higher than the test results. Therefore, the reliability and conservatism for the porous model have been demonstrated. The porous media model developed in this study can be used to estimate the temperatures for concrete cask with bird screen meshes.

REFERENCES

[1] Topical Report for Concrete Storage Cask (Rev.2), KORAD, 2014.

[2] Macini, P. et al. "Laboratory Measurements of Non-Darcy Flow Coefficients in Natural and Artificial Unconsolidated Porous Media", Journal of Petroleum Science and Eng. 77, pp.365-374, 2011.

A PSA Framework for Interim Storage Facility Subject to Aircraft Engine Crash

Sanghoon Lee[1*], Belal Almomani[2], Dongchan Jang[2], and Hyun-Gook Kang[3]
[1]Keimyung University, 1095 Dalgubeol-daero, Dalseo-gu, Daegu, Korea
[2]Korea Advanced Institute of Science and Technology, 291 Daehak-ro, Yuseong-gu, Daejeon, Korea
[3]Rensselaer Polytechnic Institute, 110 Eighth Street, Troy, NY USA
[*]shlee1222@kmu.ac.kr

1. Introduction

A new PSA (Probabilistic Safety Assessment) framework is developed for an interim storage facility of spent nuclear fuel considering a targeted aircraft crash. It includes key elements of PSA such as event tree analysis, radiological consequence analysis together with a sophisticated structural analyses for the storage building, metal cask and spent fuel assemblies to calculate the release fraction of radionuclides due to an impact of aircraft engine into the facility. The developed framework is applied to a reference storage facility which consists of a reinforced concrete (RC) building and a single cask containing 24 PWR fuel assemblies. Three levels of structural resilience are considered together with 3 burn-up rate of fuels. It was shown that the strike of an aircraft crash does not pose a significant risk to the public in all 3 levels of structural resilience.

2. Methodology Overview

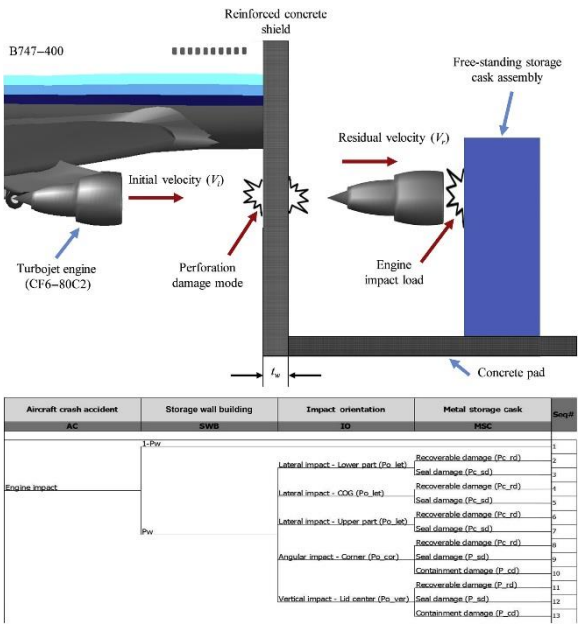


Fig. 1. Aircraft crash scenario and event tree.

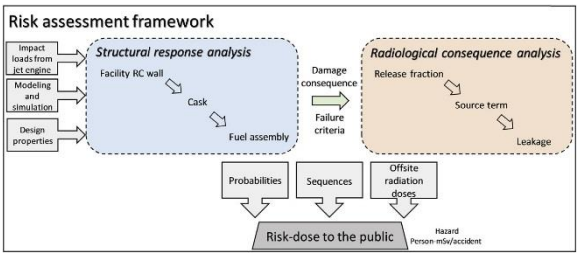


Fig. 2. Risk assessment framework.

The impact scenario and the risk assessment framework is illustrated in Fig. 1 and 2. A targeted aircraft crash is considered and its radiological consequence is calculated with inputs from a sophisticated structural analyses on the facility [2].

3. Structural Analyses

3.1 Storage building local damage analysis

As a best deterministic estimation, with a bias toward conservatism, as suggested in the NEI report [1], the empirical formulas employed in this study can predict the minimum RC wall thickness required to prevent local damage caused by the normal impact of an aircraft engine and its residual velocity. Impact speeds and compressive strengths of concrete are treated probabilistically as uncertainty.

3.2 Cask response analysis

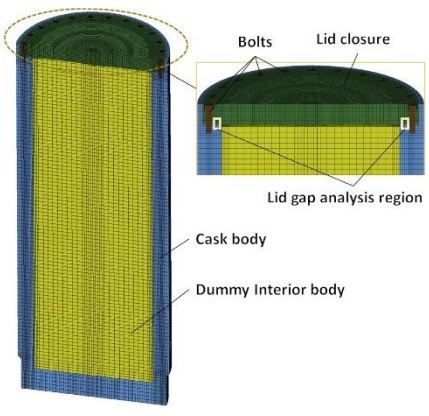


Fig. 3. Cask analysis model to calculate leak path area.

A detailed finite element model (Fig. 3) was developed to analyze the dynamic response of the lid closure system in order to calculate the leakage path area between the lid and the flange, since the lid seal plays an essential role in preventing the escape of fine particulates and radioactive gases from the cask. It is assumed that a closure opening greater than the pre-compression state of the metallic seal will cause leakage. Various velocities and impact locations were considered as sources of uncertainty.

3.3 Fuel assembly analysis

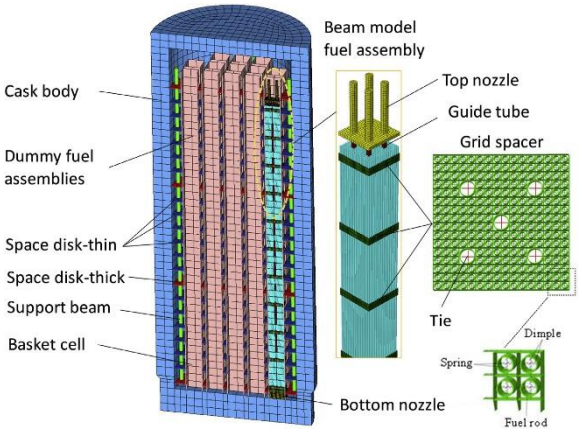


Fig. 4. Detailed fuel assembly analysis model.

Another cask model with detailed fuel assembly was developed to analyze the dynamic response of the fuel assembly and estimate the fraction of rods that fail during the impact as an essential parameter of the radiological consequences. The impact analysis studied five impact orientations. The effect of impact angle is also studied together with the impact location and the jet engine of a B747 was chosen for this study to provide an upper bound impact load on the cask body. One assembly in the proximity of impact location is modeled with full details while the other 20 assemblies are modeled as dummy weights.

4. Radiological Consequence Analysis

Three inventories for the radionuclides involved in the scenario that dominate the inhalation dose for all the chemical elements classes (volatiles, fission gases, and solid particles) are calculated using the ORIGEN-ARP of SCALE v.6.1.3 code. The computer code HOTSPOT v.3.0.2 which was developed based on the Gaussian dispersion plume model, is used in this study to estimate the radionuclide spread from the accident. The reference person is presumed to have a breathing height of 1.5 m and a breathing rate of 3.47Ee4 m^3/s. The wind speed reference height is 80 m and the release height is ground level.

5. Risk Estimation

The dose-risk elements are the product of the probabilities of the impact condition and the corresponding responses (Pw, Po, and Pc), and the fractions that lead to the release of radioactive materials that cause radiological consequences of magnitude (C). The measure of risk is given by Eq. (1), which is applied in sequence line i:

$$R_i = P_w P_o P_c \times C_i \quad (1)$$

The initiating frequency of the aircraft crash accident is assumed to be 1, representing an intentional aircraft crash. As the storage wall building is the first barrier to protect the internal spent fuel storage casks from the AI, the results of the probability of perforation (Pw) for facility walls (low, median, and high) are inserted accordingly into Column 2 of event tree. Then, the probability of each impact orientation is added in Column 3. Finally, the probability results of the cask response status for the three structural performance levels of metallic seal, are inserted into Column 4. All probability data are multiplied. The maximum possible radiological consequences for each sequence line, are inserted into the Consequence column for the three rates of fuel burnup. Finally, through Eq. (1), the expected hazard to the public can be estimated in units of mSv/accident. In all cases, the risk was calculated below the design basis accident limits.

6. Conclusions

A new PSA framework for aircraft crash into an interim storage facility has been developed and applied to a reference facility. Fire accident and secondary impact of cask with other structure will be covered in future research.

REFERENCES

[1] Nuclear Energy Institute, Methodology for performing aircraft impact assessment for new plant designs, Revision 8P (2011).

[2] Almomani, B., Lee, S., Jang, D., Kang, H.G., “Probabilistic risk assessment of aircraft impact on a spent nuclear fuel dry storage,” Nuclear Engineering and Design. 311. 104-119 (2017).

Structural Evaluation under Off-normal Condition for Concrete Storage Cask of Spent Fuels

Tae-Chul Moon*, Chang-Yeal Baeg, and Chun-Hyung Cho

Korea Radioactive Waste Agnecy, 168 Gajeong-ro, Yuseong-gu, Daejeon 34129, Republic of Korea

*tcmoon@korad.or.kr

1. Introduction

The concrete storage cask is under development with containing canister loaded with spent fuel and vertically placed on storage pad as free-standing type. The structural evaluation of the concrete storage cask must show that it secures the confinement and structural integrities under normal, off-normal and accident conditions. The evaluation results were reviewed with respect to every design criterion, in terms of whether the results satisfy the criteria, provided by US 10CFR Part 72 and NUREG-1536 [1.2]. Description of the concrete storage cask and the maintainability and assumptions include in the analysis were confirmed through detailed explanations of the acceptable standards, analysis model and analysis method. ABAQUS 6.10, a widely used finite element analysis program, was used in the structural evaluation [3]. The evaluation results of this work show that the maximum stress was below the allowable stress under off-normal condition, and the concrete storage cask satisfied the design criteria.

2. Model description

2.1 General information of concrete storage cask

A concrete cask body is a cylindrical shell structure for the storage of canisters loaded with spent fuels. Concrete for shielding is filled between the internal and external carbon steel shells of the cask body, and air intake and exhaust vents are installed at the top and bottom of the cask body to eliminate the decay heat from the spent fuel through air circulation due to natural convection. The concrete cask body of the concrete cask protects the canister from the external environment to maintain the integrity of the spent fuels, and the canister maintains the confinement boundary while it is loaded with the spent fuels as like Fig. 1.

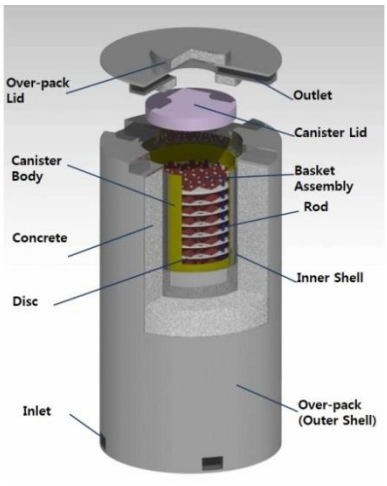


Fig. 1. The cross-section of concrete storage cask.

2.2 Load combinations of off-normal condition

The structural analysis of the concrete storage cask considered pressure load, wind load and thermal load for off-normal condition. The load combinations regarding the concrete storage cask were set according to the NUREG-1536, ANSI/ANS 57.9 and ACI criteria based on the structural analyses results on each load to conduct a stress evaluation of the concrete storage cask. The design criteria under off-normal condition are listed in Table 1.

Table 1. Design criteria under off-normal condition

Type	Criteria	Basis
Ambient temp. (Max./Min.)	35.0℃/ -25.0℃	ANSI/ANS57.9, NUREG-1536
Partial blockage of air inlets	50% (two air inlet blocked)	10CFR72,128(a)
Wind load	45m/sec (avg. 10 min)	Korea building code-Structural

2.3 Material properties

The concrete storage cask body was produced from carbon steel, and the elements other than the body were produced from stainless steel. The canister

utilized SA-240 316L material to increase the salt resistance due to the external environment under storage conditions.

2.4 Structural analysis

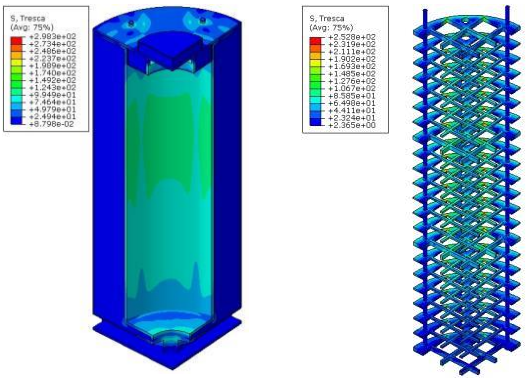
For the finite element analysis model used in the structural analysis of the concrete storage cask, one structural model was prepared and the initial condition and boundary condition were varied to apply to every analysis. Considering the symmetry of the cask, the analysis model was composed of a 1/2 model. The analysis model was composed of 809,046 nodes and 556,905 slid elements.

3. Results and discussion

The internal pressure of the canister with 10% of the internal fuel rods damaged was set as the load, and 0.09972 MPa, pressure under the off-normal condition computed from the thermal analysis results, was applied to the inside the canister. The internal elements were excluded from the analysis because the pressure load acts only inside the canister. Analysis results showed a maximum stress 15.9 MPa on the canister body.

The wind load was set with the consideration of the natural environment of Korea according to the Korean Building Code, the wind load was set as 1.831 kN/m^2 and 2.464 kN/m^2 in horizontal and vertical directions, The analysis results revealed the stress of 1.6 MPa on the external surface of the concrete cask body, and almost no influence wind load was observed.

The stress evaluations due to the thermal load at the maximum temperature of 35℃ and the minimum temperature -25℃ were conducted for the thermal loads on the concrete storage cask under the off-normal condition. An air path condition of 50% blockage was additionally considered for the maximum temperature of 35℃. The highest temperature was observed at the upper part of the concrete cask body due to the internal air circulation, and the difference between the outside and inside temperatures of the cask body was approximately 50℃. The highest stress due to the off-normal condition was observed at the disc, and satisfied the allowable stress in every part. The stress distribution with respect to the maximum and minimum outside temperatures is illustrated in Fig. 2.



(a) (b)

Fig. 2. Thermal stress distribution; (a) concrete cask body, (b) disc and rod.

4. Conclusions

This paper verified the stabilities of the structural elements that influence the safety of the concrete storage cask for spent and summarizes the structural evaluation results of a concrete storage cask with respect to the design criteria under off-normal condition. the evaluation results show that the maximum stress was below the allowable stress under off-normal condition, and the concrete storage cask satisfied the design criteria. Therefore, based on the results of the stress evaluation, the design requirements were satisfied in the off-normal condition.

REFERENCES

[1] 10CFR Part 72, Title 10 (2006), Chapter 1 of the Code of Federal Regulations, Licensing Requirement for the Independent Storage of Spent Nuclear Fuel, High-level Radioactive Waste, and Reactor-Related Greater than Class C Waste, 1-1-06 Edition.

[2] NUREG-1536 (2010), Standard Review Plan for Spent Fuel Dry Storage Systems at a General License Facility, Revision 1.

[3] Dassault Simulia (2010), ABAQUS 6.10 Documentation.

[4] TC Moon, CY Baeg, ST Yoon and IS Jung (2014), Structural evaluation and analysis under normal conditions for spent fuel concrete storage cask, Trans. of the Korean Nuclear Society Spring Meeting, Jeju, Korea, May 29~30.

A New Perspective of Hydride Re-orientation in SNF

J. S. Noh[1], Y.K. Kim[2], and M. Tayal[3]
[1]ACT Co., Ltd. , Techno 9 Ro-35, Yuseong-Gu, Daejeon, Republic of Korea
[2]KEPCO Nuclear Fuel Co., Daejeon, Republic of Korea
[3]Expert in CANDU Fuel (Consultant), Canada
jsnoh@actbest.com[1], ykkim@knfc.co.kr[2], and tayal2000@gmail.com[3]

1. Introduction

In recent years, hydride re-orientation in spent nuclear fuels (SNF) and its effects on cladding properties have become important considerations in storage, handling and transportation of SNFs. In particular, current high-burnup fuels would have more severe potential for damaging re-orientation of hydrides. The mechanism of hydride re-orientation involves dissolution of circumferential hydrides and formation of radial hydrides. Past studies have already illustrated the mechanism of hydride re-orientation and the factors that affect it, including stress, hydrogen concentration, temperature, cooling rate etc. [1~6]. In this paper, we review those studies and suggest a new perspective for additional research on hydride re-orientation.

2. Studies on Hydride Re-orientation in SNF

2.1 General

Most studies to-date on hydride re-orientation have focused on hydride re-orientation during stylized conditions pertinent to dry storage and to transportation of SNFs. Based on results from those studies [1], the U.S. Nuclear Regulatory Commission (NRC) has set some design limits to inhibit hydride re-orientation as follows [2]:

• For all fuel burnups (low and high), the maximum fuel cladding temperature should not exceed 400˚C. However, for low burnup fuel, a higher short-term temperature limit may be used when cladding hoop stress is equal to or less than 90 MPa for the temperature limit proposed.

• During loading operations, repeated thermal cycling should be limited to less than 10 cycles, with cladding temperature variations less than 65˚C each.

As can be seen in the NRC requirements, temperature and stress are recognized as the most important factors affecting hydride re-orientation in SNF cladding. Many investigations have already quantified the impacts of these two parameters on radial hydride re-orientation. Also, the effects of thermal cycles and of pre-heating on hydride re-orientation have also been investigated [3, 4].

2.2 Formation of Hydrides

Oxidation of Zircaloy cladding during reactor operation produces hydrogen. Some portion, estimated to be 5% to 20%, of the hydrogen released by this reaction is absorbed by the cladding and diffuses into the clad [4]. The absorbed hydrogen may remain in solid solution in the Zr lattice or precipitate as hydride depending on the temperature and the amount of hydrogen absorbed. When hydrogen concentration exceeds the solubility limit of hydrogen, hydrides form. The solubility of hydrogen decreases drastically with decreasing temperature in zirconium alloys. Preferred sites for hydride formation are either grain boundaries or inside the matrix, in which basal plane (0002) is the dominant habit plane [4]. Since the density of the hydride is less than that of zirconium, hydride nucleation leads to a local lattice expansion, which should be accommodated in the zirconium matrix [5].

Hydride precipitates can be seen with an optical microscope. They appear as single platelets or as a cluster of platelets, as shown in Fig. 1[6].

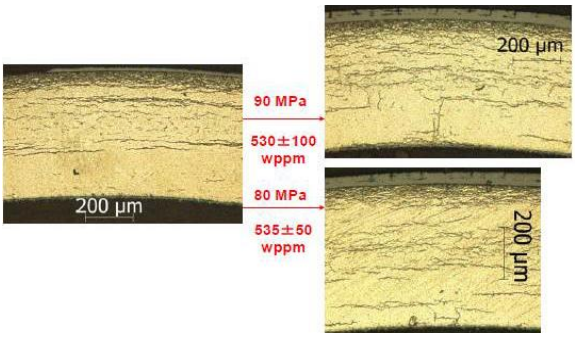


Fig. 1. Hydride Re-orientation in Irradiated ZIRLO Cladding Heated to 673˚K and Cooled under Stress[6].

2.3 Factors affecting hydride re-orientation

Threshold Stress

Radial hydride formation is believed to be driven by tensile hoop stress (along the circumferential direction). As hydrides form perpendicular to the tensile stress and parallel to the compressive stress, stress plays a major role in hydride re-orientation. Therefore, a critical stress also known as the threshold stress, under which the re-orientation takes place, has been defined. It is clear that the stress limits for hydride re-orientation appear to decrease with an increase of peak temperature.

NRC's temperature and stress limits were determined to prevent hydride re-orientation from occurring[2]. However, further research has shown that hydrides may still reorient radially even within these limits as seen in Fig. 2 [1].

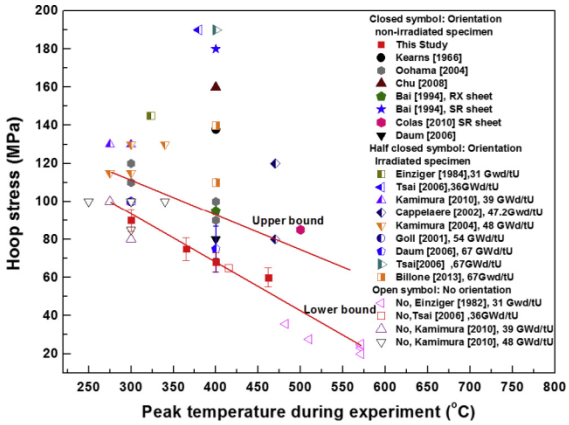


Fig. 2. Collected data on threshold stress triggering hydride reorientation in Zircaloy-4 as a function of peak temperature[1].

Temperature

As the level of re-oriented hydrides depends on the amount of dissolved hydrogen at the peak temperature of the cladding, the temperature history experienced by the cladding is of interest for hydride re-orientation in SNF. The re-orientation process is of particular concern during the drying process right after fuel is removed from the pool, at which time the cladding temperature is assumed to reach around 400˚C. This would cause a significant portion of hydrogen, about 200 wppm in Zircaloy, to dissolve back into solution. Hydrogen dissolved upon heating is available to re-precipitate as radial hydrides upon subsequent cooling. The temperature affects internal pressure of SNF: the internal pressure increases with increasing temperature. Considering the measured peak temperatures of SNF, which ranges over 400°C, the temperature of cladding should be monitored closely, especially during drying process [4].

Thermal Cycle

The percentage of radial hydrides increases as the number of thermal cycles increases until it saturates. Hence, it is believed that the effect of thermal cycling on hydride re-orientation is more significant than that of isothermal treatment [3, 4].

3. A New Perspective

Simulating the realistic conditions of SNF

Hoop Stress

Studies performed so far mostly used constant hoop stresses by using ring compression, ring tension, tapered specimen or internal gas pressure. In reality, the hoop stress decreases continually during the storage period, due to drop in temperature and cladding creep.

Temperature

Cladding temperature also decreases over time. Thus hydride re-orientation is better assessed using more realistic cladding temperatures calculated from decay heat and conduction.

Hydride Distribution

Non-irradiated cladding tested for hydride re-orientation often contained relatively uniform hydride distributions compared to the non-uniform distributions generally found in irradiated claddings. This potential difference in hydride distribution and morphologies over the cross section could be one reason for the discrepancy in test results between un-irradiated alloys and irradiated alloys.

Stress State

Stress state also impacts the threshold stress for hydride reorientation. Most results of threshold stresses for hydride re-orientation have been obtained under nearly uniaxial test conditions, thus, may not be directly applicable to re-orientation in a closed fuel rod, in which stress state would be multi-axial.

CANDU Fuel

Some differences between CANDU and PWR fuels impact Delayed Hydride Cracking (DHC) in the former. As illustrative examples: (a) Stresses near the junction between the sheath and the endcap are highly multi-axial; also much higher than in the clad; therefore hydride assessments at this location need quite detailed considerations of highly multi-axial stresses; (b) Endplates have the lowest temperature in a CANDU fuel assembly, therefore highest concentration of hydrides usually occurs in endplates and in assembly welds; (c) Variety of microstructures occur in CANDU fuel's Zircaloy. Thus DHC characteristics need to be established and analyzed for CANDU fuel differently from PWR fuels.

4. Conclusion

Considering the gaps between the conditions of laboratory hydriding tests and realistic conditions of SNF currently in dry storage, more realistic test conditions would be desirable to better understand the behaviors of hydride re-orientation in SNF.
Therefore further research is needed to better quantify the relationship between hydride re-orientation and ductility; this will improve the hydride criterion. Also, to establish the requirements for CANDU fuel, additional research is needed to reflect the several unique aspects of that fuel.

REFERENCES

[1] J.S. Kim et al., "A study on hydride reorientation of Zircaloy-4 cladding tube under stress", J. of Nuclear Materials 456(2015).
[2] NRC Interim Staff Guidance - 11, Revision 3.
[3] H.C. Chu et al., "Hydride reorientation in Zircaloy-4 cladding", J. of Nuclear Materials 373 (2008).
[4] White Paper Summary of 2nd ASTM International Workshop on Hydrides in Zirconium Alloy Cladding, 2015.
[5] IAEA-TECDOC-1410, "Delayed hydride cracking in zirconium alloys in pressure tube nuclear reactors".
[6] M. C. Billone, "DBTT for High-Burnup PWR Fuel-Cladding Alloys", 2nd ASTM International Workshop, 2015.

Determination of Uranium, Plutonium, Neodymium, Cesium, Cerium and Europium Isotopes in Irradiated Dual-cooled Annular Fuel by Isotope Dilution Mass Spectrometry and γ-Ray Spectrometry

Jung Suk Kim*, Byungman Kang, Yang-Soon Park, Young Bok Kim, Jai Il Park, and Yeong Keong Ha

Korea Atomic Energy Research Institute, 111, Daedeok-daero 989beon-gil, Yuseong-gu, Daejeon, Republic of Korea

*njskim1@kaeri.re.kr

1. Introduction

The burnup of important fissile isotopes and the composition of an irradiated fuel depend on the nature of the fuel and on the conditions of an irradiation. A detailed knowledge of these quantities is useful for a reactor work as well as for the effective utilization of a nuclear fuel. Burnup determination by destructive method, which is based on the determination of specific nuclides, e.g. U, Pu and ^{148}Nd (or ^{137}Cs) by a chemical analysis after an appropriate separation of the heavy elements and a monitoring of the fission product, is widely used as a reference method to measure the burnup of an irradiated fuel [1-3]. Of the many stable nuclides formed in the fission, Nd satisfies most of the necessary requirements for a good burnup monitor[1], can be measured using isotope dilution mass spectrometric techniques (IDMS). On the other hand, radioactive nuclides such as ^{134}Cs, ^{137}Cs and ^{144}Ce can be measured using γ-ray spectrometric techniques (GRS).

The aim of the present work is to determine the isotopic compositions and their contents of U, Pu and Nd, and the activities of Cs, Ce and Eu isotopes (γ-emitters) for the samples from dual-cooled annular nuclear fuels of UO_2 type irradiated in the Hanaro reactor at KAERI, and to determine the burnup using the measured results, so as to determine the respective validity of the methods

2. Experiments

2.1 Chemicals

The Certified ^{233}U (99.470 atom%) and ^{150}Nd (96.13 atom%) spikes were obtained from Oak Ridge National Laboratory (ORNL). These spike solutions were prepared by dissolving their oxides in 8 M HNO_3-0.01 M HF. Certified ^{242}Pu spike solution (99.9033 atom%, IRMM-044) was obtained from the Institute for Reference Materials and Measurements. The concentrations of the spike solutions were prepared by calibrating them with a standard solution.

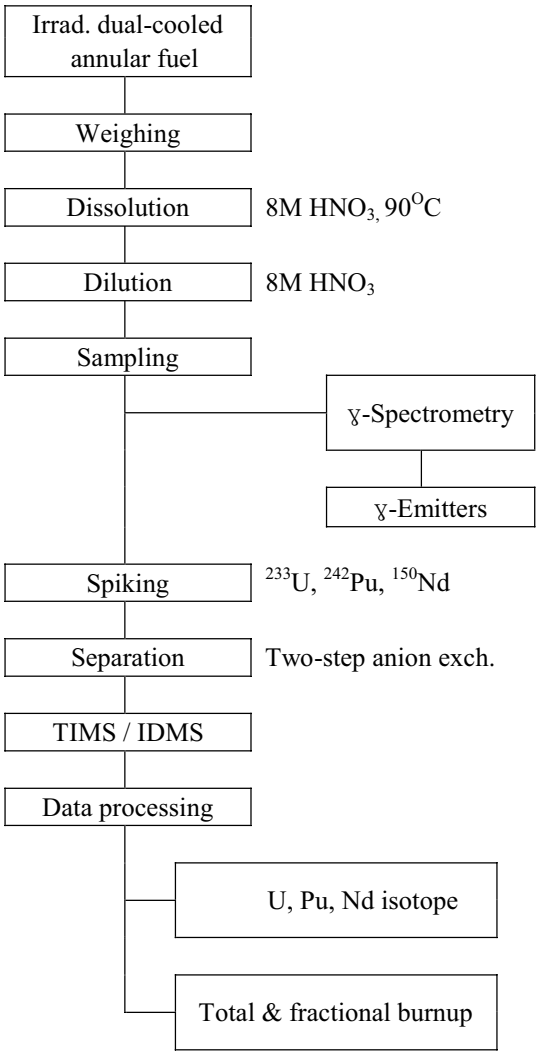


Fig. 1. Analytical Processes for the Determination of U, Pu, Nd Isotopes and γ-Emitters in an Irradiated Dual-cooled Annular Fuel Sample.

2.2 Sample Preparation and Isotopic Measurement

The basic processes in the analytical laboratory for the determination of U, Pu, Nd, γ-emitters, and burnup are shown in Fig. 1. Chemical separation was carried out for both the unspiked and the spiked sample solutions in the same experimental conditions in a glove box without any heavy shieldings. The isotopic compositions of U, Pu and Nd in the unspiked and spiked fuel samples were determined using a thermal ionization mass spectrometer (Finnigan TRITON). The activity of gamma emitters for the diluted solutions from the fuel solutions was measured with a high purity Ge coaxial detector (EG & G ORTEC) connected to a multi-channel analyzer.

3. Results & Discussion

3.1 γ-Emitters in Irradiated Fuel

The activities of γ-emitters found in the dissolved solutions of irradiated dual-cooled annular fuels are summarized in Table 1. The activities of γ-emitters in the dissolved solutions from the GRS, that is, S-1, S-2 and S-3, include the fission products ^{134}Cs, ^{137}Cs, ^{144}Ce, ^{154}Eu, ^{155}Eu, ^{106}Ru and ^{125}Sb and activation products such as ^{60}Co and ^{95}Zr.

Table 1. Distribution of Radionuclides in Irradiated Dual-cooled Annular Fuel Samples

Nucl.	Activity (Bq/g-sample)		
	S-1	S-2	S-3
^{134}Cs	1.58×10^{9} $\pm6.27\times10^{7}$	1.83×10^{9} $\pm7.23\times10^{7}$	1.76×10^{9} $\pm6.96\times10^{7}$
^{60}Co	2.17×10^{7} $\pm1.03\times10^{6}$	1.99×10^{7} $\pm1.00\times10^{6}$	2.71×10^{7} $\pm1.39\times10^{6}$
^{137}Cs	3.54×10^{9} $\pm1.44\times10^{8}$	3.48×10^{9} $\pm1.41\times10^{8}$	3.74×10^{9} $\pm1.53\times10^{8}$
^{144}Ce	2.91×10^{9} $\pm9.36\times10^{7}$	2.82×10^{9} $\pm9.23\times10^{7}$	3.00×10^{9} $\pm9.88\times10^{7}$
^{154}Eu	1.37×10^{8} $\pm6.58\times10^{6}$	1.44×10^{8} $\pm6.52\times10^{6}$	1.50×10^{8} $\pm7.10\times10^{6}$
^{155}Eu	5.97×10^{7} $\pm2.98\times10^{6}$	6.39×10^{7} $\pm3.11\times10^{6}$	7.35×10^{7} $\pm3.62\times10^{6}$
^{106}Ru	3.06×10^{9} $\pm2.06\times10^{8}$	3.10×10^{9} $\pm2.01\times10^{8}$	2.90×10^{9} $\pm1.95\times10^{8}$
^{125}Sb	1.21×10^{8} $\pm7.20\times10^{6}$	1.23×10^{8} $\pm8.53\times10^{6}$	1.46×10^{8} $\pm9.19\times10^{6}$
^{95}Zr	1.45×10^{7} $\pm2.57\times10^{6}$	1.11×10^{7} $\pm2.21\times10^{6}$	1.96×10^{7} $\pm4.59\times10^{6}$
^{140}Ba	$< 4.63\times10^{6}$	$< 7.33\times10^{6}$	$< 8.35\times10^{6}$
^{95}Nb	$< 4.42\times10^{6}$	$< 3.21\times10^{6}$	$< 7.38\times10^{6}$

3.2 Isotopic Compositions of Cs and Eu

Table 2 shows a comparison of the activity ratios for Cs and Eu in the the irradiated fuel samples, It may be inferred that there is a distinct difference between the three values with the progression of the fuel burnup.

Table 2. Comparison of Cs and Eu Activity Ratios in Irradiated Dual-cooled Annular Fuel Samples

Sample	Activity ratio	
	^{134}Cs/^{137}Cs	^{154}Eu/^{137}Cs
S-1	0.446	0.039
S-2	0.525	0.041
S-3	0.470	0.040

4. Conclusion

The contents of U, Pu, Nd, Cs and their isotopes in irradiated dual-cooled annular fuel samples and the total burnup by using Nd, Cs and Ce isotope monitors can be determined simultaneously by the isotope dilution mass spectrometric and γ-ray spectrometric techniques. The Nd and Cs isotope patterns provide information on the real irradiation characteristics which are necessary for evaluating a fuel's performance in a reactor. A comparison between independently determined burnup values provides a check on the validity of the results

REFERENCES

[1] ASTM, "Standard Test Method for Atom Percent Fssion in Uranium and Plutonium Fuel (Neodymium-148 Method)", Annual Book of ASTM Standards 12.02, E321-96 (reapproved 2012), (2012).

[2] J. S. Kim, Y. S. Jeon, S. D. Park, Y. K. Ha, and K.. Song, "Analysis of High Burnup Pressurized Water Reactor Fuel Using Uranium, Plutonium, Neodymium, and Cesium Isotope Correlations with Burnup", Nucl. Eng. & Technol., 47(7) 924-933 (2015).

[3] H. Graber, G. Hofmann and R. Berndt, "Correlations of Burnup with the ^{134}Cs/^{137}Cs and ^{154}Eu/^{137}Cs Concentration Ratios for Irradiated LWR Fuel", IAEA-SM-260/84, Nuclear Safeguards Technology, vol. I, 443-454 (1983).

Passivation of Al_2O_3-based Refractories by Air Plasma Spray Coatings of Y_2O_3

Sang-Chae Jeon*, Jae-Won Lee, Joo-Young Yoon, and Yung-Zun Cho
Korea Atomic Energy Research Institute, 111, Daedeok-daero 989beon-gil, Yuseong-gu, Daejeon, Republic of Korea
jym@kaeri.re.kr

1. Introduction

As the starting process of pyroprocessing, head-end process deals with the conversion of spent fuel into suitable feed form of uranium oxides for following electrolytic reduction process. Depending on its physical form, the fabrication process of feed materials may (or may not) include high temperature treatment. Voloxidation and sintering correspond to the high temperature processes in the preparation of porous pellet, which is one of the promising feed materials [1-3]. During the heat treatment at high enough, radioactive fission products such as Cesium (Cs) and Iodine (I) are released from the spent fuel of uranium oxides. Considering that the fission products are extremely harmful to human body, their emission to atmosphere must be strictly minimized by capturing them using appropriate filters. In other words, the released off gas should be collected at the filters connected to a furnace where the heat treatment of the spent fuel takes place.

The off-gas escapes from the spent fuel and move to the filters along with atmospheric gas flow in heating furnace, contacting inner surfaces of the refractory materials in the furnace. Most of the refractories usually contain alumina (Al_2O_3) and silica (SiO_2) due to their excellent heat tolerance. However, those likely to form mullite ($Al_6Si_2O_{13}$) phase during heating. The mullite is well known material for capturing the Cs vapor by the formation of pollucite ($CsAlSi_2O_6$) phase. Considering this, the use of those general refractories would be a critical problem. Apart from developing 'brand-new' refractory materials, which is extremely challenging, the coatings of inert materials on the surface of refractories can be a possible detour to suppress the reaction with CS. The present study explores the possible way to prevent the capture reaction of Cs with refractories by Air Plasma Spray (APS) coating of pure Y_2O_3. Both confirmation on the material and optimization of the coating process in this study would provide the applicability of this material and method for successful head-end process, especially for capturing the off-gas in pyroprocessing.

2. Experimental

The commercial insulating fire bricks with a composition of $99.3Al_2O_3$-$0.4SiO_2$-$0.1Fe_2O_3$ (wt. %) and high purity Y_2O_3 powder (> 99.9 %) were prepared for the substrate and coating material for APS coating in this experiment. The confirmation on the reactivity of the Y_2O_3 with Cs using Cs_2CO_3 powder, which is decomposes into Cs_2O and CO_2 after melting at about 610°C. The spray coating was conducted with the same conditions except the thickness of Y_2O_3 coating layer then optimized the thickness of coating layer as 500 μm. To enhance adhesion without delamination, the coated samples were heat-treated at 1520°C for 10 h in air atmosphere with heating and cooling rate of 2°C/min. For the reaction experiment between Cs and refractory material, Cs_2CO_3 powder was used as Cs source. 0.05 g of Cs_2CO_3 powder was dispersed on the surface of coated layer and heat treated at 1450°C for 1 h in 4% H_2-Ar flow (0.1 liter/min). The characterization was conducted by SEM/EDS and XRD before and after the heat treatment.

3. Results and Discussion

Fig. 1 shows the physical properties of the commercial insulating brick. It consists of pure Al_2O_3 particles ranging from few to few tens of microns as shown in the SEM and SEM/EDS results. Their particle shapes varied from rounded to elongated. The XRD pattern indicates its single phase of Al_2O_3. To exclude the possibility of mullite phase is the reason why the brick of high purity without Si was used in this experiment.

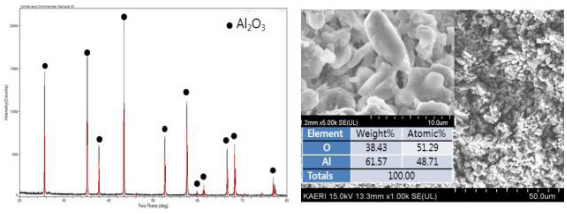


Fig. 1. XRD (left) and SEM/EDS results of the brick.

Fig. 2 shows SEM micrographs of the cross section and the surface of Y_2O_3 coated samples after heat treatment at 1520°C for 10 h in air. Clear distinction was made by different porosity in the observations. It is noting that the substrate brick was overspread with coated Y_2O_3 layer. From the micrograph showing the surface of the coated layer, well-organized small Y_2O_3 grains were observed. Severe roughness with many pores was also observed at the surface which is largely due to the original surface roughness of the surface of brick substrate. However, it did not mean the exposure of the substrate brick to atmosphere.

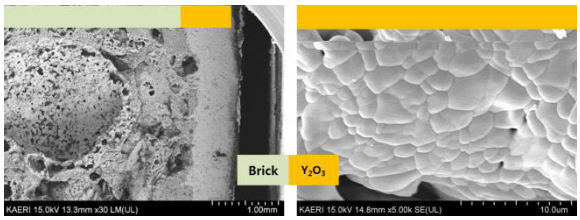


Fig. 2. SEM micrographs showing a cross section (left) and surface (right) of the APS coated samples.

The spatial chemical composition across the interface was observed by SEM/EDS line scan as shown in Fig. 3. It shows other distinction of the substrate and coated layer than the morphology shown in Fig. 2. The brick substrate and coated layer were divided by its composition with other major cation element, Al and Y, respectively. In the line scan result, some of Al was also observed at the coated Y_2O_3 layer. In contrast, from the spot analysis indicated that the coated layer was homogeneous Y_2O_3 single phase, indicating the inactivation of the coated layer based on that there was no reaction between the Y_2O_3 and Cs_2CO_3 powder.

Fig. 4 shows the photographs of cube-shaped samples before and after heat treatment at 1450°C for 1 h in 4% H_2-Ar, which is similar with real sintering process of the porous pellet fabrication.

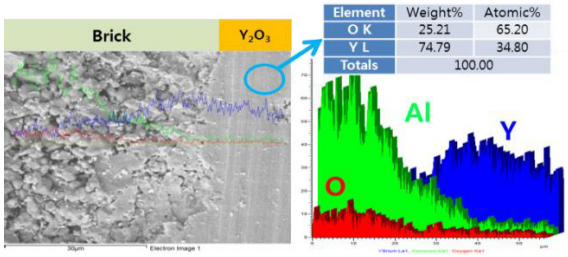


Fig. 3. SEM/EDS line scan result of across the interface between brick and coated Y_2O_3 layer.

The heat treatment was accompanied by addition of Cs_2CO_3 powder on the surface of the coated Y_2O_3 layer. After the heat treatment, the coated layer was Y_2O_3 single phase as shown in the XRD pattern as it was before the heat treatment. This clearly indicates that there would be no chemical reaction of the coated Y_2O_3 layer with Cs.

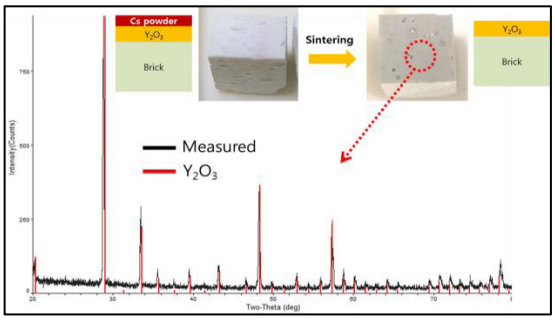


Fig. 4. Photographs of the samples before and after heat treatment (inset) and XRD pattern of the coated Y_2O_3 layer after heat treatment.

4. Conclusions

The coated Y_2O_3 layer on a commercial fire brick maintained its physical/chemical integrity with the presence of Cs during high temperature heat treatment. This provides the applicability of the APS coating of Y_2O_3 to the refractories for off-gas treatment system in pyroprocessing.

REFERENCES

[1] Y. Sakamura and T. Omori, "Electrolytic Reduction and Electrorefining of Uranium to Develop Pyrochemical Reprocessing of Oxide Fuels," Nucl. Techno., 171 (2010) 266–275.

[2] S.-C. Jeon, J.-W. Lee, J.-H. Lee, S.-J. Kang, K.-Y. Lee, Y.-Z. Cho, D.-H. Ahn, and K.-C. Song, "Fabrication of UO_2 Porous Pellets on a Scale of 30 kg-U/Batch at the PRIDE Facility," Adv. Mater. Sci. Eng., 2015 (2015) 1-8.

Spectroscopic and Electrochemical Investigation of Reactions of Oxide Ions With U^{3+} and Ln^{3+} (Ln=Nd, Ce, and La) in LiCl-KCl Melts

Suhee Choi*, Sang-Eun Bae, and Tae-Hong Park

Korea Atomic Energy Research Institute, 111, Daedeok-daero 989beon-gil, Yuseong-gu, Daejeon, Republic of Korea

*shchoi926@kaeri.re.kr

1. Introduction

Lanthanide and actinide elements in spent nuclear fuel coexist as various oxidation states in molten salt of a pyrochemical processing [1]. There is also an oxygen ion in an electro-reduction process of the pyroprocessing. It is well known that the lanthanide and actinide ions may form metal oxide precipitates if the oxygen ion exists in the solution. Therefore, the oxygen ion can give a fatal influence on the operation of electro-refining and electro-winning process. However, reactions between the uranium and the oxygen ions have not been much studied in molten salt yet. In this work, chemical reactions between the U ions and the oxygen ions in LiCl-KCl melts were investigated by electrochemical and UV-vis absorption spectroscopic methods. Raman spectroscopy and X-ray diffraction (XRD) were also employed to characterize the chemical compositions of the resulting uranium oxides.

2. Experimental

All the experiments were carried out in a glove box under Ar, where the O_2 and H_2O levels were maintained at less than 1 ppm. Lithium chloride/potassium chloride (LiCl/KCl) eutectic salts (anhydrous beads), lithium oxide (Li_2O), lithium chloride (LiCl), and silver chloride (AgCl) were obtained from Sigma Aldrich. Neodymium chloride ($NdCl_3$), cerium chloride ($CeCl_3$), and lanthanum chloride ($LaCl_3$) were purchased from Alfa Aesar (purity ≥ 99.999%). UCl_3 was prepared with a chemical method from U metal and $CdCl_2$ in a LiCl-KCl melt. Li_2O was added to the molten LiCl-KCl as 5 wt.% Li_2O-LiCl salt due to the low solubility of Li_2O in LiCl-KCl.

W wire (Alfa Aesar, diameter 0.2 mm) and glassy carbon (Alfa Aesar, diameter 3 mm) electrodes were used as the working and counter electrodes, respectively. The W wire electrode was mechanically polished with sand paper prior to use. The reference electrode was Ag wire dipped into a Pyrex tube including 1 mol % AgCl in the LiCl-KCl eutectic melt.

3. Results and Discussion

3.1 Electrochemcial study

Fig. 1 shows the CVs of UCl_3 and $LnCl_3$ in LiCl-KCl molten salts while adding Li_2O into the melt as a source of O^{2-}. The current-voltage (I-V) curves demonstrate that the electrochemical signals of U^{3+} and Ln^{3+} remained after reacting with the oxide ion in the molten salt. Prior to Li_2O addition, 1 wt.% of U^{3+} and 2wt.% Ln^{3+} show their characteristic deposition and dissolution peaks at -1.4 to -1.6 V and -2.0 to -2.2 V, respectively. Additionally, the redox couple of $U^{3+/4+}$ appears at -0.2 to -0.4 V. Then, we measured the CVs of the melt after adding aliquots of Li_2O (each ~0.25 equivalent to the U or Ln ions) to the melt and shaking the mixture to facilitate the reaction. The continuous addition of Li_2O gradually reduced the currents of U^{3+} and Ln^{3+} without inducing new signals, indicating that the U and Ln ions were consumed by the reactions with Li_2O to afford the corresponding insoluble oxide and/or oxychlorides.

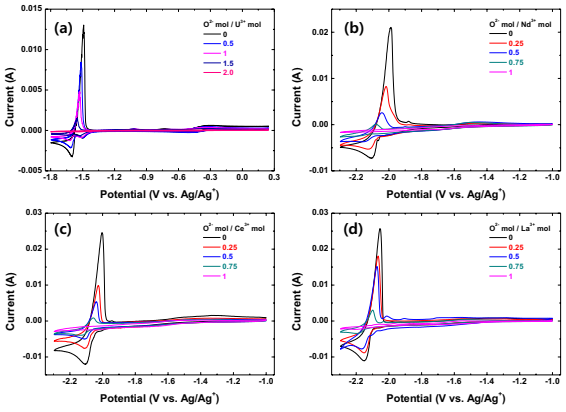


Fig. 1. CVs of LiCl-KCl melts containing (a) 1 wt.% of UCl_3, and 2 wt.% of (b) $NdCl_3$, (c) $CeCl_3$, and (d) $LaCl_3$, with the addition of Li_2O into the melts at 450 ℃. Scan rate = 200 mV/s.

3.2 Precipitations Analysis

In the Raman spectra in Fig. 2, the uranium precipitate exhibits a broad peak at 448 cm^{-1}, which is attributable to the U-O stretching mode of UO_2. On the basis of literature, the Raman modes can be assigned to NdOCl: the mode at 185 cm^{-1} has A_{1g} symmetry, the modes at 122 and 439 cm^{-1} have E_g symmetry, and that at 315 cm^{-1} can be assigned to phonons with A_{1g} or B_{2g} symmetry. Despite the slightly noisy Raman signals, the spectra of Ce and La show Raman shifts very similar to those of NdOCl, indicating that the precipitates also have the same oxychloride structure. Interestingly, CeO_2 has a Raman active Ce-O-Ce symmetric vibration at ~465 cm^{-1}. Therefore, the Raman and electronic spectroscopy study suggest that the Ce precipitate also contains CeO_2.

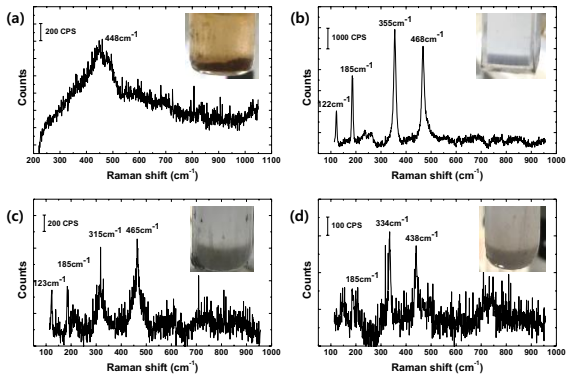


Fig. 2. Raman spectra of LiCl-KCl containing precipitates of (a) U, (b) Nd, (c) Ce, and (d) La (λ_{ex} = 625.8 nm, 20 mW; acquisition time, 1 s). Insets: photos of molten salts containing the precipitates.

Fig. 3 shows the XRD results of the mixtures of salt and precipitates obtained after the reactions. The major component LiCl and KCl exhibit much more intense signals than the reaction products. The salt containing U displays peaks of 32.7°, 55.7°, 58.4°, and 87.3°, which are attributed to UO_2. Like the Raman results, the XRD patterns of the three lanthanides were very similar and were assigned to the corresponding oxychloride structures. Meantime, it was difficult to find evidence of CeO_2 in the XRD result of the salt-precipitate mixture. After removing the salt with water, the remaining Ce precipitate was measured again by XRD. The result (shown in red in Fig. 3c) displays a clear pattern of CeOCl with trace signatures of CeO_2, indicating the reaction of Ce^{3+} and Li_2O can also form CeO_2 as a by-product, as observed in the Raman spectra. The formation of CeO_2 seems very sensitive to reaction conditions, such as the concentration and source of the oxide ion.

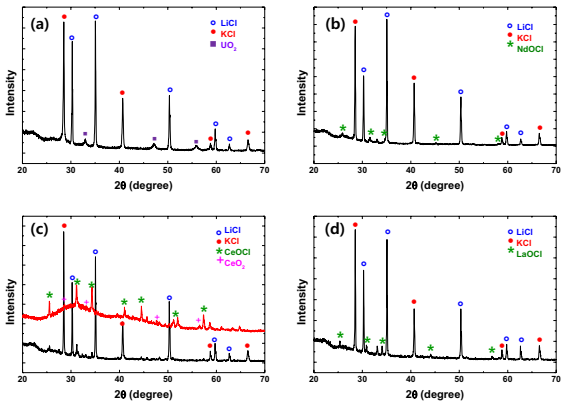


Fig. 3. XRD patterns of LiCl-KCl containing (a) U, (b) Nd, (c) Ce, and (d) La precipitates. The red trace in (c) was obtained from the solid after washing the precipitate with water.

4. Conclusions

Here, we studied the chemical reactions of U^{3+}, Nd^{3+}, Ce^{3+}, and La^{3+} with Li_2O in the LiCl-KCl melt using electrochemical tools. The CV measurements enabled in-situ monitoring of the reactions upon the addition of oxide ions, demonstrating that U^{3+} and Ln^{3+} react with two and one equivalents of the oxide ion, respectively. Raman spectroscopy and XRD analyses of the products confirmed that the precipitation reactions presented UO_2 and LnOCl. Both analyses detected a trace of CeO_2, which likely resulted from the oxidation of CeOCl during the reaction.

REFERENCES

[1] H. Lee, G.-I. Park, K.-H. Kang, J.-M. Hur, J.-G. Kim, D.-H. Ahn, Y.-J. Cho, and E.-H. Kim, “Pyroprocessing Technology Development at KAERI”, Nuclear Engineering and Technology, 43 (4), 317-328 (2011).

Re-fabrication of U-Zr Alloy System Fuel Slugs Recycling Metallic Fuel Scraps

Ki-Hwan Kim[1*], Seong-Jun Ha[2], Young-Mo Ko[1], Seok-Jin Oh[1], and Jeong-Yong Park[1]

[1]Korea Atomic Energy Research Institute, 111, Daedeok-daero 989beon-gil, Yuseong-gu, Daejeon, Republic of Korea

[2]Chungnam National University, Daejeon, Republic of Korea

[*]khkim2@kaeri.re.kr

1. Introduction

Metallic fuels such as U-Zr and U-TRU-Zr alloy are being developed for the sodium-cooled fast reactor (SFR) to be built in Korea [1-3]. TRU recovered through the pyro-electrochemical processing of spent LWR fuels are used to fabricate the metal fuel. The extracted uranium and TRU including Pu and long-lived minor actinides (MA) such as Np, Am, and Cm are used to fabricate the metallic fuel. This fuel recycling can solve the problem of PWR spent fuel accumulation by reducing the volume of PWR spent fuel, and increase the utilization of uranium resources while maintaining high proliferation resistance. A vacuum injection casting method has been applied to fabricate metallic fuel slugs of the SFR. Although the injection casting has been a well-established fabrication method for metallic fuel for decades, it has a drawback of low yield upto 55% because of the formation of lots of metallic fuel scraps such as the heel of melt residue and the butts of fuel slugs.

In this study, the fuel scraps such as the heel residue have been washed with chemical treatment. Metallic fuel slugs have been re-fabricated for the recycling of the fuel scraps. The re-fabricated fuel slugs were characterized to evaluate the feasibility of the recycling of the fuel slug scraps.

2. Methods and Results

2.1 Experimental Methods

The heel residues of U-10wt.%Zr and U-10wt.%Zr-7wt.%RE (rare-earth elements) fuels after modified injection casting were used as raw materials for re-fabrication of metallic fuel slugs. RE is a rare-earth alloy consisting of 53wt%Nd, 25wt%Ce, 16wt%Pr, and 6wt%La. The fuel scraps were pickled using 2M nitric acid for an hour using a bubble-washing equipment.

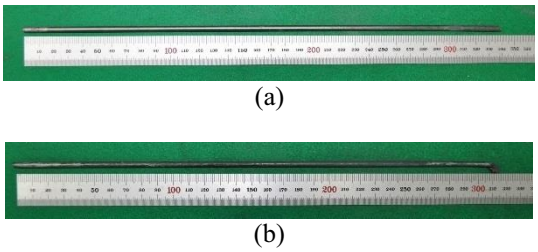
Pickled heel residues and mixed pickled heel residues with pure metals such as uranium, zirconium, and RE alloy at a ratio of 1:1 were used to fabricate U-10wt%Zr and U-10wt.%Zr-7wt.%RE fuel slug by injection casting methods. Casting variables, e.g., casting temperature and pressure, pressurizing rate, mold coating method were adjusted with graphite crucibles coated with ceramic plasma-spray coating and quartz molds coated with slurry-coating. At a predetermined superheat, the mold was lowered with pressurization of atmospheric gas, immersing the open tip into the metal melt. The metallic fuel slugs were fabricated using recycled metallic fuel scraps by injection casting method.

To examine the soundness of the metallic fuel slugs, the density of the metallic fuel slugs was measured using an Archimedean immersion method. The alloy compositions and impurities of the metallic fuel slugs were investigated using inductively coupled plasma atomic emission spectroscopy (ICP) and an elemental analysis (EA). The microstructure and the composition of the metallic fuel slugs were analyzed using scanning electron microscopy (SEM) and energy-dispersive spectroscopy (EDS). In addition, X-ray diffraction spectroscopy (XRD) was carried out for a comparison with metallic fuel slugs fabricated using pure metal materials.

2.2 Experimental Results

Metallic fuel slugs consisting of U-10wt%Zr and U-10wt%Zr-7wt%RE with a diameter of about 5.5 mm and a length of about 300 mm were fabricated per batch. They were generally sound without cracks or thin sections. The densities of the U-10wt%Zr metallic fuel slugs were measured as 15.70 (heel 100%) and 15.75g/cm^3 (heel 50%). The densities of

the U-10wt%Zr-7wt%RE metallic fuel slugs were measured as 14.93 (heel 100%) and 14.8 g/cm^3 (heel 50%). The results show that the U-10wt%Zr metallic fuel slug fabricated using the 100% heel residue was similar to that of the 50% heel residue. The results show that the U-10wt%Zr-RE metallic fuel slug fabricated using the 100% heel residue was higher than that of the 50% heel residue. The density of the metallic fuel slugs slightly differed according to the composition of fuel alloys.



(a)

(b)

Fig. 1. Typical re-fabricated metallic fuel slug; (a) U-10wt%Zr, (b) U-10wt%Zr-7wt%RE.

Table 1. Chemical composition of recycled metallic fuel slugs

Chemical Composition	U-10Zr	U-10Zr-7RE
U (wt%)	90.6	86.6
Zr (wt%)	9.6	9.9
Nd (wt%)	-	1.9
Ce (wt%)	-	1.2
Pr (wt%)	-	0.5
La (wt%)	-	0.2
C (ppm)	154	199
N (ppm)	10	210
O (ppm)	617	647
Si (ppm)	201	426

Table 1 shows the chemical compositions of re-fabricated U-10wt%Zr and U-10wt%Zr-7wt%RE fuel slugs. From the specifications of the fuel slugs, the total impurities of carbon, nitrogen, oxygen, and silicon must be less than 2,000 ppm. The total impurities of the metallic fuel slugs fabricated using a heel residue of 100% were higher than those of the slugs fabricated using a heel residue of 50%. It is originated from the high impurity content produced when fabricating a metallic fuel slug. The total impurities are satisfied with the specification requirements. The RE content of recycled U-10wt%Zr-7wt%RE fuel slugs were 3.8 weight percentage. The RE content of recycled metallic fuel slugs was increased compared with the fabricated U-10wt%Zr-7wt%RE metallic fuel slug using pure metal materials. The yield of the RE content in the recycled U-10wt%Zr-7wt%RE fuel slugs is generally low because RE elements are immiscible with U element.

3. Conclusion

The re-fabrication of the metallic fuel slugs for SFR has been studied for the recycling of fuel scraps. The fuel slugs have been refabricated for the recycling of the fuel scraps. The recast fuel slugs were characterized to evaluate the casting soundness. The fuel slugs were generally sound and fabricated to the mold length of 300 mm. The total impurities of oxygen, carbon, nitrogen, and silicon were less than 2,000 ppm for the recycled metallic fuel slugs. The feasibility of the recycling of the fuel slug scraps such as the residue heel has been demonstrated by the re-fabrication and the characterization of the metallic fuel slugs.

ACKNOWLEDGEMENTS

This work has been carried out under the Nuclear Research and Development Program supported by the Ministry of Science, Ict and Future Planning in the Republic of Korea.

REFERENCES

[1] L. C. Walters, B. R. Seidel, J.H. Kittel, “Performance of Metallic Fuels and Blankets in Liquid-Metal Fast Breeder Reactors. Nuclear Technology”, 65, 179-231, 1984.

[2] G. L. Hofman, L. C. Walters, T. H. Bauer, “Metallic Fast Reactor fuels”. Progress in Nuclear Energy, 31, 83–110, 1997.

[3] Crawford DC, Porter DL, Hayes SL. “Fuels for Sodium-cooled Fast Reactors: US Perspective”, Journal of Nuclear Materials, 371, 202–231, 2007.

2분과

사용후핵연료관리 (Poster)

An Analysis on Applicability of Temporary Onsite Storage Facilities of Spent Fuel From PWRs in Korea

Hakyun Lee and Jongsoon Song*

Chosun University, 309 Pilmun-daero, Dong-gu, Gwangju, Republic of Korea

leehakyun91@chosun.kr

1. Introduction

In South Korea, the spent nuclear fuel produced in light-water reactors is currently managed by the storage pools inside each NPP. As of the end of 2016, the cumulative amounts of spent nuclear fuel generated from the Korean nuclear plants were 16,289 and 408,797 bundles for light-water and heavy-water reactors, respectively. The Kori nuclear plant, which is scheduled to be dismantled, will trigger the shortage of the storage pools. Accordingly, interim storage facilities, which are commonly categorized into wet and dry types, are in need to resolve the issue of saturation.

Dry storage has an edge over wet storage in terms of the volume and operation of storage. Moreover, owing to its stronger economic and safety aspects, this type is currently dominant around the world. In Korea, there is a need for storage methods to address high burn-up as well as regular spent nuclear fuel generated in nuclear power plants. In particular, customization is of importance in Korea considering its limited lands. This paper examines the current status of interim storage technology for PWR spent fuel, and seeks to develop an optimal solution for Korea taking such limitations into account.

2. Main title

2.1 The Usage of Interim Storage Facilities in Korea

The used amount of the interim storage facilities versus their full capacities in NPPs in Korea at the end of 2016 are described in Table 1.

Table 1. Domestic Spent Fuel Pools saturation

Division	Capacity	Stock	Saturation
Hanbit	9,017	5,693	63.1%
Kori	6,494	5,612	86.4%
Hanul	7,066	4,855	68.7%
SinHanul	1,046	129	12.3%
WolSung	499,632	408,797	81.8%

The Hanbit and Kori plants will run out of their available capacity in 2024, Hanul in 2037 and Shin Hanul in 2038, with the overall use of 68.9% for light-water reactors only. Wolsung plant, which uses heavy water, operates a dry storage facility outside its premise, which displays a relatively high usage of 81.8% due to the large amount of spent fuel as commonly seen in PHWR.

2.2 Interim Storage Technology

The term ‘interim storage’ refers to a technique that collects and stores spent which is considered to be an intermediate phase between reusing and permanent disposal.

2.2.1 Wet Storage. Storage pools are the place where the spent nuclear fuel is collectively stored in cooling water of at least 20 ft, which is to provide sufficient protection to all workers from radiation. The bundles are moved through the bottom of the pool, so protection is needed for the staff who work nearby.



Fig. 1. Pools.

2.2.2 Dry Storage. Gas or air is used as a coolant instead of water in dry storage. Radiation shielding is provided by concrete or metal instead of water. There are three different types of dry cask storage techniques that are used in a commercial scale, i. e., metal cask,concrete silo, horizontal concrete modular storage.

2.2.2.1 Metal Cask. This method can be described rather simply the spent nuclear fuel is collected in a metal cask which is stored on a concrete pad. Some recent efforts in this area include development of multipurpose metal casks that can be used for storage/transport, or transport/storage/disposal.



Fig. 2. Metal Cask.

2.2.2.2 Concrete Silo. Concrete silo is basically similar to the metal cask technique This method is less expensive than the one using a metal cask, but has several shortcomings, including lower resistance to heat and shocks and poorer cooling performance.



Fig. 3. Concrete Silo.

2.2.2.3 Horizontal Concrete Modular Storage. This technique stores the shielded canister loaded with spent nuclear fuel on the concrete storage module in a horizontal fashion, which is established in the storage site. This method has rather complicated processing, but is known to be superior in terms of safety and economically efficient. It also has a variety of applications for other types of fuel.

2.3 Examples in the Overseas

The dry storage systems of spent nuclear fuel generally employs metal-concrete or concrete storage containers, and can be categorized into indoor and outdoor facilities depending on the storage location. .

Table 2 contains the overview of indoor and outdoor storage facilities.

Table 2. Indoors and Outdoors storage type

Type	Pros and Cons
Indoors	Good in terms of security and public acceptance, but relatively expensive to build.
Outdoors	Less expensive to build and economically feasible, but less favorable in terms of security and public acceptance as the facility is exposed.

Outdoor storage, which stores the spent nuclear fuel without water using a metal or concrete cask, or a concrete module, on top of a concrete mat, is commonly used in larger areas. For example, most of storage facilities in the United States use dry-type storages.

Indoor storage is more popular in Europe and Japan, where countries have limited lands and are densely populated. These facilities are excellent in terms of security and safety as they take into account external threats such as aircraft collision into an outside building. They tend to be better perceived by the local residents as well. In Germany, most of storages use a metal cask in the building. In addition, Japan has pursued indoor storage facilities to accommodate its spatial restraints, and built Mutsu interim storage facility, Asia's first indoor storage facility.

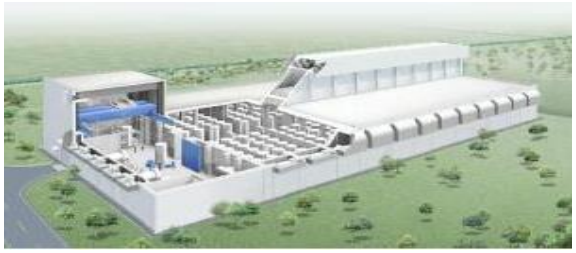


Fig. 4. Indoors Storage Type.

3. Conclusion

Korea can learn a lesson from Japan, which has longer history in NPP and became the first country in Asia to make an interim storage facility. The Korean government remains unchanged in its policy not to abandon nuclear energy despite the public opposition, and is getting warnings about the saturation of storage pools by the year of 2024. Interim storage facilities are being discussed as an alternative option that the government can choose to buy some time. Japan's Mutsu case can be a benchmark for Korea especially considering the limited space in both countries, from which Korea can refer to when selecting the type and site of interim storage facilities.

REFERENCES

[1] Ministry of Trade, Industry and Energy. (2016) High-Level Radioactive Waste Management Basic Plan (draft).

[2] Yun, H.J, "Analysis of Design Trends of Spent Fuel Intermediate Storage Facilities", Proc of the KRS 2013 autumn conference, 11(2), October 37-38, 2013, Jeju.

Estimation Radioactivity of Reference Spent Fuel With Time and Total Radioactivity of All Spent Fuel at 2035

Ara Go*, Daesik Yook, and Kyuhwan Jeong

Korea Institute of Nuclear Safety, 62 Gwahak-ro Yuseong-gu, Daejeon, Republic of Korea

*argo@kins.re.kr

1. Introduction

According to Public Engagement Commission on Spent Nuclear Fuel Management (PECOS) recommendation report, present spent fuel pools of nuclear power plant in Korea will be saturated by the middle of 2020, constructions of independent spent fuel dry storage facilities are expecting. On July 25, 2016, the Korea government announced "the basic plan for high-level radioactive waste management" based on the recommendation of PECOS. The roadmap was established based on this plan, and the roadmap includes that the Korea government will select the disposal site by 2028, complete the construction of interim storage facilities by 2035, and complete the construction of the permanent disposal facility by 2053 [1]. In order to achieve the goal, the spent fuel to be generated in future should be accurately estimated and more detailed analysis of spent fuel is requested.

The object of this study was to estimate radioactivity of reference spent fuel with time and total radioactivity of all spent fuel at 2035.

2. Materials and Methods

2.1 Spent fuel databases and applied codes

In this study, pressurized water reactors (PWRs) spent fuel data until 2015 provided from Korea Hydro and Nuclear Power (KHNP) was used. It includes fuel number, initial enrichment, mass of initial uranium, discharge burnup, and Final cycle fuel withdrawal date. According to this database, 5,549 assemblies of spent fuel were stored in Kori and Shin-Kori nuclear site, 5,693, 4,847, and 129 assemblies was stored in Hanbit, Hanul, and Shin-Wolsong nuclear site respectively.

To estimate radioactivity of reference spent fuel with time and total radioactivity of all spent fuel at 2035, Automatic Multi-batch Origen Runner for Evaluation of Spent fuel (AMORES) was used. This code was developed by the cooperation between KINS and Kyung Hee University and it can automatically generate ORIGEN-S input files and process their output files.

2.2 Estimation of radioactivity of reference spent fuel

The reference PWR spent fuel was determined based on PWRs spent fuel databases. The spent fuel with initial enrichment of 4.5wt% of ^{235}U, discharge burnup of 45,000 MWd/MTU, and mass of initial uranium of 440,000 g was adopted for reference spent fuel. For this reference spent fuel, individual nuclide radioactivity was calculated for spent fuel taken out of the reactor 1, 10, 20, 30, 40 years using AMORES.

2.3 Estimation of total radioactivity of all spent fuel

To estimate total radioactivity of all spent fuel at 2035, amount of spent fuel generated between 2016 and 2034 was estimated based on the national 7th electric power supply schedule [2]. The Eq. (1) was used to calculate the annual generation of the spent fuel,

$$Amount_{SF} = \frac{NC \cdot 365.25 \cdot CF}{\epsilon_{th} \cdot BU} \qquad (1)$$

where NC is the NPP capacity, CF is the capacity factor, ϵ_{th} is the NPP efficiency, and BU is the average discharge burnup of the spent fuels. Also, we didn't considered life extension of NPP except for Kori unit 1. For Kori unit 1, we considered life extension for 10 years.

Based on PWRs spent fuel database until 2015 and estimated amount from 2016 to 2034, individual nuclide radioactivity was calculated using AOMRES. To do this, 99 target nuclides were considered. The selected nuclides included all the actinides from thorium to californium and important fission product.

3. Results and Discussion

3.1 Results of radioactivity for reference spent fuel

Radioactivity of reference spent fuel were 1.10 × 10^{17} Bq/MTU, 2.01 × 10^{16} Bq/MTU, 1.44 × 10^{16} be numbered separately. Fig.1 show the composition of radioactivity of reference spent fuel for each times. Radioactivity of 1 year old spent fuel were mainly contributed from ^{144}Pr and ^{144}Ce, while the others were mainly contributed from ^{137}Cs, ^{241}Pu, and ^{90}Sr. This can be explained by difference of the half-life of each nuclides. ^{144}Pr ($T_{1/2}$=17.3 m), ^{144}Ce ($T_{1/2}$=285 d) have relatively short half-life, it can only affect in early time. The results of this study were similar to results of Korea Atomic Energy Research Institute [3].

3.2 Results of radioactivity for all spent fuel.

The amount of PWR spent fuel until 2015 in Korea was about 6,800 MTU, and accumulated amount of spent fuels form 2016 to 2034 was about 10,000 MTU. Based on these data, radioactivity for all spent fuel at 2035 was estimated (Table 1). Total radioactivity at 2035 was 2.26 × 10^{16} Bq/MTU, which was similar to 10 years old representative spent fuel radioactivity. ^{137}Cs occupied the biggest radioactivity (30%), and followed by ^{241}Pu (25%), ^{90}Sr (21%), ^{106}Ru (6.6%). These composition was similar to 10 years old representative spent fuel except ^{106}Ru. In 10 years old representative spent fuel, ^{106}Ru wasn't considered major nuclide, but in case of total radioactivity at 2035, ^{106}Ru was considered to be the major nuclide with more 1% ratio.

Table 1. Radioactivity of all spent fuel at 2035

Nuclide	Radioactivity of all spent fuel (Bq/MTU)			
	by 2015 y	2016~2034 y	Total	Ratio
^{137}Cs	2.38E+15	4.31E+15	6.69E+15	30%
^{241}Pu	1.40E+15	4.22E+15	5.62E+15	25%
^{90}Sr	1.63E+15	3.07E+15	4.71E+15	21%
^{106}Ru	3.60E+09	1.50E+15	1.50E+15	6.6%
^{147}Pm	8.20E+12	1.43E+15	1.43E+15	6.3%
^{134}Cs	1.73E+12	1.19E+15	1.19E+15	5.2%
^{85}Kr	6.87E+13	2.84E+14	3.53E+14	1.6%
^{238}Pu	1.05E+14	1.55E+14	2.60E+14	1.1%
^{241}Am	1.44E+14	7.94E+13	2.24E+14	1.0%
^{154}Eu	3.02E+13	1.78E+14	2.08E+14	0.9%
Other	1.10E+14	3.63E+14	4.73E+14	2.1%
Total	5.88E+15	1.68E+16	2.26E+16	100%

4. Conclusion

In this study radioactivity of reference spent fuel and total radioactivity of all spent fuel at 2035 was estimated using AMORES. Radioactivity of reference spent fuel decreased from 1.10 × 10^{17} Bq/MTU to 3.70 × 10^{15} Bq/MTU over time and radioactivity of all spent fuel at 2035 was 2.26 × 10^{16} Bq/MTU. The results of this study can be used as input for interim storage facility.

REFERENCES

[1] Ministry of Trade, Industry and Energy, "the basic plan for high-level radioactive waste management" (2016).

[2] Ministry of Trade, Industry and Energy, "7th electric power supply schedule" (2015).

[3] KAERI, "Reference spent fuel and its characteristic for the concept development of a deep geological disposal system" (1997).

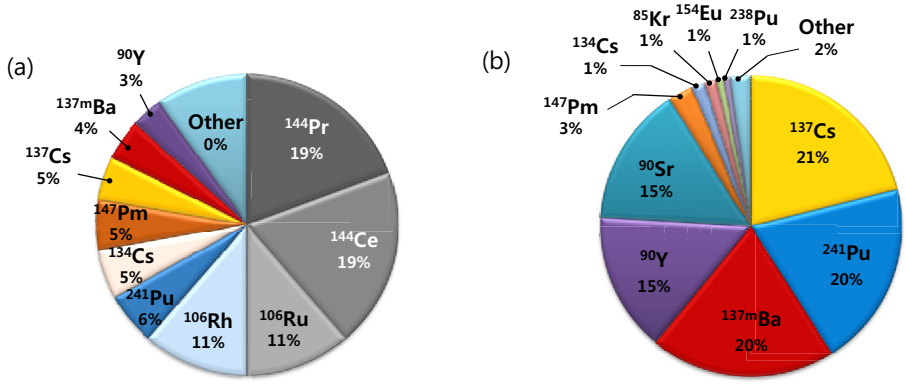


Fig. 1. Composition of radioactivity of reference spent fuel for (a) 1 year, (b) 10 years since removal from reactor.

Kr Capture in Head-End Process of Pyroprocess

Seok-Min Hong*, Ahreum Han, Jae Hwan Yang, and Yung-Zun Cho

Korea Atomic Energy Research Institute, 111, Daedeok-daero 989beon-gil, Yuseong-gu, Daejeon, Republic of Korea

*seokminhong@kaeri.re.kr

1. Introduction

A substantial interest has been generated in an accumulation of spent fuel due to its energy and environmental issue [1]. To solve this issue, Korea Atomic Energy Research Institute (KAERI) has investigated a reprocessing technology, pyroprocessing, which not only reduces the accumulated spent fuel but also increases the efficiency of fuel cycle.

In head-end process of pyroprocessing, UO_2 pellets are prepared from a fuel bundle for electrochemical reduction while various radioactive gases are released from a spent fuel during thermal treatment. Among these gases, Kr is a harmful volatile gas which has a long half-life of ~11 years and high radioactivity, and thus it is strongly required to capture Kr [2]. Several approaches such as cryogenic distillation, absorption using solvents, and adsorption on solids have been conventionally applied to Kr capture. Of these methods, adsorption has many advantages as it provides low energy-consumption processes with easy regeneration. In Kr adsorption, adsorbents such as activated carbon and zeolites have been widely used [3].

2. Experimental Section

2.1 Adsorption Column

The adsorbents were degassed at 110 ^{o}C overnight for the removal of adsorbed water and impurities. The adsorption experiment was carried using a column of a diameter of 30 mm packed with ~20 g adsorbent. The flow rate was 126 cm^3 min^{-1} and the pressure was 1 atm. The feed gas contains few parts per millions (ppm) with Ar base. The temperature of the column maintained using ethanol heat exchanger.

2.2 Gas Analysis

The gas composition was measured using a gas chromatography (DS Science, Republic of Korea) equipped with a pulsed discharge detector (PDD). He was used as a carrier gas and the 30 m of GC column (ValcoPLOT Molesieve 5A) was installed. Prior to the adsorption test, the 100 and 300 ppm Kr balanced Ar was used as standard gases.

2.3 Breakthrough Curve

In order to obtain adsorption capacity, the breakthrough time was used as:

$$q = \frac{F}{M}\int_0^{t_b}(Co - C)dt \quad (1)$$

where q represent adsorption capacity (mmol kg^{-1}), F is a flow rate (cm^3 min^{-1}), M is a mass of adsorbent (g), t_b is a breakthrough time (min). Co and C are initial and measured concentration, respectively.

3. Adsorption Test

3.1 Adsorption Column Installation

The adsorption column was installed as shown in Fig. 1. The 200 ppm Kr balanced with Ar was used as feed gas and the constant amount of feed flows from the bottom to the upper part of the column and finally reached to the GC as displayed in Fig. 2.

3.2 Adsorption performances

Dynamic results were obtained through composition of gas using GC, and the adsorption performances such as working capacities, equilibrium capacity, and kinetic. Furthermore, the effects of adsorption condition on the adsorption capacities were investigated. These parameter effects will be further applied in optimizing adsorption process.

4. Conclusion

Kr adsorption process was designed and tested using a packed bed column filled with adsorbents. The Kr adsorption performances were determined from breakthrough curves obtained from a GC, and the effects of capturing conditions on adsorption capacities were investigated.



Fig. 1. Adsorption column.



Fig. 2. Gas chromatography equipped with PDD.

REFERENCES

[1] L. Deliere, B. Coasne, S. Topin, C. Greau, C. Moulin, D. Farrusseng, “Beakthrough in Xenon capture and purification using adsorbent-supported silver nanoparticles”, Chemistry: A European Journal, 2, 9660–9666 (2016).

[2] M. Greenhalgh, T. G. Garn, J. D. Law, “Development of a hydrogen mordenite sorbent for the capture of krypton from used nuclear fuel reprocessing off-gas streams”, Journal of Nuclear Science and Technology, 51, 476481 (2014).

[3] K. Munakata, S. Kanjo, S. Yamatsuki, A. Koga, D. Ianovski, “Adsorption of noble gases on silver-mordenite”, Journal of Nuclear Science and Technology, 40, 695−697 (2003).

Salt Distiller With Mesh-covered Crucible for Electrorefiner Uranium Deposits

S.W.Kwon*, Y.S.Lee, H.B.Kang, J.H.Jung, J.H.Chang, S.H.Kim, and S.J.Lee

Korea Atomic Energy Research Institute, 111, Daedeok-daero 989beon-gil, Yuseong-gu, Daejeon, Republic of Korea

*swkwon@kaeri.re.kr

Abstract

Electrorefining is a key step in pyroprocessing. The electrorefining process is generally composed of two recovery steps – the deposit of uranium onto a solid cathode and the recovery of the remaining uranium and TRU elements simultaneously by a liquid cadmium cathode. The solid cathode processing is necessary to separate the salt from the cathode since the uranium deposit in a solid cathode contains electrolyte salt. Distillation process was employed for the cathode processing. It is very important to increase the throughput of the salt separation system due to the high uranium content of spent nuclear fuel and high salt fraction of uranium dendrites. In this study, a mesh-covered crucible was investigated for the sat distillation of electrorefiner uranium deposits. A liquid salt separation step and a vacuum distillation step were combined for salt separation. The adhered salt in uranium deposits was efficiently removed in the mesh-covered crucible. The salt distiller was operated simply since repeated cooling - heating step was not necessary for the change of the crucible. The operation time could be reduced by the use of the mesh-covered crucible and the combined operation of the two steps. A method to preserve a vacuum level was proposed by double O-rings during the operation of the distiller with the mesh-covered crucible. After the salt distillation, the salt content was measured and was below 0.1wt% after the salt distillation. The residual salt after the salt distillation can be removed further during melting of uranium metal.

Viscosities of UCl_3-LiCl-KCl Molten Salts

Sang-Heon Lee, Jong-Yun Kim, Sang-Eun Bae, and Tae-Hong Park
Korea Atomic Energy Research Institute, 111, Daedeok-daero 989beon-gil, Yuseong-gu, Daejeon, Republic of Korea
kjy@kaeri.re.kr

1. INTRODUCTION

Physical properties of high-temperature molten salt such as the viscosity, electrical conductivity, and density are very critical in designing and operating a pyroprocess. Such properties also provide important information with regard to the process operation and nuclear material accountancy. Among the many valuable physical properties, viscosity is one of the most important physical properties providing information regarding the transport properties of molten salts comprising various actinide and lanthanide elements in the pyroprocess.

However, not all commercially available measurement systems are adequate for measuring the viscosity of high-temperature corrosive molten salts [1]. Recently, we developed a new viscosity measurement system installed inside a glove box, and controlled using custom-made software based on the C# program [2].

2. EXPERIMENTAL

To develop a rotational viscometer system capable of operating on a high-temperature molten salt in a glove box under an argon atmosphere, a specially-designed viscosity measurement system is constructed using a low-viscosity LVDV-II+ Brookfield viscometer, an electric furnace capable of heating up to 900 K and keeping the temperature constant, and a special one-touch quick connector in order to mount a spindle onto the viscometer.

Software for instrument control and data acquisition was installed in a computer system for high-temperature operation after customization. The control program is capable of controlling the temperature of the electric furnace, and the torque value is displayed in real time allowing the device to be stabilized. This was designed to automatically conduct ten measurements repeatedly, and confirm the results in real time; it can therefore detect the influence of fine particles.

3. RESULTS & DISCUSSION

If a rotational Brookfield viscometer is used, the device constant values corresponding to the specific type of device and a spindle must first be determined before measuring the viscosity of the molten salt sample. Because a custom-manufactured spindle is used for corrosive and high-temperature molten salts, the spindle constant must be determined using a viscosity standard solution.

First, torque (τ_q) values in percent between 0 and 100 were measured at a specific rpm using a viscosity standard at room temperature, and the spindle constant value (C_{sm}) can then be obtained using Eq. (1) because the spring torque constant (C_t) of an LVDV-II+ Brookfield viscometer is given by the manufacturer.

$$\eta = \frac{100}{rpm} \times C_t \times C_{sm} \times \tau_q \qquad (1)$$

Once the value of C_{sm} is known, the viscosity for an unknown sample can be determined by measuring τ_q using the identical Eq. (1).

$$T_c = -0.0032 \times T_m^2 + 4.9499 \times T_m - 123.1 \qquad (2)$$

However, because the effect of the axial temperature gradient inside the vessel in a hot furnace on the viscosity measurement system cannot be elucidated accurately, a temperature correction equation (2) was obtained from the calibration curve with pure KNO_3 molten salt, whose viscosity at each temperature is well known.

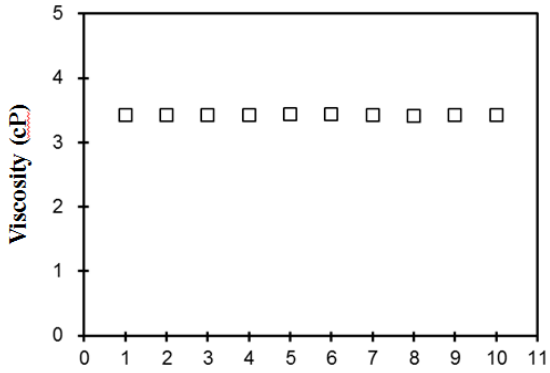


Fig. 1. Viscosities of 3 wt% UCl_3 dissolved in LiCl-KCl eutectic melt at 773 K for ten repetitive measurements.

Fig. 1 shows the results of measuring the viscosity of high-temperature eutectic LiCl-KCl molten salt containing 3wt% of UCl_3. The average and standard deviations for ten repetitive measurements were 3.43±0.02 cP at 773 K.

4. CONCLUSIONS

A rotational high-temperature viscosity measurement system was developed for the corrosive molten salts at or above 700 K. The pure KNO_3 molten salt was used as a calibration standard for the temperature correction for the accurate measurement at high temperatures. The average viscosity of uranium in a high-temperature molten salt was 3.43 cP ±0.02 cP at 773 K for 3wt% UCl_3. In a future study, various compositions of LiCl-KCl molten salt containing uranium and other lanthanide elements such as lanthanum, cerium, and neodymium will be examined to understand the viscous behavior of a multi-component molten salt system.

ACKOWLEDGEMENTS

This work was supported by a National Research Foundation of Korea (NRF) Grant, funded by the Korean government (MSIP).

REFERENCES

[1] S.F. Katyshev, Yu.F. Chervinskii, and V.N. Desyatnik, At. Energ. Vol. 53, pp. 108, 1982.
[2] J.Y. Kim, S.E. Bae, Y.S. Choi, J.W. Yeon, K. Song, International Pyroprocessing Research Conference, 2012.

Development of a Methodology for the Determination of Metal Reduction Yields of Highly Radioactive Nuclear Fuel

Young-Hwan Cho*, Ji-Hye Kim, Byung-Man Kang, Jung-Suk Kim, and Tae-Hong Park

Korea Atomic Energy Research Institute, 111, Daedeok-daero 989beon-gil, Yuseong-gu, Daejeon, Republic of Korea

*kaerisan@gmail.com

1. Introduction

One of the key steps of pyroprocessing is electrolytic reduction of metal oxide fuel into metallic form. In this step, an appropriate analytical method is required to measure the metal conversion yield of the electrolytic reduction process product. One needs to develop a reliable analytical method to determine the metallic constituents in the metal and oxide mixtures. And system establishment for the implementation of chemical analysis of highly radioactive pyroprocessing materials has become an imminent task.

2. A Standard Procedure for Selective Dissolution of metallic phases by bromine method

One of the important task for chemical analysis is determination of metallic contents in multi-component composite materials like reduced spent fuel ingot. A general approach to solve this problem is to dissolve the metallic form selectively from its oxide form and analyze the dissolved contents. For the determination of uranium, a method of selective dissolution of metallic uranium by bromine-ethyl acetate has been proposed and has been applied for various purposes.

A standard bromine method has been established to meet the process materials for Korean concept of pyro electrolytic metal reduction process.

By applying the selective dissolution method in bromine-ethyl acetate solution together with total dissolution technique, it is proved possible to determine the metallic conversion yields of actinides and lanthanides elements in the samples of electrolytic reduction process for spent nuclear fuel. And finally a standard bromine method procedure has been established, and applied to the samples from PRIDE and ACPF facilities.

3. Shielded ICP-AES system

A shielded ICP-AES system has been established. A home-made glove box system was interfaced with ICP-AES spectrometer, and performance test has been done. A standard operation manual of the system has been prepared. And a radiation resistant, hot cell space saving, modular type centrifuge has been designed and built for use inside of the chemical hot cell. And radiological assessment of hot pyrochemical samples has been done to assist minimization of radiation exposure and radioactive wastes during the chemical analysis works.

A shielded ICP-AES system, chemical hot cell and apparatus will be effectively used to provide chemical analysis data of highly active pyroprocessing materials. Fig. 1 shows the installed shielded ICP-AES system in operation.



Fig. 1. Operation of shielded ICP-AES system.

4. Conclusion

A shielded ICP-AES system, chemical hot cell and apparatus will be effectively used to provide chemical analysis data of highly active pyroprocessing materials. Various samples of importance from pyro process streams have been characterized and quantified by applying the developed chemical pretreatment method and instrumental techniques.

REFERENCES

[1] Young Hwan CHO et al “Determination of lanthanide metallic contents by selective dissolution in bromine-ethyl acetate solution”, KAERI/TR-5299/2013 (2014).

Lessons Learned From the Use of Metal Halide Lamp in the ACPF Argon Cell

Byungsuk Park*, Yunmock Jung, Jongkwang Lee, Kiho Kim, Ilje Cho, and Eunyoung Choi
Korea Atomic Energy Research Institute, 111, Daedeok-daero 989beon-gil, Yuseong-gu, Daejeon, Republic of Korea
*nbspark@kaeri.re.kr

1. Introduction

KAERI is currently developing an electrolytic reduction process that the high-heat-emitting and high-level radioactive nuclides (Cs, Sr) are efficiently removed from the spent fuels to substantially reduce spent fuels in terms of volume, heat release, and radiation intensity. In order to demonstrate the advanced technology of this process, the Advanced spent fuel Conditioning Process Facility (ACPF) has been constructed in KAERI. The ACPF consists of an air cell and an argon cell. An electrolytic reduction device was installed in the argon cell. In this paper, the failure of metal halide lamp used in ACPF argon cell and its failure countermeasures are described.

2. Lighting Device of ACPF Argon Cell

2.1 Outline of the ACPF Argon Cell [1]

The ACPF argon cell is operated to an argon atmosphere within the air cell. The argon cell (1.8L x 2D x 2.7H m) is isolated with leak tight from other air cell. The argon cell system consists of an argon cell, a remote handling device such as a crane and a master-slave manipulator, a lighting device, a material transfer system, a purifier, a cooler, a controller, utilities, etc. The argon cell maintains oxygen and moisture within 50 ppm, respectively.



Fig. 1. Constructed ACPF.

2.2 Metal halide Lamp and ballast

High-intensity discharge (HID) lamps are similar to fluorescents in that an arc is generated between two electrodes. The arc in an HID source is shorter, but it generates much more light, heat, and pressure within the arc tube. The followings are HID sources listed in increasing order of efficacy (lumens per watt); mercury vapor, metal halide, high-pressure sodium, low-pressure sodium.

Like fluorescent lights, HID also requires ballasts, and they take a few seconds to produce light when first turned on because the ballast needs time to establish the electric arc.

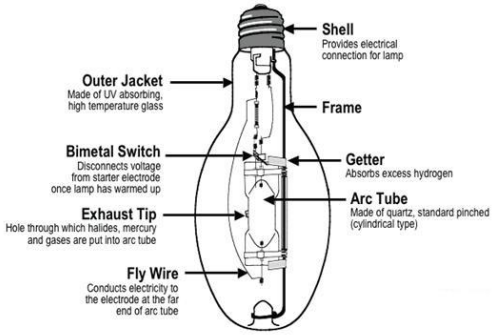


Fig. 2. Anatomy of a typical mogul-based metal halide lamp (source Venture Lighting™).

Metal halide lamps have been divided into European and American type according to the region where they are produced and used. The main difference is the lamp's tube voltage and tube current characteristics. Therefore, in Korea, they are classified as type A (European type) and type B (American type) depending on the tube characteristics. Depending on the type of ballast, CC type (high voltage generating circuit type) and RC type (peak electrostatic force type) are also called. Type A was developed to be suitable for use with CC ballast, and type B was adapted to use RC ballast. In Korea, B type lamp is mainly used.



Fig. 3. RC ballast.

2.3 Failure of cell lighting device

Fig. 4 shows the lighting device installed in the ACPF argon cell. It is equipped with one metal halide 250W lamp (B type) and one three-wavelength 100W lamp, and the ballast of the metal halide lamp is installed outside the cell.

Fig. 5 shows that an electrical spark discharge between the connector pin and the split insert carrier caused soot in the connector pin and the split insert carrier. At this time, the earth leakage breaker went down. And the CC type ballast was broken, but the RC type ballast was not broken.



Fig. 4. Cell lighting device installed in the argon cell.

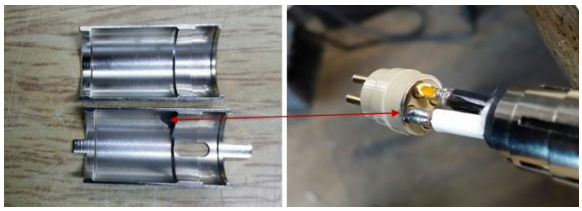


Fig. 5. Soot due to electrical spark discharge.

3. Results and Discussion

3.1 Start-up current of CC and RC type ballast

Fig. 6 shows the current up to stabilization when using the CC type ballast and the RC type ballast for a metal halide 250W lamp. In the CC type ballast, the current initially rises to 2.1A and stabilizes at 1.6A. The RC type ballast is stable at 1.2A while the current gradually increases.

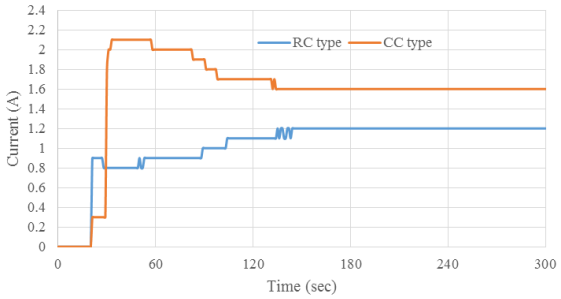


Fig. 6. Current trend until stabilization.

3.2 Failure cause analysis

If the voltage between two electrodes in the gas is increased, a spark discharge occurs at a certain value. If the electric fields between the electrodes are not equal, a light emission phenomenon occurs in a portion where the electric field on the electrode surface is large before the spark discharge, and a current of about 1~100 ㎂ flows. This is called a corona discharge. In the portion where light is generated, ionization is actively performed, current density is large, and insulation is lost.

The CC ballast has a high starting current, and the starting voltage is high when the lamp turns on. The RC ballast has a low starting current, and the starting voltage is low when the lamp turns on.

When the CC type ballast for the metal halide lamp (B type) was used in an argon environment, a corona discharge phenomenon occurred due to the high starting voltage. As a result it is considered that the dielectric breakdown occurred.

4. Conclusion

When using HID lamps in an argon environment, CC type ballasts may cause failures due to high starting currents, so RC type ballasts with low starting currents should be used. If using CC type ballasts in an argon environment, the connector pin spacing should be increased than the air environment to prevent the corona discharge [2].

REFERENCES

[1] B.S. Park, “Construction of ACPF Argon Cell using Reverse Engineering Technique”, KRS 2016 Spring Conference, 14(1), 99-100, 2016.

[2] M.L. Hayward, “Environmental Hardening of Equipment Operating in an Automated Test Bed Enclosure”, UCRL-ID-107864, LLNL, 1990.

Electrolytic Behaviors in Large-scale LCC Electrowinning System

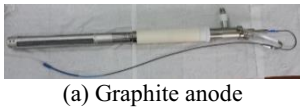
Si Hyung Kim*, Jun-Bo Sim, Han Byeol Kang, Young Sang Lee, Sungbin Park, Sang-Woon Kwon,
Moon-Sik Woo, Jae-Hoo Jung, and Sung-Jai Lee
Korea Atomic Energy Research Institute, 111, Daedeok-daero 989beon-gil, Yuseong-gu, Daejeon, Republic of Korea
*exodus@kaeri.re.kr

1. Introduction

Electrowinnng is a process to recover uranium and transuranic elements using liquid cadmium cathode (LCC) [1,2]. Major components such as electrodes should be remotely handled and relatively easily replaceable to operate the large-scale electrowinning system. In this paper, the performance of electrodes and LCC crucible was evaluated through cyclic voltammetry (CV) and electrodeposition experiments.

2. Experimental

Fig. 1 shows the photographs of graphite anode, reference, monitoring electrode and LCC assembly. Monitoring electrode is composed of glassy carbon anode and tungsten (W) electrode. In order to obtain cyclic voltammogram (CV), monitoring electrode and reference electrode are used. Graphite anode, reference and LCC assembly are used to conduct electrodeposition experiment, where LCC crucible containing LCC is loaded in the LCC assembly. Main frames of electrodes and LCC assembly are usually made of stainless steel (SUS). During the electrolysis experiment, current should flow between anode and cathode in electrolytic salt. So, insulated material is respectively inserted to the electrodes and LCC assembly to block electric current to flow to surrounding SUS parts such as lid and vessel through the salt. The insulated material is Al_2O_3 and shown in Fig. 1(a) ~ (c). LCC crucibles used at this study are Al_2O_3 and BeO. The used salt is the mixture of LiCl-KCl, UCl_3, $NdCl_3$, $CeCl_3$ and $LaCl_3$.



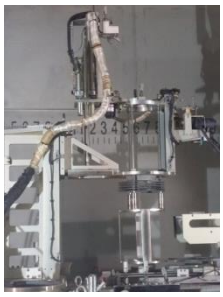
(a) Graphite anode



(b) Reference electrode



(c) Monitoring electrode

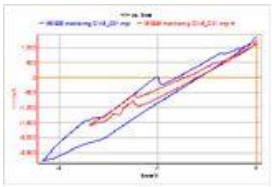


(d) LCC assembly

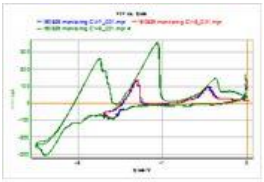
Fig. 1. Electrodes and LCC assembly used in LCC electrowinning system.

3. Results and Discussion

After the LCC assembly is loaded into the salt, CVs are acquired using the W cathode. Fig. 2 shows the current values of CVs depending on the connection/disconnection of ground cable of power source. When the ground cable is connected to the potentiostat, the value of reduction current is about -2.500 mA (Fig. 2(a)). On the contrary, when the cable is disconnected, the value is approximately -200 mA. The current values of Fig. 2(b) are more reasonable when compared with the area of the W cathode dipped into the salt. So, the following electrodeposition experiments were conducted using ungrounded potentiostat.



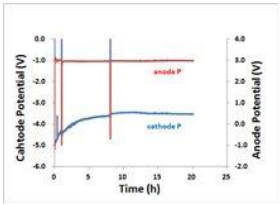
(a) grounded potentiostat



(b) ungrounded potentiostat

Fig. 2. Cyclic voltammograms at standard mode depending on the loading LCC assembly into the salt contained in the SUS electrolytic vessel.

Fig. 3(a) shows the potential change of anode and cathode at constant current density (50 mA/cm^2) for 20 hours aiming recovering 7wt%M/Cd (M=U, RE metals). Anode potential is nearly constant around 3V during the electrodeposition and cathode potential changed from -5V at initial time to -3.5V at ending time. The change of the cathode potential is thought to be related to the U/RE deposits reducing into the LCC. Fig. 3(b) shows the Al_2O_3 crucible containing salt/Cd and U/RE deposit after electrodeposition.



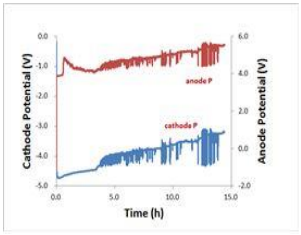
(a) potentials of anode and LCC



(b) salt/Cd/U/RE contained in Al_2O_3 crucible

Fig. 3. Electrodeposition result carried out using LCC at 50 mA/cm^2 at 500°C.

Fig. 4(a) shows the potential change of anode and cathode at constant current density (70 mA/cm^2) for 14.5 hours to recover 7wt%M/Cd. Both anode potential and cathode potential are moving upward showing similar vibration behavior. That is, the anode potential moved from 3.8V at initial time to 5.8V at ending time and the cathode potential from -4.7V to -3.2V. Fig. 3(b) shows the BeO crucible containing salt/Cd and U/RE deposit. Some deposits are seen to climb on the edge of the crucible.



(a) potentials of anode and LCC



(b) salt/Cd/U/RE contained in BeO crucible

Fig. 4. Electrodeposition result carried out using LCC at 70 mA/cm^2 at 500°C.

4. Summary

In this paper, electrolytic behavior of large-scale LCC electrowinning system was studied. Reasonable CV behavior was obtained using ungrounded power source after dipping of LCC assembly into the electrolytic salt. Electrodeposition experiments were successfully conducted at the current densities of 50 and 70 mA/cm^2.

REFERENCES

[1] Vaden, D.; Li, S.X.; Westphal, B.R.; Davies, K.B. (2008) Engineering-scale liquid cadmium cathode experiments. Nucl. Tech. 162:124-128.

[2] Kato, T.; Inoue, T.; Iwai, T.; Arai, Y. (2006) Separation behaviors of actinides from rare-earths in molten salt electrorefining using saturated liquid cadmium cathode. J. Nucl. Mater.357:105-114.

Cyclic Voltammetry Depending on the Electrode Connection Mode in Small-scale LCC Electrowinning System

Si Hyung Kim*, Taek-Jin Kim, Gha-Young Kim, Seul Gi Lee, Junhyuk Jang, Seungwoo Paek, Hansoo Lee, Hee-Chul Eun, Sung-Jai Lee, and Do-Hee Ahn

Korea Atomic Energy Research Institute, 111, Daedeok-daero 989beon-gil, Yuseong-gu, Daejeon, Republic of Korea

*exodus@kaeri.re.kr

1. Introduction

LCC electrowinning system is composed of electrodes (anode, cathode, reference), salt stirrer, SUS (stainless steel) vessel containing salt, SUS lid and SUS LCC assembly [1,2]. The liquid Cd cathode (LCC) is loaded to the salt using LCC assembly. Although currents should flow only between anode and cathode in the salt, the SUS components and electrodes can be electrically connected each other through the electrolytic salt. In this study, cyclic voltammetry behavior at the above-mentioned electrowinning system was observed depending on the electrode connection mode of potentiostat to suggest desirable connection mode.

2. Experimental

Fig. 1 shows the typical electrowinning system, where glassy carbon anode, tungsten cathode, Ag/AgCl reference electrode and stirrer are electrically insulated from the above-mentioned SUS components but SUS LCC assembly can be electrically connected to the SUS lid. The diameter of tungsten cathode is 1 mm and the dipping depth into the salt is 5 ~ 10 mm. Potentiostat made by Bio-Logic Company was used to check the effect on the CV behavior depending on the electrode connection mode. The used salt is the mixture of LiCl-KCl, UCl_3, $NdCl_3$, $CeCl_3$, $LaCl_3$ and YCl_3.

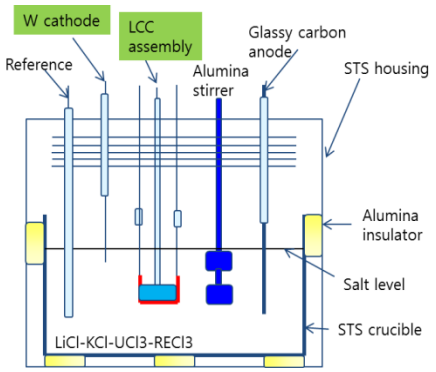
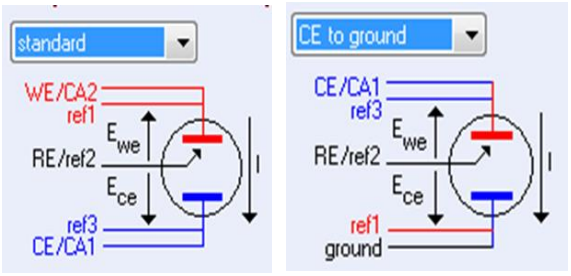


Fig. 1. Schematic diagram of LCC electrowinning system.

Fig. 2 shows the general electrode connection modes of potentiostat system. In the standard mode, a working electrode cable of potentiostat is connected to the working electrode of the cell and a counter cable to counter electrode. In the CE to ground mode, counter electrode cable of potentiostat is connected to the working electrode of the cell and ground cable to counter electrode.



(a) Standard mode (b) CE to ground mode

Fig. 2. Electrode connection mode of potentiostat system.

3. Results and Discussion

The behavior of cyclic voltammetry was compared depending on the electrode connection mode in the electrowinning system shown in Fig. 1.

3.1 Standard mode

Multi tab has normally 3 lines composed of 2 power lines and 1 ground line. The multi tab having 3 lines supplies current to potentiostat. Fig. 3 shows the cyclic voltammogram when using 3 line multi tab.

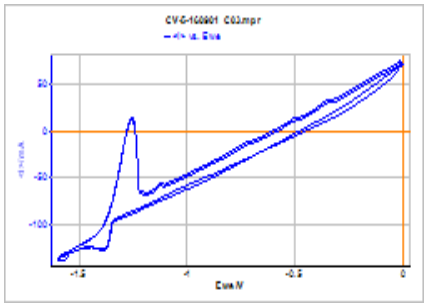


Fig. 3. Cyclic voltammogram at grounded standard mode.

Another multi tab without ground line is prepared to compare the CV behavior. Fig. 4 shows the cyclic voltammogram at the same electrowinning system when using the multi tab without ground line (ungrounded standard mode).

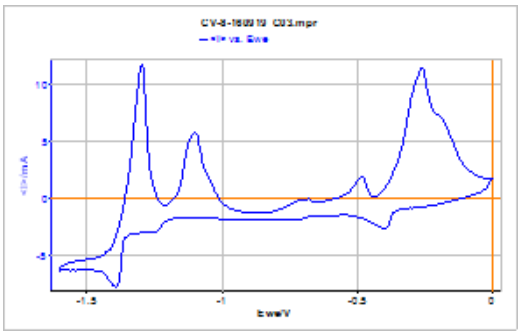


Fig. 4. Cyclic voltammogram at ungrounded standard mode.

Current values are lower when using the multi tab having 2 power lines than 3 lines. When considering the area of the tungsten cathode, current values of the ungrounded standard mode seem to be reasonable.

3.2 CE to ground mode

Fig. 5 shows the CV at the CE to ground mode. The multi tab having normal 3 lines was used for this measurement. Current values in Fig. 5 also look more reasonable than those in Fig. 3. But, in this connection mode, SUS parts connected to the ground line can be electrically connected to the anode and thereby SUS parts contacting the salt can be oxidized.

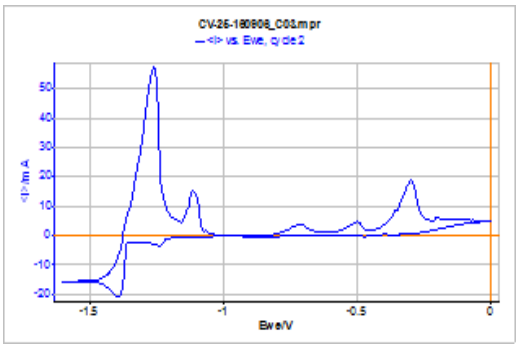


Fig. 5. Cyclic voltammogram at CE to ground mode.

4. Summary

In this paper, CV behavior of electrowinning system was studied depending on the electrode connection mode of potentiostat. In this system, currents can be flown from electrodes to SUS parts because the LCC assembly was electrically connected between the SUS parts and electrolytic salt. Standard mode without ground line of multi tab or CE to ground mode is considered to be more reasonable than standard mode when using multi tab having ground line.

REFERENCES

[1] Li, S.X.; Herrmann, S.D.; Goff, K.M.; Simpson, M.F.; Benedict, R.W. (2009) Actinide recovery experiments with bench-scale liquid cadmium cathode in real fission product-laden molten salt. Nucl. Mater. 165:190-199.

[2] Uozumi, K.; Iizuka, M.; Kato, T.; Inoue, T.; Shirai. O.; Iwai, T.; Arai, Y. (2004) Electrochemical behaviors of uranium and plutonium at simultaneous recoveries into liquid cadmium cathode. J. Nucl. Mater.325:34-43.

Effect of Electrolyte Agitation on an Electrolytic Reduction Process

Sang-Kwon Lee*, Sung-Wook Kim, Eun-Young Choi, Sun-Seok Hong, Seung-Chul Oh, and Jin-Mok Hur

Korea Atomic Energy Research Institute, 111, Daedeok-daero 989beon-gil, Yuseong-gu, Daejeon, Republic of Korea

*sklee79@kaeri.re.kr

1. Introduction

In an electrolysis system, cell voltage is a sum of the theoretical potential for each reaction on electrode and overpotentials resulted from the reaction initiation, concentration gradient and IR drops from electrolyte and apparatus [1]. As an apparatus increases in size, the effect of IR drop becomes more important. In this study, the effect of electrolyte agitation on an electrolytic reduction performance was investigated in the LiCl-1.4wt.% Li_2O molten salt at 650°C.

2. Experimental

An electrochemical cell as shown in Fig. 1 was employed for this study. A stainless steel meshed basket and Li-Pb alloy were used as a cathode and reference electrode, respectively. A platinum plate was employed as the anode electrode with alumina shroud which was connected to an exhaust pump line to prevent dispersion of oxygen in the electrochemical cell. LiCl was employed as the electrolyte and the concentration of Li_2O was 1.4 wt%. An Agilent E3633A power supply and Agilent E34405A digital multi meter were employed to apply potential or current and to measure a cathode potential, respectively.

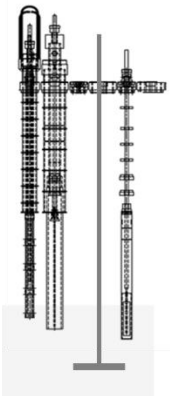


Fig. 1. Schematic experimental apparatus.

3. Results and Discussion

Fig. 2 shows the measured cell potential as a function of applied current between the cathode and anode, which were placed in different distances in the electrochemical cell. The cell potential increased with applied current and the cell potential difference with different interpolar distance, which mainly resulted from IR drop in electrolyte, increased as well.

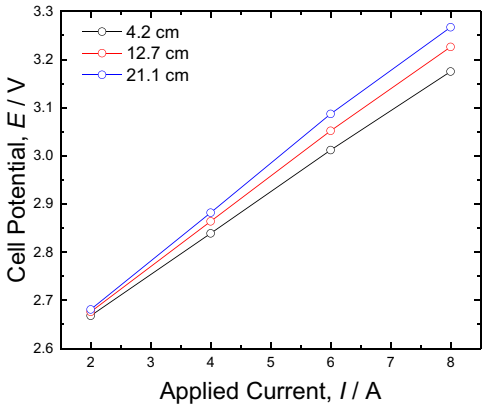
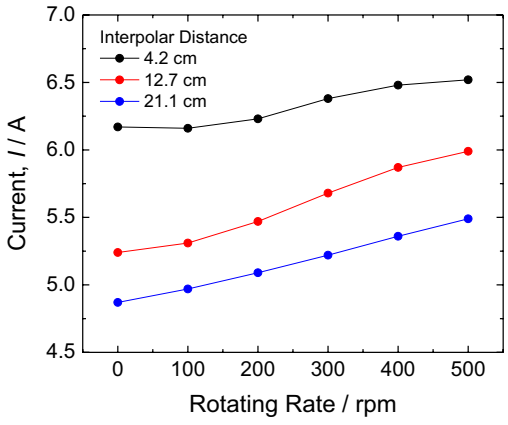


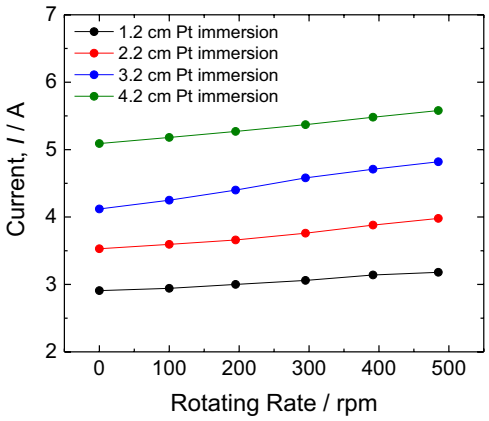
Fig. 2. Cell potential as a function of applied current.

Effect of electrolyte agitation with stirrer is shown in Fig. 3. When constant potential was applied to the electrochemical cell, current increased with increasing rotating rate of stirrer. The effect of electrolyte agitation was not significant in small interpolar distance as compared to large interpolar distance. It is recognized that decreasing interpolar distance is more effective than electrolyte agitation to improve the process in terms of production rate.

Fig. 3 (b) shows the effect of electrolyte agitation when the Pt anode was placed with different immersion depth inside the alumina shroud. Electrolyte agitation made oxygen ion mass transfer easier, but not significant. Increasing anode area is more effective than electrolyte agitation to increase current.



(a)



(b)

Fig. 3. Current with electrolyte agitation; (a) effect of interpolar distance, (b) effect of Pt immersion depth inside the shroud.

4. Conclusions

In this study, the effect of electrolyte agitation on an electrolytic reduction process was investigated in the LiCl-1.4wt.% Li_2O molten salt at 650°C. It was confirmed that current increases with increasing a rotating rate, but not significant. Effect of other experimental conditions, such as distance between electrodes, location of anode in a shroud or electrode area, on the process performance is more significant.

REFERENCES

[1] A.J. Bard, L.R. Faulkner, Electrochemical Methods; Fundamentals and Applications, 2nd edition, John Wiley & Sons, Inc., New York, 2001.

Electrolytic Reduction of 1 kg-UO_2 Using a Graphite Anode

Sung-Wook Kim*, Dong Hyun Heo, Sang-Kwon Lee, Jin-Mok Hur, and Eun-Young Choi

Korea Atomic Energy Research Institute, 111, Daedeok-daero 989beon-gil, Yuseong-gu, Daejeon, Republic of Korea

*swkim818@kaeri.re.kr

1. Introduction

Developing anode materials has been a critical issue of electrolytic reduction in pyroprocessing because of the extremely high price of Pt, which is the most common anode material. Recently, the feasibility of a C anode as a potential alternative to a Pt anode was suggested through a small-scale experiment (~50 g-UO_2) [1]. Accumulation of Li_2CO_3, a major byproduct in the C anode system, can be prevented, enabling the repeatable use of LiCl electrolyte. Cl_2 gas is expected to be dominantly generated at the anode surface during the reaction to eliminate the Li_2CO_3 byproduct. In this study, a larger-scale electrolytic reduction experiment was conducted using 1 kg of UO_2 pellets with graphite as the C anode.

2. Results

An identical reactor, which was used to test the Pt anode at the same scale (1 kg-UO_2), was used for comparison [2]. Pure LiCl was used as the initial electrolyte, which was heated to 650°C. One cathode basket containing 1 kg of UO_2 pellets and two graphite anodes were used in this experiment.

With the graphite anode, the maximum cell current was 220 A under 7-7.5 V with a constant current operation. On the other hand, the Pt anode system operated at a constant voltage of 3.4 V can only transfer 30-35 A. This implies the superiority of the graphite anode in terms of the cell current, which directly determines the reaction time. Such a high current is originated from the application of higher voltage and the higher concentration of the major anion species participating in the electrochemical reaction. Since Pt is ionized to be dissolved in a LiCl electrolyte above 3.4 V ($Pt \rightarrow Pt^{2+} + 2e^-$), it is difficult to apply high voltage with a Pt anode. However, C does not suffer from an anodic dissolution, and a higher voltage can be applied to result in an increased cell current. A Cl_2 evolution ($2Cl^- \rightarrow Cl_2(g) + 2e^-$) and O_2 evolution ($2O^{2-} \rightarrow O_2(g) + 4e^-$) are regarded as the major anodic reactions in a graphite anode and Pt anode, respectively. LiCl is the dominant phase in the electrolyte, and hence an excessive amount of Cl^- should exist around the graphite anode, which is advantageous over an electrochemical reaction.

The surfaces of the UO_2 pellets were reduced to U metal after the reaction, as shown in Fig. 1. However, the cores of several pellets remained UO_2, even though a 150-200% theoretical charge was supplied. The relatively low conversion rate was due to the limited diffusion of metallic Li, formed at the cathode surface to reduce UO_2 to U ($UO_2 + 4Li \rightarrow U + 2Li_2O$), into the core of the UO_2 pellets, and due to side reactions induced by reaction byproducts dissolved in the electrolyte. The conversion rate can be increased by supplying more charge and optimizing the operation condition to ensure the sufficient diffusion time for the metallic Li.

After the reaction, the reactor corroded severely owing to the evolution of highly reactive Cl_2 and O_2 during the reaction. The corrosion can be reduced by designing an off-gas system to minimize the residence time of the gas species in the reactor. In addition, a ceramic coating or attaching ceramic plate will be effective at prohibiting any corrosion.



Fig. 1. U metal products in a cathode basket after electrolytic reduction using a carbon anode.

3. Conclusion

An electrolytic reduction of 1 kg-UO_2 was conducted using a graphite anode. The graphite anode can transfer a 7-times higher current to the Pt anode in the same reactor. UO_2 was electrochemically converted into metallic U after the reaction, indicating the feasibility of the graphite anode at the pilot-scale. However, further investigation should be made, such as increasing the conversion rate, and developing anti-corrosion techniques for a scale-up.

REFERENCES

[1] S.-W. Kim, M. K. Jeon, H. W. Kang, S.-K. Lee, W. Park, E.-Y. Choi, S.-S. Hong, S.-C. Oh, and J.-M. Hur, "Carbon Anode with Repeatable use of LiCl Molten Salt for Electrolytic Reduction in Pyroprocessing", Journal of Radioanalytical and Nuclear Chemistry, 310(1), 463-467 (2016).

[2] E.-Y. Choi, J. Lee, M. K. Jeon, S.-K Lee, S.-W. Kim, S.-C. Jeon, J. H. Lee, J.-M. Hur, "Electrolytic reduction of 1 kg-UO_2 in Li_2O-LiCl Molten Salt Using Porous Anode Shroud", Journal of Korean Electrochemical Society, 18(3), 121-129 (2015).

Change of Oxygen Concentration According to Argon Purging of Storage Vault in ACPF

Yunmock Jung*, Byungsuk Park, Jongkwang Lee, Sunseok Hong, and Eunyoung Choi

Korea Atomic Energy Research Institute, 111, Daedeok-daero 989beon-gil, Yuseong-gu, Daejeon, Republic of Korea

jym@kaeri.re.kr

1. Introduction

When performing a pyroprocessing experiment, Uranium / molten salt ingot which are by-products are generated and need a place to store them. We have called this place a Storage Vault which is located in the ACPF (Advanced spent fuel Conditioning Process Facility). These products should always be stored in an Argon atmosphere because they have high radiation levels and high temperature.

These by-products (high temperature condition) are easy to react to the small amount of Oxygen. As a result, fire and explosion may occur. These event also cause severe accident. Thus it is essential to measure the Oxygen concentration in the storage vault. Therefore, in order to measure the change of Oxygen concentration according to the amount of Argon in the storage vault, Oximeter was installed in the storage vault outlet to measure Oxygen concentration change.

2. Experimental

The storage vault is divided into vault A and Vault B, and their specifications are shown in Table 1.

Table 1. Volume of vault A and vault B

	Specification
Vault A	Storage rack: 6 ea Volume: $0.0176\ m^3 \times 6 = 0.105\ m^3$
Vault B	Storage rack: 6 ea Volume: $0.0275\ m^3 \times 6 = 0.165\ m^3$

The Oxygen meter used in this experiment is shown in Fig. 1.



Fig. 1. Experimental apparatus (Oxygen meter).

3. Results and Discussion

(1) Vault A

An unused 47 L Argon bomb is filled with Argon gas at a pressure of about 120 bar, which has a volume of about 5,600 L at atmospheric pressure at room temperature (25℃). The initial pressure of the bomb used for Argon purging in vault A is 1,335 psi which is approximately 4,317 L at 25℃ at atmospheric pressure. The Oxygen concentration of the initial Oxygen meter was 206,400 ppm and the resolution of the Oxygen meter used was 0.0001 ppm. Table 2 shows the changes in Oxygen concentration according to amount of Argon purging of Vault A, and the graph is shown in Fig. 2. The amount of Argon needed to reach 100 ppm was analyzed to be about 278.31 L

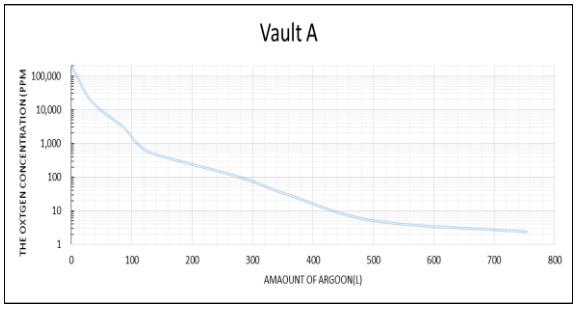


Fig. 2. The graph of change Oxygen concentration of vault A.

Table 2. The change of Oxygen concentration according to amount of Argon of vault A

Pressure (psi)	A mount of Ar (L)	Oxygen concentration (ppm)
1,335	0.00	206,400
1,327	25.59	27,500
1,320	47.98	10,000
1,308	86.37	3,000
1,301	108.76	1,000
1,293	134.35	500
1,248	278.31	100
1,223	358.28	30
1,178	502.23	5
1,099	754.95	2.36

(2) Vault B

The initial pressure of the bomb used for Argon purging in vault B is 1,211 psi which is approximately 3,920 L at 25℃ at atmospheric pressure. The Oxygen concentration of the initial Oxygen meter was 206,400 ppm and the resolution of the Oxygen meter used was 0.0001 ppm. Table 3 shows the changes in Oxygen concentration according to amount of Argon purging of Vault B, and the graph is shown in Fig. 3. The amount of Argon needed to reach 100 ppm was analyzed to be about 217.57 L

Table 3. The change of Oxygen concentration according to amount of Argon of vault B

Pressure (psi)	A mount of Ar (L)	Oxygen concentration (ppm)
1,211	0.00	206,400
1,173	123.14	10,000
1,170	132.86	3,000
1,153	187.95	1,000
1,121	291.65	200
1,113	317.57	100
1,099	362.94	50
1,065	473.11	20
1,028	593.01	10
938	884.66	2
909	978.63	1

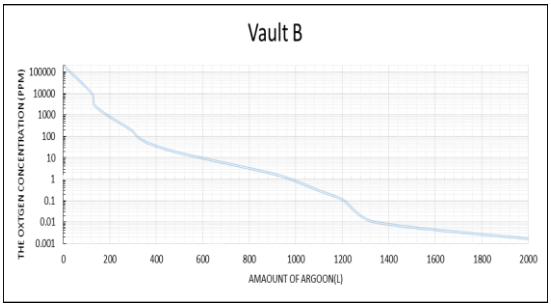


Fig. 3. The graph of change Oxygen concentration of vault B.

4. Conclusions

It uses 595.8L of Argon gas to reach 100ppm by purging Vault A and B at the same time. According to the MBRAUN data which is a famous company of making GLOVE BOX [1], it needs 11 times bigger volume of Argon gas to reach 100ppm. Also it needs 3,000L of Argon gas to purge to reach 100 ppm on this experimental volume which is 0.27m^3. There is a big gap between the MBRAUN data and our experiment result. I guess there were on error on Assuming that everything is Argon gas except Oxygen gas which was measured only. It is hard to say that other substances is Argon gas (purity 99.999%) even the Oxygen is lower than 10 ppm. But the purpose of the experiment was measuring only Oxygen level. It was not a waste of time. Also I guess there was not much error because the Oxygen concentration meter was fixed and corrected before the experiment.

REFERENCES

[1] MBRAUN Inc. Operation Manual Glove Box Systems ver 3.0, 2008.

The Oxidation Effect on The Reinforcement Particles of Al / B_4C Metal Matrix Composite

Tae Gyu Lee and Ho Jin Ryu*

Korea Advanced Institute of Science and Technology, 291 Daehak-ro, Yuseong-gu, Daejeon, Republic of Korea

*hojinryu@kaist.ac.kr

1. Introduction

Finding proper neutron absorber materials for spent fuel storage and transport is one of the biggest challenges of nuclear engineering. One of the promising neutron absorber materials for storage and transportation of spent fuel is B_4C because of its high neutron absorption cross section [1]. However, B_4C is ceramic, which means it has low ductility and machinability. Therefore, the fabrication of metal matrix composite (MMC) containing B_4C is one solution to the problem associated with the ceramic characteristic of B_4C.

However, boron carbide has a high interfacial energy with aluminum and also produces aluminum carbide, which is detrimental compound, through a chemical reaction, so there is a limit to making MMC [2].

In the case of SiC, another well-known carbide reinforcement, there have been many attempts to oxidize the surface to lower the interfacial energy and inhibit the formation of aluminum carbide [3-4]. However, in the case of boron carbide powder, oxidation occurs at a temperature higher than the melting point of boron oxide, which is an oxidized product, so, powder agglomeration occurs during the oxidation process. So far, no research has been done to oxidize the surface of boron carbide to produce high-quality MMC.

In this study, low-temperature oxidation was performed to overcome the agglomeration due to powder oxidation. MMC was made with surface oxidized boron carbide to compare mechanical properties, hardness, and flexural strength with untreated MMC.

2. Experimental procedure

2.1 Sample preparation

The fabrication procedure of MMC consists of the following steps. First, B4C particles of 3.5 μm and 40 μm in diameter were oxidized in an air environment at a temperature of 600℃ for 1, 2, and 3 hours. Then, Oxidized and non-oxidized powders are mixed with aluminum powder (ECKA 231D) in a 2: 8 ratio for 300 minutes using a 3D mixer at 40 rpm.

The mixtures were pressurized at 50 MPa for sintering in a spark plasma sintering machine, heated to 450℃ for 5 minutes and held for 5 minutes.

2.2 Hardness test

The surface of oxidized and non-oxidized MMC prepared for hardness test was polished to 2000grit using SiC polishing paper. The hardness was then measured through a Rockwell B scale hardness tester.

2.3 Bending test

For the bending test, the sintered samples were cut to a size of 2.7 * 2.0 * 11 cubic mm. Then, the flexural test was performed using a universal testing machine (UTM, Instron 5583, Instron Corporation, USA). At this time, the test was performed following ASTM C1421 – 10.

2.4 Microstructure

The dispersion of the reinforcement and the microstructure of the specimen were observed with a scanning electron microscope (SEM). To determine the mode of failure of the material, the fracture surface after the bending test was also observed with SEM.

3. Result

3.1 Hardness test

Although no investigation has been done on the

value of MMC containing B_4C, it is predicted that the hardness value will be improved by a study of the SiC reinforced MMC, which is a previous study of this researcher (Fig. 1)

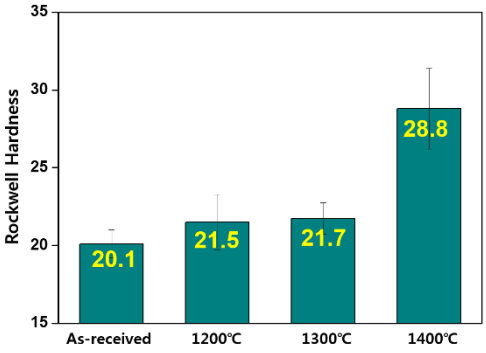


Fig. 1. Hardness data of surface-oxidized SiC / Al MMC.

In the SiC data, the oxidation temperature is variable, but in this experiment, the oxidation time of B_4C is the variable.

3.2 Bending test

The bending test has not yet been carried out, but according to previous experimental results (Fig. 2), a coherent interface is formed when B_4C is coated. Therefore, high Young's modulus and fracture toughness are expected in the case of oxidized MMC.

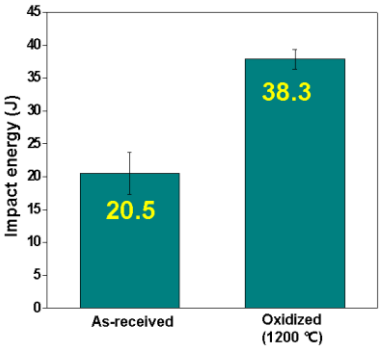


Fig. 2. Impact resistance data of surface treated B_4C and non-treated B_4C reinforced MMC.

3.3 Microstructure

The microstructure has not yet been observed, but according to existing data, the oxidized B_4C reinforced MMC will show a more dense and less porosity microstructure.

4. Conclusion

In this study, B_4C powder, which is difficult to oxidize the surface, was oxidized without agglomeration at low temperature. By doing this coating, Al / Oxidized B_4C MMC, which has not been studied previously, is prepared. As a result, the mechanical properties of the B_4C reinforced Al-based MMC were increased by the surface oxidation treatment as in the other typical carbide materials SiC.

The B_4C oxidation coating lowers the interfacial energy with aluminum and also inhibits the chemical reaction. This allowed the microstructure to produce sound MMC. Due to the sound microstructure, hardness increased and fracture toughness increased.

This result can be used for all B_4C / Al MMC applications and especially can be used as a neutron absorber, in nuclear applications where safety and robust are important.

Acknowledgments

This work was supported by the National Research Foundation of Korea (NRF, No. 2014M3C1A9060721) grant funded by the Ministriy of Science, ICT and Future Planning.

REFERENCES

[1] Zhang, P., Li, Y., Wang, W., Gao, Z., & Wang, B., "The design, fabrication and properties of B 4 C/Al neutron absorbers." Journal of Nuclear materials, 437(1), 350-358 (2013).

[2] Viala, J. C., Bouix, J., Gonzalez, G., & Esnouf, C., "Chemical reactivity of aluminium with boron carbide.", Journal of Materials Science, 32(17), 4559-4573 (1997).

[3] Urena, A., Martınez, E. E., Rodrigo, P., & Gil, L.. "Oxidation treatments for SiC particles used as reinforcement in aluminium matrix composites." Composites Science and Technology, 64(12), 1843-1854 (2004).

[4] Ribes, H., Suery, M., L'esperance, G., & Legoux, J. G.. "Microscopic examination of the interface region in 6061-Al/SiC composites reinforced with as-received and oxidized SiC particles." Metallurgical Transactions, A 21(9), 2489-2496 (1990).

Cesium Diffusion Tests in Graphite with Optimized ICP-MS Measurement Conditions

Je-Kyun Baek[1], Sunghwan Yeo[2], Young Woo Lee[2], Jeongmook Lee[2], and Ho Jin Ryu[1*]

[1]Korea Advanced Institute of Science and Technology, 291 Daehak-ro, Yuseong-gu, Daejeon, Republic of Korea

[2]Korea Atomic Energy Research Institute, 111, Daedeok-daero 989beon-gil, Yuseong-gu, Daejeon, Republic of Korea

[*]hojinryu@kaist.ac.kr

1. Introduction

Graphite has been used widely in the nuclear industry since Chicago pile-1, which was the first nuclear reactor in the world, because graphite has excellent properties as a moderator. High temperature gas-cooled reactors (HTGR) also use graphite as a moderator. The fuel design of HTGR is based on the concept of tristructural-isotropic (TRISO) particles buried into a graphite matrix. The graphite matrix works as not only the moderator but also a structural material for the TRISO particles. The coating layers of TRISO particles act as barriers of fission products that are produced from the fuel kernel. When the coating layers fail to prevent the release of the fission products due to cracking, fission products might be adsorbed in the graphite matrix. Some fission products such as cesium (Cs), silver (Ag), and strontium (Sr) are likely to cause contamination since they are released out to primary coolant channel. Therefore, evaluating the behavior of the fission products in the graphite matrix is important for safety concerns.

In the authors' previous work [1-2], the diffusion test samples preparation, the preliminary diffusion tests, and the results analysis methodology have been studied. In these studies, ICP-MS measurements were conducted to analyze the samples quantitatively. But the results showed highly scattered data even if the samples are similar. To improve the reliability of the ICP-MS measurements results, optimization of the measurement has been conducted.

2. Optimizing the ICP-MS measurement conditions

2.1 Background

ICP-MS measurements have been conducted to analyze the diffusion test samples quantitatively. The previous results showed a cesium (Cs) range of 146-652 ppm in the graphite matrix, the data is highly scattered. The solid samples have to be converted to liquid because ICP-MS measurements are applied on liquid samples only. To convert the samples, they were ground as powder. The powders were treated to dissolve out Cs from the graphite to the solution, which is called the 'pre-treatment' step. It was shown that the conditions of the pre-treatment caused the data scatter as expected. In the authors' previous work [2], the powder size effect was studied mentioning that the effect is not only from the powder size, but from other parameters that are studied in this paper.

2.2 ICP-MS optimization

In addition to the powder size effect, the powder mass effect, the pre-treatment temperature, and time were studied. Only Cs can be dissolved into the solution, and the graphite remains. Therefore, when the powder size is larger, the diffusion distance is longer and the dissolution rate is decreased. In Table 1, the powders which are coarser than 212 μm showed a lower concentration of Cs. In contrast, finer powders, which have a size range of 63~106 μm, showed a much lower concentration.

Table 1. ICP-MS results with variation of powder size range

Powder mass (mg)	Particle size (μm)	Concentration (ppm)
68.6	>212	175.1
33.2	106~212	418.8
1.2	63~106	85.4
53.4	<63	424.1

The powder mass was a vague parameter as the additional tests were conducted. The target masses

were 1 mg, 10 mg, and 100 mg, the powders were prepared to investigate the effect of mass on the Cs concentration. As shown in Table 2, the powders that have 10 mg and 100 mg masses showed similar concentrations. But the results of the 1 mg powders showed much lower concentrations. It means that both the weighting error of powder mass and the low level of Cs quantities affect the results of ICP-MS measurements.

Table 2. ICP-MS results with variation of weight of powders

Test set	Powder mass (mg)	Concentration (ppm)
1	1	78.6
	11.2	405.9
	101	394.9
2	0.8	198.8
	9.8	303.8
	93	292.7

The pre-treatment temperatures were 50°C, 100°C, 150°C, and 200°C and the results of ICP-MS measurements are shown in Table 3. The concentration results are proportional to the pre-treatment temperature. This means that the temperature affects the activation of Cs and accelerates the dissolution process.

Table 3. ICP-MS results with variation of pre-treatment temperature

Pre-treatment temperature (°C)	Concentration (ppm)
50	162.5
100	186.9
150	239.1
200	308.3

The results of ICP-MS at 200°C with different pre-treatment time are listed in Table 4. When the pre-treatment time is 30 minutes, the Cs concentration is lower than all the other cases, which have relatively similar concentrations.

Table 4. ICP-MS results with variation of pre-treatment time at 200°C

Test set	Holding time (hours)	Concentration (ppm)
1	0.5	291.5
	4	463.8
	12	466.0
2	1	495.9
	2	505.5
	3	513.3
	4	516.3

3. Conclusion

In this paper, the results of optimized ICP-MS measurements, which were used to analyze the diffusion test samples quantitatively, were obtained and discussed. To conduct ICP-MS measurements, the samples have to be converted to liquid in the pre-treatment process. The target of optimization was to change the pre-treatment conditions such as powder size, powder mass, pre-treatment temperature, and pre-treatment time to optimum values. The ICP-MS measurements will be conducted following the optimized conditions based on the results of this study. The results show that optimum conditions to get the intended results include using powders finer than 212 μm and larger than 10 mg and holding the pre-treatment time to be longer than 1 hour at 200°C.

ACKNOWLEDGMENT

This study was supported by NRF-2015M2A8A2023296. And the LA-ICP-MS analyses have been supported by Dr. Jong-Yun Kim, Dr. Sang Ho Lim, and Dr. Sun-Ho Han who are affiliated to Nuclear Chemistry Research Division of KAERI. I would like to appreciate all researchers who supported this study.

REFERENCES

[1] Je-Kyun Baek, Sunghwan Yeo, Young Woo Lee, Sun-Ho Han, and Ho Jin Ryu, “A study of cesium impregnation behavior in IG-110 graphite matrix by using Laser Ablation ICP-MS (LA-ICP-MS)”, KNS 2016 Spring Meeting, May 12-13, 2016, Jeju.

[2] Je-Kyun Baek, Sunghwan Yeo, Young Woo Lee, Jeongmook Lee, and Ho Jin Ryu, “Preparation of Cesium (Cs) Release Test for Verifying Diffusion Coefficient in the IG-110 Graphite Matrix”, KNS 2016 Autumn Meeting, Oct. 27-28, 2016, Gyeongju.

Spray Coatings of Al_2O_3 Layer for Passivation of Al_2O_3-SiO_2-based Refractory

Joo-Young Yoon*, Jae-Won Lee, Sang-Chae Jeon, Yung-Zun Cho, Ju-Ho Lee, Kweon-Ho Kang, Do-Youn Lee, Jang-Jin Park, and Kwang-Hoon Cho

Korea Atomic Energy Research Institute, 111, Daedeok-daero 989beon-gil, Yuseong-gu, Daejeon, Republic of Korea

*yjy2746@kaeri.re.kr

1. Introduction

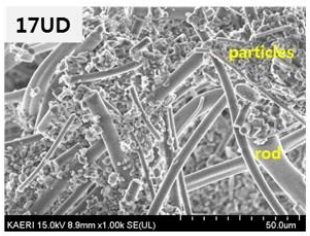
From few decades ago, pyroprocessing has been recognized as a promising dry processing technology to manage the accumulating spent fuel with less proliferation risk than wet processing. It starts with head-end process for the conversion of spent fuel into a feed material for following processes. The spent fuel generally contains various fission products as a result of nuclear reactions during operation. The preparation of feed material in the head-end process may include heat treatment at high temperatures, which leads to the release of volatile fission products from the spent fuel, so called off-gas. The emission of the off-gas from should be minimized due to its toxicity to human body.

Considering great importance of the off-gas treatment in terms of safety, many studies have focused on the capture of the off-gas by filters to reduce its emission rate [1-2]. The off-gas capture system in the head-end process should be connected to a sintering furnace where heat treatment of the spent fuel takes place. For high temperature operation, the sintering furnace is generally equipped with refractories, which contain Al_2O_3, SiO_2, etc. Those can react and form mullite ($Al_6Si_2O_{13}$) phase during heating as shown in Fig. 1. Paradoxically, the mullite phase is a major component of the filters for capturing of Cs. Cs is known to be stabilized by the formation of pollucite ($CsAlSi_2O_6$) phase with the mullite phase. It indicates that the Cs emitted from the spent fuel can be captured at the surface of refractories. This is contrary to the aim of the off-gas system and the contact between the Cs vapor and refractories should be restricted. The development of alternative composition for the refractories would be tremendous time- and effort-consuming work. In view of this, the passivation treatment on the surface of refractories by coating with inert material can be a route. From literature survey, Al_2O_3 and Y_2O_3 with high purity were chosen as possible coating materials that hardly react with Cs.

The present study aims at evaluating the possibility of the passivation by spray coating method. Cube-shaped commercial refractories containing SiO_2 were spray coated by high purity Al_2O_3 and the coated layer was examined before and after heat treatment. To this end, the applicability of this spray coating method was discussed for sintering furnace equipped with off-gas treatment system.

2. Experimental

The commercial refractory (designated as 17UD) in the form of cube (1 cm × 1 cm × 1 cm) and commercial Al_2O_3 spray (Al_2O_3, purity: 96%) were prepared. The Al_2O_3 layer was coated by spraying in air for 3 sec by 3, 4 and 5 shots for the formation of coating layer with different thickness. The sprayed cubic samples were dried in air for 10 min. The samples were then sintered under the following condition: at 1,500°C for 150 min in 4% H_2-Ar atmosphere, ramp/cooling rate was 5°C/min).



Particle

Element	Weight%	Atomic%
O	56.07	68.28
Al	43.93	31.72
Totals	100.00	

Rod

Element	Weight%	Atomic%
O	55.32	67.81
Al	34.70	25.22
Si	9.98	6.97
Totals	100.00	

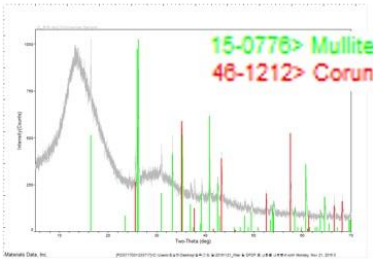


Fig. 1. Physical properties of 17 UD.

The characterization of samples were carried out by X-ray diffraction (XRD, Bruker, D8 Advanced A25) and scanning electron microscope (SEM, Hitachi, SU-8010) and energy dispersive X-ray spectroscope (EDS, Horiba, X-MAX).

3. Results and Discussion

Fig. 2 shows 17UD samples spray coated with different thickness of Al_2O_3 layers were shown before heat-treatment. After sintering at 1,500°C for 150 min in 4% H_2-Ar, regardless of the thickness of coated layers, all the samples were integrity and maintained homogeneously covered Al_2O_3 layer.

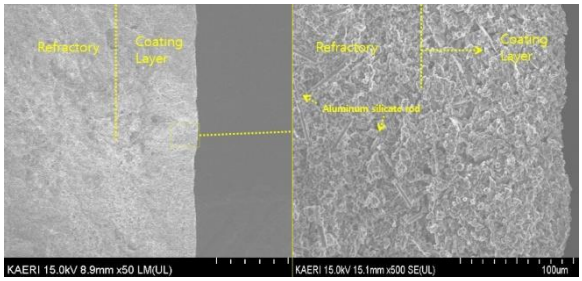


Fig. 2. Spray coated 17UD samples Al_2O_3 after drying.

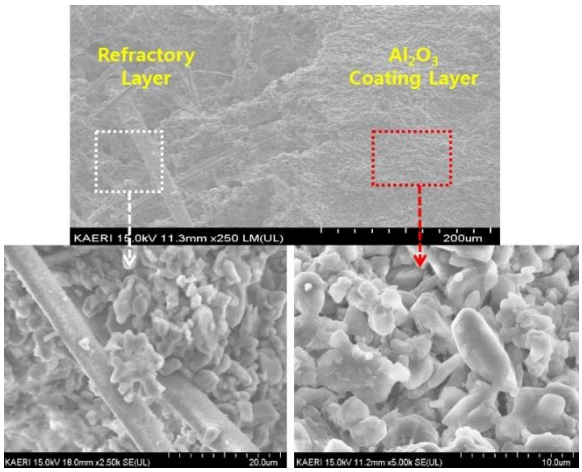
Fig. 3 shows the microstructure of interface between the 17UD substrate and coated Al_2O_3 layer. The newly formed layer was deposited uniformly and made a good adhesion possibly due to sufficient surface roughness at the surface of 17UD before coating. In addition, without polishing and other surface treatment, the interface region can be recognized by the presence of rod shape phases in the 17UD substrate but without it in the coated Al_2O_3 layer. As shown in Fig. 1, the rod shape phase was observed as aluminum silicate by SEM/EDS. The thickness of coated Al_2O_3 that contains only particle shape grains was measured as 100 μm. Considering the refractories are not contact anything during operation, although there is no evidence on the durability of coated layers, this spray coating can be an easy and effective way to deposit the protective layer on the 17UD in terms of physical stability.

4. Conclusions

The spray coating behavior of high purity Al_2O_3 on refractory material containing SiO_2 were investigated. For the formation of protective layer, the adhesion and connectivity of the coated layer were satisfactory. In a physical viewpoint, its durability also should be confirmed. Also, the reactivity of coated layers with



(a) Image of coating area



(b) Image of Al_2O_3 coating and refractory layer

Fig. 3. SEM image of Al_2O_3 coated layer and 17UD.

Cs vapor needs to be examined for the application to in the sintering furnace equipped with the off-gas treatment system. The chemical reaction of the coated samples with Cs vapor will be discussed in future study.

REFERENCES

[1] Park, J.J., Shin, J.M., Yang, J.H., et al., 2015. Fabrication and performance of fly ash granule filter for trapping gaseous cesium. Nukleonika 60, 565-570.

[2] Yang, J.H., Yoon, J.Y., Lee, J.H., Cho, Y.Z., 2017. A kaolinite-based filter to capture gaseous cesium compounds in off-gas released during the pyroprocessing head-end process. Annals of Nuclear Energy 103, 29-35.

Development of Graphene Reinforced Calcium Hydroxyaptite Matrices for the Immobilization of Radioiodine

Muhmood ul Hassan and Ho Jin Ryu*

Korea Advanced Institute of Science and Technology, 291 Daehak-ro, Yuseong-gu, Daejeon, Republic of Korea

*hojinryu@kaist.ac.kr

1. Introduction

The presence of volatile radioisotopes like radioiodine-129 (I-129) makes the immobilization of ILW somehow difficult through vitrification and other high temperature techniques because of its volatilization above 500°C. This is being one of the challenges suffered by the used nuclear fuel (UNF) reprocessing industry and requires the development of such matrices which can effectively immobilize the I-129 below its volatilization temperature as well as exhibit good durability in the geological repository environment. This is not only necessary to fully establish the worth of used nuclear fuel processing facilities in nuclear industry, also to counter the radiological effects of this long lived radioisotope. In this regard the development and adoption of effective methodologies/techniques to capture and immobilize the volatile radionuclides being evolved in the off-gas system may be one of the major licensing requirements for UNF processing facility [1].

Calcium hydroxyapatite $\{Ca_{10}(PO_4)_{10}OH_2\}$-HAP is calcium based phosphorus mineral having good corrosion resistance properties in ground environment as well as resistance against radiation damages of the loaded radioactive material [2,3]. HAP has the properties to accommodate iodine ions having an ionic radius of 196 pm at channels within its crystal structure [4].

In this study we have successfully sintered the synthesized graphene reinforced HAP at an extraordinary low temperature of <200°C by using the technique of cold sintering [5] as the first attempt. In this effort we have got 90% relative dense sintered pellet at a temperature of 180°C under a uniaxial pressure of 300MPa and has started the work for the consolidation of radioiodine loaded graphene within this ultra-low temperature sintered ceramic matrices.

2. Methods and Results

2.1 Apatite Synthesis

Initially the crystalline apatite has been synthesized by using the wet precipitation method as described elsewhere [6]. Two solutions, A & B, were prepared by dissolving each di-ammonium hydrogen phosphate $\{(NH_4)_2HPO_4\}$ and calcium nitrate $\{Ca(NO_3)_2{\cdot}4H_2O\}$ in 100ml of double deionized water respectively. The pH of the solutions was adjusted at 10.5 by using concentrated ammonia $\{NH_4(OH)_2\}$. All used materials were of reagent grade. Then solution "A" was mixed with solution "B" dropwise during one hour under continuous stirring at the rate of 150RPM and temperature was maintained at 35 ^{o}C. The pH of the solution was continuously monitored by using digital pH meter and was maintained at 10.5 throughout the synthesis period by the dropwise addition of concentrated ammonia. At the end of synthesis, precipitates were filtered and thoroughly washed with double deionized water. Finally the filtrate was room temperature dried for 12hrs in a vacuum oven.

2.2 Powder Characterization

XRD pattern of the apatite powder was obtained by using SmartLab, RIGAKU, high resolution powder X-ray diffractometer and the 2Θ range was between 10 and 70◦.

2.3 Cold Sintering of Apatite

The sintering of apatite powder by using cold sintering technique has been investigated first time in. 3 g of apatite powder was mixed with 10wt% of deionized water by using pestle and mortar. 0.5wt% of graphene nano powder reinforced was used to study the effect of this enforcement on the textural strength and on the density of the sintered matrix. The powder was then poured in a steel mold and uniaxial pressed under the pressure of 300 MPa for 3 hrs. In order to provide controlled heating during

the pressing, heating tape was wrapped around the steel mold. The pressing time was divided into three steps.

Step-I

Pressing at room temperature for 10 minutes

Step-II

Pressing with heating (25 ^{o}C to 180 ^{o}C) for 120 minutes

Step-II

Pressing during cooling for 50 minutes

After 3hrs, pressure was released and a sintered/dense pellet of the reinforced HAP was obtained.

3. Conclusion

In this work, ultralow temperature sintering of graphene reinforced apatite by using cold sintering technique was demonstrated. This leads to our final goal of development of an ultralow temperature sintered graphene reinforced matrices for the immobilization of I-129 for long term geological disposal.

REFERENCES

[1] N. R. Soelberg *et al.*, "Radioactive Iodine and Krypton Control for Nuclear Fuel Reprocessing Facilities," *Sci. Technol. Nucl. Install.*, vol. 2013, pp. 1–12, 2013.

[2] J. Wang, "Incorporation of iodine into apatite structure: a crystal chemistry approach using Artificial Neural Network," *Front. Earth Sci.*, vol. 3, no. June, pp. 1–11, 2015.

[3] C. Jiang *et al.*, "Using 'radioparagenesis' to design robust nuclear waste forms," *Energy Environ. Sci.*, vol. 3, no. 1, pp. 130–135, 2010.

[4] P. Alberius Henning *et al.*, "Iodo-oxyapatite, the first example from a new class of modulated apatites," *Acta Crystallogr. Sect. B Struct. Sci.*, vol. 55, no. 2, pp. 165–169, Apr. 1999.

[5] H. Guo, A. Baker, J. Guo, C. A. Randall, and D. Johnson, "Cold Sintering Process: A Novel Technique for Low-Temperature Ceramic Processing of Ferroelectrics," *J. Am. Ceram. Soc.*, vol. 99, no. 11, pp. 3489–3507, 2016.

[6] L. Campayo, A. Grandjean, A. Coulon, R. Delorme, D. Vantelon, and D. Laurencin, "Incorporation of iodates into hydroxyapatites: a new approach for the confinement of radioactive iodine," *J. Mater. Chem.*, vol. 21, no. 44, p. 17609, 2011.

A Quantification Approach to Pyro-electrochemical Performance for Scale-up Design

K.R. Kim*, C.M. Kim, H. Jang, S.K. Kim, J.G. Kim, C.S. Seo, H.O. Nam, and W.I. Goh

Korea Atomic Energy Research Institute, 111, Daedeok-daero 989beon-gil, Yuseong-gu, Daejeon, Republic of Korea

*krkim1@kaeri.re.kr

1. Introduction

Pyrochemical processing for the treatment of spent nuclear fuel consists of a series of molten-salt electrochemical reactors as the main processes. The pyrochemical process operated using a high-temperature molten-salt electrolyte is cost intensive since experiments are implemented under a radioactive environment.

A successful design of the electrochemical reactors is desirable for a product attainment at the planed throughput, at the projected performance and with the desired quality standards. Many trials of high cost experiment are not to predict the behavior of the commercial-sized equipment.

This is very important in the scaling of laboratory results to the engineering scale and then from engineering data to the commercial scale.

A larger scaled cell should be designed in favor of current/potential similarity to the corresponding planned electrochemical performance. It can be configured to get uniform current distribution on the electrode for scale-up.

Therefore, the perfect design and scale-up plays an important role in successful of this pyro-electrochemical technology for desired performance.

The topic of current distribution modeling is central to the analysis of electrochemical systems and has been addressed in a reference [1]. The prediction of current distribution is an essential step in the rational design and scale-up of electrochemical cells.

In this study, an approach to characterizing current/potential was proposed to quantify the electrochemical performance similarity. Focus is placed on discussing scaling parameters for the characterization of the current distribution.

2. Theoretical

For a given electrode configuration, the prediction of the current distribution is a complex problem and the difficulties further increase with increasing complexity of the cell geometry which is due to the different geometric and hydrodynamic conditions. It is possible to estimate certain objective trends, using a dimensionless group called Wagner number (Wa) given by

$$Wa = \frac{(d\eta/di)}{(1/\kappa)L} \quad (1)$$

where, (η/di) is the slope of the activation overpotential(η) to current density(i) dependence, κ is the conductivity of the electrolyte and L is a characteristic length. This number is the dimensionless ratio of the surface specific polarization resistance (η/di) and surface related ionic resistivity $(1/\kappa)L$, and is the relevant dimensional quantity determining current density distribution over electrode surface.

The Wagner number is used to characterize the relative importance of charge transfer control on the current distribution. The current distribution is expected to become more uniform as the Wagner number increases.

In addition, local Wagner number (Wa_x) can be derived throughout the electrode surface.

$$Wa_x = \left(\frac{\partial\eta}{\partial n}\right) / \left(\frac{\partial i}{\partial n}\right)\left(\frac{\kappa}{L}\right) \quad (2)$$

where, n represents the direction normal to the electrode surface. The average dimensionless Wagner number is estimated by integrating localized values over the electrode surface (S).

$$Wa_{average} = \frac{\int_S Wa_x dS}{S} \quad (3)$$

3. Results and discussion

Current and potential distributions are the most significant parameters characterizing the operation of the electrochemical cell. The current density on the electrodes is directly proportional to the reaction rate

and its distribution critically affects the refining quality.

Definition of the throwing power (*TP*) of a plating electrolyte has been used to characterize the uniformity of the thickness of the deposited metal in an electroplating system. An actual thickness of an electrodeposit obtained at different distances from the counter-electrode. Based on a semi-empirical correlation, if the Wagner number is relatively high, we expect very uniform deposit irrespective of the electrode geometry and cell scale (Fig. 1).

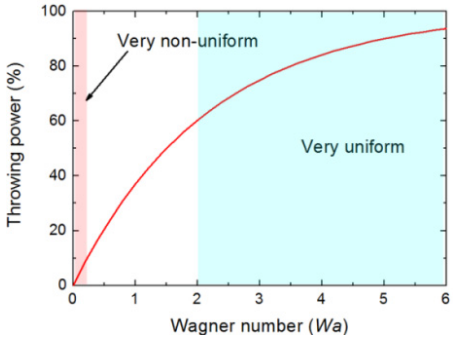


Fig. 1. Semi-empirical correlation between Wagner number and throwing power.

The Rotating Cylinder Hull (RCH) system [2] is optimized to be well suited for the study of plating processes by controlling mass-transport conditions. This system of the sophisticated design allows one to evaluate the effect of mass transport on current distribution. Theoretical expectation for the deposition rate at different distances from counter electrode is simulated by considering electrode polarization.

Copper sulphate electroplating baths are widely used in industrial applications to be informed of deposit quality standard. The current distribution on the RCH standard and corresponding quantification of deposit quality were determined. Dimensionless Wagner numbers based on cathode kinetics (activation and diffusion overpotential) were locally simulated on the rotating electrode as shown in Fig. 2.

This concept implies that for scale-up from the laboratory to the commercial scale the consequences of an enlarged size to current distribution have to be considered carefully in terms of the Wagner number.

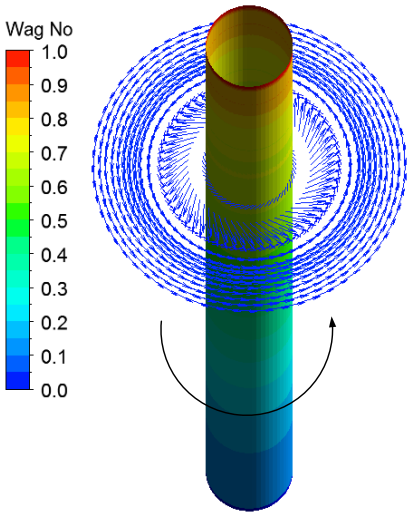


Fig. 2. Local Wagner number distribution along the rotating electrode (750 rpm).

4. Conclusion

This study shows that a theoretical approach to characterize current distribution on the cathode has been proposed for refining cell design. These means provide us design and operation guidelines to obtain a qualified deposit for specific applications.

REFERENCES

[1] J.O. Dukovic, “Computation of Current Distribution in Electrodeposition, a Review”, IBM Journal of Research & Development, 34(5), September (1990).

[2] C.T.J. Low, E.P.L. Roberts, F.C. Walsh, “Numerical Simulation of the Current, Potential and Concentration Distributions along the Cathode of a Rotating Cylinder Hull Cell,” Electrochimica Acta, 52 , 3831–3840 (2007).

The Temperature Distribution of a Fuel Rod With the Presence of a Thermocouple Using COMSOL MULTIPHYSICS

Sunwoo Park and Kwangheon Park*

Kyung Hee Univ., 1732 Deogyeong-daero, Giheung-gu, Yongin-si, Gyeonggi-do, Republic of Korea

kpark@khu.ac.kr

1. Introduction

Temperature profile is an important base in predicting and evaluating the performance of a fuel in a normal or an accident condition. A direct measurement of the temperature in a fuel rod normally is obtained by a fuel rod in which a thermocouple is inserted. However, the measured data have to be carefully interpreted, since the measured temperature may not be the value of the centerline temperature. The precise analysis for the temperature distribution in a fuel rod that has a thermocouple in it is needed for the right estimation of the centerline temperature. We have analyzed the temperature distribution of the fuel rod in the Halden Reactor experiment, i.e., IFA-432. In the NUREG/CR-6534 report, a thermocouple was installed at the bottom of the IFA-432 nuclear fuel rod of the Halden HBWR reactor to confirm the temperature distribution. Based on the results of the above report, the temperature distribution model was created using the COMSOL MULTIPHYSICS program and the results were compared to the measured temperature distribution of the fuel rod. The results of the program are intended to confirm the suitability of the 'thermocouple' when measuring the temperature of the fuel rod.

2. Methods and Results

2.1 COMSOL MULTIPHYSICS Program

COMSOL MULTIPHYSICS is a multiphysical phenomena analysis program that analyzes various complex phenomena using finite element method. In this study, thermal analysis and flow analysis module of COMSOL MULTIPHYSICS program were used to analyze the temperature profile of the fuel rod. The heat transfer equations for solid materials used in the thermal analysis process are shown in (1) and (2), and the heat transfer equations in the fluid are (1) and (3). Q_{ted} and Q_{vd} are thermal elastic damping and viscous dissipation factors which were ignored in the thermal analysis of this study. The fluid flow equation is shown in (4). In this study, only the natural convection due to the density difference was considered. The water flowing on the surface of the fuel rod was calculated through the heat flux function, and the equations used are expressed as (5) and (6).

$$\boldsymbol{q} = -k\nabla T \tag{1}$$

$$\rho Cp\frac{\partial T}{\partial t} + \rho Cp\boldsymbol{u}\cdot\nabla T + \nabla\cdot\boldsymbol{q} = Q + Q_{ted} \tag{2}$$

$$\rho Cp\frac{\partial T}{\partial t} + \rho Cp\boldsymbol{u}\cdot\nabla T + \nabla\cdot\boldsymbol{q} = Q + Q_p + Q_{vd} \tag{3}$$

$$\rho\frac{\partial \boldsymbol{u}}{\partial t} + \rho(\boldsymbol{u}\cdot\nabla)\boldsymbol{u} = \nabla\cdot[-p\boldsymbol{I} + \mu\left(\nabla\boldsymbol{u} + (\nabla\boldsymbol{u})^T - \frac{2}{3}\mu(\nabla\cdot\boldsymbol{u})\boldsymbol{I}\right] + \boldsymbol{F} \tag{4}$$

$$q_0 = h\cdot(T_{ext} - T) \tag{5}$$

$$h = h_{water}(L, U, T_{ext}) \tag{6}$$

2.2 Modeling and material setup

IFA-432r2 fuel rod of Halden HBWR reactor is used for modeling in this study. Total length of fuel rod is 579 mm and radius of it is 6.3944 mm. The thickness of the cladding is 0.9398mm and it composed with Zircaloy-2. The thickness of the initial gap is 0.1905 mm. At the bottom part, a thermocouple with radius of 0.9mm and total length of 100mm is inserted. 2D Axisymmetric dimension was used and the actual model of the fuel rod was simplified. Only the lower part where the thermocouple was inserted was described in this study. The physical properties of nuclear fuel and cladding were expressed in terms of the function of temperature.

2.3 Calculation results and analysis

In this study, the transient analysis results up to 22.64 days were examined, and the LHGR from UO_2 was averaged up to 22.64 days. Fig. 1 shows the results of the 2D Axisymmetric form analyzing the temperature profile of the fuel rod depending on the presence of the thermocouple. The black arrows indicate the convection direction of the filling gas at the GAP.

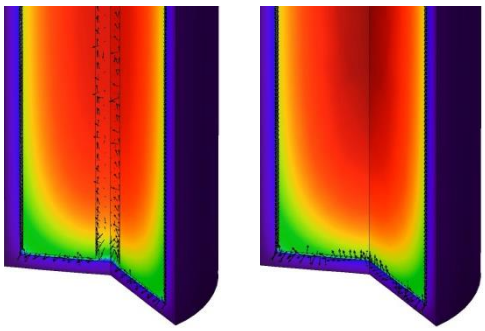


Fig. 1. The temperature distribution of the fuel rod (IFA-432rod2) depending on the presence of the thermocouple. The left fuel rod is a model with a thermocouple and the right is a model without.

For a fuel rod in which a thermocouple is inserted, the temperature difference in the centerline between the height of 105 mm and 96 mm from the bottom is about 43K. This can be seen from the results in Fig. 2. For a fuel rod which a thermocouple is not inserted, there is little temperature difference between the height of 105 mm and 97 mm from the bottom.

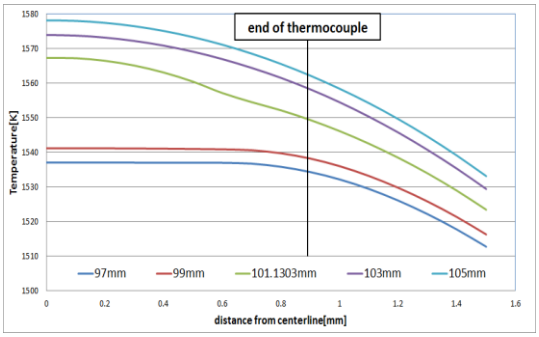


Fig. 2. Temperature profile from centerline to 0.68mm with thermocouple.

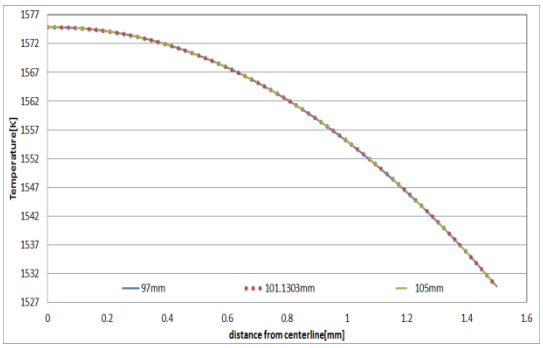


Fig. 3. Temperature profile from centerline to 0.68 mm in the absence of thermocouple.

The temperature profile at the height of 1.2 mm from the bottom of the fuel rod is shown in Fig. 4.

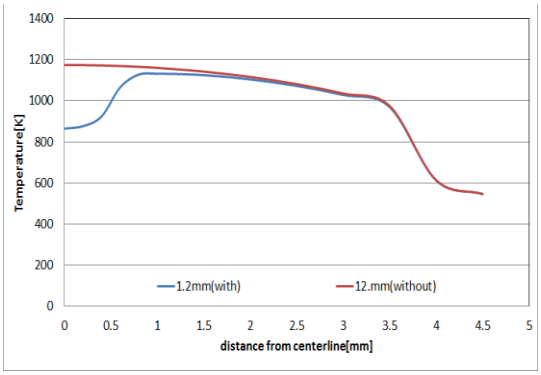


Fig. 4. Temperature distribution at 1.2 mm height of model with and without thermocouple.

The above results are caused by the fact that the heat generation and conduction are removed from the GAP and the influence of the convection of the filling gas becomes dominant.

3. Conclusion

The temperature at the height where the thermocouple is inserted is about 30-40K lower than the temperature at the height where the thermocouple is not inserted. Therefore, when measuring the temperature of a fuel rod through a thermocouple, it should be considered that the actual temperature is higher than the temperature detected through the thermocouple.

REFERENCES

[1] D.D. Lanning[(a)], C.E. Beyer[(a)], G.A. Berna[(b)], "FRAPCON-3: Integral Assessment", NUREG/CR-6534 Volume3, PNNL-11513(1997).

Example Operating Procedure for an Automation Concept of Electrochemical Process

Dongseok Ryu*, Jonghui Han, Jongkwang Lee, Kiho Kim, and Seunghyun Kim

Korea Atomic Energy Research Institute, 111, Daedeok-daero 989beon-gil, Yuseong-gu, Daejeon, Republic of Korea

*sayryu@kaeri.re.kr

1. Introduction

Various ways to reduce the toxic waste in spent fuel has been extensively explored. Pyroprocessing has been studied as one option for compressing down the waste, by recycling 95 percent of Uranium from the spent fuel. The spent fuel is highly radioactive so that the treatment should be performed in a hot cell. The human operator is not allowed to access in the hot cell, thus he or she uses remote devices in order to manipulate material or equipment from outside of the hot cell. Until now, most operations in the hot cell were manually done, and mechanical MSM (master-slave manipulator) became the main tool. However, manual operation is inefficient. Moreover, it can cause human errors. An adoption of modern automation solution has been, therefore, considered for nuclear facility, and a preliminary automation concept for Pyroprocessing was proposed at KAERI [1].

In this research, operating procedures for the proposed preliminary automation concept is discussed in detail.

2. Automation concept of electrochemical process in Pyroprocessing

To make an outline for automated Pyroprocessing, the existing manual operation in processing cell was analyzed, and the requirements for changing the manual ways into automated method were deduced. Finally a preliminary automation concept for integrated Pyroprocessing was proposed [1], as shown in Fig. 1. The proposed processing cell was composed of 4 automation zones. In the automation zone, electro chemical equipment for Pyroprocessing and the automated handling devices cooperate dynamically, and finally an automation workflow can be achieved.

The most important thing in automation is to simplify and standardize the existing methods. A design guide for the electrochemical equipment was proposed. That is to help modularize the equipment for convenient handling by the automated handling devices. Each module attaches a standardized docking knob, which can be transported by the automated handling devices.

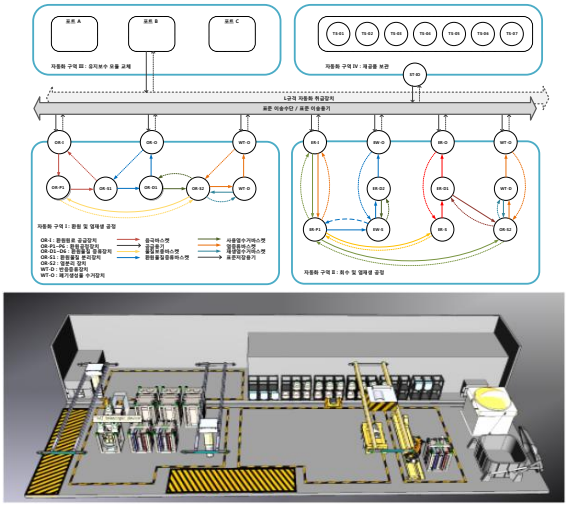


Fig. 1. Preliminary automation concept for Pyroprocessing.

Fig. 2 shows the example design of electro chemical equipment and the automated handling devices to handle the modules. Electrochemical process in automation zone I, most frequent operation is to replace basket and electrode. The basket and electrode are designed as modules which have standardized docking knob, and it can be easily replaced by using the automated handling device.

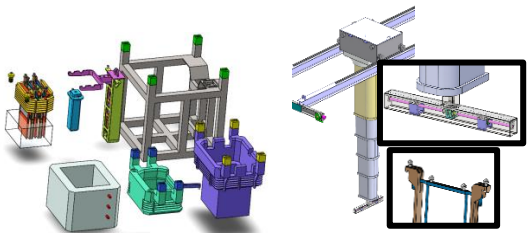


Fig. 2. Modular equipment and automated handling device.

In the proposed automation zone I, the core processes are proceeded by three pieces of equipment,

an oxide reductor, cathode processor, and the salt reprocessor. In between the core equipment, several supporting devices are located to transfer material from the previous crucible to the next crucible. Finally, 8 pieces of equipment are proposed to be located in the automation zone I. Fig. 3 shows the equipment list and the basket flow in the automation zone I.

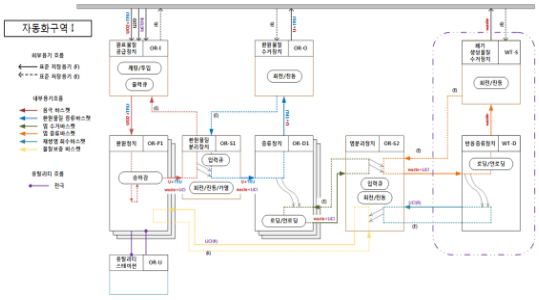


Fig. 3. Basket flow in automation zone I.

3. Example operating procedures in automation zone I

Six types of baskets are defined to transfer material in the automation zone I, as shown in Fig. 3. The basket A circulates among Equip I, II, III. The basket B successively moves from III, IV, V. and the empty basket is forwarded to III again. The basket C move the basket D. The basket D keep moving to VII, VIII continuously, then the empty basket D back to VI. The basket E carry the purified salt from VII to VI, then back to VII. The basket F get the purified salt from VII and put it into

The basket flow in Fig. 3 can be expressed as a flowchart form as shown in Fig. 4. Actually the operation of equipment happens in discrete time, and several operation is possible to proceed in parallel. Even though the flowchart does not matched in time line, it helps to figure out the causality among the operations. The detailed operation procedures in automation zone I are break down, and it is included in the flow chart.

4. Conclusion

An example operation procedure for an automation concept of electrochemical process was proposed in this research. The developed operation procedures were based on one automation zone, which was introduced in the preliminary automation concept for integrated Pyroprocessing. The example operation procedure was compiled as one flowchart form. The procedures will be utilized to develop control logics of automation system.

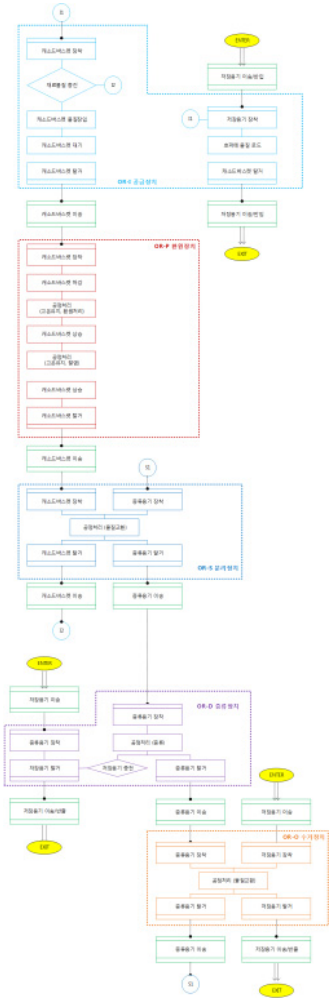


Fig. 4. Flowchart to show operating procedures in automation zone I.

REFERENCES

[1] Dongseok Ryu, et al. "Framework to Develope a Preliminary Automation Concept for Integrated Pyroprocessing", Proc. of Korea Radioactive Waste Society 2016 Spring, pp. 151-2, 2016..

[2] Dongseok Ryu and Jongkwang Lee, "Virtual Verification using 3D Simulator for a Remote Operation Procedures in PRIDE", Proc. of 2016 IPRC, pp. 66, 2016.

[3] Dongseok Ryu, et al. "Development of a Virtual 3D Simulator to Evaluate Remote Operations in PRIDE", Proc. of the D&RS 2016, July 31-August 4, 2016, Pittsburgh.

Chemical Process Safety at a Pyroprocess Facility

Seok-Jun Seo*, Hongrae Jeon, Woojin Jo, Siwan Noh, Jeong-Hoe Ku, and Hyojik Lee
Korea Atomic Energy Research Institute, 111, Daedeok-daero 989beon-gil, Yuseong-gu, Daejeon, Republic of Korea
*sjseo@kaeri.re.kr

1. Introduction

Management of spent fuels stored in nuclear power plant sites in South Korea is one of the most significant issues because of the limited capacity for available areas in South Korea. A pyroprocess, called a dry process compared to a wet process, is regarded as a fascinating technology to recycle the valuable materials and to reduce the volume of wastes. In Korea Atomic Energy Research Institute (KAERI), we have been developing each unit process for a pyroprocess in the PyRoprocess Integrated inactive DEmonstraion (PRIDE) facility as an engineering-scale inactive test as well as lab-scale facility [1].

In a pyroprocess, there are several types of chemical and electro-chemical processes with various operational conditions. Thus, different hazard factors are distributed all over the process lines, containing not only radiological materials but also chemical and toxic materials. For example, there are molten-salts of LiCl and LiCl-KCl at above 500°C, cadmium for a liquid electrode, inert argon gas in a hot-cell, and chlorine gas for an UCl_3 production, etc.

Chemical Process Safety at Fuel Cycle Facilities, NUREG-1601, was published to provide broad guidance on chemical safety issues relevant to fuel cycle facilities in 1997 [2]. This explains the role of chemical process safety, basic information needed to properly evaluate a chemical process safety, and appropriate methods to identify and evaluate the chemical hazards and assessing the adequacy of the chemical safety. In this study, chemical safety in pyroprocess is to be discussed based on the NUREG-1601.

2. Discussion

A definition of the hazardous chemicals is substances which are toxic, corrosive, flammable, explosive, or reactive. And they can cause a significant detrimental effect to the public, worker, co-worker, or environment. Although, in addition, some substances are not hazardous under a normal operational condition, they may cause a harmful situation under an extreme condition or in a circumstance with other materials. Thus, all hazards and their characteristics in a facility should be thoroughly examined and addressed. It can be divided into three types of the hazards related to the chemical hazards:

a. Chemical risk cause by inherent chemical properties, which affect occupational health or the environment;

b. Chemical risk produced by a radioactive material; and

c. Plant conditions such as fire or explosion (caused by chemical materials) which affect the safety of radioactive materials;

Interestingly, NRC does not regulate chemicals, but verifies interactions between chemicals and NRC-licensed nuclear materials and equipment. Those interactions may mislead to loss of a licensed material, degradation of equipment, and loss of containment or confinement.

Considerations to establish a methodology on the chemical safety in terms of chemical information, chemical safety evaluation, and assessment would be discussed for the purpose of chemical safety in a pyroprocess facility.

Acknowledgement

This work was supported by National Research Foundation of Korea (NRF)
(NRF-2017M2A8A5015083).

REFERENCES

[1] S.-I. Moon, W.-M. Chong, G.-S. You, J.-H. Ku, H.-D. Kim, Y.-K. Lim, H.-S. Chang, Preliminary safety study of engineering-scale pyroprocess facility, Nuclear Engineering and Technology 46 (2014) 63-72.

[2] NUREG-1601, Chemical Process Safety at Fuel Cycle Facilities, U.S. Nuclear Regulatory Commission(1997).

A Study on Characteristics of Airborne Materials for Pyroprocess Using MELCOR

Siwan Noh[1*], Jaehoon Lim[1], Hongrae Jeon[1], Jae-Uk Shin[2], Seok-Jun Seo[1], Woo Jin Jo[1], Gil Sung You[1], and Hyo Jik Lee[1]

[1]Korea Atomic Energy Research Institute, 111, Daedeok-daero 989beon-gil, Yuseong-gu, Daejeon, Republic of Korea

[2]Aritec, 40, Samsung 1-ro 1-gil, Hwaseong-si, Gyeonggi-do 18449, Republic of Korea

[*]snoh@kaeri.re.kr

1. Introduction

As unsealed radioactive materials are treated in pyroprocess, airborne materials may occur in a facility. The airborne materials are diffused as aerosol and vapor by aerodynamic process including forced flow, deposition, agglomeration, and by condensation/evaporation. The diffusion of the materials in a pyroprocess facility can cause contamination of hot cells, operation rooms, flow systems and equipment, and off –site effluent. Thus, it is important to assess the behavior of airborne materials in the facility. In this study, basic characteristics of airborne materials for pyroprocess are assessed using MELCOR code [1] to produce data as a basis of assessment for a specific facility in the future.

2. Materials and Methods

2.1 MELCOR modeling

MELCOR is a fully integrated, engineering-level computer code that models the progression of severe accidents in light water reactor nuclear power plants. Because MELCOR model the behavior of airborne radioactive materials by RN (RadioNuclide) package, however, MELCOR can be applied to pyroprocess facilities. In this study, CVH (Control Volume Hydrodynamics), FL (Flow Path), HS (Heat Structures), and RN (RadioNuclide) packages of MELCOR are used. In order to assess characteristics of airborne materials, an arbitrary hot-cell and ventilation system are modeled as Fig. 1. The volume No. 201 of the figure is location of initial airborne source term and the volume No. 901 remains in atmospheric pressure. It is assumed that temperature in the all location of the modeled system remains in room temperature.

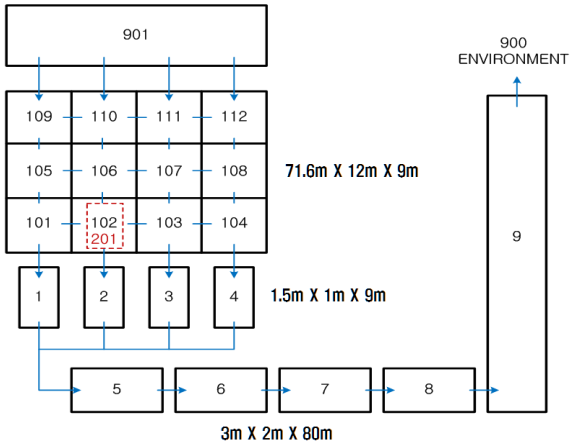


Fig. 1. MELCOR modeling of arbitrary hot-cell and ventilation system for parametric study.

2.2 Parametric study

In order to identify characteristics of airborne materials, parametric study is performed in this study. Velocity of ventilation flow, initial state of source term, and aerosol particle size are selected as parameter. In the parametric study, changes of deposition fraction and off-site release fraction are observed by changing the selected parameters. Table 1 shows the initial conditions for the parametric study.

3. Results and Discussion

Fig. 2 shows the one example result which shows mass in each volume section for 1 kg of initial Cs source term by time (vapor, 10m/s). Fig. 3 shows the one example result which shows deposited mass in all volume sections for 1 kg of initial Cs source term by time (10 μm aerosol, 10 m/s). Table 2 shows the result of parametric study. According to the results, deposition fraction of the airborne materials largely depends on the flow velocity, and aerosols whose size is

below 10 μm are hardly deposited on the structures for 10 m/s of flow velocity.

Table 1. Initial conditions for the parametric study

Parameter	Value	Fixed condition
Flow velocity	1 m/s	Cs 10 μm aerosol
	5 m/s	
	10 m/s	
Initial state of source term	vapor	Cs 10 m/s
	0.25 μm aerosol	
	0.88 μm aerosol	
	3.00 μm aerosol	
	10 μm aerosol	
Element	Cs (aerosol)	10 μm aerosol 10 m/s
	Xe (noble gas)	

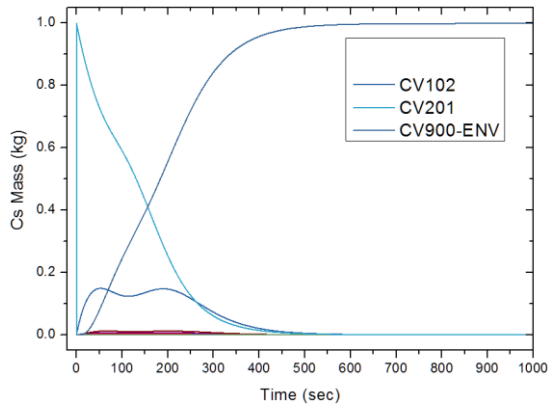


Fig. 2. Example result which shows mass in each volume section for 1kg of initial Cs source term by time (vapor, 10m/s).

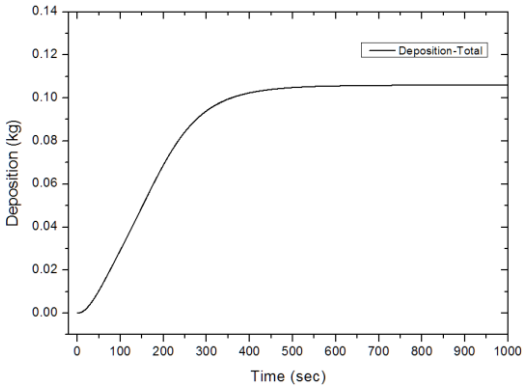


Fig. 3. Example result which shows deposited mass in all volume sections for 1 kg of initial Cs source term by time (10 μm aerosol, 10 m/s).

Table 2. Result of the parametric study

Value	Fixed condition	Deposition fraction
1 m/s	Cs 10 μm aerosol	0.628
5 m/s		0.233
10 m/s		0.106
vapor	Cs 10 m/s	0.0019
0.25 μm aerosol		0.0019
0.88 μm aerosol		0.0020
3.00 μm aerosol		0.0083
10 μm aerosol		0.106
Cs (aerosol)	10 μm aerosol 10 m/s	0.106
Xe (noble gas)		0

4. Conclusion

In pyroprocess facilities, it is important to predict the behavior of airborne materials. Thus, the study on characteristics of airborne materials for pyroprocess is performed using MELCOR code. Changes of deposition fraction of the materials are observed by changing of ventilation flow, initial state of source term, and aerosol particle size. According to the results, deposition fraction of the airborne materials largely depends on the flow velocity, and aerosols whose size is below 10 μm are hardly deposited on the structures for 10 m/s of flow velocity. The results of this study will be used in design and safety assessment for pyroprocess facilities.

ACKNOWLEDGEMENT

This work was supported by Nuclear Research & Development Program of National Research Foundation of Korea (NRF) funded by Minister of Science, ICT and Future Planning (MSIP).

REFERENCES

[1] L.L. Humphries, R.K. Cole, D.L. Louie, V.G. Figueroa, and M.F. Young, MELCOR Computer Code Manuals, SAND2015-6691R, 2015.

Thermal Analysis for Spent Nuclear Fuel Temporary Storage System in Pyroprocessing Facility

Jaehoon Lim*, Seung Nam Yu, Seok-Jun Seo, Ho Hee Lee, Won Myung Choung, Woo Jin Jo, Hongrae Jeon, and Hyo Jik Lee

Korea Atomic Energy Research Institute, 111, Daedeok-daero 989beon-gil, Yuseong-gu, Daejeon, Republic of Korea

*jhlim85@kaeri.re.kr

1. Introduction

A temporary storage system is needed to safely store the spent nuclear fuel assemblies until the process starts after the SNF (Spent Nuclear Fuel) assemblies are brought into the pyroprocessing facility.

In this paper, thermal analysis was performed on an imaginary SNF storage vault system using the concept of cooling by using natural convection.

2. Analysis Model for Spent Nuclear Fuel Temporary Storage System

The natural convection cooling system is economical and efficient because it does not use forced convection using power. The natural convection cooling system is applied to MACSTOR (Modular Air Cooled STORage) which is interim storage facility constructed at Wolsong nuclear power plant.

In case of applying this natural convection cooling system to pyroprocessing facility as a temporary storage system, it should be designed so that the decay heat generated from the SNF is sufficiently cooled because it is necessary to maintain the temperature of SNF cladding and concrete to be lower than the limit temperature.

In this paper, thermal analysis was performed on the present SNF storage vault system to verify its cooling capability.

ANSYS CFX, a commercial computational fluid dynamics analysis tool, is used to obtain the mass flow of the inlet and outlet and MELCOR is used to obtain the cladding and concrete temperature.

The established analysis model for ANSYS CFX is shown in Fig. 1. The dimension of the present temporary storage system is shown in Table 1.

The established thermal analysis model using MELCOR are shown in Fig. 2. The heat transfer of the present SNF temporary storage system is mainly performed by the flow from the inlet to the outlet. In addition, the heat conduction to the upper space which is a hot cell with air atmosphere is considered in the present analysis model.

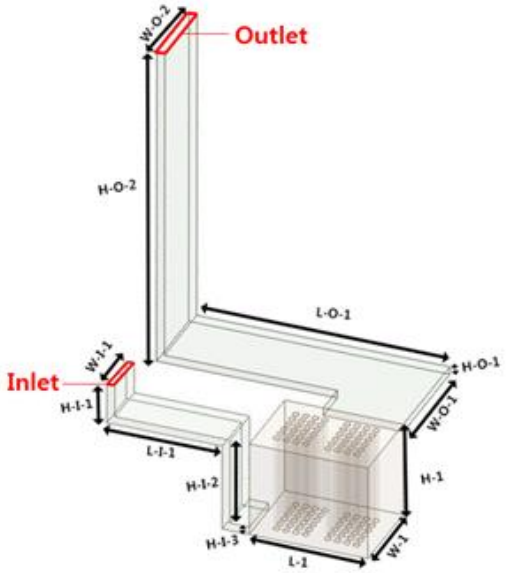


Fig. 1. Analysis domain of ANSYS CFX (flow only).

Table 1. Main dimension of the present temporary storage system

W-1(in Fig. 1)	7.4 m
L-1 (in Fig. 1)	5.5 m
H-1 (in Fig. 1)	5.5 m
W-I-1	3,000
L-I-1	7,200
H-I-1	2,500
H-I-2	5,500
H-I-3	500
W-O-1	7,200
W-O-2	5,000
L-O-1	15,800
H-O-1	500
H-O-2	20,500

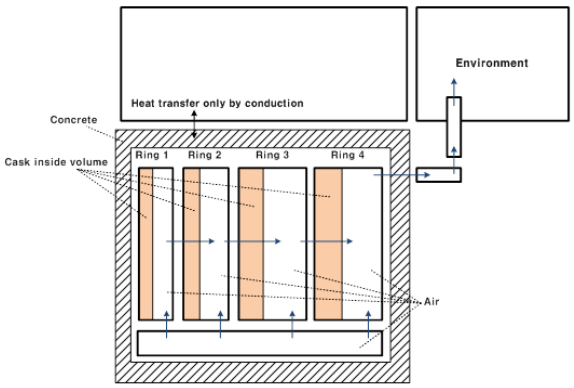


Fig. 2. Analysis domain of MELCOR (heat transfer).

The initial and boundary conditions for the present analysis are shown in Table 2.

Table 2. Initial and boundary conditions

Inlet/outlet boundary condition	Opening (1 atm)
Ambient temperature	30.7°C
Heat flux of SNF	140.591 W/m^2 (=1.06 kW/SNF)

3. Numerical Results

The analysis results are shown in Table 3. The resulted cladding temperature is compared with the temperature limit of the interim dry storage system of Wolsong nuclear power plant [1] and the resulted concrete temperature is compared with the temperature limit of ACI 349-06 [2].

Table 3. Maximum temperature during normal operating condition

Location	Maximum Temperature	Temperature limit
Cladding	118.8°C (21% margin)	150.5°C [1]
Concrete	40.5°C (37% margin)	65.0°C [2]

As a result, the resulted cladding and concrete temperature are lower than those of the limit values. Therefore, it is concluded that there exists sufficient temperature margin compared to those temperature limit values.

However, the present facility is designed at normal air atmosphere including moisture, not dry air atmosphere. Despite the short storage period (up to one year), it is considered necessary to further examine whether the application of the dry air atmosphere is necessary, such as the long-term dry storage facility of Wolsong nuclear power plant.

4. Conclusion

It was investigated that the imaginary SNF storage vault system for pyroprocessing facility using the concept of cooling by using natural convection. Computational flow and thermal analysis were conducted to verify its cooling capability. As a result, it was concluded that there exists sufficient temperature margin between the obtained maximum temperature and those temperature limit values. Application of the dry atmosphere is required to be discussed in the future and further analysis for the accident condition will be needed to be conducted.

REFERENCES

[1] Kim, Y. J, "Preliminary Study for the Evaluation of the Safety of Spent Nuclear Fuel in Dry Storage System in Wolsong," Korea Radioactive Waste Society Conference, Oct. 2015.

[2] ACI 349-06, Code Requirements for Nuclear Safety-Related Concrete Structures and Commentary, Appendix E - Thermal considerations.

Preliminary Safety Evaluation of Nuclear Criticality in a Large-scale Pyroprocess Facility

Woo Jin Jo*, Seok-Jun Seo, Hun Suk Im, Hongrae Jeon, Siwan Noh, and Hyo Jik Lee

Korea Atomic Energy Research Institute, 111, Daedeok-daero 989beon-gil, Yuseong-gu, Daejeon, Republic of Korea

*wjjo@kaeri.re.kr

1. Introduction

Korea Atomic Energy Research Institute (KAERI) has been developing a pyroprocess technology to reduce the waste volume and recycle some elements in a spent nuclear fuel. Because the operation with some fissionable materials such as pyroprocess operations may cause very high risks of criticality accident resulting in high radiation doses for facility worker or collocated worker, the safety evaluation of nuclear criticality is prerequisite to pyroprocess facility design. However, there are few published studies on the criticality evaluation for the pyroprocess facility due to lack of the facility information. KAERI conducted the preliminary conceptual (pre-conceptual) design of the large-scale pyroprocess facility. Preliminary safety assessment of nuclear criticality was evaluated using the pre-conceptual design data and SCALE/KENO code [1].

2. Nuclear criticality requirements

In Korea, article 90, 91, and 99 of enforcement regulations of Nuclear Safety Act require that the fuel storage, handling, and operation systems must be designed to be maintained subcritical [2]. NRC regulation also demand that the risk of criticality accidents must be limited by assuring that under normal and credible abnormal conditions, all nuclear processes are subcritical, including use of an approved margin of subcriticality for safety [3]. The table 1 shows the application of regulation for nuclear criticality safety.

Table 1. Application of regulation for nuclear criticality safety

	Application
Regulation	• Article 90, 91, 99 of the Enforcement regulations of Nuclear Safety Act • Article 5(7) of the Enforcement rule of the Radiation Safety Criteria • 10CFR Part 70 subpart H
Guide	• NUREG-1520 (Rev.2), • REG. Guide 3.4, 3.71 • IAEA Safety Standard No. NS-R-5 • DOE-STD-3007 • ANSI/ANS-8.1, 8.3, 8.15, 8.19, 8.20, 8.22, 8.23, 8.26

3. Validation of calculation method

For use in safety related analysis, the ability of a calculational methodology to accurately predict the subcriticality of a system must be well understood. The understanding of a calculational methodology's bias in predicting subcritical systems is obtained through the validation process. Validation includes identification of the difference between calculated and experimental results. This difference, called the bias, and the uncertainty associated with the bias are used in combination with additional subcritical margin to establish an upper safety limit (USL) [4]. In this study, the USL was set by following equation:

$$\mathrm{USL} = 1.0 + \mathrm{Bias} - \sigma_{bias} - \Delta_{SM} - \Delta_{AOA} \quad (1)$$

Where the critical experiments are assumed to have a k_{eff} of unity, the bias is calculated as the difference between the calculated k_{eff} and the critical experiment modeled. The statistical uncertainty in the bias is represented by σ_{bias} and the subcritical margin is represented by Δ_{SM}. The term Δ_{AOA} is an additional subcritical margin to account for extensions in the area of applicability. The following condition must be demonstrated for all normal and credible abnormal operating conditions:

$$k_{calc} + 2\sigma_{calc} < USL \quad (2)$$

Where k_{calc} is the calculated k_{eff} returned by the method and σ_{calc} is the uncertainty. In this study, SCALE/KENO Monte Carlo code was used for calculation of k_{eff} and uncertainty. Critical experiments from the International Handbook of

Evaluated Criticality Safety Benchmark Experiments (IHECSBE) are used for validation of calculation [5]. Over 350 cases are used in validation of KENO code and USL was determined. As a result of validation process, k_{eff} should be satisfied the following condition for being subcritical:

$$k_{eff} = k_{calc} + 2\sigma_{calc} < 0.9419 \quad (3)$$

4. Evaluation objects

According to the general arrangement of large-scale pyroprocess facility which was developed from pre-conceptual design, temporary spent nuclear fuel assembly (SFA) storage vault and product (U ingot and U/TRU ingot) storage cell which has a high priority for the nuclear criticality safety were evaluated. The capacity of temporary SFA storage vault is up to 48 SFAs corresponding to 20 tHM. For the storage of product such as U ingot and U/TRU ingot, KAERI developed the vessel consists of inner-canister and container. Design requirements of product storage cell demand that 1 year of production for U ingot and 1 quarter for U/TRU ingot should be temporary stored. Thus, the amount of containers produced by designed storage container is 180 and 13, respectively. Source term were calculated by material flow sheet of pyroprocessing and ORIGEN code. Normal condition and abnormal condition which means flooding were evaluated respectively.

5. Results

Table 2 and 3 shows the results of k_{eff} of temporary SFA storage vault and product storage cell, respectively. All area indicates being subcritical under the normal and abnormal condition by calculated k_{eff} and equation (3).

Table 2. Calculated k_{eff} of temporary SFA storage vault

	Standard SFA (PLUS7, 10 years cooling)	Fresh fuel(PLUS7)
Normal	0.126056 ± 0.000093	0.15717 ± 0.00012
External flooding	0.34487 ± 0.00024	0.51832 ± 0.00027
Internal and external flooding	0.58022 ± 0.00033	0.91645 ± 0.00036

Table 3. Calculated k_{eff} of product storage cell

	U ingot container	U/TRU ingot container (1 quarter)	U/TRU ingot container (1 year)
Normal	0.26472 ± 0.00014	0.59457 ± 0.00033	0.62865 ± 0.00031
External flooding	0.33472 ± 0.00023	0.64929 ± 0.00033	0.67895 ± 0.00039
Internal and external flooding	0.35154 ± 0.00023	0.69687 ± 0.00034	0.70626 ± 0.00036

6. Conclusion

Criticality evaluation concerning the high priority area of large-scale pyroprocess facility was performed by pre-conceptual design data and Monte Carlo codes. The results indicate that there are no criticality risks corresponding to temporary SFA storage vault and product storage cell under any condition. However, the nuclear criticality safety of a storage arrangement requires a very careful contingency analysis as well as k_{eff} calculation. To reach a criticality safety conclusion requires a detailed nuclear criticality safety evaluation where credible contingencies are evaluated.

REFERENCES

[1] ORNL/RSICC, SCLAE 6.1.2, 2013.

[2] ROK, Enforcement rule of the Radiation Safety Criteria, 2016.

[3] USNRC, Additional requirements for certain licensees authorized to possess a critical mass of special nuclear material, 10CFR 70 Subpart H.

[4] USNRC, Guide for validation of nuclear criticality safety calculational methodology, NUREG/CR-6698, 2001.

[5] W.J. Marshall and B.T. Rearden, Criticality Safety Validation of SCALE 6.1, ORNL/TM-2011/450, 2011.

Wall-tube Flange Refurbishment for Securing Gas-tightness of Telemanipulators in the ACPF Hot-Cell

Kiho Kim

Korea Atomic Energy Research Institute, 111, Daedeok-daero 989beon-gil, Yuseong-gu, Daejeon, Republic of Korea

khkim5@kaeri.re.kr

ACPF (Advanced spent fuel Conditioning Process Facility) was constructed in the basement of the Irradiated Materials Examination Facility (IMEF) at KAERI (Korea Atomic Energy Research Institute) in 2005. ACPF, an alpha-gamma type hot-cell, was operated in an air atmosphere. This hot-cell had two cells: a maintenance cell for repairing damaged equipment or devices and a process cell for conducting experiments. In 2015, this hot-cell was refurbished to demonstrate an electrolytic reduction process of pyroprocessing in an argon atmosphere. One of the major features of the ACPF refurbishment was the construction of an additional argon cell inside the ACPF process cell with an air atmosphere. Relevant remote handling systems including telemanipulators and an argon supply system implemented to make the argon cell more functional.

The ACPF hot-cell has a configuration of 8.1 x 2.0 x 3.4 (LxWxH) m and five shielding window workstations. Each workstation is equipped with a pair of telemanipulators. Each telemanipulator consists of three modules: a master arm (installed outside the cell), a through-tube (penetrated and installed through the wall-tube), and a slave arm (installed inside the cell). The ACPF hot-cell before refurbishment was equipped with one-piece telemanipulators, in which theses three modules were connected together in one body. In an one-piece telemanipulator, these modules cannot be remotely separated in modules after being installed in the cell. Thus, when the slave arm is broken inside the cell, it is not possible to remotely replace it by a new one inside the cell without having a whole telemanipulator outside of the cell. To overcome remote replacement of the one-piece telemanipulator, three-piece telemanipulators were applied to the refurbished ACPF hot-cell in 2015. The master arm, through-tube, and slave arm of the three-piece telemanipulator are connected together through modules, and can also be separated into modules. The broken slave arm of three-piece telemanipulator, as the cell is active, can be replaced by a new one in a remote manner inside the cell without extracting the entire telemanipulator.

This technical note deals with the wall-tube flange refurbishment for replacing the one-piece telemanipulators by three-piece versions in the refurbished ACPF hot-cell. The gas tightness of the three-piece telemanipulator in the ACPF hot-cell is achieved through the contact between the wall-tube flange and the two o-rings seated in the through-tube flange. The wall-tube flange surfaces were rough and damaged after dismantling the one-piece telemanipulators from the ACPF hot-cell. The front surfaces of the wall-tube should be refurbished so that the tightness between the wall-tube flange and the through-tube flange can be secured. This refurbishment included the flange surface machining of the wall-tube such as drilling, tapping, grinding, and tightness identification in sequence. A total of ten wall-tube flanges were machined. For each wall-tube flange surface, six holes were accurately drilled and tapped at intervals of 60 degrees so that the through-tube flange of the telemanipulator can completely fit into the wall-tube flange. The flange surface was ground flat enough using specially designed tools to secure a complete gas-tightness. After completing the wall-tube flange machining, tightness tests were followed. Three-piece telemanipulators were installed through the refurbished wall-tube in the refurbished ACPF hot-cell. Currently, telemanipulators are under use by conducting various types of remote tasks in the refurbished ACPF hot-ell.

Development of a Virtual 3D Simulator Working With an Actual Hardware Testbed to Verify Element Technologies for Pyroprocessing Automation

Doyeon Kim*, Dongseok Ryu, Jongkwang Lee, Kiho Kim, and Jonghui Han

Korea Atomic Energy Research Institute, 111, Daedeok-daero 989beon-gil, Yuseong-gu, Daejeon, Republic of Korea

*doyeon1301@kaeri.re.kr

1. Introduction

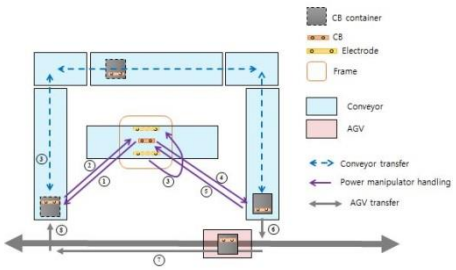
Pyroprocessing, a method to recycle spent fuels, has been studied at KAERI (Korea Atomic Energy Research Institute). The process should be performed in a hot cell due to high radiation. The human workers cannot access in the hot cell, and all operation should be done out of the hot cell by using remote devices. Thus, all procedures should be thoroughly verified in advance. Since the existing remote devices and procedures were complicate and difficult, simplification and automation of handling procedures were issued. The preliminary automation concept for integrated Pyroprocessing was proposed [1], and virtual 3D simulator was developed to verify the concept. However, the simulation assumed only ideal situation. The simulator was hard to show real physical behavior, especially for the case of hand over the basket. To overcome this problem, hardware in the loop simulation (HILS) were proposed [2].

In this study, a simulation framework for interlinking a virtual simulator and a real physical testbed is discussed to verify element technologies for Pyroprocessing automation.

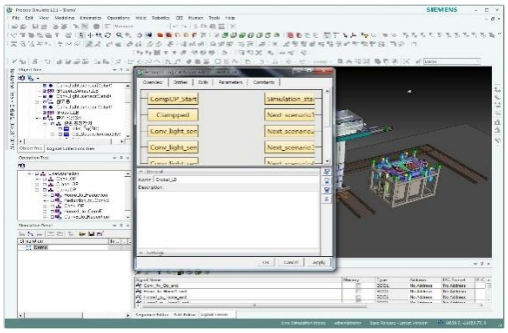
2. Virtual 3D simulator to verify element technologies for Pyroprocessing automation

The preliminary automation concept for integrated Pyroprocessing requires several element technologies, such as, transferring electrode, moving basket, replacing sensor module, and etc. An actual physical hardware testbed to verify the element technologies was integrated at KAERI. The testbed was composed of various handling devices, i.e., power manipulator, gripper, AGV (automated ground vehicle), and conveyor, so that it can performed experiment to move dummy baskets and electrode automatically. An example scenario using the handling devices was planned as shown in Fig. 1. (a).

A virtual 3D simulator for working with the real physical testbed is implemented by using Tecnomatix. The first step to construct a virtual environment is importing a 3D CAD data. The 3D data for the handling devices in testbed were prepared by using Solidworks 3D modeling software. Because the Tecnomatics only accepts JT format, the 3D models of the handling devices were converted to JT files. The kinematics of the handling devices was implemented, and logic block were defined to describe moving algorithm, as shown in Fig. 1 (b) [3].



(a) Example operation scenario to verify element technologies for Pyroprocessing automation



(b) Development of virtual 3D simulator using Tecnomatix

Fig. 1. Virtual 3D simulator to verify element technologies for Pyroprocessing automation.

In the 3D simulator, a virtual sensor was attached to mimic a real sensor on the handling device. The automation logics for the simulator can be driven by either the actual sensor data or the virtual sensor data, whereas the actual handling devices only works with

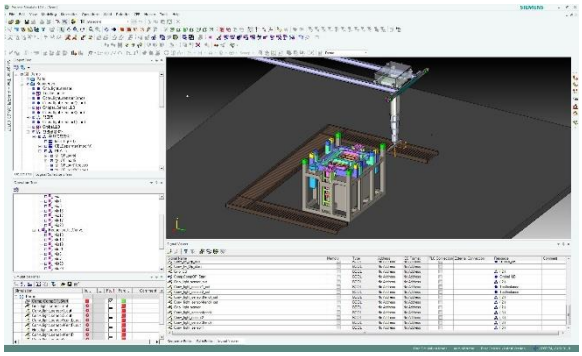
actual sensor. Similarly, the operation logic of each handling device can be simulated by logic block in Tecnomatix or actually controlled by the PLC controller on the hardware [2]. The operator monitors all the parameters on the simulation and the hardware status. For the running method of the simulation, the operator chooses the controller and the sensing data either virtual or actual, when the simulation starts.

3. Interlinking with an actual hardware testbed to verify element technologies for Pyroprocessing automation

Fig. 2 (a) shows the actual physical hardware testbed to verify the element technologies for Pyroprocessing automation, based on the experimental scenario as sown in Fig. 1 (a). The 3D simulator was implemented as same configurations of the testbed, as shown in Fig. 2 (b).



(a) Actual handling devices in the real physical testbed



(b) Virtual 3D simulator interlinking with the testbed

Fig. 2.Cyber physical experimental setup, using a virtual simulator and an actual testbed.

To interlink the simulator and the actual hardware, OPC (OLE for Process Control) communication was utilized. OPC is widely used in industrial fields for factory or plant automation. In this research, the sensing and control data was shared in one data base on the OPC server between the virtual simulator and the actual testbed in real time. Fig. 3 shows the control architecture to share the data for interlinking the virtual simulator and actual testbed. The selected memory addresses in the PLC controller were synchronized on the data base in OPC server. Tecnomatix also update data in 10 millisecond. In the virtual 3D simulator, the updated OPC variable was used signals to drive the simulation scenario.



Fig. 3. Control architecture for interlinking the simulator with actual hardwares.

4. Conclusion

In this paper, the virtual 3D simulator working with an actual hardware testbed was developed. Siemens Tecnomatix was used to integrate the 3D simulator for enhancing reliability of the simulation. CAD 3D models of the handling devices in the testbed were imported, and the kinematics and control logics were implemented. The simulation data were shared with the actual testbed via an OPC server. Finally, the developed virtual 3D simulator was interlinked to the actual hardware testbed. The integrated system will be utilized to perform experiments to verify element technologies for Pyroprocessing automation.

REFERENCES

[1] Dongseok Ryu, et al. "Framework to Develope a Preliminary Automation Concept for Integrated Pyroprocessing," Proc. of Korea Radioactive Waste Society 2016 Spring, pp. 151-2, 2016.

[2] Dongseok Ryu and Jongkwang Lee, "Virtual Verification using 3D Simulator for a Remote Operation Procedures in PRIDE," Proc. of 2016 International Pyroprocessing Research Conference, pp. 66, 2016.

[3] Dongseok Ryu, Sunghyun Kim, Jonghui Han, Jongkwang Lee, and Kiho Kim, “Development of a Virtual 3D Simulator to Evaluate Remote Operations in PRIDE, Proc. of the D&RS 2016, July 31-August 4, 2016, Pittsburgh.

Adaptability Study of Hybrid ISA-PSA Method on Safety of Pyroprocess Facilities

Gilsung You*, Seokjun Seo, Siwan Noh, Hongrae Jeon, Hyojik Lee, Woojin Jo, Hyunsook Im, Hohee Lee, Wonmyung Choung, Seungnam Yu, Jaehoon Lim, and Jeonghoe Ku
Korea Atomic Energy Research Institute, 111, Daedeok-daero 989beon-gil, Yuseong-gu, Daejeon, Republic of Korea
*yougil@kaeri.re.kr

1. Introduction

KAERI is being developed pyroprocessing technology for spent fuel recycling. For this it is necessary to establish the facility development technology [1]. In this paper the Hybrid ISA-PSA method developed by US NRC was introduced and studied the adaptability on safety of pyroprocess facilities.

2. Safety study and Hybrid ISA-PSA method of US NRC

2.1 Safety Study of US NRC for SF recycling facilities

US NRC recommends and regulates fuel cycle facilities to follow ISA method through the code 10CFR70 [2, 3]. The main reason to use the ISA method is that the fuel cycle facilities have some chemical processes which are different from the nuclear reactors.

Recently US NRC is studying and suggesting the consequence thresholds and qualitative risk bins by risk indexing method for SF recycling facilities as following Table 1 and 2 [4-7].

Table 1. Consequence thresholds

	Workers	Offsite Public	Environment
Very High Consequence Event	RD>>1Sv CD>endanger life	RD>1Sv CD=endanger life	Radioactive release >500,000 x Table 2 of 10CFR20, Appendix B
High Consequence Event	RD>1Sv CD>endanger life	RD>0.25Sv sol U intake>30mg CD=long-lasting health effects	Radioactive release >50,000 x Table 2 of 10CFR20, Appendix B
Intermediate Consequence Event	RD>0.25Sv CD=long-lasting health effects	RD>0.05Sv CD=mild transient health effects	Radioactive release >5,000 x Table 2 of 10CFR20, Appendix B
Low Consequence Event	Accidents of lower radiological and chemical exposures than those above in this column	Accidents of lower radiological and chemical exposures than those above in this column	Radioactive releases producing lower effects than those referenced above in this column

Table 2. Qualitative risk bins

		Likelihood (Events Per Year)			
		Very Highly Unlikely (<1E-6)	Highly Unlikely (<1E-5)	Unlikely (<1E-4)	NOT Unlikely (>1E-4)
Consequence	VHCE	Acceptable	Not Acceptable	Not Acceptable	Not Acceptable
	HCE	Acceptable	Acceptable	Not Acceptable	Not Acceptable
	ICE	Acceptable	Acceptable	Acceptable	Not Acceptable
	LCE	Acceptable	Acceptable	Acceptable	Acceptable

US NRC is considering several methods for evaluation of SF recycling facilities including ISA and PSA, and suggests using the Hybrid ISA-PSA method for present time and the PSA method for the future [7].

2.2 Hybrid ISA-PSA method of US NRC [7]

The Hybrid ISA-PSA method, suggested by US NRC, processes according to the following steps. :

- Quantify all analyses to the extent practical and as supported by the state of the art.
- Use a quantified ISA to identify all credible accident sequences.
- Identify a subset of HCEs based upon attributes that significantly increase consequences above the high-

consequence thresholds, and designate this subset as VHCEs.
- Apply safety controls to render the likelihood of intermediate events, HCEs, and VHCEs acceptable.
- Conduct probabilistic risk analyses on HCEs and VHCEs to the extent practicable and consistent with the state of the art.
- Use the PRA results to aggregate risk from a subset of accident sequences for potential receptors.
- Adjust risk as needed to meet the appropriate NRC risk limits and criteria.
- Minimize the total risk to receptors beyond the minimum requirements.
- Identify GDC and/or other controls that reduce the risk beyond the minimum requirements as items supporting safety for accident situations.
- Require routine updates to the safety analyses, and establish a facility-specific program.
- Identify processes for ranking the various IROFS and events according to their risk importance.
- Identify processes for risk-informed safety review, inspection, and surveillance programs.

3. Adaptability of Hybrid ISA-PSA method to pyroprocess facilities

A PSA method needs a large data base including equipment reliability and test data, etc. For pyroprocess facilities, these data are too small when compared to other fuel cycle facilities. Pyroprocess facilities have some dry type process equipment and don't require large amounts of cooling water to prevent accidents. Although large amounts of radioactive fission products are stored and processed in hot cells, these fission products do not have large energy sources that could affect the integrity of hot cell walls. In this manner pyroprocess facilities are similar to wet recycling facilities described in [8]. PSA can give an insight to total risk of facility, but ISA can also be useful to determine the needed safety requirements for pyroprocess facilities. It can also give semi-quantitative risk values and a limited risk insight. The inspection processes for pyroprocess facilities can be risk informed by focusing resources on IROFS based on the ISA, which have similar properties to wet recycling facilities described in [8].

According to above considerations, it would be concluded that sole ISA, not Hybrid ISA-PSA, can be a good method to evaluate the safety of pyroprocess facilities.

4. Conclusions

In this paper, the Hybrid ISA-PSA method, suggested by US NRC, for safety evaluation of SF recycling facilities was introduced and studied the adaptability to pyroprocess facilities. According to this study, it is concluded that sole ISA, not Hybrid ISA-PSA, can be a good method to evaluate safety of pyroprocess facilities.

Acknowledgements

This study was supported by the Ministry of Science, ICT and Future Planning through its National Nuclear Technology Program**.**

REFERENCES

[1] Gil-Sung You, et al., Concept and safety studies of an integrated pyroprocess facility, Nuclear Engineering Design, No. 241, pp. 415～424, (2011).
[2] US NRC, "Integrated safety analysis guidance document, " NUREG-1513 (2001).
[3] US NRC, "Standard review plan for the review of a license application for a fuel cycle facility," NUREG-1520-rev.2 (2015).
[4] US NRC, "Regulatory option for licensing facilities associated with the Global Nuclear Energy Partnership," SECY-07-0081 (2007).
[5] US NRC, "Regulatory structure for spent fuel reprocessing," SECY-08-0134 (2008).
[6] US NRC, "Update on reprocessing regulatory framework summary of gap analysis," SECY-09-0082 (2009).
[7] US NRC, "Draft regulatory basis for licensing and regulating reprocessing facilities," SECY-11-0163 (2011).
[8] NEI, "Integrated Safety Analysis: Why it is appropriate for fuel recycling facilities," NEI white paper attachment (2010).

Review of Spent Nuclear Fuel Dry Storage Demonstration Programs in US

Sanghoon Lee[1] and Daesik Yook[2]

[1]Keimyung University, 1095 Dalgubeol-daro, Dalseo-gu, Daegu, Republic of Korea

[2]Korea Institute of Nuclear Safety, 62 Gwahak-ro, Yuseong-gu, Daejeon, Republic of Korea

*shlee1222@kmu.ac.kr

1. Introduction

US have carried out several notable demonstration programs for the initiation and license extension of dry storage of spent nuclear fuel (SNF). At the very early stage of dry storage, the demonstration programs were focused on the proof of the safety of dry storage systems and a demonstration project named dry cask storage characterization project (DCSCP) was performed for the license extension of low burn-up fuel dry storage. Currently, a demonstration program for the license extension of high burn-up fuel dry storage is under way and it is expected to continue at least 10 years from now. Korea has not begun the dry storage of PWR fuel yet and those programs of US can be a good reference and lessons to safely begin and operate dry storage in Korea. In this paper, the past and current of the demonstration programs of US are analyzed and several recommendations are provided on the demonstration programs for dry storage of spent nuclear fuel in Korea.

2. Regulations on SNF Integrity

2.1 Storage regulations

The regulatory requirements on the integrity of spent nuclear fuel are stipulated in 10 CFR 72, NRC Interim Staff Guidance (ISG) and NUREG documents. 10 CFR 72.122(h) states that (1)The spent fuel cladding must be protected during storage against degradation that leads to gross ruptures or the fuel must be otherwise confined such that degradation of the fuel during storage will not pose operational safety problems with respect to its removal from storage, and (5) The high-level radioactive waste and reactor-related GTCC waste must be packaged in a manner that allows handling and retrievability without the release of radioactive materials to the environment or radiation exposures in excess of part 20 limits. The definition of the term “retrievability” is defined in ISG-2 which was recently revised in 2016 to accommodate the retrieval of spent fuel in canister and storage cask. The requirements on the retrievability do not apply to the accident conditions.

2.2 Transportation regulations

In the transportation regulation, 10 CFR 71, the requirements on the integrity of spent nuclear fuel is not explicitly stipulated. In the regulations for fissile material transportation, 10 CFR 71.55, it states that (1) The contents would be subcritical; (2) The geometric form of the package contents would not be substantially altered in normal conditions of transportation. As the degradation of fuel cladding and other structural parts of fuel assembly may lead to the gross rupture of fuel assembly in the presence of transportation loading such as vibration, the requirements on transportability shares some aspects with the requirements on retrievability.

3. SNF Dry Storage Demonstration Program

3.1 Demonstration at early stages

The purpose of the demonstration programs at early 1980’s was the verification of the performance and safety of the dry storage systems and set-up of the dry storage procedure at reactor site. This early stage demonstration was initiated by the Nuclear Waste Policy Act of 1982. It includes the demonstration with the Sealed Storage cask (Fig. 1) at Nevada Test Site (NTS) and the demonstration performed at Surry nuclear power plant with CASTOR V/21 cask, demonstration at H.B. Robinson power plant with NUHOMS system and the demonstration at INEEL(currently INL) with several types of casks (Fig. 3). Through these demonstration programs, the DOE staffs successfully validated and verified their computational model for shielding and computational fluid dynamic codes such as COBRA-SFS, HYDRA.

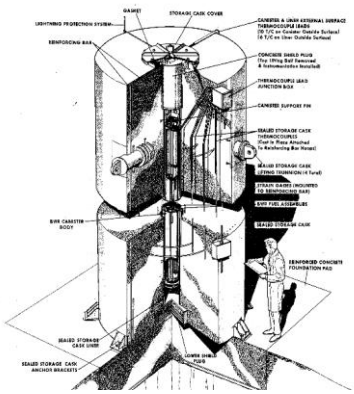


Fig. 1. Sealed Storage Cask used in NTS demo.



Fig. 2. Demo casks stored at INTEC of INL [1].

3.2 Dry Cask Storage Characterization Project

The purpose of DCSCP [2] was to produce data to support the license renewal of dry storage of SNF after the first 20 years of storage period. DOE, NRC and EPRI opened the CASTOR V/21 cask which was stored at INL after the first stage demonstration and performed examinations on the cask systems and the fuel elements to find any clue of degradation that can hinder the extension of license for dry storage. The Cask system and fuel assembly exterior were examined at INL and the fuel rods were examined at ANL for residual creep life and any sign of hydride reorientation. It was concluded that there was no sign of significant degradation of fuel and cask system and the license could be extended. However, the facts that the fuel was loaded dry in a hot-cell omitting the process of vacuum drying, and the 'before-storage' fuel condition was not characterized are the limitation of the data obtained by DCSCP.

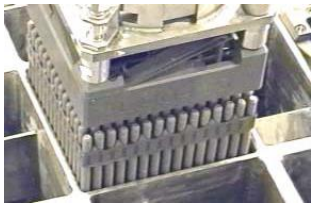


Fig. 3. Fuel assembly visual inspection at INL.

3.3 The High Burnup Confirmatory Data Project

Currently US DOE leads a joint project with NRC and EPRI named as high burnup confirmatory data project (HBU-CDP) [3]. The purpose of this project is to generate technical data to support the licensee extension of high burnup fuel dry storage. It is now under way and will continue at least 10 years from now. This demo focuses on the data acquisition during the loading and drying process of dry storage, which were missed in earlier demo, DCSCP. For this purpose, the lid of TN-32 cask were modified so that instruments for temperature and gas monitoring can be inserted into the cask (Fig. 4). 4 different types of fuel will be loaded into the cask. Sister rods, which have almost identical history and material with demo fuels were selected and sent to DOE labs for destructive examinations to characterize the 'before-storage' condition of the demo fuel's cladding. The loading of the demo cask is planned to start at latter part of 2017.

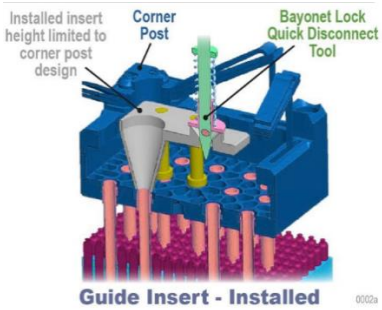


Fig. 4. Instrumentation for thermocouple insert.

4. Conclusions

Since Korea has not started the dry storage of PWR fuel yet, those demonstration programs of US can of great lessons to learn. Korea also needs such demonstration programs for various purpose: 1) to confirm the safe storage conditions of SNF that can guarantee retrievability of SNF after storage 2) to monitor the integrity of spent fuel in case the storage period is extended 3) to verify the performance and quality of the domestic storage systems.

REFERENCES

[1] B. Hanson, H. et al, Gap analysis to support extended storage of used nuclear fuel, Rev. 0, US Department of Energy (2012).
[2] Electric Power Research Institute, 1002882, Dry cask storage characterization project – final report (2002).
[3] EPRI, High burnup dry storage cask research and development project – final test plan (2014).

Safety Strengthening for On-Site Spent Nuclear Fuel Dry Storage Facilities

Sunghwan Chung* and Jwayoung Kim

Central Research Institute, Korea Hydro & Nuclear Power Co., Ltd., 7, 1312-gil, Yuseong-daero, Yuseong-gu, Daejeon, Republic of Korea

*sunghchung@khnp.co.kr

1. Introduction

Intentional aircraft crashes on containment and fuel buildings of new NPPs are regulated to be assessed as raising protection issues of national key facilities including nuclear power plants (NPPs) since 911 terrorist attacks in the Unites States, but the regulatory requirements for on-site spent nuclear fuel (SNF) dry storage facilities are not yet provided. Each country is preparing measures to cope with aircraft crashes at SNF dry storage facilities. Here, regulations and regulatory policies to strengthen the safety of on-site SNF dry storage facilities against intentional aircraft crashes were analyzed.

2. Subject

2.1 Intentional aircraft crash

Anxiety about large-scale human damage, economic loss and severe environmental pollution to accidents of NPP facilities caused by terrorism is very high, but vulnerable facilities to actual terrorism are oil refineries or chemical plants that are weaker structures and security than NPPs. Terrorists select targets with a high probability of success (success means total number of casualties or scale of building destruction), but it is estimated that NPP facilities including SNF dry storage facilities are unlikely to be selected as a terrorist target due to strong structures made of reinforced concrete with high security. Aircraft crash resistance to the SNF dry storage facilities is relatively advantageous compared to other NPP facilities because it is difficult to hit correctly by an aircraft, only some SNF storage casks are destroyed, the damage to facility is local and the accident is easy to catch. Whether or not to assess aircraft crashes against NPP facilities differs from country to country, and Europe often assesses the crash of light aircraft or military aircraft. Since 911 terrorist attacks and Fukushima accidents, there is a growing concern about Beyond Design Basis Accident (BDBA) or Beyond Design Basis Threat (BDBT), so there is a growing demand for increased safety against aircraft crashes.

2.2 United States

NRC requests an assessment of aircraft crashes against new NPPs, although BDBA including aircraft crashes are unlikely to occur unlike Design Basis Accident (DBA) and is not reflected in the design. However, since the SNF dry storage facilities are not to be assessed, NRC investigated problems of NPPs and notified them of Security Order for NPP's storage facilities in 2002. In addition to the requirements of 10CFR72 and 10CFR73, it is regulated under Security Order. In 2003, NRC carried out Security Assessment of NRC-regulated facilities to review the necessity of measures or safeguards in addition to Security Order. The assessment includes large commercial aircraft strikes against SNF dry storage facilities and various ground attacks. There is no urgent need to add to the security requirements of existing SNF dry storage facilities. As the security requirements of SNF dry storage facilities are complex and confusing, NRC has arranged through Federal Registers 72FR12705 (Design Basis Threat) and 74FR13935 (NPP Security Requirements). NRC added aircraft crash to Design Basis Threat (DBT) at 72FR12705 and said that there is no possibility of serious leakage of radioactivity due to aircraft crashes and there is no need for additional measures such as barrier installation. Regarding the requests for installation of external barriers for SNF dry storage facilities, NRC noted at 74FR13935 that aircraft crashes are military issues that the government must respond to and that it is possible to respond due to the Security Order to mitigate damage to NPPs. And NRC noted that it is not the duty of NPP operators. NRC said that as attacks to NRC-regulated facilities is not a responsibility of NPP operators, measures for aircraft crashes are not regulatory requirements and the regulation stipulates the actions

of NPP operators in order to minimize the damage of SNF dry storage facilities against aircraft crashes. NRC requires to establish a mitigation strategy for operating NPPs against aircraft crashes and specifies mitigation strategies and response procedures for aircraft crashes at 10CFR50.54(hh) in 2009. This provision includes NPP's mitigation strategies and precautionary measures for large fire and explosions when NPPs are subjected to potential aircraft crashes. 10CFR50.150 requires that structural/impact/fire assessments for the impact of aircraft crashes to new NPPs built after July 2009 shall be carried out. In this regard, NRC provided guidance and procedure on assessment of aircraft crashes.

2.3 Germany

Although the license for NPPs requires guarantee of suitable protection system, the responsibility of NPP operator is exempted because the war is the responsibility of national defense. It is not clear, however, whether terrorism by aircraft is regarded a war action. In the 1980s, the regulatory authority prepared guidelines for evaluation of aircraft crashes, basically a phantom-type military aircraft crash was assumed and collision-relate missiles, aviation fuel fire and vibration was considered.

2.4 IAEA

IAEA Safety Series No.SSR-2/1 subdivides the accident classification system, introduces Design Extension Conditions including intentional aircraft crashes that cover BDBA and major accident areas to exceed DBA, and requires accident prevention, accident mitigation, accident management, radiation mitigation measures and emergency response outside NPPs.

2.5 Domestic

Aircraft crash as an artificial accident to NPP facility is included in the design criteria for external factors in Article 13 of Reactor Rules. For intentional aircraft crashes, criteria for new NPPs are preparing and criteria for existing NPPs were established in accordance with 10CFR50.54(hh). Operators of NPPs shall submit Accident Management Plan including severe accident management plan for disasters in accordance with Article 20 of Nuclear Safety Act, and the scope of accident management is in accordance with Article 85-19 of Reactor Rules. According to NSSC Notice No.2016-2 (Detailed criteria for scope and assessment of accident management) accident management scope covers natural and artificial disasters including intentional aircraft crashes. Therefore, as on-site SNF dry storage facilities are the NPP-related facilities, Accident Management Plan shall be prepared and submitted in accordance with NSSC Notice No.2016-3 (How to prepare an accident management plan, published in June 2016) and precautionary measures and accident mitigation for aircraft crashes shall be taken.

Table 1. Regulatory requirements for aircraft crashes

Items		Domestic	US
Artificial aircraft crash		To assess according to crash probability	
Intentional aircraft crash	New NPPs*	Preparing	10CFR10.150
	Existing NPPs*	NSSC Notice No.2016-3	10CFR50.54

* including NPP-related facilities

3. Conclusion

In order to strengthen the safety of NPP facilities against intentional aircraft crashes, regulations for new domestic NPPs have been made like the United States, and operating NPPs shall establish Accident Management Plan for disasters including aircraft crashes against NPP-related facilities like on-site SNF fuel dry storage facilities and submit it to the Nuclear Safety and Security Commission in accordance with NSSC Notice No.2016-3.

REFERENCES

[1] US National Research Council, Making the Nation Safer : The Role of Science and Technology in Countering Terrorism, 2002.

[2] US National Academies of Science, Safety and Security of Commercial Spent Nuclear Fuel Storage, 2005.

[3] US Federal Register 72 FR 12705, Design Basis Threat, 2007.

[4] US Federal Register 74 FR 13935, Power Reactor Security Requirements, 2009.

[5] IAEA SS No.SSR-2/1(Rev.1), Safety of Nuclear Power Plants : Design, 2016.

[6] IAEA NSS No.4, Engineering Safety Aspects of Protection of Nuclear Power Plants against Sabotage, 2007.

Stepwise Approach on Spent Nuclear Fuel Integrity Evaluation R&D Work in Korea

Donghak Kook*, Jaeyong Kim, Yongsik Yang, and Changwhan Shin

Korea Atomic Energy Research Institute, 111, Daedeok-daero 989beon-gil, Yuseong-gu, Daejeon, Republic of Korea

*syskook@kaeri.re.kr

1. Introduction

The national plan on SNF management was announced by MOTIE in 2016. Dry storage business will be visualized after the relevant Act is approved soon. Safety evaluation on our domestic SNF is essential work in order to support the success of this coming business. Review on USA case, especially dividing burnup range, is very useful to establish our R&D strategy for the long time frame. The review result recommends that a stepwise approach on burnup range with low and high is desirable in Korean case.

2. Status of SNF Management

2.1 National Basic Plan by MOTIE

MOTIE (Ministry of Trade, Industry, and Energy) which is in charge of nuclear promotion and also radioactive waste management announced the Basic Plan of High-Level Radioactive Waste Management [1] and AEC (Atomic Energy Commission) approved the plan in 2016. Based on this plan, Storage, transportation and disposal business of spent nuclear fuel could be more tangible and implemented just after the relevant Act which is now tentative and waiting for Congress approval.

2.2 Urgency in storage business

SNF inventory database of KHNP (Korea Hydro and Nuclear Power) indicated that unloading PWR SNF from pool to dry storage should be started at least 2024 and 80% of SNF belong to the lower burnup level (less than 45 GWd/MtU) [2].

2.3 Importance of SNF integrity

Lessons learned [3] from foreign predecessors shows us the importance of SNF integrity evaluation because storage time frame is getting longer without visible disposal progress, there is almost no more chance to check SNF condition after the initial loading into the first dry storage, and uncertainty of SNF status after several decades storage could be a huge threat to SNF delivery from utility to the government, to long distance transportation and to safe handling before disposal packaging.

3. Reference on burnup consideration

A EPRI report [4] picture (Fig. 1) shows SNF cladding material degradation along burnup level. Data tendency in low burnup level (less than 45 GWd/MtU inside #2 line area) is easily predictable, however in high burnup range (from #2 to #4 line area), data dispersion & deviation is getting more significant along burnup increase. Regulatory history in USA has experience of two step approach on burnup range. Regarding to urgent PWR SNF dry storage, it is necessary to consider stepwise approach on R&D.

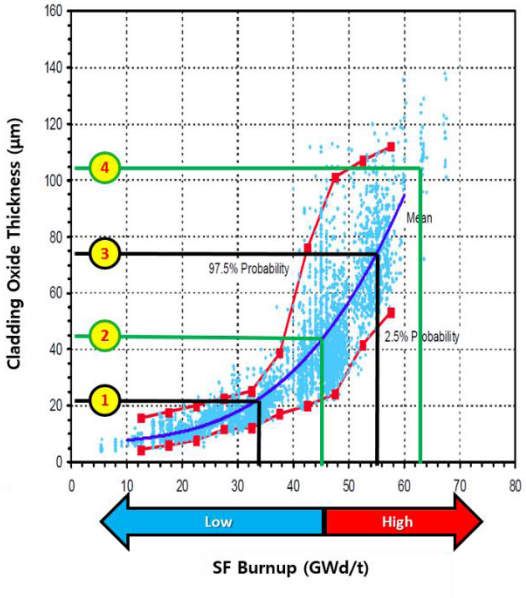


Fig. 1. SNF burnup vs cladding oxidation.

3.1 Low Burnup

SNF testing data in PNNL (Pacific Northwest National Lab.) before 1985 when the first commercial dry storage was started was concentrated on 33 GWd/MtU range with 45 GWd/MtU maximum data (Fig. 2) [5]. This means that majority of #1 data covers up to #2 area even though material degradation tendency is getting severe along burnup increase.

Type of Operating Conditions	Fuel Design	Rod-Average Burnup, MWd/kgM	Rod Pressure, psi
Upper Bound Operating Conditions	PWR 15 x 15	33	1707
		45	2416
	BWR 7 x 7	28	1094
Average Operating Conditions	PWR 17 x 17	33	1293
	BWR 8 x 8R	28	142

Fig. 2. USA Low Burnup SNF testing in 1980's.

3.2 High Burnup

The first high burnup SNF dry storage license with 20 years in USA will be expired in 2025, however SNF testing data in high burnup range is precious because hotcell work in laboratories is getting difficult with many reasons even though data dispersion is huge in this area. In order to support above license renewal, 'High Burnup Demo' by US DOE and EPRI [6] utilizes around 54 GWd/MtU level (#3) SNF and tries to cover up to #4 area. A recent research result [7] on SNF inventory in USA shows the majority of high burnup SNF is near #3 line area and this raises the justification of the Demo work.

4. Stepwise Approach on R&D

4.1 Low Burnup

The ongoing research program funded by MOTIE is now focusing on low burnup range first because low burnup SNF occupies the majority of PWR SNF inventory and Korea needs to improve R&D infra which is dedicated on SNF testing and evaluation technique. In this framework, the 'fast follower' strategy is adapted and the main target of R&D is to verify whether our domestic SNF testing data satisfy the already well-organized regulatory requirements or not. If there are some extreme results, then we need to establish our own strategy to treat those SNFs.

4.2 High Burnup

Most concern about high burnup SNF is 'transportability' after several decades storage. Material degradation according to decreasing temperature in storage system could cause brittle condition and mechanical integrity with this embrittled material(especially cladding) is not secured at impact situations like fuel handling, transportation and repackaging. No one has experience mentioned above and that is why high burnup remains a big problem. Infra structure established and verified with low burnup range could be expanded to high burnup range and it is expected to produce reliable SNF testing data with various cladding materials.

5. Conclusion

The national SNF management plan has been announced in 2016 and this could construct a strong cornerstone which supports storage business and research work on SNF. A Stepwise approach on PWR SNF R&D by dividing low and high burnup area is reasonable in considering urgency of storage and infra structure of R&D.

ACKNOWLEDGEMENT

This work was supported by the Korea Institute of Energy Technology Evaluation and Planning (KETEP) granted financial resource from the Ministry of Trade, Industry and Energy, Republic of Korea (No. 2014171020166A)

REFERENCES

[1] MOTIE, "National Basic Plan on High Level Radioactive Waste", 2016.
[2] KHNP, SNF Inventory Data Analysis, 2013.
[3] US DOE, "Gap Analysis to Support Extended Storage of Used Nuclear Fuel. Rev.0", 2012.
[4] EPRI-1015048, "Spent Fuel Transportation Applications-Assessment of Cladding Performance", 2007.
[5] PNL-6189, "Recommended Temperature Limits for Dry Storage of Spent Light Water Reactor Zircaloy-Clad Fuel Rods in Inert Gas", 1987.
[6] PNNL-25374, "High Burnup Spent Fuel Data Project-Sister Rod Test Plan Overview", 2016.
[7] EPRI, "Technical Issue-Cladding", Regulatory Conference-Division of Spent Fuel Management 2015, 2015.

Methodology of Delayed Hydride Cracking Assessment of Spent Fuel Cladding

Jong-Dae Hong*, Euijung Kim, Yong-Sik Yang, and Dong-Hak Kook

Korea Atomic Energy Research Institute, 111, Daedeok-daero 989beon-gil, Yuseong-gu, Daejeon, Republic of Korea

*jongd@kaeri.re.kr

1. Introduction

During dry storage, the spent fuel claddings could degrade through hydrogen-related degradation mechanisms. DHC (Delayed Hydride Cracking), which is a time dependent crack growth process resulting from stress assisted hydrogen diffusion to the crack tip, is considered as a main concern. In this regard, NRC, DOE, and EPRI also recognized that DHC is a potential cladding breach mechanism after ~100 years of dry storage, but relevant test data are limited. Moreover, there is no methodology to evaluate or regulate DHC phenomenon, because DHC was important only for CANDU pressure tube. In this regard, DHC assessment procedures using threshold stress intensity factor (K_{IH}) are proposed and applied to PWR spent fuel cladding.

2. DHC Assessment Procedure

In spite of scatter in the published data [1-3], the maximum CGR by the DHC phenomenon is estimated to be within the range of 10^{-7}m/s at which the cladding can rupture within a year at high temperature during the early stage of the dry storage period [4]. Thus, to maintain the integrity of cladding during long-term storage, DHC crack growth not supposed to happen.

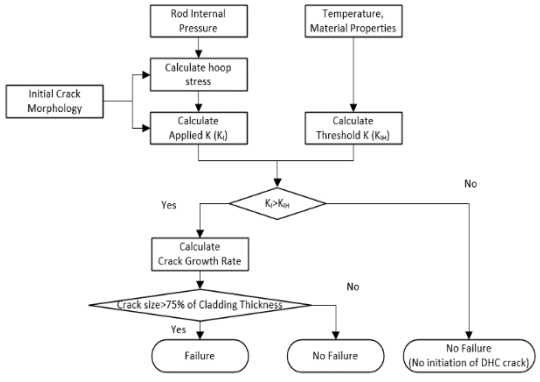


Fig. 1. Flow chart of integrity assessment for DHC [4].

In this regard, the threshold stress intensity factor (SIF), K_{IH}, is selected as principal criteria for DHC assessment. If crack grows, crack length increases according to crack growth model based on the IAEA CRP test data. Also, the cracks are judged as a failure when the grown crack size is greater than 75% of the cladding thickness. The overall flow of DHC assessment procedure is described as **Fig. 1**. Used model is summarized in **Fig. 2**.

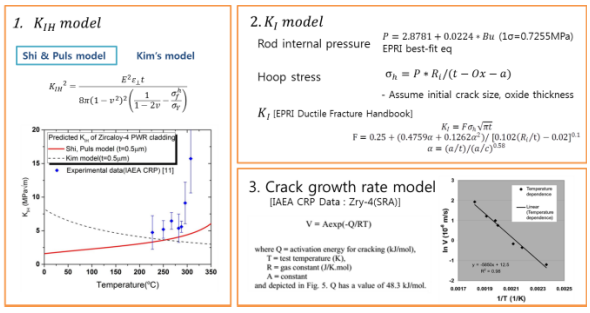


Fig. 2. Used model for DHC assessment.

2.1 Threshold stress intensity factor model (K_{IH})

To predict K_{IH} of Zircaloy-4 fuel cladding, many tests had been performed. But their results are limited and wide scattered with large uncertainties. Instead, theoretical estimations from fracture mechanics approaches were conducted using previous proposed for Zr-2.5Nb pressure tube by Shi and Puls [5]. It is function of hydride thickness, temperature and material properties. More detail is described on previous paper [4].

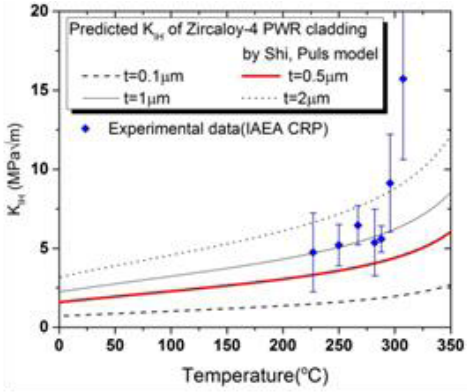


Fig. 3. K_{IH} prediction for Zircaloy-4 PWR cladding [4].

$$K_{IH}{}^2 = \frac{E^2 \varepsilon_{\perp} t}{8\pi(1-v^2)^2\left(\frac{1}{1-2v} - \frac{\sigma_f^h}{\sigma_Y}\right)}$$

Also, material properties of Zircaloy-4 accounting for spent fuel cladding were used. The predicted values are described on **Fig. 3**.

2.2 Applied stress intensity factor model (K_I)

Applied SIF is also calculated for a comparison with K_{IH} using axial part-through wall internal flaw model in the EPRI ductile fracture handbook. That reflects the pre-existing crack morphology, hoop stress, and burn-up effect. As fuel burn-up increases, increased rod internal pressure and oxide thickness effects are reflected.

2.3 Crack growth model

The crack growth rate (CGR) of Zircaloy-4 cladding was estimated by following equation according to the IAEA CRP best-fit equation [1,2] once DHC crack growth occurs. The equation is only valid under the temperature below 283°C.

$$\mathrm{CGR(m/s)} = 10^{-8} * \exp(-5850 * \mathrm{T(K)} + 12.5)$$

3. Application to PWR spent fuel cladding

Case analyses were conducted to evaluate the degradation of PWR spent fuel cladding. Basic input values for the case analysis are shown in **Fig. 4**. For simulate low burn-up and high burn-up cladding, two kinds of fuel burn-up values were used. And three different initial crack sizes on Westinghouse 17X17 type cladding (OD = 9.5 mm) are assumed with conservatism.

	Case 1	Case 2	Case 3	Case 4	Case 5	Case 6
Burnup (BU, GWd/MTU)	45	60	45	60	45	60
Initial crack depth (a, μm)	18.6	18.6	160	160	250	250
Rod internal pressure (P, MPa)	4.6116	4.9476	4.6116	4.9476	4.6116	4.9476
Oxide thickness (o, μm)	40	100	40	100	40	100

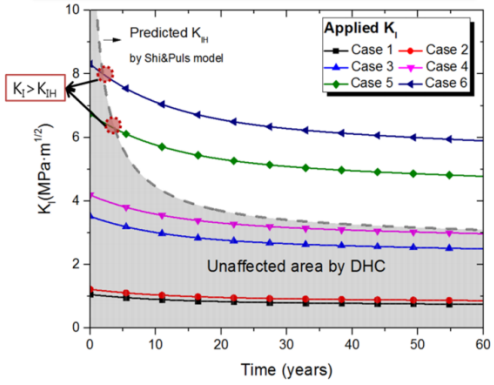


Fig. 4. Estimated applied stress intensity factor of PWR spent fuel during dry storage [4].

Fig. 4 shows estimated applied SIF of PWR spent fuel during dry storage with comparison to the predicted threshold SIF. As shown in **Fig. 4**, DHC does not degrade cladding integrity for general cases of low burn-up and high burn-up fuels. But for some limiting cases considering damaged fuel (Case 5, 6), DHC crack grows occurs. Nevertheless, PWR spent fuel cladding during dry storage is not immune to DHC because used models were derived from limited data. By obtaining more information on spent fuel, a more accurate and reliable analysis may be possible.

4. Conclusion

DHC is considered as a most potential cladding breach mechanism for spent fuel cladding. The assessment procedures of that using threshold stress intensity factor (K_{IH}) are proposed and applied to PWR spent fuel cladding. From the analysis, degradation of PWR spent fuel by DHC could occur only for some limiting cases considering damaged fuel. But for a more accurate and reliable analysis, it need to obtain more information on spent fuel.

ACKNOWLEGMENTS

This work was supported by the Korea Institute of Energy Technology Evaluation and Planning (KETEP) and the Ministry of Trade, Industry & Energy (MOTIE) of the Republic of Korea (No. 2014171020166A).

REFERENCES

[1] C.E. Coleman et al, “Delayed hydride cracking in zircaloy fuel cladding - An IAEA coordinated research programme”. Nucl. Eng. Technol. 41, 171-178 (2009).

[2] IAEA, “Delayed hydride cracking of zirconium alloy fuel cladding”. IAEA-TECDOC-1649, 2010.

[3] IAEA, “Evaluation of conditions for hydrogen induced degradation of zirconium alloys during fuel operation and storage”. IAEA-TECDOC-1781, 2015.

[4] J.-D. Hong et al, “Delayed hydride cracking assessment of PWR spent fuel during dry storage”, Submitted to Nucl. Eng. Des.

[5] S.Q. Shi, M.P. Puls, “Criteria for fracture initiation at hydrides in zirconium alloys- I. Sharp crack tip”. J. Nucl. Mater. 208, 232-242 (1994).

Sensitivity Analysis of COBRA-SFS for Dry Storage of Spent Fuel

ChangHwan Shin*, Kyong-won Seo, and Dong-hak Kook

Korea Atomic Energy Research Institute, 111, Daedeok-daero 989beon-gil, Yuseong-gu, Daejeon, Republic of Korea

*shinch@kaeri.re.kr

1. Introduction

The storage in the spent fuel pool for spent fuels of the domestic power plant is expected to be saturated from 2024 [1]. As a practical alternative to solve this problem, an intermediate storage through the dry storage of spent fuel is considered. Studies about spent fuel for the dry storage are performing for the low burnup fuels, which accounts for 80% of the domestic spent fuels. The degradation of the spent fuel during the dry storage depends on the temperature profile. Thus the temperature profile is suggested as the first item on the gap analysis report [2]. The sensitivity analysis with COBRA-SFS, a thermal hydraulic analysis code for spent fuel storage and transportation casks [3] is performed to decide the priority of the model development and experiment variables.

2. Sensitivity parameter and results

For the sensitivity study, a dry storage cask, TN24p is used from sample input in this analysis. The explicit data in fluid flow model, the properties of backfill gas, and thermal conductivity of conduction heat transfer are consider to analysis sensitivity of the peak and the minimum temperature of cladding surface.

2.1 Fluid flow models

The momentum exchange terms are a primary source of empiricism in the fluid flow equations in COBRA-SFS. In this paper, three parameters of wall friction, form drag of spacer grids, and turbulent mixing for momentum exchange between subchannels is estimated.

The friction factor used in COBRA-SFS is the Darcy-Weisback friction factor, a dimensionless number determined from experimental measurement. Idelchik [4] suggested the following relation for rectangular array of the rod bundle geometry.

$$f_{bundle} = \frac{64}{Re}\left(0.96\frac{p}{d} + 0.63\right) \quad (1)$$

As shown in table 1, when the friction factor of 64~124 is applied, the variation of minimum temperature is less than 3℃ and the effect of friction on the peak temperature is negligible.

The flow area due to local obstructions result in axial pressure losses. However the flow velocity in the natural convection is much less than 5 of Reynolds number. The pressure loss coefficient for the low Reynolds number was suggested as 5 by Idelchik. For the range of 0.01 to 10 of the form loss coefficient, the temperature variation is neglible as shown in Table 1.

Table 1. Cladding temperature for variation of friction factor and form loss of spacer grid

Friction Factor	Temperature (℃)		Form Loss	Temperature (℃)	
	Peak	Min.		Peak	Min.
64	222.29	85.27	0.01	222.41	87.07
100	222.41	87.07	1	222.41	87.07
124	222.42	87.87	10	222.41	87.08

2.2 Helium properties

In dry storage cask, the helium gas will be filled for heat transfer within a cask. The helium properties of enthalpy, specific heat and volume, thermal conductivity, and viscosity are necessary to calculate heat transfer in the cask. The variation of the property is ± 20% of NIST property data at the 0.1 MPa. As shown in Fig. 1, the thermal conductivity is dominant for the peak temperature and the specific volume and enthalpy is dominant for the minimum temperature. The deviation of temperature prediction is less than 3%.

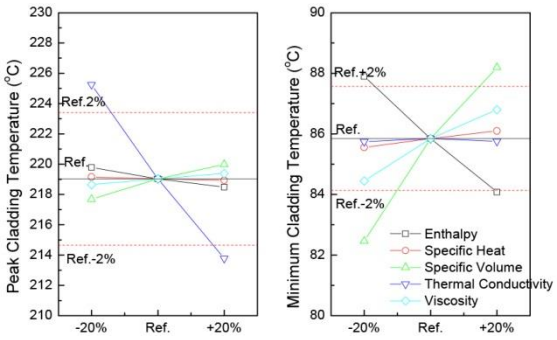


Fig. 1. Sensitivity for helium properties.

2.3 Slab material and fuel conductivity

A dry storage cask of TN24P for the sample input consists of fuel basket of aluminum, steel body, neutron shield, and shell. The fuel conductivities of pellet and cladding is related to conduction heat transfer in a fuel rod. As the heat generation rate of spent fuel is extremely low to 1 kW or less for a spent fuel assembly, the effect of the thermal conductivities of fuel pellet and cladding can be neglected.

Radiation heat transfer from fuel rods, which are the heat source transfers to the fuel basket made of aluminum alloy. The main radiative heat transfer occurs between the fuel and the fuel basket. Thus, as shown in Fig. 2, the variation in the thermal conductivity of the fuel basket of aluminum alloy has a great influence on the cladding temperature. A 10% change of the thermal conductivity results in 0.5% for the peak temperature and 1% for the minimum temperature of cladding.

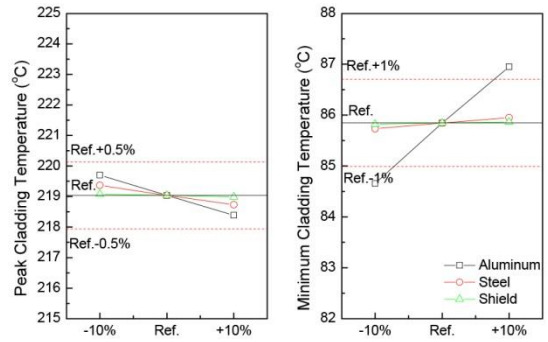


Fig. 2. Sensitivity for the thermal conductivity of slab materials.

3. Conclusions

The sensitivity on the peak and the minimum of fuel cladding surface temperature is evaluated with COBRA-SFS. For the fluid flow, the friction factor causes the variation of less than 3 ℃ for the minimum temperature and the effect of friction on the peak temperature is negligible. The form loss caused by flow area change is also negligible.

The properties of a backfill gas such as helium cause a difference of about 3%. In particular, it can reduce error by providing precise properties for thermal conductivity, enthalpy, and specific volume.

Although the thermal conductivity of the fuel basket connected by radiation heat transfer to fuel rod has the greatest effect, the difference is less than 1% for a change of 10%.

The sensitivity analysis about the energy exchange models, which is expected to cause major deviation is currently in progress.

ACKNOWLEDGEMENT

This work was supported by the Korea Institute of Energy Technology Evaluation and Planning (KETEP) granted financial resource from the Ministry of Trade, Industry and Energy, Republic of Korea (No. 20141710201660A)

REFERENCES

[1] Ministry of Trade, Industry and Energy, “Roadmap for Disposal of High-level Radioactive Wastes” (2016).

[2] B. Hanson, et al., “Gap Analysis to Support Extended Storage of Used Nuclear Fuel, Rev. 0”, PNNL-20509 (2012).

[3] T. Micherner, et al., “COBRA-SFS, A Thermal-Hydraulic Analysis Code for Spent Fuel Storage and Transportation Casks, Cycle 4”, PNNL-24841 (2015).

[4] I. Idelchik, “Handbook of Hydraulic Resistance”, 2nd Edition, Hemisphere Publishing Corporation, (1986).

.

Assessment of COBRA-SFS Cycle4 With Various Single Phase Flow Tests

Kyong-Won Seo*, Chang-Hwan Shin, and Dong-Hak Kook

Korea Atomic Energy Research Institute, 111, Daedeok-daero 989beon-gil, Yuseong-gu, Daejeon, Republic of Korea

*nulmiso@kaeri.re.kr

1. Introduction

COBRA-SFS (Coolant Boiling in Rod Arrays - Spent Fuel Storage) code [1] has widely been used to analyze flow field and temperature profile in spent fuel storage canisters. The code was derived from the COBRA-IV [1], abilities to analyze spent fuel storage systems such as radiative and conductive heat transfer were added while two-phase flow related features were removed. And the code has been validated for many spent fuel storage systems and has shown the predicted temperatures agree well with measured. The flow mechanism within spent fuel storage system is natural circulation driven by temperature difference. It is hard to find a validation work about COBRA-SFS's ability to predict flow field rather than temperature profile under natural circulation. In this reason, we have assessed the COBRA-SFS Cycle4 code with various tests were performed at single phase flow.

2. Assessment

2.1 Flow Mixing Test at CNEN 4x4 Rod Bundle

This test measured flow velocity distribution at the subchannel exits at five different flow conditions at CNEN 4x4 Rod Bundle[3]. The measured values were integrated into a subchannel average velocity. This test can show the ability of COBRA-SFS of predicting turbulent mixing between subchannels. The turbulent mixing was modeled with a coefficient of 0.02 as listed in Eq.(1).

$$w'_T = 0.02 s_k \overline{G} \qquad (1)$$

The predicted values agreed well with the measured at center and side subchannels as shown in Fig. 1. However COBRA-SFS under-predicted velocity at corner subchannel and the discrepancy becomes the larger as the flow rate increases.

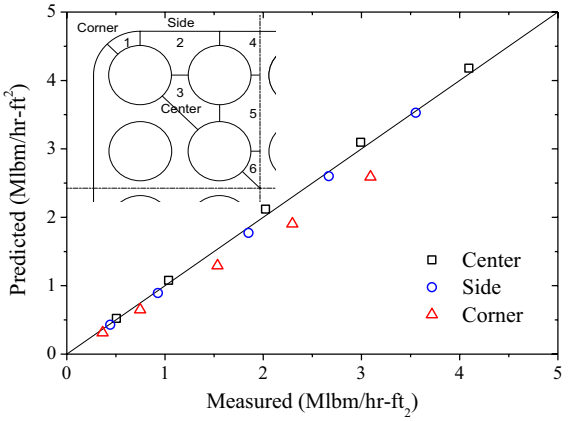


Fig. 1. Analysis of the Flow Mixing Test.

2.2 Flow Redistribution Test at WH Two-Assemblies

This test at Westinghouse observed flow re-distribution between two adjacent assemblies when one assembly was blocked [4]. The flow blockage at the right side was simulated by reducing the flow rate by 550 gpm whereas flow rate remains at 1100 gpm for the left. Each assembly consists of 38-inch long 196 rods in 14x14 square lattice.

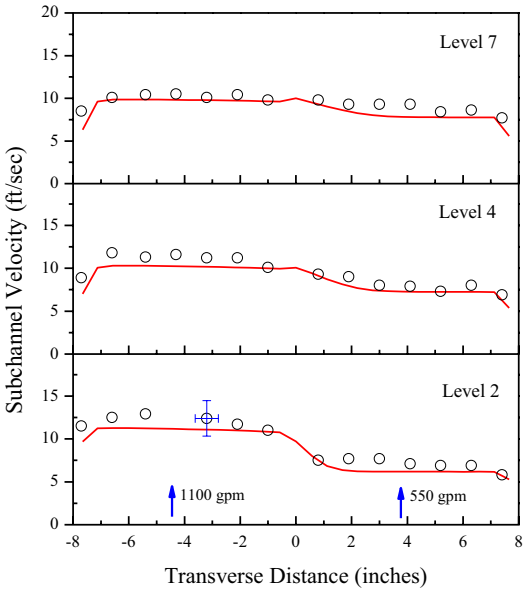


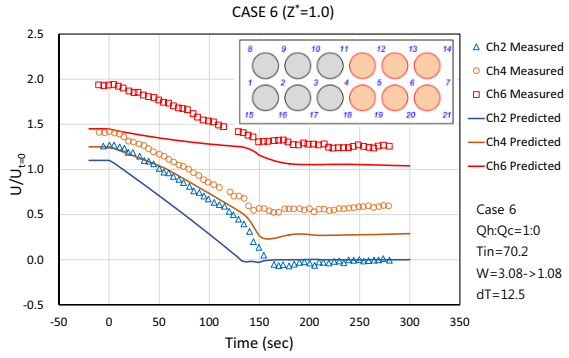
Fig. 2. Analysis of the Flow Redistribution Test.

Fig. 2 shows the flow redistribution between two assemblies and flow profile becomes uniform at the level 7 both of the measured and the predicted.

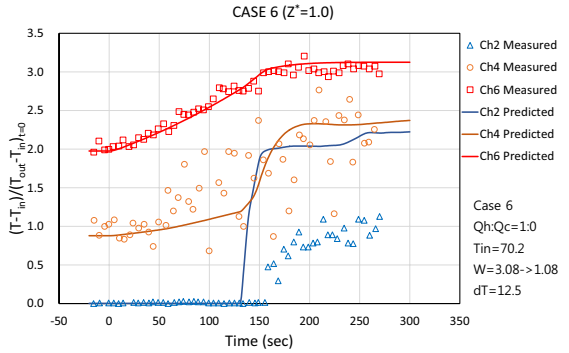
2.3 Low Flow Test at PNL 2x6 Rod Bundle

This test was performed under steady states and flow reduction transients at PNL 2x6 rod bundle [5]. The test measured the local flow velocity and temperature profile. The temperature profiles were measured with various non-uniform radial power distributions.

Fig. 3 shows the flow velocity and temperature profiles at the subchannel no. 2, 4, and 6 for the test case 6. The test case 6 was a flow reduction transient during 150 seconds while right half six rods were heated and the others were unheated. The measured flow velocity at the subchannel 2 dropped below zero after the transient ended as shown in Fig. 3(a). The predicted flow velocity at that subchannel became slightly negative around 130 seconds which was earlier than the measured. Fig. 3(b) shows the transients of non-dimensionalized temperature rise for the case 6. Temperature rises at the subchannel 4 and 6 agreed well with the measured whereas that of subchannel 2 was under-predicted.



(a) Flow Velocity



(b) Flow Temperature

Fig. 3. Analysis of the Flow Reduction Transient.

3. Conclusion

We have assessed COBRA-SFS Cycle4 code with three single phase flow tests before we apply the code to analyze temperature profile in a certain spent fuel storage system. The test cases used in this study are flow mixing test at CNEN 4x4 rod bundle, flow redistribution test at Westinghouse two 14x14 rod bundles, and low flow transient test at PNL 2x6 rod bundle. In the flow mixing test at CNEN 4x4 rod bundle, the flow velocity at the corner channel was under-predicted. In the low flow transient test at PNL 2x6 rod bundle, flow velocity at the cold channel became negative earlier than the measured and the temperature rise was over-predicted at that subchannel.

Acknowledgement

This work was supported by the Korea Institute of Energy Technology Evaluation and Planning (KETEP) granted financial resource from the Ministry of Trade, Industry and Energy, Republic of Korea (No. 2014171020166A)

REFERENCES

[1] T.E. Michener et al., “COBRA-SFS: A Thermal Hydraulic Analysis Code for Spent Fuel Storage and Transportation Casks,” PNNL-24841, Pacific Northwest National Laboratory, 2015.

[2] C. W. Stewart et al. COBRA-IV: The Model and the Method,” BNWL-2214. Battelle Northwest Laboratory, 1972.

[3] V. Marinelli, et al., “Experimental Investigation on Mass Velocity Distribution and Velocity Profiles in an LWR Rod Bundle,” Trans. ANS 15, pp.413-415, 1972.

[4] H. Chelemer, et al., “THINC-IV – An Improved Program for Thermal Hydraulic Analysis of Rod Bundle Cores,” WCAP-7956, Westinghouse Electric Corp., 1973.

[5] J. M. Bates and E. U. Khan, “Investigation of Combined Free and Forced Convection in a 2x6 Rod Bundle during Controlled Flow Transients,” PNL-3135, Pacific Northwest Laboratory, 1980.

Preliminary Approach of Impact Simulation for the Simplified Unit Grid

Sunguk Lee*, Jaeyong Kim, Sooho Kim, Yongsik Yang, Hyochan Kim, and Donghak Kook
Korea Atomic Energy Research Institute, 111, Daedeok-daero 989beon-gil, Yuseong-gu, Daejeon, Republic of Korea
*leesunguk@kaeri.re.kr

1. Introduction

As the amount of Spent Nuclear Fuel (SNF) in domestic spent fuel pool substantially increases, the storage capability for the SNFs will be expected to be saturated in 2020 [1]. The SNFs in the pool have to transfer to a designated wet or dry spent fuel storage facility. Among the issues of the SNF treatment, the handling and transportation of the SNF have been considered as key factors. Experimental evaluation about the soundness of the mechanical behavior during the SNF management requires a lot of time and effort. The computational methodology like FE simulation is usually employed as a technical solution instead of experiment. Lee et al. [2] conducted the drop impact simulation using dynamic properties. The study was conservative approach by applying the simplified properties.

In this study, we investigate the effect of strain rate on the impact simulation through experiment and simulation of the simplified unit grid in order to verify the dynamic analysis of the SNF.

2. Simulation of the drop impact test

2.1 Drop impact modeling

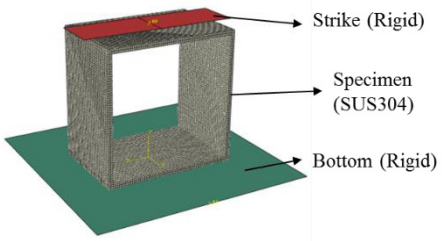


Fig. 1. Finite element model for drop impact simulation.

Fig. 1 shows the finite element model of the strike and specimen for drop test. The specimen was modeled using ABAQUS/explicit 6.14.5, C3D8R (8-node linear brick reduced integration element) was used for the specimen, and analytic rigid elements were used for the strike and bottom. Total number of elements and nodes are 722,459 and 831,875 respectively. The material of the specimen is stainless steel (SUS304).

2.2 FE analysis considering the strain rate

Metal can behave very differently at the higher strain rates like drop tests and impacts. SUS304 is highly strain-rate dependent [3]. Stain-rate sensitivity can be included in a number of different explicit dynamics material models. For metals, Cowper-Symonds and Jonson-Cook models are often used. These models, and others like them, are readily available in commercial FE analysis software codes like LS-Dyna, ANSYS and ABAQUS. The flow stress of Jonson-Cook model, which includes strain hardening, stain rate, and temperature effect, was used as constitutive equation in this model.

$$\begin{aligned}\sigma\left(\varepsilon_p,\dot{\varepsilon},T\right) &= f_1\left(\varepsilon_p\right)\cdot f_2\left(\dot{\varepsilon}\right)\cdot f_3\left(T\right)\\ &= \left(A+B\varepsilon_p^n\right)\left(1+C\ln\dot{\varepsilon}^*\right)\left(1-\left(T^*\right)^m\right)\\ \text{where}\quad \dot{\varepsilon}^* &= \frac{\dot{\varepsilon}}{\dot{\varepsilon}_0},\ T^* = \frac{T-T_r}{T_m-T_r}\end{aligned} \tag{1}$$

The used Jonson-Cook parameters of SUS304 are presented in table 1 [4].

Table 1. SUS304 properties

A [MPa]	B [MPa]	n	C
310	1,000	0.65	0.07
$\dot{\varepsilon}_0$ [/s]	M	T_r [K]	T_m [K]
1	1.0	293	1,673

These properties were applied to a 2 mm thick rectangle box impacted by a 22.9 kg rigid block travelling at 2.09 m/s. The total impact energy is 50 J.

3. Result & discussion

3.1 Result of drop impact test

The drop impact test for rectangle box was carried out in order to evaluate the simulation result. Fig. 2

shows the experimental apparatus and the deformed specimen for drop impact test.

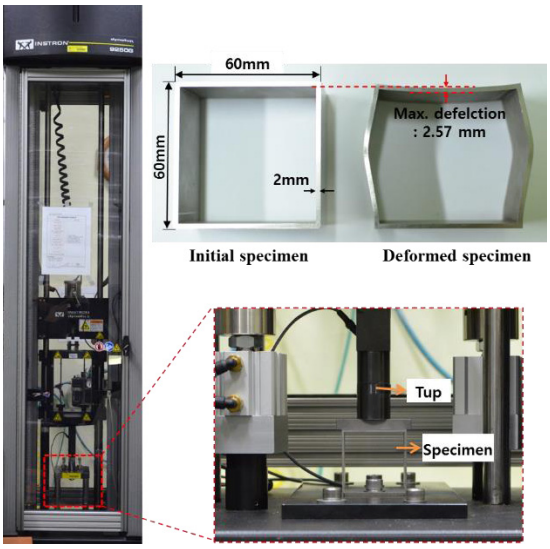
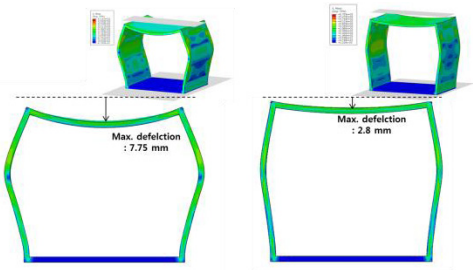


Fig. 2. Experimental apparatus and tested specimen.

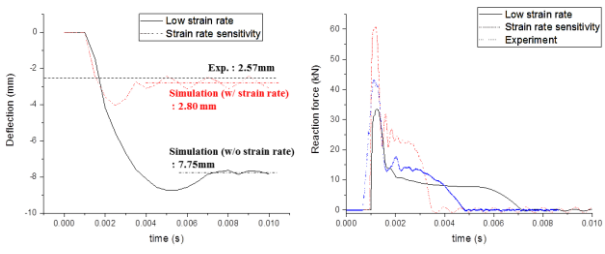
3.2 Results of the finite element analysis



(a) (b)

Fig. 3. Deformed shapes for drop impact simulation (50 J)
(a) Low strain rate and (b) Stain-rate sensitivity model.

Fig. 3 shows the deformed shapes of the specimen for 50 J drop impact test. In comparison with the cross-section of the experimental results shown in Fig. 2, the extent of deformation with FEM is higher than that of the test. The reason could be thought as that in the FE analysis the model was considered ideally.



(a) (b)

Fig. 4. Comparison between experiment and simulation
(a) Max. deflection and (b) Reaction force.

Fig. 4 shows the resulting maximum deflection and reaction force versus time for the strain-rate sensitivity Jonson-Cook plastic model, for the same plasticity model but without the strain-rate sensitivity, and for experiment. It's obvious that the deformation and reaction force are significant influenced by the strain-rate. Also, a check of maximum deflection for the model with the strain-rate sensitivity shows that the value is close to the experimental result.

4. Conclusion

Drop impact test for the simplified unit grid was performed to evaluate the dynamic model of SNF. The finite element analyses considering strain rate and not considering that were carried out. By comparing the two results with or without strain rate, the material input data at the simulation should contain the rate-dependent effect to simulate the impact behavior of the grid made with a property which is very sensitive to the strain rate.

ACKNOWLEDGMENTS

This work was supported by the Korea Institute of Energy Technology Evaluation and Planning(KETEP) and the Ministry of Trade, Industry & Energy(MOTIE) of the Republic of Korea (No. 2014171020166A).

REFERENCES

[1] H.J. Choi, D.K. Cho. D.H. Kook, and J.W. Chol, "Current status of spent fuels and the development of computer program for the PWR spent fuel management in Korea", Progress in Nuclear Energy, 53(3), 290-297 (2011).

[2] Y.S. Lee, C.H. Ryu, H.S. Kim and Y.J. Choi, "A study on the free drop impact of a cask using commercial FEA code", Nuclear Engineering and Design, 235, 2219-2226 (2005).

[3] H. Nordberg, "Note on the sensitivity of stainless steels to strain rate", AvestaPolarit Research Report No 04.0-1, 1-10 (March 2004).

[4] S. Lee, F. Barthelat, J.W. Hutchinson, and H.D. Espinosa, "Dynamic failure of metallic pyramidal truss core materials – Experiments and modeling", International Journal of Plasticity, 22, 2118-2145 (2006).

Correlation Between Hydrogen Contents and Stiffness of Oxidized Spacer Grid for Calculating Spent Fuel Rod Response to Impacting Force

Young-Ho Lee*, Hyun Gil Kim, and Donghak Kook

Korea Atomic Energy Research Institute, 111, Daedeok-daero 989beon-gil, Yuseong-gu, Daejeon, Republic of Korea

*leeyh@kaeri.re.kr

1. Introduction

Discharged spent fuels from light water reactors are temporarily stored in spent fuel storage pools of each plant site, but it reaches saturation in the near future. So, dry storage method is regarded as one of the most practical and alternative solutions for resolving the spent fuel accumulation problems in Korea [1]. However, domestic technologies and industrial know-how for operating dry storage facilities are in the beginning stage while the first dry storage installation in the US was licensed by the Nuclear Regulatory Commission (NRC) in 1986 at the Surry Nuclear Power Plant in Virginia. The spent fuels are safely stored by applying the dry storage methods of various concepts such as Vaults, Silos, metal and concrete cask.

The final objectives of spent fuel dry storage are to prevent a gross rupture of the spent fuel during operation and to keep its retrievability until transportation because dry storage means an intermediate method before a permanent decision [2]. In other words, integrities of spent fuel rods and their structural supporting parts should be maintained against temperature-induced failures (i.e., creep, hydrogen reorientation, etc.) and interaction between fuel rod and spacer grid during handling and transportation, respectively. This study focus on the later issue that external force to spent fuel rods mainly exerted by spacer grid springs and dimples. It is well known that Zr-based claddings of spent fuel rods show brittle characteristics due to the formation of hydrides and oxidation in high temperature pressurized water. In addition, it is expected that structural parts of fuel assembly also degraded by the same environment. During the transportation and handling, external force on spent fuel rod exerted by spacer grids that their stiffness values are increased by thermal relaxation and irradiation embrittlement. In this study, the variation of spring stiffness of spacer grid with increasing oxidation time in high temperature pressurized water were examined focusing on effect of hydrogen contents and oxide thickness for calculating spent fuel rod response during the transportation and handling.

2. Experiments and Results

2.1 Oxidation tests

The spacer grid specimens were prepared with 10.9 mm in width and 40 mm in length and oxidized in an autoclave up to 360 days and then examined their stiffness values, oxide thickness and hydrogen contents.

2.2 Specimen analysis

The stiffness of oxidized spacer grids were measured by a simplified p-δ (force-displacement) tester with 10 N of maximum applied force. The oxide thickness and hydrogen contents were also measured by SEM and a hydrogen determinator, respectively.

2.3 Variation of stiffness & oxide thickness

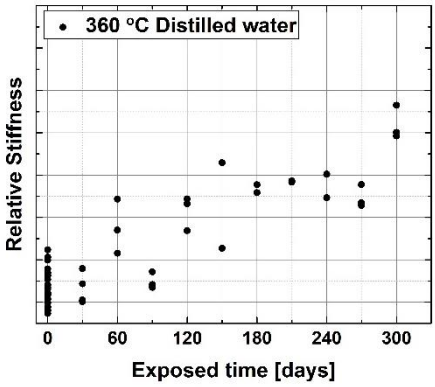


Fig. 1. Variation of stiffness with exposed time.

Fig. 1 shows the variation of stiffness with increasing oxidation time. When compared with as-received specimen (i.e., before oxidation), stiffness of oxidized grid spring gradually increased. However, oxide thickness rapidly increased at 60~90 days and then gradually increased as shown in Fig. 2. This means that thin oxide did not affect the variation of thickness.

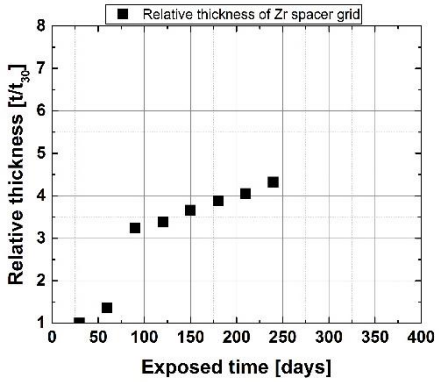


Fig. 2. Measurement results of oxide thickness.

2.4 Hydrogen contents

Fig. 3 shows the variation of hydrogen contents with increasing oxidation time. As expected, amount of hydrogen increased with oxide thickness and oxidation time. However, these amount seem to be small rather than conventional Zr cladding because of different microstructures.

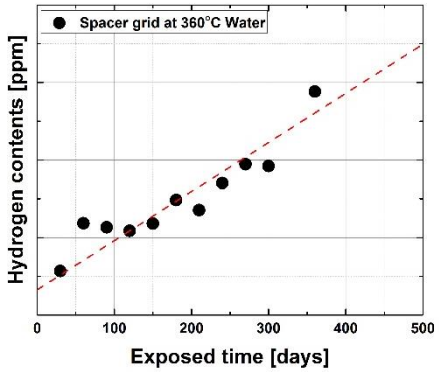


Fig. 3. Measurement results of hydrogen contents.

3. Summary

In this study, the stiffness of spacer grid gradually increased with oxide thickness and hydrogen contents (i.e., oxidation time). Previous results [3] indicated that average cell size of spacer grid enlarged rather than as-built condition. So, increased stiffness of spacer grid should be examined for calculating the spent fuel rod response to impact force during the transportation and handling. However, the key factor affecting the stiffness variation is not apparent and further studies focus on the effect of hydrogen contents without surface oxidation.

ACKNOWLEGEMENTS

This work was supported by the Korea Institute of Energy Technology Evaluation and Planning (KETEP) and the Ministry of Trade, Industry & Energy (MOTIE) of the Republic of Korea (No. 2014171020166A).

REFERENCES

[1] Ministry of Knowledge and Economy of Korea, “Fundamental Energy Plan of Korea for 2008~2030” (2009).

[2] 10 CFF 72, “Licensing requirements for the independent storage of spent nuclear fuel, high-level radioactive waste”, USA.

[3] Technical Report, “Development of cell spring test technique for the irradiated spacer grid of a nuclear fuel assembly in hot cell”, KAERI/TR-4637/2012.

Confirmatory Procedure of Spent Fuel Information for Spent Fuel Transport to the Interim Storage Facility

Daesik Yook*, Ara Go, Gyeong-uk Kang, and Kyuhwan Jeong

Korea Institute of Nuclear Safety, 62 Gwahak-ro, Yuseong-gu, Daejoen, Republic of Korea

*dsyook@kins.re.kr

1. Introduction

The national basic policy for high level radioactive waste management of Korea was established and promulgated, taking into consideration the national/international trends on policy and technology development in 2016. According to the national plan, the siting for deep geological disposal facility of high level radioactive waste will be proceeded by 2028. Once the site was selected at somewhere, centralized spent fuel storage facility will be constructed by 2035 at the same site while research program is ongoing to determine the compatibility of the site for disposal facility. Additionally, spent fuel will be expected to store at onsite dry storage cask until finishing the central interim storage facility in Korea. Therefore, spent fuel will be transported to the onsite storage facility or offsite storage facility in the future. Once spent fuel stored in storage cask, it is almost impossible to inspect the integrity of spent fuel through visual inspection, etc. For that reason, the aim of this study is to establishment the procedure to ensure the status and the integrity of spent fuel before storing into the dry storage cask.

2. Confirmatory procedure of spent fuel information

2.1 Regulatory position of spent fuel information

The comprehensive spent fuel information can be divided 3 categories. First information will be composed of foundation data like as the characteristics of nuclear fuel, operational histories in nuclear reactors, positions in spent fuel pool, etc. Second information is derived through calculation or evaluation of 1st information like as burnup of spent fuel, radioactive isotope inventory in spent fuel, etc.

Third information is related to the integrity of spent fuel cladding through confirming the cladding status, etc.

These multi-layered information should be produced or updated whenever spent fuel are generated and moved, and these are stored in the comprehensive spent fuel DB system. Information related to radionuclide inventory with axial or in assembly, as a second information, are needed to be secured through destructive analysis or non-destructive analysis methods for the accuracy of information. Axial radionuclide inventory should be evaluated by the exact simulation computer code, Fig. 1 shows how this computer code should be developed.

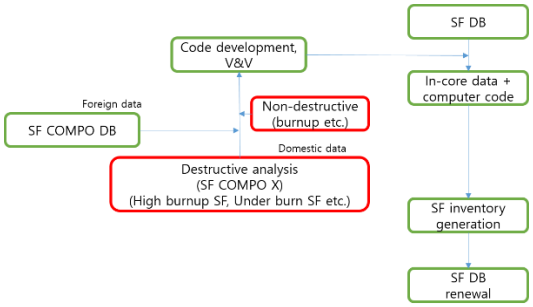


Fig. 1. Spent fuel inventory evaluation computer code development procedure.

As a third information, data related to spent fuel integrity should be obtained by direct inspection methods like as visual inspection before transporting spent fuel to the dry storage cask. These data should be stored in the comprehensive spent fuel DB system as well.

2.2 Confirmative procedure for spent fuel information

The comprehensive spent fuel DB system should be developed and operated by national authority or organization which is responsible to manage spent fuel. Spent fuel information which is generated, collected, and managed by utility should be transferred to the competent organization who operate comprehensive spent fuel DB. Before

transferring spent fuel DB to the competent organization, spent fuel DB should be confirmed and updated by the following procedure as shown in fig. 2. Since spent fuels have been stored in spent fuel pool for a few decades, spent fuel should be confirmed its integrity and matched both physical spent fuel and its information of document. As shown in fig. 2, spent fuel information should be generated in accordance with QA program which was approved by the regulatory body in advance. If it can't meet the QA procedure, spent fuel information should be reconfirmed by various methods like as direct or indirect measurement as shown in fig. 2. If spent fuel transferred to the dry storage cask which burnup credit was approved, burnup of spent fuel should be measured to prevent misloading. In case dry storage cask is not applied burnup credit, burnup measurement may be skipped and spent fuel can be loaded to dry storage cask directly. However, burnup of target spent fuel should be measured randomly because it should be confirmed the match physical spent fuel and its information of document. Finally, whole implementation following the procedure of fig. 2 should be recorded in comprehensive spent fuel DB.

3. Conclusion

Reliability of the safety information on spent fuel is very important because safety information will be used as basic data for safety evaluation and verification for transportation, storage and disposal of spent fuel. For this reason, this study proposed regulatory position and confirmatory procedures for verifying spent fuel safety information. These are suggested after reviewing domestic and international technology level [1,2,3] and confirming actual applicability of domestic nuclear industry.

Regulatory position and confirmatory procedures will be applied to the development of review guidelines for spent fuel safety information in the future.

ACKNOLEDGEMENT

This work was supported by the Nuclear Safety Research Program through the Korea Radiation Safety Foundation (KORSAFe), granted financial resource from the Nuclear Safety and Security Commission (NSSC), Republic of Korea (No. 1503003)

REFERENCES

[1] NRC, Review of information for spent nuclear fuel burnup confirmation, NUREG/CR-6998, 2009.

[2] IAEA, Data Requirements and Maintenance of Records for Spent Fuel Management, TECDOC-1519, 2006.

[3] OECD/NEA, Spent Nuclear Fuel Assay Data for Isotopic Validation, NEA/ NSC/ WPNCS/ DOC (2011)5, 2011.

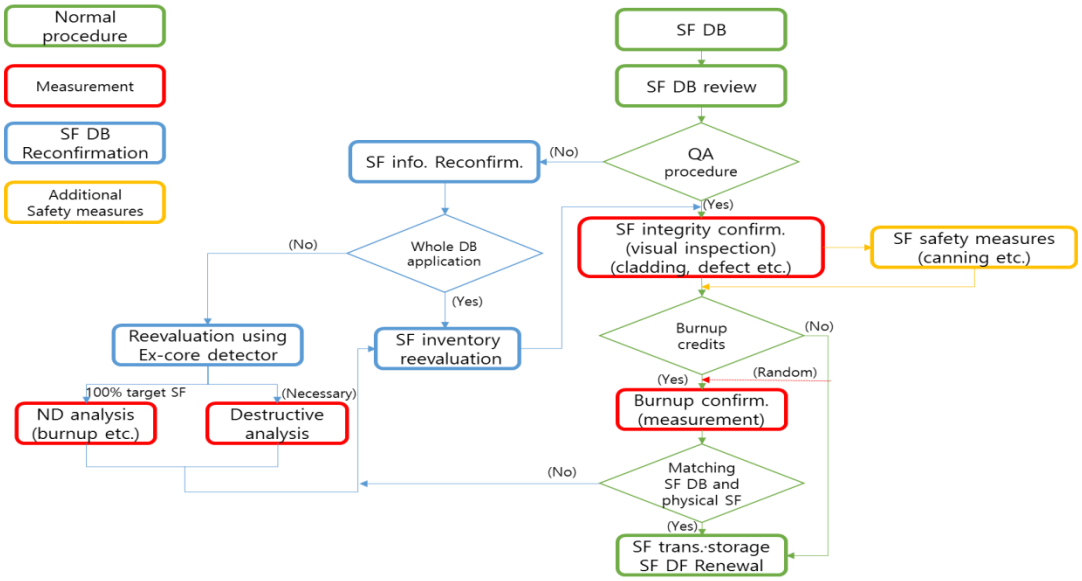


Fig. 2. Confirmative procedure of spent fuel information.

Preliminary Numerical Simulation and Test Plan for Actual Drop Accident Condition

Woo-seok Choi[1*], Sangsoon Cho[1], Ki-seog Seo[1], Yun-young Yang[1], Sanghyeok Han[2] , and Yong-hui Park[1]

[1]Korea Atomic Energy Research Institute, 111, Daedeok-daero 989beon-gil, Yuseong-gu, Daejeon, Republic of Korea

[2]Sungshin ENG, 29, Insadong 5-gil, Jongno-gu, Seoul, Republic of Korea

[*]wschoi@kaeri.re.kr

1. Introduction

As we construct a safety case of transport cask and spent fuel, there are actual accident conditions in the life-cycle, which are beyond the regulatory hypothetical accident conditions. To ensure the safety of spent fuel transportation, it is necessary to select the accident conditions for the safety evaluation based on the analysis of accident scenarios and to perform a safety assessment under these actual accident conditions.

2. Test plan for actual accident conditions

2.1 Evaluation of actual accident conditions

Actual operation scenarios of spent fuel handling and transportation were derived by analyzing spent nuclear fuel storage facilities, transport systems and transport procedures in domestic nuclear power plants.

Among them, it was analyzed that there could be a possibility of a drop of nuclear fuel due to the shortage of the crane cables, the damage of the fuel handling device, or the operator's mistake during withdrawal, movement and loading of the fuel in the spent fuel wet storage tank.

In case of underwater fall, the maximum drop height was estimated to be about 5 m. The nuclear fuel would be damaged, but no radioactivity or radiation leakage would occur. In addition, when the cask is moved from the decontamination tank to the transportation vehicle, it is possible to cause a drop of 9.5 ~ 14 m due to the various reason described above.

One of the worst accident conditions in which the cladding of the spent nuclear fuel assemblies is damaged is dropping of cask from the high height without the impact limiter which is shock absorbing component. Therefore, it is necessary to evaluate the safety of the actual accident condition when the cask without impact limiter drops down from 15 m height.

In this study, structural integrity of cask, nuclear fuel assemblies, cladding tubes and support grids is evaluated when a transport cask without shock absorbers drops down to concrete pad at a maximum of 15 m.

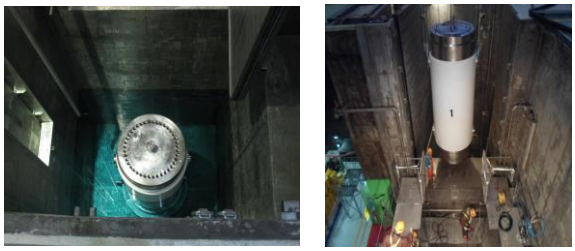


Fig. 1. Cask transportation w/o lid bolt fastening (Loading pit -> Decon. pit).

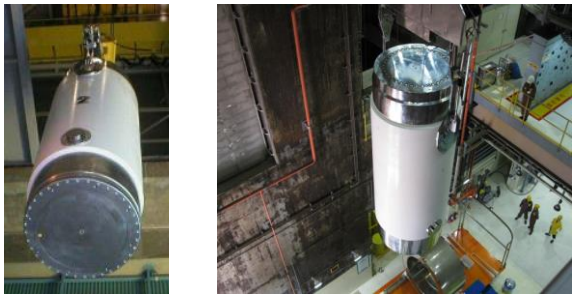


Fig. 2. Cask transportation w/o impact limiters (Decon. pit -> Truck bay).

2.2 Test plan simulating actual accident condition

To assess the actual accident conditions, KAERI will conduct a non-absorbing drop test with a drop height of 15 m. The schematic diagram of the overall drop test is shown in Fig. 3.

In order to carry out the ultimate drop impact test, we considered where to place the test. At the KAERI's safety test facility, tests have been carried out according to the IAEA Regulation SSR-6 and the Nuclear Safety Commission Act No. 2014-50, which are falling to a non-deformable rigid pad at a height of 9 m. Drop test at 15 m height is not possible at KAERI test facility.

We have also examined concrete pads installed on vacant lots, closed buildings, or factory sites, and tested after people's access control. However,

significant problems such as operation of the hydraulic equipment that releases the cask in the air (440V needed), movement of structures, power supply (using generators or batteries), and coping with the unexpected weather have been found. Finally, it was decided to carry out the test by modifying and repairing a part of the facility in KAERI.

The scenario we want to simulate is to drop cask without impact limiter onto a concrete pad, which represent the second floor of a building. Therefore, we will construct the concrete pad laid over the ground through reinforcement work on the empty space of test facility in Fig. 4. The protecting structure will be installed to prevent accidents caused by the rebound of the transport cask after the impact. We decided to use a portable heavy car crane to lift the cask to a height of 15 m and to drop it. It is expected that a lot of budget will be required for the series of works such as modifying of test facility, performing drop test, and restoration of facility after test.

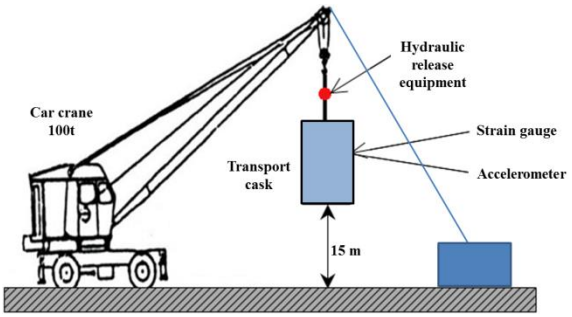


Fig. 3. Conceptual schematic drawing for test.

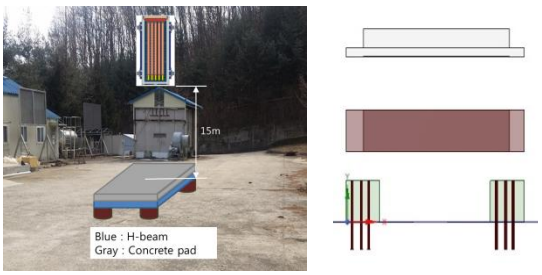


Fig. 4. Conceptual drawing of concrete pad.

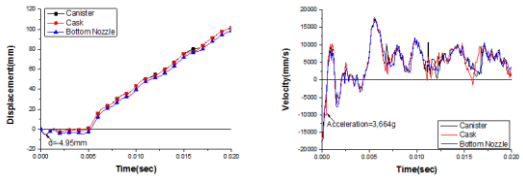
2.3 Preliminary numerical simulation

Displacement and velocity history of cask, canisters, and bottom nozzle of the fuel assembly after a 15 m fall are shown in Fig. 5. In Fig. 5(a), the displacement history of each component showed that the concrete pads were compressed to a maximum of 4.95 mm after impact, and that the cask was rebounded upward after about 5 ms. In Fig. 5(b), the speed of the cask was rapidly reduced during 1 ms at the beginning. The maximum deceleration was about 3,664 g.

Generally, a deceleration is about 100 to 300 g, and contact holding time is about 10 to 25 ms, when the impact limiter is assembled into a cask. However, the impact energy is hardly absorbed in this actual accident condition such as the drop of high height and without impact limiter.

The plastic deformation of the canister occurred from the bottom to the middle height, which resulted in the expansion of the diameter. As a result of the expansion of the canister, the outer wall of the canister has come into contact with the inner wall of the cask.

In other words, since the contact area after the drop occurred widely from the bottom of the canister to the middle height, it is estimated impossible to recover the canister from the cask after the actual drop accident condition of 15 m height.



(a) Displacement (b) Velocity

Fig. 5. Displacement and velocity time history.

The average axial stress acting on the bolt was 1,615 MPa and the average shear stress was calculated to be 231 MPa. The allowable tensile stress and allowable shear stress of the bolts applied in this analysis are 557 MPa and 334 MPa, respectively. Therefore, stress evaluation for multiple loads was performed, and as a result, all bolts were evaluated to be damaged.

3. Conclusions

The actual accident conditions beyond regulatory accident conditions were evaluated. Among them, preliminary structural integrity evaluation was carried out for the actual drop accident condition in which the transport cask without impact limiter drops at a maximum of 15 m. As a result, it was estimated that all the cladding, supporting guide tube, bottom nozzle and lower support grid in the spent fuel assembly were damaged and all the bolts in the cask lid were also damaged. For the further evaluation, KAERI will perform the test to simulate the drop condition with 15 m height and without impact limiter.

Comparison of Permeability Calculation Inside a Spent Nuclear Fuel in a Dry Storage

Seung-Hwan Yu*, Kyung-Sik Bang, Ju-Chan Lee, and Woo-Seok Choi

Korea Atomic Energy Research Institute, 111, Daedeok-daero 989beon-gil, Yuseong-gu, Daejeon, Republic of Korea

*shyu80@kaeri.re.kr

1. Introduction

The porous media model and effective thermal conductivity are used to simplify the fuel assembly. USNRC, 2010 recommend that an approach to calculate the friction factors should be to perform a computational fluid dynamics (CFD) analysis for a fuel assembly. From the detailed CFD analysis of a single fuel assembly, the friction factors could be calculated by wall shear stresses.

In this study, computational modeling of a fuel assembly was used to numerically investigate the fluid flow characteristics in a basket containing a nuclear fuel assembly. Three different methods of calculating the permeability were used and their results compared.

2. Calculation model

The calculation model represents a spent nuclear fuel assembly loaded in a fuel basket. The canister in a dry storage system is filled with helium. Helium flows from the bottom to the top of the basket because of the natural convection produced by the decay heat of the spent nuclear fuel. The complex geometry of the nuclear fuel assembly induces a shear stress on the helium flow.

Fig. 1 shows a model of the fuel assembly. The target fuel assembly for modeling was a PLUS7 fuel assembly (16 × 16 type). The PLUS7 fuel assemblies were for OPR1000 and APR1400s in Korea. More than 2,300 PLUS7 fuel assemblies were supplied to the OPR1000 nuclear power plants from 2006 [1]. The fuel cladding had a diameter of 9.5 mm. A total of 11 spacer grids were located at regular intervals along the fuel rod, except at the upper and lower end fittings. The vanes and other small parts of the spacer grid were not considered. The purpose of the vanes was to enhance the heat transfer rate by introducing a turbulent water flow in the reactor vessel of a nuclear power plant. However, the effect of the vane on the flow was negligible in the dry storage cask because the flow velocity of helium was very slow compared to that of the water flow in the reactor vessel. The lengths of the upper and lower end fittings were relatively short compared to the total height of the fuel assembly. The flow resistance inside the basket was inversely proportional to the flow area. The flow resistance generated by the upper and lower end fittings was negligible. Therefore, the upper and lower end fittings were not considered in the fuel assembly model.

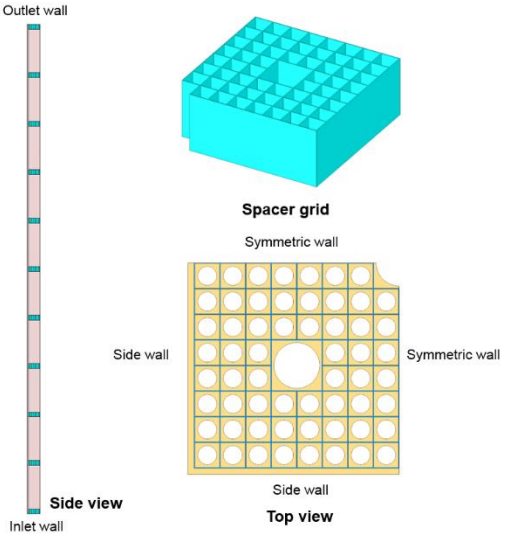


Fig. 1. Modeling of fuel assembly.

3. Permeability calculation

Permeability was calculated using three different methods. The first method was a theoretical approach using the friction factor. The second method was a CFD calculation using the wall shear stress, while the third method was a CFD calculation using the pressure drop.

The porous media flow resistance model was defined by the Darcy–Forchheimer law [2]:

$$\frac{\Delta P}{L} = D\mu V + C\left(\frac{1}{2}\rho V^2\right) \quad (1)$$

where ΔP is the porous media pressure drop; V is the superficial fluid velocity; L is the length of the porous media; D is the viscous resistance parameter (permeability); and C is the inertial resistance parameter. In the dry storage cask (vertical type), the flow velocity inside the basket was very low. D was more dominant than C because of the low velocity. Therefore, the permeability (D) is defined as follows:

$$D = \frac{\Delta P}{L\mu V} \tag{2}$$

The frictional pressure drop is defined by the following equation:

$$\frac{\Delta P}{L} = \frac{f}{D_h}\frac{1}{2}\rho V^2 \tag{3}$$

The Reynolds number is as follows:

$$\mathrm{Re} = \frac{\rho V D_h}{\mu} \tag{4}$$

The frictional pressure drop is rearranged by the Reynolds number as:

$$\frac{\Delta P}{L} = \frac{f\,\mathrm{Re}}{2}\frac{\mu}{D_h^2}V \tag{5}$$

The Darcy friction factor (f) was experimentally obtained by [3] when the flow was laminar and the rod bundle was as follows:

$$f = \frac{110}{\mathrm{Re}} \tag{6}$$

The permeability could be obtained in Eqs. (1) and (6) as follows:

$$\frac{\Delta P}{L} = \frac{55\mu}{D_h^2}V \tag{7}$$

Thus,

$$D = \frac{55}{D_h^2} \tag{8}$$

The friction factor can be expressed as follows:

$$f = \frac{4\tau_w}{\frac{1}{2}\rho V^2} \tag{9}$$

The permeability could be calculated from the combination of Eqs. (1), (2), and (8) as follows:

$$D = \frac{4\tau_w}{\mu V D_h} \tag{10}$$

Table 1 shows the calculated permeability using each of the three different methods described earlier. The result obtained by the friction factor method was 30%, which was 32% less than that acquired by the CFD calculations using the wall shear stress and the pressure drop. The effect of the spacers could be the reason for the difference. Accordingly, the Darcy friction factor needs to be modified to calculate the exact shear stress of the fuel assembly, including the effect of the spacer grid.

Table 1. Results of permeability calculation

Method	Friction factor	Wall shear stress	Pressure drop
Permeability	3.61×10^5	5.17×10^5	5.34×10^5

4. Conclusions

The flow inside a fuel basket that contains a fuel assembly is analyzed using CFD. Three different methods were used to calculate the permeability and their results were compared. The friction factor method could be used to determine the approximate permeability without performing a CFD calculation. However, the permeability from the friction factor method is 50% less than the permeability from wall shear stress and pressure drop using CFD.

ACKNOWLEDGEMENT

It is gratefully acknowledged that this research was supported by MOTIE, Korea, under the Radioactive Waste Management Technology Development Project (20161720200930).

REFERENCES

[1] KEPCO and KHNP, PLUS7 Fuel Design for the APR1400, APR1400-F-M-TR-12001-NP, 2012.

[2] A. Bejan, Convective heat transfer, John Wiley & Sons, Inc., 1984.

[3] F. Engle, R. Markley, A. Bishop, “Laminar, transition, and turbulent parallel flow pressure drop across wire-wrap spaced rod bundles, Nuclear science and Engineering”, 69(2), 290-286 (1979).

Measurement Plan of Residual Moisture

K.S. Bang*, S.H. Yu, J.C. Lee, K.S. Seo, and W.S. Choi

Korea Atomic Energy Research Institute, 111, Daedeok-daero 989beon-gil, Yuseong-gu, Daejeon, Republic of Korea

*nksbang@kaeri.re.kr

1. Introduction

In order to maintain the integrity of spent nuclear fuel when spent nuclear fuel is stored in the dry storage system, water within the canister is drained, residual moisture in the canister and spent nuclear fuel must be removed, and spent nuclear fuel have to be stored in inert gas atmosphere. Drying equipment is required to remove the residual moisture remaining in the canister of the spent nuclear fuel storage system and spent nuclear fuel. In order to evaluate the amount of residual moisture remaining in the canister after drying the moisture present in the canister of the spent nuclear fuel storage system using the drying equipment, measurement system capable of measuring moisture content should be established. Therefore, the method of measuring the residual moisture according to the vacuum drying and the gas dehydration drying method was analyzed. The residual moisture measuring equipment was investigated and selected, and a schematic diagram of the measurement system for dryness evaluation was derived.

2. Key Parameters for Dryness Evaluation

In the United States, the University of South Carolina, South Carolina State University, University of Florida and AREVA are participating in experiments on vacuum drying and gas dehydration drying method under the Nuclear Energy University Programs (NEUP).

In this program, key conditions for simulating drying of spent nuclear fuel storage system are as follows;

- Vacuum and forced circulation
- Sequence, number, timing of stages in drying process
- Power to simulate decay heat with heater rods
- Ice formation

The main parameters for measuring or evaluating in experiment of this program are “temperature, chamber pressure, gas composition, gas flow rate, water removed as a function of time, indication of ice formation”.

The experiments conducted in this program are as follows;

- Design and fabrication of mock fuel assembly with heater rods and hardware
- Design and fabrication of vacuum chamber
- Testing with small chamber (vacuum and forced circulation)
- Instrument testing (guided wave, IR camera, thermocouples, etc.)
- Optical emission spectrometer (OES) was applied to a small chamber, and experiments were performed to obtain calibration curve as shown Fig. 1 to quantify the moisture content by analyzing the emission spectrum of dry and humid nitrogen under the pressure condition of 3 torr.

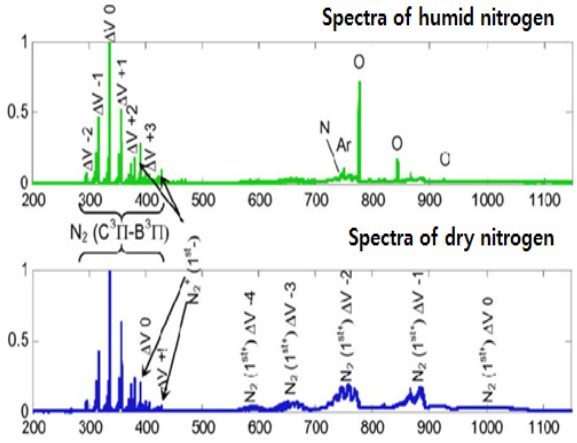


Fig. 1. Spectra of humid and dry nitrogen.

Regarding the evaluation of the integrity of the cladding in the drying of canister, the regulatory requirements for a dry storage system are prescribed as follows;

- Maximum fuel cladding temperature : < 400°C
- Repeated thermal cycling : < 10 cycles with cladding temperature variations more than 65°C
- Pressure : 3 torr for 30minutes (vacuum drying)
- Cold trap temperature : -7°C (gas dehydration drying)

Therefore, the following items were determined as the measurement items for drying evaluation in the drying process experiment.

- Temperature of the mock fuel rod, heater rod, and gas
- Pressure within chamber
- Flow rate at outlet and after remove the moisture

The following items will be included within the budget allowed.

- Gas composition after moisture removal
- Special glass window for preventing the distortion of wave and observation of the ice formation

3. Measurement System

According to the regulatory guidelines and standards for dry storage of spent nuclear fuel, it is estimated that the drying is sufficiently performed when the internal pressure is maintained within 3 torr for 30 minutes in case of the vacuum drying method [1], and when the cold trap temperature is maintained below -7°C for 30 minutes in case of the gas dehydration drying method [2]. We can perform a dryness evaluation as well as calculate the amount of the residual moisture in the canister of the dry storage system, if we could be known the pressure in the canister of the dry storage system and the temperature in the cold trap of the drying system when drying the canister of the storage system using drying equipment. Therefore, pressure and temperature measurements are required.

The regulatory guidelines and standards for dry storage of spent nuclear fuel specify that the integrity of spent nuclear fuel must be maintained during the drying process. Therefore, it is necessary to evaluate whether the temperature of the simulated fuel rod is maintained within allowable temperature.

While the temperature or pressure is deeply relate to the state or quality of the drying process, the flow rate mainly determines the balance of the process material relative to the amount of water in the drying process. Therefore, it is necessary to measure the mass flow rate in the drying process and the dehydration efficiency of the dehydrator or the condenser by measuring the mass flow rate of the gas from the outlet of the test chamber and the dehydrator.

Accordingly, the main items and measurement positions that need to be measured for the dryness evaluation in drying experiment of the spent fuel dry storage system were determined as follows;

- Pressure in the test chamber
- Temperature in dehydrator of drying system
- Mass flow rate at outlet of test chamber
- Mass flow rate through dehydrator or condenser
- Moisture content of the gas passing through the dehydrator or condenser
- Analysis of the composition of the gas passing through the dehydrator or condenser (provided that the budget permits)

The measurement system capable of measuring pressure and flow rate will be added in the temperature measurement system that is currently owned by the Korea Atomic Energy Research Institute. In addition, a moisture analyzer capable of directly measuring the moisture content of the gas passing through the dehydrator or condenser was selected and the purchase was completed.

We plan to install an emission capable of analyzing the composition of the gas under the condition that the budget allows. Fig. 2 shows the configuration of the measurement system

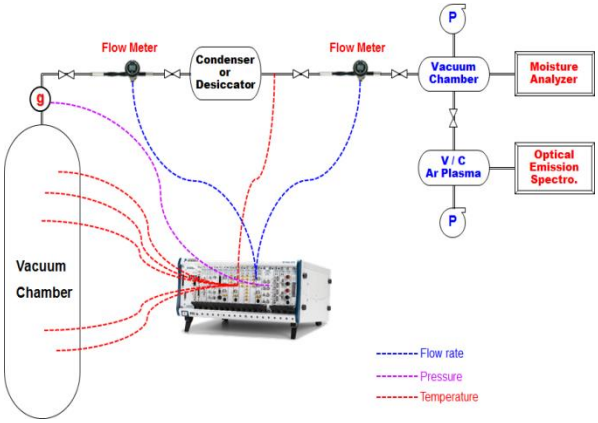


Fig. 2. Configuration of Measurement System.

ACKNOWLEDGEMENTS

It is gratefully acknowledged that this research was supported by MOTIE, Korea, under the Radioactive Waste Management Technology Development Project (20161720200930).

REFERRENCES

[1] NUREG-1536, Rev. 1, "Standard Review Plan for Spent Fuel Dry Cask Storage Systems", U.S. NRC Washington, DC, July 2010.

[2] Dry Storage Handbook, 2015 Edition "Fuel Performance in Dry Storage", ANT International, Molnlycke, Sweden, 2015.

Structure Integrity Evaluation of Fresh Nuclear Fuel

Yun-Young Yang*, Sang Soon Cho, Ki-seog Seo, and Woo-seok Choi

Korea Atomic Energy Research Institute, 111, 989 beongil, Daedeok-daero, Yuseong-gu, Daejeon, Republic of Korea

*yang0124@kaeri.re.kr

1. Introduction

For safe transport and storage of fuel, the integrity evaluation should be performed. But, considering the current research infra such as test facility, it is considerably difficult to implement test evaluation about many kinds of fuel. Therefore, finite element analysis evaluation can be more efficient alternative solution.

IAEA Safety Standard Series No.SSR-6[1], According to the notification 2014-050 from Nuclear Safety and Security Commission, the radioactive transport cask for the accident transport condition evaluation should be performed with such as 9 m free drop test, 1 m puncture test, thermal test and water immersion test. Through this process, the structure integrity of the transport cask can be evaluated.

In this study, the 9m free drop analysis was performed and the structure integrity evaluation was implemented about fresh nuclear fuel FEM model which is located in the transport cask.

2. Analysis

2.1 FEM model of fresh nuclear fuel

Fig 1. Shows the finite element model of the fresh nuclear fuel. Because the fuel meat and fuel cladding consisted of very thin plate, the shell element is used, and the side plate and end fitting are modeled as the solid element. The finite element model of the fresh nuclear fuel consists of 219,356 of elements and 184,172 of nodes.

Fuel cladding is constrained to side plate with tie conditions. PF foam is designed to absorb the impact force at the top, bottom, and side of the fresh nuclear fuel. End fitting and side plate consists of Al6061-T6 and fuel cladding is made of Al6061.

The transport cask usually carries 12 of fresh nuclear fuels assemblies. But this study modeled the 1 fresh nuclear fuel FEM model in the cask in order reduce the analysis time.

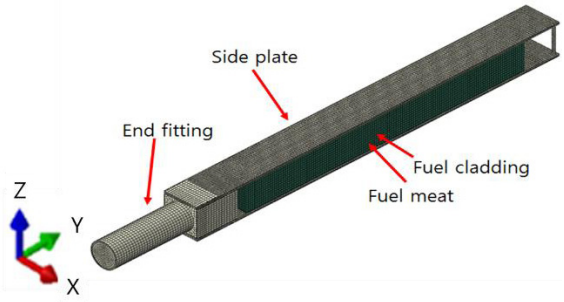


Fig. 1. FEM model of fresh nuclear fuel.

2.2 Drop analysis of the fresh fuel model

The free drop analysis of the transport cask including fresh nuclear fuel was performed using ABAQUS 6.14 [2]. Free drop was analyzed for four times in total, two times of horizontal drops, bottom vertical and Lid vertical drops. Horizontal drop was analyzed in two times, when the fuel cladding is arranged in vertical, and when it is arranged in horizontal. Fig. 2. Shows the finite element model of transport cask.

The floor target is rigid wall which is conservative condition. The drop velocity is 13.288 m/s corresponding to a height of 9 m.

Table 1 shows the results of fuel cladding and side plate stress for each drop posture. Fig. 3 shows the drop analysis results and focuses on fuel cladding. The left is the strain, and the right is the result of von Mises stress.

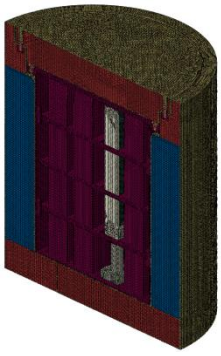
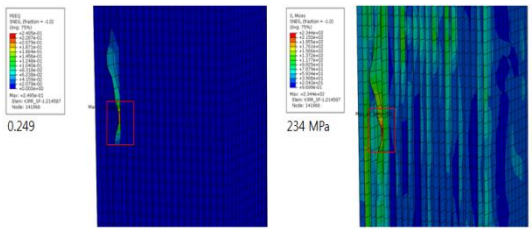


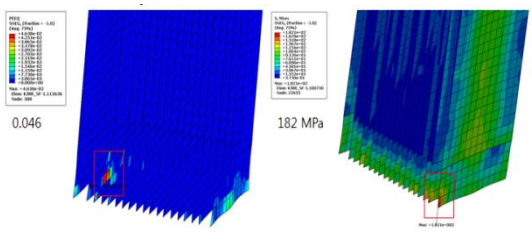
Fig. 2. Finite element model of transport cask.

Table 1. Max. von-Mises stress (unit:MPa)

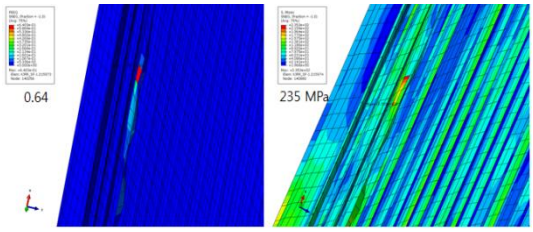
Direction	Cladding	Side plate
Bottom Vertical End Drop(Y)	234	259
Lid Vertical End Drop(Y)	182	324
Cask-Horizontal(Z) Fuel- Horizontal(X)	235	293
Cask-Horizontal(Z) Fuel- Vertical(Y)	228	240



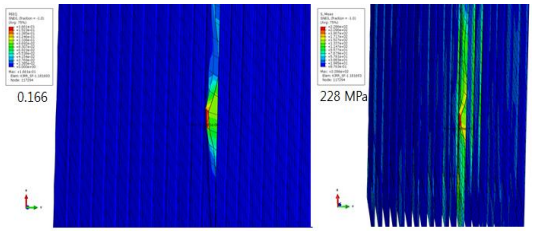
(a) Bottom Vertical End Drop(Y)



(b) Lid Vertical End Drop(Y)



(c) Cask-Horizontal(Z) Fuel- Horizontal(X)



(d) Cask-Horizontal(Z) Fuel- Vertical(Y)

Fig. 3. Distributions of the effective plastic strain and von-Mises Stress for each drop conditions.

In the case of bottom drop and lid drop, the direction of fresh nuclear fuel only changed, but not significantly different, and the upper side of the side plate showed some buckling.

In the case of a horizontal drop, the shape in which the stress appears depends on the direction of the fresh nuclear fuel. When the fresh nuclear fuel dropped horizontally, cladding caused a lot of stress due to bending, and when the fresh nuclear fuel dropped vertically, it appeared to come out higher at the part contacting the side plate.

3. Conclusion

The structural integrity of fresh nuclear fuel was evaluated by carrying out several 9 m drop analysis of the transport cask including fresh fuel. The local permanent deformation of the fuel cladding occurred in all 9-m drop conditions. In addition, it was observed that there was a considerable difference depending on the direction of the fresh nuclear fuel even though the drop directions of the cask are same. However, we did not conclude yet if the structural integrity of the fresh nuclear fuel is able to be maintained since there are so many stress localization in the analysis results.

In the future, we will conduct again model verification of the fresh nuclear fuel model and evaluate the structural integrity of it more precisely.

REFERENCES

[1] IAEA safety standard series No.SSR-6, “Regulation for the safe transport of Radioactive Material”, 2009.

[2] ABAQUS(6.14) analysis user manual.

Thermal Analysis of Transportation and Storage Cask of Spent Nuclear Fuel for Forced Gas Drying Condition

Suk-Nam Lim[1*], Gyung-Sun Chae[1], Jae-Hyun Han[1], Jae-Seok Park[1], and Dong-Gyu Lee[2]

[1]SAE-AN ENGINEERING Co., 481-10 Gasan-dong, Geumcheon-gu, Seoul, Republic of Korea

[2]Korea Nuclear Engineering & Service Corporation, 65, Myeongdal-ro, Seocho-gu, Seoul, Republic of Korea

[*]limsn@sae-an.co.kr

1. Introduction

The national high level radioactive waste management plan indicates that dry storage systems are to be installed for expending on site storage capacity of NPPs and establishing a centralized interim storage.

A Test grade Forced gas Drying equipment (TFD) is being developed as the drying process system to remove moisture in a cask.

As a part of the dry storage of the spent nuclear fuel (SNF), a canister of a dual-purpose cask (DPC) is loaded with the SNF under water. After draining the majority of the water, the remaining water in the canister must be removed using drying system to prevent corrosion and hydrating of the SNF.

The NUREG-1536 describes that the maximum calculated fuel cladding temperature should not exceed 400℃ for normal conditions of storage and short-term loading operations, including cask drying and backfilling.

Thermal analysis of DPC of PWR SNF during drying operation by TFD was conducted to identify compliance with the drying criteria after completing detailed design of TFD.

This paper presents thermal analysis results of transportation/storage cask during cask drying with the TFD to identify drying performance and fuel cladding integrity.

2. Thermal analysis

2.1 General information

The design features of TFD are as follows

- Flow rate: 65㎥/hour
- Operating pressure: 70 psig
- Inlet /outlet temperature: 150℃/180℃
- Cooling temperature: Max. - 20℃

The Fig. 1 shows a simplified TFD diagram including canister.

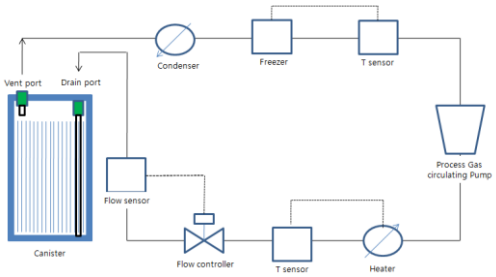


Fig. 1. Simplified diagram of TFD.

The key specifications of KORAD-21 DPC are provided in the Table 1.

Table 1. Design specifications of DPC

Item	Specification
Storage capacity	21 PWR (WH & CE)
Maximum Burn up	45 GWd/MTU
Max-average enrichment	4.5wt.% U-235
Minimum Cooling time	10 years
Max-decay heat	16.8 kW /canister
Free volume of canister	6,456 L

2.2 Thermal analysis model

The heat transfer modes in each process are provided in the Table 2.

Table 2. Heat transfer modes in each process

Item	Internal environment of canister		
	Wet	Drying	Dry
Medium	Water	-	He
Transfer mode	-Conduct -Natural convect	-Forced convect -Conduct	-Conduct -Convect -Radiat

Based on the canister drying condition and the heat transfer mode, a three-dimensional finite volume model was constructed to perform the thermal analysis. The thermal analysis was carried out using FLUENT 13.0.

The modeling included all components such as the SNF assembly, neutron absorber, basket, disk, canister, cask body, neutron shield, and canister lid. Especially, the thermal analysis model for the SNF assembly was modeled in the form of a homogeneous model, so as to simulate heat transfer characteristics of the assembly.

Simulations were performed with 21 hours of transient analysis under 3 conditions. During drying process, the inlet and outlet boundary condition of canister was established and modeled to describe the drying gas circulating process.

Thermal analysis conditions of each process are shown in the Table 3.

Table 3. Thermal analysis conditions of process

Item	Process		
	Wet	Drying	Dry
Duration(hr)	15	3	3
Medium	Water	Water/He	He
Ambient(℃)	38	38	38
Initial condition	46 ℃ equiv.	From former	From former
Decay heat	Maximum	Maximum	Max.

The drying operation process occurs in the spent fuel facility and the cask is installed vertically.

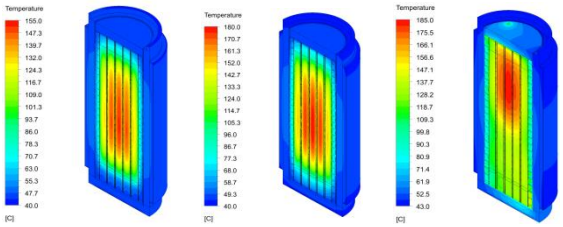
Boundary condition in the form of convection and radiation heat transfer was defined at the cask surface.

2.3 Analysis results

Short term loading operations consists of wet process (loading SNF in the pool), cask drying process (Helium recirculation and moisture removal) and dry process (backfilling). The analysis results of calculated maximum cladding temperature in each process are shown in the Table 4 and Fig. 2.

Table 4. Calculated maximum cladding temperature

Process	Wet	Drying	Dry
Temperature (℃)	152.1	179.4	184.1



Wet (15hr) Drying (3hr) Dry (3hr)

Fig. 2. Temperature distribution in the DPC at the end of the each process.

3. Summary

The thermal analysis of transportation and storage cask for SNF was conducted during short term loading operations for forced gas drying condition.

The fuel cladding temperature in 6 regions of SNF in the cask during the short term loading operations for forced gas drying condition is shown in the Fig. 3.

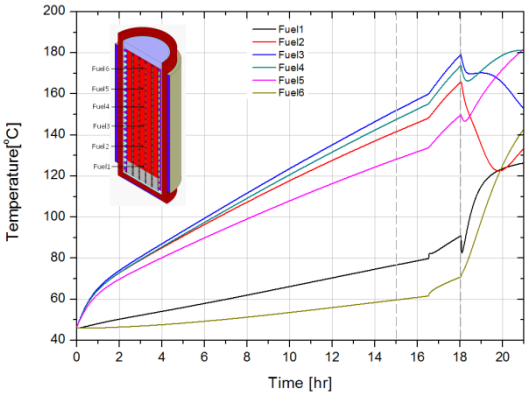


Fig. 3. Fuel cladding temperature history in 6 regions of SNF.

The thermal analysis results of calculated maximum cladding temperature in each process demonstrate that operating scenario of TFD in detailed design maintain well below the temperature limits of 400℃.

REFERENCES

[1] NUREG-1536 Revision 1 Standard review plan for spent nuclear fuel dry storage system at a general license facility.

Structural Integrity Evaluation of Spent Nuclear Fuel Assembly Under Normal Transportation Drop Conditions

Sang Soon Cho*, Woo Seok Choi, Ki-Seog Seo, and Yun-Young Yang

Korea Atomic Energy Research Institute, 111, Daedeok-daero 989beon-gil, Yuseong-gu, Daejeon, Republic of Korea

*sscho96@kaeri.re.kr

1. Abstracts

In this study, the structural integrity of the spent nuclear fuel assemblies was evaluated by carrying out a 0.3 m drop impact analysis, one of the normal transportation conditions of the nuclear fuel assemblies. For this purpose, the spent nuclear fuel assembly was modeled in detail as beam elements, and a coupled model for impact analysis was developed by inserting the modeled nuclear fuel assemblies into a cask.

2. Introduction

2.1 General information

Recently, the assessment of the integrity of spent fuel cladding for normal transport conditions as well as the hypothetical impact accident condition is becoming an increasingly important. The failure mode of the spent fuel cladding varies depending on the input conditions of the accident load, the shape of the fuel, and the material properties. It has been known that the elongation is known to be 1 ~ 4% and the maximum elongation varies with load and boundary conditions according to the results of physical properties of spent fuel cladding [1]. Therefore, in order to evaluate the integrity and failure mode of the cladding tube against for normal transport conditions as well as the hypothetical impact accident load, the influence of the cladding, the spacer grid, the tie plate and so on should be considered.

Sandia National Lab. suggested finite element modeling and analytical methodology for drop impact analysis of single spent fuel cladding and spent fuel assemblies, and describes the methodology for evaluating the integrity of spent fuel cladding [1].

USNRC and PNNL have described the finite element modeling method and the evaluation method using the shell and beam elements for the drop analysis of a single spent fuel cladding on the basis of the reference [1] [2].

In this study, the spent fuel assemblies were modeled in detail as beam elements [3], and a coupled model for impact analysis was developed by inserting a modeled fuel assembly finite element model into the cask.

The impact analysis of 0.3 m drop height, one of the normal transport conditions of the spent nuclear fuel assemblies, was performed and the integrity of the nuclear fuel assemblies was evaluated.

2.2 Analysis Conditions

The drop impact analysis in the normal transport condition was carried out with the finite element model including the fuel assemblies developed in Reference [3] as shown in Fig. 1, and the 0.3 m vertical and 0.3 m horizontal drop impact analysis were performed.

The following assumptions was made for the analysis of vertical and horizontal drop impacts.

- The spent fuel assemblies are CE type
- The drop height is 0.3 m
- The shock absorber is an isotropic material with a yield stress of 12.2 MPa
- Allowable failure strain of cladding is 0.04

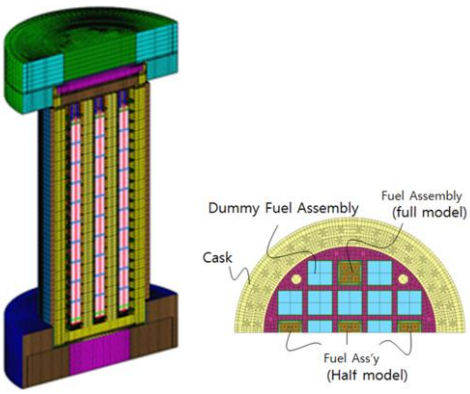


Fig. 1. Coupled Finite Element Model of Transport /Storage Cask and Spent Nuclear Fuel Assemblies.

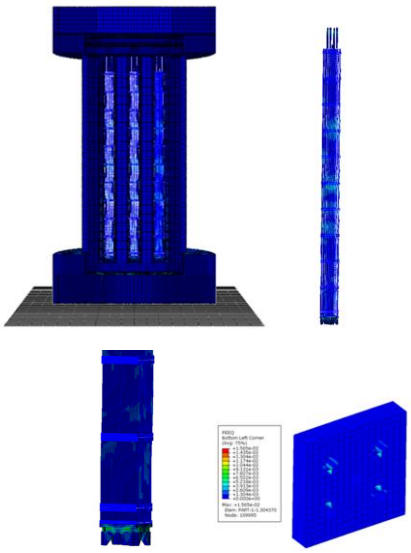


Fig. 2. Analysis Results for 0.3 m Vertical End Bottom Drop.

3. Analysis Results

3.1 0.3 m Vertical End Drop Analysis

Fig. 2 show the effective plastic strain distribution of the cask, the spent nuclear fuel assemblies and grid for the 0.3 m vertical end drop analysis.

No plastic deformation occurred in the cladding of the fuel assembly in the transport cask, and a small plastic strain of 0.018 was generated in the supporting grid

3.2 0.3 m Side Drop Analysis

No plastic deformation occurred in the cladding of the fuel assembly in the transport cask, but a relatively large plastic strain of 0.291 occurred in the supporting grid as shown in Fig. 3.

Table 1. Analysis Results for 0.3 m Drop Height in Normal Transportation Conditions

Drop Direction	Cask Acceleration G	Impact Limiter Deformation mm	Max Plastic Strain @ Cladding	Max Plastic Strain @ Grid
Bottom	40.67	11.69	0.000	0.016
Horizontal	22.32	23.55	0.000	0.291

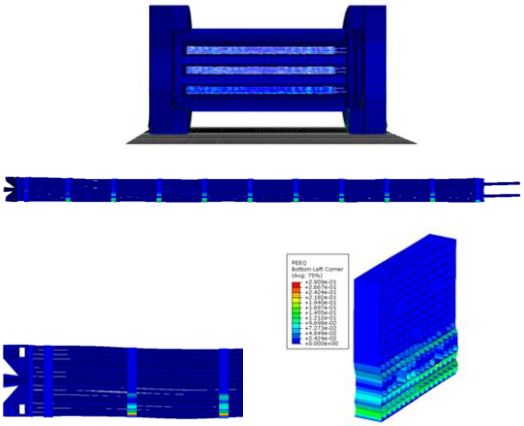


Fig. 3. Analysis Results for 0.3 m Horizontal Drop.

4. Conclusions

It was concluded that there is no problem in the integrity of the cladding of the nuclear fuel assemblies as well as the transport cask in the vertical and horizontal drop impact analyses at the normal transport condition of 0.3 m. However, in the case of a horizontal drop of 0.3 m under normal transport conditions, a relatively large plastic deformation or local failure may occur in some grids supporting the fuel claddings.

REFERENCES

[1] T. L. Sanders, et al., “A Method for Determining the Spent-Fuel Contribution to Transport Cask containment Requirements”, Sandia National Laboratories, SAND90-2406, TTC-1019 (1992).

[2] D. T. Tang, J. Guttmann, B. J. Koeppel and H. E. Adkins, “High Burn-up Spent Nuclear Fuel Structural Response when subjected to a Hypothetical Impact Accident”, Proc. of ASME/JSME Pressure Vessels and Piping Division Conference, July 25-27, 2004, USA.

[3] S.S. Cho, W.S. Choi, K.S. Seo and Y.Y. Yang, “Drop Analysis of Spent Nuclear Fuel including Cladding”, Proc. of the KRS 2016 Fall Conference, 14(2), Oct. 12-14, 2016, Jeju.

Remote Operation and Maintenance of Crane System for Use in ACPF Argon Cell

Jong Kwang Lee*, Byungsuk Park, Sunghyun Kim, Kiho Kim, Il-Je Cho, and Eun-Young Choi
Korea Atomic Energy Research Institute, 111, Daedeok-daero 989beon-gil, Yuseong-gu, Daejeon, Republic of Korea
*leejk@kaeri.re.kr

1. Introduction

The Advanced spent fuel Conditioning Process Facility (ACPF) at the Korea Atomic Energy Research Institute (KAERI) has recently been successfully renovated to demonstrate lab-scale electrolytic reduction process using the spent fuel. One of the highlights of this renovation project was the installation of a small argon compartment within the atmospheric hot cell of the facility [1, 2]. A special crane system for use inside the compartment was also developed and tested under the renovation project. In this paper, we describe the remote operation and maintenance of the crane system.

2. Remote crane system

2.1 Key features of the design

In general, the electric drive unit of a bridge crane is connected directly to the mechanical drive unit at high elevation. However, this configuration is not proper for the argon cell crane considered in this study because of the limited space reserved for the crane as well as the reach limitation of the MSM. We devised a remote actuation mechanism where the mechanical and electrical parts of the crane system are separated, located far from each other, and connected through power transmission shafts and bevel gears. The electrical parts consisting of servomotors, position sensors, and limit switches were lowered in place inside the workspace of the MSM. They transmit power to the mechanical parts installed near the ceiling. Even though this configuration does not provide an optimal solution, as the mechanical parts are placed outside the workspace of the MSM, it can become a widely used practical solution because it makes it easier to enhance the durability of the mechanical parts to minimize or eliminate the possibility of mechanical failure within the expected lifetime of the crane.

In addition to the use of a remote actuation mechanism, the use of a linear drive mechanisms for precise motion, modular design of electrical components for easy maintenance, and the use of appropriately dimensioned, commercially proven components to ensure durability are implemented to design a smaller crane that is easily maintainable by the MSM. Furthermore, the cable tray is shifted from a high location near the mechanical parts of the crane and installed on a wall near the electrical parts. Therefore, this maximizes the working volume of the crane. Fig. 1 shows a three-dimensional computer-aided design model of the crane system.

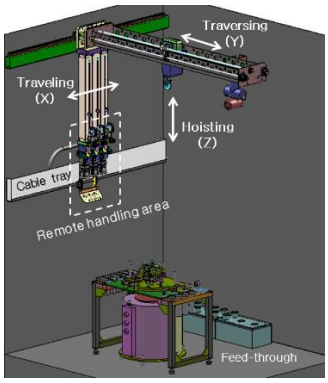


Fig. 1. 3D CAD model of the crane system.

Another key feature of the design is modular design for easy maintenance which is a major goal in the design of a remote handling system because it reduces service downtime and associated costs with quick troubleshooting. One common approach involves duplicating the same module for redundant use: for instance, the spare module is used in an emergency, whereas the damaged module is repaired in a maintenance area. Instead, an on-site replacement method is used that takes into consideration the limited space available for the crane. As shown in Fig. 2, two modular design concepts are introduced for a drive module and a sensor module, focusing particularly on their easy remote maintenance.

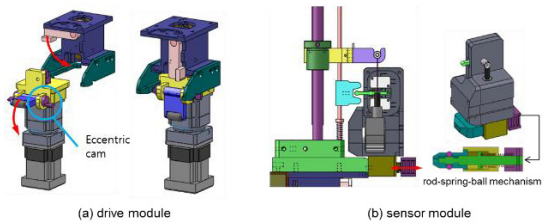


Fig. 2. Modular design for easy maintenance of drive module and sensor module.

2.2 Control system

An accurate servo-control system is also developed based on absolute positioning measurement to allow for the safer performance of perform through automatic operation. The motion controller integrates camera controller, therefore, the operator can operate the crane system by watching the camera monitor as well as looking through the lead-glass shield window. Several control modes, such as the jog mode, the absolute positioning mode, and the sequential operation mode, are prepared to be selectively assumed using the touch pendant in which several graphical pages are linked to each control mode.

2.3 Remote operation and maintenance

The crane system was tested and qualified at a full-scale evaluation mock-up facility prior to installation in the hot cell. After introducing the crane system to the hot cell, several mechanical and electrical tests were performed to check whether the crane system performed at the desired level. The maximum deflection of the girder frame at a load of 1.5 kN was measured at approximately 0.3 mm. The overall height of the trolley hoist including the load hook was 271 mm: this meant that the hook could be placed over the MSM, thereby achieving the design requirement for remote maintenance on it.

As shown in Fig. 3, several remote maintenance experiments were conducted to verify that the driving modules, sensor modules, and a hook of the crane can be replaced using an MSM only. For successful remote operation and easy maintenance, following design considerations were also considered in the design of the crane system,

- Alignment mark for visual guidance
- Proper guiding structure
- Modular design considering handling device
- Direction of the force applied from the remote system
- Initial pose of MSM
- Use of the camera to enhancement of work efficiency

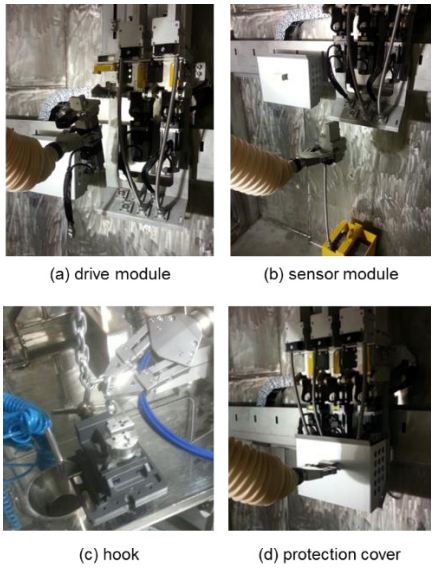


Fig. 3. Remote maintenance test of crane system modules.

3. Conclusion

Several operation and maintenance tests of the crane system showed that all design goals were achieved in general, especially remote maintainability. Based on the experimental results, the remote operation and maintenance procedures were established. The ACPF is right before hot operation, and further work is underway on the production of document for responding to normal and abnormal situation.

REFERENCES

[1] Yu, S.N., Lee, J.K., Park, B.S., Cho, I.-J., Kim, K., “Hot cell renovation in the spent fuel conditioning process facility at the Korea Atomic Energy Research Institute,” Nuclear Engineering and Technology, 47, 776–790 (2015).

[2] Lee, J.K., Park, B.-S. Yu, S.-N., Kim, K., Cho, I.-J., “Crane system with remote actuation mechanism for use in argon compartment in ACPF hot cell”, Nuclear Engineering and Design, 307, 144-154 (2016).

3분과

고준위폐기물처분 (Oral)

Vitrification of Radioactive Waste Salt Using Modified Si-Al-P Composites

Ki Rak Lee*, Hwan-Seo Park, Ahreum Han, Jung-Hoon Choi, and Seung Youb Han
Korea Atomic Energy Research Institute, 111, Daedeok-daero 989beon-gil, Yuseong-gu, Daejeon, Republic of Korea
*kirakki@kaeri.re.kr

1. Introduction

SAP (SiO2-Al2O3-P2O5) composite has been suggested by KAERI to immobilize the radioactive waste salts generated from pyroprocessing. In Korea, LiCl used at electro-reduction process and LiCl-KCl used at the electro-refining process are generated as radioactive waste salts containing small amounts of fission products. Vitrification method using conventional glass matrix are not suitable to deal with these reactive salts wastes. However, SAP composite successfully convert the highly unstable salt waste to stable compounds via dechlorination process. SAP waste forms exhibit good performances such as high waste loading, high chemical durability and suitable physical properties. In previous study, SAP composites were synthesized by sol-gel method. This method is expensive and is not suitable for mass production to treat large amounts of salt wastes. Therefore, development of economical method to treat salt wastes without performance loss is needed.

2. Experimental

Same composition of previous SAP material was selected. Adjusted amounts of SiO_2, $Al(OH)_3$, $(NH_4)H_2PO_4$, B_2O_3, Fe_2O_3 were mixed. The mixture was heat-treated at 500℃ and the material containing $AlPO_4$ or SAPO-20 was synthesized. LiCl with 0wt%, 10wt% 20wt% and 30wt% ratio of nuclides ($SrCl_2$, CsCl) were used as surrogate radioactive salt waste. The prepared salt waste and K-SAP were mixed with various ratio for wasteform synthesis. Each sample was labeled K-SAP n where the n was assigned to the ratio of K-SAP/waste salt. Additionally amount of nuclides was indicated at end of labels ; K-SAP2-1 (10wt%), K-SAP2-2 (20wt%), K-SAP2-3 (30wt%). Dechlorination process of the mixture was heat-treated at 650℃ and dechlorination product was vitrified with 1300℃ heat-treatment. XRD, SEM, and TGA were conducted for physical characterization. Chemical durability was evaluated using ASTM Standard C 1285-02 (PCT-A).

3. Results and discussion

From XRD result of K-SAP, $AlPO_4$ and Fe_2O_3 peaks were indicated. However, $AlPO_4$ peaks were similar with SAPO-20 material. Further analysis is needed. From XRD results of dechlorination products, unreacted LiCl and Lithium chloride borate existed in K-SAP1. Main crystaline phases were Li-aluminosilicate and $AlPO_4$. In higher ratio of K-SAP/salt, unreacted Cl compounds were removed, and Li_3PO_4 and $AlPO_4$ were formed. It is means that over capacity which can react with waste salt remain in K-SAP. Dechlorination ratio was calculated via TGA results. Weight loss value of K-SAP 1 and K-SAP 1.5 was 15wt % and 4.5wt %, respectively deu to unreacted salt compound. For over ratio 2, weight loss over 500℃ was below 1wt%. it means that metal chlorides are almost dechlorinated under the given condition. Therefore, optimized ratio of K-SAP and salt might be ratio 2 with perfect dechlorination reaction. Using ratio 2 of K-SAP, K-SAP 2-1, K-SAP 2-2, and K-SAP 2-3 with surrogate salt was prepared. Uniform wasteforms were formed over 1300℃. Amorphous phases were indicated from XRD results. From SEM images, dense and defect-free surfaces o K-SAP wasteforms were detected. In the case of durability test, PCT-A method was used. Cs and Sr show high durability of 10^{-2} ~ 10^{-3} g $m^{-2}day^{-1}$ and compositions of matrix such as Si, Al, P, B, and Fe show 10^{-1} ~ 10^{-2} g $m^{-2}day^{-1}$.

4. Conclusion

All wasteforms with wide range of composition except K-SAP 1 showed glassy monolithic shapes. A wide range of wasteform ratio for a monolithic form is essential property as wasteform due to inaccuracy of waste compositions and amounts. Using XRD and SEM analysis, amorphous, dense, and monolith wasteforms were detected.

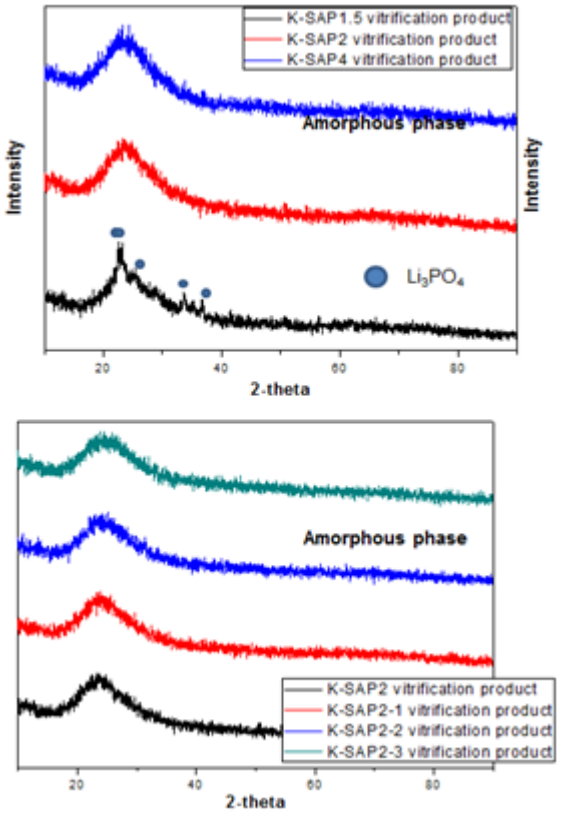


Fig. 1. XRD results of K-SPA wasteforms.

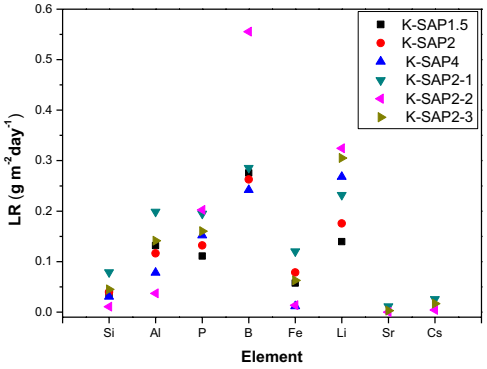


Fig. 2. PCT-A results of K-SAP wasteforms.

REFERENCES

[1] H-S. Park, I-H. Cho, H-C. Eun, I-T. Kim, Y-Z. Cho, and H-S. Lee, "Stabilization/Solidification of Radioactive LiCl-KCl Waste Salt by Using SiO_2-Al_2O_3-P_2O_5 (SAP) Inorganic Composite: Part 1. Dechlorination Behavior of LiCl-KCl and Characteristics of Colsolidation", Environ. Sci. Technol., 45, 1932 (2011).

[2] I.-H. Cho, H.-S. Park, S.-N. Ahn, I.-T. Kim and Y.-Z. Cho, "Stabilization/Solidification of Radioactive LiCl-KCl Waste Salt by Using SiO_2-Al_2O_3-P_2O_5 (SAP) Inorganic Composite: Part 1. The Effect fo SAP Composition on Stabilization/Solidification", J. Kor. Rad. Waste Soc., 10(1), 45 (2012).

Review of Anion Diffusion in Highly Compacted Montmorillonite for Copper Corrosion Modeling

Heui-Joo Choi*, In-Young Kim, Minsoo Lee, and Dong-Keun Cho

Korea Atomic Energy Research Institute, 111, Daedeok-daero 989beon-gil, Yuseong-gu, Daejeon, Republic of Korea

*HJCHOI@kaeri.re.kr

1. Introduction

KAERI has developed the geological disposal systems for high-level wastes (HLW). The main safety function of the disposal system is the isolation of HLW from the human environments for a very long period. Generally, the HLW is isolated with the engineered barrier system composed of a disposal canister and buffer.

The authors have developed the engineered barrier system consisting of a copper disposal canister and a Ca-bentonite buffer for the geological repository. The cold spray coating technique was used to manufacture a disposal canister, and a very long-term corrosion experiment is in progress at the KURT for ensuring the long-term performance of a copper canister.

Recently, the parts of long-term corrosion test results conducted at the KURT were published [1]. According to the report, the major corroding agent for copper is the dissolved oxygen in groundwater, since the water was taken from a borehole not too deep. The authors developed a numerical model for the corrosion test.

It is well-known that the corroding agents of copper under the repository condition are chloride ion, sulphide ion, and dissolved oxygen, which are all anionic ions. In the geological repository the disposal canister is surrounded by a bentonite buffer, in which no groundwater flow is allowed. Thus, the copper is corroded by the diffusion of corroding agents through a compacted montmorillonite buffer.

In general, the diffusion of anion in the compacted montmorillonite is explained by pore water diffusion and anion exclusion. In this study, the effect of anion diffusion on the copper corrosion was examined, and the diffusion of anion in compacted montmorillonite was reviewed and documented in detail to develop a copper corrosion model.

2. Copper corrosion

2.1 Corrosion test at the KURT

The long-term corrosion tests were performed under the simulated conditions at the KURT to verify the corrosion resistance of a copper canister. The column test (marked [B] in Fig. 1) at 70°C was carried out for approximately 3 years from 2009 to 2012. The groundwater from a borehole in the KURT was supplied at a flow rate of 15 cc/min. Fig. 2 shows the corrosion depth of copper specimens for three years.

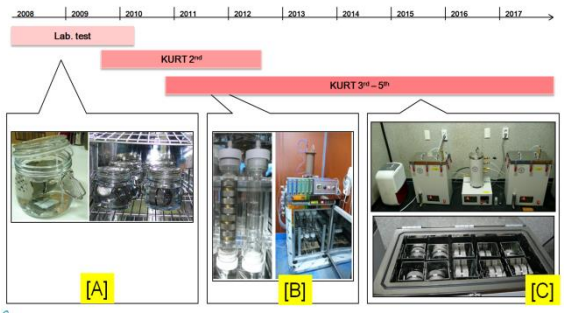


Fig. 1. Long-term corrosion test at the KURT.

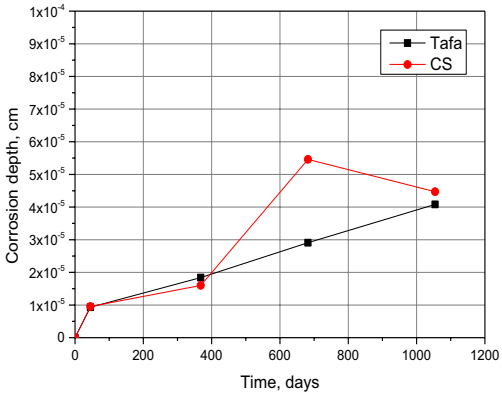


Fig. 2. Corrosion depth of copper specimens.

2.2 Corrosion modeling

The transport mechanism of anions such as dissolved oxygen or sulphide through highly compacted bentonite buffer is mainly diffusion. Then, the one-dimensional diffusion equation in bentonite buffer is described in equation (1):

$$\frac{\partial C}{\partial t} = D_a \frac{\partial^2 C}{\partial x^2} \quad (1)$$

The apparent diffusion coefficient (D_a) of anion in equation (1) is generally identical to pore diffusion coefficient (D_p). The corrosion depth of copper is proportional to the cumulative diffusive flux of corroding agent through the bentonite buffer, and the cumulative diffusive flux is given as follows:

$$Cflux = -D_p \cdot \varepsilon \cdot Area \cdot \int_0^T \frac{\partial C}{\partial t} dt \qquad (2)$$

The porosity in equation (2) for anion is generally expressed as an effective porosity due to anion exclusion. There is a large difference between the effective porosity and total porosity for highly compacted montmorillonite.

3. Anion diffusion

3.1 Previous Study on diffusion coefficients

J. O. Lee et al. measured the diffusion coefficient of Iodide for the domestic Ca-bentonite. The effective diffusion coefficient was 1.25×10^{-12} m^2 s^{-1} at dry density of 1.7 Mg m^{-3}, which was one order of magnitude lower than the apparent diffusion coefficient [2]. S.P. Yim et al. investigated the diffusion of iodide in compacted bentonite containing Ag_2O [3]. They measured the diffusion coefficient of 8.7×10^{-12} m^2 s^{-1} at dry density of 1.6 Mg m^{-3} with no addition of Ag_2O.

T. Kozaki et al. measured the diffusion of Chloride ions in sodium montmorillonite to understand the diffusion mechanism [4]. They reported the apparent diffusion coefficient of around 3.7×10^{-11} m^2 s^{-1} at dry density of 1.6 Mg m^{-3} at 25°C.

3.2 Anion Exclusion

It is well-known that anion transport through the stacks of montmorillonite does not take place because of Donnan exclusion [5]. This means that anion diffusion takes place through a part of total porosity in bentonite buffer.

According to the previous study by J.O. Lee et al., this ratio is around 9% of the total porosity at the dry density of 1.7 Mg m^{-3}. Pusch et al. reported that the volume of interlayer water takes 10% of total water volume [5]. Also, it was reported that in case of a high ionic strength solution, the charges on the surface led to a lower exclusion effect [6].

As given in equation (2), the corrosion depth of copper depends only on the effective porosity, through which anion can transport. It is very crucial to distinguish and estimate the interlayer porosity and inter-particle porosity.

4. Conclusion

A copper disposal canister may be corroded under the geological repository conditions. It has been known that most of corroding agents are anions such as dissolved oxygen and sulphide. The corrosion depth of copper is proportional to the effective diffusion coefficients of anions in bentonite buffer, which were influenced much by the anion exclusion. To this end, a more sophisticate diffusion model should be developed to explain the anion exclusion in detail.

Acknowledgement

This work was supported by the Ministry of Science, ICT and Future Planning within the framework of the national long-term nuclear R&D program (NRF-2017M2A8A5014856).

REFERENCES

[1] Minsoo Lee, Heui-Joo Choi and Jong Youl Lee, KAERI/TR-6764/2017, 2017.

[2] J.O. Lee, W.J. Cho, P.S. Hahn, and H.H. Park, “Diffusion Characteristics of Iodide in a Domestic Bentonite of Korea”, Journal of Korean Nuclear Society, 26(2), 285-293, 1994.

[3] Sung Paal Yim, Ji Hyun Lee, Heui-Joo Choi, Jong-Won Choi, and Cheo Kyung Lee, An Investigation of Diffusion of Iodide Ion in Compacted Bentonite Containing Ag_2O, J. of the Korean Radioactive Waste Society, 9(1), 33-40, 2011.

[4] Tamotsu Kozaki, Koichi Inada, Seichi Sato, Hiroshi Ohashi, Diffusion mechanism of chloride ions in sodium montmorillonite, Journal of Contaminant Hydrology, 47, 159-170, 2001.

[5] Roland Pusch, Ola Karnland, Harald Hokmark, SKB-TR-90-43, p20, 1990.

[6] Luc R. Van Loon, Martin A. Glaus, Werner Muller, Anion exclusion effects in compacted bentonites: Towards a better understanding of anion diffusion, Applied Geochemistry, 22, 2536-2552, 2007.

Complex Behavior of Radionuclides in a Disposal Environment

Jae-Kwang Lee*, Seung-Yeup Lee, and Min-Hoon Baik

Korea Atomic Energy Research Institute, 111, Daedeok-daero 989beon-gil, Yuseong-gu, Daejeon, Republic of Korea

*jklee1@kaeri.re.kr

1. Introduction

A study on the complex behavior of radionuclides in a deep geological disposal environment for radioactive wastes is necessary to predict their migration and retardation. A disposal system for radioactive waste was mainly consists of a disposal canister, buffer/backfill material and natural barrier. It is generally known that the geochemical behavior between radionuclides and the components of disposal system is a main retardation process of radionuclide migration in a deep geological environment. The geochemical reaction of radionuclides is highly affected by various geochemical conditions such as pH, redox potential, ionic strength, microbe and ionizing radiation.

This work is focused on the reaction between radionuclides and corrosion products, the alteration of bentonite and its effect on the sorption/diffusion of radionuclides, the microbial effect on the migration of radionuclides and the combined reaction of radiation and microbe.

2. Materials and Methods

2.1 Materials

Copper disks (99.90% Cu), Kyungju bentonite, KURT granite and goethite were used as a component of a geological disposal of radioactive wastes. All the solutions were prepared with deoxygenated ultrapure water with a resistivity of 18.3 MΩ/cm (Milli-Q system, Millipore) under anaerobic conditions in a glove box filled with Ar.

2.2 Methods

Gas generation was measured by gas chromatography (7890A, Agilent) using a packed column and thermal conductivity detector. The composition and morphology of corrosion products on copper specimen was analyzed using XRD and SEM. XRD patterns were taken using Cu-Kα radiation and a Rigaku D/MAX 2200 Ultima X-ray diffractometer. The surface morphology was observed using FE-SEM (JSM-7000F, JEOL) and the chemical composition of corrosion products formed on the copper specimen were analyzed using Energy Dispersive X-ray analysis (EDS). Copper in aqueous solution dissolved from the copper sample was measured using ICP-MS (Ultramass 700, Varian).

3. Results

The distance of the interlayers of bentonite can be reduced when Cu^{2+} exchanged with ions (Na^{+}, Ca^{2+}) located in the interlayer of the raw bentonite owing to the differences of the hydration energy among Cu^{2+}, Na^{+}, and Ca^{2+}. Consequently, the contraction of the basal plane spacing resulted in the reduction of swelling pressure of bentonite. However, copper exchanged bentonite sorbed uranium and cesium more than the raw bentonite. The exchange of copper with ions of bentonite interlayer could reduce the mobility of radionuclides.

A γ-irradiation increased the H_2 gas generation and the dissolution of copper ions from the metallic copper. The generation of H_2 gas was mainly affected by the total irradiation dose and chloride concentration. After γ-irradiation, cuprite (Cu_2O) was observed as a major corrosion product and very few tenorite (CuO) was also observed. A microbial activity induced the generation of H_2(g) and H_2S(g) and formed the corrosion products of copper and irons as chalcocite(Cu_2S) and mackinawite(FeS) respectively.

The microbes inhabiting in Kyungju bentonite were isolated and identified and the changes in the microbial community existed in fracture filling minerals were observed. Different kinds of sulfate reducing bacterium were identified from Kyungju bentonite and the *Veillonella* genus was observed

from the matured fracture fillings. In the presence of bacteria and H_2, the sorption of uranium by Kyungju bentonite and fracture fillings increase as a function of the growth time due to the changes in the microbial community in natural minerals.

Gamma-irradiation did not affect the viability of bacteria and the combined reaction between gamma-irradiation and the microbial activity resulted in the increase of uranium sorption due to the changes in redox environments and forming a strong binding between uranium and newly formed secondary mineral from goethite.

The formation of CuI induced by the microbial activity immobilized the iodide in a copper exchanged bentonite. Microbial activity also reduced the mobility of uranium in the compacted bentonite by the formation of mackinawite with a high sorption affinity to uranium when the sulfate was added.

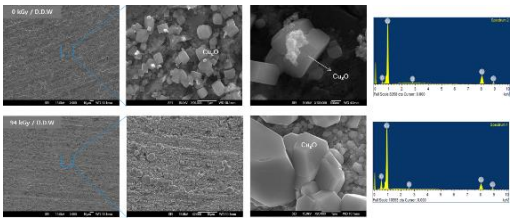


Fig. 1. Effect of γ-irradiation on the formation of copper corrosion products.

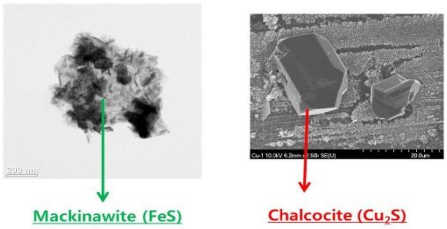


Fig. 2. Effect of microbial activity on the formation of iron/copper corrosion products.

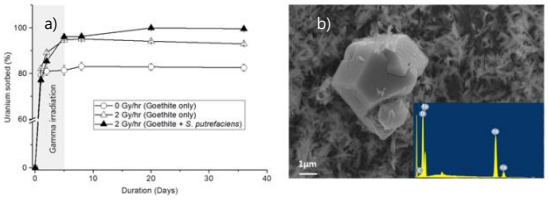


Fig. 3. Effect of microbe and γ--irradiation on U sorption and formation of magnetite.

4. Conclusion

The results of a study on the complex behavior of radionuclides and the relative technologies can be directly utilized for the disposal of the spent fuel generated in Korea. Models and data obtained from this work can be also applied to the development of the safety case. Moreover, the reliability of the safety for the disposal of radionuclides can be enhanced by presenting the scientific evidences on the complex behavior of radionuclides in a deep geological environment to the public.

REFERENCES

[1] N.A. Chapman, I.G. McKinley, and M.D. Hill, “The Geological Disposal of Nuclear Waste”, John Wiley & Sons, Chichester (1987).

[2] I.G. McKinley and J. Hadermann, Radionuclide Sorption Database for Swiss Safety Assessment, NTB 84-40. Nagra, Baden (1985).

Investigation of Dry Unit Weight for Bentonite Buffer Block

Seok Yoon[1], Seungrae Lee[2*], Jinseop Kim[1], Geonyoung Kim[1], Donghwa Noh[2] , and Minjun Kim[2]

[1] Korea Atomic Energy Research Institute, 111, Daedeok-daero 989beon-gil, Yuseong-gu, Daejeon, Republic of Korea

[2]Korea Advanced Institute of Science and Technology,291 Daehak-ro, Yuseong-gu, Daejeon, Republic of Korea

*srlee@kaist.ac.kr

1. Introduction

The geological disposal of high level waste (HLW) is designed to isolate the radioactive materials from human being until the radionuclides decay [1]. The principal of engineered barrier system (EBS) was suggested for this reason, and EBS is composed of a disposal canister with packed spent fuel, a buffer material, backfill material, and near field rock mass (Fig. 1). The role of a buffer material is very important to guarantee the disposal safety of HLW, and play a role to protect the waste and canister against any external mechanical impact. In terms of dry unit weight, its value should be higher at least 1600 kg/㎥ in order to satisfy the performance criteria [2], and it is necessary to investigate dry density of buffer material exactly. Therefore, this paper analyzed the method for investigating dry unit weight of cylindrical bentonite buffer block.

2. Experimental Setup

2.1 Theoretical background

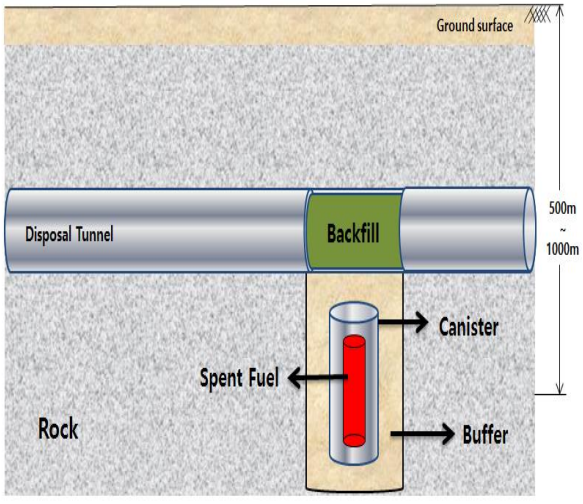


Fig. 1. Concept of engineered barrier system.

The diameter of cylindrical bentonite block was 30cm, and height was 40mm. Three samples were prepared and water dried for 48 hours in the oven. The relationship between dry unit weight (γ_d) and moist unit weight (γ_t) is like Eq. (1).

$$\gamma_d = \frac{W_s}{V_t} = \frac{\gamma_t}{1+\omega}, \quad \gamma_t = \frac{W_s + W_w}{V_t} \qquad (1)$$

Here, V_t means total volume of bentonite block, W_s is weight of dried bentonite block, ω is water content, and W_w is weight of water.

2.2 Results and Discussion

Table 1 shows the moist unit weight and dry unit weight for three bentonite block samples. Initial moist unit weight was obtained by dividing weight by volume. Initial volume was measured with vernier caliper. Calculated dry unit weight was obtained by Eq. (1) with initial moist unit weight and water content. Also, measured value of dry unit weight was obtained with dried weight and volume. Dried volume was also measured with vernier caliper after 48 hours in the oven. Measured value showed 3~5% higher than calculated one.

In real geological disposal system, bentonite buffer block is confined with rock mass and backfill materials, and it is thought that volume change may not occur according to temperature and water content variation. Therefore, it is more accurate to use calculated value in order to obtain dry unit weight of benotonite buffer material, not measured value after drying in the oven.

3. Conclusion

This paper investigated methods to obtain dry unit weight for bentonite buffer material which is a very important component in the EBS system for the geological disposal of HLW. Three different

Table 1. Results of dry unit weight value

	Calculated value from Eq. (1)	Measured value	Note
Dry unit weight, γ_d (kg/cm^3)	1,769	1,821	Initial γ_t=1,952
	1,714	1,802	Initial γ_t=1,917
	1,684	1,768	Initial γ_t=1,903

cylindrical sample of bentonite buffer block were prepared. Dry unit weight was valued from two different methods. One method describes that dry unit weight was obtained from Eq. (1) with water content and initial moist unit weight. The other method is that dry unit weight can be obtained by measuring dried volume and weight. Measured value showed 3~5% higher than calculated one. Since bentonite buffer block is confined with rock mass and backfill materials in the real disposal condition, volume change may not occur according to temperature and water content variation. Therefore, it might be more accurate to use calculated value in order to obtain dry unit weight of benotonite buffer material, not measured value after drying in the oven.

ACKNOWLEDGEMENT

This research was supported by the Nuclear Research and Development Program of National Research Foundation of Korea (NRF) funded by the Minister of Science, ICT and Future Planning.

REFERENCES

[1] Lee, M.S., Choi, H.J., Lee, J.W., Lee, J.P., Improvement of the thermal conductivity of a compact bentonite buffer, KAERI/TR-5311(2013).

[2] Lee, J.W., Choi, H., Lee, J.Y., Thermal conductivity of compacted bentonite as a buffer material for a high-level radioactive waste repository, Ann Nucl Energy 94(2016a), 848-855.

Prediction of Inflow and Wetting Behaviors of Bentonite in Deposition Hole Under In-Situ Geological Features

Jin-Seop Kim*, Chang-Soo Lee, Jae-Won Lee, and Geon-Young Kim

Korea Atomic Energy Research Institute, 111, 989 beon-gil, Daedeok-daero, Yuseong-gu, Daejeon, Republic of Korea

*kjs@kaeri.re.kr

1. Introduction

Äspö Task Force is a forum of the international organizations for modeling of groundwater flow and transport of solute (GWFT) in fractured rocks. SKB Task 8 primarily focuses on the evaluation of the hydraulic interaction between the bentonite backfill material and near-field host rock [1]. The objective of this study is to calculate inflows into 30 cm diameter open boreholes and to evaluate the resulting wetting of the bentonite installed in the borehole.

2. Approach

Numerical model development is based on the use of TOUGH2 and FLAC3D. A lot of computer resources are generally required in TOUGH2 and FLAC3D with regard to application of smeared fracture model to all the elements in model domain. Equivalent permeability, therefore, is estimated from fracture statistics around TASO tunnel by application of an imaginary tunnel (2×2×20 m) into model domain. Equivalent permeability is obtained by assuming that the inflow estimated from TOUGH2 code is same to that from FLAC3D code in which site-specific DFN is evaluated by applying the smeared fracture model with regard to the hydraulic properties. Three deterministic large fractures and small-scale fractures with large transmissivity (log10(T) > -11.6) intersecting probing borehole are directly embedded to the model geometry. They are assumed to have a thickness of 5 cm

3. Model setup

The mode geometry is presented in Fig. 1 below. In contrary to Task 8c, additional monitoring boreholes surrounding probing borehole and site-specific small fractures intersecting probing boreholes are further embedded in Task 8d. Material properties used in TOUGH2 analysis and other input parameters including initial & boundary conditions are same to those used in Task 8c. Total mesh number in Task 8d is 74,184 within a domain of 40x40x40 m (Fig. 1).

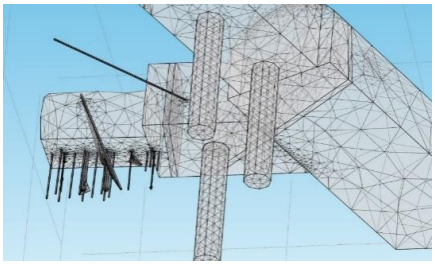
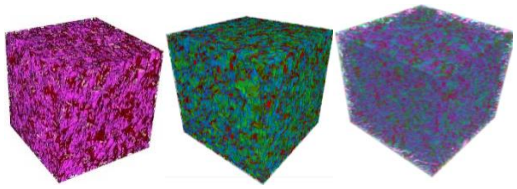


Fig. 1. Model geometry for Task 8d.

Site specific-stochastic fracture statistics are given as intensity, size and orientation data, and serve as the basis for the hydraulic properties. DFN generated from FracMan is applied to FLAC3D for equivalent permeability calculation (Fig. 2).



(a) FracMan (b) FLAC3D (C) EPM

Fig. 2. DFN generation and EPM (Equivalent Porous Medium).

4. Main Results

4.1 Estimation of groundwater inflow into probing holes

When the permeability of intact rock is assumed to be 1.02×E-21 m^2, the inflow into an imaginary tunnel is calculated as 1.652E-7 kg/sec from FLAC3D. While the inflow from TOUGH2 code is calculated to be 0.911E-7 kg/sec. It should be noted that some

difference is found in the estimated flow between TOUGH2 and FLAC3D codes even under the identical input condition without discrete fractures. The value from FLAC3D is consistently 1.81 times larger than that from TOUGH2 code in this study.

Therefore, the calibration factor between two codes should be taken into account with regard to inflow estimation when using TOUGH2 code. Equivalent permeability of 1.125E-19 m^2 is selected to be used in this study.

Based on this information, the inflow into borehole is calculated from TOUGH2 code and listed in Table 1. In the borehole of BEN18, relatively large difference is found at inflow estimation between simulation and BRIE data. It is likely that there are some geological features or processes such as impermeable zone around the BEN18 (KO018). As more data became available, the model should be adjusted to better reproduce the observations made in probing boreholes.

Table 1. Inflow into boreholes after excavation at 0.1 yr

Borehole	KO20	BEN18 (KO18)	BEN17 (KO17)
Inflow (ml/min)	0.48	1.00	0.95
BRIE (ml/min)*	0.01	0.0 (0.01-0.03)**	1.0 (0.12-0.25)**

* inflows from short duration test (approx. 15 min)

** values in parenthesis indicate inflow into 300 mm diameter open boreholes

4.2 Variations in saturation and pressure around TASO tunnel

The required time for full saturation of bentonite is around 100 years or more. These values are much longer than the time from Task 8c (less than 5 years).

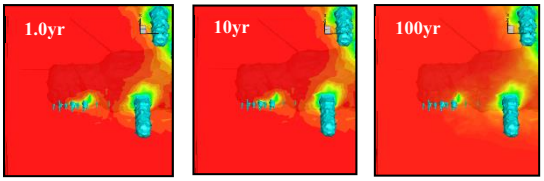


Fig. 3. Saturation distribution at the middle of probing hole.

Pressure distribution around TASO tunnel is presented in Fig. 3 with time. The pressure does not show substantial difference with time and remains relatively low value around the boreholes.

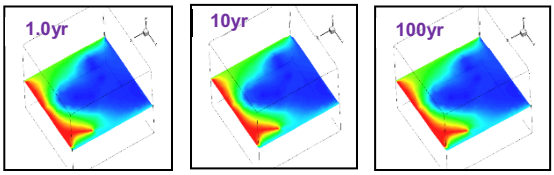


Fig. 4. Pressure distribution at the middle of probing hole.

5. Discussion

The time required for the full saturation of benonite in Task 8d is estimated to be much longer than that in Task 8c although additional fractures are taken into account and the inflow is larger. It is likely that additional boreholes and fractures intersecting tunnel and boreholes results in slow saturation in Task 8d. In particular, various monitoring boreholes surrounding each probing borehole give rise to low pressure distribution.

It is worthwhile to notice that the borehole KO17 shows very slow saturation profile (Fig. 2). Even after 100 years, some location does not show fully saturated. This is attributable to the fact that a large fracture is intersected with the tunnel inside which has a constant atmospheric pressure. Subsequently, more information on the geological features near the deposition holes, such as interconnection of fractures is also required for improving prediction of inflow as part of deposition hole characterization.

6. Conclusion

Better prediction of the hydraulic interaction between the near-field rock and bentonite depends on how well the site-specific features around the deposition are identified. Subsequently, more information on the geological features near the deposition holes, such as interconnection with man-made structures is also required for improving prediction of inflow. In addition, model adjustment and calibration based on the available data measured in situ are necessary to better reproduce the observations.

REFERENCES

[1] SKB (2012), Task 8-Modelling the interaction between engineered and natural barriers: An assessment of a fractured bedrock description in the wetting process of bentonite at deposition tunnel scale, SKB report P-16-05, Stockholm.

Numerical Analysis of Thermo-Hydro-Mechanical Coupled Behavior in Multi-level HLW Repository Concept

Changsoo Lee*, Won-Jin Cho, Jaewon Lee, and Geon-Young Kim

Korea Atomic Energy Research Institute, 111, Daedeok-daero 989beon-gil, Yuseong-gu, Daejeon, Republic of Korea

*leecs@kaeri.re.kr

1. Introduction

High-level radioactive waste disposal facility based on Korean Reference HLW disposal System (KRS) will be constructed at depth of 500 m underground and the estimated total area of the facilities is approximately 8 km^2 [1]. This would be a constraint for site selection of repository. Therefore, it is necessary to consider multi-layer disposal concept in order to lessen the area of disposal facility. In this study, numerical modeling was conducted to investigate thermo-hydro-mechanical coupled behavior in multi-layer concept base on the KRS.

2. Numerical model

Numerical analysis was performed to investigate THM coupled processes in the multi-layer HLW repository concept using TOUGH2-MP/FLAC3D. Modeling cases are listed in Table 1. The first case is numerical modeling for double layer disposal system where is located at depth of 400 m and 500 m. And the second case is numerical modeling for triple layer disposal system where is located at depth of 400 m, 500 m, and 600 m. Tunnel spacing and disposal holes interval are listed in the Table. 1. Temperature criterion is 100℃ for all modeling cases.

Table 1. Modeling cases

Modeling case	Depth	Tunnel spacing and disposal holes interval
1	400 m & 500 m	40 m & 8 m
2	400 m, 500 m, 600 m	40 m & 10 m

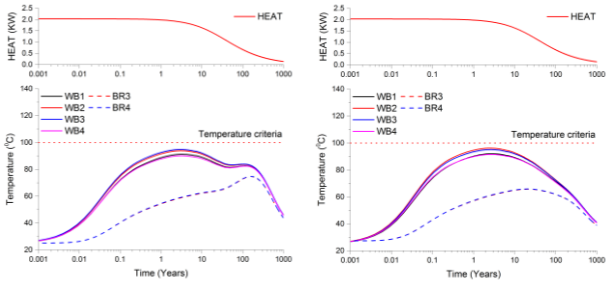
The used input parameters, function of decay heat, initial and boundary conditions are presented in the [1]. And monitoring points at each level (400 m, 500 m, 600 m) are same as that is presented in Lee et al. [2]. The excavation sequence was simulated for 10 years, and then the waste canister, bentonite buffer, and backfill are installed instantaneously and the post closure simulation can start for all modeling cases.

3. Results

3.1 Thermo-hydraulic analysis

Maximum temperature is calculated below 100℃ for the two modeling cases. Temperature evolutions are analogous to that is described in Lee et al. [2]. But, temperature evolution is slightly different at depth of 500 m in triple layer disposal system (modeling case 2) as shown in Fig. 1. In the triple layer disposal system, the temperature generated at depth of 500 m (middle level disposal system) could be difficult to escape, because temperature of upper and lower disposal system act as thermal boundaries. Therefore, a secondary peak temperature due to superposition phenomenon is shown after about 1.5 hundred years.

According to Lee et al. [2], fluid pressure is slowly increased until several years, after then, the pressure is rapidly increased and becomes hydrostatic pressure after decades. However, fluid pressure is rapidly increased after ten years and becomes hydrostatic pressure after one hundred years for the modeling case 1 and 2. And the liquid saturation evolutions in the buffer are analogous to that presented in Lee et al. [2]. Degree of saturation decreases to a minimum of about 0.2 after a few years, after then saturation starts to increase and finally reaches 1.0.



(a) Temperature evolution at depth of 500 m (b) Temperature evolution at depth of 600 m

Fig. 1. Temperature evolution for modeling case 2.

3.2 Mechanical analysis

Thermal stress, sum of swelling stress and fluid pressure can influence the stress filed at BR1 and BR2 where is described in the Lee et al. [2] as shown in Fig. 2. Therefore, stress path at BR1 and BR2 was calculated to investigate the potential rock failure using Mohr-Coulomb criterion [3] is used to investigate the evolution of the stress field and potential for rock failure.

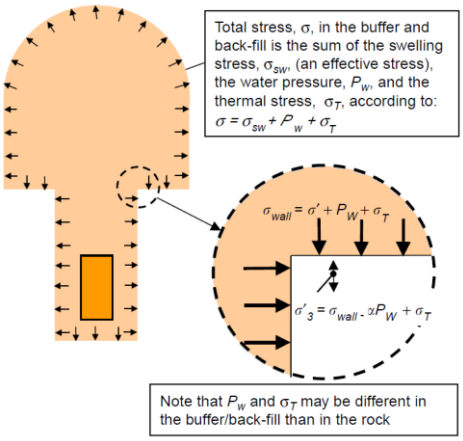
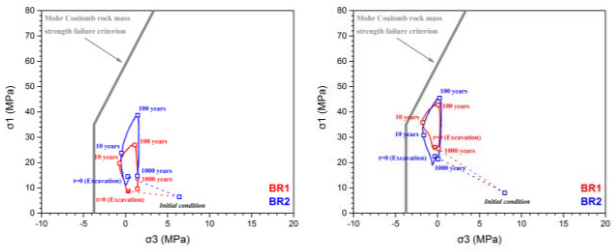


Fig. 2. Illustration of the effect of compressive stress, σ, in the backfill on minimum compressive principal effective stress, σ'_3, in the floor of the drift [4].

Fig. 3 and Fig. 4 show the evolutions of minimum and maximum principal effective stresses at BR1 and BR2 with the Mohr-Coulomb failure envelopes. The stress path in multi-layer disposal system is analogous to that presented in the Lee et al. [2]. The stress state of rockmass stays below that required for failure, however, stress state at depth of 500 m is relatively close to the failure envelope in the double layer disposal system (Fig. 3). In case of triple layer disposal system, stress state at depth of 500 m is relatively higher after 1,000 years (Fig. 4), because temperature is higher than others.



(a) Stress path at depth of 400 m (b) Stress path at depth of 500 m

Fig. 3. Principal stress path in relation to Mohr-Coulomb failure criterion in double layer disposal system.

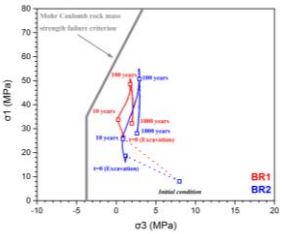


Fig. 4. Principal stress path at 500 m in modeling case 2.

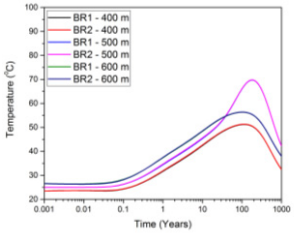


Fig. 5. Temperature evolution in modeling case 2.

4. Conclusions

Numerical modeling was performed to investigate influence of THM processes on multi-layer disposal system based on KRS during 1,000 years after operation. The maximum temperature can satisfy temperature criteria of 100 ℃ and stress state of rockmass stays below the failure criterion for all measuring points in multi-layer concept. However, it is necessary to investigate the stress state is below the spalling criterion as presented in Lee et al. [2].

Acknowledgements

This research was supported by the Nuclear Research and Development Program of National Research Foundation of Korea (NRF) funded by the Minister of Science, ICT and Future Planning.

REFERENCES

[1] Lee, J.; Cho, D.; Choi, H.; Choi, J. (2007) Concept of a Korean Reference Disposal System for Spent Fuels. Journal of Nuclear Science and Technology. 44: 1565–1573.

[2] Lee, C.; Cho. W. -J.; Lee, J.; Kim, G. -Y. (2017) Numerical Analysis of Thermo-Hydro-Mechanical coupled behavior in Korean Reference HLW disposal System (KRS). Abstract of Proc. of the Korean Radioactive Waste Society Spring 2017.

[3] Jaeger, J. C.; Cook, N. G. W.; (1979) Fundamentals of Rock Mechanics. Chapman and Hall, London.

[4] Rutqvist, J.; Chijimatsu, M.; Jing, L; Millard, A.; Nguyen, T. S.; Rejeb, A.; Sugita, Y.; Tsang, C. F. (2005) A numerical study of THM effects on the near-field safety of a hypothetical nuclear waste repository-BMT1 of the DECOVALEX III project. Part 3: Effects of THM coupling in sparsely fractured rocks. Int J Rock Mech Min Sci 42: 745-755.

Earthquake Modelling and Application to Long-term Safety Analysis of a Final Repository of Spent Nuclear Fuels in Forsmark Sweden

Jeoung Seok Yoon[1*], Arno Zang[1], Ove Stephansson[1], Ki-Bok Min[2], Fabrice Cotton[1], and Flavio Lanaro[3]

[1]Helmholtz Centre German Research Centre for Geosciences, Potsdam, Germany

[2]Seoul National University, Seoul, Republic of Korea

[3]Swedish Radiation Safety Authority, Stockholm, Sweden

[*]jsyoon@gfz-potsdam.de

1. Introduction

In 2011, the Swedish Nuclear Fuel and Waste Management Company (SKB) has submitted a license application to the Swedish Government to obtain a license for construction of a final repository for spent nuclear fuels at Forsmark. This study was conducted as a part of the review by the Swedish Radiation Safety Authority (SSM) on SKB's application. This study addresses one of several scenarios that could impair the physical integrity of the repository of spent nuclear fuel at the Forsmark site, which is a seismic event, i.e. earthquake, occurring at a nearby fault. The effect relevant to the repository safety is the shear displacement of rock fractures induced by an earthquake. In SKB's assessment, a shear displacement of 50 mm of a target fracture that crosses a canister position in the repository area is regarded as the upper limit of canister failure. For such analysis, we developed a numerical modelling work flow using a discrete element model and applied to this task.

2. The Forsmark Repository Model

The Forsmark repository model is generated based on the integrated deterministic geological model [1] shown in Fig. 1. Our discrete element based Forsmark model is generated to contain the deformation zones (green traces) and the discrete fracture network (red) distributed in the repository rock mass at the depth of the repository, i.e. depth = 450 m [2]. The arrows indicate the orientation of the maximum horizontal stress at present day in situ stress condition.

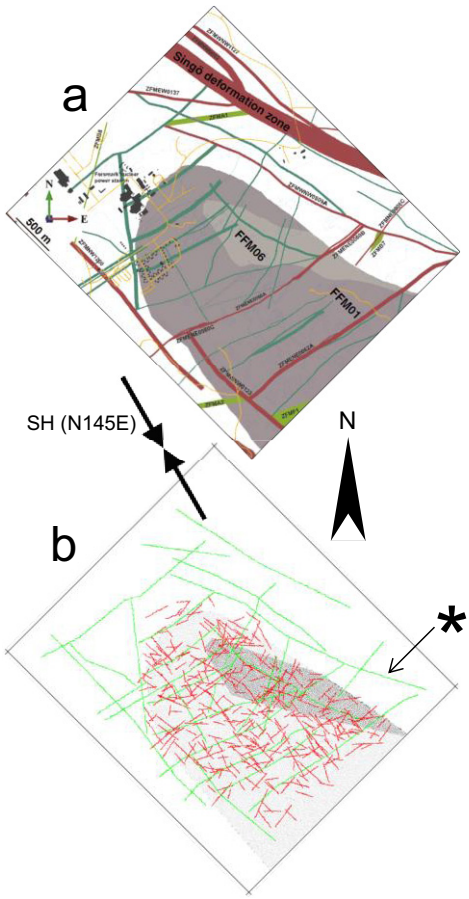


Fig. 1. (a) Integrated deterministic geological model of the Forsmark site at the depth of the repository [1], (b) the Forsmark repository model generated in this study using discrete element model [2].

3. Modelling Earthquake Source: Dynamic Fault Rupture, and Fracture Slip

For simulation of an earthquake, we chose a deformation zone named ZFMWNW0809A (indicated * in Fig.1b). An earthquake is simulated by releasing the strain energy that is accumulated along the trace of ZFMWNW0809A under a given

stress field. Upon releasing the strain energy, a seismic wave is generated from the rupturing fault trace and travels through the model and at the same time attenuates due to the damping of the rock mass, failure of the rock mass and slip of the discrete fracture network where the seismic energy is partially consumed. After a seismic wave passes through the repository rock mass, a redistribution of the stress field follows due to permanent deformation (slip) of the ruptured fault which further induces repository rock mass failure and post-seismic slip of the discrete fracture network. In this way, a main-shock and an after-shock of an earthquake are truly simulated. Here in this study, we only analyze the coseismically induced slip of the discrete fracture network. Fig. 2 demonstrates the results showing the hypocentre of the fault rupture (black star with M4.9) and coseismically induced slip of the discrete fracture network.

We also show in Fig. 2b distribution of the fracture slip induced by the same fault rupture under glacially induced stress condition, especially when the glacial ice cover approaches the repository area and results in lithosphere forebulge. The comparison shows that in both cases, there is no fracture with slip displacement exceeding the 50 mm canister damage limit, which led to a conclusion that for the tested cases (activation of the fault ZFMWNW0809A) the integrity of the repository can be ensured.

4. Application to Seismic Risk Study of Kyeong-Ju Repository

Recent Kyeong-Ju earthquakes occurred on 12 September 2016 have resulted in uprising attentions in Korea. The earthquake was followed by 365 aftershocks (as of 18 Sep. 2016; 341 M1.5-3, 14 M3-4, 1 M4-5). The seismic risk of the earthquake is higher than any other cities as the city of Kyeong-Ju hosts an underground repository for low and intermediate nuclear wastes at 500 m depth and Wolseong Nuclear Power Plant (NPP) which are 25 km distance from the epicenter of the earthquake.

The modelling method we present in this paper can be applied to a study of seismic risk of Kyeong-Ju repository and NPP. Such study would be highly needed as there is an ongoing debate that the repository was build in a geological condition where the presence of the nearby faults and their reactivation potential are poorly investigated at the time of site selection and construction of the repository. The three recent earthquakes near Kyeong-Ju with M>4 have clearly demonstrated that the nearby faults have potential to reactivate. In particular, seismic risk of resulting from Yang-San fault earthquake should be carried out using a numerical modelling of this kind, as it is the largest fault in that area and estimated to host M>6 earthquakes in the future.

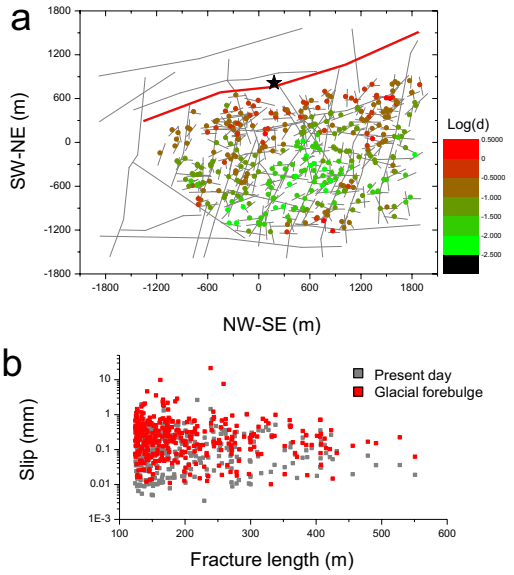


Fig. 2. (a) Distribution of the coseismically induced slip, d, (mm) of the discrete fracture network, colored by log(d), (b) Comparison of the fracture slip distributions induced by an earthquake occurring under present day stress (gray) and glacially induced forebulge stress (red) conditions.

REFERENCES

[1] MB. Stephens, S. Follin, J. Petersson, H. Isaksson, C. Juhlin, A. Simeonov, “Review of the deterministic modelling of deformation zones and fracture domains at the site proposed for a spent nuclear fuel repository, Swede, and consequences of structural anisotropy”, Tectonophysics, 653, 68-94 (2015).

[2] JS. Yoon, O. Stephansson, A. Zang, KB. Min, F. Lanaro, “Numerical modelling of earthquakes and induced seismicity under various in situ stress conditions at Forsmark, the site for a final repository of spent nuclear fuel”, In Proc of the 7th Int Symp on In-Situ Rock Stress – RS2016 Symposium, May 2016, Tampere, Finland.

Study on the 3D Site-descriptive Model for the HLW Disposal Site Characteristics Evaluation

Soo-Gin Kim, Jae-Yeol Cheong, Jeong-Hwan Lee, and Jeong-Hyoun Yoon*
Korea Radioactive Waste Agency, Deajeon 34129, Republic of Korea
*jhyoon@korad.or.kr

1. Introduction

Despite the growing number of voices wanting to stop the nuclear power generation after the Fukushima nuclear accident, nuclear power has continued to rise in many countries, and an increasing number of energy demands and efforts to reduce greenhouse gas emissions have taken place. One of the important issues to be addressed for the sustainable development of nuclear power is to present a solution for the safe management of spent nuclear fuel. Since the 1950s, various high-level radioactive waste (HLW) management methods have been proposed, including ocean disposal, space disposal, and glacier disposal. One of them, the deep geological disposal, is a direct disposal of HLW that emits high heat and radiation to the bedrock, which is located deep in the underground for completely isolating it from the ecosystem. The International Atomic Energy Agency (IAEA) recommends deep geological disposal as long-term solution for HLW disposal when considering economic and safety considerations. The most important factor of the deep geological disposal is to select an optimal site and implement a disposal system that meets safety, technical and environmental requirements. The system may slightly depend on the geological conditions and the type of waste in each country, but the ultimate goal is to secure long-term safety. Thus, it is very important to understand the characteristics of the site, before designing to maintain the performance of the disposal system for a long time.

This study analyzes the case of site-descriptive modelling (SDM) in Sweden and Finland for future HLW disposal projects in Korea.

2. Domestic and overseas case

2.1 Definition of Site-descriptive modelling (SDM)

The Olkiluoto (crystalline rock) region of Finland is the world's first deep geological repository (DGR) site and is now in the construction phase. Following, Sweden and France selected Forsmark (crystalline rock) and Bure (sedimentary rock) for disposal sites. Germany and the US selected Goreleben (rock salt) and Yucca Mountain (volcanic rock) as disposal sites, but now they are reviewing the project. Thus, depending on the geological characteristics of each country, the preference for disposal sites is different. The role of the geological formation is to provide stable mechanical conditions, favorable hydro-geochemical conditions, low movement of groundwater and effective retention of radionuclides, if released from the disposal site [1]. These site characteristics affect the performance of the disposal system, so it must be understood before engineering barrier design. SDM is a detailed description to help understanding of the site characteristics based on the interpretation of the quality assurance databases generated by the site investigation. The geo-scientific disciplines forming the base for the SDM models included geology, thermal properties, rock mechanics, bedrock hydrogeology, bedrock transport properties and surface ecology [1]. These are related to each other by the feedback based on the geological model, which is an essential element of the SDM (Fig. 1.). Therefore, the SDM should be performed with multidisciplinary project.

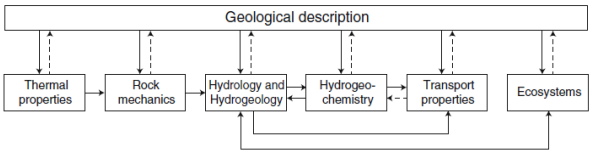


Fig. 1. The framework of SDM.

2.2 Comparison of SDM for Olkiluoto and Forsmark

Finland and Sweden are countries on the Baltic coast which share broadly similar geological histories and geography. However, there are obvious differences between the two such as hydrogeochemistry, hydrogeology, and rock

mechanics. Considering also that site safety is a composite of multiple barrier functions, the impact of these differences, in terms of overall site suitability, is difficult to judge without a full safety assessment of each site that includes an analysis of how these differences and associated uncertainties may influence safety [2].

2.3 Domestic case

In Korea, a low and intermediate-level radioactive waste (LILW) repository, comprising a total size of 800,000 drums, are under development. The 1st phase of the construction, which is an underground silo-type, was completed in 2014. The 2nd phase for a surface-type is under construction. The safety analysis report (SAR), which is a document related to licensing, provides a description of site characteristics. In this report, the results of the site investigation are shown with a diagram and a picture with explanations.

2.4 3D geological modeling

The key process in the SDM is the visualization of the site. When displaying natural phenomena with tools such as maps, it is helpful to improve understanding by expressing them as images, rather than just writing them. In particular, the 3D geology model is very similar to the actual view of the natural landscape. It also helps to simulate and interpret invisible underground space. In fact, Posiva and SKB estimated the deep structure and volume through SDM geological modeling.

The commercial software used for building a 3D geological model is SKUA-GOCAD from Paradigm, Leapfrog from ARANZ Geo, etc. SKB developed a unique system called Rock Visualization System (RVS) to perform 3D geological modeling (Fig. 2.).

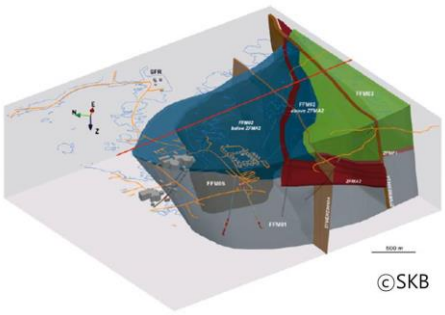


Fig. 2. 3D model (fracture domains and their relation).

3. Conclusion and future work

This study analyzed the necessity and method of SDM to improve the understanding of disposal site characteristics based on site investigation data in the case of Finland and Sweden. These countries are in the stage of construction or construction license permit reviewing by demonstrating the performance of DGR through site investigation and safety assessments over a decade. The center of SDM is a geological model, so it is recommended that they build a 3D structure. Korea Radioactive Waste Agency has carried out preliminary 3D geological modeling based on geological survey data, compiled in the SAR, of Gyeongju LILW repository [3]. The model is currently being complemented by reflecting the results of the second stage site investigation. In order to enhance the understanding of site characteristics, SDM will be constructed by integrating modeling results of groundwater flow, fault and geochemistry. The building process and the results of the models will be useful to evaluate HLW disposal site characteristics in the future.

Acknowledgement

This work was supported by the Korea Institute of Energy Technology Evaluation and Planning(KETEP) and the Ministry of Trade, Industry & Energy(MOTIE) of the Republic of Korea (No.20141720100570).

REFERENCES

[1] J. Andersson, K. Skagius, A. Winberg, T. Lindborg, A. Ström, “Site-descriptive modelling for final repository for spent nuclear fuel in Sweden”, Environ Earth Sci, 69, 1045-1060 (2013).

[2] J. Geirer, A. Bath, O. Stephansson, “Comparison of site descriptive models for Okiluoto, Finland and Forsmark, Sweden”, STUK, TR-14 (2012).

[3] S. Kim, J. Cheong, H. Jung, “3D Geological Modeling for Gyeongju LILW Repository”, Proc. of the KRS 2015 Fall Conference, 193-194, October 14-26, 2015, Busan.

3분과

고준위폐기물처분 (Poster)

Dissolution Characteristics of Uranium From the KURT Granite in Various Geochemical Conditions

Wan Hyoung Cho*, Min Hoon Baik, and Jae Kwang Lee
Korea Atomic Energy Research Institute, 111, Daedeok-daero 989beon-gil, Yuseong-gu, Daejeon, Republic of Korea
cho0714@kaeri.re.kr

1. Introduction

The studies on long-term behavior of radionuclide have been progressing in the field of radioactive waste disposal. After a long period of radioactive waste disposal, radionuclides released from a radioactive waste repository will be contacted with groundwater and radionuclides will be dissolved by groundwater. Therefore, the study on dissolution characteristics of radionuclide is important part in understanding the long-term behavior of radionuclide in disposal environment.

The objective of this study is to understand dissolution characteristics of uranium from KURT (KAERI Underground Research Tunnel) granite by groundwater in relevant geochemical conditions.

2. Samples and dissolution test

2.1 Samples

Samples for dissolution experiments were obtained from DB-1 core of KURT granite (depth of sampling: 108 ~ 109 m), Granite core samples from KURT were grinded into particles with a size less than 74 um (200 mesh) and then homogeneously mixed. After washing the samples 5 times, samples and deionized water were mixed in 1 (20 g) : 20 (400 mL) ratio. After the mixed samples were precipitated for 10 minutes by gravitation, suspending turbid water was removed. The washed samples were dried in oven at 60℃ for 48 h and then completely dried at 90℃ for 6 h.

2.2 Leaching test

Seven reaction solutions were prepared considering the relevant geochemical conditions of KURT groundwater in order to confirm the dissolution characteristics by groundwater (Table 1). Samples and seven reaction solutions were reacted in 1 : 10 (5 g : 50 mL) ratio and stirred in an agitator at 100 rpm continuously. Dissolution tests were carried out during 8 different time steps (0 day, 2 day, 5 day, 1 week, 2 weeks, 1 month, 3 months, 5 months). After the end of reaction periods, pH of reaction solutions were measured and supernatant samples (2.5 mL) were taken and then analyzed by ICP-MS after filtration with 0.22 μm syringe filter (Fig. 1).

Table 1. Scheme and conditions of the dissolution experiments

Code	Solution	What to see
UD-Bl (pH 1)	0.1M HNO_3	Effects of blank solution on U dissolution
UD-Bg (pH 8.8)	0.6mM $NaHCO_3$ 0.4mM $CaCO_3$ 0.3mM $Na_2SiO_3 9H_2O$	Effects of Background solution on U dissolution
UD-CO_3 (pH 8.8)	0.5 mM $NaHCO_3$ 0.5mM $CaCO_3$	Effects of Carbonate on U dissolution
UD-Na (pH 8.8)	1mM $NaClO_4$	Effects of Na^+ on U dissolution
UD-Ca (pH 8.8)	1mM $Ca(ClO_4)_2$	Effects of Ca^{2+} on U dissolution
UD-CaSii(pH 8.8)	0.5mM $CaCO_3$ 0.5mM $NaSiO_3$	Effects of ($Ca+SiO_2$) on U dissolution
UD-Si (pH 8.8)	1mM $NaSiO_3$	Effects of SiO_2 on U dissolution

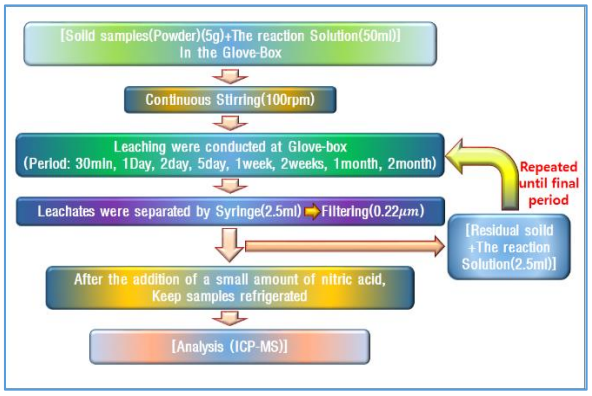


Fig. 1. Leaching test procedure.

3. Results and Discussion

As expected, uranium showed a higher amount of dissolution in the reaction solution (UD-Bl). Since uranium is well dissolved in mixed solution with HNO_3[1], the uranium dissolved by HNO_3 shows several tens to hundreds times greater concentration than other solutions in the UD-Bl. The dissolved amount of uranium is increased up to 5 day and then decreased after 1 week with a fluent curve. This result may be due to the fact that dissolution of uranium tends to decrease since the dissolution of uranium will be limited by the solubility of uranium in a given condition. The amount of uranium dissolved in other solutions (UD-Bg, UD-CO_3, UD-Na, UD-Ca, UD-CaSi) increases with increasing time although the amount of uranium dissolved is very small (less than 7 ug/L) (Table 2). Because uranium^{+} forms stable complexes with carbonates (CO_3^{2-}) [1], the samples UD-Bg and UD-CO_3 show higher amount of dissolved uranium than other reaction solution (UD-Na, UD-Ca, UD-CaSi). But the dissolution rate is decreased as the reaction (contact) time increases because the formation of uranium carbonate complex decreases by decreasing carbonate concentration as the reaction proceeds.

In addition, the dissolved amount of uranium shows a tendency to increase consistently with increasing reaction time in the solutions of UD-Na, UD-Ca, and UD-CaSi although the amount of uranium dissolved is very small. This result implicates that the presence of Na+, Ca2+, and SiO2 would not greatly influence on the dissolution of uranium from the KURT granite samples.

Table 2. The concentrations of dissolved uranium from the KURT granite samples with increasing contact time (ug/L)

U	UD-Bl	UD-Bg	UD-CO_3	UD-Na	UD-Ca	UD-CaSi	UD-Si
0 D	20.53	0.78	0.68	0.35	0.09	0.44	0.73
1 D	188.46	2.80	2.68	0.82	0.38	0.71	0.81
2 D	251.73	3.73	4.20	1.03	0.50	0.85	0.72
5 D	298.11	4.30	4.60	1.37	0.81	0.81	0.60
1 W	298.71	4.58	5.13	1.84	1.03	0.86	0.54
2 W	287.79	4.52	5.01	2.42	1.52	0.99	0.50
1 M	277.66	5.31	5.96	3.63	2.36	1.66	0.57
2 M	262.84	5.74	6.29	5.26	3.62	3.11	0.75
3 M	247.29	-	-	-	-	-	-
5 M	247.95	9.25	10.06	10.15	9.95	7.60	5.25

4. Conclusion

Our result shows that dissolution of uranium from the KURT granite is estimated to be affected by at the presence of CO_3^{2-}. According to collected KURT groundwater properties and composition at DB-1 core of KURT (91.7 ~ 199.7 m), pH and HCO_3^{-} of groundwater were identified as 8.3 ~ 8.5 and64.1 ~ 85.4 mg/L, respectively, and the main chemical species of uranium was a calcium-uranyl-carbonate complex, $Ca_2UO_2(CO_3)_3(aq)$ [2]. Since $CaCO_3$ is also present at KURT granite, KURT groundwater is estimated to have a sufficient condition for uranium to be dissolved by CO_3^{2-}. Therefore, under the geochemical conditions of KURT, uranium can be dissolved from the KURT granite by interactions with groundwater. Furthermore, the dissolved uranium by interaction with groundwater is able to migrate through fractures in the KURT granite. Besides, our result can explain why the concentration of uranium in groundwater shows an anomalously higher value in a certain part of DB-1 borehole.

REFERENCES

[1] N.A. Titayeva, “Nuclear Geochemistry”, CRC press, Moscow, 296p (1994).

[2] M. H. Baik et al., “Determination of uranium concentration and speciation in natural granitic groundwater using TRLFS”, J. Radioanl. Nucl. Chem., Vol.305, p.589 (2015).

Analyses of Double Layered Disposal System for the Spent Nuclear Fuels Considering the Deposition of Time Difference

Jongyoul Lee*, Hyeona Kim, Minsoo Lee, Heuijoo Choi, and Kyungsu Kim
Korea Atomic Energy Research Institute, 111, Daedeok-daero 989beon-gil, Yuseong-gu, Daejeon, Republic of Korea
*njylee@kaeri.re.kr

1. Introduction

The electricity from the nuclear power plants is about 30 % of total electricity in Korea. And as long as the nuclear power plants are operating continuously, the spent nuclear fuels from them are increasing and accumulating. Accordingly, it is expected that the disposal area for them is also becoming huge. With this reason, a study on the improvement of the disposal efficient such as reduction of disposal area is needed. There can be lots of ways to reduce the repository area, such as a longer term storage, improvement of the EBS (Engineered Barrier System) performance and a reprocessing of the spent nuclear fuels, etc.

In this study, for the purpose of reduction of disposal area, the multi-level repository and the deposition of time difference were considered. To do this, a double layered disposal concept was drawn. After then, preliminary thermal analyses were carried out to confirm the thermal stability of the disposal system. These results will be used in the optimization of the disposal system lay-out.

2. Reference disposal system

With the current technology, a deep geological disposal is considered as the safest disposal concept for spent nuclear fuels, where the spent fuels are encapsulated into disposal canisters and disposed of in a repository excavated deep into bedrock (Deep geological repository (Fig. 1).

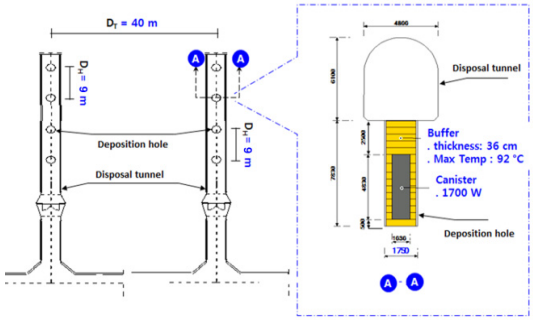


Fig. 1. Reference disposal concept.

The most important design requirement is that the peak temperature of buffer should be lower than 100°C. That is to assure the long-term integrity of EBS, that is to say, to preserve the physical and chemical properties of buffer(bentonite blocks). The result of thermal analysis for the reference concept is shown in Fig. 2 and the thermal requirement was satisfied.

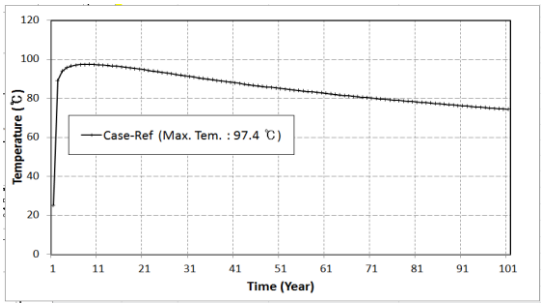


Fig. 2. Result of analysis for reference concept.

3. Double layered repository concept

Based on the reference concept, several concepts for multi-level repository concepts can be drawn. In this study, a double layered repository concept with the distance 100 m upward direction from the depth of 500 m which is the location of reference repository depth (Fig. 3).

With this concept, the deposition of time differences for each layer was considered. Also, the case of the first deposition of lower layer and the case of the first deposition of upper layer were considered.

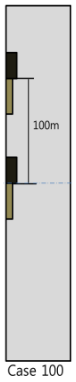


Fig. 3. Double layered repository concept.

The thermal analyses to check whether the thermal requirement of the system was satisfied were carried out (Fig. 4).

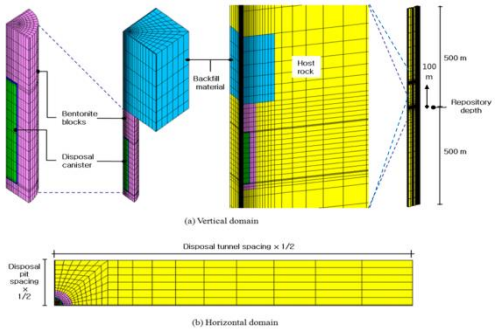


Fig. 4. Repository model for the thermal analysis.

A model for the thermal analysis of a geological repository is implemented in a three-dimensional quarter model, as shown in Fig. 4. The initial conditions were set up with the assumptions that the temperature of the groundwater at the surface was 10℃, and the thermal gradient was 3℃ for every 100 m depth. So, the top and the bottom of the analyzed domain were considered to be constant temperatures boundary and set 10℃ and 40℃, respectively according to the geothermal condition of the repository [3]. The density, thermal conductivity and specific heat of the rock, buffer, backfill and canister were shown in Table 1.

Table 1. The material properties for the analyses

Items	Density (kg/m^3)	Thermal Conductivity (W/m℃)	Specific Heat (J/kg℃)
Cast insert	7,200	52	504
Outer shell	8,900	386	383
Buffer	1,970	1.0	1,380
Backfill	2,270	2	1,190
Rock	2,650	3.2	815

4. Results and Discussion

The results of the thermal analyses for the double layered repository concepts were shown in Fig. 5 and Fig. 6.

As show in the figures, for the reduction of disposal area, the double layered repository concept with the proper distance from reference disposal depth can be an available option.

When considering the deposition of time difference, the shorter the deposition time difference, the lower the maximum temperature of the system. And, in the case of the first deposition of lower layer, the time difference can be up to 50 years, but in the case of the first deposition of upper layer, the time difference can be up to 30 years.

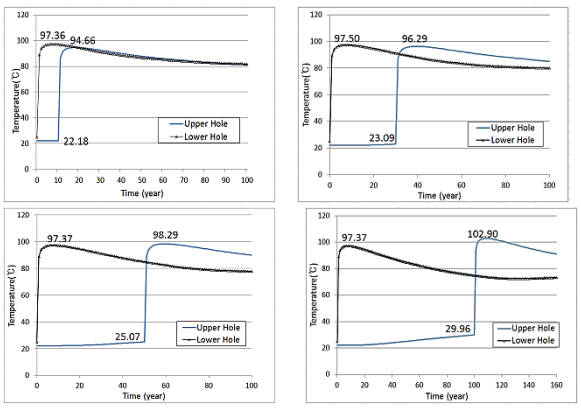


Fig. 5. Results for the case of the first deposition of lower layer.

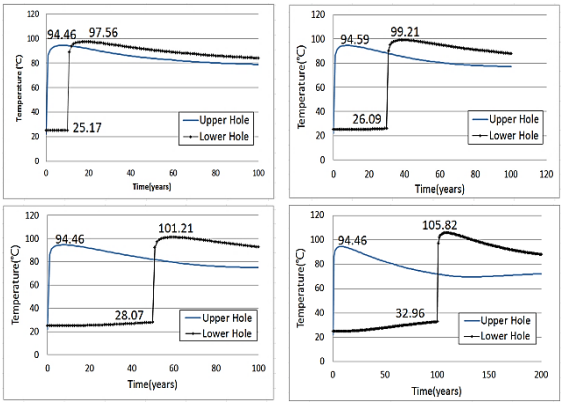


Fig. 6. Results for the case of the first deposition of upper layer.

5. Concluding Remarks

In this study, to reduce the disposal area, the concepts of the double layered repository concept was drawn and the thermal analyses for the concepts were carried out. From this study, followings were described as concluding remarks.

For the efficiency of the spent nuclear fuels disposal, the double layered repository concept with the proper distance from reference disposal depth could be an available option.

And for the deposition of time difference, the case of first deposition of lower layer is more advantageous than the other case.

The results need to be checked by real disposal site data later. And the results of this study can be used in the optimization of the disposal system lay-out.

Acknowledgement

This work was supported by the Long-term Nuclear Research & Development Program (NRF-2017M2A8A5014856) of the National Research Foundation funded from the Ministry of Science, ICT and Future Planning.

REFERENCES

[1] J. Y. Lee, D. Cho, H. Choi, J. Choi, Concept of a Korean Reference Disposal System for Spent Fuels, JNST, Vol. 44, No. 12, 1565-1573 (2007).

[2] H. J. Choi, J. Y. Lee, J. W. Choi, Korean Reference HLW Disposal System, Korea Atomic Energy Research Institute, KAERI/TR-3563/2008, pp. 23-35 (2008).

[3] J. Y. Lee, H. A. Kim, M. S. Lee, G. Y. Kim, H. J. Choi, "An Analysis of the deep geological disposal concepts considering spent fuel rods consolidation, Journal of Nuclear Fuel Cycle and Waste Technology, 12(4), 287-297 (2014).

Review on the Foreign Uncertainty Management Programs on the Safety Case for a HLW Repository

Jongtae Jeong*, Dong-Keun Cho, and Min Hoon Baik

Korea Atomic Energy Research Institute, 111, Daedeok-daero 989beon-gil, Yuseong-gu, Daejeon, Republic of Korea

*jtjeong@kaeri.re.kr

1. Introduction

Recently, many countries are implementing a repository development program for the disposal of high level wastes including spent fuels. And they are developing a safety case based on the long-term safety assessment for the smooth implementation of a repository development program. However, the safety assessment results of a HLW repository are subject to uncertainty, and the management of uncertainties is recognized as an important element of a safety case. In this paper, we review an uncertainty management program of several countries and identify the challenges related to the uncertainty management for the safety case.

2. Review of uncertainty management programs

2.1 Sweden

SKB performed a study on the repository layout accounting for uncertainty concerning the location and size of fractures [1]. According to the safety analysis of a repository, they found that a canister may fail if subjected to a sufficiently large shear movement due to earthquakes. However, such failure can be avoided by avoiding canister deposition in or close to fracture zones and in positions where intersection with a large single fracture is indicated. By conditioning these rules, the calculated risk contribution associated with earthquakes is greatly reduced. There are, however, large uncertainties with the network of single fractures between major zones. In order to find the fracture sizes to be avoided, they performed a study by simulating detailed process models, and found that it depends on the magnitude of earthquake, distance to earthquake-generating fault, size, and position and orientation of target fracture. And they estimated the fracture size to be avoided as a function of distance to potential earthquake-generating fault.

2.2 Finland

According to the regulatory guidelines in Finland, the uncertainties included in the safety analysis shall be assessed by means of appropriate methods, e.g., sensitivity analysis or probabilistic methods. Therefore, POSIVA has developed a systematic approach (Fig. 1) for the management of uncertainties in the safety case based on iterative process [2]. The overall strategies for uncertainty management are: identify, avoid, reduce, and assess. Uncertainties have to be described and quantified, and their relevance to safety needs to be considered. They recognized that uncertainties can be reduced by gaining new knowledge and understanding of the system behavior through appropriate researches. Some uncertainties will always remain and have to be assessed in terms of their relevance to the final conclusions on safety.

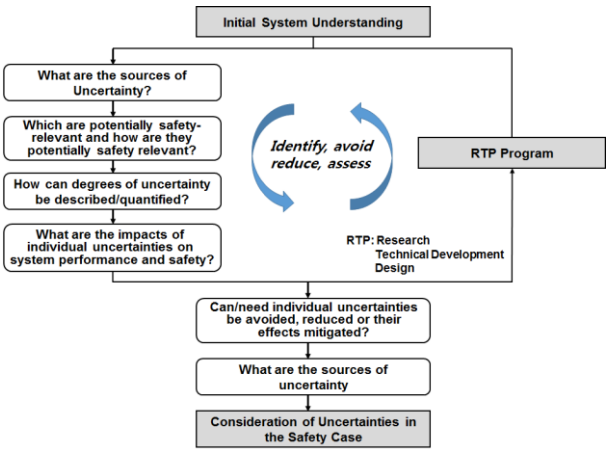


Fig. 1. POSIVA's iterative approach to the management of uncertainties [2].

2.3 USA

The USNRC emphasized the importance of an appropriate assessment of the uncertainty in performance assessment (PA) for both WIPP and YM repositories. In the conceptual and computational structure of 2008 YM PA, three uncertainties are considered: the uncertainty in the occurrence of future events; models for predicting the physical behavior and evolution of the repository system; and the uncertainty associated with analysis inputs. They recognized the uncertainty and sensitivity analysis as an important role in the development of potential solutions for radioactive

waste disposal. In addition, they developed several kinds of methods for uncertainty and sensitivity analysis and applied them to the PA of WIPP and YM repositories. The typical representation of uncertainty analysis results included in the safety assessment of the YMP [3] is shown in Fig. 2.

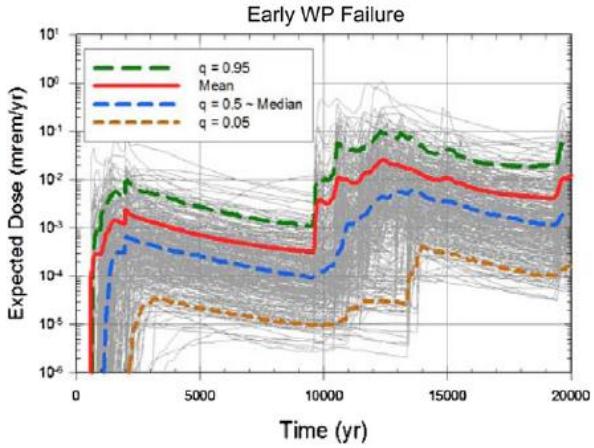


Fig. 2. Typical representation of uncertainty analysis results of YMP [2].

2.4 France

ANDRA developed a qualitative safety analysis (QSA) to examine the uncertainties regarding: the characteristics of each component; its evolution over time; and its interactions with other components. The QSA can be used to explore possible dysfunctions of the repository components, to propose design measures, and to identify scenarios to be quantified. Examples of uncertainty management using QSA are as follows: analysis of the primary vitrified waste package; analysis of the over-container for vitrified waste packages; analysis of galleries seals; and analysis of the host rock.

2.5 Belgium

Belgium has been developing and using tools for uncertainty management to steer the RD&D of a geological disposal program. They are developing and implementing a long-term management system for a repository by considering uncertainties. For parameter uncertainty, they considered parameter uncertainty expressed using PDF and uncertainty factor. However, they acknowledged that the use of PDF irrespective of their aleatory or epistemic characteristics may be ill-defined and mislead the characterization of the uncertainty. Therefore, they considered the expert management by asking experts to estimate two ranges of parameter value: expert range and source range. Finally, they put more emphasis on the identification of the uncertainty associated with the parameter than on the search of a single best estimate value.

2.6 England (UK)

In the UK, the regulatory body insist that the developer of a repository should: 1) establish and maintain a register of significant uncertainties; 2) develop clear strategies for managing uncertainties; 3) assess whether uncertainties can be reliably quantified. NDA uses two approaches (bottom-up and top-down) to develop a model hierarchy (process-component-total system models) from two different viewpoints. They insisted modeling is recognized as having several roles, for example, to aid process and system understanding, inform R&D and optimization, in addition to calculating risks; and it has found its appropriate place in safety case development and presentation.

3. Conclusion

Appropriate strategies for uncertainty management have to be established and an efficient communication skill for uncertainty to the public is necessary for the implementation of a repository development program successfully. The challenges to be resolved related to the management of uncertainty are as follows: 1) how to determine which uncertainties are matter; 2) how to make decisions when there are significant uncertainties; 3) how to demonstrate confidence in the safety case when there are still uncertainties; 4) how to regulate in the face of uncertainty; 5) how to communicate uncertainties to the public.

Acknowledgements

This work was supported by the Nuclear Research and Development Program (No. 2017M2A8A 5014856) of the National Research Foundation of Korea (NRF) funded by the Ministry of Science, ICT, and Future Planning (MSIP).

REFERENCES

[1] A. Hedin and R. Munier, Repository Layout Accounting for Uncertainty Concerning the Location and Size of Fractures, Topical session on analyzing and addressing uncertainties and sensitivities in 16-th IGSC Meeting, Paris (2015).

[2] POSIVA, Safety Case for the Disposal of Spent Nuclear Fuel at Olkiluoto – Synthesis 2012, POSIVA 2012-12 (2012).

[3] J.C. Helton, et al., Uncertainty and Sensitivity Analysis in Performance Assessment for the proposed high-level radioactive waste repository at Yucca Mountain, Reliability Engineering and System Safety, Vol.122, pp.421-435, 2014.

A Review of Process-based Total System Performance Assessment Model for A Geological Disposal System

Jung-Woo Kim*, Jaewon Lee, and Dong-Keun Cho

Korea Atomic Energy Research Institute, 111, Daedeok-daero 989beon-gil, Yuseong-gu, Daejeon, Republic of Korea

*jw_kim@kaeri.re.kr

1. Introduction

A geological disposal system of radioactive wastes generally consists of multiscale components, such as engineered barrier system (EBS), natural barrier system (NBS), etc., and multiphysical processes are involved in the system. Thus, the general performance assessment process can be represented as a pyramid in Fig. 1 [1]. Based on the massive information and knowledge, detailed process models are developed and tested. The detailed process models are abstracted and then finally the total system models can simulate the integrated behaviors of the entire disposal system [1].

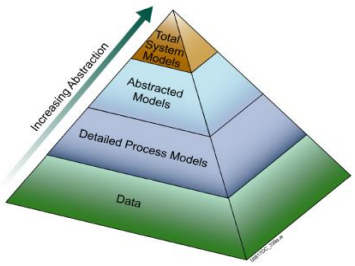


Fig. 1. Performance assessment pyramid [1].

In the most disposal projects, the post-closure safety assessments have been conducted by using the total system models until recently. KAERI's post-closure safety assessment tool was also the total system model developed with GoldSim until now.

Since many important processes are highly abstracted in the total system models, the advanced knowledge from state-of-the-art researches is seldom applied into the safety assessment. In addition, it is impossible or very difficult to verify the total system models due to the absence of the system-scale experimental data.

To cope with the total system models' limitations above, US has been trying to use high-performance computational codes to move the total system model closer to the process model level [2] and EU has developed and been using a multiphysics simulation framework by coupling COMSOL Multiphysics and PHREEQC [3]. To keep up with the trends, recently, KAERI has also proposed developing a process-based total system performance assessment (TSPA) model for a geological disposal system.

In this study, therefore, some precedent studies abroad were reviewed and the general considerations in the process-based TSPA model development were stated.

2. General Considerations in Multiphysics

2.1 Multiphysics system [4]

Multiphysics system can be classified by whether the multi-components in the system are coupled in the bulk (bulk-coupled multiphysics system) or on the lower dimensional interface (interface-coupled multiphysics system). The reactive transport in subsurface flows and the fluid-structure dynamics would be a typical example of bulk- and interface-coupled multiphysics systems, respectively.

Multiphysics application can be considered from algorithmic and architectural perspectives. Both mathematical analysis and computational complexity would be dealt with algorithmic perspective, and both software and hardware environments with architectural perspective.

2.2 Multi- concepts in multiphysics system [4]

2.2.1 Multi-scale. Lifting is the coarse-to-fine transformation which may means populating an ensemble of particles according to a distribution, and restriction is the fine-to-coarse transformation which may means averaging.

2.2.2 Multi-rate or multi-resolution. A chemical kinetics in the reactive transport model where the relaxation time should be modulated is the typical example of multi-rate.

2.2.3 Multi-level. The modeling system may be distinguished by only different mathematical formulations or even different discretizations.

2.2.4 Multi-model. Even single component may be analyzed using systems of partial differential equations of different types.

2.3 Operator splitting (OS)

Operator splitting (OS), where numerical computations are separated for each components and/or processes, is generally considered in multiphysics problem due to its expeditiousness. The general algorithm of OS is as follows [4]:

Given initial values $\{u_1(t_0), u_2(t_0)\}$
for $n = 1, 2, \ldots, N$ **do**
  Evolve one timestep in $\partial_t u_1 + f_1(u_1, u_2(t_{n-1})) = 0$ to obtain $u_1(t_n)$
  Evolve one timestep in $\partial_t u_2 + f_2(u_1(t_n), u_2) = 0$ to obtain $u_2(t_n)$
end for

Among various OS techniques [5], the appropriate OS scheme for the multiphysics should be decided keeping in mind the error propagation.

3. Process-based TSPA Models

3.1 PFLOTRAN

PFLOTRAN is "A recently developed code for modeling multi-phase, multi-component subsurface flow and reactive transport using massively parallel computers" from US's national laboratories [2]. It is written in Fortran, and the reactive transport equations can be solved using either a fully implicit Newton-Raphson algorithm or OS method [2]. Followings are current capabilities of PFLOTRAN [6]:

- Richard's Equation
- Thermo-Hydro-Chemical
- Multiphase Water-Supercritical CO2
- Surface Flow
- Discrete Fracture Network
- Aqueous Complexation
- Sorption
- Mineral Precipitation and Dissolution
- Multiple Continuum for Heat
- Subsurface Flow-Reactive Transport Coupling
- Multiphase Ice-Water-Vapor Flow

And, followings are under development in PFLOTRAN [6]:

- Community Land Model Coupling
- Surface-Subsurface Flow Coupling
- Geomechanics
- Multiple Continuum for Reactive Transport

3.2 iCP [3]

iCP is a numerical interface "Which couples two standalone simulation programs: the general purpose Finite Element framework COMSOL Multiphysics and the geochemical simulator PHREEQC" by Amphos 21, Spain. Fig. 2 is the iCP's computing algorithm.

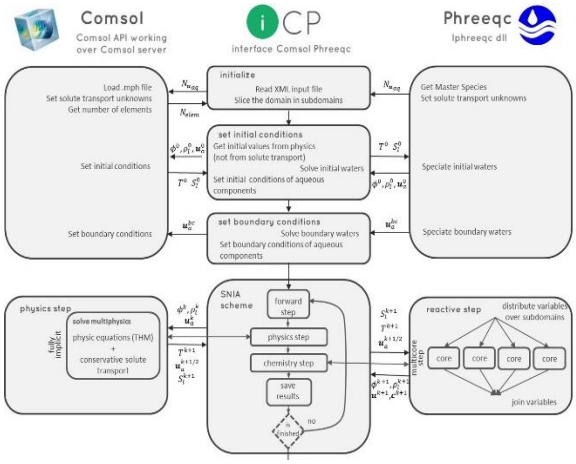


Fig. 2. iCP's computing algorithm [3].

4. Conclusion

The current trend of process-based TSPA model will contribute to the diversity and robustness of the post-closure safety assessment tools as well as will decrease uncertainty.

ACKNOWLEDGEMENT

This work was supported by the Nuclear Research and Development Program (No. 2017M2A8A5014856) of the National Research Foundation of Korea (NRF) funded by the Ministry of Science, ICT and Future Planning (MSIP).

REFERENCES

[1] SNL, Total System Performance Assessment Model Analysis for the License Application, Sandia National Laboratories MDL-WIS-PA-000005 REV00 (2008).

[2] R. T. Mills et al., "Simulating Subsurface Flow and Transport on Ultrascale Computers using PFLOTRAN", Journal of Physics: Conference Series, 78, 012051 (2007).

[3] A. Nardi et al., "Interface COMSOL-PHREEQC (iCP), an efficient numerical framework for the solution of coupled multiphysics and geochemistry", Computers & Geosciences, 69, 10-21 (2014).

[4] D. E. Keyes et al., "Multiphysics simulations: Challenges and opportunities", The International Journal of High Performance Computing Applications, 27(1), 4-83 (2013).

[5] J. Carrayrou et al., "Operator-splitting procedures for reactive transport and comparison of mass balance errors", Journal of Contaminant Hydrology, 68, 239-268 (2004).

[6] www.pflotran.org

Conceptual Study on Thermal Analysis for Disposal System of Spent Nuclear Fuel

Seunghyun Kim*, Jeonghwan Lee, and Jeonghyoun Yoon

Korea Radioactive Waste Agency, 168 Gajeong-ro, Yuseong-gu, Daejeon 34129, Republic of Korea

*shkim@korad.or.kr

1. Introduction

One of the basic options in spent nuclear fuel management is a geological repository. Many phenomena and processes have to be understood when considering the safety of the engineering barrier system (EBS) of the spent nuclear fuel repository. In a conceptual design the repository is in the depth of 500 m. the maximum temperature in a canister is limited to the design temperature of 100 ^{o}C. Due to uncertainties in thermal analysis parameters and natural variation in thermal analysis parameters the allowable calculated maximum canister temperature is set to 90°C causing a safety margin of 10 ^{o}C [1]. A single canister causes a maximum temperature of 75 ~ 90°C in the heat generating canister depending on the decay heat power. Fig. 1 shows the dimensions and layout of the disposal hole and backfill from the SKB. In this study, thermal analysis results for the KBS-3(V) type are verified and based on this model, the results of the thermal analysis for determining the interval of the disposal space to minimize the area of the Korean HLW repository system. The spacing between disposal holes is one of the important factors in minimizing the disposal area. Therefore, the result of thermal analysis over time is an important parameter to determine the spacing between disposal holes. For this, Numerical thermal heat analysis was performed by finite element method (FEM). The present paper briefly describes the thermal analysis of steady state and transient analysis of spent nuclear fuel canister are also presented in this results.

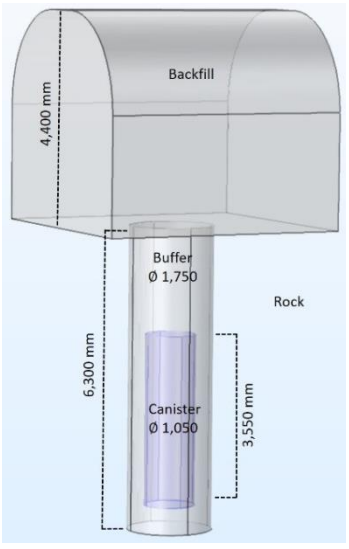


Fig.1. Dimensions of disposal hole and backfill of SKB.

2. Governing equations and boundary conditions

2.1 Governing equations, Heat transport

Heat transport by conduction must be included in the model, because in many cases there is a heat source of some kind in the system. The temperature field, T(x, t) obeys the equations. All other outer boundaries are perfectly insulated. The convective and conductive heat transfer inside the canister is described by the following equation.

$$\rho C_p \frac{\partial T}{\partial t} + \nabla \cdot (-k\nabla T) = -\rho C_p u \cdot \nabla T + Q \quad (1)$$

where C_p denote the heat capacity (J/(kg·K)), k is the thermal conductivity (W/(m·k)), and Q refers to the power density (W/m^3) in the canister that serves as a heat source.

2.2 Boundary conditions

The container is emplaced vertically in boreholes drilled into the emplacement gallery floor and surrounded by buffer. The copper container is represented as a in order to ensure no-flux boundary conditions at the container wall. Table 1. Summarizes thermos-mechanical properties of solid materials used in the analysis [3]. At the inner surfaces of canister, radiation is descrived by surface-to-surface radiastion. This mean that the mutual

irradiation from the surfaces that can be seen from a particular surface an radiation to the surroundings are accounted for. At the outer surfaces, radiation is described by surface-to-ambient radiation, which means that there is no reflected radiation from the surroudings. The canister was assumed to be homogeneous with uniform power generation over its volume and the contents of it was not modelled in detail.

Table 1. Thermo-mechanical properties used in the analysis [3]

Parameters	Values	Unit
Canister conductivity	390	W/m/K
Buffer conductivity	1.0	W/m/K
Canister volumetric capacity	2.4	MJ/m^3/K
Buffer volumetric capacity	2.2	MJ/m^3/K
Rock conductivity at 60 ^{o}C	2.61	W/m/K
Rock volumetric capacity	2.15	MJ/m^3/K

3. Results and discussion

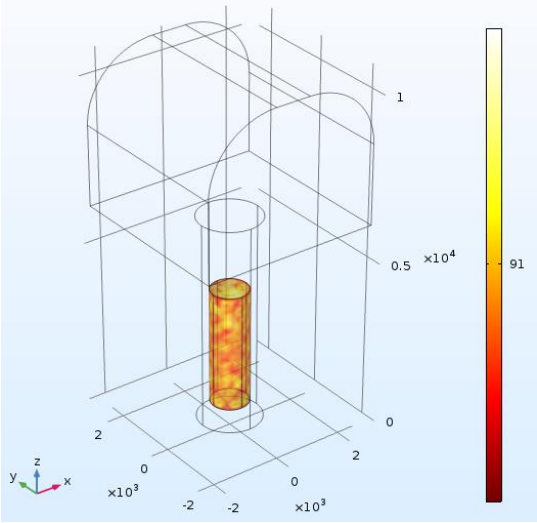


Fig. 2. 3D Temperature profile of canister after 10 years.

Temperature dependence of the conductivity of air, rock, canister material and volumetric heat capacity as shown in Table 1 were applied. Fig. 2 indicate that temperature distribution of bore hole after 10 years operation in the vertical type of canister. The temperature profile is unsymmetrical with the vertical plane of the canister. Thus different height of the buffer above and below the canister and the different conductivity of the backfill tunnel material have minor effect.

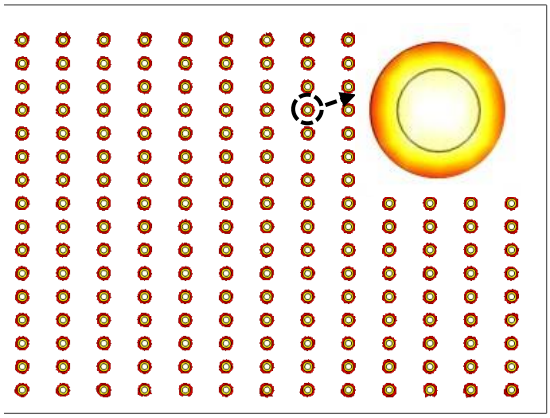


Fig. 3. Temperature distribution of one panel after 20 years operation in the vertical plane. And zoomed temperature profile around canister.

Fig. 3 show the temperature profile after 20 years, when the highest temperature of 92.8^{o}C is encountered and canister spacing is 7 m. Since the copper shell has very high thermal conductivity (390 W/m/K) causing nearly uniform temperature distribution on the outer surface of the canister.

4. Conclusion and further studies

The heat source model may thus estimate successfully the temperature of the canister, where the highest temperature is encountered. The numerically and analytically calculated temperature profile histories on the disposal area is an important results, since it proves that the analytic solution using effective design for disposal hole. For more robust representation of the repository, processes such as time dependent defect size, corrosion, water flow and transport of radionuclides from used nuclear fuel and multiple nearby defective containers can be examined in more detail.

REFERENCES

[1] Koari lkonen, “Thermal analysis of spent nuclear fuel repositoty”, POSIVA 2003.

[2] Markus Olin, Merja Tanhua-Tyrkko, Veli-Matti Pulkkanen,“Thermo-Hydro-Mechanical-Chemical (THMC) Modeling of the Bentonite Barriers in Final Disposal of High Level Nuclear Waste”, COMSOL Conference, 2008, Hannover.

[3] Agelskog L, Jansson P, “Heat propagation in and around the deep repository”, Swedish nuclear fuel and waste management Co. Technical report TR-99-02. 14(1), Jan 35, 1999.

Correlation Study Between Fracture Zone and Geophysical Logging Data in Crystalline Rock

Kyung-Woo Park*, Dae-Hee Kim, and Hong-Yung Jung

Korea Atomic Energy Research Institute, 111, Daedeok-daero 989beon-gil, Yuseong-gu, Daejeon, Republic of Korea

*woosbest@kaeri.re.kr

1. Introduction

Geophysical logging is the conventional investigation method for understanding the chemical and physical environment in the subsurface area. Though some logging methods can be applied to detect fracture in the bedrock, they are generally used for identifying a relatively large-scale open fracture and fracture zone. Also, the fracture and fracture zone from the geophysical method is very difficult to consider as deterministic features because of the lack of fracture geometry data. Thus, the relation study between fracture data, which are used for fracture network modeling, and geophysical logging data were needed.

In this paper, we aimed to understand the relation between statistically obtained fracture zone and geophysical logging data.

2. Study area

2.1 Geology

The study area is located at a northern part of Daejeon city. The topography of the site is well characterized as rolling hills surrounded by upland of EL. 300-500 m and the lowland of about EL. 50 m. The geology of the study area is mainly composed of Mesozoic plutonic rock, Precambrian metamorphic rock and a dike. The geologic formation of the Mesozoic plutonic rock is Jurassic schistose granite and two mica granite. The Cenozoic alluvium is distributed over a wide area through the surface basin system in research area with a 3-11 m depth. So, the geological unit of the study area below the surface soil layer is defined as crystalline rock which includes fractures and a fracture zone.

2.2 Boreholes

Total 3 boreholes (AH1, AH2 and AH6) were used for the correlation study in this paper. These boreholes, drilled in 2014 and 2015 around KURT(KAERI Underground Research Tunnel), are for an understanding of the deep geologic environment with a depth of -400～-500 m (GL.) (Table 1, Fig. 1). Statistics of fracture data were applied to define the fracture zone intersecting boreholes such as fracture spacing and frequency analysis. And, fracture data were obtained in the boreholes by borehole acoustic televiewer.

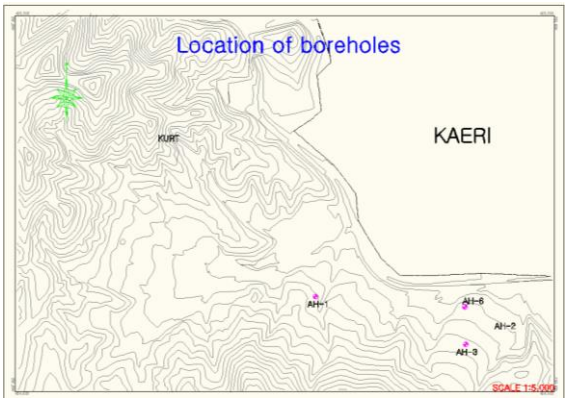


Fig. 1. Location of boreholes (All borehole are located at south-eastern area from KURT).

Table 1. Summary of boreholes around study area

AH-1	424745.4	232989.1	400	89.8	3 in.	Vertical
AH-2	424648.7	233489.6	450	74.8	3 in.	Vertical
AH-6	424718.2	233385.5	400	73.5	3 in.	Vertical

2.3 Geophysical logging method

To compare borehole logging data with fracture zone, we used total 5 logging data including 4 geophysical data which are temperature, electric conductivity, self-potential and gamma lay, and 1 borehole diameter data by caliper logging. Because fracture frequency is defined by number of total

fractures each meter, geophysical data also obtained at same interval.

3. Result

Total 3498 fractures were obtained from the borehole acoustic televeiwer and projected to a stereo net. The results showed that main orientation of fractures has a tendency of the NS direction. Also, NW and EW trend fractures could be found around the study area (Fig. 2).

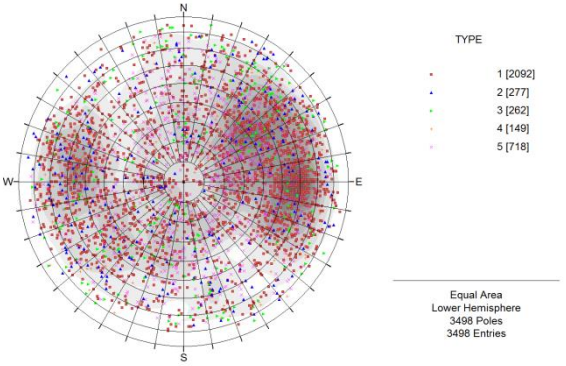


Fig. 2. Orientation of fractures in the boreholes.

Based on the fracture spacing analysis, the fracture zone in the boreholes was determined below the 0.33m of fracture spacing, which is identical to the 3 fractures per meter of the fracture frequency.

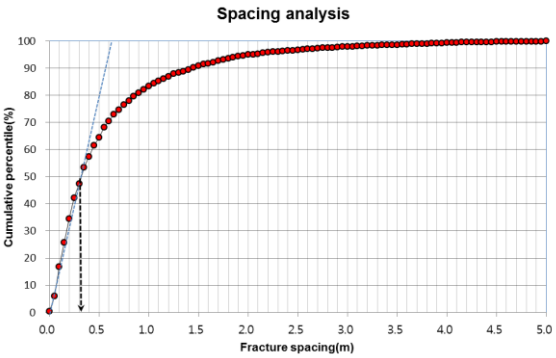


Fig. 3. Result of fracture spacing analysis.

The correlation study between fracture frequency data and geophysical logging data were performed. Furthermore, fracture zone data were also compared with geophysical logging data. Table 2 and 3 showed that self-potential logging data were related to the fracture frequency data and fracture zone. And, it seems that there is a little relation between caliper data and fracture frequency. Because the values of correlation coefficient were very low, it was difficult to suggest that SP logging was most significant logging method for identifying the fracture zone.

Table 2. Correlation coefficient between fracture frequency data and geophysical logging data

	SP	Caliper	Gamma	EC	Temp
AH1	0.27	0.10	-0.01	-0.06	-0.09
AH2	0.34	0.18	0.10	0.02	0.04

Table 3. Correlation coefficient between fracture zone and geophysical logging data

	SP	Caliper	Gamma	EC	Temp
AH1	0.23	0.08	-0.02	0.05	-0.04
AH2	0.32	0.17	0.06	0.01	0.06
AH6	0.21	0.16	-0.04	0.07	-0.09

4. Conclusion

Geophysical logging data and statistically obtained fracture data were compared to understand their relation. The result explained that the self-potential logging and borehole diameter (caliper) data were more related to fracture data than other logging method such as Gamma, EC, Temperature logging data. Because the value of correlation coefficient is about 0.2-0.3, it is difficult to suggest that SP and caliper logging is most effective logging technique to recognize the fracture zone. Nevertheless, the result from the comparison with other geophysical logging data is about zero, so we could conclude that there is a little relation between fracture data and SP, caliper data.

Microstructure and Corrosion Properties Zr-Cr-Si-NM Alloy Metallic Waste Form for Long-term Disposal

Seung-Youb Han*, Seon-Ah Jang, and Hwan-Seo Park

Korea Atomic Energy Research Institute, 111, Daedeok-daero 989beon-gil, Yuseong-gu, Daejeon, Republic of Korea

*hsy@kaeri.re.kr

1. Introduction

Technologies used in solidification processing by melting spent nuclear fuel assembly materials and hulls for metal waste reduction that occurs during the pyro-processing have been studied, mainly in the United States [1-3]. A cladding hull in a spent fuel assembly to be applied to a domestic PWR is composed of a metal alloy such as Zircaloy-4, ZIRLO accounts for the highest volume and weight ratio in the generation of process waste. Recently, at KAERI, we have been conducting research on the recycling of a cladding hull as a solidification host matrix in order to solidify and handle highly radioactive anode sludge residue including noble metal (NM) that occurs from electro-refining from pyro-processing. If we produce an MWF (Metallic Waste Form) by adding and melting the alloying elements and anode sludge in the cladding hull, the effect on the volume reduction and weight loss can be maximized because the cladding hull can be 100% recycled to the solidification host matrix of MWF. According to the existing results of MWF alloys manufactured in the US, although a stable production of MWF is possible with SS-15Zr alloy, it is disadvantageous in terms of the domestic cladding hull recycling efficiency, because the Zr content is low. In addition, the mechanical stability and corrosion resistance of Zr-8SS is relatively low [3]. As a result of the new composition with Zr-Cr-Si-NM in KAERI, a stable MWF was formed without cracks. Moreover, it was possible to confirm the possibility that the cladding hull and anode sludge generated from the pyro-processing can be fabricated MWF alloy with an excellent corrosion resistance

2. Experimental Results

The Zr-22Cr-3Si composition of the three kinds of solidification host matrix compositions has the eutectic point composition, and the Zr-27Cr-3Si and Zr-17Cr-3Si compositions have a Cr composition difference of ±5wt.% respectively. A total of 6 specimens were prepared and evaluated by adding 8wt.% of NM to each solidification host matrix composition and selecting three Zr-based MWF alloy compositions. All specimens were fabricated by high frequency induction heating in a silica crucible in an Ar atmosphere after forming a vacuum of 5×10^{-5} torr. To ensure the integrity of the specimen, it was held at 1600 to 1800℃ for 5 minutes. After forming the melt completely, it was kept at 1350℃ for about 15 minutes, furnace cooling was then applied to reduce the solidification shrinkage cracks and porosity. All prepared specimens were cut and polished, and XRD, SEM, and EDS analyses were performed for a microstructure and phase analysis.

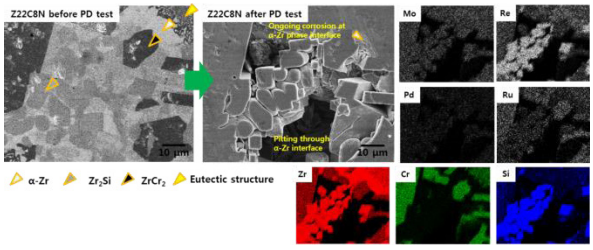


Fig. 1. SEM micrographs and EDS mapping results of the Zr-Cr-Si-NM specimen before and after potentiodynamic test.

For an evaluation of the corrosion properties, potentiodynamic (PD) and potentiostatic (PS) tests were carried out in the acidic brine aqueous solution condition (0.0001 mol·kg^{-1} H_2SO_4 + 0.01 mol·kg^{-1} NaCl in demineralized water, pH 4), and the leach solution was analyzed using ICP.

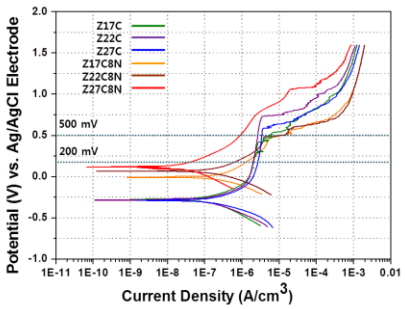


Fig. 2. The potentiodynamic polarization plots for Zr-Cr-Si-NM specimens.

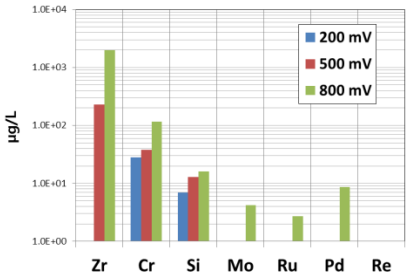


Fig. 3. ICP analysis results of electrolyte after potentiostatic test.

3. Conclusion

The main phases composing the Zr-Cr-Si-NM alloy consist of α-Zr, $ZrCr_2$, and Zr_2Si. The eutectic structure and $ZrCr_2$ phase increased with increasing Cr content. Pd was concentrated on α-Zr, Ru on α-Zr and $ZrCr_2$, Re on Zr_2Si phase. Electrochemical accelerated corrosion tests such as PD and PS were carried out on the Zr-Cr-Si and Zr-Cr-Si-NM alloys prepared in this study. The Zr-Cr-Si-NM alloys exhibited a high corrosion resistance and low corrosion rate owing to their low I_{corr} values with high E_{corr} values compared to conventional materials. As a result of the analysis of the composition of the leachate after the PS test, there was no NM element leaching below 500 mV, or leaching of the elements excluding Re, which is a surrogate Tc at 800 mV. In particular, the Zr_2Si phase, which is encapsulating phase of Re, was very stable, and showed no shape change or leaching of Re after the corrosion test, suggesting that the Tc immobilization ability is excellent.

REFERENCES

[1] D. D. Keiser Jr, D. P. Abraham, and J.W Richardson Jr, “Influence of technetium on the microstructure of a stainless steel-zirconium alloy”, J. Nucl. Mater, 277(2-3), 333-338 (2000).

[2] S. M. McDeavitt, D. P. Abraham, and J. Y. Park, “Evalution of stainless steel-zirconium alloys as high-level nuclear waste forms”, J. Nucl. Mater, 257(1), 21-34 (1998).

[3] W. L. Ebert and D. Kolman, Alloy Waste Form Testing Strategy Roadmap, U.S. Department of Energy Report, FCRD-SWF-2013-000226 (2013).

Microstructure and Corrosion Properties of Zirlo-Inconel718-SS304-NM Metal Waste Form Alloys for Improving Stability of Metal Waste Generated by Pyro-Process and Long-term Disposal Stability

Seon-Ah Jang*, Seung-Youb Han, and Hwan-Seo Park

Korea Atomic Energy Research Institute, 111, Daedeok-daero 989beon-gil, Yuseong-gu, Daejeon, Republic of Korea

*sajang@kaeri.re.kr

1. Introduction

Pyroprocessing has been studied based on the electrochemical separation technology in molten salts for the recycling of spent fuel (SF). In the pretreatment and electrorefining processes, various metal wastes including cladding hull tubes, NFBC (Non-Fuel Bearing Components), and NMs (noble metals) in the anode sludge are generated as a process waste in the pyroprocess [1]. Among them, Zirlo cladding hulls have the highest weight ratio, which reaches about 62wt.%, excluding the SF, whereas NFBC has the highest volume ratio. Many researchers are studying technologies for the treatment of the metal wastes by melting or compaction, followed by a solidification process. The metal waste solidified by the melting process can easily be alloyed with other elements to improve the corrosion resistance and stability for long-term disposal. However, most of the studies have focused on the alloys based on stainless steel (SS) cladding materials and NM, which are generated from the fast breed reactors [2]. Since the pyroprocessing studying at KAERI is targeting the SF from PWRs (Pressurized Light Water Reactors), it is essential to develop waste form alloys that include Zr-based cladding hull wastes with NMs. In particular, by recycling the cladding hull waste and NFBC as a solidification medium for immobilizing the NMs, we can have a great advantage not only in the volumetric reduction effect but also in the reduction of the waste amount, and in the simplification of the waste treatment process.

In this study, Zirlo-Inconel 718-SS304-NM based alloys including all the metal waste components were fabricated by the induction melting process to evaluate the long-term disposal stability of the metal wastes generated from pyroprocess using microstructure analysis and corrosion tests.

2. Experiments

The induction melting process was performed using a Y-coated silica crucible with 99.9% pure Zr, Inconel718, SS304, and NM samples mounted in a vacuum induction melting furnace.

The metal waste form of about 3 x 3 cm^2 in size based on 100 g of the specimen was produced by melting at the temperature range of 1200^oC to 1400 ^oC and by slowly cooling down. The various Zr-Inconel-SS-NM alloys were produced by controlling the content of Inconel and SS304. The prepared specimens were evaluated for soundness and long-term stability of the waste form by examining the microstructure and by corrosion tests.

3. Results and discussion

We fabricated six waste form specimens including three different Zr-Inconel-NM alloys by controlling the content of Inconel718 and three Zr-Inconel-SS403-NM alloys added with Cu and Cr based on the composition of NFBC (Fig. 1). All the waste form specimens were fabricated in almost uniform size and shape without any apparent cracks due to a slow cooling rate.

	ZIN 195	ZIN 245	ZIN 295	ZINS5_#9	#10	#11
Top						
Side						
Crack	X	X	X	X	X	X

Fig. 1. Pictures of metal waste forms at various compositions.

In the result of SEM observation, the microstructures of representative samples were shown to consist of three different colors; bright grey, grey, and dark grey (Fig. 2).

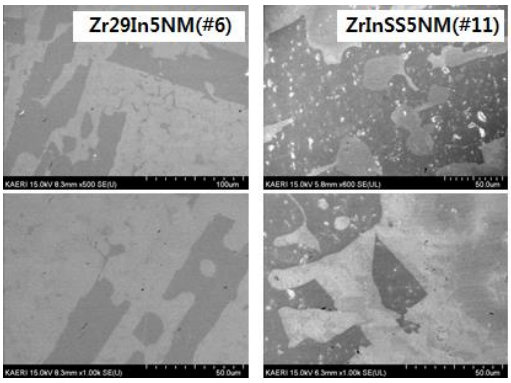


Fig. 2. SEM images of the microstructure for Zr-29Inconel-5NM and Zr-Inconel718-SS304-5NM.

For the two different kind of alloys, Cr and Ni were distributed in the regions of Fe and Zr, respectively, while NMs were evenly distributed over the entire surface. From the corrosion tests, E_{corr} and i_{corr} depending on the composition of specimens were shown in Fig. 3. Relatively higher E_{corr} were evident for all the compositions of Zr-Inconel-NM alloy specimens and a lowest i_{corr} was found at the lowest concentration of Inconel718, showing a superior resistance to corrosion. On the other hand, for the NFBC composition, both E_{corr} and i_{corr} were measured to be relatively low. The addition of Cu and Cr enhanced the resistance to corrosion of the waste forms based on NFBC composition.

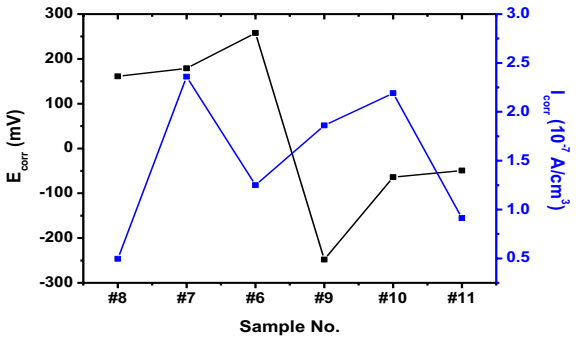


Fig. 3. E_{corr} and i_{corr} for the specimens with various compositions.

4. Conclusion

In this study, we fabricated metal waste forms using an induction melting process and evaluated the performance thereof to recycle the cladding hull and NFBC wastes generated from pyroprocess thereby reducing the volume of the waste.

REFERENCES

[1] K.H. Kang, C.H. Lee, M.K. Jeon, Y.L. Lee, Y.T. Choi, and G.I. Park, “Treatment Technology of Hull Wastes”, KAERI/TR-5288/2013 (2014).

[2] D. P. Abraham, S. M. McDeavitt, J. Y. Park, “Microstructure and Phase Identification in Type 304 Stainless Steel-Zirconium Alloys”, Metallugical and Materials Transactions A, 27A, 2151-2159 (1996).

Estimating Arrival Time of Crack Wave by Using Moving Window

Young-Chul Choi*, Jin-Seop Kim, and Tea-Jin Park

Korea Atomic Energy Research Institute, 111, Daedeok-daero 989beon-gil, Yuseong-gu, Daejeon, Republic of Korea

*cyc@kaeri.re.kr

1. Introduction

Acoustic emission (AE) is produced due to an elastic wave generated from the damage in solid materials. However, an accurate determination, by a non-destructive manner, of localization on where the damage happened in solids still remains challenging. Here, we report a novel crack wave arrival time determination algorithm of AE suitable to identify crack wave with low signal-to-noise ratios generated in rocks. Calculation of variances resulted from moving windows as a function of their size differentiates the signature from noise and from crack signal, which lead us to determine the crack wave arrival time. To validate our algorithm, we have performed the pencil lead break test using rock samples, which resulted in successful determination of the wave arrival time and crack localization.

2. Proposed Method

Fig. 1 shows a clear difference between the crack wave and the noise after the frequency analysis on crack wave as a function of time domain (see the inset). The crack wave signal has a narrower frequency range with higher amplitude, whereas the noise signal has the frequency distribution of a wide band with lower amplitude. The frequency analysis result from the crack wave possesses a specific frequency range, while that from the noise signal does a wide frequency distribution.

The main idea comes from the frequency characteristics. Fig. 2 (b) shows that the variance of a windowed noise signal in the time domain is not changed with varying length of window. This is because the noise has wide band frequency range. However, because the crack signal has narrow frequency range, the variance of a windowed crack signal is changed depending on the widow size as shown in Fig. 2 (a).

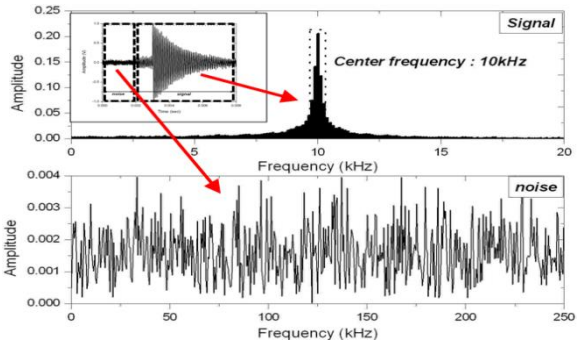
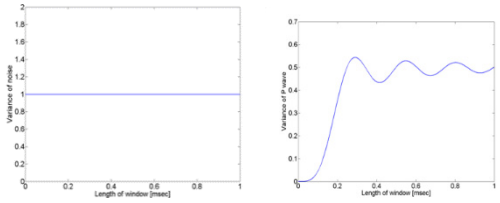


Fig. 1. Results of a crack wave generated from the rock and the frequency analysis of the noise signal.



(a) (b)

Fig. 2. Signal variance as the window size of (a) noise signal and (b) crack wave.

3. Validation using the experiment

In this paper, to verify the accuracy of the proposed algorithm for measuring the arrival time of the wave, the experiment was performed on the surface of the rock.

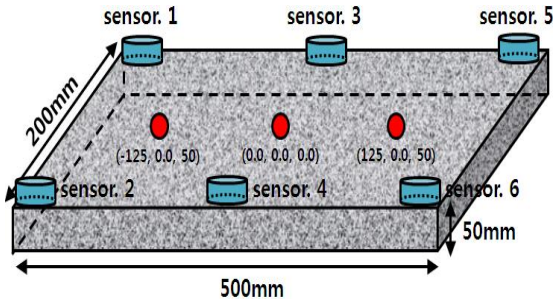


Fig. 3. Location of AE sensors on the granite rock and the schematic diagram of the pencil lead break for the accuracy of the source localization.

The AE signal is generated by using the pencil lead break. Fig. 3 shows the location of the three hit points and the coordinate information of the six sensors used in the experiment. The three red circles denote the pencil lead break points.

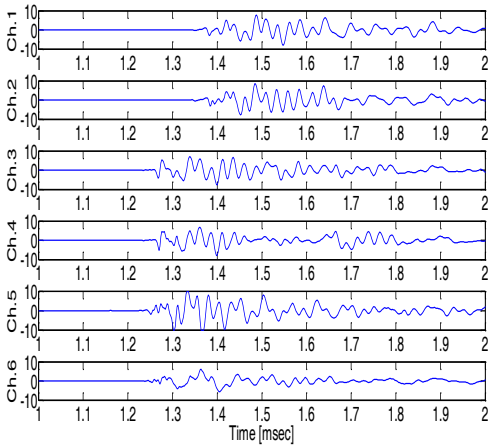


Fig. 4. Measured AE signals when the pencil lead break test was performed at (125 mm, 0.0 mm, 50 mm).

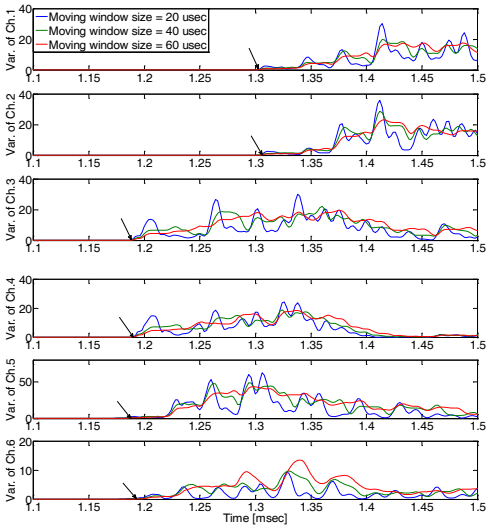


Fig. 5. Experimental results by using the proposed moving window method when the pencil lead break test was performed at (125 mm, 0.0 mm, 50 mm).

Fig. 4 shows the measured raw signal from each AE sensors. It is difficult to find the starting point of the each wave. However, we can detect the arrival time easily by using the proposed method as shown in Fig. 5.

To verify the result of the Fig. 5, we have performed source localization. In the Fig. 6, the estimated source location was (125.8 mm, 2.7 mm, 50 mm) when the true source location was (125 mm, 0 mm, 50 mm). Therefore, the result shows that the proposed method can estimate the arrival time of crack wave accurately.

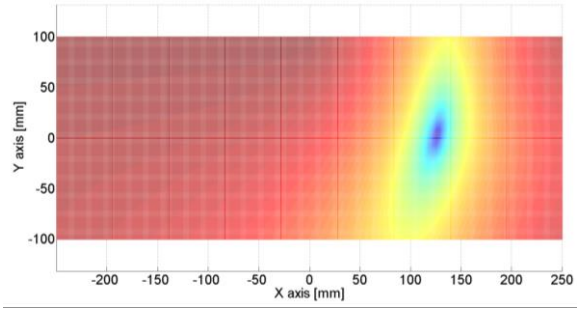


Fig. 6. Source location was estimated by calculating the variance of velocities, where the minimum value of variance indicated source location.

4. Conclusion

In this paper, we suggested how to predict the arrival time of the crack wave by using the moving window. To verity the method, the experiment for the rock specimen was performed. The result shows the method is quite powerful for estimating the arrival time of crack wave in nosy environment.

REFERENCES

[1] Tsang, C. F., Bernier, F. and Davies, C. (2005), "Geohydromechanical processes in the excavation damaged zone in crystalline rock, rock salt, and indurated and plastic calys-in the context of radioactive waste disposal", Int. J. Rock Mech. Min. Sci., Vol.42, No.1, pp.109-125.

[2] IAEA, (2001), "Monitoring of geological repositories for high level radioactive waste:, IAEA-TECDOC-1208, IAEA, Vienna.

[3] EU (2004), "Thematic network on the role of monitoring in a phased approach to geological disposal of radioactive waste", Final report to the European Commission Contract FIKW-CT-2001-20130, pp.1-16.

[4] hardy, H. R. (1994), "Geotechnical field applications of AE/MS techniques at the Pennsylvania state university: a historical review," NDT&E International, Vol.27, No.4, pp.191-200.

Implementation of Damage Model to TOUGH2-MP/FLAC3D Coupled Code

Jaewon Lee*, Changsoo Lee, and Geon Young Kim

Korea Atomic Energy Research Institute, 111, Daedeok-daero 989beon-gil, Yuseong-gu, Daejeon, Republic of Korea

*jwl@kaeri.re.kr

1. Introduction

In the case of a repository for radioactive waste, corrosion of metallic materials under anoxic conditions will lead to the formation of hydrogen. If the rate of gas production exceeds the rate of gas diffusion within the pores of the barrier, gas will continue to accumulate until its pressure becomes sufficiently large for it to enter the surrounding material. In the case of plastic clays and in particular bentonite, classic concepts of porous medium two-phase flow are inappropriate and continuum approaches to modelling gas flow may be questionable. However, the detail of the dilatant mechanisms controlling gas entry, flow and pathway sealing are unclear and such features may impair barrier performance, in particular, acting as preferential flow paths for the movement of radionuclides. Because of that, development of new and novel numerical representations for the quantitative treatment of gas in clay-based repository systems are therefore required. In this study, the damage model is adopted to model the gas migration phenomena, and implemented to TOUGH2-MP/FLAC3D coupled code for hydro-mechanical modeling.

2. Numerical code

TOUGH2-MP and FLAC3D were used to perform thermal-hydraulic-mechanical interaction analysis. TOUGH2-MP is an abbreviation of TOUGH2 Massively Parallel, and is the parallel version of TOUGH2 software. TOUGH2 has a strong point in multiphase/multi-component flow analysis and heat transfer analysis. In case of TOUGH2-MP, parallel analysis is made possible and the analysis speed is dramatically improved. FLAC3D is a code that has strengths in the mechanical analysis of soil and rock. The algorithm of the TOUGH2-MP/FLAC3D coupling analysis module is shown in Fig. 1.

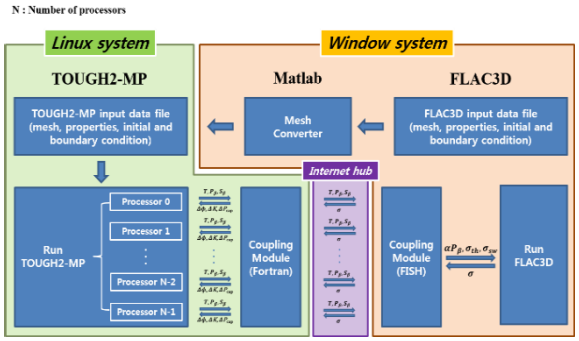


Fig. 1. TOUGH2-MP/FLAC3D coupling module algorithm.

3. Damage model [1]

Tang et al. proposed a flow-stress damage (FSD) coupling model of saturated rocks by taking into account the growth of existing fractures and the formation of new fractures [1].

In elastic damage mechanics, the elastic modulus of the element may degrade gradually as damage progresses, and the elastic modulus of the damaged element is defined as follows:

$$E = (1-D)E_0 \tag{1}$$

where D represents the damage variable, and E and E_0 are the elastic moduli of the damaged and undamaged elements, respectively.

When the tensile stress in an element reaches its tensile strength f_t, the damage variable can be described as:

$$D = \begin{cases} 0 & \varepsilon_{t0} \le \varepsilon_3 \\ 1 - \dfrac{f_{tr}}{E_0 \varepsilon_3} & \varepsilon_{tu} \le \varepsilon_3 \le \varepsilon_{t0} \\ 1 & \varepsilon_3 \le \varepsilon_{tu} \end{cases} \tag{2}$$

where f_{tr} is the residual tensile strength, and ε_3 is tensile principal strain.

To describe the element damage under a

compressive or shear stress condition, we choose the Mohr–Coulomb criterion as the second damage criterion. The damage variable under uniaxial compression is described as:

$$D=\begin{cases}0 & \varepsilon_1 \le \varepsilon_{c0} \\ 1-\dfrac{f_{cr}}{E_0\varepsilon_1} & \varepsilon_{c0} \le \varepsilon_1\end{cases} \quad (3)$$

where f_{cr} is the residual compressive strength, and ε_3 is tensile principal strain.

Fig. 2 shows elastic damage constitutive law for elements under uniaxial compressive stress and tensile stress.

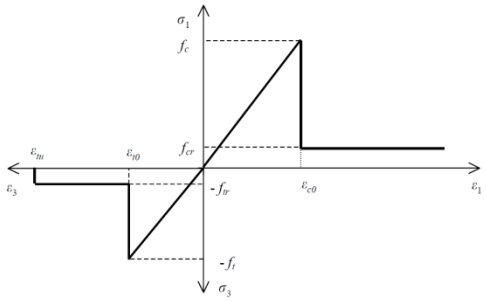


Fig. 2. Elastic damage constitutive law for elements under uniaxial compressive stress and tensile stress.

4. Implementation to TOUGH2-MP/FLAC3D

This section describes the numerical implementation of the FSD model in the framework of the TOUGH2-MP/FLAC3D coupled code. Stress analysis, based on the effective stress principle, is carried out to obtain the stress field. The coupled FS model is used to analyse the coupling problem between flow and stress, and the coupled FD model is used to analyse the coupling problem between flow and damage. The stiffness and strength of the damaged elements will be reduced whereas their porosity and permeability will increase accordingly.

For porosity change, we assume the solid volume is constant. That means porosity increase in proportion to the volumetric strain as described below:

$$\phi=\frac{V_p}{V}=\frac{V_p+\Delta V}{V_0+\Delta V}=\frac{V_p+\varepsilon_v V_0}{(1+\varepsilon_v)V_0} \qquad \left(\varepsilon_v=\frac{\Delta V}{V_0}\right) \quad (4)$$

where V_0 is the initial total volume and V_p is the pore volume.

In this case, permeability is assumed porosity dependent model as described below [2, 3]:

$$k=k_0\exp\left[A\left(\frac{\phi}{\phi_0}-1\right)\right] \quad (5)$$

where k_0 is initial (zero stress) intrinsic permeability, ϕ_0 is initial porosity, and A is the empirical factor.

5. Conclusions

In this study, the damage model is adopted to model the gas migration phenomena, and implemented to TOUGH2-MP/FLAC3D coupled code for hydro-mechanical modeling. Elastic modulus is varied according to damage variable D, and porosity and permeability is changed based on the volumetric strain. In the future, we plan to conduct the validation process using the laboratory test results for the damage model of TOUGH2-MP/FLAC3D.

ACKNOWLEDGEMENTS

This research was supported by the Nuclear Research and Development Program of National Research Foundation of Korea (NRF) funded by the Minister of Science, ICT and Future Planning.

REFERENCES

[1] C.A. Tang, L.G. Tham, P.K.K. Lee, T.H. Yang, and L.C. Li, “Coupled analysis of flow, stress and damage (FSD) in rock failure”, International Journal of Rock Mechanics & Mining Sciences, 39, 477-489 (2002).

[2] J.P. Davis and D.K. Davis, “Stress-dependent permeability: characterization and modeling”, Society of Petroleum Engineers, SPE Paper no. 56813 (1999).

[3] J. Rutqvist, Y.S. Wu, C.F. Tsang, and G. Bodvarsson, “A modeling approach for analysis of coupled multiphase fluid flow, heat transfer, and deformation in fractured porous rock”, International Journal of Rock Mechanics & Mining Sciences, 39, 429-442 (2002).

High Speed Boreshear Tests of an Engineered Barrier System for High Level Waste Disposal

Minsoo Lee*, Heui-Joo Choi, Jongyoul Lee, and Sung-Hoon Ji

Korea Atomic Energy Research Institute, 111, Daedeok-daero 989beon-gil, Yuseong-gu, Daejeon, Republic of Korea

*minm@kaeri.re.kr

1. Introduction

Korean peninsula is not completely free of seismic activity, since it is near to the active volcano belt of the Pacific Rim. Recently, in 2016, there was a fairly strong earthquake around Gyeong-Ju Province. To cope with such seismic influences on the disposed canister in a underground borehole, some foreign organizations in Japan (JAEA) and Sweden (SKB) have been investigating the effects of seismic movement on the underground repository for many years [1, 2]. In Korea, KAERI has also been studying seismic influence on an underground repository.

The countries which are concerned about fault movements at a repository have established the allowed conditions for fault movement in their canister design, which are summarized in Table 1. The disposal canister must not be ruptured by fault movement.

Table 1. The maximum allowed conditions for fault movement for a disposal canister

	Korea (KAERI)	Japan (JAEA)	Sweden (SKB)
Fault Velocity		1 m/sec	
Fault movement	10 cm	10 cm	5cm

It is difficult to conduct boreshear testing of a disposal canister in real scale to determine whether it can resist the expected magnitude of a fault movement crossing a borehole. Thus the testing is generally conducted at a reduced scale, to try and simulate the behavior using computational modeling, to develop a reliable evaluation tool. KAERI has also tried this approach since 2010, and created a 1/30 scale miniature boreshear testing module.

However the maximum test speeds of fault module in laboratories were much below than the requirement limit of 1.0 m/sec so far as described in Table 2. Thus the high speed boreshear module was designed, and its performance was tested at above 1m/sec experimentally in this study.

Table 2. Comparison of KAERI shear module with those of JAEA [1] and SKB [3] (Unit: mm)

Org./Scale	Canister	Hole size	Test condition
KAERI 1 : 30	D30, L60	D76, L124 t3.0(1㎛), t1.5(10㎛)	Disp. 20 SR(Shear rate) 100 ㎜/min
JAEA 1 : 20	D50, L100	D150, L350	Disp. 70, 40 SR 10, 100 ㎜/sec
SKB 1 : 10	D80, L450	D158, L622 t20 (max 12㎛) CylinderFilter L300x2	Disp. 28, 30, 21 SR 20, 100, 1000 ㎜/min

2. Module Design

Two shear modules were made at 1/30 scale of the A-KRS [4]. A module was composed of two cylindrical half parts, which can slip into each other. And the inner space diameter was 70 mm with a length of 120 mm, in which a copper rod (D30 x L60) was placed with compact bentonite blocks. There were 6 stress sensors around the module boundary of the stationary part to measure stress changes in the bentonite buffer when a shearing occurs.

A high speed shearing was achieved by punching down the other movable part with a free dropping of 97 kg mass above 20 cm high position as shown in Fig. 1. The impact velocity of the mass was about 2.0 m/sec, and it has a 196.2 J of kinetic energy.

For the water saturation of bentonite buffer, KURT underground water was supplied with 2.0 MPa pressure, and the supplied amount was monitored to know the degree of saturation. The test modules were placed in mini-environmental chambers to control them at 30˚C.

Two kinds of bentonite buffers were used in this experiments, which were pure Gyeong-Ju bentonite and the 3wt% graphite added one. Those were compacted to be 1.6 g/cm^3 in dry density.

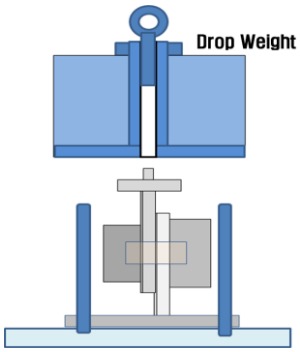


Fig. 1. Schematic drawing of a high speed boreshear test module.

3. Experiment

After reaching the equilibrium of water supply, a heavy mass was dropped onto the shear module above 20 cm high. The shear displacement by the first drop was approximately 2~3 mm in two modules, which was much lower than expected. Thus more free drops were repeated 3~4 times to reach a 19 mm shear displacement.

The stress increases around shear module were suggested for 3wt% graphite bentonite buffer in Fig. 2. The maximum stress increase was about 2 MPa at bottom position near the shear plane. And the total stress increase after 19 mm shear displacement was below 5 MPa. After the test, the copper rod was examined to know if any shear deformation was occurred on it, but no deformation was observed.

The rotational angle of a copper rod was measured after dismantling of them. The rotational angle by the 19 mm shear displacement was about 23~24˚, which was a bit higher than 18˚ of a theoretical angle as shown in Fig. 3.

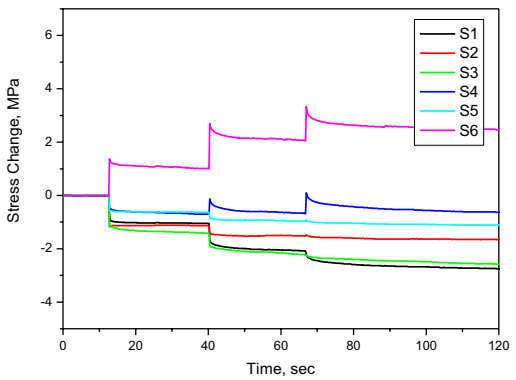


Fig. 2. The increase of shear stress by several free drops of heavy mass for 3wt% graphite bentonite.



Fig. 3. Shear rotated copper rod in a pure bentonite and a 3 wt% graphite added bentonite.

4. Conclusion

High speed boreshear tests were performed above 1.0 m/sec velocity at 1/30 scale of A-KRS. The stress increase in the buffer was not higher than 5.0 MPa after 19 mm shear displacement. Thus it was concluded that the saturated bentonite buffer can reduce the mechanical impact by a fault movement to a moderate level not to damage the inner canister. However, the development of simulation model was needed for the clear evaluation of the full-scale boreshear safety of a disposal canister.

Acknowledgement

This work was supported by the Ministry of Science, ICT and Future Planning within the framework of the national long-term nuclear R&D program (NRF- 2017M2A8A5014836).

REFERENCES

[1] Yuya Saito, Kenji Tanai, Hirohito Kikuchi, and Mayuka Nishimura, JAEA Research 2008-010, "Assessment on Mechanical effect of Engineering Barrier System to Fault Movement (II)", 2008.

[2] Lennart Borgesson, Jan Hernelind, SKB TR-10-33, “Earthquake induced rock shear through a deposition hole”, 2010.

[3] Swedish Nuclear Fuel and Waste Management Co., SKB Technical Report, TR-01-23, Copper corrosion under expected conditions in a deep geologic repository, 2001.

[4] KAERI Research Report, "High-Level Waste Long-term management Technology Development", KAERI/RR-3100 (2009) in Korean.

Evidence From Fracture Filling Minerals for the Interpretation of Uranium Isotopes in Investigating Ancient Redox in Granitic Rock in KURT Site

Ji-Hun Ryu* and Hong-Yun Jeong

Korea Atomic Energy Research Institute, 111, Daedeok-daero 989beon-gil, Yuseong-gu, Daejeon, Republic of Korea

*jryu@kaeri.re.kr

1. Introduction

The study of past groundwater condition is of particular interest in the context of potential waste repository site characterization. It is because of the need to predict the future behavior of the groundwater system over timescales of relevance to safety assessment. It is necessary to develop an understanding of how the groundwater system has changed over time in response to changing driving forces for groundwater flow and hydrogeochemical evolution. The generation of fracture filling minerals contains geochemical record of the compositions of the groundwaters from which they precipitated. The combination of isotopic characteristics of fracture filling minerals provides very important information of paleo-hydrology of a geological site. In this study, to advance the understanding of uranium isotopes in fracture filling minerals and its response to groundwater flow and chemical evolution, we measured U isotopes such as ^{238}U, ^{235}U, ^{234}U in fracture filling minerals in KURT site.

2. Methods

The study site is located at KURT (KAERI underground Research Tunnel) site in Korea Atomic Energy Research Institute, Yuseong area, the northern part of the Daejeon city, Korea. Boreholes MB1, KP3 and KP4 were drilled inside KURT, MB2 and DB2 outside KURT, respectively.

Fracture filling minerals were obtained from the drill cores from MB1, MB2, KP3, KP4 and DB2 boreholes that they were drilled into the highly fractured domain. Fracture coatings from drill cores were collected from drilled cores at various depths up to ~1000 m. Samples from the surface of fractures were crushed into powder using a pestle and mortar. Samples were prepared by MW-assisted digestion in HNO_3 + HCl + HF mixture. $^{238}U/^{235}U$ isotope ratio measurements were carried out by MC-ICP-MS (NEPTUNE, ThermoScientific). $^{235}U/^{234}U$ isotope ratio measurements were carried out by ICP-SFMS (ELEMENT XR, ThermoScientific) at ALS Scandinavia AB, Sweden. The determination of U, Fe, Mn concentrations was performed at the Korea Basic Science Institute using an ICP-AES (Perkin Elmer) and an ICP-MS(VG, PQ3).

3. Results

3.1 Redox front

The concentrations of Mn and Fe in fracture filling minerals indicated they were enriched at similar depths. Mn and Fe are believed to have formed in oxidized forms. The presence of significant concentrations of U suggests that the groundwater from which it precipitated was reducing. The enrichment patters of Mn, Fe and U indicated the location of redox front in KURT site, which was the range of 100 – 200 m depths (Fig. 1).

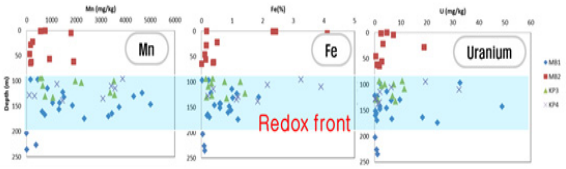


Fig. 1. Enrichment patterns of Mn, Fe and U in the KURT site indicated the presence of redox front.

3.2 $^{234}U/^{238}U$

At the shallow depths in the site, $^{234}U/^{238}U$ AR showed various values as shown in Fig. 2. At the deeper depths (below ~ 600 m depth), the values of $^{234}U/^{238}U$ AR became constant, which might indicated the secular equilibrium of U bearing minerals in fracture filling minerals. Thus, it indicated that the mobility of U was very slow to

reach the secular equilibrium in the groundwater system, while the scatter patterns of $^{234}U/^{238}U$ AR resulted from weathering and precipitation. During weathering process, ^{234}U is preferred to be removed from mineral matrix and it is enriched in groundwater interacting with the solid phase [1]. The U bearing minerals was formed from groundwater that was enriched in ^{234}U resulted in higher values of $^{234}U/^{238}U$ AR, which is believed to happen continuously [1].

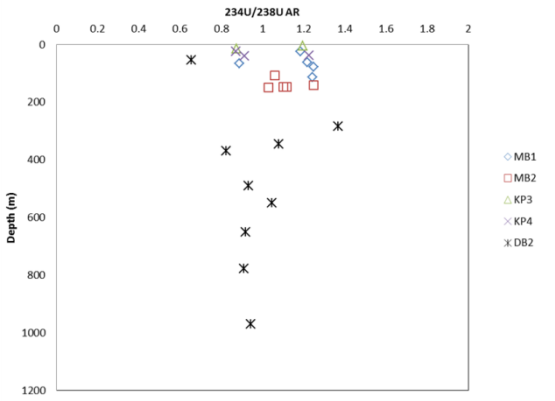


Fig. 2. Patterns of $^{234}U/^{238}U$ AR with depths in KURT site.

3.3 $^{238}U/^{235}U$

At the shallow depths uranium reduction process prefer ^{235}U over ^{238}U. Thus ^{238}U was enriched in U bearing fracture filling minerals by uranium reduction [1]. But the enrichment of ^{238}U is limited by microbiological uranium reduction. Thus, the large number of $^{238}U/^{235}U$ ratio in U bearing minerals indicated that U reduction was not the only process to occur but more processes involved in the formation of U bearing minerals. At shallower depths in KURT site, the values of $^{238}U/^{235}U$ ratio were scattered (Fig. 3), which shows the different sources of uranium. Thus it indicates groundwater was mixed at shallower depths. At deeper depths, the values of $^{238}U/^{235}U$ ratio became constant. It indicated that the groundwater system at the depths was not mixed and U reduction was the major process influenced $^{238}U/^{235}U$ of U bearing minerals.

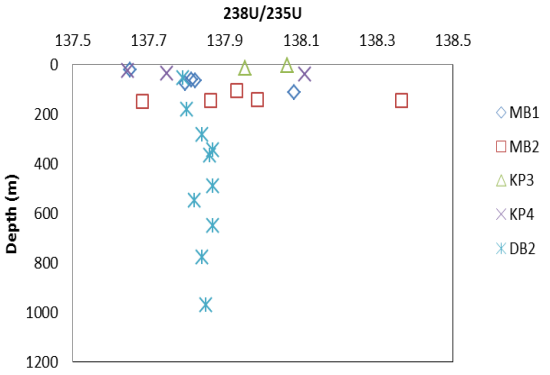


Fig. 3. Patterns of $^{238}U/^{235}U$ with depths in KURT site.

This study evaluated the location of redox front based on the patterns of concentrations of Mn, Fe and U in fracture filling minerals. Also, we evaluated paleo-hydrology condition which showed paleo-groundwater mixing, weathering and U precipitation at shower depths while very slow U mobility enough to reach the secular equilibrium at deeper depths (below ~ 600 m depths) in KURT site (Fig. 4).

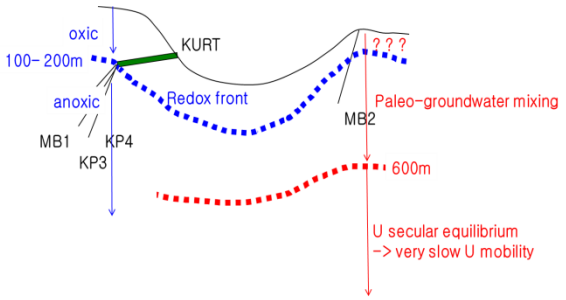


Fig. 4. A conceptual model for redox front and secular equilibrium in U, which indicated very slow U mobility to reach the secular equilibrium in KURT site.

REFERENCES

[1] D.M. Bonotto, “A comparative study of aquifer systems occurring at the Parana sedimentary basin, Brazil: U-isotopes contribution”, Environ. Earth Sci., 68, 1405-1418 (2013).

[2] M. J. Murphy, C. H. Stirling, A. Kaltenbach, S.P. Turner, and B.F. Schaefer, “Fractionation of $^{238}U/^{235}U$ by reduction during low temperature uranium mineralization processes”, Earth and Planetary Science Letters, 388, 306-317 (2014).

Thermal Design Concept of Gap Between Canister and Buffer in an HLW Repository

Jae Owan Lee* and Geon Young Kim

Korea Atomic Energy Research Institute, 111, Daedeok-daero 989beon-gil, Yuseong-gu, Daejeon, Republic of Korea

*jolee@kaeri.re.kr

1. Introduction

When the buffer is installed in the excavated deposition borehole in the HLW repository, there will be an empty space, i.e. gap between the canister and the buffer and between the buffer and the deposition borehole. These gaps around the buffer may give a significant influence on the release of decay heat from the waste through the canister and buffer into the surrounding host rock.

This study presents the influence of the gap between the canister and buffer (hereafter, referred to as the inner gap) on the peak temperature of the buffer and its thermal considerations in the buffer design of Korean Reference disposal System (KRS).

2. Numerical model

The present KRS design concept has no consideration of gaps between the canister and the buffer and between the buffer and the deposition borehole: The high-level waste encapsulated in the canister is deposited in the deposition borehole, and after its emplacement, the empty space between the canister and the wall of the deposition borehole is filled with compacted bentonite buffer without any gaps (Fig. 1). This study assumes there are gaps between the canister and the buffer and between the buffer and the deposition borehole, analyzing the change in the buffer thermal performance by gap-filling options of the inner gap when the outer gap between the buffer and the surrounding host rock is filled with bentonite pellets.

Numerical simulations are carried out for a 3-D quarter of model geometry using the Heat Transfer Module of COMSOL Multiphysics Ver. 5.1, which is a finite element computer code. The Heat Transfer Module is expressed by the following governing equation which is applicable to a conductive heat transfer in a porous medium:

$$\rho C_p \frac{\partial T}{\partial t} + \nabla \cdot (-\lambda \nabla T) = Q, \quad (1)$$

where T is the temperature as a dependent variable, ρ is the density of porous media, C_p is the specific heat capacity, λ is the thermal conductivity, t is the time, and Q is the heat source. The meshes for the numerical simulation are made using free tetrahedral elements, and more elements are made near the buffer and its surrounding gaps.

For model simulation, the thermal conductivity of bentonite pellets used as gap-fills is calculated from Beziat et al.'s equation [1]:

$$\lambda_{pellets} = {\lambda_s}^{1-n} \cdot {\lambda_w}^{n \cdot s_r} \cdot {\lambda_a}^{n \cdot (1-s_r)} \quad (2)$$

where $\lambda_s, \lambda_w, \lambda_a$ are the thermal conductivities of solid, water, and air, respectively. n is the porosity of the bentonite pellets and s_r is the degree of saturation.

3. Results and conclusions

The location of the peak temperature in the buffer was determined by examining the temperature distribution along the interface boundary between the inner gap and the buffer. The highest temperature in the buffer was located at the central point of the inner gap which is in contact with the buffer in the axial direction of the deposition borehole.

The peak temperature in the buffer, when the inner and outer gaps were left unfilled with gap-fills, was much higher than when no gap around the buffer was considered. This is probably because air significantly interferes with the release of decay heat from the canister containing waste to the surrounding host rock.

However, when both the outer gap and inner gap were filled with the gap-fills of bentonite pellets, the peak temperature was much reduced to 110℃ (Fig. 2), which suggests that the bentonite pellets are

effective in improving the heat release through the gaps. Fig. 2 also shows the calculated peak temperature when the outer gap is filled with the gap-fills of bentonite pellets and the inner gap is left empty without gap-fills. We knew in this figure an interesting fact unlike our expectations: the peak temperature for the case of no gap-fills in the inner gap (107.5℃) was lower than that of the case of gap-fills (110℃). This suggests that it is favorable for the heat release to leave the inner gap empty without filling it with gap-fills.

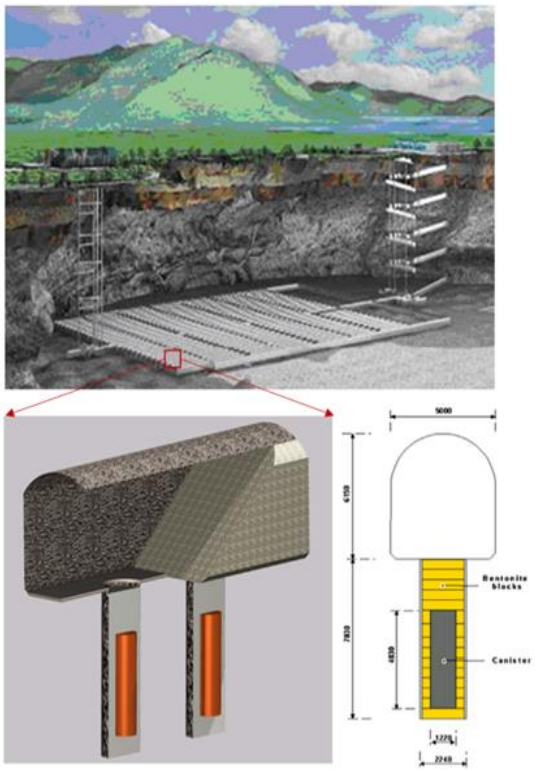


Fig. 1. Schematic picture of Korean Reference disposal System (KRS) and engineered barrier system.

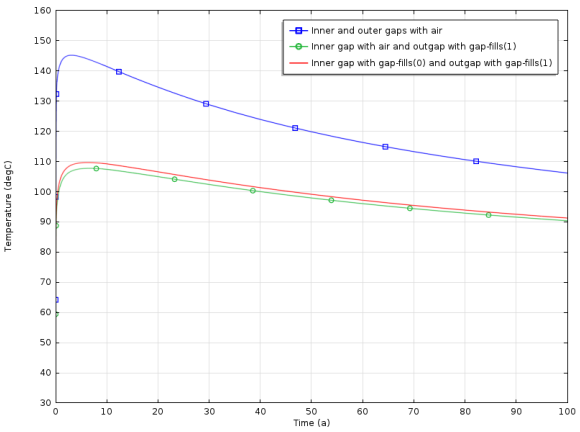


Fig. 2. Temperature evolution curves at peak temperature point for three gap-filling options of the inner gap.

Acknowledgement

This work was supported by Nuclear Research & Development Program of the National Research Foundation of Korea (NRF) Grant funded by the Ministry of Science, ICT and Future Planning (MSIP).

REFERENCES

[1] A. Beziat, M. Dardaine, V. Gabis, Effect of compaction pressure and water content on the thermal conductivity of some natural clays", Clays and clay Minerals, 36(5) (1988).

Preliminary Study on Optimization of Disposal Facilities Against Human Intrusion

Dong-Keun Cho*, Jung-Woo Kim, Jongtae Jeong, and Min-Hoon Baik

Korea Atomic Energy Research Institute, 111, Daedeok-daero 989beon-gil, Yuseong-gu, Daejeon, Republic of Korea

*dkcho@kaeri.re.kr

1. Introduction

It is the preferred option to contain the radwaste and isolate it from the human environment for a long-term management of the radwaste. The concentration and containment of the waste in one location, however, could make future generation be in hazard condition if someone were to disturb the disposed waste.

In this study, protective measures to increase robustness of disposal facilities against human intrusion were proposed on the basis of methodology developed HIDRA project, with the assumption that the intrusion occurs after loss of knowledge of the hazardous nature of the disposal facility.

At first, the assumption regarding disposal facilities and assessment methodology of human intrusion were briefly explained, followed by assessment of potential measure to propose protective measure against inadvertent human intrusion scenarios.

2. Conditions and Assumptions

2.1 Safety framework

It was assumed the safety framework regarding human intrusion were the same as the ones described in references 1 and 2. The important things are as follows. The main purpose of assessing human intrusion is to optimize the disposal facility with higher robustness rather than to check whether the disposal facility satisfies dose constraint. And, protective measures against human intrusion should not jeopardize safety function of the disposal facility.

2.2 Hypothetical Disposal facilities

It was assumed that silo-type geological disposal facility is under operation stage for intermediate-level wastes. The silo which conceptually has diameter of 25 m and height of 50 m, respectively, is located at 100-150 m from the sea level. The radwaste to be composed of contains 10% of long-lives nuclide in terms of radioactivity.

2.3 Premises of human intrusion

It was assumed that human intrusion occurs after loss of knowledge of the hazardous nature of the disposal facility. It is definite that future generation will have advanced technologies than current generation, but it was assumed that future generation would have the level of current technologies to exclude uncertainty induced from speculation. Representative human intrusion scenario were also driven on the basis that future generation would have the same human activities and residential habits as those current generation has.

2.4 Assessment method for optimization

In this paper the methodology to assess human intrusion developed through HIDRA project by IAEA, in which the main purpose to derive protective measure against human intrusion is to make disposal facility robust as an optimization process, was adopted. In this methodology, to derive protective measure, safety framework is defined at first, and then the potential measure on the basis of general measures and specific disposal system is derived. Finally, the potential measure is accepted as protective measure after assessing the conflict with safety function of the facility, implementation of the potential measure, and effectiveness of the reduction of potential for and/or consequence of human intrusion. Here, general measures means all kinds of measures which can be considered as a potential measure. And, the potential measure means appropriate candidate to derive eventual protective measure. Please refer to references 1 and 2 for more detailed information.

3. Scenario and Potential Measures

3.1 Human intrusion scenario

Drilling scenario was considered as a representative human activity. Drilling a borehole through disposal facilities results in radwaste or contaminated material to be brought to the surface. This activity can causes acute exposure to the borehole driller and field scientists. If the radwaste or contaminated material is spread to a farmland, it can also cause chronic exposure to residents who could ingest crops and vegetable cultivated on contaminated soil.

3.2 Potential measures

Two plausible potential measures were considered: one is transmute long-lived nuclides in waste and the other is implement 2.5 m-thick reinforced concrete slab beneath ground surface. The former one is transmute long-lived radionuclides contained in radwate by using accelerator or nuclear reactor to

reduce radioactivity and hazard of radwaste itself. The latter one is install implement 2.5 m-thick reinforced concrete slab beneath ground surface just over silo-type disposal facility. A reinforcing rod frame installed to prevent drill bit from intruding the concrete silo is contained within concrete. The total thickness of the reinforced concrete is 30 cm and it is installed at a depth of 2 m from the ground surface. The diameter and pitch of each mesh to compose of the reinforcing rod frame are 1 cm and 5 cm, respectively. The rod frame is composed of 8 mesh plates that are staggered by 5 cm each. Fig. 1 shows conceptual drawing representing geological disposal facility with reinforced concrete slab.

Table 1. Potential Measures

ID	Candidate Potential Measures
PM-1	Transmutation of long-lived nuclides in radwaste
PM-2	Insertion of a 2.5 m-thick reinforced concrete slab over near surface

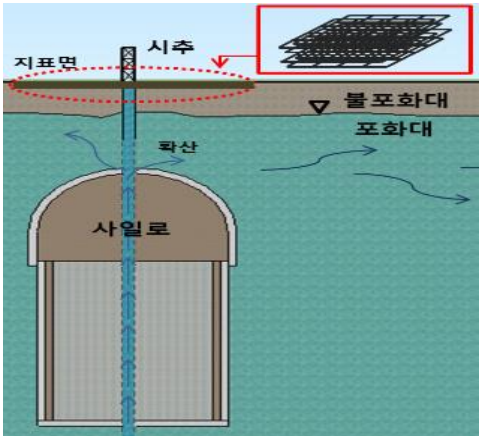


Fig. 1. Conceptual Drawing of Facilities.

4. Derivation of Protective Measures

According to references 1 and 2, protective measure is derived through four steps. In this paper, however, the last 4th step was only considered.

First, it was assessed whether PM-1 could be accepted as a protective measure. According to the data announced in Scottland, the probability of installing a borehole at a depth of 150 m and 250 m are 1.5×10^{-10}/m^2-yr and 7×10^{-11}/m^2-yr, respectively. Therefore, increasing the depth of the silo by 100 m can be a highly effective protective measure in terms of reducing the likelihood of human intrusion. However, since the construction of silos is already completed, this potential measure can't be a adopted as measures in terms of implementation.

According to the assessment methodology of human intrusion developed by HIDRA project, protective measure is identified until an appropriate protective measure is derived. Therefore PM-2 was assessed as an iteration process. The method of installing reinforced concrete is to install reinforced concrete with a thickness of 2.5 m at a depth of 2.5 ~ 5.0 m below ground surface. Because of reinforcing rod frame, it is very hard for drill bit with a diameter of 5 cm or more to pass through the silo. Generally, the strength of reinforcing rod is significantly higher than that of ordinary rock. This method can delay and deter the human intrusion into the disposal facilities due to the operation time and the breakage of the drill bit. The next important thing is feasibility of the implementation of PM-2 to geological facility. The reinforced concrete containing reinforcing bars with a depth of 2.5 m below ground surface does not require much cost compared to the cost of construction of the disposal facility. Although the reinforced concrete is installed above the silo containing radwaste, the load from the installed reinforced concrete is negligible. Therefore PM-2 does not jeopardize safety function of geological disposal facility. Therefore, it is reasonable to adopt reinforced concrete over the footprint of the silo as a protective measure to reduce the risk of human intrusion.

5. Summary and Conclusion

In this paper, protective measure against human intrusion was derived on the basis of assessment methodology developed by HIDRA project, for an optimization of geological disposal facility. Only drilling human intrusion scenario and the 4th step for the derivation of protective measure were considered. Feasibility of implementation, economic cost, and conflict with safety function were considered when the potential measure was assessed qualitatively. As a result, installation of reinforced concrete over concrete silo was adopted as protective measure. In this paper, the protective measure was derived through simple qualitative consideration, but the implementer should submit comprehensive safety case for the derivation of protective measure against human intrusion to support their justice.

ACKNOWLEDGEMENT

This work is based on the outcomes from HIDRA (Human Intrusion in the context of Disposal of RadioActive Waste) Project by International Atomic Energy Agency [8] and was supported by the National Research Foundation of Korea (NRF) grant funded by the Korea government (the Ministry of Science, ICT & Future Planning (MSIP)) (No. 2017M2A8A5014856)

REFERENCES

[1] IAEA, - HIDRA -The International Project on Human Intrusion in the context of Disposal of RadioActive Waste, Version 1.1, 2015.

[2] D. K. Cho et al., Review on Assessment Methodology for Human Intrusion Into a Repository for Radioactive Waste, Journal of Nuclear Fuel Cycle and Waste Technology. Vol. 14 No.3 pp.297-305, September 2016.

Spectroscopic Characterization of Aqueous Am(III) Species

Hee-Kyung Kim*, Euo Chang Jung, Hye-Ryun Cho, and Wansik Cha

Korea Atomic Energy Research Institute, 111, Daedeok-daero 989beon-gil, Yuseong-gu, Daejeon, Republic of Korea

*hkim11@kaeri.re.kr

1. Introduction

Minor trans-uranic (TRU) radionuclides including Am in spent nuclear fuels are the major concerned long-lived radionuclides in the high-level radioactive waste managements. Understanding their physicochemical interactions in groundwater systems is essential for the safety assessments of the high-level radioactive waste managements. Due to relatively weak luminescent properties (luminescence half-life: ~23 ns) [1] and high specific radioactivity (radioactivity half-life ^{241}Am: 432 yr), there are limited number of spectroscopic studies on aqueous Am(III) species [2-4]. Upon complex formation with hydroxyl group [2] or organic ligands [3,4], Am(III) absorption peak shifts towards longer wavelength [2,3], while luminescence intensity and lifetimes increase [4]. However, many of the thermodynamic properties of Am(III) species are still adapted from the results of Cm(III) and Eu(III) studies [5]. In this study, we directly characterized the spectroscopic properties Am^{3+} and its hydrolysis products progressively formed upon increase in the pH conditions. Temperature-dependent changes of the spectroscopic properties will be also discussed in relation to the species distribution.

2. Experimental

2.1 Am(III) sample preparation

^{241}Am was used as a Am(III) source. Am(III) samples were prepared in the concentration of 2-6 μM in 0.1 M $NaClO_4$ under the Ar condition to prevent dissolution of CO_2. Pre-estimated amount of diluted NaOH was added to adjust the pH. Precipitation was separated from supernatant by centrifugation at 18000 rpm for 1 hour. Concentration of Am(III) in the supernatant was measured by Liquid Scintillation Counting (TriCarb, PerkinElmer). Presence of colloidal particles in the supernatant was determined by Laser Induced Breakdown Detection (LIBD) method. pH of each sample was measured by combined glass electrode (Orion) at the last step of the experiments.

2.2 Time-Resolved Laser Fluorescence Spectroscopy (TRLFS)

Nd:YAG pumped OPO laser (Vibrant, Opotek Inc.) was used as an excitation source of 503 nm. Emission per wavelength was collected by a spectrometer (Semrock) connected to an ICCD (Andor Tech.). A delay generator triggered by the laser flashlamp was set to control the timing of the Q-switch of the OPO laser and the ICCD gating times. Series of luminescence measurements were carried out as increasing the ICCD gating delay time in stepwise to measure luminescence decay curves. Luminescence half-lives were calculated from linear regression of the luminescence intensity decays in natural log unit as a function of gate delay time.

3. Results and Discussion

3.1 pH-dependent Luminescence Spectra

Luminescence spectra of Am(III) solutions under different pH conditions were obtained for the $^5D_1 \rightarrow {}^7F_1$ transition as shown in Fig. 1. The center of the peak is 689 nm with FWHM of 15 nm at pH 2. As increasing the pH of the solutions, the concentrations of the supernatants decreased as measured by LSC, indicating formation of $Am(OH)_3(s)$ precipitations. Luminescence intensity of Am(III) in the supernatants decreased accordingly. While the peak positions of the supernatants do not change, peak widths become slightly broadened towards longer wavelength region. These observations indicate formation of $Am(OH)_n(aq)$ upon increase of the available hydroxyl groups at high pHs. Our results support a previous report by showing red-shifted absorption as hydrolysis reaction progresses [2]. Currently, we are working on measurements of luminescence spectra at different temperatures in attempt to increase the signal to noise

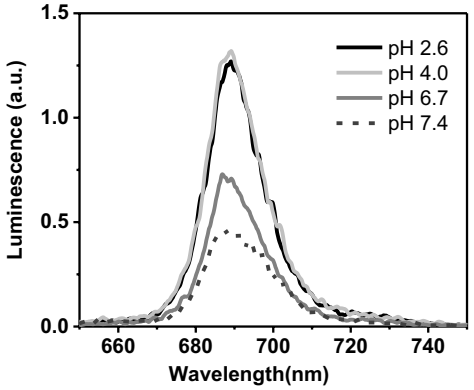


Fig. 1. Luminescence spectra of Am(III) at different pHs in 0.1 M $NaClO_4$. Concentrations of the Am(III) in the supernatants decreased from 5.8 μM to 1.1 μM as Am(OH)3 precipitated upon increasing the pH of the solutions from pH2.6 to pH7.4. Spectra were averaged over 2000 shots at a 30 ns delay from the excitation at 503 nm (3.5 mJ) with a gate width of 150 ns (pH 2.5).

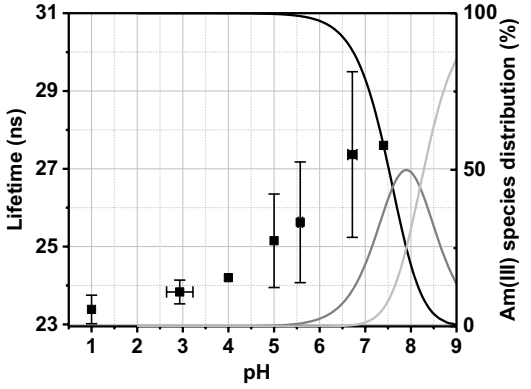


Fig. 2. Luminescence lifetimes (square) of Am(III) under the different pH conditions. Lifetimes were obtained from linear fitting of luminescence decays in the natural log scale as a function of gate delay time. Gradual increase in the lifetimes are displayed along with distribution changes of Am^{3+} (black line), $Am(OH)^{2+}$ (gray line), and $Am(OH)_2^{+}$ (light gray line), calculated from formation constants of $\log {}^{*}\beta_{1,1}$ = -7.6, $\log {}^{*}\beta_{1,2}$ = -15.8, $\log {}^{*}\beta_{1,3}$ = -26.9 at I = 0.1 M $NaClO_4$ [5].

ratio, which can enable luminescence measurements of higher pH conditions with lower Am(III) concentrations. Spectral deconvolution results will be also discussed.

3.2 pH-dependent Luminescence Lifetimes

Lifetimes of the Am(III) luminescence were measured from linear regression of the luminescence decays in the natural log scale as a function of ICCD gate delay time. Under the acidic conditions (pH 1-2.6), where all the Am(III) present as Am^{3+}, the lifetime was measured to be 23.4 ± 0.4 ns, as previously reported [1]. As increasing the pH, lifetimes also gradually increased as shown in the Fig. 2. These results suggest that displacing water molecules by hydroxyl group also results in the increased luminescence lifetimes as other organic ligands [4]. Based on the results from spectral deconvolutions, speciation and their distributions will be presented.

4. Conclusions

We demonstrate here that luminescence of Am(III) can be useful in the study of Am speciation. pH-dependent luminescence spectral changes were observed along with increased lifetimes. Our results suggest that hydrolyzed Am(III) species have distinguished luminescence properties and can be resolved from the TRLFS studies. Luminescence measurements at different temperatures will be discussed in attempt to probe higher pH conditions, where more hydrolyzed Am(III) species are present. Temperature-dependent speciation distribution changes will be discussed in relation to the thermodynamic properties of the hydrolysis of Am(III).

REFERENCES

[1] J.V. Beitz, “f-state luminescence of trivalent lanthanide and actinide ions in solution." J. Alloys Compd. 207/208, pp. 41-50 (1994).

[2] S. Stadler and J.I. Kim, “Hydrolysis reactions of Am(III) and An(V)." Radiochim. Acta 44/45, pp. 39-44 (1988).

[3] M. Müller, M. Acker, S. Taut and G. Bernhard, “Complex formation of trivalent americium with salicylic acid at very low concentrations." J. Radioanal. Nucl. Chem. 286, pp. 175-180 (2010).

[4] A. Barkleit, G. Geipel, M. Acker, S. Taut and G. Bernhard, "First fluorescence spectroscopic investigation of Am(III) complexation with an organic carboxylic ligand, pyromellitic acid." Spectrochim. Acta A 78 (1), pp. 549-552 (2011).

[5] R. Guillaumont, T. Fanghänel, J. Fuger, I. Grenthe, V. Neck, D.A. Palmer, M.H. Rand. In: “(OECD, NEA-TDB): Chemical thermodynamics". "Update on the chemical thermodynamics of uranium, neptinum, plutonium, americium and technetium", vol 5. Elsevier, North-Holland, Amsterdam, (2003).

Coffinite in the KURT Environments and in Natural Analogue Sites

Tae-Jin Park*, Wan Hyoung Cho, and Jae-Kwang Lee

Korea Atomic Energy Research Institute, 111, Daedeok-daero 989beon-gil, Yuseong-gu, Daejeon, Republic of Korea

*etjpark@kaeri.re.kr

1. Introduction

Coffinite, $USiO_4$, is the second most abundant uranium(IV) mineral [1] and one of the major uranium(IV) sources in reduced uranium ore deposits. Thus, from the perspective of radioactive wastes disposal, coffinite is considered as an important secondary phases that could be formed during radioactive wastes leaching and/or after the long-term contact of groundwater to dissolve the UO_2 matrix. Under preferable geological conditions, coffinite is expected to precipitate and then to impact the uranium release based on the relative stability of coffinite and uraninite.

KAERI has been investigating the long-term behaviors of uranium under the Korean granite environments. Thus, the understanding and analysis of the coffinite existence under the KURT (KAERI Underground Research Tunnel) environments provides insights into the long-term uranium behaviors under the Korean granite environments. Here, we analyze and compare the coffinite in the KURT environments and the natural analogue sites. Based on the favorable environments and thermochemical perspectives, we conclude that the coffinite will be one of the major U(IV) mineral to control the U concentration with time after the disposal of radioactive wastes.

2. Coffinite

With its importance in geology and radioactive waste disposal among uranium minerals, coffinite belongs to the nesosilicate group with crystal structure of tetragonal ($I4_1/amd$) and is isostructural to orthosilicates zircon ($ZrSiO_4$) and thorite ($ThSiO_4$). We note that the area of the metamictization in $ZrSiO_4$ contains the activity of coffinite ($USiO_4$), thorite ($ThSiO_4$), and/or uranothorite ($(U,Th)SiO_4$, a solid-solution of coffinite and thorite).

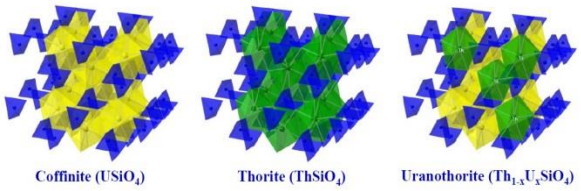


Fig. 1. The structure of (a) coffinite, (b) thorite and (c) uranothorite. Yellow, green, and blue polyhedra represent U, Th, and Si sites, respectively.

3. Occurrence of coffinite in KURT environments and natural analogue sites

We analyzed the KURT rock samples and observed an occurrence of uranothorite phase [2]. It is found that the uranium coexists mostly with thorium under the KURT environments. This accords with thermodynamics perspectives since the pure coffinite phase cannot be synthesized directly from uraninite and quartz whereas the thorite can from thorite and quartz. Also, the uranothorite are more abundantly found than the pure coffinite.

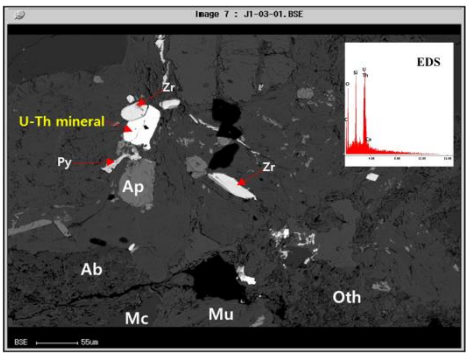


Fig. 2. Electronmicroprobe results obtained from a representative KURT rock sample. Inset shows spectrums from energy dispersive X-ray spectroscopy (EDS).

In several natural analogues study sites, such as Cigar Lake, Oklo, and Palmottu, the coffinitization of UO_2 were observed. The existence of the coffinite phase from the uranium mineralization at Cigar Lake

underwent quite a substantial characterization by the use of XRD, SEM, and XPS, followed by EMPA and BSE imaging. The samples from borehole 615, 620 both indicate the presence of coffinite in cavities of the hosting uraninite, which implies its secondary formation. The results from microprobe analysis of the samples from Oklo RZ 10 indicate significant alteration of uraninite through partial dissolution along grain coundaries, volume diffusion and finallyreplacement by coffinite. Results from Palmottu samples also indicate the coffinite was formed soon after uraninite precictation and it would have involved uranium remobilization because it is found in association with fracture infillings.

We analyzed and compared the groundwater characteristics associated with the rock/borehole samples (Table 1). We note that the major elements in groundwater that most likely impacted the occurrence of coffinite under given environments are Na, Ca, and Si, along with U and Th.

Table 1. Comparison between groundwater compositions of KURT and Cigar lake

	Cigar Lake [2]			KURT
	Clay zone	Basement	Ore zone	
Na mg/l	3.40 – 18.00	55.00 – 59.00	**19.20 – 31.20**	**17.01 – 23.42**
K	1.24 – 2.10	5.50 – 5.60	5.64 – 8.81	0.39 – 2.80
Ca	3.00 – 6.80	5.40 – 6.76	**10.90 – 14.80**	**11.98 – 16.36**
Mg	1.37 – 1.89	2.75 – 3.09	3.40 – 5.30	1.34 – 2.44
Fe	0.81 – 3.40	< 0.01 – 0.49	< 0.01 – 5.50	0.00 – 0.01
Si	6.32 – 9.80	4.29 – 4.30	4.30 – 6.10	8.46 – 9.80
U ug/l	1.05 – 54.74	5.44 – 12.39	**5.81 – 25.50**	**5.17 – 14.66**
Th	< 0.02 – 0.11	0.09 – 0.17	< 0.02 – 0.23	< 1

4. Conclusion

The existence of coffinite phase under the KURT environments and under the natural analogue sites (including Olko, Palmottu, Cigar lake, etc.) was compared and analyzed. The major elements in groundwater that likely impact the coffinite existence under the given environments include Na, Ca, Si, U and Th. We note that the coffinitization can be realized under the KURT environments when groundwater dissolve UO_2 and transport U(VI) ion to the more reducing environments with silica-rich conditions.

Acknowledgements

We acknowledge the Korean government, Ministry of Science, ICT and Future Planning (MSIP), for support (No. 2017M2A8A5014859).

REFERENCES

[1] Plant, J. A., Simpson, P. R., Smith, B., Windley, B. F., Rev. Mineral, 38, 255-319 (1999).

[2] Cho, W. H., Baik, M. H., Park, T.-J., in preparation.

[3] V P. Vilks, J. J. Cramer, D. B. Bachinski, D. C. Doern, and H. G. Miller, “Studies of colloids and suspendedd particles, Cigar Lake uranium deposit,” Saskatchewan, Canada. Appl. Geochem. 8, 605-616 (1993).

Basic Research to Reconstruct Paleo-geological Evolution Model Around KURT Area

Soolim Jung[1*], Chang-Whan Oh[2], K.S. Yengkhom[2], Yong-Kwon Koh[1], and Sung-Hoon Ji[1]

[1]Korea Atomic Energy Research Institute, 111, Daedeok-daero 989beon-gil, Yuseong-gu, Daejeon, Republic of Korea

[2]Chonbuk National University, 567 Baeje-daero, Deokjin-gu, Jeonju-si, Jeollabuk-do, Republic of Korea

[*]sljung@kaeri.re.kr

1. Introduction

Disposal facilities for radioactive waste shall be sited to provide isolation from the accessible biosphere. The features shall aim to provide this isolation for several tens to hundreds of years after closure. For the safety assessments of repository, the long-term natural evolution and possible events of the site, that can cause disturbances to the facility over the period of interest, should be considered. The objective of this research is to reconstruct the paleo-tectonic evolutions for pre-research of long-term safety and of developing the effective methodology of constructing a geological evolution model.

2. Literature investigation

2.1 Research area

The research is performed around the KURT (Korea Underground Research Turnnel), Daejeon, Korea. Regional scale of the target area is defined by [1]. For the study of geological evolution, regional and site scale area boundaries are used. The regional scale area is called “Yuseong area” and the site scale area is called “KURT site”. The regional boundary is modified from [1] along the hydrological drainage basin.

2.2 National investigation

To understand the regional scale geological evolution history, it is required to understand the geological history of the Korean peninsula. The geological map is the most basic information around the Yuseong area. The pre-studied information on the Yuseong area will give a direction to develop the evolution model.

2.3 International investigation

Japan Atomic Energy Agency (JAEA) has studied the reconstruction and estimation of long-term geological evolution around URL sites [2]. The Finnish organization for final disposal of nuclear waste (POSIVA) and other European countries already have their own technology to construct a structural model for the target area. The preliminary survey of examples and methods of preceding international research will contribute to developing specific evolution model for the Korean environment.

3. Field works and sample preparations

3.1 Field works

To reconstruct the geological evolution history, it is necessary to have field works on the study area. Lithological boundaries marked in the geological map of Yuseong area were investigated to increase the accuracy of the evolution history and to construct fracture networks of the area. Host rock (granite) and dyke rock samples were gathered for age dating.

3.2 Deep borehole- core sampling

The borehole geophysical surveys have been performed for several drillholes adjacent to the KURT to collect geological information of the deep underground. Drilling core samples were taken from

host rock interval, dykes and fracture zones at 300-1000m depth.

4. Sample analysis

4.1 Structural analysis

Brittle and ductile deformation histories will be evaluated using structural analysis data from the field works, geophysical surveys and drilling core investigations. The quantitative analysis of structural characteristics around KURT area will contribute to evaluating hydrogeological processes.

4.2 Age-dating

K-Ar and Zircon age dating will be carried out to decide the age of rocks and fractures consisting of the Yuseong area. Through the SHRIMP zircon age dating, the intruded ages of granite body will be confirmed. The K-Ar age dating will indicate the estimated uplift ages and the intruded ages of dykes.

5. Conclusion

The study on long-term history of geological evolution will be applied to understand hydro-geological and geochemical characteristics, and to predict future processes of geological evolution. The reconstruction of the paleo-geological evolution model is fundamental to estimate long-term history. To construct the paleo-tectonics in next step, it is necessary to do more field works and age dating for confirming and improving the history and for understanding more detail on the relationships between the history and fracture system in the study area.

REFERENCES

[1] Park, K.W.; Kim, K.S.; Koh, Y.K.; Kim, G.Y. (2009) “Site characterizations around KURT area-Geologic model (version 1)”, KAERI/TR-3870/2009.

[2] Kosaka, H; Saegusa, H; Yasue, K; Kusano, Y; Onoe, H. (2011) “Development of a Methodology for the Characterisztion of the Long-term Geosphere Evolution (2) Estimation of the long-term evolution of goundwater flow conditions in a Tono area case study”, Proceeding of ICONE19, ICONE19-43567, 2011, Japan.

Numerical Analysis of Thermo-Hydro-Mechanical Coupled Behavior in Korean Reference HLW Disposal System (KRS)

Changsoo Lee*, Won-Jin Cho, Jaewon Lee, and Geon-Young Kim

Korea Atomic Energy Research Institute, 111, Daedeok-daero 989beon-gil, Yuseong-gu, Daejeon, Republic of Korea

*leecs@kaeri.re.kr

1. Introduction

Decay heat can influence temperature distribution at Engineered Barrier System (EBS) and at Natural Barrier System (NBS) in Korean Reference HLW disposal System (KRS). Water inflow from the rockmass can influence thermal conductivity of buffer materials. It can affect the thermal behavior. And thermal stress due to decay heat and swelling pressure due to the water inflow can change the stress condition at the disposal system and at the rock mass near the system. Therefore, the understanding of the THM coupled behavior is essential for the site selection, design, as well as the operation of the repository. In this study, numerical modeling was performed to enhance the understanding of THM coupled processes in the KRS.

2. Numerical model

2.1 Numerical code

TOUGH2-MP [1] was used to perform TH analysis using 60 processors in Linux system and FLAC3D [2] was used to conduct M analysis using 8 processors in Window system. Data can be exchanged through an internet hub.

2.2 Initial and boundary conditions

Fig. 1 presents the initial and boundary conditions for a coupled THM simulation. The initial conditions are defined at the pre-excavation stage. The vertical gradients of temperature, fluid pressure, and in-situ stress applied as shown in Fig. 1. In the numerical model, tunnel spacing and disposal holes interval was set to be 40 m and 8 m, respectively.

2.3 Input parameters

Decay heat was applied as a function (Eq. 1) and 30 years cooling time was assumed in the model. Van Genuchten model was used to consider capillary pressure. Power law was applied for relative permeability function. Mohr-coulomb model was used for mechanical analysis of buffer, backfill and host rock. Physical, thermal, hydraulic, and mechanical properties are listed in Table 1.

$$\text{power} = 1.844 \times 1.455 \times 10^4 \times (t + 30)^{-0.758} \quad (1)$$

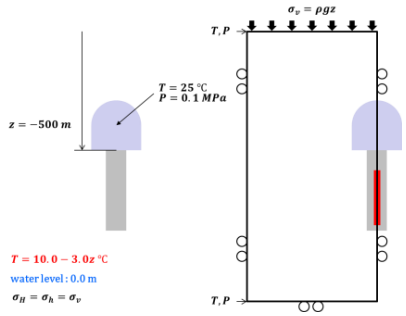


Fig. 1. Initial and boundary conditions in the model.

Table 1. Input parameters in the model

Parameters	Buffer	Back fill	Rock	Waste
Dry density (kg/m^3)	1,600	1,600	2,650	6,577
Porosity (-)	0.41	0.40	0.01	0.001
Thermal conductivity (W/mK)	0.72 – 1.20	1.09 – 2.149	2.853 - 3.165	49.02
Specific heat of solid (J/kg/K)	966.0	981.0	820.0	1000.0
Linear expansion coefficient (1/K)	2.5 E-5	2.5E-5	7.5 E-6	1.7 E-5
Intrinsic Permeability (m^2)	1.5E-20	1.6E-19	1.0E-18	0.0
λ	0.2941	0.5	0.6	-
$1/P_0$	2.6E-7	3.3E-7	5.0E-7	-
Klinkenberg parameter	1.0E09	1.0E08	6.86E5	-
Young's modulus (GPa)	0.59	0.59	33.34	155.0
n for relative permeability function (S^n)	1.9	1.9	3.0	-
Poisson's ratio(-)	0.20	0.20	0.3	0.285
Maximum swelling stress (MPa)	5.0	3.0	-	-
Friction angle (°)	37.0	37.0	46.66	-
Cohesion (MPa)	1.0	1.0	10.4	-
Tensile strength (MPa)	3.0	3.0	3.75	-
Dilation angle (°)	10.0	10.0	10.0	-

2.4 Modeling procedures

The excavation sequence was simulated for 10 years, with the elements in the tunnel removed and with fixed fluid pressure (0.1MPa) and relative humidity (100%). After 10 years, the waste canister, bentonite buffer, and backfill are installed instantaneously and the post closure simulation can start. The post closure simulation was performed for 1,000 years. The monitoring points are shown in Fig. 2.

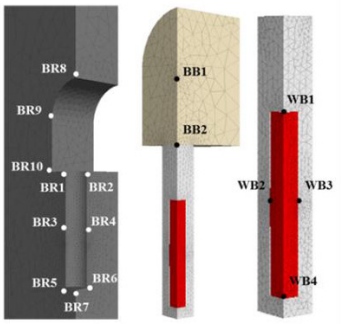


Fig. 2. Monitoring points of time dependent results.

3. Results

3.1 Thermo-hydraulic analysis

Fig. 3 presents temperature, fluid pressure, and degree of saturation evolutions with decay heat in the simulated waste canister. Maximum temperature is calculated below 100℃. Fluid pressure is slowly increased until several years, after then, the pressure is rapidly increased and becomes hydrostatic pressure after decades. The liquid saturation in the buffer decreases to a minimum of about 0.3 after a few years, after then saturation starts to increase and finally reaches 1.0 over 200 years.

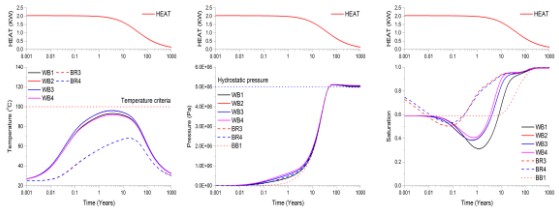


Fig. 3. Evolution of temperature, fluid pressure and saturation in KRS.

3.2 Mechanical analysis

In this study, the linear elastic (LE) swelling model was used and the model input parameters was be determined analytically to achieve a desired maximum swelling stress which is listed in Table 1. And Mohr-Coulomb criterion [3] is used to investigate the potential for rock failure. Fig. 4 presents the path of minimum and maximum principal effective stresses in relation to the Mohr-Coulomb failure envelopes. The stress state of rockmass stays below that required for failure.

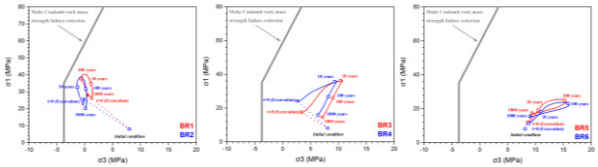


Fig. 4. Principal stress path in relation to Mohr-Coulomb failure criterion for rock mass.

4. Conclusions

Numerical modeling was performed to investigate influence of THM processes on KRS involving the interaction of multi-components including buffer materials, canister, and rockmass over 1000 years. The maximum temperature at the interface between canister and buffer can satisfy temperature criteria of 100℃. The stress state of rockmass stays below the failure criterion, but it is necessary to check that the stress state is below the spalling criterion based on the compressive strength.

Acknowledgements

This research was supported by the Nuclear Research and Development Program of National Research Foundation of Korea (NRF) funded by the Minister of Science, ICT and Future Planning.

REFERENCES

[1] Zhang, K.; Wu, Y. -S.; Pruess, K. (2008) User's Guide for TOUGH2-MP: A Massively Parallel Version of the TOUGH2 code. Report LBNL-315E. Lawrence Berkeley National Laboratory, Berkeley, California.

[2] Itasca. (2012) FLAC3D V5.0, Fast Lagrangian Analysis of Continua in 3Dimensions, User's Guide, Itasca Consulting Group, Minneapolis, Minnesota.

[3] Jaeger, J. C.; Cook, N. G. W.; (1979) Fundamentals of Rock Mechanics. Chapman and Hall, London.

4분과

방사성폐기물관리 (Oral)

Site Selection Process in Germany for Radioactive Waste Disposal

Jeoung Seok Yoon*, Arno Zang, Ove Stephansson, and Fabrice Cotton
Helmholtz Centre German Research Centre for Geosciences, Potsdam, Germany
*jsyoon@gfz-potsdam.de

1. Introduction

This paper summarizes the key issues evolved over the past several years in Germany in the field of radioactive waste management and disposal. As Korea will face problems and challenges in managing high-level radioactive wastes and especially in selecting a site for a final repository, the intention of this paper is to provide those Korean implementers and the regulatory authorities in this field with the know-hows and lessons learned in Germany.

2. The Fukushima Disaster and Reaction of Germany: Immediate Policy Reversal

On March 11, 2011, the Daiichi-Fukushima nuclear disaster broke out, after which 50k households had to be displaced after radiation contaminated air, soil and sea. After Fukushima disaster, a nationwide opinion poll in Germany showed that 80% of Germans opposed the government policies to extend nuclear power. In the end, on May 30, 2011, the Chancellor Angela Merkel completed the full reversal of her nuclear policy, announcing that all of Germany 17 NPPs (Nuclear Power Plants) are to be shut down by 2022.

3. The Repository Site Selection Act and Procedure for Site Selection

With the decision of shutting down all NPPs by 2022, an initiative was raised to discuss when and how to start looking for a site for a radioactive waste repository. For the search for an appropriate repository site in Germany, the Repository Site Selection Act (Standortauswahlgesetz – StandAG, in German) became effective on 27 July 2013. The Act provides a national, science-based and comparative site selection procedure for the best possible repository.

According to the Act, host rocks suitable for the disposal of high-level radioactive waste (HLRW) in deep geological formations may basically be granite, salt and clay.

The site selection process took the following steps. First, a 32-member Commission was formed (the Commission of Storage of High-Level Radioactive Waste Materials) by the Parliament in May 2014. The task of the Commission was to develop, for two years, the criteria, processes and decision bases to evaluate the Act to make proposals for public participation and transparency. The Commission published a report on July 2016. Among five major proposals by the Commission, the one for organizational requirements draws an attention. This is described in Section 4. Second, the Act is evaluated based on the report of the Commission, which is followed by (1) identification of eligible site regions, (2) development of site-related exploration programmes and examination criteria, (3) in-depth geological exploration, (4) concluding site comparison and site proposal, (5) site decision and conclusion of the site selection procedure by 2031, and (6) licensing for the construction, operation and decommissioning of the repository.

4. Key Players and Tasks

With the Act on the Organisational Restructuring in the Field of Radioactive Waste Management, the federal government has reorganized responsibilities in the field of radioactive waste disposal to ensure a clear allocation of responsibilities and tasks in the field of radiation protection and radioactive waste disposal. These organizations are *BfS*, *BfE* and *BGE mbH*.

The *BfS (The Federal Office for Radiation Protection)* is an organizationally independent, scientific-technical, higher federal authority responsible for radiation protection, nuclear safety, transport and storage of nuclear fuels, and radioactive

waste disposal. With the Act became effective in July 2016, the federal tasks of supervision and licensing in the field of nuclear energy, interim storage, repository site selection and repository surveillance are transferred to a new federal authority called *BfE*.

4.1 The Federal Office for the Safety of Nuclear Waste Management (BfE)

On the basis of the Act, *BfE* takes over the task of the central supervisory, licensing and regulatory authority in the field of radioactive waste management. It is responsible for the repository site selection procedure. This is a licensing and regulating authority under nuclear and mining law and responsible for public participation and also supervisory authority under nuclear law for radioactive waste repositories. The execution of the associated tasks that had so far been distributed to different federal and state authorities was difficult for the citizens to follow. At times, for example, the false impression was given that the *BfS* was acting at the same time as operator and regulator in the same area.

4.2 The Federal Company for Radioactive Waste Disposal (BGE mbH)

This newly formed *BGE mbH* performs the planning, construction, operation and decommissioning of repositories. As the so-called project developer pursuant to the Repository Site Selection Act, the federally owned company is also tasked with the search for a repository for high-level waste materials in Germany. It is currently in its formulation stages. After it has been ensured that the company is able to act, the corresponding tasks will be transferred from the *BfS* to the *BGE mbH*.

5. Public participation

The Act demands active public relations work by both the *BfS* and *BfE*, for example, in all stages of the site selection procedure. In the Act, it has been regulated which milestones the public shall participate in and the minimum forms of participation to be applied. It is planned to perform public participation in a dialogue-oriented process including dialogue between citizens, public meetings and information provided via the Internet, citizens' offices and by other suitable media. The followings are the cases where the public shall be given the opportunity to make comments:

(1) on proposals by the Commission for the bases for decision-making and on all other tasks,
(2) on proposals for eligible site regions and the selection of sites to be explored from the surface,
(3) on proposals for the site-specific exploration programmes and examination criteria,
(4) on the report of the results from the exploration from the surface and their evaluation,
(5) on the proposal for the sites to be explored underground,
(6) on the proposals for the in-depth geological exploration programmes and examination criteria,
(7) on the findings and evaluations of the underground exploration, and
(8) on the proposal of the site for the future repository.

6. Closing

In review of the German system of site selection procedure for a final repository for radioactive wastes, we found three major issues that drew our attention. Firstly, the 32 members of the Commission formed by the Parliament represent diverse groups in the society which are State Governments, Parliamentary Groups of Federal Parliament, Sciences, Environmental Groups, Churches, Industry and Trade Unions. Such diverse fields of background of the Commission members could provide unbiased view of the site selection criteria. It is also worth noting that detailed protocols of all the meetings of the Commission have been archived in the website (www.bundestag.de/endlager/) and were made accessible easily to the public. Secondly, through the Act and by the proposal of the Commission, the responsibilities of the relevant organizations (*BfE*, *BfS*, *BGE mbH*) were clearly defined and a clear cut was made between the operators and the regulatory authorities. Thirdly, we have found that public participations are planned in all stages of the site selection procedure. Such measure may in some cases significantly delay the programmes. However, at the same time such measures mentioned above significantly improve transparency and help gain people's trust.

Glass-Ceramic Waste Forms for Immobilization of Cs Trapping Filters

Jae Hwan Yang*, Ahreum Han, Joo Young Yoon, Hwan-Seo Park, and Yung-Zun Cho
Korea Atomic Energy Research Institute, 111, Daedeok-daero 989beon-gil, Yuseong-gu, Daejeon, Republic of Korea
*yjh98@kaeri.re.kr

1. Introduction

Cesium gas is evolved from spent nuclear fuel during the head-end process of Pyroprocess. Capture of Cs has been performed with aluminosilicate-based ceramic filters at high temperatures [1]. This study presents a simple and novel scheme to immobilize the Cs trapping filters in glass-ceramic waste forms.

2. Materials and methods

2.1 Cs trapping experiment using the SA filter

The silica-alumina (SA) filter composed with aluminosilicates was prepared with kaolinite powder. The synthesis of SA filter was described elsewhere [2]. Typically, a polyvinyl alcohol (PVA) solution and the kaolinite powder were mixed to make a slurry. Then, a polyurethane (PU) sponge was coated with the slurry. The slurry-filled sponge was sufficiently dried and the coating process was repeated several times. The sponge was thermally elevated at 1200°C to remove the PVA and the PU sponge.

Cesium hydroxide ($CsOH{\cdot}H_2O$) placed in a boat crucible and the SA filters were loaded in an alumina tube. The filters were thermally treated at 800°C and then cesium hydroxide was volatilized at 900°C in flowing 4%H_2/Ar gas.

2.2 Synthesis and characterization of waste forms

A glass frit was prepared and the compositions were presented in Table 1. The glass frit and the Cs-trapping filter (Cs-SA filter) were mixed and heat-treated at 1000°C in the air. Characterization of the specimens was performed by X-ray diffraction (XRD) and scanning electron microscope (SEM) equipped with energy dispersive spectra (EDS). Leaching of the specimens was examined by MCC-1 test at 90 °C.

Table 1. Compositions of the glass frit prepared in this research

Oxide	Reagent	Mass fraction (wt%)
SiO_2	SiO_2	47.4
B_2O_3	B_2O_3	30.1
Na_2O	Na_2CO_3	22.5

3. Results & discussion

Fig. 1 shows the XRD patterns of the Cs-SA filters after heat-treatment with different temperatures for 3 h. It is seen that the structure of $CsAlSiO_4$ in the Cs-SA filter is present during the heat treatment at 800°C. $CsAlSiO_4$ peaks are decreased and pollucite peaks are developed from 900°C. In particular, $CsAlSiO_4$ peaks are significantly lowered and the intensity of pollucite peaks becomes very prominent at 1200°C. It suggests that the formation of pollucite is possible by the simple heat process of the Cs-SA filter.

The XRD patterns of the waste forms are presented in Fig. 2. Peaks were not found at 10−20 wt% of waste fraction, suggesting that a glassy phase was formed during the thermal elevation. However, peaks appear at 30−50wt% of waste fraction, which were all identified as pollucite. In addition, the intensity of pollucite peaks became higher as waste fraction grows, suggesting that the growth of waste fraction led to the increase of the crystallinity of pollucite.

Fig. 3 shows morphology of the waste form surfaces investigated by SEM. It is seen that there are many round particles with diameters of 100–600 nm (Fig. 3(a)). The irregular and agglomerated particles were also observed (Fig. 3(b)). EDS analysis reveals

that the particles are pollucite.

Leaching rates of the specimens were presented with respect to major elements at 3, 7, 14, and 28 d of duration (Fig. 4). The leaching rates of most elements are gradually declined with the increase in the leaching period. In addition, the increase in the waste fraction generally lowers the leaching rates of all elements. In particular, the Cs leaching rate at 3 d was 8.3×10^{-3} g·m^{-2}/d for the 10wt%-waste specimen (Fig. 4(a)), which was two orders of magnitude higher than that for the 50wt%-waste specimen (7.21×10^{-5} g·m^{-2}/d). This result originated from the difference of main Cs-incorporated phases in the waste forms. Most Cs was contained in an amorphous Cs-aluminosilicate phase at low waste fraction; however, the major Cs phase became pollucite at higher waste fractions.

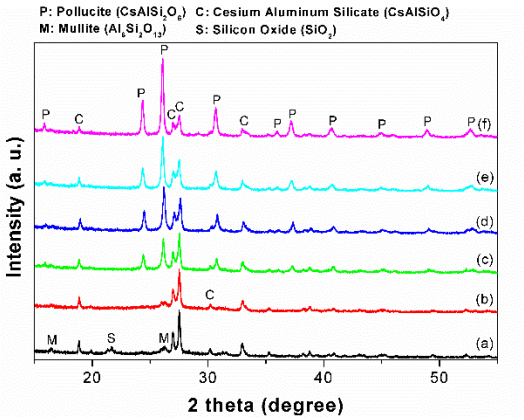


Fig. 1. XRD patterns of the Cs-SA filters after heat treatment for 3 h at different temperatures: (a) no heat treatment, (b) 800°C, (c) 900°C, (d) 1000°C, (e) 1100°C, and (f) 1200°C.

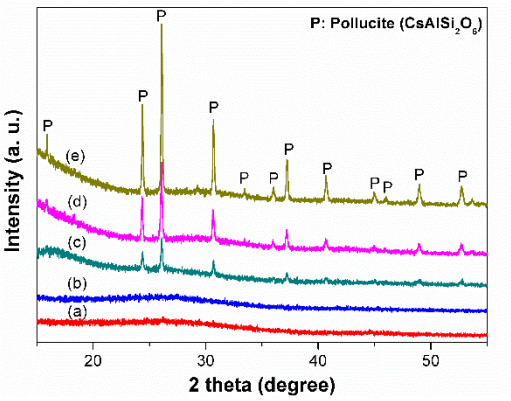


Fig. 2. XRD patterns of the monolithic waste forms at different waste fractions: (a) 10wt%, (b) 20wt%, (c) 30wt%, (d) 40wt%, and (e) 50wt%.

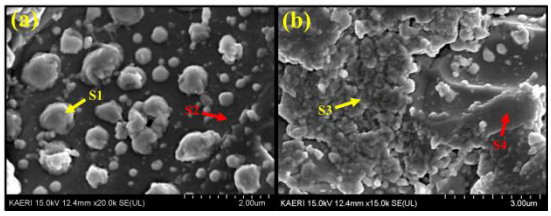


Fig. 3. SEM images of the specimen at 40wt% of waste fraction with different magnifications ((a) 20,000 times and (b) 15,000 times).

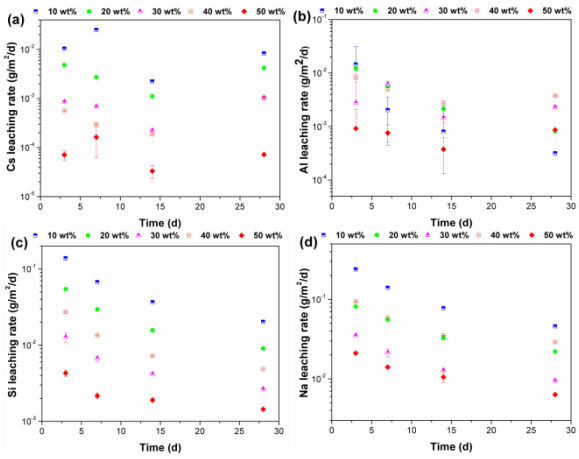


Fig. 4. Normalized leaching rates of (a) Cs, (b) Al, (c) Si, and (d) Na for different specimens obtained from an MCC-1 leaching test performed for 28 d.

4. CONCLUSIONS

The Cs-SA filter was transformed to monolithic waste forms for the final storage of Cs. A glass frit was synthesized and mixed with the Cs-SA filter, which was heat-treated at 1000°C for 3 h to for the synthesis of waste forms. Characterization revealed that pollucite was the major Cs phase when the waste loading was not less than 30wt%.

REFERENCES

[1] Lee, H.S.; Park, G.I.; Kang, K.-H.; Hur, J-M.; Kim, J.-G.; Ahn, D.-H.; Cho, Y.-Z.; Kim, E.H. (2011) Pyroprocessing technology development at KAERI. Nucl. Eng. Technol., 43 (4): 317.

[2] Yang, J.H.; Yoon, J.Y.; Lee, J.H.; Cho, Y.-Z. (2017) A kaolinite-based filter to capture gaseous cesium compounds in off-gas released during the pyroprocessing head-end process. Ann. Nucl. Energy, 103:29.

Hydrogeochemical Changes in the Groundwater System at the Gyeongju LILW Disposal Site After Construction

Nam C. Woo[1*], Eunhye Kwon[1], Jae-Min Lee[1], Youn-Tae Kim[1], Sang Min Ryu[2], and Soon-Il Ok[3]

[1]Dept. Earth System Sciences, Yonsei University

[2]Hyundai Engineering Co., Ltd.,

[3]Korea Radioactive Waste Agency

[*]ncwoo@yonsei.ac.kr

1. Introduction

This study is objected to understand the hydrogeochemical change and its long-term perspective in the groundwater system at the Gyeongju LILW disposal site during the site operation period.

2. Methods

2.1 Monitoring Site

This study uses the long-term monitoring data obtained from the LILW site monitoring program by KORAD. Groundwater and sea-waer monitoring data were analyzed [1].

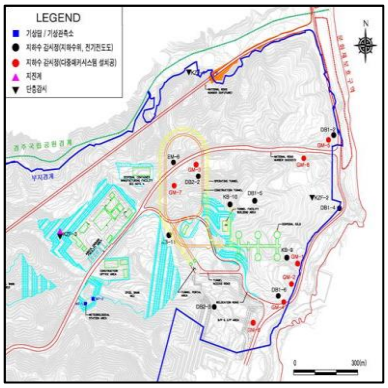


Fig. 1. Location of groundwater monitoring wells.

2.2 Data analysis

The obtained monitoring data were analyzed using various techniques including plotting for hydrochemistry, statistical analysis, and time-series analysis.

3. Results & Discussion

3.1 Hydrogeochemical characteristics

Hydrogeochemical type of the groundwater samples are presented in Fig. 2. They show significant variation in location of monitoring wells and depths of monitored interval.

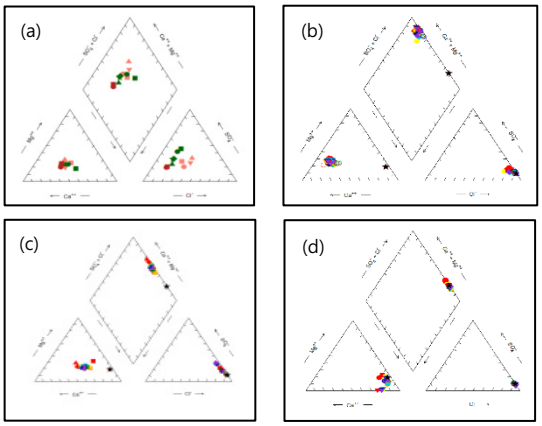


Fig. 2. Hydrogeochemical types of groundwater plotted in the Piper diagram: (a) background waters, (b) Type I, (c) Type II, (d) Type III.

3.2 Time-series of EC

Observed electrical conductivities of groundwater samples, implying the dissolved content of the samples, show three types of time-series changes.

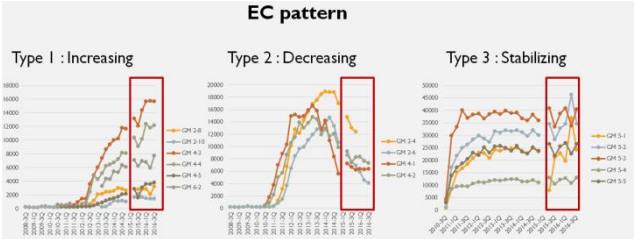
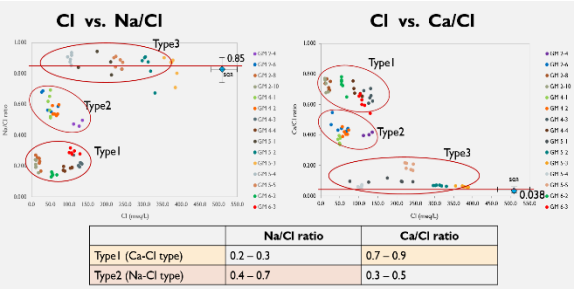


Fig. 3. Time-series data of groundwater EC's.

Type I shows the changes in the groundwater system started relatively later and the change is still on-going process. Type II indicated the change has past the highest point and now is moving backward to the original state. Type III represents the new equilibrium states after some changes, however, the variation is not settled yet.

3.3 Hydrogeochemical reactions

Groundwater of different types indicate that they are experiencing different hydrochemical reactions [2].



	Na/Cl ratio	Ca/Cl ratio
Type1 (Ca-Cl type)	0.2 – 0.3	0.7 – 0.9
Type2 (Na-Cl type)	0.4 – 0.7	0.3 – 0.5

Fig. 4. Hydrochemical reactions related to different types of groundwater.

Hydrogeochemical reactions in the coastal groundwater system is related to the degree of influence by the sea-water intrusion (Fig. 4). Most significant reaction can be explained using the ion-exchange process (Fig. 5).

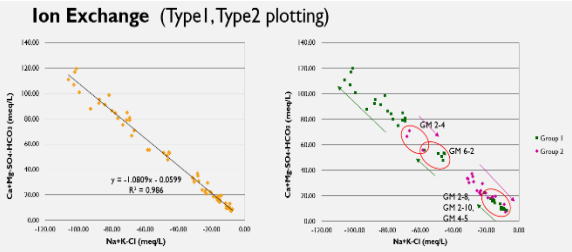


Fig. 5. Ion-exchange process of Type I and II groundwater samples.

4. Conclusion

In this study, we tried to understand the time-series change in hydrogeochemistry of the groundwater system at the LILW disposal site since 2015, when the site operation began.

Water-rock interaction of fresh groundwater with the intruded saline-water is clearly observed in the chemistry change of groundwater monitoring data.

Partly, groundwater system is still changing, and some parts show returning to the original state, and even approaching new equilibriums. These changes in time warrant the long-term monitoring of the site, and the interpretation and evaluation of the site safety and integrity based on those changes will provide significant scientific information that can improve the public acceptance of the LILW site operation.

REFERENCES

[1] KORAD, Monitoring and Surveillance of Radioactive Waste Disposal Facility during pre-operation (2015).

[2] Anders, R., Mendez, G.O., Futa, K. and Danskin, W.R., “A geochemical approach to determine sources and movement of saline groundwater in a coastal aquifer”, Groundwater, 52 (5), 756-768 (2014).

Management Plan for the Intermediate Level Liquid Waste From the Fission ^{99}Mo Production Process in the KIJANG Research Reactor

Chul Gyo Seo*, Seung-Kon Lee, and Jong-Sik Shon

Korea Atomic Energy Research Institute, 111, Daedeok-daero 989beon-gil, Yuseong-gu, Daejeon, Republic of Korea

*cgseo@kaeri.re.kr

1. Introduction

Korea Atomic Energy Research Institute (KAERI) has been developing a new research reactor, which is named the KIJANG Research Reactor (KJRR). The KJRR is a radioisotope production reactor and one of its main purposes is producing fission ^{99}Mo, which is the most widely used medical radioisotope [1]. The waste generation from the fission ^{99}Mo production process is inevitable and disposal plan for the radioactive wastes should be set up for mass production of the fission ^{99}Mo.

2. Waste generation

2.1 Target

The most fission ^{99}Mo has been produced from highly enriched uranium (HEU) targets. However, to reduce the use of HEU for nonproliferation, ^{99}Mo producers are forced to convert their HEU-based process to use low enriched uranium (LEU) targets. KAERI will use the plate-type LEU target composed of UAl_x powder dispersed in Al matrix and Al-6061 cladding. The powder is produced by the KAERI's centrifugal atomization technology. 8 plates are combined into a target assembly, which is irradiated about 7 days in the core. There are 6 fission moly irradiation holes in the reactor core [2].

2.2 Waste

The irradiated target assembly is cooled during 1 day and transported into the dissolving hotcell. In the hotcell, the target assembly is dissolved in sodium hydroxide solution in the dissolver. The overall process scheme of the KAERI process is similar to the conventional alkaline digestion process, which has been used for the HEU-aluminum alloy targets. Using the LEU targets, radioactive wastes increase by decreased production yield. The use of LEU targets will cause increase of radioactive waste production about 200% [3]. In particular, reduction of the intermediate level liquid waste (ILLW), directly resulting from the dissolution of target, is very important because of their high activity and the difficulties in the waste treatment for final disposal. KAERI developed new technology to facilitate the waste treatment by converting sludge-type waste, which is difficult to handle, into independent solid and liquid wastes [4]. The scheme for the KAERI process is presented in Fig. 1 [5]. During the dissolution, unreacted uranium and majority of other fission products form precipitates, and are removed from the solution via filtration. Emission of radioactive noble gas such as Xenon is controlled via the gaseous waste treatment system with multiple steps of mitigation and confinement. The uranium precipitates will be stored during the lifetime of the KJRR. Aluminum precipitates in low level activity can be managed as solid wastes, but it is difficult to convert the ILLW into the proper form for final disposal.

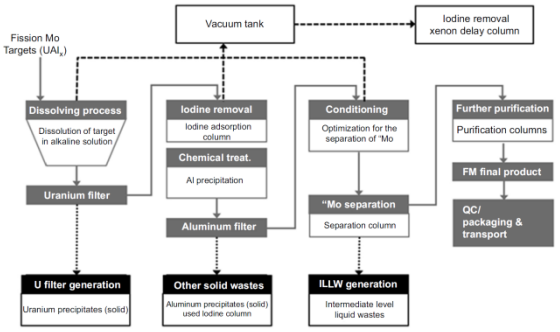


Fig. 1. Process scheme of KAERI fission ^{99}Mo production.

3. Waste management

3.1 Management plan

The ILLW will be solidified and transported to the Gyeongju low and intermediate level radioactive waste disposal facility for final disposal. The ILLW is

generated the FMPF (Fission Moly Production Facticity) and treated in the RWTF (Radioactive Waste Treatment Facility). The ILLW generated in the hotcell requires a decay time of 2 years for easy handling. The operation strategy is to store the ILLW at the FMPF for at least 4 years and to transport it to the RWTF for solidification treatment and temporary storage.

3.2 Solidification treatment

KAERI does not have any experience on solidification process of the ILLW, but there are several countries producing ^{99}Mo. We have considered the treatment processes of other countries with the following basic principles:

1) The process should be specific to the waste characteristics.
2) The process should be authorized.
3) The process should be simple.
4) The process should be controllable in remote.
5) The process should not produce any secondary waste.
6) The solidified waste should fulfill the acceptance criteria of the Gyeongju facility.

KAERI has selected the conventional cementation method for solidification treatment as the first priority option. The cementation method is authorized in Belgium and South Africa, but the characteristics of the ILLW might be different. The cementation method optimized to the KAERI ^{99}Mo production process should be developed. The development schedule is depicted in Fig. 2. The cementation method is selected as the first option, but new technologies such as Synroc [6] will be considered if the technology is authorized.

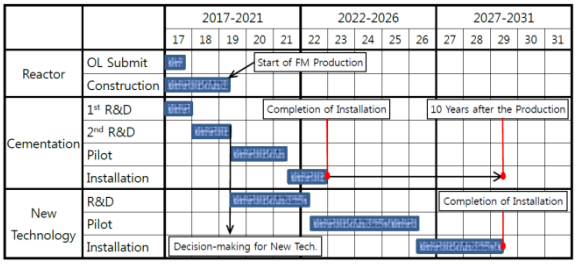


Fig. 2. Schedule for the solidification process.

4. Conclusions

KAERI has developed the ^{99}Mo production process and the production of ^{99}Mo will be followed soon after the criticality of the KJRR. The ILLW in the production process has been a critical issue, but the treatment process of the ILLW is not developed yet.

This paper introduces the treatment plan of the ILLW. KAERI has selected the conventional cementation method and development study was started last year. The development plan shows that the treatment facility could be operable within 4~10 years after start of the production. KAERI has prepared enough storage of 20 years in the KJRR.

REFERENCES

[1] W.C. Eckelmann, "Unparalleled contribution of technetium-99m to medicine over 5 decades," JACC Cardiovasc Imaging 2(2009) 364-368.
[2] Chul Gyo Seo, et al., "Silicide Fueled Core for the KIJANG Research Reactor," *KNS Autumn Meeting*, Gyeongju, Korea, 2013.
[3] International Atomic Energy Agency (IAEA), "Non-HEU production technologies for molybdenum-99 and technetium-99m," IAEA Nuclear Energy Series, No. NF-T-5.4, IAEA, Vienna (Austria), 2013.
[4] Seung-Kon Lee, et al., "Development of Fission Mo-99 Process for LEU Dispersion Target," *KNS Spring Meeting*, Jeju, Korea, 2015.
[5] Seung-Kon Lee, et al., "Development of Commercial-scale Fission Mo-99 Production System," *KNS Fall Meeting*, Gyeongju, Korea, 2016.
[6] R. B. Rozsa and C. L. Hoenig, "Synroc Processing options," LLNL UCRL-53187, 1981.

Numerical Simulation on the Diffusion and Sorption of Radionuclides Along the Heterogeneous Microstructures in Rock Matrix

Dongkyu Park* and Sung-Hoon Ji

Korea Atomic Energy Research Institute, 111, Daedeok-daero 989beon-gil, Yuseong-gu, Daejeon, Republic of Korea

*dkpark@kaeri.re.kr

1. Introduction

The SKB Task Force is a forum for the international organizations supporting the Äspö Hard Rock Laboratory (HRL), Sweden, to interact in the area of conceptual and numerical modelling of groundwater flow and solute transport in fractured rock. The 9th task of this forum was intended to increase realism in solute transport modelling on the in-situ experiments performed at the Äspö HRL (LTDE-SD) and the ONKALO underground rock characterization facility in Finland (REPRO). For the 2nd step of this task (Task 9B), particularly, the inverse modelling have been carried out to characterize the matrix diffusion and sorption of radionuclides in the crystalline rock based on the LTDE-SD experimental results.

2. LTDE-SD and Task 9B

2.1 Summary of the LTDE-SD test

Understanding of matrix diffusion and sorption of radionuclides in the crystalline rock is important in safety assessments for geological disposal of radioactive waste [1]. For this, the LTDE-SD test was performed in a borehole installed at the Äspö HRL during 198 days. The experimental section is surrounded by Ävrö granodiorite and includes a natural fracture at the end of the borehole. Within the section, both of the fracture surface and the wall of slimhole, drilled in the inner rock, were exposed to the cocktail mixed with 22 radioactive tracers (Fig. 1). After the termination, the rock surrounding the borehole was overcored and then small core samples were drilled axially (A-core) from the fracture surface section and radially (D-core) from the slimhole section (Fig. 1). The surfaces of A-cores have fracture coating and alteration while the surfaces of D-cores might include damaged zone created from the drilling process of slimhole.

One of the main results from the LTDE-SD test must be the penetration profile of ^{137}Cs having two slopes. In the profile, particularly, the flat slope of tailing part might imply the tracers reaching much longer into the rock matrix than that expected from a homogeneous diffusion/sorption model [2]. The primary objective of Task 9B was to interpret and understand this anomalous result of LTDE-SD test through more realistic modelling work.

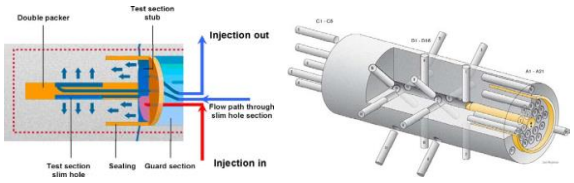


Fig. 1. The schematic diagrams of LTDE-SD experimental section (left) and overcored rock (right) [2].

2.2 Modelling approach in this study

In microscopic scale, open and sealed micropores along mineral grain boundaries or inside mineral grains are observed in rock. Particularly, well-connected micropores could act as a potential path of radionuclide migration in the rock matrix [2, 3, 4]. Cs, which had been detected throughout all the core samples in this experiment, has been known to sorb selectively onto dark and mafic or altered minerals, i.e. biotite and chlorite [2, 4]. This study focused on possible effects of the microstructures such as micropores and mineral grains on the LTDE-SD results. Assuming a core sample, a 2-D model domain (24 mm × 93 mm) was formulated (Fig. 2). Due to lack of real data on the microstructures, their geometry was obtained from the polarizing micrograph on a thin section of gneiss sampled in the KAERI underground research tunnel. In order to avoid computational burden from simulating intergranular pore boundary with several μm of aperture, we incorporated the 1-D solute transport

along them within the 2-D model domain. Inverse modeling in this work was carried out to find the five parameters of microstructures fitted to the LTDE-SD results: diffusion (D_e) and distribution coefficients (K_d) of the dark minerals located at fracture surface and rock matrix, respectively, and D_e of intergranular pore boundary.

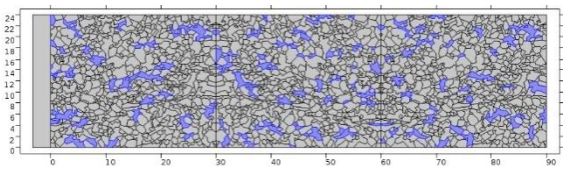


Fig. 2. 2-D Model domain with dark minerals (blue).

3. Results and Discussion

As shown in Fig. 3, both of the curves fitted with considering microstructures seems to be in accordance with the LTDE-SD results. The estimated parameters could be explained by the difference of Cs sorption on altered or unaltered minerals and the relatively fast diffusion along open mineral grain boundary. The fluctuation of penetration profile were highly relevant to the geometry of microstructures such as distribution and content of dark minerals and the connectivity of micropores. From this result, it is inferred that the high activity of steep slope in penetration profile of Cs resulted from its strong sorption onto the dark minerals located at the core surface directly exposed to the tracer cocktail. Also, due to the fast diffusion along the well-connected micropores, the tracer could reach the dark minerals located at the inner part of core sample and it might finally lead to the long tailing in the penetration profile.

4. Conclusion

This study provided a possibility that the microstructures in rocks leaded to the anomalous behavior of a tracer shown in the LTDE-SD results. One of the most influential factors on the simulation results must be the heterogeneity in geometry of microstructures. Particularly, it was observed on this work that the shapes of resulting curves were totally dependent on their geometry considered. This fact again highlighted that the microstructures could be critical to the fate of radionuclides in the rock matrix, as well as the LTDE-SD results. From this conclusion, additional modelling work on the effects of distribution and contents of mineral grains and connectivity of micropore networks is in progress.

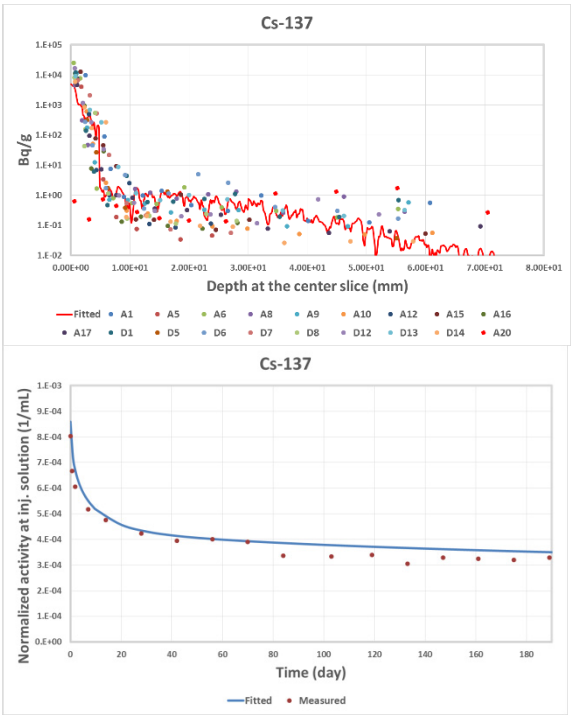


Fig. 3. Fitted results for penetration profile (upper) and temporal change in activity of tracer cocktail (lower).

REFERENCES

[1] P. Simbierowicz and M. Olin, “Investigation of the Influence of Heterogeneous Porosity on Matrix Diffusion: A Novel Approach Using Adaptive Tree-Multigrid Technique and Real Porosity Data”, Mat. Res. Soc. Symp. Proc., 45, 847-854 (1997).

[2] K. Nilsson, J. Byegård, E. Selnert, H. Widestrand, S. Höglund, and E. Gustafsson, “Long Term Sorption Diffusion Experiment (LTDE-SD): Results from rock sample analyses and modelling”, SKB-R-10-68, 298pp (2010).

[3] P. Sardini, E. Moreau, A. Meunier, and G. Touchard, “2D Connectivity of Soultz Granite Primary Minerals”, Microsc. Microanal. Microstruct., 7, 491-497 (1996).

[4] Y. Tachi, T. Ebina, C. Takeda, T. Saito, H. Takahashi, Y. Ohuchi, and A.J. Martin, “Matrix Diffusion and Sorption of Cs^+, Na^+, I^- and HTO in Granodiorite: Laboratory-scale Results and Their Extrapolation to The In Situ Condition”, J. Contam. Hydrol., 179, 10-24 (2015).

Electrochemical Behavior of Ce ion and Bi ion in LiCl-KCl Molten Salt

Beom-Kyu Kim*, Hwa-Jeong Han, Ji-Hye Park, Won-Ki Kim, and Byung Gi Park,
Soonchunhyang University, Soonchunghyangro 22, Asan, Chungnam 336-745, Republic of Korea
*qu@sch.ac.kr

1. Introduction

Pyro process is currently being studied worldwide, the Republic of Korea has been conducting the most active research to prepare solutions for spent fuel. The pyro-process is the main purpose of efficiently separating actinides through a sufficient recovery process of fission products [1]. Liquid-liquid extraction processes have been important to co-extract minor actinide for minimizing high-level waste. While both liquid metals support the co-extraction capability, it is reported to the CRIEPI, that liquid bismuth is better than liquid cadmium in terms of lanthanide to actinide separation factor [2-3]. Lanthanide and actinide elements coexist as various compounds in molten salt waste produced from pyrochemical-process. PyroRedSox process has been proposed to separate lanthanides from used salt include trans-uranium elements using cathodic liquid bismuth and bismuth chloride. That processes consist of electrowinning and selective oxidation [4]. Lately studies on the intermetallic compounds of liquid metals and lanthanides have been carried out in various fields. Therefore, the electrochemical reaction of cerium present in the LiCl-KCl molten salt was confirmed by using electrochemical method, and the characteristics study of the existence of Bi ion was carried out.

2. Experimental

Experiments were carried out in a glove box under an argon atmosphere in which oxygen and moisture were kept at 1 ppm or less. And were performed to experiment at an elevated temperature using an electric furnace at the bottom of the glove box. LiCl-KCl and $CeCl_3$, $BiCl_3$, and Bismuth as a liquid electrode were all purchased from Alfa aesar and electrochemical measurements were performed in Quartz Cell. Working Electrode (WE) and Counter Electrode (CE) were Tungsten wire (1 mm diameter), the Pyrex guide tube was used to prevent contact between electrodes. The reference electrode was consisted of an one-end closed Pyrex tube, in which LiCl-KCl eutectic salt containing 1wt% AgCl was placed and a silver wire (Alfa-Aesar, 99%, OD: 1 mm) was immersed in the salt. All electrochemical measurements were performed using PAR Versastat3 potentiostat with Versastudio software. Temperature of the salt was measured with Chromel-Alumel thermocouple. The temperature was always 773K.

3. Results and Discussion

Results of Cyclic voltamograms of LiCl-KCl-$CeCl_3$ at 773K are shown in Fig. 1.

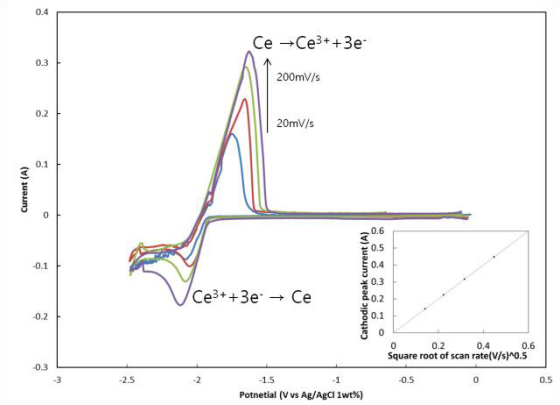


Fig. 1. Cyclic voltammogram obtained for Ce^{3+} in LiCl-KCl melt using the tungsten electrode (A=0.664 cm^2) at 773K, 1wt%, scan rate: 20, 50, 100, 200mV/s.

The values of the red-ox currents are shown in Table 1.

Table 1. The Value of the Current at at 773K

		Current(A)
20mV/s	$Ce \rightarrow Ce^{3+} + 3e^-$	0.1585
	$Ce^{3+} + 3e^- \rightarrow Ce$	-0.0335
50mV/s	$Ce \rightarrow Ce^{3+} + 3e^-$	0.2243
	$Ce^{3+} + 3e^- \rightarrow Ce$	-0.04655
100mV/s	$Ce \rightarrow Ce^{3+} + 3e^-$	0.2934
	$Ce^{3+} + 3e^- \rightarrow Ce$	-0.0818
200mV/s	$Ce \rightarrow Ce^{3+} + 3e^-$	0.3202
	$Ce^{3+} + 3e^- \rightarrow Ce$	-0.10904

We gradually added $BiCl_3$ in LiCl-KCl-$CeCl_3$ to investigate the effect of Bi ion on the Ce ion. The results of the measured CV are shown in Fig. 2.

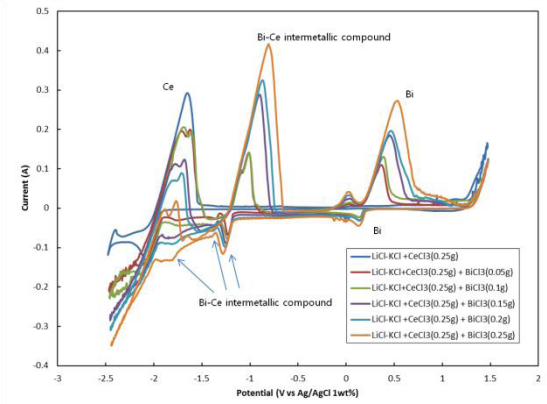


Fig. 2. Cyclic voltammograms of LiCl-KCl-$CeCl_3$(5wt%) at with $BiCl_3$(0.9~4.5wt%) using tungsten electrode and scan rate 100mV/s.

Comparison of the cyclic voltemmograms obtained in LiCl-KCl-$CeCl_3$ and after the addition $BiCl_3$ (0.9~4.5 wt%) is shown in Fig. 2.

The results are consistence with those obtained Ce peak, correspond to the formation of a Ce^{3+}/Ce in the first time. And Cathodic/anodic peak around 0.1~0.6 V should be ascribed to the deposition/dissolution of Bi Metal, respectively. Many anodic and cathodic peaks Ce-Bi alloys observed, so expected to the formation of Ce-Bi intermetallic compounds.

And we have derived a Potential-Current Voltammogram summarized from the Cyclic Voltammetry method.

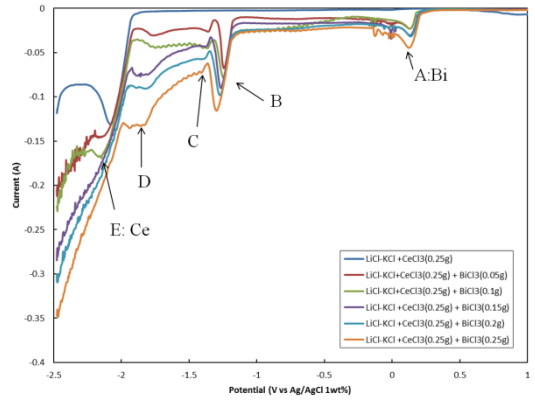


Fig. 3. Potential-Current Voltammogram for the reduction (from 1 to -2.5V) of Ce ion with Bi ion (Ce-Bi alloy) in the LiCl-KCl on the tungsten electrode (A=0.664cm2) at 773 K.

As a result of Fig. 3, various peak current appeared (A, B, C, D, E). In order to consider the reduction of intermetallic compound, potential was applied in the positive to negative direction.

A and E was a reduction of the Bismuth Cerium ion. And a sequential curve, which is a potential curve corresponding to the reduction of the dissimilar metal alloy.

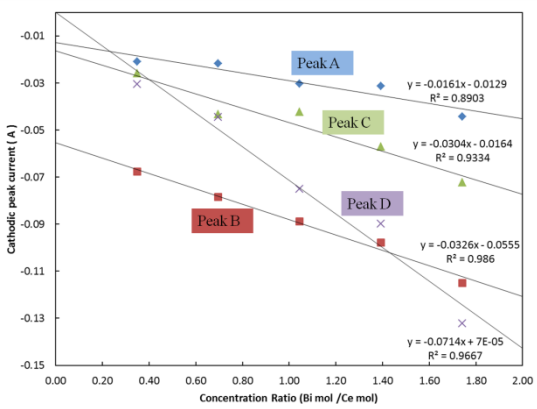


Fig. 4. Peak current according to mole concentration ratio (Bi/Ce).

Fig. 4 shows bismuth and Cerium reduced peak value as the concentration of bismuth ion increases. As a Result, Bi ions affect to the Ce ion.

4. Summary

In this paper, electrolytic behavior of Cerium and Ce-Bi ion system was studied. The electrochemical behavior of Ce was studied in LiCl-KCl-$CeCl_3$ molten salts using electrochemical techniques Cyclic Voltammetry on tungsten electrodes at 773K. During the process of CV electrolysis, intermetallic compound were observed of Ce, Cex-Biy.

Further study, in order to determine clarity of diffusion coefficient in this experiment, we will compare result of electrochemistry method and we also need to quantitative research.

REFERENCES

[1] H. Lee, G.-I. Park, K.-H. Kang, J.-M. Hur, J.-G. Kim, D.-H. Ahn, Y.-J. Cho, and E.-H. Kim, “Pyroprocessing Technology Development at KAERI”, Nuclear Engineering and Technology, 43 (4), 317-328 (2011).

[2] M. Sakata et al., “Equilibrium distribution of rare earth elements between molten Kcl-LiCl eutectic salt and liquid cadmium,”Journal of Nuclear Materials, Vol. 185, pp. 56-65, (1991).

[3] Kensuke Kinoshita et al., “Separation of uranium and transuranic elements from rare earth elements by means of multistage extraction in LiCl-KCl/Bi system,”Journal of Nuclear Science and Technology, Vol. 36, pp. 189-197, (1999).

[4] H. O. Nam, "All the Spent Nuclear Wastes to Low and Intermediate Level Wastes: PyroGreen", Proceedings of Global 2009, Paris, France, September 6-11, (2009).

Uranium Removal by Tributyl Phosphate-Coated Hydroxyapatite

HyunJu Kim* and Wooyong Um

Division of Advanced Nuclear Engineering (DANE), Pohang University of Science and Technology (POSTECH, 77 Cheongam-Ro, Nam-Gu, Pohang, Korea

*hyunju1157@postech.ac.kr

1. Introduction

Efficient and rapid removal of radioactive contaminants is crucial when they are released into the environment following nuclear accidents. Here, different types of apatite were synthesized using tributyl phosphate (TBP) and tested for uranium removal from various solutions using different reaction times and uranium concentrations.

2. Experimental

2.1 Synthesis of different apatite materials

Hydroxyapatite was prepared by solution-precipitation method [1]. Tributyl phosphate (TBP)-coated hydroxyapatite was prepared using surface functionalization with TBP using the method developed by WANG et al [2]. TBP-coated hydroxyapatite was prepared at different pHs (pH=4, 7, 10), respectively. The hydroxyapatite was washed repeatedly three times with deionized water (DIW), and dried at 60°C for 2 h prior to use. The TBP (20ml) was diluted in 100 ml ethanol, and this mixing solution was adjusted pH 4, 7 and 10 with 1M hydrochloric acid and 1M sodium hydroxide. After that, 5 g synthesized hydroxyapatite was added to prepared mixing solution. The mixture was placed in a heating mantle at 100℃ until the ethanol was evaporated. This remained mixture were baked in an oven at 130°C for 2 days. And then this material was washed with DIW and ethanol and dried at 60°C for 2 h. The final powder is TBP-coated hydroxyapatite materials.

2.2 Batch U adsorption and isotherm experiment

Uranium adsorption experiments were conducted using the synthesized apatite materials at a solid to solution ratio of 5 g L^{-1} under different background solution in open system. Uranium removal was evaluated under different reaction times and U concentrations.

Uranium adsorption isotherm experiments were conducted using different U initial concentrations. For isotherm experiments, a series of 15 mL polypropylene test tubes were used. Each test tube was filled with a synthesized adsorbents and 200 ppm of the initial U concentration in a 0.01 M $NaHCO_3$ solution at different solid/solution ratios. Langmuir and Freundlich models were applied for the experiment data.

3. Results & Discussions

3.1 Characterization of synthesized materials

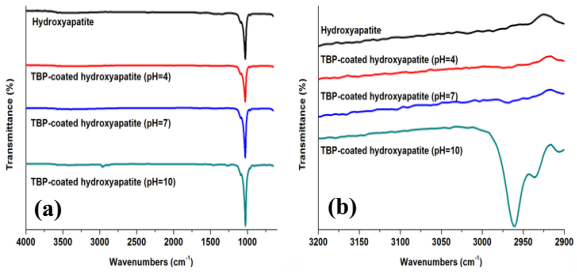


Fig. 1. FTIR spectra of the synthesized apatites: (a) analysis of the 4,000–650 cm^{-1} region; (b) an expanded view of the 3,200–2,900 cm^{-1} range of the C-H functional group.

In Fig. 1, the FTIR results showed that main peaks were shown at 3570 cm^{-1} in all materials. It indicates the stretching hydroxyl group from hydroxyapatite. Phosphate functional group was observed around at 1040 cm^{-1}. The C-H containing functional group (3000-2950 cm^{-1}) from TBP was found in the TBP-coated hydroxyapatites prepared at different pHs.

In Fig. 2, the ^{31}P NMR spectra show that all phosphorus in the synthesized apatite are PO_4^{3-} functional group, but TBP-apatite prepared at pH=10 condition show additional peak at around δ = -2 ppm due to $O=P(OR)_3$ structure from TBP structure.

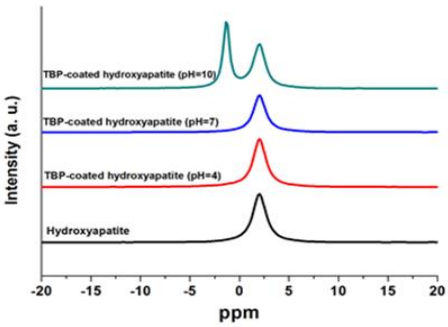


Fig. 2. Solid-state ^{31}P MAS NMR spectra for the synthesized apatites.

From the TC data for hydroxyapatite and TBP-coated hydroxyapatite, TBP-coated hydroxyapatite sample prepared at pH = 10 has 8–13 times more carbon present compared to other hydroxyapatite samples.

Based on the various characterization results, more TBP coating occurred on the hydroxyapatite surfaces at pH = 10 than other pH conditions.

3.2 Uranium Batch Adsorption Results

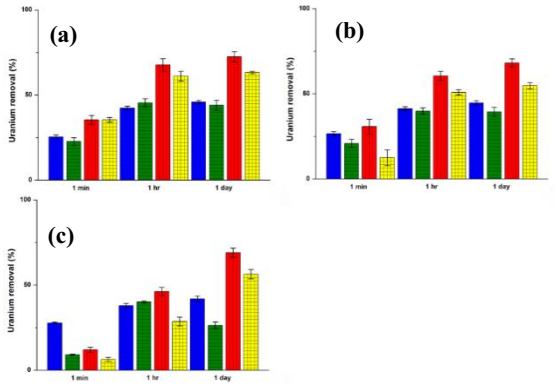


Fig. 3. Uranium removal (%) using different synthesized apatites at different initial U concentrations (a) 10 ppb, (b) 100 ppb, and (c) 1,000 ppb in 0.1 M $NaHCO_3$ background solution at 293.15 K [blue: hydroxyapatite; green: TBP-coated hydroxyapatite (pH = 4); red: TBP-coated hydroxyapatite (pH = 7; yellow: TBP-coated hydroxyapatite (pH = 10)].

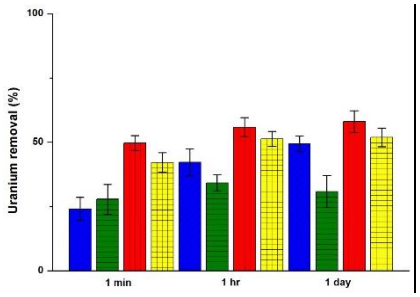


Fig. 4. Uranium removal % of synthesized apatites using the simulated seawater (0.7 M NaCl) spiked with 10 ppb U(VI) in at 293.15 K [blue : Hydroxyapatite; green : TBP-coated hydroxyapatite; red : TBP-coated hydroxyapatite (pH = 7); yellow: TBP-coated hydroxyapatite (pH = 10)].

In Fig. 3, TBP-coated hydroxyapatites show better U removal than hydroxyapatite. Especially, TBP-coated hydroxyapatites prepared at pH=7 condition shows the best U removal. The results of U adsorption experiments in simulated seawater (0.7 M NaCl) showed that the TBP-coated hydroxyapatite prepared at pH = 7 still had the best U removal capacity among the four solids, suggesting that TBP-coated hydroxyapatite can be used an efficient adsorbent to recover U from seawater.

According to the fits, the maximum adsorption capacity for U removal is close to 38 mg·g-1 for the TBP-coated hydroxyapatite prepared at pH = 7. And, the Freundlich isotherm gives a better fit to the U adsorption by TBP-coated hydroxyapatites prepared at pH = 7. It suggests multilayer U(VI) adsorption sites on their surfaces.

4. CONCLUSIONS

The adsorbents were successfully fabricated and tested for the removal of U from various solution conditions. Under the same conditions, TBP-coated hydroxyapatite showed better U removal capability than pure hydroxyapatite. In particular, TBP-coated hydroxyapatite synthesized at pH 7 showed the highest U adsorption capacity (38 mg g^{-1}). The results of this study indicate that TBP-coated hydroxyapatite can be used as a new adsorbent to efficiently and selectively remove U from seawater.

REFERENCES

[1] I. Mobasherpour, M. S. Heshajin, A. Kazemzadeh, and M. Zakeri, Synthesis of nanocrystalline hydroxyapatite by using precipitation method. Journal of Alloys and Compounds, Vol. 430, pp. 330-333, 2007.

[2] Wang, H.; Shao, X. Z.; Tian, Q.; Ji, Y. Q., Synthesis of TBP-coated magnetic Pst-DVB particles for uranium separation. Nucl. Sci. Tech. 2014, 25 (3).

Development of Treatment Equipment for Spent Resin Mixture in Heavy Water Reactors (HWR)

Kyu-Tae Park*, Jung-Min Yoo, and Young-Ku Choi
Sunkwang T&S Co.,Ltd, Sunkyung Officetel 20F, #3, Gongwon-ro, Guro-gu, Seoul 08298, Republic of Korea
*paradoxno1@hanmail.net

1. Introduction

To purify the liquid radioactive waste generated in the process of operating the Nuclear Power Plants (NPPs) are using the ion exchange resin. This spent resin is currently stored in the spent resin storage tanks in the NPPs as the treatment method has not been determined. The treatment method of the stored spent resins will be determined and the spent resins will be disposed according to the NPP decommissioning plan. The spent resin from Heavy Water Reactor (HWR) NPPs contains various radionuclides, and particularly a high concentration of C-14, a long half-life nuclide.

According to the domestic radioactive waste classification system, the currently stored HWR spent resin mixture is classified as Intermediate-Level Waste (ILW), and must be disposed of in rock caverns. However, the total activity of C-14 in the spent resin from Wolsung NPPs Units 1 through 4 is about 10 times as much as the total C-14 limit (1.66×10^{14} Bq) of rock-cavern disposal facilities specified in the Safety Analysis Report (SAR) of Korea Radioactive Waste Agency (KORAD). Accordingly, to reduce disposal quantities and disposal costs, it is necessary to separate the resins containing highly-concentrated radionuclides from the spent resin mixture, and remove C-14 from the separated spent resin.

2. Methods and Results

The purpose of this study is to develop a HWR spent resin mixture treatment system based on the results of collecting spent resin mixture samples from the spent resin storage tank #2 in Wolsung NPPs Unit 1, and analyzing the properties and the spent resin storage tank.

2.1 Spent resin mixture disposal scenario

As about 20% of the spent resin mixture of HWR NPPs is the active carbon and zeolite mixture and 80% of it is the mixed (anion and cation) resin, a disposal scenario was developed to reduce disposal quantities and disposal costs.

To dispose of the spent resin mixture of HWR NPPs, the spent resins must be separated from active carbon and zeolite, and the validity of deregulation must be reviewed, and to dispose of the spent resin corresponding to the ILW as Low-Level Waste (LLW) or Very-Low-Level Waste (VLLW), C-14, a highly-concentrated long half-life radionuclide, must be removed. The removed C-14 must be collected in a chemically stable form, and the disposal volume must be reduced and disposal safety must be ensured. Also, the validity of recovering and recycling the radioisotope C-14, an expensive resource, generated in the treatment process from the spent resin rather than disposing of it will be reviewed.

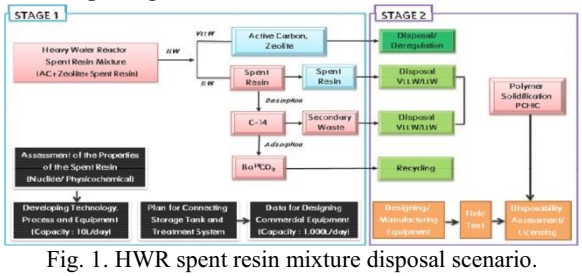


Fig. 1. HWR spent resin mixture disposal scenario.

2.2 Sampling the spent resin mixture and analyzing properties

Samples of the spent resin mixtures were collected from the spent resin storage tank #2 in Wolsung NPPs Unit 1. According to the results of sampling, the composition of the spent resin mixtures varied depending on their location in the storage tank. As illustrated in Fig. 2, zeolite, active carbon and spent resin were mixed in the sample collected from the manhole, whereas most of the samples consisted of spent resin at other locations.

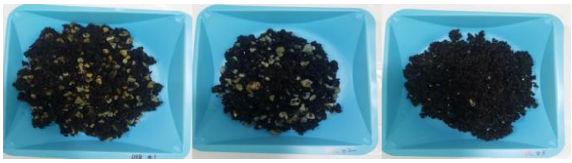

Fig. 2. Spent resin mixture samples from Wolsung NPPs Unit 1.

Table 1. Analysis of the properties of the spent resin from Wolsung NPPs Unit 1

Classification	Particle size (Spec.)	Particle size (Mesh experiment)
Resin	0.3mm~1.18mm	Less than 0.50mm on average
Active carbon	1.0mm~3.35mm	0.71mmor more on average
Zeolite	1/8" Pellets 4×8 Beads	0.71mmor more on average

Based on the particle size data in the purchase specifications of the zeolite, active carbon and resin from Wolsung NPPs Unit 1, meshes of various sizes were selected, and a multi-level separation experiment was conducted. In the separation experiment, most active carbon and zeolite did not

pass the 850μm sieve. All resin passed the 850μm sieve, and resin was distributed on several layers depending on particle size, but it was confirmed that only a small quantity (friability resin) passed the 300μm sieve.

2.3 Development of the spent resin mixture separator

Based on the result of analyzing the properties of the spent resin, appropriate meshes were selected, and it was confirmed that if Mesh 20 (0.85mm) and Mesh 50 (0.30mm) are used to separate the mixture, the resin can be effectively separated from active carbon and zeolite.

In the same way as the spent resin mixture is treated in the field, the spent resin mixture separator was connected to the resin outlet at the bottom of the storage tank, and a simulation was conducted. The simulation was done horizontally and vertically.

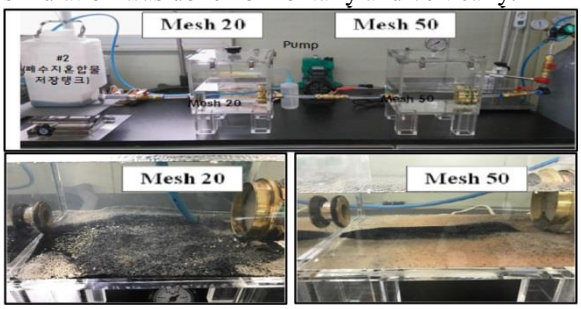


Fig. 3. Lab scale spent resin mixture separator (horizontal).

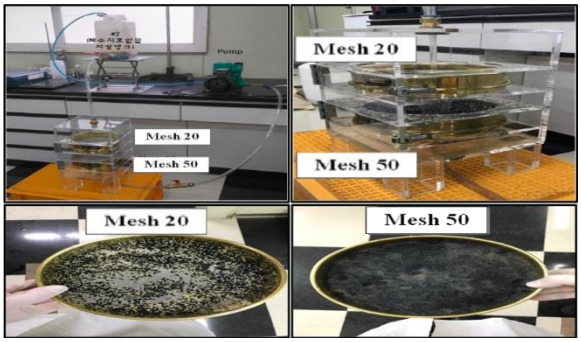


Fig. 4. Lab scale spent resin mixture separator (vertical).

The vertical structure separator in Fig. 4 had a shorter separation time than the horizontal structure in Fig. 3, and the vertical structure had a very high separation rate. Also, it was very easy to treat the separated waste at each level in the vertical structure separator. Based on these experimental results, the spent resin mixture separator was developed as shown in Fig. 5.

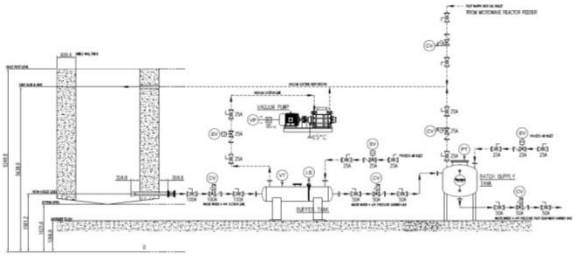


Fig. 5. Spent resin mixture separator.

2.4 Spent resin treatment system

To remove C-14 in the separated spent resin, this study used microwave. As the conventional C-14 removal technology uses the desorption solution, the cation and anion materials remain in the spent resin besides the spent resin. So there are residues and secondary waste after desorption. However, the heating and desorption method using can raise the temperature quickly, and as no materials are added in the desorption, there is no secondary waste, and the resin can be dried.

Table 2. Properties of the microwave

Classification	Microwave	Simple heating
Characteristics	- directly heating the molecules in the sample	Indirect heating (heat conduction)
Strengths	- quickly raising the temperature - uniform heating - selective heating - temperature control - high efficiency (80%) - easy to operate - No noise/heat/exhaust gas	General purpose
Weaknesses	- Limited applicability due to the chemical structure	Nonselective

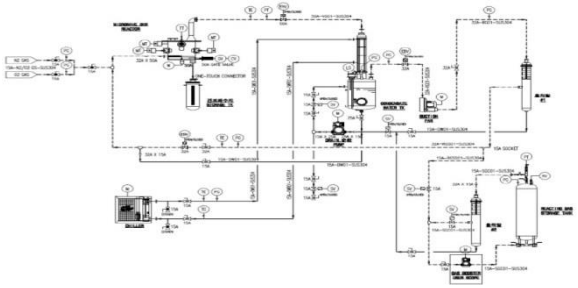


Fig. 6. Spent resin treatment system.

3. Conclusions

The purpose of this study is to come up with a scenario for disposing of the spent resin mixture from HWR NPPs, and develop the technology for securing disposal stability by optimizing and demonstrating the technology for removing C-14 in the spent resin of NPPs.

The technology for disposing of the spent resin of NPPs is expected to improve the stability of NPPs. Also, it is deemed possible to develop products that can reduce disposal costs by more than 50%, and flexibly establish NPPs operation and radioactive waste management policies.

REFERENCES

[1] Jianlong Wanga, Zhong Wan, Treatment and disposal of spent radioactive ion-exchange resins produced in the nuclear industry, Progress in Nuclear Energy, Volume 78, January 2015, Pages 47.

4분과

방사성폐기물관리 (Poster)

The Study of an Additional Liquid Waste Collection Tank Arrangement on the GA Drawings

Keun-Pack CHANG *, Mu-Gap SHIN, Gi-Won HWANG, and Dong-Jae LEE
KEPCO Engineering & Construction Company .Inc, 269 Hyeokssin-ro, Gimcheon-si, Gyeongsangbuk-do, Republic of Korea
* kpchang9@kepco-enc.com

1. Introduction

The liquid radwaste system(WV) in the nuclear power plant processes radioactive and potentially radioactive liquid wastes. These wastes include equipment, floor and chemical drains that are transferred from Containment, Auxiliary and Compound Building sumps or equivalent tanks. Also the wastes from the steam generator blowdown system, the auxiliary steam condensate receiver tank wastes and the condensate demineralizer regeneration wastes are included, if significantly contaminated by primary to secondary leakage [1]. There are several tanks as shown on the Table 1 to accommodate these wastes in the nuclear power plant. These tanks should have the enough storage capacity to accommodate all liquid radioactive wastes.

The SKN 5&6 nuclear power plants are now being constructed with improvements resulting from operation experience of previous plants. As a result of construction permit by regulatory body, it has been decided that an additional waste tank needs to be introduced in the system in the light of increased waste volumes generated during operation abnormally which capacity attains 20,000 gallons.

This paper presents chiefly an example of an additional waste tank arrangement on the general arrangement (GA) drawings to put it on in the SKN5&6 compound building.

2. Waste Collection Tanks in the Liquid Radwaste system for SKN5&6

Various kinds of waste tanks are available to accommodate liquid radioactive wastes in the WV system. The liquid waste input sources are originated from various kinds of drains from related buildings such as leakage from equipment, equipment & floor drain, leakage from spent fuel pool, equipment decontamination, primary sampling drain, laundry drain, and human body decontamination, etc. And the quantities of liquid waste generated during operation are dependent upon several factors, including design conditions, type of equipment, equipment arrangement, and operating rate, etc. [2].

These wastes are collected in three different categories reflecting three process trains in the nuclear power plant; floor drain, equipment waste and chemical waste. Segregation of wastes is done according to the processing required in the plant [1]. Table 1 below shows various kinds of waste collection tanks and their capacities in the SKN5&6.

Table 1. Waste Collection Tanks and their Capacity

Tank Name	Capacity (gallon)	Quantity (EA)	Sum (gallon)
Floor Drain Tank	18,000	2	36,000
Equipment Waste Tank	18,000	2	36,000
Chemical Waste Tank	15,000	2	30,000
Laundry Drain Tank	6,000	2	12,000
Total			114,000

Besides of the tanks above, auxiliary waste tank named tentatively for an additional tank (20,000 gallons) will be newly added in the WV system for SKN5&6.

3. An example of an additional waste tank arrangement on the GA drawings

When a feasibility study is done from the lay-out perspective, the study has been done with some preconditions in order to minimize the effect on the current GA drawings. They are:

(a). The current other waste tanks are not changed so as not to add a pump and other process equipment in the WV system .

(b). Current civil structural columns are still maintained.

(c). A compartment for additional waste tank is prepared at CPB 63ft, 77ft and 85ft near to other waste tanks in viewpoint of efficient interconnection in the system.

From the example of arrangement, an auxiliary waste tank will be installed in the compound building along with other waste tanks; floor drain tank, equipment waste tank, and chemical waste tank. In order to reserve the space of 20,000 gallons of an additional waste tank, the civil structure needs to be revised at the 63ft, 77ft and 85ft areas. The revised portions in the GA are seen in the Fig. 1, 2 and 3 below.

As liquid waste tanks are seen in the Fig. 1 and 3, they are installed in each compartment. This is for the observation of criteria which is required in the design of radioactive waste management system from the view of mainly structural resistance and occupational radiation exposures to operating personnel.

Consequently, a compartment is prepared for an additional waste tank next to the equipment waste tank.

According to Fig. 1(IS) below, a couple of chemical waste tank, floor drain tank and equipment waste tank are seen downward from the top. And, each pump room is there by each tank. The size of each pump room is reduced to prepare a compartment for an additional waste tank next to the equipment waste tank. This makes it efficient for related pumps and piping to be interconnected in the design.

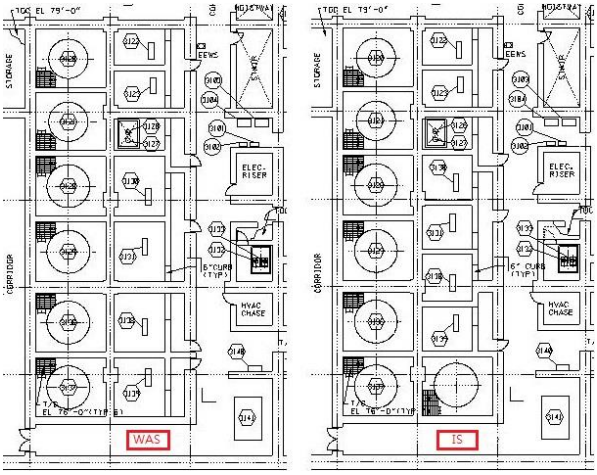


Fig. 1. Arrangement of Waste Tanks in the CPB 63ft.

Equally, a revision of civil structure at CPB 77ft and 85ft is envisaged as shown on Fig. 2 &3. The Fig. 2 shows a necessity of revision of the hot pipe way while Fig. 3 valve room and access way to the tanks. The hot pipe way is revised to prepare a space for an additional waste tank which measures 12ft (Dismeter) x 29ft (Height) supposedly as shown on Fig. 2.

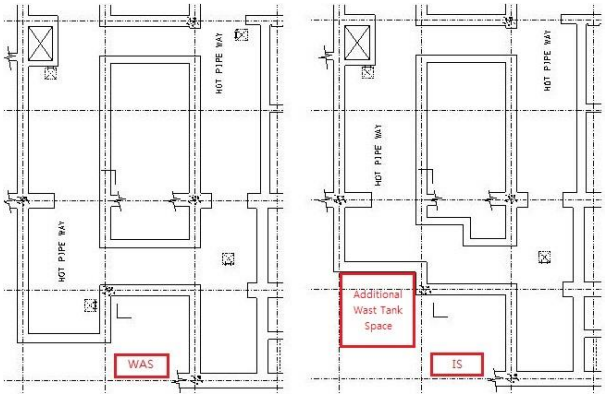


Fig. 2. Hot Pipe Chase Arrangement in the CPB 77ft.

The Fig. 4 below shows a flow diagramt of liquid radwaste system (WV). It shows many major components of WV system such as various tanks, pumps, Reverse Osmosis (R/O) packages, associated piping which contribute to waste collection, waste processing through R/O package and LRS monitor tank, etc. It also shows that it is designed to do necessary process to produce effluent of quality suitable for discharge or recycle. That is, the waste gone through the process is collected in the monitor tanks, and sampling is carried out. The contents inside monitor tank is decided either to go for recycle or for discharge to environment.

The effluent shall meet the requirement of NSSC Notice No.2014-34, Standards on Radiation Protection [4]. In the flow diagram, an additional extended waste tank in red is seen. It is designed to accommodate all kinds of wastes without differentiation of equipment, floor or chemical drain. And it shows its role of buffer storage in case of a temporarily increase of liquid waste in the process. And there are links with other related tanks and a couple of equipment waste pumps for interconnection network.

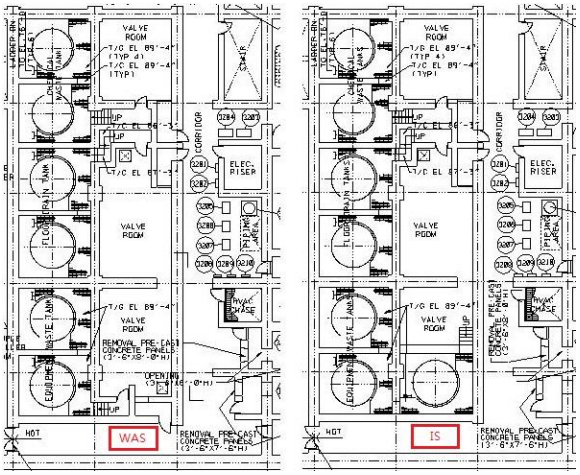


Fig. 3. Arrangement of Waste Tanks in the CPB 85ft.

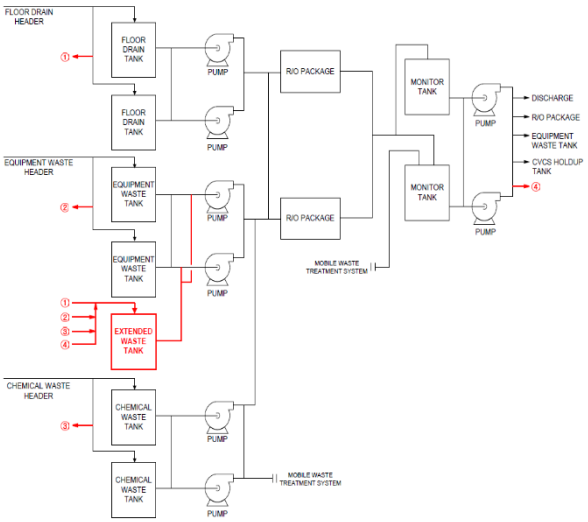


Fig.4. A flow diagram of Liquid Radwaste System (WV).

4. Conclusions

The liquid radwaste system (WV) should be designed to control and manage of liquid radwaste generated as a byproduct of nuclear power plant. It should be designed to accommodate total volumes generated from routine operation including abnormal operation which result in a great quantity of liquid wastes.

This paper has reviewed its possible location on the GA drawings according to the introduction of 20,000 gallons of an additional waste tank.

By introducing a new tank in the system, many advantages are expected with enhanced system reliability, operability and availability.

REFERENCES

[1] Liquid Radwaste System(WV) System Functional Description, 0-472-N403-001, KEPCO-E&C, 2016.
[2] ANSI/ANS-55.6-1993, Liquid radioactive waste processing system for light water reactor plants.
[3] Plant Manual, Liquid Radwaste System(WV), 0-472-N442-001, KEPCO-E&C, 2015.
[4] NSSC Notice No.2014-34, Standards on Radiation Protection.

Analysis of Inlet Air Characteristics of Air Cleaning Unit in Nuclear Power Plants

Hak-Soo Kim* and Cho-Rong Kim

KHNP Central Research Institute, 7, 1312-gil, Yuseong-daero, Yuseong-gu, Daejeon, Republic of Korea

*hskim0071@khnp.co.kr

1. Introduction

Air Cleaning Unit (ACU) as an Engineering Safety Features (ESF) in Nuclear Power Plants (NPP) is adopted to remove radioactive waste as well as toxic materials from operation and accidents. ACU in NPP composed to various components to clean air such as pre-filter, HEPA and adsorber which is filled with TEDA (Tri-Ethylene-Di-Amine) impregnated activated carbons (TEDA-AC). The removal performance and shelf-life of TEDA-AC is affected by the operating environment such as temperature, humidity and toxic materials. This paper deals with the analysis results of inlet air characteristics into ACU to establish experimental variables for TEDA-AC aging evaluation

2. Inlet Air Characteristics Analysis

2.1 Representative Sampling

The NPP to collect the representative samples were selected for reactor type. The selected NPPs are Hanbit Unit-2, Shin Wolseong Unit-2, Hanul Unit-2 and Wolseong Unit-4. The representative samples are collected at full power, de-synchronizing, overhaul and synchronizing based on NPP operation modes, and the sample locations are Containment Building, Fuel Building and Auxiliary Building. Table 1 is shown the selected NPPs, sampling time and locations

Table 1. NPPs, Sampling Time and Location for Representative Sampling

NPPs	Sampling Time	Locations
Hanbit 2 Shin Wolseong 2 Hanul 2 Wolseong 4	Full Power De-Sychronizing Overhaul Sychronizing	Containement Bldg. Fuel Bldg. Auxiliary Bldg.

2.2 Analysis of Representative Sample

The representative sampling was carried out at the inlet of ACU using a commercial portable air sampler and a 5 liter Tedlar Bag. The analysis items of air samples were determined by type and concentration of volatile organic compounds, oxides (NOx, SOx) and aldehydes based on the related studies and organic solvents used in NPP. Typically, the analysis of aldehydes used the High Performance Liquid Chromatography (HPLC) and the analysis conditions are shown in Table 2.

Table 2. Analysis Conditions of HPLC

Parameters	Conditions
Column	Inno C_{18}(250x4.6 ㎜, ㎛)
Mobile Phase	ACN/H_2O = 60/40 (v/v%)
Detector	UV 360 ㎚
Flow Rate	1.0 ㎖/min
Injection	20 ㎕

2.3 Analysis Results of Representative Samples

○ Analysis results of organic compounds

The analysis results of type and concentration of organic compounds are shown in Table 3 and Fig. 1.

Table 3. Type and Concentration of Organic Compounds

Organic compound	Molecular Formula	Concentration (㎍/㎥)
Formaldehyde	CH_2O	95.91
Accetaldehyde	C_2H_4O	52.62
Benzene	C_6H_6	8.58
Toluene	C_6H_6-CH_3	95.72
Ethylbenzene	C_8H_{10}	48.42
m, p-Xylene	C_8H_{10}	98.85
Stylene	C_8H_8	2.55
o-Xylene	C_8H_{10}	57.09

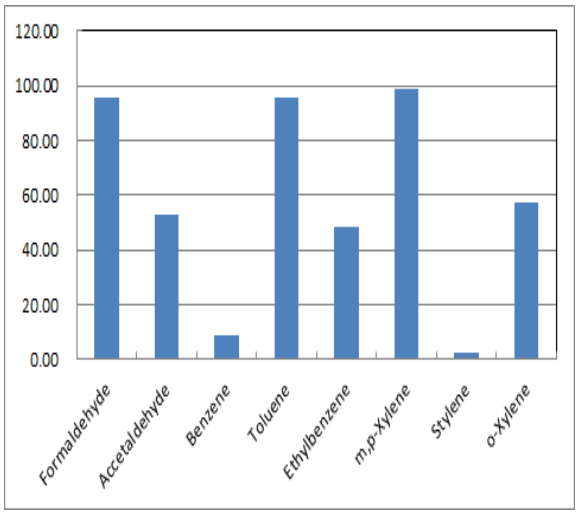


Fig. 1. Distribution of Organic Compounds in Inlet Air.

The total concentrations of organic compounds with NPPs are shown in Fig 2. The total organic compound concentration of Shin Wolseong Unit-2 is higher than that of other NPPs because its commercial operation is short and the large amount of organic compounds contained in the coating materials on the wall and equipment surface was continuously volatilized.

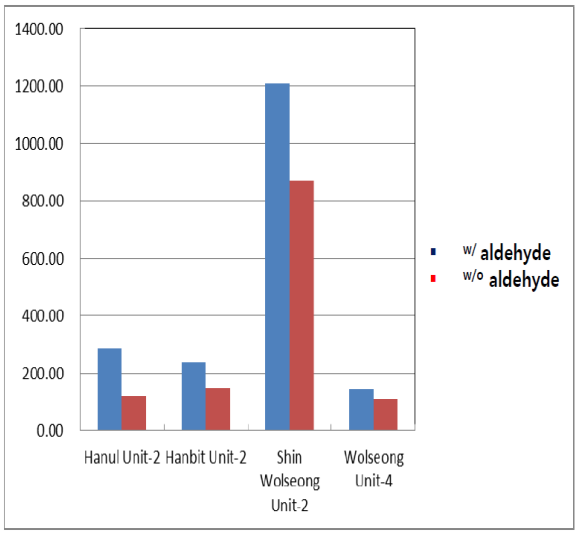


Fig. 2. Total Concentrations of Organic Compounds with NPPs.

○ Analysis results of oxides

The analysis results of type and concentration of oxides are shown in Fig. 3. As shown in Fig. 3, the concentrations of NO_2 and SO_2, which are known to affect the shelf-life of TEDA-AC, are negligible as about 1/100 $\mu g/m^3$, and there is no significant difference according to the NPPs.

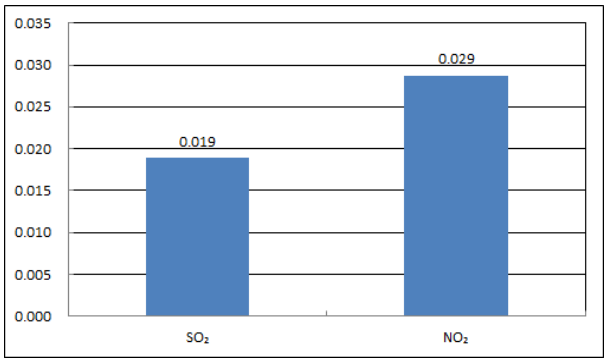


Fig. 3. Concentration of Oxides in Inlet Air.

3. Conclusion

The types and concentrations of organic compounds and oxides in inlet air into ACU were analyzed for representative nuclear power plant. The representative organic compounds were identified as Formaldehyde, Accetaldehyde, Benzene, Toluene, Ethybenzene, m,p-Xylene, Stylene and o-Xylene, and the concentrations of Formaldehyde, Toluene and m,p-Xylene are relatively higher than that of other organic compounds. In addition, it was confirmed that NO_2 and SO_2 exist as oxides in inlet air and their concentrations were analyzed as 0.02 ppm. The results of organic compounds and oxides in inlet air into ACU will be used as the poisoning parameters in aging test of TEDA-AC.

REFERENCES

[1] M. Nakayama, et al., 'Effects of weathering on impregnated charcoal removal efficiency for radioactive methyl iodide,' 28th ISNATT (2004).

[2] H.S. KIM, et al., 'An Analysis Report: The Chemicals in Inlet Air of NPP's ACU,' KHNP CRI, 2016-50003339-전-0540TC, (2016).

Development of Silver-Graphene Fiber Composites as Sorbents for Radioactive Iodine Gas

Minseok Lee and Ho Jin Ryu*

Korea Advanced Institute of Science and Technology, 291 Daehak-ro, Yuseong-gu, Daejeon, Republic of Korea

*hojinryu@kaist.ac.kr

1. Introduction

There has been a lot of effort to remove ^{129}I from the gas streams of reprocessing facilities to protect the environment and human health from the radiographic exposure. Therefore, various methods, such as wet scrubbing or solid sorbents, have been suggested to capture iodine. Due to the simplicity of designing the removal systems, solids sorbents are more preferred than other methods. Silver (Ag) impregnated solid sorbents, such as Ag-zeolites or Ag-silicate, have been developed especially because of the chemisorption properties of Ag for iodine [1]. Recently, graphene-based materials have been studied as potential iodine sorbents. They showed better performance than other conventional iodine sorbents in the laboratory scale [2]. In this work, composites of graphene fiber [3] hybridized with silver as sorbents have been prepared for the effective removal of iodine gas. By preparing the fiber-type adsorbent, it is expected that the pressure drop of gas streams will be lower than powder-type sorbents and the adsorption kinetics will be faster than granular-type adsorbents [4].

2. Preparation

2.1 Preparation of graphene oxide (GO)

Expanded graphite was first prepared by the microwave irradiation (720W, 2.45 GHz) of graphite intercalated compounds. After that, GO solution was synthesized by oxidizing the expanded graphite using Kovtyukhova's method and Hummers's method.

2.2 Preparation of graphene fibers

To obtain the GO liquid crystals, the prepared GO solution was concentrated by centrifuge. And then, the GO solution was placed in the syringe and injected into a rotating coagulation bath. The coagulation bath contained the $CaCl_2$ aqueous solution. The GO solution was coagulated and formed a gel-state fiber. The gel fiber was stretched and suspended on a pair of spaced parallel sticks. The GO fiber can be obtained by drying the gel fiber at air for 1 day and at vacuum oven for 12 hours. The prepared GO fiber was chemically reduced by hydroiodic acid at 80 ^{o}C for 12 hours. After that, the reduced GO fiber was dried at a vacuum oven for 1 day.

2.3 Hybridization with silver

The silver-graphene composites were fabricated by electroplating methods. The reduced graphene fiber was soaked in a silver nitrate solution with metallic silver. Then, a voltage of at least 0.8V, which is the reduction potential of silver, was applied on the two ends of the fiber (Fig. 1).

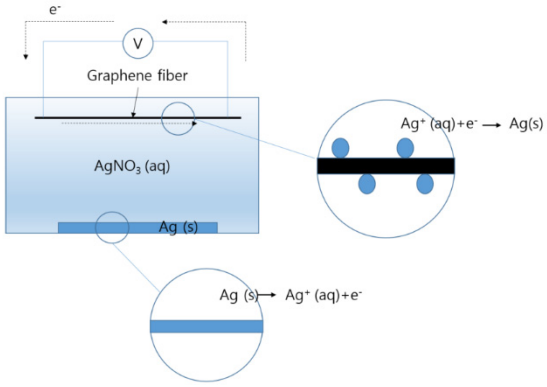


Fig. 1. The process of Ag-graphene fiber hybridization.

3. Results and Discussions

Fig. 2 and Fig. 3 show the morphologies of the silver-graphene fiber composite. Since the large-size graphene oxide plates were shrunk into small-diameter cylinder-like shape fibers, the surface of the fiber has a lot of wrinkles that enhance the surface

area. In addition, numerous defects on the graphene sheet can provide the space for the growth of silver nanocrystalline.

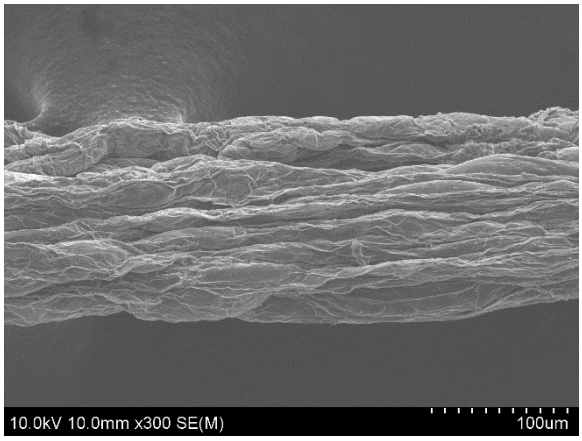


Fig. 2. SEM image of the Ag-graphene fiber.

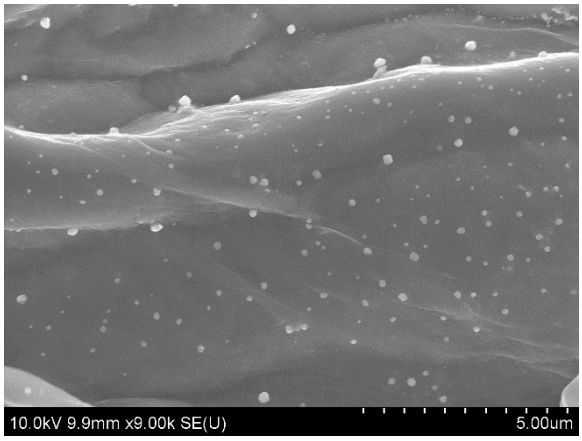


Fig. 3. Nano-sized silver particles attached on the graphene fiber.

4. Conclusion

In this paper, the silver-hybridized graphene fiber composites were synthesized to be used in radioactive iodine gas removal. The electrodeposition method showed evenly deposited silver nanocrystalline on the surface of the graphene fiber. For the future work, the composites will be characterized using various analysis techniques such as EDS, XRD, or XPS. Based on the results, the hybridization process conditions will be optimized. Lastly, the iodine sorption kinetics and the gas permeability of the composite sorbents will be estimated.

Acknowledgement

This study was supported by the Ministry of Science, ICT and Future Planning. (NRF-2016M3A7B4905630)

REFERENCES

[1] B. J. Rieley et al, Materials and processes for the effective capture and immobilization of radioiodine: A review, Journal of Nuclear Materials, 470, 307, 2016.
[2] S. M. Scott et al, “Graphene-based sorbents for iodine-129 capture and sequestration”, Carbon, Vol. 90, p. 1, 2015.
[3] Z. Xu, C. Gao, “Graphene chiral liquid crystals and macroscopic assembled fibers”, Nature communications, 2, 571, 2011.
[4] M. Suzukiet al, “Activated carbon fiber: Fundamentals and applications”, Carbon, 32, 577, 1994.

Preliminary Test of ^{3}H and ^{14}C Analysis Methods in Radioactive Waste

Kahee Jeong*, Eun Kyung Jung , Kyu-Min Song , and Seung Chul Park

KHNP Central Research Institute, 70-1312 gil, Yuseong-daero, Yuseong-gu, Daejeon, Republic of Korea

*kaheejeong@khnp.co.kr

1. Introduction

The radiochemical analysis is an essential necessity for the management and disposal of radioactive wastes. The demand of radiochemical analysis is expected to increase rapidly as the decommissioning of NPP K-1 unit which will be starting in the near future. KHNP-CRI has been building the infrastructure for the contribution of the smooth progress of decommissioning like the radiochemical analysis laboratory and analysis instruments.

In this study, separation and analytical methods for the quantitative analysis of ^{3}H and ^{14}C are investigated from radioactive waste generated from nuclear power plants. Also, preliminary tests are carried out to establish analytical methods using pyrolyser equipment, one of the analytical methods.

2. Sample pre-treatment and separation methods

2.1 Distillation method

Distillation method is one of basic methods for analyzing ^{3}H and ^{14}C. An oxidizing agent is added to the sample to be oxidized. The flask containing sample and oxidizing agent is connected to distillation unit and then the impinger. It is heated to 100-150℃ and the ^{3}H and ^{14}C as form of HTO and CO_2 are collected in the impinger. Reaction is carried out for 5 hours or more to sufficiently extract ^{3}H and ^{14}C from the sample. One of disadvantages of this method is any leakage through the connection of glasses.

2.2 Oxidation method

Oxidation method is a method to completely combust the sample at 900℃ using a combustion oven, a combustion bomb, a oxidizer, and etc. In order to select proper one of them, it is important that the separation method of the objective nuclide should be investigated through the preceding studies on the characteristics of the sample. A combustion oven is also known as tube furnace. The type and amount of sample depend on the size of the tube. The oxidation method with a combustion bomb oxidizes the sample under high pressure oxygen condition. This method takes shortly processing time. However, this method has a disadvantage that post treatment is difficult. The oxidizer method is simple and takes shortly processing time because the entire process is automated. The amount of sample is limited to 1 mg or less. It is hard to control the flowrate of gas for performing this experiment.

2.3 Separation of ^{3}H and ^{14}C in concrete samples using pyrolyser equipment

The pyrolyser equipment is composed of three furnaces, sample zone, mid zone and catalyst zone (Fig. 1). The pyrolyser should be heated to 900 ℃ for desorption of ^{3}H and ^{14}C from the sample. In the mid zone, it can be separated by condensing some volatile radionuclide (^{99}Tc, etc.) into a tube while maintaining 500℃. The catalyst zone is filled with Pt catalyst, where CO, generated by incomplete combustion, is oxidized to CO_2. The trap solution of ^{3}H and ^{14}C is 0.01 M HNO_3 and Carbo-sorb E, respectively.



Fig. 1. Configuration of the pyrolyser [1].

3. LSC calibration and sample measurement

^{3}H and ^{14}C can be measured by LSC (Liquid Scintillation Counter). Fig. 2 shows the detection efficiency curve using a CRM (Certified Reference Material). The separation is performed using simulated samples with concrete and CRM and recovery tests are measured by LSC.

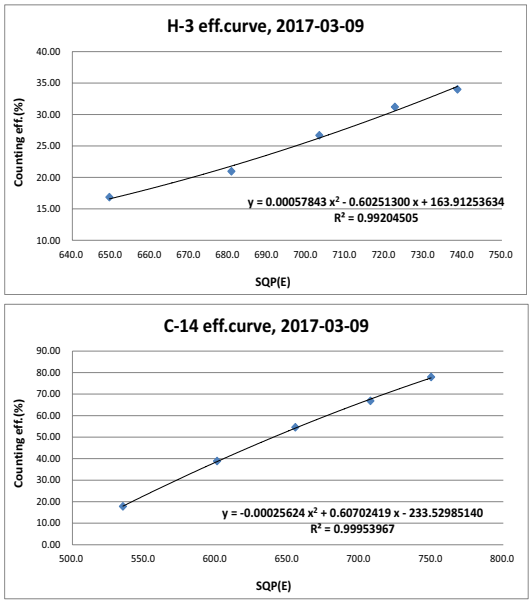


Fig. 2. Detection efficiency curve.

4. Results

The specific radioactivity, recovery rate and MDA of ^{3}H and ^{14}C are calculated from the LSC measurement results. The results are shown in table 1.

Table 1. Results of simulated sample with concrete and CRM measured by LSC

	Sample			Activity (As)	Recovery	MDA
H-3	Name	Taken(g)	Analyzed (g)	(Bq/g)	(%)	(Bq/g)
	STD 1	5.102	7.9178	3.108	91.082	0.0095
	STD 2	5.158	7.9502	3.152	92.464	0.0095

	Sample			Activity (As)	Recovery	MDA
C-14	Name	Taken(g)	Analyzed (g)	(Bq/g)	(%)	(Bq/g)
	STD 1	5.102	7.8013	1.654	96.019	0.0055
	STD 2	5.158	7.8458	1.680	98.560	0.0053

5. Conclusion

In this study, separation and analytical methods for the quantitative analysis of ^{3}H and ^{14}C are investigated from radioactive waste generated from nuclear power plants. ^{3}H and ^{14}C are analyzed by pyrolyser equipment and LSC in the simulated sample with the standard source. Good specific radioactivity, MDA and recovery rate of more than 90% are obtained.

REFERENCES

[1] RADDEC user of pyrolyser presentation, Effective extraction of ^{3}H & ^{14}C using the Raddec Pyrolyser (2014).

[2] Hou X. L., Rapid analysis of ^{14}C and ^{3}H in graphite and concrete for decommissioning of nuclear reactor, Appl Radiat Isot 62(2005) 871-882.

[3] J. M. Lim, M. J. Kang, K. H. Chung et al., Application of high-temperature tube furnace and liquid scintillation counter for radioactivity determination of ^{14}C and ^{3}H in solid waste samples, J. Radioanal Nucl Chem(2015) 303:111.

Comparative Study on Electrothermal Radioactive Waste Dryer & Non-Electronic Power Source Radioactive Waste Dryer Utilizing Air Circulation of Ventilation / Exhaust System in NPP

Kwang-sik Seo, Hyo-cheol Kim, Dong-hyun Park, Sang-tae Lee, Soon-hwan Yang, and Sang-uk Lim

Hana Nuclear Power Engineering Co., Ltd, 84, Hanam-daero, Hanam-si, Gyeonggi-do, Republic of Korea

shmhg@hanarad.com

1. Introduction

Most of dry radioactive waste created in the radiation management areas of domestic NUCLEAR POWER PLANT contain moisture. The waste containing moisture uses a radioactive waste dryer equipped with a suction fan in the heating device for drum disposal (free water content in drum : high integrity container less than 1%, other containers less than 0.5%). This dryer has low efficiency of use due to the fact that it is not only vulnerable to fire hazards, but also has lots of limitations of use. Therefore, it was necessary to develop a NEPS (Non-Electric Power Source) and an air-circulating dryer without fire hazard and electricity. This study compare the fire hazards and continuous operating conditions with the previous electrothermal waste dryer. Therefore, we have been studied to optimize drying efficiency and manpower utilization to draw a optimal operating technic of high quality drumming work.

2. Body

2.1 A comparison of the operating characteristics in electrothermal dryer and NEPS dryers

2.1.1Operating characteristics of Electrothermal dryer. The electrothermal dryer which is operated by electricity has a high possibility of fire hazard due to malfunction of the temperature sensor and safety device, dust deposited on the coil of the heater, and overheating during operation due to the flammable materials. so, the electrothermal dryer needs to be approved by the MCR (Main Control Room) and the HP (Health Physics) Room before and after operation. In addition, the drying operation time is limited to 6 hours per day, and also it is necessary to observe 1 hour preheating before the use and 1 hour cooling after the use. Also, it cause increase of personal exposure dose because operator has to be located at drying facility during the operation.

2.1.2 Operation characteristics of NEPS dryer. The purpose of NEPS dryer which is developed by characteristics of Nuclear power plant's operation is to reduce an unnecessary radiation exposure and to prevent fire. The NEPS dryer utilize the ventilation/exhaust suction system, and it is different from the electrothermal dryer that obtains dry heat source from a source of electric power. The NEPS dryer utilize a suction system (1,200CFM) which induced air flow from the lower part to the upper part. And it can be operated without any limitation. These characteristics make it possible to use the dryer continuously for 24 hours regardless of the residence of the operator. Therefore this structure improve the dry ability of any solid waste and reduce possibility of unnecessary radiation exposure.

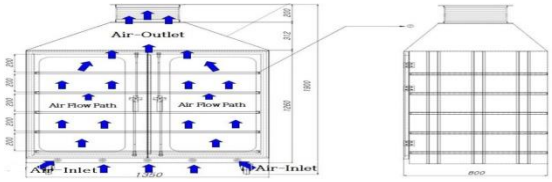


Fig. 1. NEPS dryer structure drawing.

2.2 A comparison of the with performance test in electrothermal dryer and NEPS dryers

2.2.1 *Testing method.* Step1: Measure the weight of dried papers (4 kg) and cottons (8 kg). Step2: Make two samples of each kind of papers (11 kg) and cottons (13 kg) dehydrated by adding enough moisture. Step3: Add one sample of each kind of papers and cottons which the moisture is sufficiently added to the electrothermal dryer and the NEPS dryer, and dry them. Step4: The drying time is measured by separating by natural drying, electrothermal dryer drying, and NEPS dryer drying until the weight is the same as measured at the initial drying state. Step5: The experimental results

are derived by comparing the drying time of each dryer based on the weight of the sample before drying (step 1) and the weight of the sample after drying.

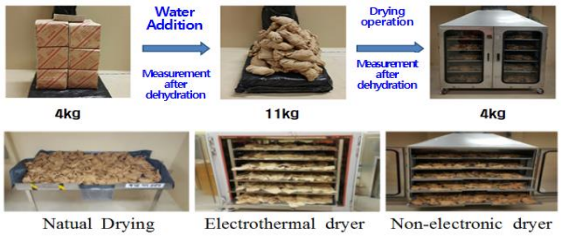


Fig. 2. Paper's sampling and measuring weight for each step.

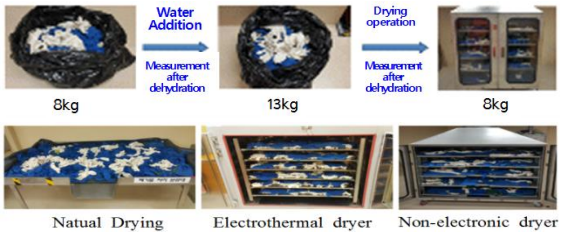


Fig. 3. Cotton's sampling and measuring weight for each step.

2.2.2 Operation restriction requirement. Limit the operating time (8 hours / day) due to the fire hazard of the electrothermal dryer and make sure that the operator is operated with the resident. The operation is 1 hour of preheating, 6 hours of drying, 1 hour of cooling, and the actual drying operation is 6 hours. Operators may contact the MCR before operation and obtain approval for operation. However, since the NEPS dryer does not have a fire hazard, it is possible to operate for 24 consecutive hours without the need of a operator. As a result, it was possible to improve drying ability and reduce manpower.

2.2.3 Test Result

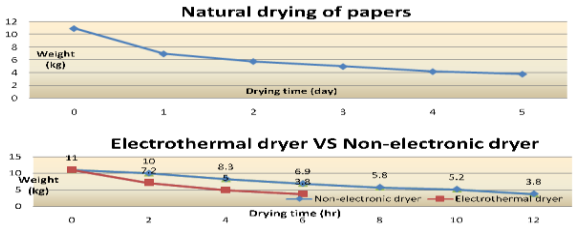


Fig. 4. Comparison graph of paper's drying time.

Table 1. Test result of papers

Division		Drying possible time/day	Ref1)Drying finished time	Drying finished days
Papers	Electrothermal dryer	Ref2)6 hour/day	6 hour	1.0 day
	Non-electric dryer	24 hour/day	12 hour	0.5 day

Ref1) This is drying completed time about 11kg of moisture-containing papers regard to operating restriction requirement
Ref2) Consider the preheating 1 hour before the operation and cooling 1 hour after the shutdown for 8 hours(working time)

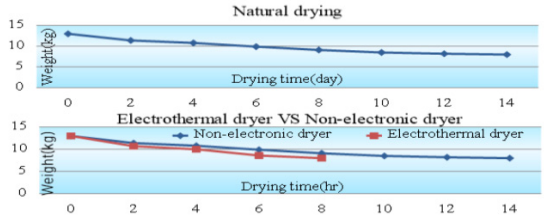


Fig. 5. Comparison graph of cotton's drying time.

Table 2. Test result of cottons

Division		Drying possible time/day	Ref1) Drying finished time	Drying finished days
Cottons	Electrothermal dryer	Ref2) 6 hour/day	8 hour	1.3 day
	Non-electric dryer	24 hour/day	14 hour	0.6 day

Ref1) Drying amount per 13kg of moisture -containing cottons taking into account the restricted driving condition.
Ref2) The operator considers the preheat time and the cooling time after shutdown of the dryer for 8 hours.

2.2.4 A comparison of the operation efficiency in electrothermal dryer and NEPS dryers. Although the electrothermal dryer dried the moisture-containing waste about 2 times faster than the NEPS dryer, the drying time was limited to 6 hours during 8 hours/day. Unlike the electrothermal dryer, the NEPS dryer was able to operate without fire hazard for 24 hours continuously. Calculating the number of drying completed dates, It was confirmed that which was dried by NEPS dryer had a 2 times higher efficiency of the paper type and a 2.2 times higher efficiency of the cotton type.

3. Conclusion

The NEPS dryer is facility not using the power supply and using the negative pressure of ventilation or exhaust system, there is no anxiety of overheating during the operation. There was no fire hazard unlike the electrothermal dryer, and continuous and safe operation was possible even the inflammables are mixed without the need for the operator resident. It reduced the unnecessary radiation exposure dose and maximized the utilization of the human resources by converting the previous operator to other tasks. So, the work quality was improved ultimately. This study figured out that the operation time (1day) of NEPS dryer increased 4 times more and drying ability improved 2 times more than electrothermal dryer.

REFERENCES

[1] Guideline for the delivery of low-level.
[2] radioactive waste (2014-64).
[3] Criteria for the acceptance of low-level radioactive waste (disposal facility safety analysis report).

The Effect of Fractured Rock to Radionuclides Transport Through Unsaturated Zone

Won-Seok Kim*, Sangsoo Han, and Wooyong Um

Pohang University of Science and Technology (POSTECH), ChungAm-Ro 77, Pohang, South Korea

*wkim23@postech.ac.kr

1. Introduction

The potential release of radionuclides from low and intermediate-level radioactive waste (LILW) may pose environmental problems to adjacent areas. In addition, the presence of released radionuclides can affect human health [1]. Released radionuclides can be transported by the flow of rainfall, exist with pore water through fractures in unsaturated zone, and is reached to groundwater flow. Released radionuclides to vadose zone and ultimately groundwater can be transported by groundwater flow through porous materials or fractures [2]. It is important to investigate the effect of fractured rock to radionuclides transport through vadose zone. In this study, batch adsorption, batch diffusion, and flow-through column experiments were conducted to understand the sorption and transport behavior of radionuclides under fractured rock in unsaturated zone, and the safety assessment and long-term performance of repository.

2. Materials and methods

2.1 General information

To investigate the relationship between the sorption of radionuclide and site characteristics which fractured rock in vadose zone, batch sorption, batch diffusion, and flow-through column experiment for radionuclides such as ^{3}H, ^{99}Tc, and ^{90}Sr were conducted using groundwater and solid materials from the LILW repository site. Fractured rock samples were collected in the LILW repository site, and it was characterized by X-ray microtomography (XMT) analysis and fractured filling/coating material was investigated by X-ray diffraction (XRD).

2.2 Experiments

Solid material of fractured rock sample (1.0 g for ^{3}H, 1.0 g for ^{99}Tc, 0.5 g for ^{90}Sr) was used in 10 mL of groundwater for the batch sorption experiments. Specimen sample (2 × 2 × 0.5 cm) was used for batch diffusion experiments. Column sample (5.0 × 12.5cm) was used for flow-through column. In order to compare the radionuclide adsorption to fracture filling/coating material, experiments were done with and without fracture filling/coating materials. The size of solid material is 75-250 μm.

Solid material was pre-equilibrated through contact with a sufficient amount of groundwater for one day for the sorption experiments. Pre-equilibrated step was repeated until the pH of the solution was maintain with the pH of groundwater (pH=6.8). After pre-equilibration, control batch test which without radionuclide was performed to determine the initial concentrations of the radionuclides and the mass loss by sorption onto bottle walls. The radionuclide was spiked into the pre-equilibrated reacting bottles to attain the required radionuclide concentration (^{3}H: 100 Bq/mL, ^{99}Tc: 100 Bq/mL, ^{90}Sr: 20 Bq/mL). Solid material was shaken at 80 rpm with radionuclide spiked groundwater for 14 days. The pH was adjusted to maintain the initial pH of the groundwater by 0.1M HNO_3 or NaOH solution during experiment. After finish the batch sorption experiment, the solution was separated by using a syringe filter of 0.45 μm pore size (Whatman) and stored to determine the concentration of radionuclides. All batch sorption experiments were carried out in triplicate.

The diffusion of radionuclide were investigated using diffusion reactors which shown in Fig. 1, and it was divided by two part. Tracer and radionuclide was inserted to one part and it was transported to the other part by diffusion through specimen which installed in middle of reactor.

The fractured rock sample was setting inside of column and the condition of column was controlled in unsaturated (water content: 35%) by syringe pump. The flow of groundwater with radionuclide was controlled by syringe pump.



(a) (b) (c)

Fig. 1. Experiment for (a) batch sorption, (b) diffusion, and (c) flow-through column.

3. Results and discussion

The XMT and XRD results show the characterization of fractured rock sample. The distribution coefficient of radionuclide was calculated after experiment and compared with and without fracture filling/coating material.

3.1 XMT and XRD

XMT, a nondestructive three-dimensional imaging technique, was applied to demonstrate its capability to visualize the mineralogical alteration and microstructure changes in rock sample. Fig. 2 shows the XMT images of fractured rock surface. XRD result (Fig. 3) shows that heulandite and laumontite was major component of fracture filling/coating material.

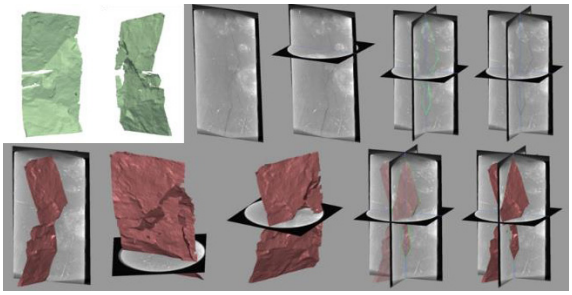


Fig. 2. X-ray microtomography image of fractured rock surface.

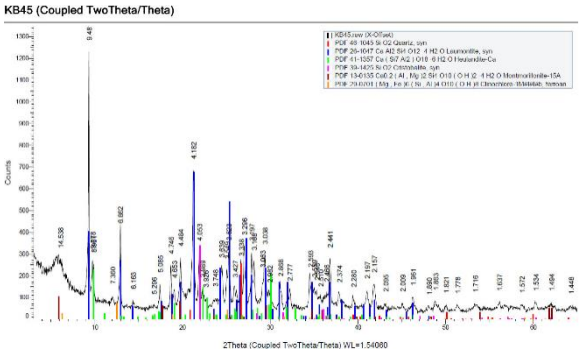


Fig. 3. X-ray diffraction results of fractured rock.

3.2 Radionuclide transport behavior

The fracture filling/coating materials were significantly affect to the distribution coefficient of radionuclide sorption. The distribution coefficient of ^{90}Sr (45.1 mL/g) with fracture filling/coating materials is higher than without fracture filling/coating materials (30.3 mL/g). In case of ^{99}Tc, there are similar distribution coefficients in both with and without fracture filling/coating materials (0.9 and 1.1 mL/g). The batch diffusion and flow-through column experiments were also conducted using the same fractured rock sample, and the results of diffusion and column experiments showed similar trend of radionuclide sorption and transport to sorption experiment.

4. Conclusion

When the fracture filling/coating materials are exist, distribution coefficient of radionuclide is higher than without fracture filling/coating materials. This study involved a geochemical characterization of the LILW repositroy, and was performed as a part of the site characterization effort. The results of this study provide more basic information and insight for the safety assessment of LILW repository.

REFERENCES

[1] V. Höllriegl, H.Z. München, “Strontium in the Environment and Possible Human Health Effects”, Encyclopedia of Environmental Health, 21, 268–275 (2011).

[2] K.A. Rod, W. Um, M. Flury, “Transport of Strontium and Cesium in Simulated Hanford Tank Waste Leachate through Quartz Sand under Saturated and Unsaturated Flow”, Environ. Sci. Technol, 44, 8089-8094 (2010).

Preliminary Analysis on Radionuclides Transport in the Unsaturated Environment

Jaechul HA*, Jeonghwan LEE, and Jeonghyoun YOON
Korea Radioactive Waste Agency, 168 Gajeong-ro, Yuseong-gu, Daejeon, Republic of Korea
*jcha@korad.or.kr

1. Introduction

The assessment of the Wolsong LILW Disposal Center (WLDC) as a repository of radioactive wastes critically depends on the performance of the engineered containment system, and the natural, geologic system underlying the repository. The inventory of radionuclides, their mobilization and release from the repository, and their transport through the unsaturated zone (UZ) to the groundwater table and eventually to the biosphere are key factors and processes affecting the long-term performance of the system [1].

This study is performed using TOUGH2 code for multiphase flow and transport simulator [2]. And preliminary modeling has done to predict radionuclide transport using a physically based description of the relevant processes. In other words, simulations were performed and analyzed to the development of a simplified model of the WLDC.

2. Modeling approach

As shown in Fig. 1, 2-dimensional (2D) model representing the LILW second disposal facility was developed. It includes the host rock (saturated and unsaturated zone) and engineering barriers that consist of waste, concrete lining and cover.

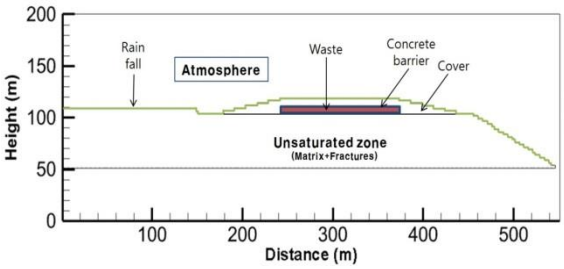


Fig. 1. Geometry and boundary conditions of the model.

Boundary conditions (specifically infiltration rates) and their implementation were appropriately adjusted in the model as well as steady-state simulation to obtain hydrological initial conditions under long-term infiltration.

Initial condition is shown as Fig. 2 and steady-state hydraulic head obtained from hydrological initial conditions under long term infiltration is shown as Fig. 3. Simplified groundwater flow path is shown as Fig. 4.

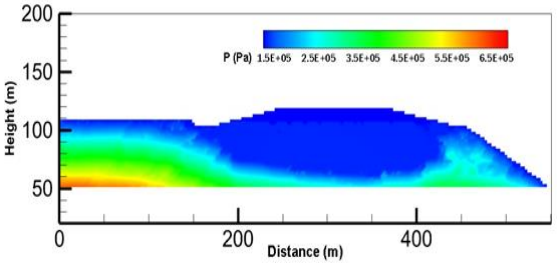


Fig. 2. Initial condition of unsaturated modeling area.

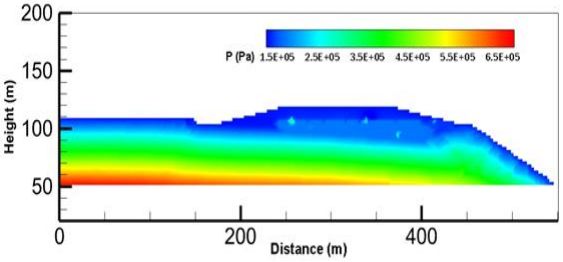


Fig. 3. Hydraulic head on the steady state.

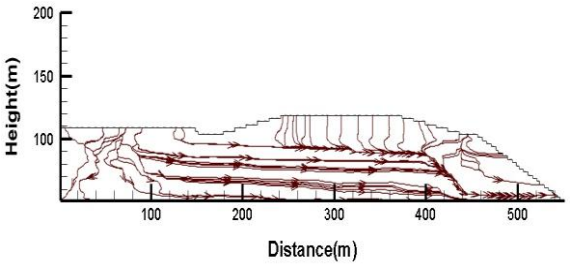


Fig. 4. Vector of groundwater flow path .

As for radionuclide property data set (specifically for the C-14 → N-14 decay chain), it was developed simple sub-model behavior of radionuclides in a simplified representation of the repository. Waste element in the modeling as represented by C-14 only.

Radionuclides transportation by advection and diffusion was simulated from the repository into unsaturated zone [3].

3. Results

Radioactive nuclide C-14 transportation was simulated for 300 years after closure, and the result is shown in Fig. 5. Most of C-14 including in the LILW disposal facility transported along ground-water flow path to east-south direction.

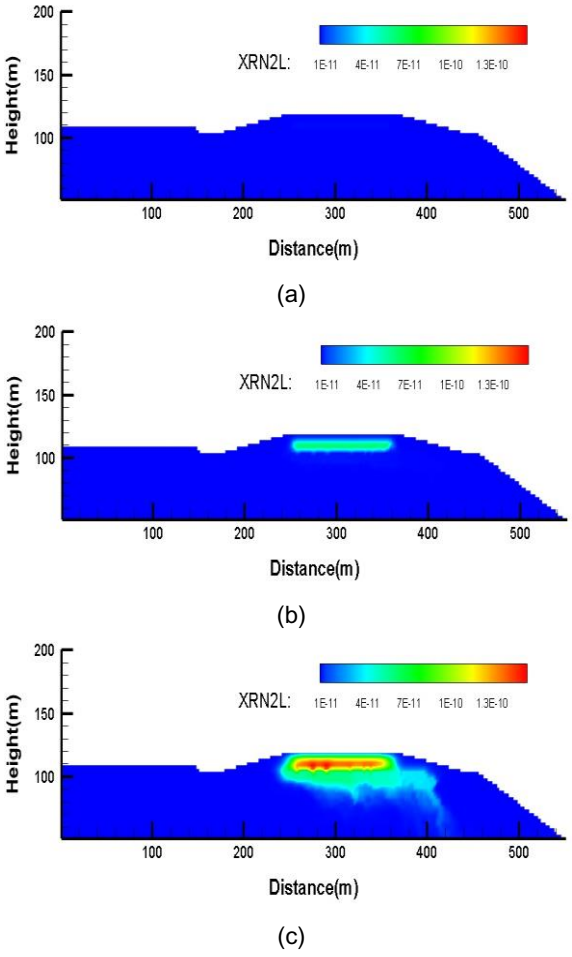


Fig. 5. Radioactive nuclide C-14 transport at (a) after 1 year, (b) after 50 years, and (c) after 300 years.

4. Conclusion

The preliminary modeling was carried out to analyze the RNs transportation in the LILW second phase disposal facility in Korea which is under licensing. In this modeling the amount of groundwater penetrating into the ground is important. The most important factors determining the unsaturated environment are the infiltration rate and medium permeability. For accurate modeling, validity of physical properties is required.

As a further detailed model to develop, it is essential to calculate the source term and condition in and around the repository. Such a model may either implement some conservative scenarios and assumptions about containment breaching and waste mobilization.

Acknowledgements

This work was supported by the Radioactive Waste Management of the Korea Institute of Energy Technology Evaluation and Planning (KETEP) grant funded by the Korea government Ministry of Trade, Industry and Energy.

REFERENCES

[1] Van Genuchten, M.Th., “A closed-form equation for predicting the hydraulic conductivity of unsaturated soils. Soil Sci. Soc. Am. J. vol. 44 (1980).

[2] Pruess, K., Oldenburg, C., Moridis, G.,” TOUGH2 user`s guide, Version 2.0, LBNL Report, LBNL-43134, Berkeley,CA (1999).

[3] Hinds, J., “Development of Numerical Grids for UZ Flow and Transport Modeling”, US DOE, 70p. (2001).

Basic Study on Development of Solidification Agent for Disposal Container Recycled From Paste Powder at Concrete in Decommissioning Nuclear Power Plant

Youngbum Mun[1], Jeahyung Lee[1*], Hyunkook Choi[1], Jaeyung Kim[1], and Chulwoo Chung[2]

[1] Sung Shin Cement, 48-37 Bugang oecheon-ro, Bugang-myeon, Sejong, Korea

[2] Pukyung Natl. Univ., 45 Yongsoro, Nam-gu, Busan, Korea

[*]Jhlee@sscem.com

1. Introduction

For the first time, the nuclear power plant will be decommissioned as Kori unit 1 has been operated for over 40 years. In decommissioning nuclear power plant, various type of waste is generated and over 80 % is concrete in these wastes. There is volume reduction technology as method for reducing volume of concrete.

Generally, since portion of activation is only paste excluding the aggregate, it is need to separate paste and aggregate. The aggregates will be recycled and pastes will be disposed.

In this paper, study is conducted for hydration recovery by re-heating paste. The re-heat paste will be used to solidification agent for disposal container using separated paste. This study aims to obtain basic data necessary for the development of solidification agent for radioactive waste disposal container.

2. Experiments

2.1 Materials

The paste was made W/B = 40% and cured for 28 days. For making the paste as the sample powder of solidification agent, crashed to a size of several millimeters using jaw-crasher. And they were dried at 100°C to remove un-acted water. To reflect 40 years old period, two type samples which are carbonation paste (CP) and non-carbonation paste (NP) were made according to KS K 2584. Also it was ground as same particle size to cement using ball mill.

2.2 Experiment methods and items

After heat temperature conditions have been selected by 500, 600, 700°C for hydration recovery of the pastes, the pastes were heated in electric furnace during one and half hour. And then they were cooled in desiccators during the same time. To reflect carbonation environment in atmosphere over 40 years, carbonation paste (CP) and non-carbonation paste (NP) were mixed at 50:50%. Dehydrate gypsums were added by 4% to enhance compressive strength.

As experimental items, the specific gravity of each heat temperature was measured according to KS L 5110. Mortar compressive strength was measured according to KS L ISO 679 for evaluation of strength development.

2.3 Mortar mix design

Rate of fine aggregate : cement : water is 3 : 1: 0.5 according to KS L ISO 679. Mix 1, 2 were designed to this method and table of mix proportion is shown to Table 1. But Mix 3 was designed to different amount of cement according to specific gravity.

Table 1. Mixing Design of Mix 1 and 2

Type		Temp	NP	CP	Gypsum	W/B	Sand
		(°C)	(%)				(g)
Mix 1	1	0	96	0	4	0.6	1350
	2	500	96	0	4	0.6	
	3	600	96	0	4	0.6	
	4	700	96	0	4	0.7	
Mix 2	1	0	48	48	4	0.6	
	2	500	48	48	4	0.6	
	3	600	48	48	4	0.6	
	4	700	48	48	4	0.7	

Generally, specific gravity of cement is 3.15 g/cm^3. At this time, requested amount of cement is 450 g. If specific gravity of cement was decreased by 2.6 g/cm^3 after heating, cement volume of 450 g is same to that of 270 g. Like this, amount of cement is

varied depending on the change of specific gravity after heating. Mix proportion and specific gravity of each heating temperature were shown to Table 2. In case of 700°C, unit water content is increased to ensure the same flowability.

Table 2. Mixing Design and Density of Mix 3

Type		Density	Temp	NP	CP	Gypsum	W/B	Sand
		(g/cm^3)	(°C)		(%)			(g)
Mix 3	1	2.63	0	48	48	4	0.75	1350
				376 g				
	2	2.67	500	48	48	4	0.75	
				382 g				
	3	2.85	600	48	48	4	0.75	
				407 g				
	4	3.01	700	48	48	4	0.8	
				429 g				

2.4 Result of compressive strength

Compressive strength of Mix 1, 2 at 28 days is shown to Fig. 1. Compressive strength of Mix 1 and 2 increased with increasing heating temperature and compressive strength is highest at 600°C. But compressive strength at 700°C decreased due to the increase in mixing water for ensuring flowability. Mix 2 of mixing CP is lower compressive strength then Mix 1 because it is judged to limestone formed by carbonation.

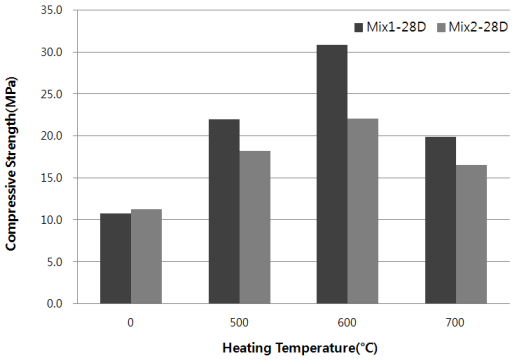


Fig. 1. Compressive strength of Mix 1, 2.

Compressive strength of Mix 3 at 7, 28 days is shown to Fig. 2. Compressive strength of Mix 3 is lower than Mix 1, 2 due to decreasing paste amount according to specific gravity. Also compressive strength increases with increasing heating temperature and the difference between 600°C and 700°C was not significant.

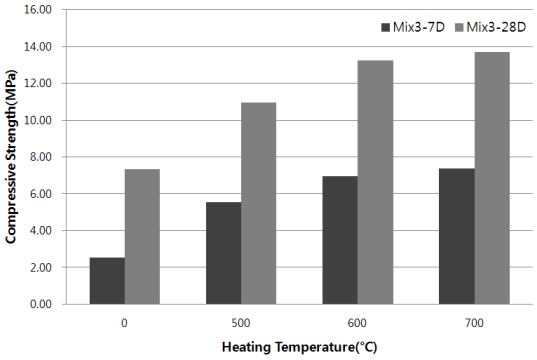


Fig. 2. Compressive strength of Mix 3.

3. Conclusion

Specific gravity of CP was as low as 2.63 g/cm^3. But Specific gravity was increased with increasing heating temperature due to water evaporation. Compressive strength at 600°C was highest and mixing water was needed at 700°C for ensuring flowability. Result of compressive strength experiment, it is judged that 600°C is more suitable than 700°C.

Acknowledgement

This work was supported by the Energy Technology Program of the Korea Institute of Energy Technology Evaluation and Planning (KETEP) granted financial resource from the Ministry of Trade, Industry & Energy, Republic of Korea (No. 20161510300420)

REFERENCES

[1] Ahn. Jae-Cheol, “Properties of recycle cement made of cementitious power from concrete waste by conditions of burning”, Architectural Institute of Korea, 19-11 (2003).

[2] Cho. Min-chol, “A study on the development of recycling cement using the waste concrete power”, Korea concrete institute (2002).

Modelling of the Spent Nuclear Fuel Assembly Using the Monte Carlo Method

Hwa Jeong Han, Beom Kyu Kim, Ji Hye Park, Won Ki Kim, and Byung Gi Park*
Soonchunhyang Univ., Soonchunhyang-ro 22, Asan, Republic of Korea
*byunggi@sch.ac.kr

1. Introduction

After irradiation of a uranium fuel assembly during its operation in a fission nuclear reactor core, many radionuclides are generated by fission and activation of ^{235}U, ^{238}U and other nuclides present in the assembly. Thus spent nuclear fuel difficult to measure material because of the complexity of the isotopic composition and high neutron and gamma-ray emission rates. In particular, an independent determination of spent fuel assembly characteristics, such as initial enrichment, burnup, cooling time, and/or plutonium content, poses a challenging task [1-2].

The purpose of this paper is to develop and test simulated model to improve safeguards measurements of spent nuclear fuel. This model can be used to measure of gamma and alpha radiation emitted from a spent nuclear fuel assembly. A detailed combine modeling and evaluation of the additional instrument to independently assess spent fuel assembly characteristics will be performed in future work using GEANT4.

2. Method and Calculations

2.1 The GEANT4 simulation code

To simulate the passage of various particles emitted from the spent nuclear fuel, the GEANT4 Monte Carlo calculation code was selected. GEANT4 is a toolkit that simulates accurately the passage of particles through matter. It contains a complete range of functionalities including tracking, geometry, physics models and hit.

2.2 Characteristics of the spent nuclear fuel assembly

Generally, the fuel assembly consists of 265 fuel rods in a 17 by 17 square array. The center position in the fuel assembly has a guide thimble that is reserved for in-core instrumentation. The remaining 24 positions in the fuel assembly have guide thimbles. The guide thimbles are joined to the top and bottom nozzles of the fuel assembly and provide the supporting structure for the fuel grids.

We chose to consider the features of a spent nuclear fuel with a burnup of 47GWd. The fuel was initially enriched to 3.1wt%^{235}U and the most important radionuclides contributing to alpha activity are UO_2. They lead to an alpha activity of 4.73E+08Bq after 15 years of alpha decay and the average value of emitted alpha particles is 5.3MeV. The simplified chemical composition considered in the calculations is $^{238}UO_2$, with a mass density of 10.8 g/cm^3 [2].

2.3 Description of spent nuclear fuel

First, in order to be representative of the UO_2 fuel shape, we considered to geometrical shape of a single fuel rod. A single spent fuel rod was designed to consist of a three-layer cylindrical tube which is consist of Fuel, Gap, and Cladding. Where a single fuel rod consists of enriched uranium, in the form of UO_2 pellets, contained in Zircaloy-4 tubing. And rods are pressurized internally with helium during fabrication to reduce clad creepdown during operation and thereby prevent clad flattening.

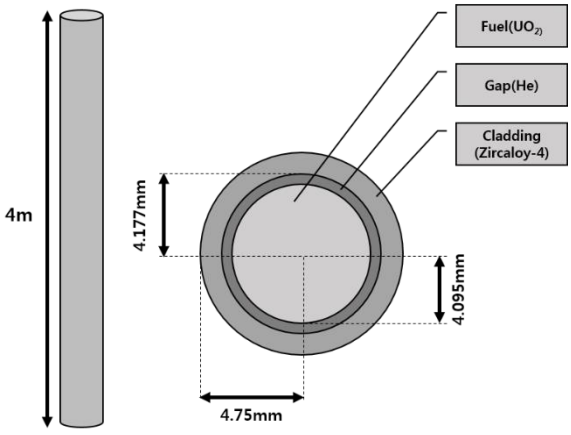


Fig. 1. Plant view of a single rod with the geometric characteristics.

Guide tube was designed to the cylindrical stainless steel tube. The designed single fuel rod and guide tube arranged 17 by 17 type.

Second, to give the simple approach to the spent fuel in the water, spent fuel was considered as a material which emission of alpha particle was isotropic and homogeneous.

A schematic layout of modeled systems is presented in Fig. 1. Also, the main parameters taken into account in the GEANT4 calculations are given in this figure.

3. Results

Fig. 2 shows the cross-sectional view of 17 by 17 spent nuclear fuel assembly model visualized using GEANT4. The red circles represent the guide tube and the white circles represent the spent nuclear fuel rods.

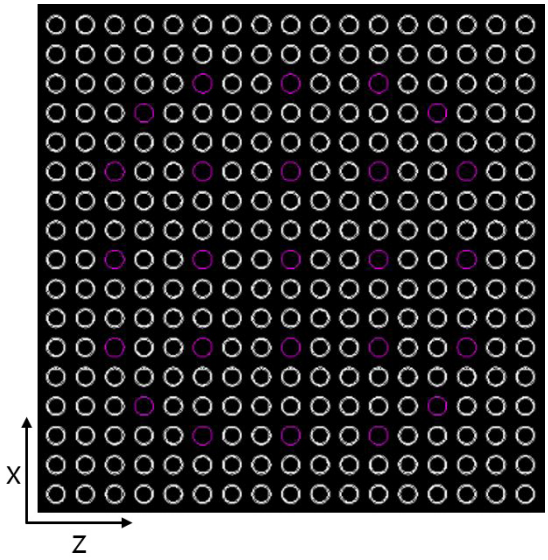


Fig. 2. GEANT4 geometry view of a 17 by 17 PWR Fuel Assembly.

As previously mentioned, the average energy of alpha particles was 5.3 MeV. Therefore, the effect of alpha particles on the spent nuclear fuel assembly was simulated using this model.

3.1 The effect of alpha particle emission

We observed the effect of alpha particle emission at 10, 100, 1000, and 10000, respectively.

The increase of alpha particles had more impact on the assembly area. These results are shown in Fig. 3. The yellow dots shown in this figure are result of the particles hitting each rod.

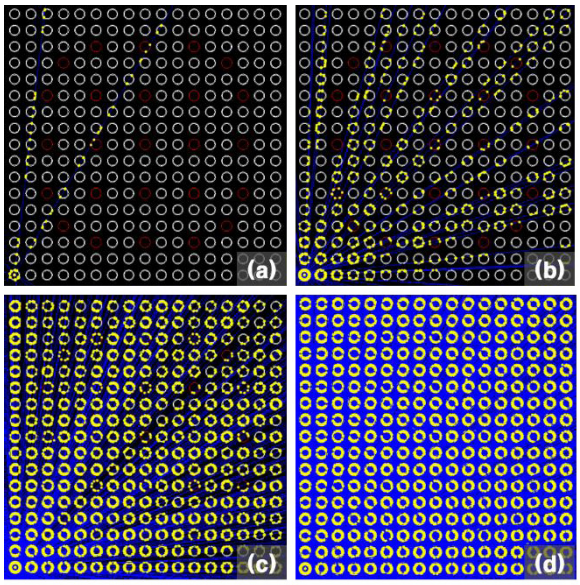


Fig. 3. Simulation results by amount of alpha particle emission (a) 10, (b) 100, (c) 1000, (d) 10000.

4. Discussion and Conclusion

In this work developed and test simulated fundamental model to improve safeguards measurements of spent nuclear fuel. The single fuel rod was modeled. And then the spent nuclear fuel assembly was created by arranging the designed fuel rod as 17 by 17. We investigated the effect of alpha particles emitted from fuel rods using the developed model. The simulation results showed that the increase of alpha particle effects more areas.

This work should be supplemented in the future. The model should be added the various physical processes and the detailed definition of radioactive source. In order to be suitable for the purpose, it is considered that further improvement of this model.

REFERENCES

[1] L. Viererbl et al, “Measurement of gamma and neutron radiations inside spent fuel assemblies with passive detectors”, Nucl. Inst. and Meth. A, 652(1), 90-93(2011).

[2] M. Tribet et al, “Spent nuclear fuel/water interface behavior: Alpha dose rate profile determination for model surfaces and microcracks by using Monte-Carlo methods”, Journal of Nuclear Materials, 488(1), 245-251(2017).

Decontamination Technology of Spent Resin From PHWR

Young-Soo Jo* and Jin-Hyun Sung

HuvisWater Co., 16, Gongdan 1-daero 322beon-gil, Siheung-si, Gyeonggi-do, Republic of Korea

*jys@huviswater.com

1. Introduction

Spent resin from Pressure Heavy Water Reactor(PHWR) are stored in concrete storage tanks near the reactor. Spent resin storage tanks have been reaching saturation point due to the prolonged operation time of nuclear power reactors.

Therefore, it is necessary to develop a proper method to handle and transfer the spent resin. However, because the spent resin contains a large amount of β-nuclides(^{14}C, ^{3}H) and ɣ- nuclides(^{60}Co, ^{137}Cs), the spent resin is currently under long-term storage.

Particularly with ^{14}C, which is mainly generated from $^{17}O(n, \alpha)^{14}C$ reaction in reactor system [1], it requires proper decontamination method because it emits high radiation due to its large amount that is bond to the anion resin in $H^{14}CO_3^-$ and $^{14}CO_3^{2-}$ form.

This paper focuses on introducing the ^{14}C desorption, as well as removal, technique within the spent resin storage.

2. Experiment method

2.1 ^{14}C adsorption experiment

Before proceeding with the desorption and precipitation experiment, in order to evaluate the adsorbability of ^{14}C and produce model sample of the spent resin from PHWR, ^{14}C standard solution was added to the anion resin to measure the amount of ^{14}C within the anion resin.

2.2 ^{14}C desorption and precipitation experiment

Then, in order to desorb ^{14}C that has been bonded to the anion resin, sulfuric acid solution was used because ^{14}C gets released in gaseous form of CO_2 at low pH [1]. The core technique in decontaminating ^{14}C is desorbed in $^{14}CO_2$ form from the anion resin, collecting the generated precipitate to remove ^{14}C. Such method can be verified through two stages. First stage is about generating precipitate within $Ca(OH)_2$ aqueous solution by desorbing the ^{14}C bond to the anion resin at low pH condition, and the second stage is about assuring if the precipitation of ^{14}C from the first stage had been done properly by collecting ^{14}C from the generated precipitate. The experimental equipment was installed as below for the first stage experiment.



Fig. 1. ^{14}C desorption and precipitation equipment.

The CO_2 gas, which was generated after injecting sulfuric acid into the previously produced ^{14}C adsorption sample resin, was collected by using NaOH solution. Also, N_2 gas and vacuum pump were subsidiarily used to smooth out the flow of and minimize the external release of the generated CO_2. ^{14}C was re-collected by using the below equipment after collecting and natural drying $CaCO_3$ that was generated at the first stage.

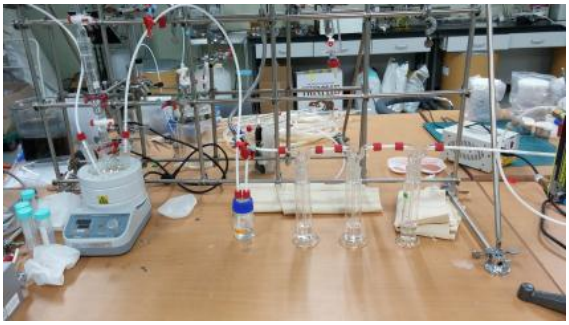


Fig. 2. Precipitate oxidation and collection equipment.

The CO_2 gas was generated by reacting $CaCO_3$ with HC1, and the generated $^{14}CO_2$ was collected with NaOH solution. The effectiveness of precipitation was verified by measuring the amount of ^{14}C within the generated $CaCO_3$ from the first experiment. Like the first experiment, in order to smooth out the flow of the generated CO_2, N_2 gas and vacuum pump were subsidiarily used.

3. Results and discussion

Table 1. Anion resin before and after the experiment; ^{14}C activity of $CaCO_3$

1st Performance	^{14}C activity(Bq)		Recovery factor
Anion Resin Before Desorption	39	Amount of Desorbed ^{14}C: 37.3	72%
Anion Resin After Desorption	1.7		
Precipitated $CaCO_3$ Powder	27		
2nd Performance	^{14}C activity(Bq)		Recovery factor
Anion Resin Before Desorption	65	Amount of Desorbed ^{14}C: 63.2	81%
Anion Resin After Desorption	1.8		
Precipitated $CaCO_3$ Powder	51.25		

As shown in the above table, the total amount of ^{14}C within the anion resin changed from 39 Bq, 65 Bq to 1.7 Bq, 1.8 Bq after the experiment, meaning that almost all ^{14}C was desorbed. Also, it was assured that ^{14}C amount within the generated precipitate is 27 Bq, 51.25 Bq, meaning that 72%, 81% of the desorbed ^{14}C was collected.

4. Conclusion

Through the desorption and precipitation experiment of ^{14}C bond to the anion resin, it was affirmed that ^{14}C can be collected by using $Ca(OH)_2$ aqueous solution, and it can be predicted that there will be considerably less amount of secondary waste than the ^{14}C adsorption using the LiOH filter.

Thus, from now on, if the spent resin from PHWR is decontaminated by applying these techniques, it will be effective towards developing the technique to dispose of and transfer spent resin with minimum amount of secondary waste.

REFERENCES

[1] Ho-Yeon Yang, besides 7, “Ion Adsorption Charateristics of IRN-150 Mixed Resin and Removal Behavior of ^{14}C”, J. of the Korea Radioactive Waste Society, 4(4), 373-384 (2006).

A Feasibility Study of the Quantification of C-14 by Photocatalytic Oxidation

Byungman Kang*, Jung Suk Kim, Jai Il Park, Hong-Joo Ahn, and Yeong-Keong Ha
Korea Atomic Energy Research Institute, 111, Daedeok-daero 989beon-gil, Yuseong-gu, Daejeon, Republic of Korea
*bkang@kaeri.re.kr

1. Introduction

The regulations of radioactive waste discharges and disposals require the radiochemical waste characterization for major radionuclides such as ^{3}H, ^{14}C, and ^{129}I, which provides important criteria for establishing disposal principles based on the concentration of radionuclides. Moreover, to identify the need for further treatment of radwastes or their suitability for storage, numerous analytical procedures have been developed for radionuclides of interest. Among those radionuclides, the determination of radioactive ^{14}C in low- and intermediate-level radwastes (LILW) has been getting more and more attention due to concerns about the radiological impacts to the environment. As ^{14}C is a pure beta emitter with a half-life of 5,730 years, it should be chemically separated from other radionuclides present in LILW for accurate quantification. Compared to non-volatile radionuclides, the successful analysis of ^{14}C relies mainly on how efficiently organic or inorganic carbon in radwastes is converted to gaseous carbon dioxide through an oxidation reaction. Although several methods have been developed for the radiochemical analysis of ^{14}C in LILW, for example, combustion, wet oxidation, and acid stripping techniques [1], it is still a challenge to determine the accurate radioactivity of ^{14}C effectively. In terms of processing time, complicated procedures including the decomposition of a sample along with the purification of ^{14}C might be considered a major obstacle to the practical application. In this study, advanced oxidation process (AOP) based on the UV light source was adopted as a promising technique for the quantification of ^{14}C in LILW via *in situ* decomposition of samples. As an initial step to demonstrate the feasibility of the proposed method, various radioactive ^{14}C standards were investigated to evaluate the recovery of ^{14}C: ^{14}C-labeled methanol ($^{14}CH_3OH$), lauric acid ($CH_3(CH_2)_{10}{}^{14}COOH$), sodium carbonate ($Na_2{}^{14}CO_3$), and toluene ($C_6H_5{}^{14}CH_3$). These compounds were oxidized with chemical oxidants such as H_2O_2 or $K_2S_2O_8$ under photocatalytic conditions, and the generated $^{14}CO_2$ was collected in Carbo-Sorb E solution. The individual solution was then mixed with a scintillation cocktail and counted using a liquid scintillation counter (LSC).

2. Methods and Results

2.1 Photocatalytic oxidation

Photocatalytic oxidation of organic or inorganic carbon was carried out in an immobilized batch reactor. Fig. 1 describes a schematic diagram of the UV photo-reactor. A cylindrical photo-reactor made of borosilicate glass with capacity of about 250 mL was employed with water circulation arrangement to maintain the temperature below 30°C. The UV lamp (131 mm arc length) was mercury 450 W with the wavelength range of 280 ~ 400 nm. It was inserted symmetrically into the reactor and immersed directly in the solution. In a preliminary study for the optimization of photocatalytic reaction, non-radioactive lauric acid was chosen as the target organic compound, and mixed with $K_2S_2O_8/AgNO_3$ or H_2O_2 oxidant in an acidic solution. To evaluate the effect of reaction parameters on the decomposition of lauric acid, the corresponding lauric acid in aqueous solution was extracted with HPLC grade ethyl acetate (EtOAc) and then analyzed using GC-FID with an external standard of myristic acid. In the case of radioactive compounds, the resulting gaseous $^{14}CO_2$ was trapped by Carbo-Sorb E solution with a supply of nitrogen carrier gas, followed by the measurement of its radioactivity using LSC.

2.2 Quench calibration for C-14 measurement

To determine the counting efficiency from the quench levels obtained during ^{14}C counting, 14,878 Bq of a ^{14}C standard (Packard) were each placed into 10 scintillation vials. Subsequently, both 10 mL of Carbo-Sorb E and 10 mL of Permafluor E+ were added to the above vials. As a quenching agent, nitromethane (CH_3NO_2), was finally added in the range of 0 ~ 200 μL. A quench indicator, in which the gamma activity of ^{133}Ba was used as a standard to monitor external quenching prior to application, was adjusted to the transformed spectral index of external

standard (tSIE/AEC) mode. In the resulting quench correction curve, as the amount of CH_3NO_2 was increased, we confirmed that the quench level was increased while the counting efficiency was decreased. Furthermore, an increase in the counting efficiency was observed with an increase in the tSIE.

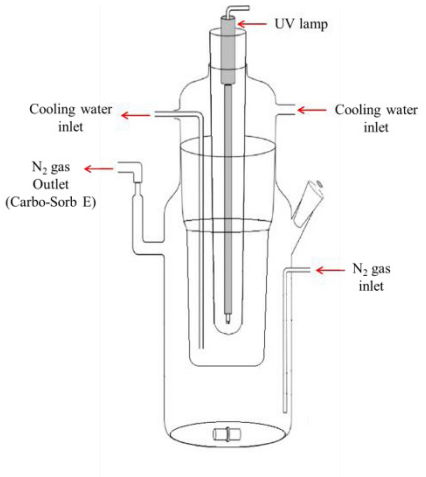


Fig. 1. Schematic diagram of UV photo-reactor.

2.3 Minimum detectable activity (MDA)

The MDA (Bq/g) for radioactive ^{14}C samples is determined as follows [2]:

$$MDA = \frac{2.71+4.65\sqrt{C_b T_b}}{E_{ff} \times V_s \times T_s \times 60} \quad (1)$$

Where E_{ff} is the counting efficiency of LSC, V_s is the sample weight (g), C_b is the background count rate, T_s is the sample counting time, and T_b is the background counting time. As shown in Eq. (1), the MDA can be decreased by increasing the counting efficiency, sample weight, and sample counting time. Using these parameters and the maximum allowable weight of simulated samples, MDA of ^{14}C for the proposed photocatalytic oxidation can be calculated from Eq. (1). Table 2 provides MDA results for different amount of simulated ^{14}C resins, which were obtained using the LSC parameters shown in Table 1. When the maximum 20 g of sample was applied, MDA of the ^{14}C radionuclide was 8.6×10^{-4} Bq/g.

Table 1. LSC parameters for the calculation of MDA

Radionuclide	E_{ff}	C_b (cpm)	T_b (min)	T_s (min)
^{14}C	0.91	1	30	30

Table 2. MDA of ^{14}C for different amount of simulated resins

Sample	Weight (g)	MDA (Bq/g)
Simulated resins	5	3.4×10^{-3}
	10	1.7×10^{-3}
	20	8.6×10^{-4}

2.4 C-14 measurement

From the result of recovery rate for various inorganic and organic ^{14}C standards, it was identified that the overall recoveries of ^{14}C were above 90%. However, toluene was found to be difficult to decompose due to the absence of an activating group such as hydroxyl on benzene ring.

3. Conclusion

UV-assisted photocatalytic reaction was optimized and evaluated using various ^{14}C standards for the application to determine the ^{14}C concentration in LILW. During the photocatalytic oxidation, inorganic and organic ^{14}C compounds were found to be efficiently oxidized and separately recovered with yields above 90%. Furthermore, the corresponding data were compared with those of reported wet-oxidation method.

REFERENCES

[1] Å. Magnusson, K. Stenström, and P.-O. Aronsson, "^{14}C in spent ion-exchange resins and process water from nuclear reactors: A method for quantitative determination of organic and inorganic fractions", Journal of Radioanalytical and Nuclear Chemistry, 275(2), 261-273 (2008).

[2] H. J. Ahn, B. C. Song, S. C. Shon, M. H. Lee, K. Song, and K. Y. Jee, "Application of a wet oxidation method for the quantification of ^{3}H and ^{14}C in low-level radwastes", Applied Radiation and Isotopes, 81, 62-66, 2013.

Reaction Characteristics of $CsNO_3$ by Different Adsorbents

Dasom Yang*, Jinmyeong Shin, and Sangho Na

Korea Atomic Energy Research Institute, 111, Daedeok-daero 989beon-gil, Yuseong-gu, Daejeon, Republic of Korea

*dsyang@kaeri.re.kr

1. Introduction

Semi-Volatile cesium(Cs) can be released during the operation of radioactive waste incineration and melting of radioactive metal waste at nuclear facilities. Cs is the most significant semi-volatile fission product which is highly radioactive and heat generating fission product. Cs is very leachable under disposal environment. ^{134}Cs, ^{135}Cs and ^{137}Cs are radioactive isotopes, ^{135}Cs has a long half-life of about 2.3×10^6 years, while ^{134}Cs has a short half-life of about 2years. ^{137}Cs has an intermediate half-life of 30.2years. Among these isotopes, ^{137}Cs is a major concern because of its high abundance, intense gamma radiation and high heat generation.

Cesium oxide can be readily incorporated into aluminosilicate compounds by thermal reaction, and the resulting cesium aluminosilicate compounds are stable. This stability of cesium in aluminosilicate structures may be exploited in the fixation of nuclear waste, by the trapping radioactive cesium into stable cesium aluminosilicate phases.

This study was carried out to analyze the reaction characteristics of $CsNO_3$ with sintered kaolin, fly ash and pyrophyllite, respectively.

2. Experimental

Kaolin, fly ash and pyrophyllite were sintered at 1,150℃ for 2 hours, cooled and powdered for the experiment. The analyzed particle size of kaolin, fly ash, pyrophyllite used in this study is around 0.15 mm (200 mesh), 0.2~0.35 mm (70 mesh), 0.15 mm (200 mesh), respectively. The particle size of $CsNO_3$ (Sigma Aldrich) is 0.2 ~0.35 mm (70 mesh). The reaction experiments of $CsNO_3$ with sintered kaolin, fly ash and pyrophyllite were maintained at 1,000℃ for 3 hours under air condition. Melting point of $CsNO_3$ is 414℃ and it begins to volatilize near at 700℃. And 98% of $CsNO_3$ is volatilized.

The $CsNO_3$ and kaolin, fly ash and pyrophyllite were mixed with Cs, Al and Si in the mole ratio of 1:1.02:1.07, 1:1.02:1.76, 1:1:3.60, respectively.

The trapping quantity of cesium on adsorbents and weight change were calculated as follows.

Table 1. Reaction quantity of cesium on different adsorbents

Adsorbent	Before reaction(g)	After reaction(g)	Reaction quantity (g-Cs/g-adsorbent)
Kaolin	1.5593	1.2511	0.78
Fly Ash	1.5272	1.2678	0.45
Pyrophyllite	1.5390	1.3427	0.34

The weight loss of before and after reaction of kaolin is 19.5%, fly ash is 17% and pyrophyllite is 12.8%. Based on these results, the reaction quantity of kaolin, fly ash and pyrophyllite is 0.78 g-Cs/g-kaolin, 0.45 g-Cs/g-fly ash, 0.34 g-Cs/g-pyrophyllite, respectively. As shown in Table 1, reaction quantity of cesium indicated the formation of cesium aluminosilicate compounds of three adsorbents exposed to cesium vapors.

In this study, to confirm the presence of cesium reacted with adsorbent, cesium peak is analyzed by XRD (X-Ray Diffraction Analyzer). The XRD was applied to analyze the phases of the reaction product. The scanning rate was 0.2°/min and the angle, 2θ, was within the range of 10° to 90°.

The cesium reaction product of sintered kaolin gave XRD peaks that indicate Cs-nepheline ($CsAlSiO_4$) and pollucite ($CsAlSi2O_6$) phases as shown in Fig. 1. As shown in Fig. 1, XRD pattern confirmed that Cs-nepheline ($CsAlSiO_4$) phase was mainly formed.

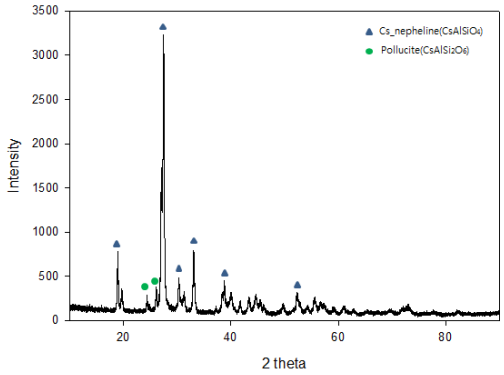


Fig. 1. X-ray diffraction patterns of cesium reaction product of sintered kaolin.

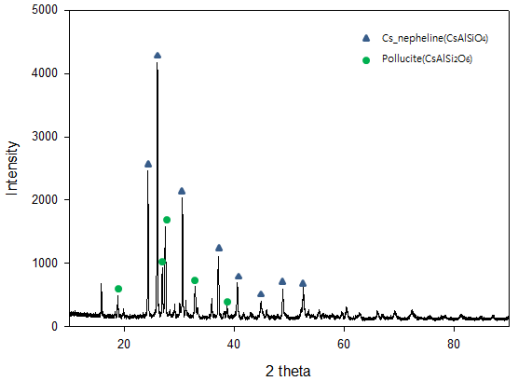


Fig. 2. X-ray diffraction patterns of cesium reaction product of sintered fly ash.

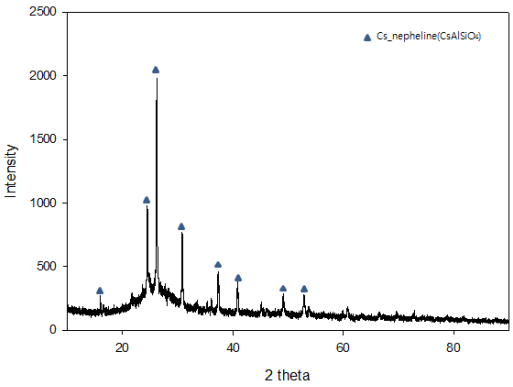


Fig. 3. X-ray diffraction patterns of cesium reaction product of sintered pyrophyllite.

Fig. 2 shows the XRD pattern of the cesium reaction product of sintered fly ash. The XRD pattern confirmed pollucite phase and Cs-nepheline phase were formed.

Fig. 3 shows the X-ray diffraction patterns of cesium reaction product of sintered pyrophyllite. The XRD pattern confirmed the existence and the crystal structure of the single phase Cs-nepheline.

The SEM image results are shown in Fig. 4. SEM image indicates that sintered kaolin has platy particles stuck to together to form agglomerates and irregular shapes (Fig. 4(a)). SEM image also indicates that sintered kaolin reacted with $CsNO_3$ is bulky crystals with a rough surface (Fig. 4(b)).

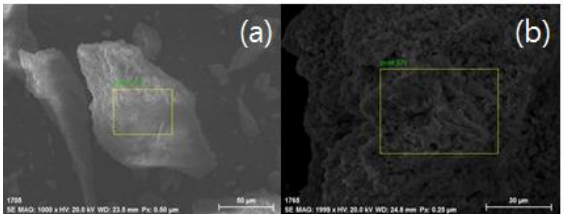


Fig. 4. (a) SEM image of sintered kaolin, (b) SEM image of sintered kaolin after reaction with cesium.

3. Conclusion

Reaction characteristics of $CsNO_3$ with sintered kaolin, fly ash and pyrophyllite were studied respectively. The high trapping quantity of these sintered adsorbents is believed to due to the formation of pollucite ($CsAlSi_2O_6$) phase and Cs-nephline ($CsAlSiO_6$) of the reaction products. Because of their high performance, easy availability and low cost, kaolin, fly ash and pyrophyllite are expected to be utilized as adsorbents for trapping gaseous cesium.

REFERENCES

[1] J.J. Park, J.M. Shin, M.S. Yang, K.S. Chun, H.S. Park, “Trapping characteristics for gaseous cesium generated from different cesium compounds by fly ash filter”, IAEA-SM-357/71.

Study on Vitrification of Slag From Metal Melting Process

Mi-hyun Lee*, Young Hwan Hwang, Seok Ju Hwang, Cheon-Woo Kim
KHNP CRI, 70, 1312-gil, Yuseong-daero, Yuseong-gu, Daejeon, Republic of Korea
*mihyun.lee@khnp.co.kr

1. Introduction

More than 90% of the wastes generated during nuclear dismantling are metal waste. Most of radioactive metal waste is carbon steel and stainless steel. Since these metal wastes are bulky, effective volume reduction techniques are required. One of the effective methods is melt decontamination [1], [2]. However, slag, which is a secondary waste, is generated during the melting decontamination process. And it has high melting temperature and is difficult to handle. In this study, vitrification using iron phosphate glass was studied to lower the melting point of slag and effectively treat it.

2. Experiment

2.1 Carbon Steel Melting Test

The sample used in the experiment is carbon steel. The melting point of carbon steel is 1430℃. Alumina crucibles were used to melt the samples in the furnace. The temperature of furnace was increased to 1550℃ with 10℃/min.

2.2 Slag Analysis Method

XRD and SEM/EDS analysis were performed to analyze the chemical composition and crystallinity of the slag.

2.3 Vitrification of Slag Using Iron Phosphate Glass

Alumina crucibles were used to melt the raw chemical ($FeO:P_2O_5$ = 0.5:0.5) in the furnace The temperature of furnace was increased to 1150℃ with 10℃/min. After melting for two hours, glass was mixed using quartz rod. After that was poured the glass into the graphite mold.

3. Result

3.1 Carbon Steel Melting Test Result

Fig. 1 shows of carbon steel before and slag after melting.



Fig. 1. Carbon steel before melting(left) and slag after melting(right).

3.2 Slag Analysis Result

The SEM/EDS analysis of slag is shown in Fig. 2. Fig. 2 indicates that the slag is consisted of FeO and Al_2O_3. It seems that Al_2O_3 is diffused from the crucible.

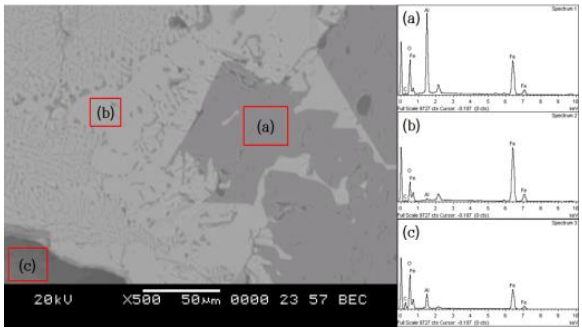


Fig. 2. SEM/EDS image of slag.

The XRD analysis shown in Fig. 3 indicated that the slag is consisted of 90% of FeO and 10% of Fe_3O_4. Since the physical properties, such as melting temperature, structure, etc., strongly depends on the oxidic state of Fe, accurate analysis of chemical species of Iron oxide is important.

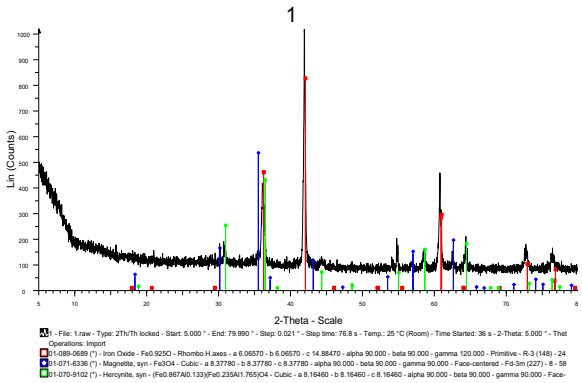


Fig. 3. X-Ray Diffraction of slag.

3.3 Characterization of Iron Phosphate Glass

Discharge was fair when the glass was poured into the graphite mold as shown in Fig. 4 (a), and the raw chemical was fairly dissolved in visual appearance as shown in Fig. 4 (b). The prepared glass was visually smooth on the surface and homogeneous as shown in Fig. 4 (c).

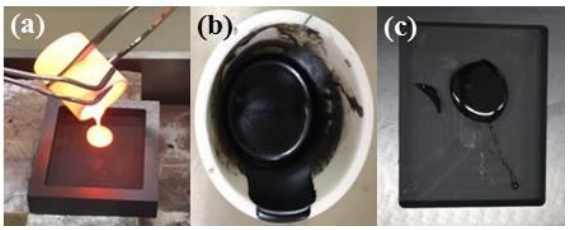


Fig. 4. (a) Glass pouring, (b) Crucible, and (c) Fabricated glass.

According to the evaluation of surface homogeneity through SEM/EDS analysis of Iron phosphate glass, a very homogeneous glass phase was analyzed as shown in Fig. 5. A homogeneous glass phase with Fe and P as the main composition was observed according to Fig. 5.

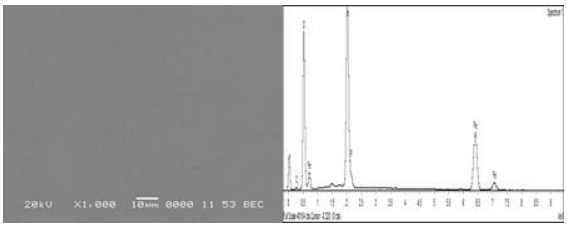


Fig. 5. SEM/EDS image of Iron phosphate glass.

4. Conclusion

When dismantling nuclear power plants, a large amount of carbon steel waste is generated. The main component of the slag generated during the carbon steel melt decontamination is FeO. Since the primary chemical species of slag was FeO, the Iron phosphate, which enables high waste loading, was studied for the vitrification of slag. As a result of the production of the iron phosphate glass to vitrify the slag, the experiment was successfully carried out. The physical and chemical properties of the resulting glass will be examined and a vitrification feasibility study will be conducted.

REFERENCES

[1] Hopkinson, K. L., Bishop, A., Cross, M. T., Harrison, J. and Selgas, F. (1998) Recycling and reuse of radioactive material in the controlled nuclear sector, EUR18041EN, European Commission.

[2] Nieves, A. and Tilbrook, R. W. (1996) Potential radioactive scrap metal quantities from Nuclear power plants worldwide, Radwaste, Vol. 3, No. 1, pp. 45-53.

Study on Long-term Performance of Reinforcing Concrete Structures in Subsurface Environment

Ki-jung Kwon*, Hyun-jin Cho, and Jung-hyun Yoon

Korea Radioactive Waste Agency, 168 Gajeong-ro, Yuseong-gu, Daejeon 34129, Republic of Korea

*kjkwon@korad.or.kr

1. Introduction

Concrete is one of the most widely used materials for the construction of structures, and concrete structures have been considered to be durable with large life.

In a LILW disposal facility located in subsurface environment, a silo concrete plays an important role to limit the release of radionuclides from the silo geosphere. However, the performance of the concrete structure decrease over a period of time because of several physical and chemical processes. After a long period of time in the future, the concrete would lose its effectiveness as a barrier against groundwater inflow and the release of radionuclides.

Although a number of process are responsible for the degradation of the silo concrete, it is concluded that a reinforcing steel corrosion cause the failure of the silo concrete. Hence, a concrete silo failure time is calculated based on a corrosion initiation time which takes for chloride ions to penetrate through the concrete cover, and a corrosion propagation time. This paper aims to analyze the concrete failure time in the Wolsung Low- and intermediate-level wastes Disposal Center (WLDC)

2. Design of concrete silo

The detail design information of concrete silo is shown in Table 1.

Table 1. Design information of concrete silo

Silo diameter	Silo length	Diameter of Reinforcing steel	Cover depth Of concrete
26.8 m	57.1 m	43 mm	100 mm

3. Degradation process for concrete

3.1 Sulfate attack

Through a chemical reaction, sulfate ion penetrates into the surface of concrete and weakens the concrete wall. The model for sulfate attack was already proposed by Atkinson and Hearne [1]. The degradation rate of concrete from sulfate attack is estimated by:

$$R = \frac{EB^2 c_0 C_E D_0}{\alpha\gamma(1-\nu)} \qquad (1)$$

Where, B is linear strain caused by one mole of sulfate reacted in 1 m^3 (1.8E-6 m^3/mol), c_0 is sulfate concentration in water (mol/m^3), C_E is concentration of reacted sulfate as ettringite (mol/m^3), D_0 is intrinsic diffusion coefficient (m^2/s), E is Young's modulus (20 GPa), α is roughness factor for fracture path (assumed to be 1.0), γ is fracture surface energy of concrete (10 J/m^2), ν is Poisson's ratio (0.3), and the rate of degradation, R, is in (m/y). The concentration of sulfate (c_0) in groundwater was measured at 119 mg/L. However, in the estimation of sulfate attack, 1,190 mg/L of sulfate concentration was applied for a conservative estimation.

3.2 Calcium hydroxide leaching

A shrinking core model proposed by Atkinson and Hearne [2] is adopted here. The model assumes the calcium removal from concrete exterior is rapid compared to the movement of calcium through the concrete. Thus, the transport of calcium in the concrete is controlled by diffusion. The depth into the concrete affected by Ca removal is then given by:

$$X = \left(2D\tau\emptyset\frac{C_t - C_{gw}}{C_b}\right) \qquad (2)$$

Where, D is the diffusion coefficient of Ca^{2+} ions in concrete (m^2/s), τ is the tortuosity factor (-), $\emptyset$ is the porosity (-), C_t is the concentration of Ca^{2+} ion in the pore space (mmol/kg), C_{gw} is the concentration of Ca^{2+} in groundwater (mmol/kg), and C_b is the bulk concentration of Ca^{2+} ions in solid concrete (mmol/kg).

3.3 Corrosion of reinforcing steel

There are several mathematical models available to predict the chloride diffusion in concrete, based on varying levels of simplifying assumptions. The commonly used ones are presented below:

Fick's second law of diffusion deals with one-dimensional diffusion [3] and given by,

$$\frac{\partial C}{\partial t} = D\frac{\partial^2 C}{\partial x^2} \qquad (3)$$

For one-dimensional flow into a semi-infinite medium a closed-form solution can be derived for equation (3) as follows,

$$C(x,t) = C_0\left(1 - erf\frac{x}{2\sqrt{Dt}}\right) \qquad (4)$$

Where, C(x,t) = concentration at depth x (m), at time t (% by mass); t = time of exposure(seconds); C_0 = surface chloride concentration (% by mass); D = constant diffusion coefficient (m^2/s); *erf* = error function.

The equation (4) can be used only if the diffusion coefficient, *D*, and surface chloride concentration, C_0 remain constant during the time of diffusion. It has been shown by previous researchers that these conditions do not apply in practical conditions. The equation (1) can be modified to take account of the variation of *D* with time as shown by Crank:

$$\frac{\partial C}{\partial t} = D(t)\frac{\partial^2 C}{\partial x^2} \qquad (5)$$

The reinforcing steel starts to corrode after depassivation process of passive of passive film. US DOE assumed that a concrete vault fails completely once 50 volume percent of the reinforcing steel has corroded.

Korean Concrete Institute (KCI) reviewed the US DOE approach applying strength design method to calculate the mineral volume of the reinforcing steel for the structure safety of the reinforcing steel for the structure safety of the silo concrete. KCI concluded that the US DOE approach is conservative for the estimation of failure time of the silo concrete.

The US DOE [2] applied a conservative corrosion rate of 10^{-5} m/y to calculate a corrosion propagation time. Under the pore water conditions of the silo concrete, the corrosion rate of the reinforcing steel was reported to be in the range of 10^{-8} to 10^{-9} m/y. However, a corrosion rate of 10^{-5} was applied in the estimation of a corrosion propagation time in the WLDC.

50 volume percent of the reinforcing steel was also used to determine complete failure of the concrete silo in the WLDC based on the KCI review on the US DOE approach.

In this model service life of reinforcing steel is divided into two parts initiation and propagation. Initiation time means time required to initiate the corrosion when chloride concentration of the concrete reaches to its threshold value. The next stage is degradation when delamination, cracking and spalling of the concrete occur [3].

4. Conclusions

The concrete silos were initially assumed to be intact and have low permeability. The effects of sulfate and magnesium attack, calcium hydroxide leaching, and the corrosion of reinforcing steel were analyzed on the degradation of concrete in WLDC.

Groundwater samples were collected from the disposal site to estimate the amounts of sulfate, chloride, dissolved oxygen (DO) and other ions. In the sulfate attack process, the concrete degradation rate was calculated to be 1.313E-2cm/y. For the concrete thickness of 100 cm in the disposal silo, this rate is negligible over 3,800 years, and, therefore, sulfate attack is assumed to be negligible for this analysis.

In the model of calcium hydroxide leaching, the Ca^{2+} concentration in the concrete was calculated to be 15.7 mmol/kg. After 5,000 y, the depth of calcium hydroxide leaching is estimated to be approximately 3 cm.

Hence, it is concluded that this mechanism is negligible over 80,000 y for the disposal facility.

In the evaluation of Eq. (5), it is unveiled that the degradation rate of the concrete silo due to chloride attack is much faster than the rates estimated from sulfate attack and calcium hydroxide leaching.

Based on the DOE approach which estimated that concrete fails completely once 50 volume percent of the reinforcing steel corrodes, a corrosion propagation time was calculated to be 640 y, which is the time it takes for corrosion to penetrate 0.640 cm of the reinforcing steel.

In addition to the corrosion propagation time, a diffusion equation was used to calculate a corrosion initiation period. A corrosion initiation time was calculated to be 1,284 y, after closure of the WLDC when added to the 640 y corrosion propagation period.

REFERENCES

[1] A. Atkinson and J.A. Hearne, Mechanistic models for the durability of concrete barriers exposed to sulfate-bearing groundwater, Vol. 176, p. 149, 1990.

[2] US DOE, The US DOE Idaho National Laboratory Site DraftSection 3116 Waste Determination For Idaho Nuclear Technology And Engineering Center Tank Farm Facility, 2006.

[3] ACI, 2000, ACI 365R, Service –Life Prediction.

Estimation of Centerline Temperature of the Rare Earth Glass Waste Form

Jung-Hoon Choi*, Tae-Kyo Lee, Ki-Rak Lee, Seung-Youb Han, Na-Young Kim, Seon-Ah Jang, and Hwan-Seo Park
Korea Atomic Energy Research Institute, 111, Daedeok-daero 989beon-gil, Yuseong-gu, Daejeon, Republic of Korea
*mrchoijh@kaeri.re.kr

1. Introduction

High level glass waste forms are to be stored in the storage building before final disposal. The waste form storage vault should be operated using mechanically induced cooling system to remove the decay heat preventing overheat of the vault and devitrification of glass waste form in the canister [1,2]. However, even with the air cooling system in the storage vault, when the waste loading of heat generative nuclides are high, the centerline temperature of a glass waste form could exceed its glass transition temperature, leading to the increase of leaching rate of radioactive nuclides due to the devitrification of glass waste form [3]. Therefore, the estimation of centerline temperature of glass waste form for each waste stream is very essential in the period of storage. Here, the centerline temperature of rare earth glass waste form generated from pyrochemical process has been estimated [4].

2. Experimental

2.1 Fabrication of rare earth glass waste form

The rare earth glass waste form was fabricated using a SiO_2-Al_2O_3-B_2O_3 glass frit and Nd_2O_3/Gd_2O_3 as a surrogate waste material of rare earth fission products. For a vitrification of mixed oxides, the crucible was heated to 1,450°C with a heating rate of 6°C/min and maintained at 1,450°C for 4 hours. Thermal conductivity that is required in the centerline temperature calculation was measured using NETZSCH-LFA457 under an Ar atmosphere with a sample size of 12.7 mm in diameter and 2 mm in thickness.

2.2 Centerline temperature calculation

Centerline temperatures of waste forms for each transuranic elements (TRU) recovery ratio in the electrowinning process of the pyrochemical process were calculated using steady-state conduction equation (see equation (1) and (2)) in a long and solid cylinder with uniform heat generation and constant thermal conductivity. The heat generations of the waste form for each TRU recovery ratio were calculated using ORIGEN-S code.

$$\frac{1}{r}\frac{\partial}{\partial r}\left(kr\frac{\partial T}{\partial r}\right)+\frac{1}{r^2}\frac{\partial}{\partial \phi}\left(k\frac{\partial T}{\partial \phi}\right)+\frac{\partial}{\partial z}\left(k\frac{\partial T}{\partial z}\right)+\dot{q}=\rho c_p\frac{\partial T}{\partial t} \quad (1)$$

$$T_c = T(r=0) = \frac{-A+\sqrt{A^2+2B\left(AT_S+\frac{B}{2}{T_S}^2+\frac{\dot{q}}{16}D^2\right)}}{B} \quad (2)$$

3. Results and Discussion

During the pyrochemical process, TRUs could be involved in the rare earth waste owing to the TRU recovery ratio (hereafter TRR) in the electrowinnng process. The nuclide formulation of each waste form after electrowinning process was calculated according to the TRR, where TRR-100 indicates 100% TRU recovery ratio. TRR-99, TRR-95, TRR-90, TRR-85, and TRR-80 indicate TRU recovery ratio of 99%, 95%, 90%, 85%, and 80%, respectively.

The centerline temperatures of each waste form having 0.3 m diameter were calculated according to the scheme in Fig. 1 and the results are summarized in Table 1. In case of TRR-100, when there are no TRUs in the rare earth waste, the centerline temperature was 138.34°C at the initial stage of storage. The centerline temperature was increased according to the decrease of TRU recovery ratio, however, even the TRR-80 case showed the centerline temperature of 201.62°C, which is far below the glass transition temperature of the rare earth glass waste form (T_g=769.46°C). Therefore, it is concluded that thermal stability of waste form in case of 0.3 m diameter is not affected by the TRU recovery ratio (even with the TRR-80 case) in the electrowinning process.

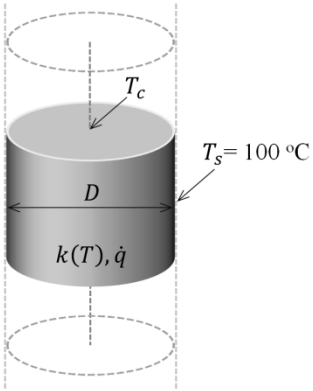


Fig. 1. Scheme of centerline temperature (Tc) calculation (Ts :surface temperature, k: thermal conductivity, q: heat generation, D: diameter).

Table 1. Centerline temperatures of the rare earth glass waste form with 0.3 m diameter

Year	Centerline temperature of the waste form [°C]					
	TRR-100	TRR-99	TRR-95	TRR-90	TRR-85	TRR-80
0.3	138.34	142.09	156.36	172.77	187.80	201.62
1	135.59	139.34	153.64	170.08	185.14	198.98
3	129.35	133.10	147.41	163.86	178.92	192.77
10	116.04	119.71	133.72	149.83	164.57	178.13
30	103.18	106.45	118.95	133.34	146.54	158.70
100	100.03	102.34	111.20	121.45	130.88	139.61
300	100.00	101.36	106.56	112.60	118.19	123.38
1000	100.00	100.55	102.65	105.11	107.40	109.53

4. Conclusion

In order to determine thermal stability of the waste form immobilizing rare earth waste generated from the electrowinning process of the pyrochemical process, the centerline temperature of the rare earth glass waste form was calculated using steady-state conduction equation in a long and solid cylinder type waste form of constant thermal conductivity and uniform heat generation. To verify the effects of TRU content in the rare earth waste on the centerline temperature, the TRU recovery ratio (TRR) was varied from 80% to 100%. It was revealed that thermal stability of waste form in case of 0.3 m diameter was not affected by the TRU recovery ratio in the electrowinning process, meaning that the waste form size is thermally reasonable due to the low centerline temperature being far below the glass transition temperature of the rare earth glass waste form.

REFERENCES

[1] R. Rainisch, Alternative design concept for the second glass waste storage building, WSRC-TR-92-466 (1992) 1-23.

[2] B.J. Hardy, Temperatures in DWPF glass waste storage building, WSRC-RP-93-1177 (1993) 1-10.

[3] D.B. Spilman, L.L. Hench, D.E. Clark, Devitrification and subsequent effects on the leach behavior of a simulated borosilicate nuclear waste glass, Nucl. Chem. Waste Man. 6 (1986) 107-119.

[4] J.H. Choi, H.C. Eun, T.K. Lee, K.R. Lee, S.Y. Han, M.K. Jeon, H.S. Park, D.H. Ahn, J. Nucl. Mater. 483 (2017) 82-89.

Thermogravimetric Analysis on External Wall Coating Material of Cold Crucible Induction Melter

Young Hwan Hwang*, Seokju Hwang, Mi-Hyun Lee, and Cheon-Woo Kim

KHNP-CRI, 70, 1312-gil, Yuseong-daero, Yuseong-gu, Daejeon, Republic of Korea

*yhhwang7@khnp.co.kr

1. Introduction

The cold crucible induction melter (CCIM) of HanUl Vitrification Facility (UVF) consists of 48 sectors with mica sheet spacers. The temperature of external wall maintains designed temperature with help of cooling water system, while the temperature of melted glass in the CCIM is 1,100~1,200°C. The mica spacer, located between the sectors, attributes the electrical insulation of the sectors and mechanical flexibility of the CCIM. The external wall coating material maintains the physical structure of the CCIM and obstructs the emission of internal heat energy transfer, as shown in Fig. 1.

The composite structure, hybrid structure of glass fabric and chemical, is usually used for the fabrication of external wall coating to achieve both mechanical strength and high temperature resistivity.



Fig. 1. Photo of external wall coating material of CCIM.

2. Experiment

2.1 General information

The glass fabric and chemical, usually epoxy or silicon resin, based composite structure is used for external wall coating materials. Since the primary object of coating material is the obstruction of high thermal energy from the melted glass, the selection of suitable coating material with good heat resistance is important.

In this study, the thermal property of the glass fabric and chemical based composite structures were studied.

2.2 Fabrication of glass fabric and epoxy composite structure

The epoxy, bisphenol A type, resin and curing agent were mixed for 0.5 hr with adequate mixing ratio. The prepared glass fabrics (W/L=5/10 cm) were immersed for 0.5 hr to achieve sufficient surface reaction. And they were dried for 24 hrs at the ambient atmosphere as shown in Fig. 2.

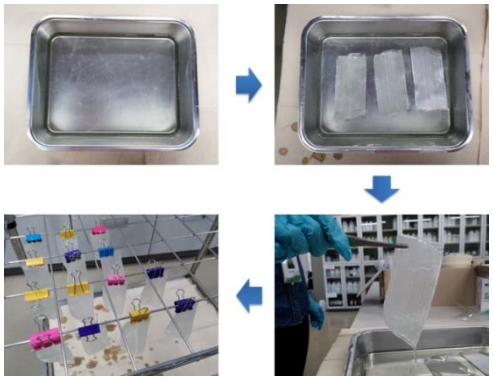


Fig. 2. Fabrication of glass fabric and epoxy composite structure.

2.3 Fabrication of glass fabric and silicon composite structure

The silicon resin for heat resistance purpose was manually coated on the prepared glass fabrics (W/L=5/10 cm) at the room temperature. Since the viscosity of the silicon resin is far higher than epoxy resin, the previous immersion method was not applicable for the silicon coating. The coated samples were dried for 24 hrs as shown in Fig. 3.

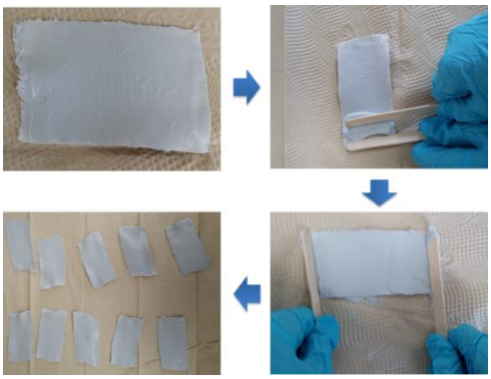


Fig. 3. Fabrication of glass fabric and silicon composite structure.

3. Discussion

The designed operation temperature of CCIM external wall surface is around 110°C. Since the heat conduction in inorganic material is lower than metal, it was suggested that the standard temperature for analysis is 150°C. All the thermogravimetric analysis (TGA) was repeated 3 times for accurate characterization. The measurement condition of TGA is O_2/N_2 atmosphere with 10°C/min (30~800°C).

3.1 TGA of glass fabric

The TGA of glass fabric, shown in Fig. 4, indicates that the glass fabric is thermally stable under 800°C. The gradual weight loss was observed from 200 to 800°C. It seems that the weight loss of 1.47% is originated from surface coating of glass fiber for the separation and synthesis of fabric [1].

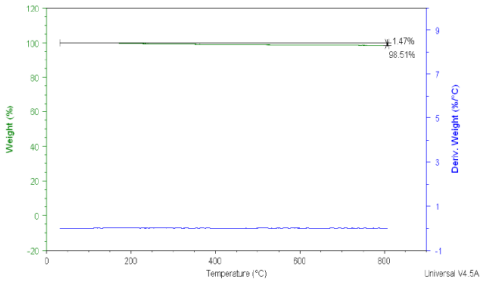


Fig. 4. TGA of glass fabric.

3.2 TGA of glass fabric and epoxy composite

The TGA of glass fabric and composite is shown in Fig. 5. The result indicates that all the organic materials convert to CO_2 and evaporate, when the temperature reaches 650°C. The weight loss ~100°C is attributed to thermal decomposition of thermally unstable carbon related component.

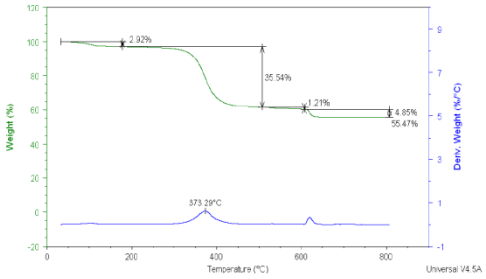


Fig. 5. TGA of glass fabric and epoxy composite structure.

3.3 TGA of glass fabric and silicon composite

The TGA of glass fabric and composite is shown in Fig. 6. It is generally known that the functional group, attached to the silicon, determines the property of the silicon resin. The composite is stable until the temperature reaches 200°C. It seems that the carbon based functional groups are gradually decomposed, above 200°C. According to the analysis, the glass fabric and silicon composite is thermally stable at ~110°C, designed operation temperature of CCIM external wall.

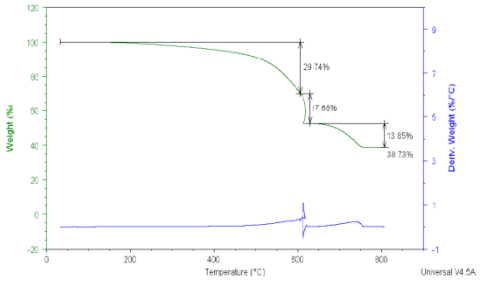


Fig. 6. TGA of glass fabric and silicon composite structure.

4. Conclusion

The glass fabric and chemical, epoxy and silicon resin, composite was studied for the application of external wall coating materials for CCIM. The TGA of composites indicated that the glass fabric and heat resistance silicon composite was stable until the temperature reaches 200°C.

REFERENCES

[1] Soo Lee, “Modification of Glass Fiber Bundle with Functionalized Coupling Agent and Phenolic Resin”, Journal of the Korean Oil Chemistry Society, 33(1), 168-175 (2016).

Study on Thermal-Flow Analysis of the Cold Crucible Induction Melter

Seokju Hwang*, Young Hwan Hwang, Mihyun Lee, and Cheon-Woo KIM
KHNP-CRI, 70, 1312-gil, Yuseong-daero, Yuseong-gu, Daejeon, Republic of Korea
*hsjhhhhh@khnp.co.kr

1. Introduction

Vitrification has been developed to treat radioactive wastes and considered a promising technology that can be applied to enhance the safety of radioactive waste disposal and to reduce the volume of radioactive wastes.

For efficient use of the vitrification technology, there is a need to perform academic research with the aim of establishing the optimum operating conditions for vitrification facility and determining the heat flow characteristics inside the Cold Crucible Induction Melter (CCIM) for acquiring high-quality vitrified solids.

2. Thermal-Flow Analysis

2.1 Analysis strategy

Thermal-Flow Analysis in the FLUENT 15.0. Under the presumption of abnormal state and incompressible flow, the volume of fluid (VOF) model, and standard k-ε turbulence model were applied to simulate the bubble behavior, molten glass and interface.

2.2 Assumptions for Efficient CFD analysis

Since the difference in electrical conductivity within the solid parts of the CCIM, melted glass, air, and water is very large, numerous grids are required for the accurate calculation of the temperature gradient and electrical conductivity gradient.

The effect of electromagnetic field from a coil to melted glass in CCIM is magnificent, while the effect to water and air is negligible.

The height of bubbler is not considered. Although the diameter of bubbler is only 3.6% of the CCIM diameter, the consideration of height bubbler doubles the number of grids.

The input height of the sparger was 200 mm in this study for the efficient calculation. Many case studies have proven that the height of the sparger has negligible influence on the temperature and electromagnetic field distribution.

The domain and grid configuration of CCIM in this study is shown in Fig. 1 and Fig. 2.

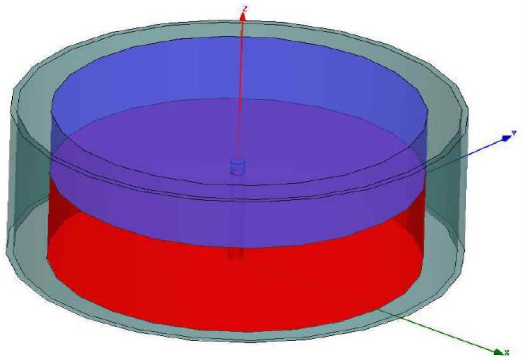


Fig. 1. Modeling of CCIM.

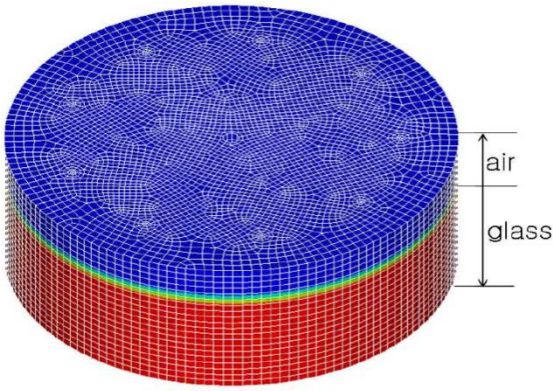


Fig. 2. Grid configuration of CCIM.

In the initial setup, the molten glass was placed from the bottom to the height of 0.15 m, and the air was placed from the height of 0.15 m and 0.3 m. For the analysis, around 3 million unstructured grids were used.

2.3 Analysis Conditions

The heat transfer by the electromagnetic field inside the CCIM was ignored in this study for the efficient calculation. In an actual CCIM, however, an electromagnetic field is induced by the current flowing through the coil and the temperature of molten glass increases. To solve the disagreement, the initial temperature was set as actual internal temperature of CCIM, which is 1150°C. Fig. 3 shows the initial temperature distribution used in this study. The physical properties and boundary conditions used in this study are shown in Table 1 and Table 2.

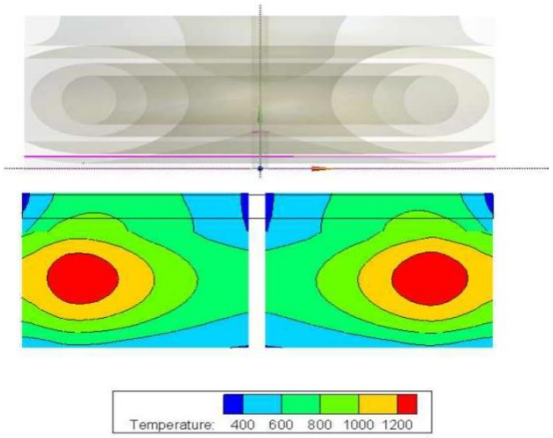


Fig. 3. Initial temperature distribution (y-section).

Table 1. Physical properties of the air and glass

	Density (kg/㎥)	Cp (j/kg·K)	Thermal Conductivity (W/m·K)	Viscosity (kg/m·s)	Molecular Weight (kg/kgmol)
Air	1.225	1006.23	0.0242	1.7894e-5	28.966
Glass	2350	1290	3	4.278	69.62

Table 2. Boundary conditions for interfaces

	Interface	Bottom Wall	Side Wall Air	Side Wall Glass
Heat Transfer Coefficient	80 W/m^2·K	300 W/ m^2·K	80 W/ m^2·K	30 W/ m^2·K
Free Steam Temperature	30℃	24℃	30℃	30℃

Fig. 4 shows the dimensions and boundary conditions of the CCIM.

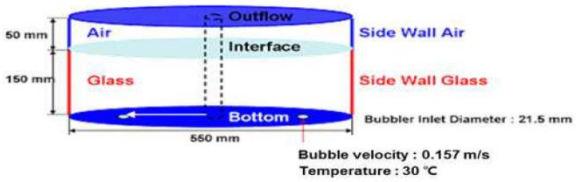


Fig. 4. Dimensions and boundary conditions of CCIM.

2.4 Analysis results

Fig. 5 shows the temperature distribution in the CCIM with respect to the time.

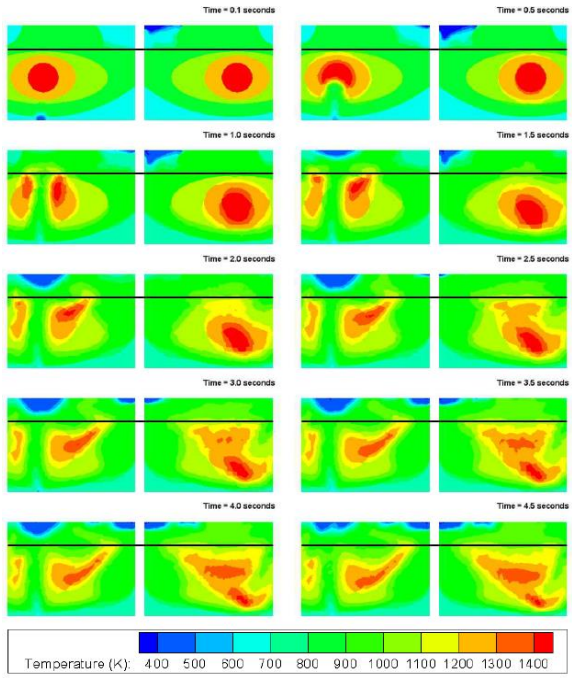


Fig. 5. Temperature distribution of central section.

3. Conclusion

The simulation model for CCIM is constructed with ~ 3 million unstructured grids. The temperature gradient, valuable information for the evaluation of stable operation of CCIM, was successfully simulated by performing the heat transfer and fluid dynamics analysis of CCIM.

REFERENCES

[1] G. Sugilal, “Experimental study of natural convection in a glass pool inside a cold crucible induction melter”, International Journal of Thermal Sciences, 47(2008) pp. 918-925.

Leaching Characteristics of Intermediate Level Liquid Radwastes

Jong Sik Shon*, Won Hyuk Jang, Dong Ju Lee, and Dae Seok Hong

Korea Atomic Energy Research Institute, 111, Daedeok-daero 989beon-gil, Yuseong-gu, Daejeon, Republic of Korea

*njsshon@kaeri.re.kr

1. Introduction

The intermediate level liquid radwastes (ILLW) will be generated during Mo-99 production at KIJANG research reactor [1]. The liquid radioactive waste over intermediate level will shift to final disposal site after solidification.

In this study, we performed leaching test for cementation of ILLW, and evaluated the results meet the acceptance criteria for disposal.

2. Experiments

2.1 Liquid Radwastes

The chemical composition and concentration of liquid radwastes in this study are NaCl 64.28 g/L and Na_2SO_4 106.53 g/L. The liquid waste stored for 4~5 years to reduce some nuclide which has short half-life [2].

2.2 Materials and Methods

Portland cement (type1) was used for solidification, and chemically simulated liquid wastes were used.

The cement and wastes were mixed following mechanical mixing method (KS-L-5109, KS). The concentration of Cs, Co and Sr are 3,000 ppm, 1,000 ppm, 1,000 ppm, respectively. We prepare 3 samples per each conditions and averaged the results.

The Leachability Index (LX) is defined as followings.

$$\mathrm{LX} = -\log D_e \qquad (1)$$

,where D_e = effective diffusion coefficient [cm^2/sec]

De can be obtained by eq. (2)

$$\mathrm{f(t)} = CFL = \frac{\sum \alpha_n}{A_0} = 2\frac{S}{V}\left[\frac{D_e}{\pi}\right]^{1/2} \cdot t^{1/2} \qquad (2)$$

CFL : Cumulative Fraction Leached

The slop can be calculated using $\frac{\sum \alpha_n}{A_0}$ term vs. $t^{1/2}$ term.

3. Results and Discussion

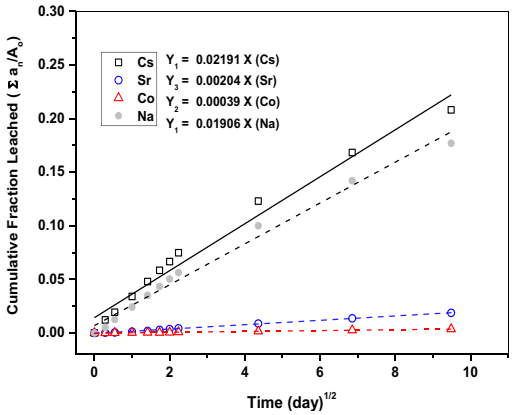


Fig. 1. Cumulative fraction leached and slope of each nuclide in cementation samples.

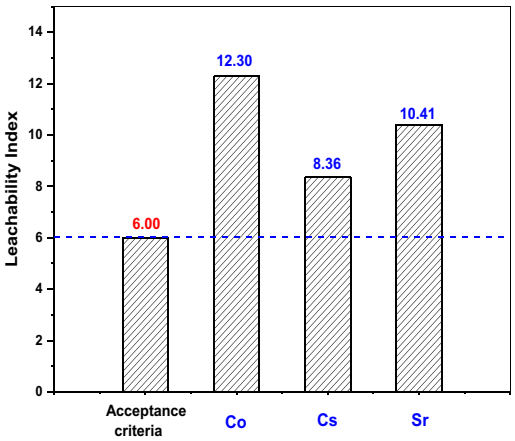


Fig. 2. Leachability index of each nuclide in cementation samples.

Fig. 1 shows cumulative fraction leached and slope for all nuclides in cementation. It clearly shows that they are following typical diffusion model.

Fig. 2 shows leachability index of each nuclide in cementation samples. All cases are meet the acceptance index of final disposal site.

4. Conclusion

4.1 De (effective diffusion coefficient) for each nuclide in cementation follow the typical diffusion model

4.2 The nuclides, high leaching rate to lowest leaching rate are Co, Sr, and Cs, the leachability indexes are 12.30, 10.41 and 8.36, respectively.

4.3 Leachability index for all nuclides in cementation meet acceptance criteria of final disposal site.

REFERENCES

[1] Martin W. A. Stewart, “Immobilisation of higher activity wastes from nuclear reactor production of 99Mo”, Australian Nuclear Science and Technology Organization (ANSTO), 2013.

[2] Korea Radioactive Wastes Agency.

[3] “Safety analysis report of Low-and intermediate-Level Radioactive Waste Disposal Facility”, 2008.

Treatment and Disposability of Intermediate Level Liquid Radwastes Generated by Fission Moly Production

Jong Sik Shon*, Jongjin Kim, Dae Seok Hong, and Chul Gyo Seo

Korea Atomic Energy Research Institute, 111, Daedeok-daero 989beon-gil, Yuseong-gu, Daejeon, Republic of Korea

*njsshon@kaeri.re.kr

1. Introduction

The intermediate level liquid radwastes (ILLW) will be generated during Mo-99 production at KIJANG research reactor which is planning by KAERI. Currently, the KIJANG research reactor is on the construction regulation phase, and it require ILLW storage capability at least 20 years.

All radwastes treatment processes of KIJANG research reactor should be certified, and all treated radwastes can shift to final disposal site. Furthermore, the treatment processes have to fit for the radwastes from the research reactor because, the radwastes of research reactor differ from that of nuclear power plants.

In this study, we developed the treatment method for ILLW, and evaluated the disposability

2. Experiments

2.1 Characteristics of ILLW

The ILLW will be generated 3.0 m^3/yr and, and chemical characteristics are shown in Table 1.

Table 1. Chemical characteristics of ILLW

Chemical Composition	Concentration [g/L]	Solubility (water, 20°C) [g/L]	Density [g/cm^3]
NaCl	64.28	359.00	2.165
Na_2SO_4	106.53	139.00	2.664
Sum	170.81		

The radioactivity of ILLW is dramatically decrease for 2years, and after 5years most nuclide with short half-life are naturally decayed. Table 2 summarized activity of ILLW after 5yeasrs.

Table 2. Activity of ILLW after 5years

Nuclide	Half-life [day]	Activity [Bq/ml]
Ag-110m	2.504E+02	1.921E+00
Co-60	1.924E+03	1.316E+03
Cs-134	7.526E+02	7.351E+03
Cs-137	1.095E+04	6.531E+06
Fe-59	4.460E+01	1.381E-08
I-129	5.731E+09	1.106E-02
Ru-103	3.935E+01	7.873E-07
Te-125m	5.800E+01	6.090E-09
Te-127m	1.090E+02	1.106E-01
Te-129m	3.360E+01	4.129E-12

As shown in Table 2, our target nuclide is Cs-137 which has highest activity after 5years [1].

2.2 Materials

Portland cement (type1) was used for solidification, and chemically simulated liquid wastes were used.

2.3 Method and evaluation

The mixture of cement and liquid wastes were mixed following “Testing method for mechanical mixing of hydraulic cement pastes and mortars of plastic consistency” (KS-L-5109). The operation range were determined using mixability, free standing water test and water immersion test (90days). The workability was adopted from “cement test flow table” (KS-L-511, KS).

In order to evaluate the disposability of cementation, we decided test contents and method

following the acceptance criteria of Gyeongju disposal site [2].

We prepared 3 cementation samples and averaged 3 results per each case.

3. Results and Discussion

Amount of salt in the cementation proportional to liquid wastes mixed with cement. That is, it proportional to w/c (water/cement) ratio. Over the 0.65 w/c ratio, there is free standing water, and there is no mixability under 0.35. Thus, the operating range is 0.40 ~ 0.60 w/c ration. In this case, the salts contents in the cements is 6.83 ~ 10.25wt.%. Considering safety and economics such as scale up factor, human error and so on, the optimum condition would be 0.50 ~ 0.55, and in this case the salts contents would be 8.54 ~ 9.39wt.%. Fig. 1 shows operation range and optimum condition for cementation.

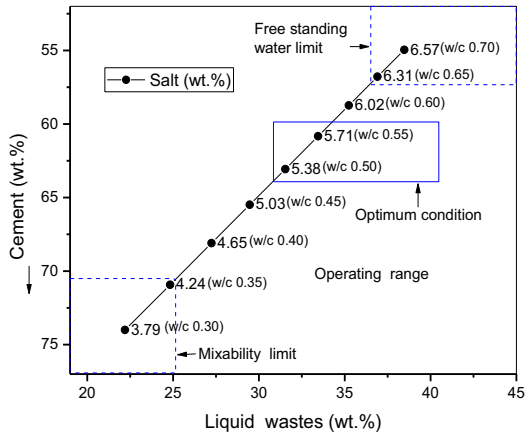


Fig. 3. Optimum condition of cementation for liquid radwastes.

3.1 Evaluation for Disposability

We performed compressive strength test and re-measured compressive strength after thermal cycling test, water immersion test and irradiation test using samples solidified with 0.50 w/c ratio. Also we performed free standing water test using crushed sample. The result of compressive strength (188~276 kg_f/cm^2) after all test is higher than acceptance criteria of Gyeongju disposal site (35.2 kg_f/cm^2). Fig. 2 shows the evaluation for acceptance criteria of FM radwastes for final disposal.

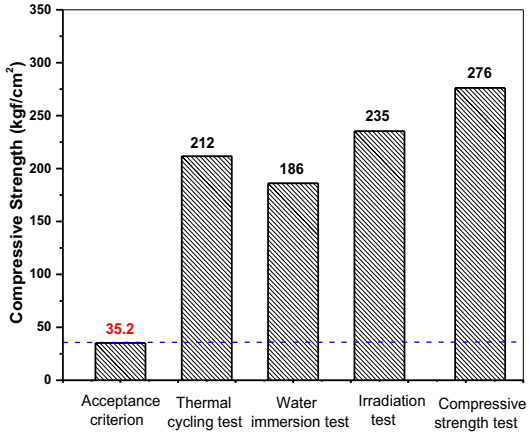


Fig. 4. Evaluation for acceptance criteria of FM radwastes for final disposal.

4. Conclusion

4.1 Cementation is a certified technology, and the activity of solidification is 3.01E+06 Bg/g. Thus, it classified as intermediate level wastes by atomic energy act. And can be disposed to Gyeongju disposal site.

4.2 The operation range is 0.40 ~ 0.60 of w/c ratio, and the salts contents are 6.83 ~ 10.25wt.%.

4.3 Optimum condition is 0.50 ~ 0.55 of w/c ratio, and the physical and chemical properties of cementation meet the acceptance criteria of Gyeongju disposal site.

REFERENCES

[1] Martin W. A. Stewart, “Immobilisation of higher activity wastes from nuclear reactor production of 99Mo”, Australian Nuclear Science and Technology Organization (ANSTO), 2013.

[2] Korea Radioactive Wastes Agency, “Safety analysis report of Low-and intermediate-Level Radioactive Waste Disposal Facility”, 2008.

Safety Analysis of Cementation Including Deliquescent Na Compound for Final Disposal

Jong Sik Shon*, Ki Baek Shin, Jongjin Kim, Dae Seok Hong, and Gi Yong Kim
Korea Atomic Energy Research Institute, 111, Daedeok-daero 989beon-gil, Yuseong-gu, Daejeon, Republic of Korea
*njsshon@kaeri.re.kr

1. Introduction

According to acceptance criteria of disposal site, deliquescent Na and its compound not be accepted in humid environments [1]. The representative Na compounds are $NaNo_3$, Na_2SO_4 and NaCl, and liquid radwastes including them have to solidify to disposal.

The purpose of this work, in order to dispose cementation of radwastes including Na compounds, evaluate the stability as varying temperature and humidity of disposal site.

2. Materials and Methods

For the experiments, simulated $NaNO_3$ and KNO_3 were used and Portland cement type 1 was used for the cementation.

The mixture of cement and liquid wastes were mixed following "Testing method for mechanical mixing of hydraulic cement pastes and mortars of plastic consistency" (KS-L-5109, KS). We prepared 3 cementation samples and averaged 3 results per each case.

The temperature and humidity were constantly kept for 12 hours using a thermo-hydrostat. Considering the temperature of disposal site, the experiment temperature varied as 5, 10 and 15℃, the humidity also changed as 100, 80, 70, 50, 30 and 10% per each temperature. We measured extracted salt by the humidity changes.

3. Results and Discussion

3.1 Relationship between $NaNo_3$ contents and deliquescent



Fig. 1. Picture of cement waste form samples with $NaNO_3$ and extracted salt.

Fig. 1 shows the picture of cement waste form samples with $NaNO_3$ and extracted salt from the sample.

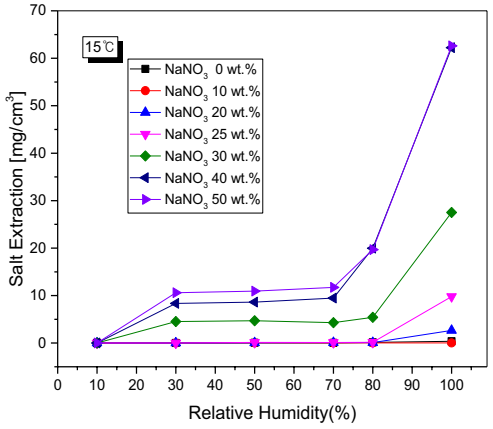


Fig. 2. The amount of extracted salt from cement waste form with different $NaNO_3$ contents and relative humidity at 15℃.

Fig. 2 shows the amount of extracted salt from cement waste form with different $NaNO_3$ contents and relative humidity at 15℃. The deliquescent increased after 70% humidity, and it was observed that the higher $NaNO_3$ contents, the higher deliquescent, and rapidly increased after 100%.

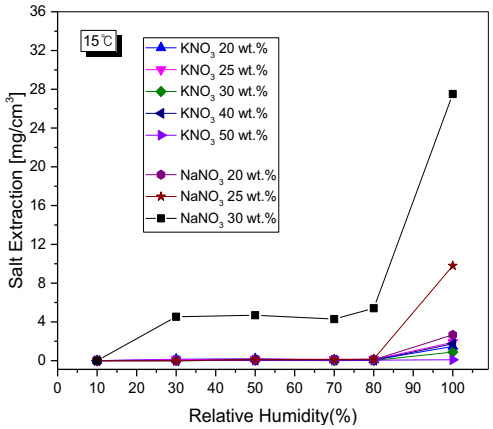


Fig. 3. The amount of extracted salt from cement waste form with different $NaNO_3$ and KNO_3 contents in varying humidity condition at 15℃.

Fig. 3 shows the amount of extracted salt from cement waste form with different $NaNO_3$ and KNO_3 contents, which has no deliquescent, in varying humidity condition. Up to 20wt.% of $NaNO_3$, the amount of extracted salt is almost same with that of KNO_3 even in 100% humidity, over the 20wt.%, while, the amount of extracted salt is larger than that of KNO_3.

4. Conclusion

According to our results, the cementation of $NaNO_3$ up to 20wt.% shows no deliquescent properties in disposal site environments. Thus, it has stability for final disposal.

REFERENCES

[1] Korea Radioactive Wastes Agency, “Safety analysis report of Low-and intermediate-Level Radioactive Waste Disposal Facility”, 2008.

Recovery of the Magnetic Adsorbent for Cs Separation from Liquid Waste by Using the Magnetic Liquid-Solid Separation Method

Hyo-Jeong Lee*, Jung-Weon Choi, Seung-Yeon Cho, Won-Zin Oh, and Sang-June Choi

Kyung pook National University, Dae-Hak ro 80, Buk-gu, Dae-Gu, Republic of Korea

*pinetree93@knu.ac.kr

1. Introduction

To remove Cs from waste aqueous solutions, traditional techniques such as ion-exchanges, adsorption and electrocoagulation are used. Among the mentioned methods, adsorption is one of the most popular methods for removal Cs in aqueous waste solution due to simplicity, selectivity and efficiency. Especially, nanostructured adsorbents have emerged as strong candidates for removal of contaminants in wastewaters because of large specific surface area and high adsorption capacities. However, it is difficult to recover. Therefore, the application of magnetic nanostructured adsorbents can overcome this weakness [1-3]. It is possible using magnetic force to recover the magnetic adsorbents instead of column.

In our previous works, we reported the synthesis method of adsorbents (magnetic MWCNTs-ZnFC-1 and magnetic MWCNTs-ZnFC-2) and their maximum adsorption ability (0.8951 ± 0.0045 mmol/g (R^2=0.9989), 1.4476 ± 0.0630 mmol/g (R^2=0.9702), respectively) [1]. However, with low recovery efficiency, it is not outstanding adsorbents. Therefore, in this paper, we prepared adsorbents with same synthesis method as previously. Then, we evaluate recovery efficiency with permanent magnet.

2. Experiments

2.1 Preparation of the adsorbents

In order to obtain magnetic MWCNTs, mixing reaction was carried out at 280℃ for 1 hours under Ar gas with 100 mg of $Fe(acac)_3$ (2,4-pentanedionate, 99%), pristine MWCNTs and TREG (Triethylene glycol, 99%). Then, washed with ethanol and DI-water, and dried. The next procedure for Zinc ferrocyanide functionalized magnetic MWCNTs was as follow. Firstly, shaking magnetic MWCNTs at 25℃, 100 rpm for 3 hours under N_2 gas with 0.1 M $K_4Fe(CN)_6 \cdot H_2O$. Then, shaking at 25℃, 200 rpm for 3 hours under N_2 gas with 0.3 M $ZnCl_2$ (magnetic MWCNTs-ZnFC-1). For magnetic MWCNTs-ZnFC-2, 0.2 M $K_4Fe(CN)_6 \cdot H_2O$ and 0.6 M $ZnCl_2$ are used instead of 0.1 M and 0.3 M respectively.

2.2 Measure the Particle Size

The particle size of magnetic nanostructured adsorbents is one of the most important things in magnetic separation. PSA (Particle Size Analyzer, N5/LS-13320, Beckman Coulter) measures particle size and their distribution by principles of diffraction.

2.3 Experiment of Magnetic Separation

The efficiency of separation is evaluated by batch magnetic process. The permanent magnet captured magnetic MWCNTs-ZnFC-1 and magnetic MWCNTs-ZnFC-2 while 700 mL DI water stirred with 250 rpm for 1 minute. Fig. 1 shows the separation procedure.

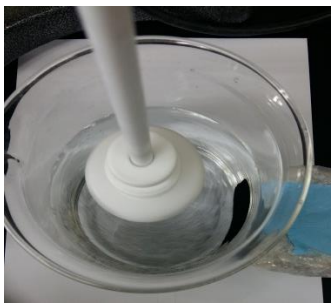


Fig. 1. Magnetic separation with permanent magnet.

The separation efficiency of permanent magnet was computed on Equations (1) :

$$E = \left(\frac{W_{captured}}{W_0}\right) \times 100(\%) \quad (1)$$

where E is percent of separation, $W_{captured}$ is captured adsorbent mass (g) by permanent magnet, W_0 is the initial adsorbent mass (g) dispersed in the batch reactor.

3. Results

3.1 Particle Size Distribution

Particle size analysis result data of magnetic MWCNTs-ZnFC-1 and magnetic MWCNTs-ZnFC-2 is shown Fig. 2 and Table 1.

Table 1. Diameter Information of magnetic MWCNTs-ZnFC-1 and magnetic MWCNTs-ZnFC-2

	magnetic MWCNTs-ZnFC-1	magnetic MWCNTs-ZnFC-2
D10	23.604	17.940
D50	56.099	57.967
D90	233.547	238.510
Mean	111.725	105.620
Median	56.099	57.967

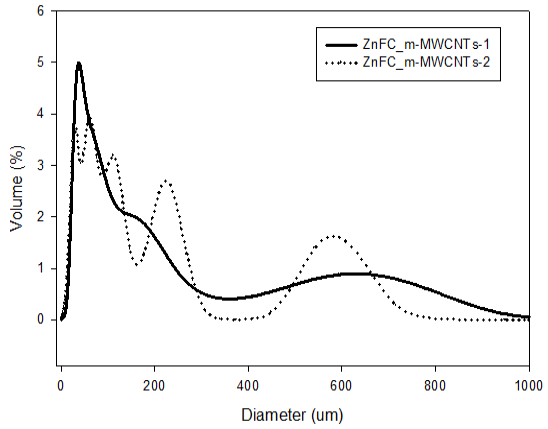


Fig. 2. Particle Size Distribution Curve of magnetic MWCNTs-ZnFC-1 and magnetic MWCNTs-ZnFC-2.

The sizes of magnetic MWCNTs-ZnFC-1 ranged from 0.6 μm to 1142 μm, magnetic MWCNTs-ZnFC-2 ranged from 0.375 μm to786 μm. The D10 of magnetic MWCNTs-ZnFC-2 is smaller than magnetic MWCNTs-ZnFC-1. However, their D50, D90 and mean diameters are similar.

3.2 Magnetic Separation Efficiency

Separation Efficiencies are shown Table 2. Efficiency of magnetic MWCNTs-ZnFC-1 is 95.81% and magnetic MWCNTs-ZnFC-2 is 91.01% for 1 minute.

Table 2. Separation Efficiency of Adsorbents

Adsorbent	Initial adsorbent mass [g]	Captured adsorbent mass [g]	Separation efficiency [%]
magnetic MWCNTs-ZnFC-1	0.2005	0.1921	95.81
magnetic MWCNTs-ZnFC-2	0.2003	0.1823	91.01

4. Conclusion

In the previous study about the magnetic MWCNTs-ZnFC-1 and magnetic MWCNTs-ZnFC-2, the latter with the two times higher ZnFC contents has higher adsorption ability than the magnetic MWCNTs-ZnFC-1 [1]. We obtained the following conclusion based on the recovery efficiency of the two adsorbents: increase in the Cs adsorption sites by ZnFC has little influence on the magnetic recovery efficiency due to little change in the particle size distribution.

Acknowledgement

This work was supported by National Research Foundation of Korea (NRF) grant funded by the Korea government (MSIP: Ministry of Science, ICT and Future Planning). (NO.2012M2B2B1055496)

REFERENCES

[1] Hyo-Jeong Lee et al., “Study of making MWCNTs magnetic adsorbent using zinc ferrocyanide for selective adsorption of Cs ions”, Korean Radioactive Waste Society AUTUMN, 16(2), OCT, 12-14, 2016, Je-Ju.

[2] Anthony M.Muliwa et al., “Magnetic adsorption separation(MAS) process: An alternative method of extracting Cr(Ⅵ) from aqueous solution using polypyrrole coated Fe3O4 nanocomposites”, Separation and Purification Technology, 158, p.250-258 (2016).

[3] A.M. El-Kamash, “Evaluation of zeolite A for the sorptive removal of Cs+ and Sr2+ ions from aqueous solutions using batch and fixed bed column operations”, Journal of Hazardous Materials, 151, p.432-445 (2008).

Recovery Tests for Analysis of Radionuclides in Spent Resin Using Elution and Microwave Digestion Method

Simon Oh*, Jaesik Hwang, Kwang-Soon Choi, and Hong-Joo Ahn

Korea Atomic Energy Research Institute, 111, Daedeok-daero 989beon-gil, Yuseong-gu, Daejeon, Republic of Korea

*simon@kaeri.re.kr

1. Introduction

Ion-exchange resins are widely used in the nuclear power plant for purification of various aqueous streams. As spent resins are the relatively high activity, an evaluation of radionuclide inventories should be carried out to permanently dispose these resins based on the Korean Nuclear Safety and Security Commission (NSSC) Notice No. 2015-4, in which the acceptance criteria for LILWs are specified. Elution and microwave digestion method was tested for recovery tests of radionuclides in spent ion-exchange resins.

Elution method using a column is a process that the radioactive nuclide is eluted from the resins using the eluent. However, the former is complicated for the control of flow rate and produces secondary waste such as column material. The spent resins are difficult to achieve standard requirement after elution, so it is used to treat some low level radioactive spent resin [1]. Elution method needs concentration process because of much of eluent used.

Closed vessel microwave digestion system offers several distinct advantages such as lower acid consumption, avoiding the loss of volatile elements, rapid reaction time. However, closed microwave digestion system has only one disadvantage, namely, explosion and cracking of digestion tubes due to simultaneous build-up of pressure along with temperature increase.

In this study, we compared recovery tests in fresh ion-exchange resin between elution method and closed vessel microwave digestion method.

2. Experimental

2.1 Preparation

For evaluation of recovery tests, the fresh IRN-150 resin was used. IRN-150 (Amberite^{TM}) is 1:1 mixtures of IRN-77 and IRN-78. The IRN-77 is a strongly acidic cation resin and IRN-78 is a strongly basic anion resin. Approximately 1 g of the sample was dried in an oven at 60℃ for 24 hr in a beaker. After cool, 20 mL distilled de-mineralized water (DDW) was added to the beaker and 0.5 mL of each of Ni, Nb, Re, and Sr (10 mg/L) were added. 12 hr waited for the adsorption of metallic ions, and the ion-exchange resins was separated by a filter paper with 25 μm pore size. The concentration of each element in solution was determined using ICP-AES to know the amount of each element being adsorbed in IRN-150.

2.2 Elution method

A column (D 0.7 cm) was plugged at the bottom with a polyethylene bed support. The column was packed with 1 g of ion-exchange resin with soft tapping to ensure dense packing, and a bed support was packed with a bed support on top of the resin bed for prevention of disturbance during addition of the eluent. The resin bed height was adjusted to 5 cm. Ten mL of DDW, 50 mL of 4 M HCl, 50 mL of 10 M HNO_3, 50 mL of 5 M HNO_3 including 0.2 M HF, and 10 mL of DDW was transferred to the column at a flow rate of 1 mL/min, respectively. The concentration of each element in the elution was determined using ICP-AES.

2.3 Closed vessel microwave digestion system

For recovery test, about 1 g of ion-exchange resin was used to desorb the metal ions in the resin adsorbed using a microwave digestion system (MDS) including mixed acid (10 mL of HNO_3, 4 mL of HCl, 0.25 mL of HF). After operation of MDS, the solution was transferred to a volumetric flask. The concentration of each element in the solution was determined using ICP-AES. Fig. 1 shows elution method and closed microwave digestion system in the glove box.

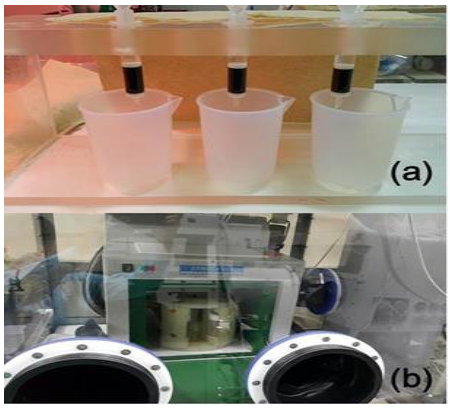


Fig. 1. Elution method (a) and closed vessel microwave digestion system (b).

3. Results & discussion

Fig. 2 shows the result of recovery between elution method and microwave digestion method. The mean recovery of 4 elements for the microwave digestion system was 98.1±2.8%. The recovery of Re and Nb for microwave digestion method was 97.1±3.1% and 94.8±6.3%, respectively.

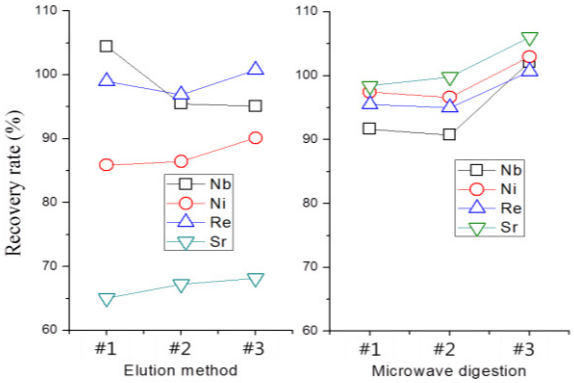


Fig. 2. Comparison of recovery between elution method and microwave digestion method.

However, the average recovery of 4 elements for elution method was 87.9±15.0%. The recovery of Re and Nb for elution method was 98.9±2.0% and 98.3±5.3%, respectively. Especially, although the cause of low recovery for Sr is unknown, the recovery of Sr using elution method was very low as 66.8±1.6%. The recovery of Re and Nb for microwave digestion method was similar to that of the elution method. A standard deviation of both methods was less than 5% except Nb.

4. Conclusion

Nb, Ni, Re, and Sr in the resin adsorbed using the microwave digestion method were quantitatively recovered. The results of microwave digestion method were superior to those of the elution method. Further study will be performed to investigate the cause of low recovery of Sr using elution method.

REFERENCES

[1] Jianlong Wang, Zhong Wan “Treatment and disposal of spent radioactive ion-exchange resins in the nuclear industry”, Progress in Nuclear Energy, 78, 47-55, (2015).

Recovery Rate of Fe, Nb, Ni, Re, Sr According to Elution Speeds in the Column Examination for the Pretreatment of Spent Resin

Jaesik Hwang*, Simon Oh, Kwang-soon Choi, and Hong-Joo Ahn
Korea Atomic Energy Research Institute, 111, Daedeok-daero 989beon-gil, Yuseong-gu, Daejeon, Republic of Korea
*jaesikhwang@kaeri.re.kr

1. Introduction

Ion-exchange resins are widely used for the purification of various water streams [1]. In addition, spent resins are contain activation products generated by irradiation of structural materials in the reactor core, along with fission products and isotopes of uranium and transuranium elements that escaped from the irradiation nuclear fuel or have been generated by irradiation of the slight surface contamination of nuclear fuel elements [2].

The management of spent ion-exchange resins demands the determination of their radioactive inventory as a first and fundamental step. The activity concentration of some typical radionuclides contained in spent ion-exchange resins can be measured directly by gamma-ray spectrometry of samples or gamma-ray scanning. However, many other radionuclides commonly found in spent ion-exchange resin are pure alpha, pure beta or low-energy photon emitters not amenable to direct measurement. The chemical separation technique of their radionuclides in spent ion-exchange resins were developed [3].

Pretreatment methods of spent ion-exchange resin for chemical separation were commonly used elution method using the column and microwave digestion method. The present work describes the chemical recovery of the metallic ions in elution method with elution speed change.

2. Experimental

2.1 Preparation

For evaluating the chemical recovery, we used IRN-150. IRN-150 (Amberite^{TM}) is 1:1 mixtures of IRN-77 and IRN-78. The IRN-77 is a strongly acidic cation resin and IRN-78 is a strongly basic anion resin. The resins were put in a beaker containing 250 mL DI water and filtered using vacuum pump. Approximately 1 g of the sample was weighted that was dried in an oven at 60℃ for 24 hr in a beaker. 2 ml of 10 mg/L Fe and Nb solution, 0.2 ml of 10 mg/L Ni solution, 0.3 ml of 10 mg/L Re and Sr solution were added. After adsorbing for 12hr, the precipitate was separated by filter paper with 25 um pore size. The effluent solution made a determination to ICP-AES.

2.2 Elution method

Elution system is present in the picture below. About 1 g of the prepared resin was placed in 8 ml plastic column and packed with separation membrane for prevent of sample loss. 10 ml of DI water was added to remove air bubbles in resins and then added 50 ml of 4 mol HCl, 50 ml of 10 mol HNO_3, 50 ml of 5 mol HNO_3 + 0.2 mol HF in regular sequence. The elution speed of system was controlled within the range of 0.5 ml/min and 2.0 ml/min.

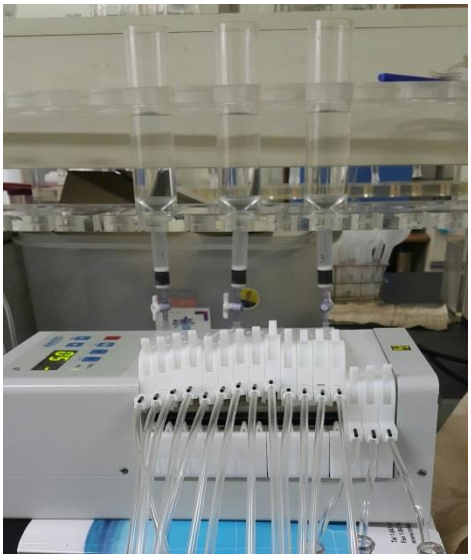


Fig 1. Elution system for evaluation of chemical recovery rate according to eluting speed.

3. Result

The adsorption rate of metallic ions in prepared resin was observed above 99.99 percent. Chemical recovery of metallic ions according to elution speeds is shown in Fig. 1. In 1 ml/min for the elution speed, chemical recovery were 98.2% for Fe, 49.3% for Nb, 69.3% for Ni, 86.2% for Re, 73.1% for Sr. The chemical recovery in 2 ml/min for elution speed were 85.8% for Fe, 43.4% for Nb, 62.9% for Ni, 80.1% for Re, 60.2% for Sr.

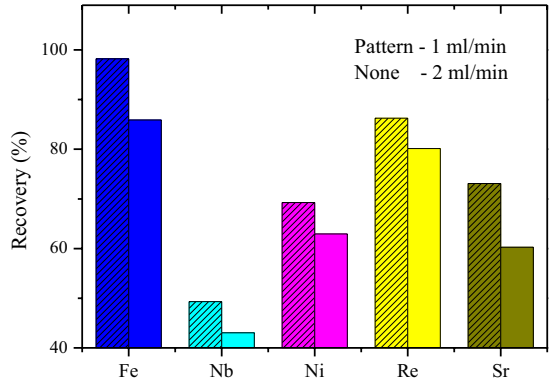


Fig. 2. Recovery of metallic ion according to eluting speed.

4. Conclusion

For evaluation of chemical recovery, we investigated the effect of the eluting speed in elution method for pretreatment of spent resin. The recovery rate decreased as increasing the eluting speed.

REFERENCES

[1] International Atomic Energy Agency, “Management of spent ion-exchange resins from nuclear power plants”, Technical Document Issued, 238, 1981, Vienna.

[2] M. H. T. Taddei, R. Viecnte, J. T. Marumo, S. K. Sakata, L. A. A. Terremoto, “Determination of long-lived radionuclides in radioactive wastes form the IEA-R1 nuclear research reactor”, Journal of Radioanalytical and Nuclear Chemistry, 295, 951-957 (2013).

[3] J. T. Marumo, “Progress in the characterization of radioactive waste in brazil”, Annual meeting of the international network of laboratories for nuclear waste characterization, December 10-12, 2013, Vienna, Austria.

Dissolution of Large Amount of Ash Produced From Radioactive Waste Using High-Performance Microwave Digestion Systems

Kwang-Soon Choi*, Jaesik Hwang, Simon Oh, Young-Bok Kim, and Hong Joo Ahn
Korea Atomic Energy Research Institute, 111, Daedeok-daero 989beon-gil, Yuseong-gu, Daejeon, Republic of Korea
*nkschoi@kaeri.re.kr

1. Introduction

Drums of low and intermediate levels of dry radioactive waste (DAW) containing paper, cotton, vinyl, and plastic have been managed temporarily in Korea atomic energy research institutes (KAERI) site. For permanently disposal of these wastes in a repository, the activity of ^{60}Co, ^{137}Cs, ^{55}Fe, ^{94}Nb, ^{59}Ni, ^{90}Sr, and ^{99}Tc in DAW based on the radioactive waste acceptance criteria specified by nuclear safety and security commission (NSSC) should be determined. A dry ashing method [1,2] has been used for sample pretreatment owing to advantages such as allowing the decomposition of a large sample size, no requirement of reagents, relatively safe techniques, and capability of mass production.

2. Dissolution of ash

2.1 Amount of ash produced

To treat 80 to 100 g of sample, a dry ashing method was selected due to the decomposition of a large sample size and the concentration effects of the sample. The weight difference of DAW between before and after ashing was usually big from 80 g to 2-3 g. However, the amount of ash produced from DAW including cotton gloves coated with rubber and surgical gloves was significantly large about 20 g.

2.2 Dissolution of large amount of ash produced

We have established a sample pretreatment procedure of ash produced from DAW. However, the established procedure couldn't be applied to the large amount of ash produced. Therefore studies on the dissolution of the large amount of ash produced with a high-performance microwave digestion system (HP-MDS) containing HNO_3-HCl-HF were performed owing to the difficulty in dissolving certain oxides after heating.

3. Results & discussion

The large amount of ash produced was not completely dissolved by the established sample pretreatment procedure [3]. The sample was not absolutely dissolved with 12 mL of aqua regia and 0.25mL of HF using an HP-MDS. In addition, the ash sample was also not dissolved with fusion method using lithium metaborate and lithium tetraborate (50:50, wt%) as a flux. Although the sample was not completely dissolved, a qualitative analysis using inductively coupled plasma atomic emission spectrometry (ICP-AES) showed the highest concentration of silicon.

Owing to the highest contents of silicon, the volume of HF increased from 0.25 mL to 0.5 mL. Finally the 0.1 g of sample was absolutely dissolved with 12 mL of aqua regia and 0.5 mL of HF using the HP-MDS. A qualitative analysis using the ICP-AES showed the presence of Si, Al, Fe, Ti, Ca, and K in order of high concentration. Analytical results of the ash samples are shown in Table 1.

Table 1. Analytical results of the ash sample

Item	Results (%)	
	Measured	Calculated
Al	0.24	0.44 (as Al2O3)
Ca	0.16	0.23 (as CaO)
Fe	0.24	0.34 (as Fe2O3)
K	0.09	0.11 (as K2O)
Si	43.4	92.97 (as SiO2)
Ti	0.20	0.34 (as TiO2)
Total	44.33	94.44

4. CONCLUSIONS

A sample treatment procedure for the dissolution of a large amount of ash produced by heating the dry radioactive waste including cotton gloves coated with rubber and surgical gloves was established. We found over 90 percent of the ash was SiO_2. This procedure will be applied to the dissolution of the large amount of ash produced.

REFERENCES

[1] Ming Y, Bing L (1998) Determination of rare earth elements in human hair and wheat flour reference materials by inductively coupled plasma mass spectrometry with dry ashing and microwave digestion. Spectrochim Acta 53B:1447.

[2] Sahayam AC, Chaurasia SC, Venkateswarlu G (2010) Dry ashing of organic rich matices with palladium for the determination of arsenic using inductively coupled plasma-mass spectrometry. Anal Chim Acta 661:17.

[3] Kwang-Soon Choi, Chang Heon Lee, Hee-Jung Im, Hong-Joo Ahn, Kyuseok Song (2014) Sample pretreatment for the determination of gamma emitting nuclides in dry radioactive waste using a dry ashing and high-performance microwave digestion system. J Radioanal Nucl Chem 301:567.

Development of Nuclear Waste Filter Sampling Device and Process

Kyung-Ho Kim[1*], Hyeon-Oh Park[1], Mi- Rang Lee[2], and Young-Ku Choi[1]
[1]Sunkwang T&S Co.,Ltd Sunkyung Officetel 20F, #3, Gongwon-ro, Guro-gu, Seoul, Republic of Korea
[2]KOREA HYDRO&NUCLEAR POWERCO.,LTD, 696-13 Donghaean-ro, Yangnam-myeon, Gyeongju-si, Gyeongsangbuk-do, Republic of Korea
[*]kyungho0121@naver.com

1. Introduction

About 2,500 drums of intermediate-level and low-level radioactive waste are produced annually by 4 nuclear power plants in Korea, and as of September 2016, 92,008 drums (200L) are stored in the temporary storage facilities at the NPPs. The Nuclear Safety and Security Commission Notification #2015-4 requires that the concentration of the radionuclides that need to be declared during the disposition of the intermediate-level and low-level radioactive waste, possessed by possessed by Korea Hydro & Nuclear Power Co., Ltd. (KHNP), particularly the radionuclides in drums, emitting the alpha ray and beta ray, that cannot be directly measured by radiation dosimeters, should be measured. An assessment technology of the radionuclide inventory, the scaling factor, which is a method of predicting the concentration of radionuclides, was developed for the waster produced between 2004 and 2008, and the scaling factor will be used to assess the radionuclide inventory in the intermediate-level and low-level radioactive waste drums that were generated prior to 2004.

The purpose of this study is to develop a sampling device and process for analyzing nuclide in order to permanently dispose of nuclear waste filters generated before 2004.

2. Methods and Results

2.1 Establishing the plan to collect sample waste filters

As the intermediate-level and low-level radioactive waste, which were generated prior to 2004, e.g. dry active waste (DAW), spent resin and concentration waste fluid powder, except for the waste filter, is cement-solidified, the waste filter was selected as the sample. In case of Pressurized Water Reactor NPPs, 6 systems are using filters to purify the liquid waste, and the waste filter for purifying the coolant is sampled, and different filters are used for the Pressurized Water Reactor (PWR) and the Pressurized Heavy Water Reactor (PHWR). Various filters are used respectively, and Fig. 1 and Table. 1 show the representative filters and dimensions. Also, to minimize workers' radiation exposure, radiation protection plans will be established based on the surface dose inside the storage rack where samples are collected.



Fig. 1. The image of the filters used in Wolsong nuclear power plant.

Table 1. The size of waste filter used in Wolsong nuclear power plant

Filter type		Size	
		#1	#2,3,4
[1)]PHT	Primary Heat Transport	Ø482.6×1400L	
[2)]MOD	Moderator	Ø381×1090L	
[2)]SFB	Spent Fuel Bay	Ø384×1090L	
[3)]F/M	Gland Seal	Ø127×1320L	
[3)]G/S	Fuel Machine	Ø127×1080L	

2.2 Waste filter sampling

2.2.1 Designating the radiation controlled area. In this study, samples will be collected from the storage facility of Wolsung Unit 1, which was designated as the radiation controlled area for collecting waste filter samples, and during the sampling period, it will be off limits to people other than workers.

2.2.2 Making preparations for sampling. For this study, a shielding board and tent for preventing the proliferation of contamination and equipment for collecting samples were developed, and Fig. 2 shows them.



Fig. 2. Equipment for preventing the proliferation of contamination and collecting samples.

2.2.3 *Sampling procedure.* The intermediate-level and low-level radioactive waste filter that were generated prior to 2004 was sampled as illustrated in Fig. 3.



Fig. 3. The procedure for sampling old waste filters.

1) Select the waste filters to be sampled, and open the rack from which samples will be collected.
2) After opening the rack, measure tritium and surface dose of the storage container
3) Remove the lid of the storage container, and measure the surface dose.
4) Measure the concentration of tritium in the workspace.
5) Check the waste filter storage status, and recover the waste filter and measure the dose.
6) Go to the waste filter tent for preventing the proliferation of contamination, measure the dose of the sampling location and make preparations for sampling.
7) Use the sampling device to collect waste filter samples.
8) Use the sealing bag to pack it, and put it in a container for transporting radioactive materials.

3. Conclusion

In this study, we developed the sampling device and process for the waste filters, and 22EA of Waste filters(PHT: 7, MOD: 2, SFB: 3, F / M: 6, G / S: 4) from Wolsong nuclear power plant were sampled. The collected waste filter samples are used for analyzing nuclide to verify the scale factor.

REFERENCES

[1] Yong Joon Park, Hong Joo Ahn, Byoung Chul Song, Kyuseok Song, Periodic Verification of the Scaling Factor for Radwastes in Korean NPPs, WM2013 Conference (2013).
[2] K. W. Jee and H. J. Ahn, “"Estimation of hard-to-measurement radionuclides in low & medium level radwastes from Korea NPP"", ICEM’'05 conference (2005).

CaO Absorbent Development for ^{14}C Immobilization Generated From Waste Resin of Heavy-Water Reactor and Mechanism Study

Hyeon-Oh Park[1], Hwan-Seo Park[2], Ki-Rak Lee[2], Kyu-Tae Park[1], Jung-Min Yoo[1] , and Young-Ku Choi[1]

[1]Sunkwang T&S Co.,Ltd, Sunkyung Officetel 20F, #3, Gongwon-ro, Guro-gu, Seoul, Republic of Korea

[2]Korea Atomic Energy Research Institute, 111, Daedeok-daero 989beon-gil, Yuseong-gu, Daejeon, Republic of Korea

gusdhtpgml@nate.com

1. Introduction

Domestic Heavy-Water Reactor Nuclear Power Plants (NPPs) produce a lot of spent resin in the process of operation. Nuclides are captured in a spent resin by ion exchange. It is treated using a unique method different from a method to treat general radioactive waste. Conventional methods of treating the spent resin include activity stripping, the PLO process, acid stripping and thermal stripping, and all of them aim to selectively separate ^{14}C, a long half-life nuclide, and reduce the volume of spent resin. Currently in Korea the method of treating the spent resin is not determined, and it is stored in storage tanks inside the NPPs. Looking at the spent resin treatment process under investigation, gaseous ^{14}C, generated from the spent resin, is immobilized again, and disposed of as a solid. The existing CO_2 removal technique has an advantage in terms of volume reduction, but it is not enough to stabilize the radionuclide.

CaO has been considered as a good absorption material for CO_2 capturing process due to high efficiency of CO_2 capturing and high stability of $CaCO_3$, final product. However, there is a disadvantage to handle a CaO as absorbent because it exists as powder form without support material.

In this study, CaO was synthesized as cylindrical form without support. Porosity of CaO structure was controlled using organic solvent. FT-IR analysis was conducted for mechanism study of CaO structure formation.

2. Experimental

To make the absorbent for removing gaseous ^{14}C, desorbed from the spent resin, calcium acetate was dissolved in the DI water, and ethylene glycol was added to it. Calcium hydroxide was added to the resulting mixture, and the mixture was mixed, and aged for 24 hours at room temperature. An organic solvent was added to the aged mixture, and a paste was made. It was treated with heat, i.e. 90°C, 300°C and 900°C, and the absorbent was made. Ethanol and isopropyl alcohol (IPA) were used as organic solvents, and a paste without the organic solvents was also assessed to compare properties. The physical properties of the absorbent were analyzed through the XRD and SEM analysis, and the FT-IR analysis was conducted to analyze the changes in the absorbent formation mechanism.

3. Result and discussion

3.1 Comparison of properties by absorbent manufacturing method

To analyze properties depending on the heat treatment temperature of the absorbent, samples, plasticized at 300°C and 900°C, were used to conduct the XRD analysis. Fig. 1 illustrates the result of the XRD analysis of properties depending on the temperature of the absorbent. When the absorbent was treated at 300°C, it existed in the form of $Ca(OH)_2$, and there was a small quantity of $CaCO_3$. $CaCO_3$ is thought to have been formed by CO_2 or Calcium acetate in the air. When the absorbent was treated at 900℃, $Ca(OH)_2$ and $CaCO_3$, which existed at 300℃, were turned into CaO through dehydration and decarbonation. What follows are the reaction formulas.

$$Ca(OH)_2 \rightarrow CaO + H_2O \quad (1)$$

$$CaCO_3 \rightarrow CaO + CO_2 \quad (2)$$

The SEM analysis was conducted with regard to the differences in the porosity of absorbents depending on the organic solvent added when absorbents are manufactured, e.g. alcohol-free,

ethanol and IPA. Fig. 2 illustrates the result of the SEM analysis by organic solvents. It was confirmed that when alcohol-free was added, no porosity was formed, and when ethanol was added, porosity was formed, but it was less than the porosity resulting when IPA was used.

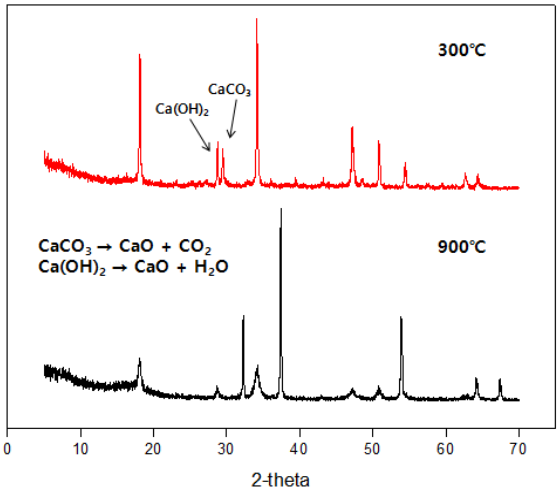


Fig. 1. XRD patterns of Calcium absorbent.

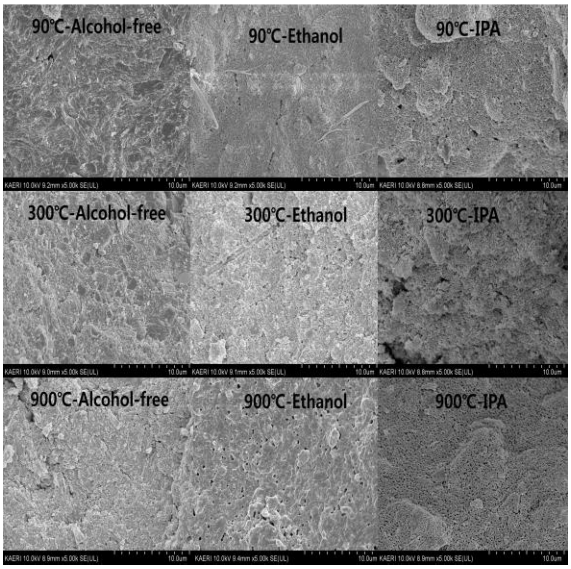


Fig. 2. SEM images by organic solvent and temperature.

3.2 Changes in the absorbent formation mechanism

The esterification between ethylene glycol and calcium acetate was used to manufacture an absorbent with free porosity without using any inorganic support or polymer. The FT-IR analysis was conducted to see if this esterification affected the absorbent formation mechanism. Fig. 3 shows the result of FT-IT by aging time. It was similar to the result of FT-IT analysis of calcium acetate. The peak appearing at 3630 cm^{-1} was reduced, indicating that $Ca(OH)_2$ reacts and decreases with time. As FT-IR alone did not show much difference, however, it was difficult to analyze the mechanism. Accordingly, the mechanism will be analyzed using additional methods like NMR.

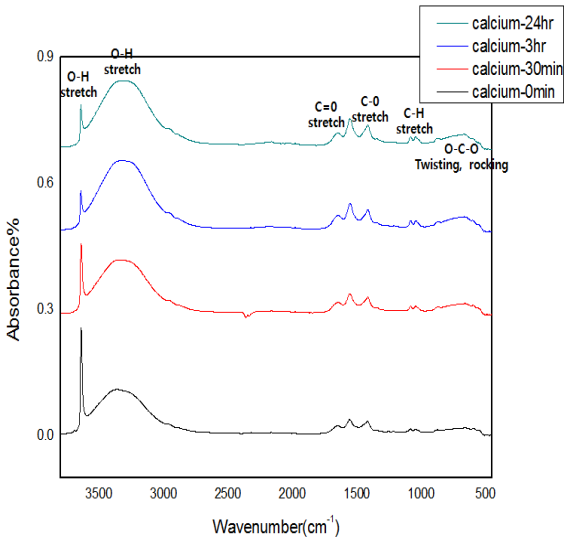


Fig. 3. FT-IR analysis of calcium absorbent by aging time.

4. Conclusion

In this study, CaO structures for CO_2 capturing were successfully synthesized. Porosity of CaO structure was controlled by organic solvent. IPA shows the high and uniform porosity. Form XRD results, it was confirmed that calcium hydroxide still exist after heat-treatment at 300°C and calcium oxide was formed after heat-treatment at 900°C. Uniform and porous surfaces of absorbent were indicated from SEM images. The FT-IR analysis was not enough to analyze changes in the absorbent formation mechanism. Accordingly, the mechanism will be analyzed using additional methods like NMR.

REFERENCES

[1] KAREI, “Development of Adsorbent for C-14 Gas Trapping and Characteristics Evaluation, 2005.

[2] V. P. Yadav “Kinetics of Esterification of Ethylene Glycol with Acetic Acid Using Cation Exchange Resin Catalyst, 2011.

Separation Characteristics of Fission Products in LiCl-KCl Waste Salt by Layer-melt Crystallization

Tae-Kyo Lee*, Jung-Hoon Choi, Ki-Rak Lee, Seung-Youb Han, and Hwan-Seo Park

Korea Atomic Energy Research Institute, 111, Daedeok-daero 989beon-gil, Yuseong-gu, Daejeon, Republic of Korea

*tklee@kaeri.re.kr

1. Introduction

The wastes arising from pyrochemical process after sufficient use of chloride salts as molten state electrolytes are LiCl waste salt from the electrolytic reduction process, and LiCl-KCl eutectic waste salt from the electrorefining and electrowinning processes. In particular, the waste salts have highly heat generative group II fission product such as Sr and Ba nuclides and highly radioactive generative rare earth fission products. Therefore, the fission products within the waste salt should be separated and concentrated in small volume to reduce the volume of final waste [1].

In this study, layer melt crystallization process was tested for separation Group Ⅰ & II and rare earth nuclide from the LiCl-KCl molten salt.

2. Experimental

Layer melt crystallization process was carried out in a 2 Kg/batch lab-scale apparatus. LiCl-KCl crystals were recovered by layer-melt crystallization, where crystallization plate is rectangular shape with thickness of 15 mm, 60 mm wide, and 200 mm height. Module of crystallizer consisted of three thermocouples, three crystallization plates [2]. Crystallization process was controlled by temperature monitoring of around crystallizer module: outer surface of crystallization plate (Crystallizer TC), center of two crystallization plate (Center TC) and molten salt (Salt TC), as shown in Fig. 1. All the parts are located in a glove box which was kept in Ar atmosphere. 2 kg LiCl-KCl having impurities of 1wt.% Group Ⅰ & Ⅱ nuclides and 0.5wt.% rare earth nuclide respectively were melted at 440°C in a furnace. For the growth of LiCl-KCl crystal on the crystallization plates which were cooled by Ar gas with stepwise flow rate of 5 L/min to 1min and 20 L/min to 300min. After crystallization process, concentration of impurities in purified LiCl-KCl salt was analyzed using an Inductively Coupled Plasma Spectrometer.

3. Results

Solid-liquid phase diagram was identified to determine temperature condition of crystallization process and separation possibility. Fig. 2 is the solid-liquid phase diagram for the LiCl-KCl-$SrCl_2$ system drawn using the FactSage software. As shown it showed not solid solutions at 330-350°C. Therefore, it thought that separation of Group I and II nuclides and recovery of purified LiCl-KCl salt can possible in this temperature conditions of crystallization process. The purified LiCl-KCl crystals are obtained below its melting temperature of around 350°C on the crystallization plates which is cooled by Ar coolant. Solid-liquid phase diagram of LiCl-KCl-$LaCl_3$ system is shown in Fig. 3. The temperature of solid state of only LiCl-KCl eutectic is none. The phase diagram shown that this system exist temperature zone of formation of K_2LaCl_5.

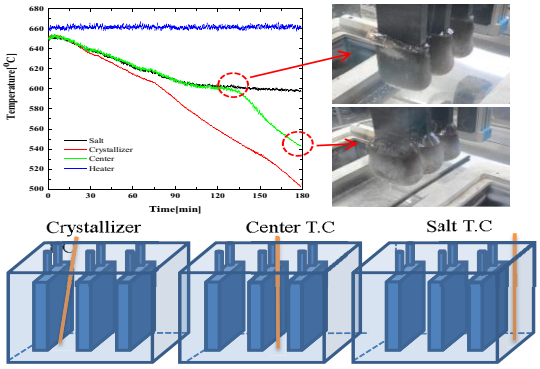


Fig. 1. Scheme of crystallizer module and temperature monitoring.

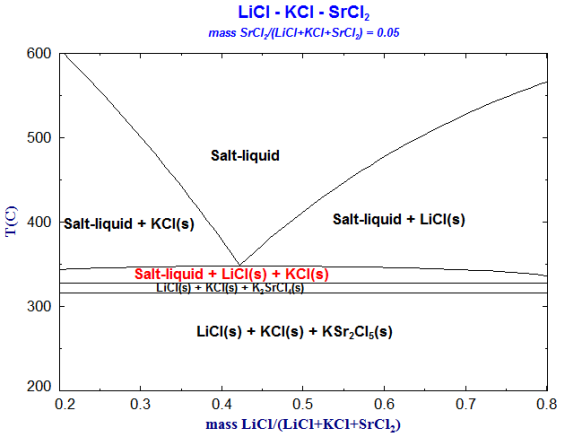


Fig. 2. Phase diagram of LiCl-KCl-$SrCl_2$ system.

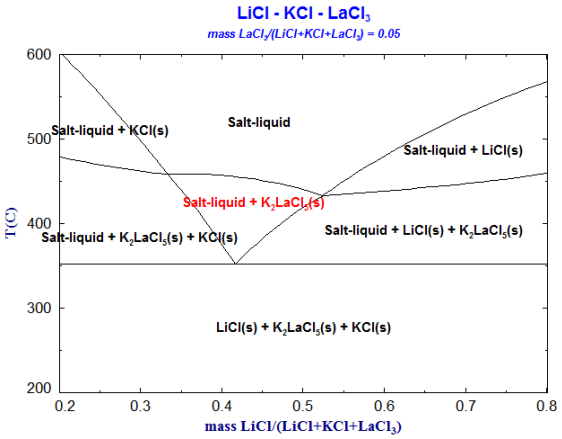


Fig. 3. Phase diagram of LiCl-KCl-$LaCl_3$ system.

REFERENCES

[1] J. H. Choi, H. C. Eun, H. S. Park, D. H. Ahn, "Study on a separation and solidification of Sr and Ba nuclides from LiCl waste salt generated from pyrochemical process", JNFCWT, 13(S), 77 (2015).

[2] Y. Z. Cho, G. H. Park, H. S. Lee, I. T. Kim and D. S. Han, " Concentration of cesium and strontium elements involved in a licl waste salt by melt crystallization process", Nucl. Technol., 171, 325 (2010).

5분과

제염해체 (Oral)

Development of Level 1 Schedule for Nuclear Power Plant Decommissioning Project in Korea

Wanil Jung*, Hae Jeong Lee, Myung Duck Yang, and Yong Beom Kwon

KEPCO E&C, 269 Hyeoksin-ro, Gimcheon-si, Gyeongsangbuk-do, Republic of Korea

*wanil@kepco-enc.com

1. Introduction

With the arrival of the permanent shutdown of Kori Nuclear Power Plant unit 1, scheduled in June 2017, the decommissioning is emerging as one of the hottest social issues. In preparation for it, this paper presents the overall project schedule at top-tier level through a comprehensive review on the anticipated tasks, interdependencies, business conditions and surroundings of the whole decommissioning process.

2. Main Discussion

2.1 Activity Listing

As the activities for this top-tier schedule, the work category and items of level 1 and 2 in the draft Work Breakdown Structure for NPP decommissioning developed previously by the author are adopted [1]. The activities consists of 8 items such as Decommissioning Planning and Licensing, Permanent Shutdown, Characterization and Environmental Evaluation, Decommissioning Engineering and Preparatory Works, Decontamination and Dismantling, Waste Management, Site Restoration, and Project Management. These items are subdivided into second level according to their own characteristics as shown in the left column of Fig. 1.

2.2 Project Milestones Setting

In order to manage large-scaled projects over a long period of time, the operation of project milestones has been believed to be very essential for the successful project control. The project milestones in Table 1 are incorporated into this top-tier schedule.

Table 1. Project Milestones, draft [2]

▪ Submit Operation Change Request	
▪ **Operation Change Permit / Permanent Shutdown**	**<Key Milestone>**
▪ Complete Characterization	
▪ Submit Draft Decommissioning Plan	
▪ **Submit Decommissioning Permit Request**	**<Key Milestone>**
▪ Start Interim Storage Facility Operation	
▪ **Decomm. Permit / Start Decont. & Dismantling**	**<Key Milestone>**
▪ Complete Transportation of Spent Fuel to Interim Storage Facility	
▪ Complete Large Components Removal	
▪ Complete Remaining System and Components Removal	
▪ Complete Building Demolition	
▪ Complete Site Restoration and Final Status Survey	
▪ **Complete Decommissioning**	**<Key Milestone>**

2.3 Duration of Major Steps in Each Phase

❍ Decommissioning Planning and Licensing Phase
- ➢ Decommissioning Plan needs to be drafted within 4 years after the permanent shutdown, and then Decommissioning Permit Request shall be filed, through the public review process including public hearing, within 5 years after the permanent shutdown.
- ➢ Planning tasks such as D&D scenario development, cost estimates, waste management planning, etc. need to be completed 1 year before submitting of Decommissioning Plan.

❍ Permanent Shutdown Phase
- ➢ 2 years are given for plant permanent shutdown, drainage, drying, and removal of system fluids and operational waste.

❍ Characterization and Environmental Evaluation Phase
- ➢ As the result of this phase is needed for decommissioning planning, it needs to be done within 2 years after the permanent shutdown.

❍ Decommissioning Engineering and Preparatory Works Phase
- ➢ Primary system decontamination is carried out right after the permanent shutdown. Modification of the existing utilities, building structures and boundary security facility follows, and waste management facility is installed.

- The design and licensing of the spent fuel storage facility is carried for two years, and 2 years are given for its manufacturing and installation.

❍ Decontamination and Dismantling Phase

- 6 months are given for the mobilization, purchase and testing of various equipment.
- 9 months for the dismantling of the Steam Generator, Reactor Cooling Pumps and pressurizer, 15 months for Reactor Vessel Internal segmentation, and 12 months for the cavity drain and drying are assumed respectively.
- Demolition of buildings and yard structures starts 1 year after the commencement of component removal and finishes in 3 years after the component removal.

❍ Waste Management Phase

- The waste management proceeds in parallel with the dismantling work.

❍ Site Restoration

- After the building demolition, the demolition of remaining facilities, site decontamination, environmental restoration work and final status survey proceeds for 1 year, followed by the submitting of decommissioning completion report and deregulation process for another one and half years.

2.4 Level 1 Schedule, Draft

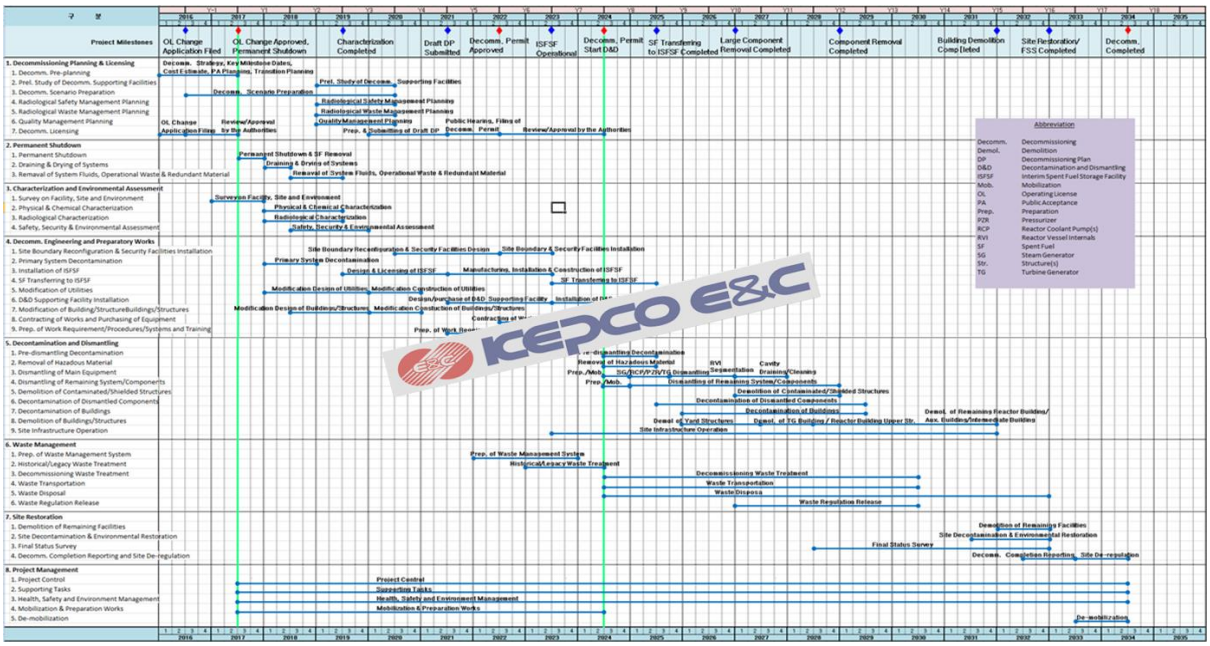


Fig. 1. Project Top-tier Schedule for NPP Decommissioning (Level 1), draft.

3. Conclusion

This paper introduces the top-tier overall schedule for the whole phases of the decommissioning project in Korea with a view to provide overview of the decommissioning sequence and duration.

Henceforward, this schedule is expected to be elaborated through the discussion by relevant parties on the various aspects including contract structure, spent fuel interim storage facility, applied decontamination technology, dismantling method, licensing requirement, site release criteria, etc.

REFERENCES

[1] Wanil Jung, Yong Beom Kwon, and Byung-sik Lee, “Development Direction of Work Breakdown Structure for Nuclear Power Plant Decommissioning Project”, Journal of Power Engineering, Vol. 66, 2015.

[2] Wanil Jung, Yong Beom Kwon, and Jai Hoon Jung, “Development of Draft Project Milestones for Nuclear Power Plant Decommissioning Project”, Proceedings of the KRS 2016 Spring Conference, 2016.

Fabrication and Cs Removal Performance of Various Metal-ferrocyanide Functionalized Magnetic Adsorbents

Kyu Sun Hwang, Chan Woo Park, In-Ho Yoon, Kune-Woo Lee, and Hee-Man Yang*

Korea Atomic Energy Research Institute, 111, Daedeok-daero 989beon-gil, Yuseong-gu, Daejeon, Republic of Korea

*hmyang@kaeri.re.kr

1. Introduction

A huge amount of radioactive contaminants have leaked and spread over a large area of soil and water from the nuclear accident sites at Fukushima Daiichi nuclear power station in 2011.

Radioactive cesium (^{137}Cs) is the most dangerous radioactive contaminant associated with nuclear fall out and radioactive liquid waste due to its long half-life (30.2 years), high-energy gamma ray (γ-ray) emissions, and biological interactions, which are similar to those of potassium [1].

A variety of cesium adsorbents, including zeolites, ammonium molybdophosphate (AMP), silicotitanate (CST), and metal-ferrocyanide were extensively investigated for their ability to remove radioactive cesium from water [2].

Metal-ferrocyanide; such as iron ferrocyanide (prussian blue) is known as a low cost adsorbent which has a high selectivity for cesium and high stability for decomposition. However, very fine powder forms of metal-ferrocyanide are difficult to collect the adsorbents used after applying them into the environment [3].

In the present study, metal-ferrocyanide functionalized magnetic nanoclusters were fabricated for the removal of cesium and rapid magnetic separation of absorbent from contaminated water.

2. Materials and methods

2.1 Fabrication of magnetic adsorbents

The procedure used to synthesize the MFC-MNCs (M = Co, Ni, Cu) for the removal of Cs is illustrated in Fig. 1. First, the as-synthesized magnetic nanoclusters (MNCs) were synthesized via a hydrothermal reaction in the presence of succinic acid (SA), 1,6-Hexanediamine (HMD), and citric acid (CA) as a capping ligand. Naming the SA-MNCs, HMD-MNCs, and CA-MNCs, respectively.

Succinic acid (SA) with the carboxylate have strong coordinative affinity towards metal ions. In case of SA-MNCs, the negatively charged carboxylate ions. These carboxylate ions capture the toxic metal ions by forming chelate complexes.

Polyethyleneimine (PEI) was employed as a foundation material to functionalize the surfaces of the HMD-MNCs and CA-MNCs with CuFC due to the outstanding adsorption properties of PEI toward heavy metals, such as Cu ions.

After immobilizing the MFC onto the SA-MNCs and PEI-MNCs surfaces, we conducted adsorption tests using inactive and radioactive cesium (^{137}Cs) to evaluate their cesium removal performance.

2.2 Characterization of magnetic adsorbents

The fabricated CoFC-MNCs, NiFC-MNCs, CuFC-MNCs-1, and CuFC-MNCs-2 were characterized by X-ray diffractometer (XRD), Fourier transform infrared spectroscopy (FTIR), Transmission electron microscopy (TEM), and Dynamic light scattering instrument (DLS), vibrating sample magnetometer (VSM).

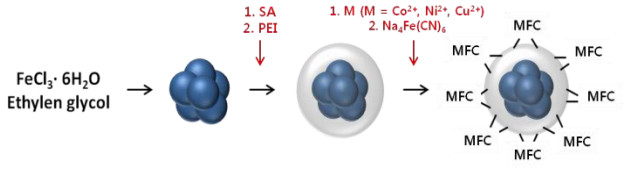


Fig. 1. Synthesis of magnetic adsorbents for the removal of cesium.

3. Results and Discussion

The crystalline structure of the MCNs was determined by XRD, as shown in Fig. 2. The XRD analysis revealed six characteristic peaks at 2θ = 30.1, 35.5, 43.1 53.4, 57.0, and 62.6°, corresponding to the (220), (311), (400), (422), (511), and (440) phases of Fe_3O_4, respectively, indicating that the magnetic

nanoclusters consisted of a Fe_3O_4 phase. The peaks in the XRD results confirmed that the Fe_3O_4 in the SA-MNCs, HMD-MNCs, and CA-MNCs had a high crystallinity.

FTIR analysis also revealed the successful coating of CoFC, NiFC, and CuFC onto the MNCs surfaces. As shown in Fig. 3, a strong absorption peak corresponding to the cyanide groups of hexacynoferrate appeared at 2100 cm^{-1} in the FTIR spectra, indicating that the CoFC-MNCs, NiFC-MNCs, CuFC-MNCs-1, and CuFC-MNCs-2 were successfully functionalized with MFC.

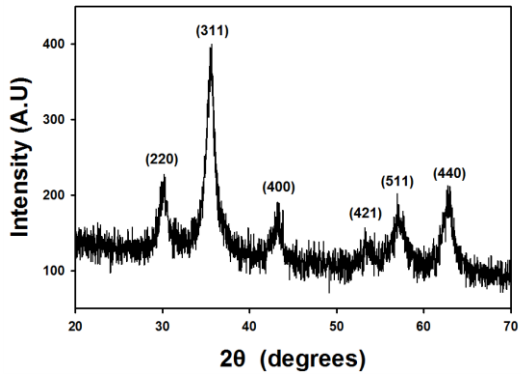


Fig. 2. XRD patterns obtained from the MNCs.

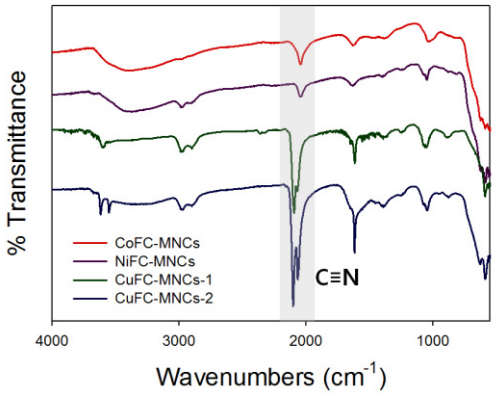


Fig. 3. FTIR spectra of the MFC-MNCs.

The Cs removal performance of the MFC-MNCs were evaluated by measuring the adsorption isotherms using inactive Cs. The experimental isotherm data were analyzed as Langmuir isotherm (Fig. 4). The excellent fit to the Langmuir isotherm curve suggested monolayer adsorption of Cs onto the MFC-MNCs surfaces. The maximum adsorption capacity (q_{max}) of the adsorbents were 15.63 mg/g (CoFC-MNCs), 12.11 mg/g (NiFC-MNCs), 125 mg/g (CuFC-MNCs-1), and 166.7 mg/g (CuFC-MNCs-2), respectively

The MFC-MNCs provided a high removal efficiency exceeding 99.09% of the ^{137}Cs.

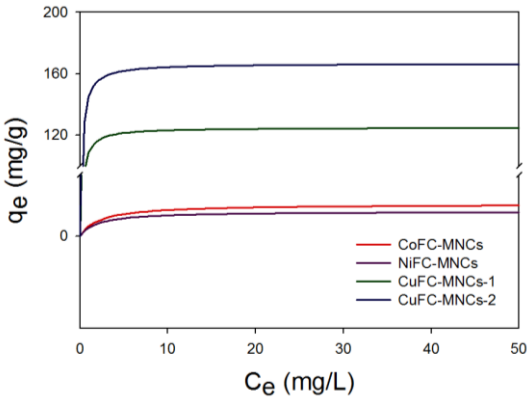


Fig. 4. Adsorption isotherm data obtained from the MFC-MNCs. The curve fits were obtained from the Langmuir isotherm.

4. Conclusions

In this study, we successfully fabricated metal-ferrocyanide modified magnetic nanoclusters (MFC-MNCs). The MFC-MNCs exhibited high removal efficiency of cesium in water and showed rapid magnetic separation of the adsorbents from the water after treatment. They have great potential for the treatment of liquid waste containing radioactive cesium (^{137}Cs). The magnetic adsorbents can be easily recovered once spread into an open environment.

REFERENCES

[1] Brumfiel G, "Fukushima set for epic clean-up", Nature, 472, 146-147 (2011).

[2] E.H.Borai, R.Harjula, L.Malinen and A.Paajanen, “Efficient removal of cesium form low-level radioactive liquid waste using natural and impregnated zeolite minerals”, J. Hazard. Mater, 172(1), 416-422 (2009).

[3] P .A. Hass, “A review of information on ferrocyanide solid for removal of cesium from solutions”, Sep. Sci. Technol, 28, 2479-2506 (1993).

Effects of Site Characteristics on Dose Assessment in NPP Decommissioning

Sanghyun Hong[1*], Woongik Hwang[1], Yongmin Kim[2], Seokyoung Ahn[3], and Jong Seh Lee[1]

[1]Hanyang University, 55 Hanyangdaehak-ro, Sangnok-gu, Ansan, Gyeonggi-do, Republic of Korea

[2]Catholic University of Daegu, 13-13 Hayang-ro, Hayang-eup, Gyeongsan-si, Gyeongsangbuk-do, Republic of Korea

[3]Pusan National University, 2, Busandaehak-ro 63beon-gil, Geumjeong-gu, Busan, Republic of Korea

[*]jerom1st@hanyang.ac.kr

1. Introduction

In the decommissioning of a nuclear power plant (NPP), the principal objective of a site remediation is to prevent contamination occurring. According to IAEA's Safety Guide [1], the site release and the reuse are considered as the final step of NPPs decommissioning. The six phases for the remediation are listed in Table 1 [2]. These phases are based on the data of a site characterization which requires a site-specific suite of radionuclides. For the NPP decommissioning, the characterization survey, which is consisting of identifying the environmental problems, collects the appropriate data necessary to demonstrate that the site meets the release criterion. In the case of advanced countries, a contractor is experienced and will leverage lessons learned from other decommissioning projects. In Korea, however, there is a limit to the use of base information.

This study aims at selecting the parameters of the site characterization for the NPPs decommissioning. To that end, the effects of the parameters are investigated by using RESRAD.

Table 1. Project Phases for NPP Decommissioning [2]

Phases	Actions
1	Problem definition
2	Remedial investigation
3	Remedy planning
4	Remedial action
5	Project closeout
6	Institutional control

2. Parameters based on site characterization

A dose modeling for the site release involves using radiological exposure pathways to determine the dose to an individual from residual radioactive material as shown in Fig. 2. In this study, a resident farmer scenario, which is more conservative than other scenarios, is considered for the critical population group. For comparison, four parameters are selected and tabulated in Table 2.

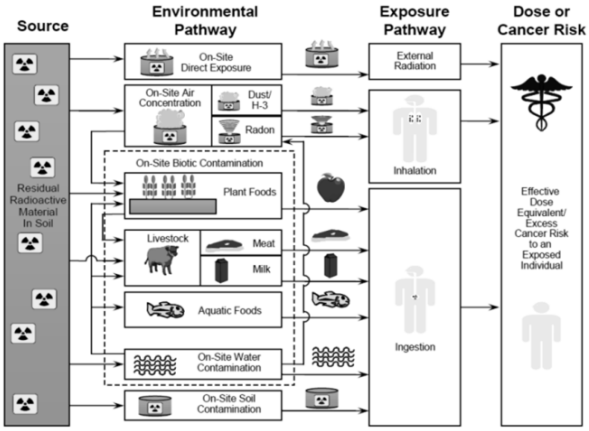


Fig. 1. Exposure Pathways Considered in RESRAD [3].

Table 2. Parameters for Case Studies

Case	Parameters
A	Area of contaminated zone
B	Thickness of contaminated zone
C	Initial concentration of radionuclide
D	Cover depth (Erosion rate 0)

3. Case studies and results

To examine the effect of the parameters, the reference model used by KINS-GR-297 [4] is considered by using RESRAD-ONSITE code. Fig. 2 shows the total effective dose equivalents (TEDE) of each case for four parameters.

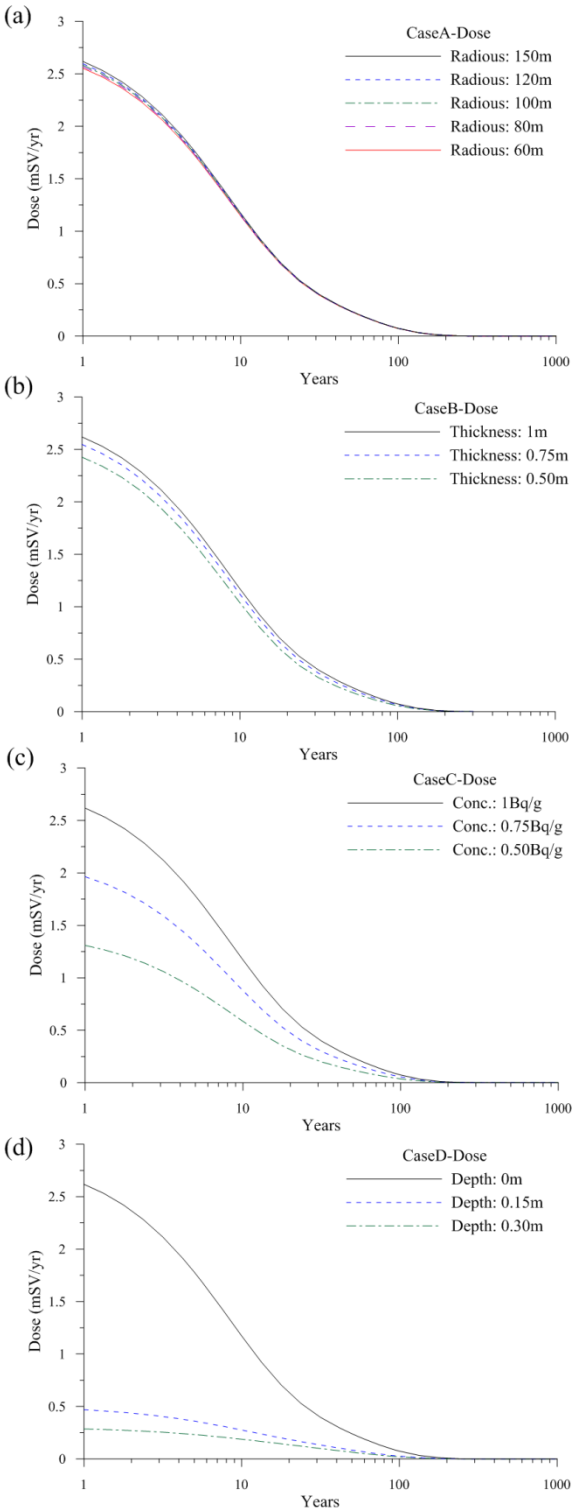


Fig. 2. TEDEs for All Pathways: (a) Area, (b) Thickness, (c) Cover depth, (d) Concentration of Radionuclide.

It is shown that, the area (Case A) and the thickness (Case B) of the contaminated zone have little effect on the dose assessment. On the other hand, the initial concentration of radionuclide (Case C) and the cover depth (Case D) can significantly reduce the TEDE. When the cover depth is increased to about 30 cm, it is possible to reduce the exposure dose most effectively and to shorten it to about 31 years in order to satisfy the site release criterion (0.1 mSv/yr).

4. Conclusion

In this study, the effects of the site characteristics for NPP Decommissioning are investigated by using RESRAD code which includes Co-60 and Cs-137. Through the case studies, it is shown that the cover depth for the site remediation is greatly influenced to the dose assessment. This is because the cover is reduced the external exposure to the contaminated soil. In addition, to restore the NPP site to Greenfield, an appropriate dose assessment should be performed on the cover condition.

ACKNOWLEDGEMENT

This research was supported by a Korea Foundation of Nuclear Safety (KoFONS) grant funded by the Nuclear Safety and Security Commission (NSSC) (No. 1305009-0416-CG100).

REFERENCES

[1] IAEA, Release of sites from regulatory control on termination of practices, International Atomic Energy Agency, IAEA Safety Standards, Safety Guide No. WS-G-5-1 (2006).

[2] OECD-NEA, Nuclear site remediation and restoration during decommissioning of nuclear installations, NEA No. 7192 (2014).

[3] Argonne National Laboratory (ANL), User's manual for RESRAD, Version 6, ANL/EAD-4 (2001).

[4] Korea Institute of Nuclear Safety (KINS), Development of regulatory technology for radioactive waste, KINS-GR-297 (2005).

Integration of the Unit Modules of the Nuclear Facility Dismantle Simulation System

Ikjune Kim*, ByungSeon Choi, Dongjun Hyun, JeiKwon Moon, Jonghwan Lee, KwanSeong Jeong, and Shinyoung Kang
Korea Atomic Energy Research Institute, 111, Daedeok-daero 989beon-gil, Yuseong-gu, Daejeon, Republic of Korea
*ikjunekim@kaeri.re.kr

1. Introduction

The dismantling of nuclear facilities takes a very long time and is a dangerous procedure. Thus, it should go through a process optimization procedure based on the process simulation. The process simulation pre-evaluates the operation time and cost, and checks the possibility of danger of the dismantling procedures, thereby enhancing the safety of the dismantling [1]. We developed unit modules for flexible dismantle simulation system, Cutting simulation module, Human dose calculation module and Scenario assessment module. And we integrate all the modules we implement to use for scenario assessment.

2. Unit modules

In this chapter, we introduce the modules of the main functionalities of the dismantle simulation system.

2.1 Cutting Simulation module

The Cutting simulation module provides the instant cutting function of the target model. Also a user can input arbitrary cutting path of various combinations of the cutters and carriers to create a cutting activity by haptic device as well as Graphical User Interface (GUI). And the cutting activity can be updated during scenario modeling procedure. Fig. 1 shows an example scenario of cutting simulation. In the Fig. 1 target model (upper internal) is cut by a circular saw which is carried by robot manipulator.

2.2 Human dose calculation module

The worker dose rate is calculated based on worker path and working time in the simulation system. A user can easily model the working path and working motion of the worker by using the human manikin model in the simulation system and based on the dose rate of the model we can calculate a worker dose rate. Fig. 2 shows an example of worker dose calculation.

2.3 Scenario assessment module

After modeling the scenario, using the Scenario assessment module, a user can calculate the cost and time of the scenario based on each activity in it.

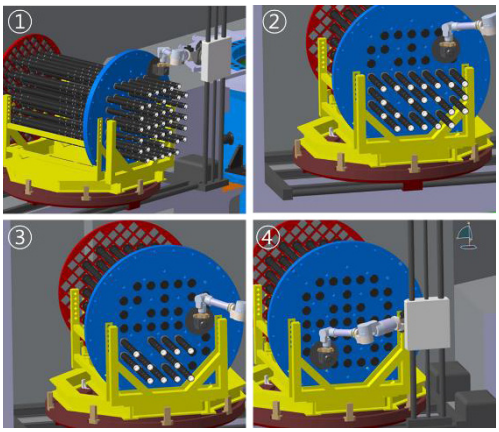
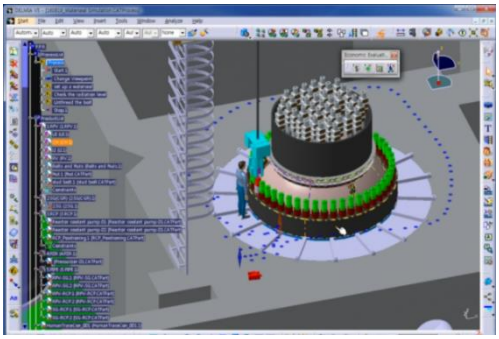


Fig. 1. Cutting Simulation.


Fig. 2. Example of worker dose calculation.

3. Integration of the modules

Each module is implemented as a Dynamic Linked Library (DLL). And all modules are bound to the simulation system at runtime. The system structures are shown in Fig. 3. Functional module are placed top position of the diagram and those modules refer to the common module which provides interfaces of the Delmia System.

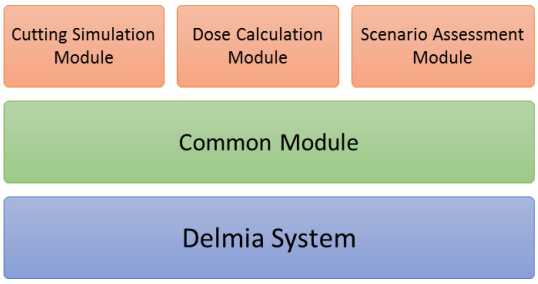


Fig. 3. System Integration Scheme.

4. Conclusion

Previously, we implemented necessary functions to simulate the dismantle process of the nuclear facility which are implemented in each module. And finally we integrate all the modules to evaluate the dismantle scenario quantitatively. In the future, this system framework can be used scenario optimization based on scenario assessment result.

Acknowledgements

This work was supported by the nuclear research and development program through the national research foundation of Korea funded by the Ministry of Science, ICT & Future Planning.

REFERENCES

[1] I. Kim, B. Choi, D. Hyun, J. Moon, J. Lee, K. Jeong, et al., A framework for a flexible cutting-process simulation of a nuclear facility decommission, Annals of Nuclear Energy, vol. 97, pp. 204-207, 2016.

[2] G. Ryu, et al., Guidance weapon assembly simulation using the DELMIA. KSAS Conference 2008, Vol. 2, p. 1220-1223, 2008.

[3] I. Kim, et al., Cutting Method of the CAD model of the Nuclear facility for Dismantling Simulation, Transactions of the Korean Nuclear Society Spring Meeting, Jeju, Korea, May 7-8, 2015 Journal of Nuclear Fuel Cycle and Waste Technology, 1(1), 1-10 (2015).

Estimation of Waste Volume for Kori # 1 Decontamination Using SP-HyBRID Process

Sang Yoon Park*, Wang Kyu Choi, Seong Byeong Kim, Hui Jun Won, and Man Soo Choi
Korea Atomic Energy Research Institute, 111, Daedeok-daero 989beon-gil, Yuseong-gu, Daejeon, Republic of Korea
*nsypark@kaeri.re.kr

1. Introduction

Kori # 1, the first pressurized water reactor (PWR) in Korea will permanently shut down in this year. Before decommissioning of shut-downed nuclear power plant, the primary side of the plant should be decontaminated. And it is necessary to review the radioactive waste minimization methods for system decontamination. The CORD process or CITROX process are the chemical decontamination processes currently used due to the low amount of secondary waste produced using in situ decomposition of oxalic acid. Large volume of spent ion-exchange resin, however, is generated because of primary waste such as radioactive materials, corrosion products and residual citric acid/nitric acid etc.

KAERI has been developing a new decontamination process that does not contain any organic chemicals in the decontamination solution and minimizes the use of ion exchange resin in the solution purifying step [1-3]. The process is hydrazine base reductive metal ion decontamination for decommissioning (HyBRID) and consists of N_2H_4, H_2SO_4 and Cu^{2+} ions. A sulfuric acid permanganate process (H_2SO_4 + $KMnO_4$) is used in HyBRID as a pre-oxidative decontamination step. To minimize the waste volume, residual hydrazine is decomposed with hydrogen peroxide and the sulfate ions are precipitated by the addition of $Ba(OH)_2$ or $Sr(OH)_2$ followed by filtration with a candle filter.

In this study, we performed small-scale and bench-scale experiments of hydrazine decomposition, sulfate precipitation and solid-liquid separation. And the waste volume for Kori #1 system decon-tamination using SP-HyBRID process was calculated and was compared with NP-CITROX or HP-CORD process.

2. Waste Treatment for SP-HyBRID

2.1 On-Line Monitoring of Decontamination Process

Fig. 1 shows the on-line monitoring system to demonstrate the decontamination chemical make-up, the permanganate and hydrazine decomposition, $BaSO_4$ precipitation and process monitoring of SP-HyBRID process.

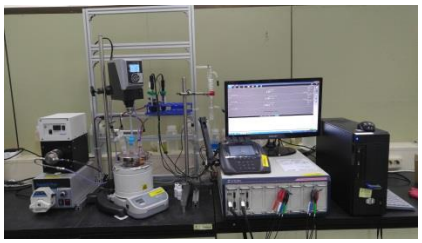


Fig. 1. On-Line Monitoring System.

2.2 Oxidative Step Process

Sulfuric acid permanganate is used in oxidative decontamination step at 95°C with various durations depending on the operating conditions. Typical concentrations of $KMnO_4$ and H_2SO_4 are 6.33 mM and 3.25 mM, respectively. After pre-oxidation treatment, residual permanganate is decomposed with N_2H_4 as follows:

$$4KMnO_4 + 5N_2H_4 + 6H_2SO_4 \rightarrow 4K^+ + 4Mn^{2+} + 5N_2 + 16H_2O + 6SO_4^{2-}$$

The solution after $KMnO_4$ decomposition can be used in the next reductive step with no refill or drain.

2.3 Reductive Step

In reductive decontamination step, 50 mM N_2H_4 + 0.5 mM Cu^{2+} ions + 25 mM H_2SO_4 of solution is used at 95°C for 10 h. After the reductive step, there are several sorts of metal ions, potassium ions and sulfate in the decontamination solution. The necessary concentration of barium hydroxide to precipitate of 28.25 mM sulfate is about 30 mM. Because of the very low value of the solubility

product for $BaSO_4$ (i.e., 1.084 x 10^{-10} at 25°C), sulfate ions can be removed from the solution with the addition of the same concentration of barium ions, which is then followed by solid-liquid separation of the precipitated particles. There are several kinds of metal ions in the used solution at the end of the HyBRID process, such as primary wastes (e.g., corrosion products including Fe^{2+}, Ni^{2+}, Cr^{3+}, etc.), secondary wastes (e.g., Mn^{2+}, Cu^{2+}, etc.) and radioactive materials (e.g., Co-60, Co-58, Mn-54, Cr-51, etc.).

3. Results and Discussion

3.1 Process Monitoring

Fig. 2 shows a typical ORP monitoring result for SP-HyBRID process: the oxidative step, decomposition of permanganate, reductive step, decomposition of hydrazine, precipitation of sulfate ions, etc. It is very useful for making the decision to add chemicals or to stop, which is valuable to the waste minimization.

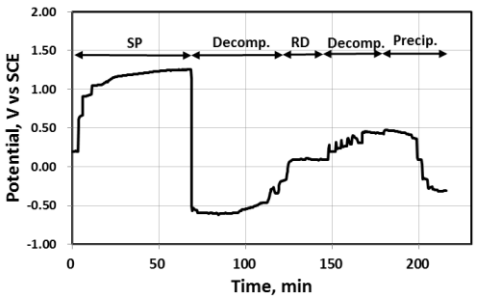


Fig. 2. Typical ORP Monitoring Curve.

3.2 Final Waste Treatment

The simulated decontamination solution was made-up and mixed with $Ba(OH)_2$ solution to remove the sulfate ions in the form of BaSO4 precipitates. After precipitation of sulfate ion, the precipitated particulate should be removed from liquid waste solution. Fig. 3 shows the morphology of the cake made by candle filtration of simulated liquid waste for a 1 cycle SP-HyBRID process. Apparent density of the cake was 2.56 g/cm^3 which will be used to calculate the waste volume for Kori #1 decontamination with the SP-HyBRID process. Before and after precipitation, the chemical concentration in the solution was analyzed with AA and it was conformed that most of sulfate ions and metal ions (higher than 99.5%) were removed from the decontamination solution to solid. It means that only 0.5% of anion and metal ions can be removed by ion-exchange resin.



Fig. 3. Cake Morphology of $BaSO_4$ Precipitates.

4. Conclusion

SP-HyBRID decontamination process can be used to decontamination of Kori # 1 with a minimization of spent ion-exchange resin before decommissioning. The total volume of solid waste can be reduced 1/10 less than that of a commercial process and spent ion-exchange resins can be reduced to 1% of that of a commercial process.

ACKNOWLEDGEMENTS

The authors would like to express their appreciation to National Research Foundation of Korea (NRF) for the Future Planning (MSIP) of the Republic of Korea, in support of the authors' work through the Nuclear Research and Development Program (NRF-2012-M2A8A5025655).

REFERENCES

[1] S.B. Kim, H.J. Won, J.K. Moon, and W.K. Choi, Magnetite dissolution using hydrazine-acid solution for chemical decontamination, Transactions of the American Nuclear Society, Vol. 115, Las Vegas, USA (2016).

[2] S.Y. Park, H.J. Won, M.S. Choi, S.B. Kim, W.K. Choi, and J.K. Moon, Waste Minimization of HyBRID Decontamination Process, WM2017 Conference, March 5-9, Phoenix, Arizona, USA (2017).

[3] H.J. Won, W.S. Lee, C.H. Jung, S.Y. Park, W.K. Choi, and J.K. Moon, Asian J. Chem. 25, 5, p. 1327-1330 (2014).

Studies on the Behavior of Spontaneous Reductive Decomposition of Hydrogen Permanganate in Water for HP/CORD Process

Hyun-Kyu Lee*, June-Hyun Kim, Won-Zin Oh, and Sang-June Choi

Kyungpook National University, 80 Daehakro, Bukgu, Daegu 41566, Republic of Korea

*lhk7933@knu.ac.kr

1. Introduction

The permanganic acid ($HMnO_4$) as oxidizing agent is usually used to dissolve the NPP oxide layers containing Cr (III) in HP/CORD process [1]. However, little attention has been made for the spontaneous reductive decomposition of $HMnO_4$, which is a competing reaction with the oxidation of the chromium oxide by permanganate. The objective of this study is to investigate the spontaneous reductive decomposition behavior of $HMnO_4$ for HP/CORD process, depending on the variation of initial concentration of $HMnO_4$.

2. Materials and methods

2.1 Reagents

All reagents were analytical grade and were used without further purification. Deionized water (18.3 MΩ·cm), which was prepared using a water purification system (Nex Power 1000, Human corporation, Korea) was used to prepare all aqueous solutions. Potassium permanganate ($KMnO_4$, above 99.3%) was purchased from DAEJUNG, Korea. Ambelite IRN-77 (cation exchange resin) was obtained from Rohm and Haas, USA.

2.2 Preparation of $HMnO_4$

$HMnO_4$ was prepared in the following manner: A known amount of potassium permanganate ($KMnO_4$) was dissolved in a known volume of deionized water. Then, the $KMnO_4$ solution was passed through the packed glass column containing cation exchange resin at a flow rate of 5 BV/h. After passing through the glass column, the pH value and K^+ concentration of the source solution were measured by pH meter (STARA211, Thermo Orion, USA) and ICP-OES (Optima 2100DV, PerkinElmer Co., USA), respectively, for determining whether the cation exchange ($K^+ \rightarrow H^+$) was completely conducted.

2.3 Apparatus and procedure

All experiments were carried out in 500 mL glass reaction vessels equipped with reflux condenser, thermometer, mechanical stirrer, and electric heating mantle. Reaction volumes were nomally 200 mL and were stirred at 250 rpm. The temperature was maintained at 90°C. Aliquots obtained from each experiment were quickly cooled, diluted, and placed in a dark bottle to avoid further reaction. The concentration of residual permanganate was determined by UV-visible spectrophotometer (Agilent 8453, Agilent technologies, USA) after filtration (0.2 um, Whatman, nylon membrane filters).

3. Results and discussion

3.1 Effect of the initial concentration of $HMnO_4$

The change of concentration of residual permanganate against time at different initial concentration (1, 2, 3, 6 mM) of $HMnO_4$ is shown in fig. 1. Although, during the first 10 min of the reaction, the spontaneous reductive decomposition behavior of $HMnO_4$ appeared to be a first-order reaction, the overall reaction has almost approached equilibrium after 60 min reaction. These phenomenons are because the rapid, reversible equilibrium between permanganate and manganous ions, according to the following chemical equations [2]:

$$4MnO_4^- + 12H^+ \leftrightarrow 4Mn^{2+} + 5O_2 + 6H_2O \quad (1)$$

$$Mn^{2+} + MnO_4^- + H_2O \leftrightarrow Mn^{3+} + HMnO_4^- + OH^- \quad (2)$$

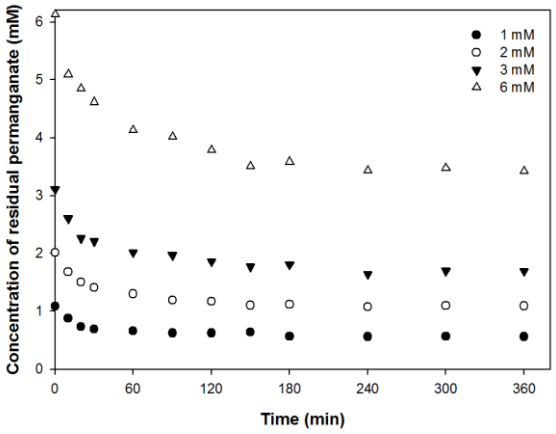


Fig. 1. Concentration of residual permangante according to time with different initial concentration of $HMnO_4$.

The difference of the initial concentration of $HMnO_4$ did not affect the rate of spontaneous reductive decomposition of $HMnO_4$ (Fig. 2). The fractions of residual permanganate were similar in all conditions after 360 min reaction.

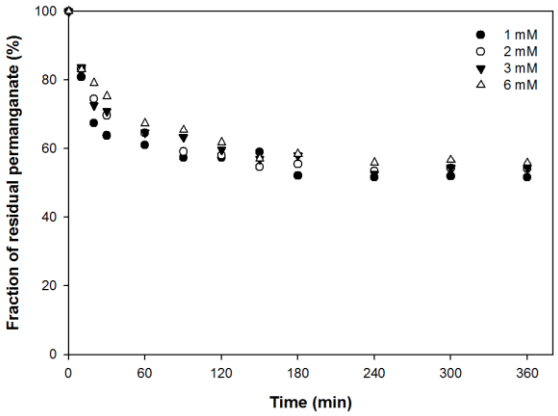


Fig. 2. The fraction of residual permanganate according to time with different initial concentration of $HMnO_4$.

3.2 Effect of manganese dioxide

The effect of decomposition product MnO_2 on the reaction of spontaneous reduction of $HMnO_4$ was studied. In Fig. 3, the spontaneous reduction of $HMnO_4$ was rapidly processed within 30 min and nearly reached to equilibrium after 60 min, which was maintained for 630 min. However, after filtering the produced MnO_2 particles from $HMnO_4$ in the reaction at 210 and 420 min, the spontaneous reduction of $HMnO_4$ was again processed, even if the reaction of spontaneous reduction of $HMnO_4$ was in equilibrium before filtering MnO_2. The removal of MnO_2 from a solution approached equilibrium reaction of spontaneous reductive decomposition of $HMnO_4$ could lead to spontaneous reduction of permanganate again.

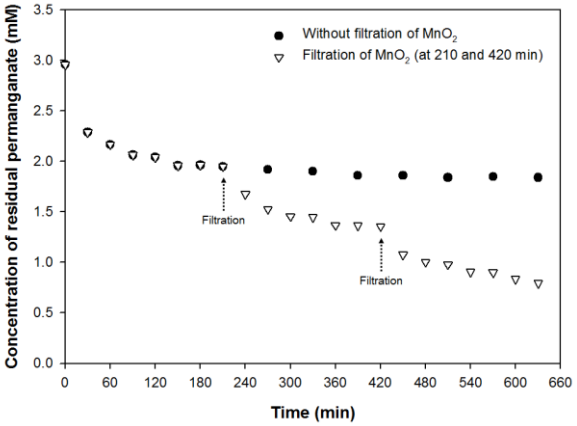


Fig. 3. Effect of removal of MnO_2 on spontaneous reductive decomposition of $HMnO_4$ during the decomposition reaction.

4. Conclusions

The spontaneous reductive decomposition of permanganate in $HMnO_4$ showed the slow decomposition behavior followed by the rapid decomposition in the early times. The decomposition product (MnO_2) is considered to take the main roles on the decomposition kinetics in the early stage of the crystal growth.

ACKNOWLEDGMENTS

This work was supported by the Korea Institute of Energy Technology Evaluation and Planning (KETEP) and the Ministry of Trade, Industry & Energy (MOTIE) of the Republic of Korea (No. 20141510300310).

REFERENCES

[1] P. Kinnuen, ANTIOXI-Decontamination techniques for activity removal in nuclear environments. Brussels (Belgium): VTT Technical Research Centre of Finland (2008) Report no. VTT-R-00299-08.

[2] A. W. Adamson, The kinetics of the manganous-permanganate reaction. Journal of physical chemistry, 55(2), 293-303 (1951).

5분과

제염해체 (Poster)

Fluidity of Cement Solidification of Residual Radioactive Waste

Daeseo Koo*, Hyun-Hee Sung, Seung-Soo Kim, Sang Bum Hong, Bum Kyoung Seo, and Jong-Won Choi
Korea Atomic Energy Research Institute, 111, Daedeok-daero 989beon-gil, Yuseong-gu, Daejeon, Republic of Korea
*ndskoo@kaeri.re.kr

1. Introduction

About ten-thousand drums of uranium soil waste from the demolition of a uranium conversion facility have been stored from 2010 until now at KAERI. The cost of their permanent disposal is very expensive. To solve this pending problem, a study on electrokinetic decontamination of uranium soil waste has been conducted. The technology of electrokinetic decontamination eliminates contaminated material in soil using a direct current. It enables various contaminated materials such as heavy metals, radioactive elements, and organic materials in soil to be removed with low permeability. Residual radioactive waste is generated from the process of electrokinetic decontamination of uranium soil waste [1-2]. To perform permanent disposal of residual radioactive waste, a study on its cement solidification has been conducted [3-5].

In this study, a fluidity experiment of cement solidification has been conducted to analyse the characteristics of cement solidification on residual radioactive waste. The compressive strength of the specimens of moulding cement solidifications has also been measured and analyzed.

2. Main title

2.1 Experiment and measurement

2.1.1 Specimen preparation. To prepare the specimens, cement (Portland cement type I) and water were mixed, and waste was also mixed together using a mortar mixer (HJ-1150) according to Table 1. The mixed materials were solidified for 4 weeks by covering vinyl on them. The cylindrical moulding cement solidifications were cut into 50mm diameter and 100 mm height using a micro cutter. The equipment (HCT-DC50) shown in Fig. 1 was used to measure the compressive strength of cement solidification. The receiving criterion on the compressive strength of KORAD (Korea Radioactive Waste Agency) is 34 kg·f/㎠.

Table 1. Condition of Flow Test for Cement Solidification

Specimen	Waste(g)	Cement(g)	Water(g)
C-2.0-60	2.0(106.95)	1(53.481)	1.80(96.253)
C-2.0-70	2.0(97.560)	1(48.786)	2.10(102.44)
C-2.0-80	2.0(89.687)	1(44.849)	2.40(107.62)
C-1.8-60	1.8(103.56)	1(57.541)	1.68(96.657)
C-1.8-70	1.8(94.435)	1(52.471)	1.96(102.83)
C-1.8-80	1.8(86.788)	1(48.221)	2.24(108.00)
C-1.6-45	1.6(116.60)	1(72.890)	1.17(85.270)
C-1.6-50	1.6(110.30)	1(68.970)	1.30(89.640)
C-1.6-60	1.6(99.620)	1(62.270)	1.56(97.130)

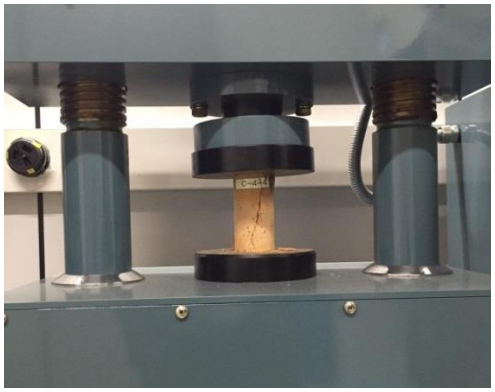


Fig. 1. Measurement of compressive strength.

2.1.2 Fluidity analysis of cement solidification. Tables 2~4 show the fluidity results of cement solidification (C-1.6, C-1.8, C-2.0) for residual metal hydroxide waste. The fluidity of cement solidifications is different from the ratio of cement to waste. As the quantity of water increases, the fluidity of cement solidifications showed an increasing trend. The workability of cement solidifications based on the receiving criterion of the compressive strength of KORAD was about 175~190%. Table 5 shows the compressive strength of cement solidification (C-1.6, C-1.8, C-2.0). The compressive strength of the cement solidifications (C-1.6-45, C-1.8-60, C-2.0-60),

which have relatively small ratios of waste and cement to water, showed an increasing trend. The compressive strength of all cement solidifications (C-1.6, C-1.8, C-2.0) was acceptable for the receiving criterion of the compressive strength of KORAD. As the amount of water of each cement solidification increases, the compressive strength of its cement solidification showed a decreasing trend.

Table 2. Condition Result of Flow Test for Cement Solidification(C-1.6)

Round	C-1.6-45	C-1.6-50	C-1.6-60
1	166%	182%	240%
2	168%	184%	217%
3	164%	185%	216%
4	162%	181%	219%
Average	165.0%	183.0%	223.0%

Table 3. Condition Result of Flow Test for Cement Solidification(C-1.8)

Round	C-1.8-60	C-1.8-70	C-1.8-80
1	183%	209%	220%
2	185%	212%	219%
3	190%	207%	225%
4	188%	200%	226%
Average	186.5%	207.0%	222.5%

Table 4. Condition Result of Flow Test for Cement Solidification(C-2.0)

Round	C-2.0-60	C-2.0-70	C-2.0-80
1	170%	200%	210%
2	175%	200%	225%
3	180%	210%	220%
4	174%	204%	213%
Average	174.8%	203.5%	217.0%

Table 5. Compressive Strength of Cement Solidification

Specimen	Compressive Strength (kg·f/㎠)		
C-2.0-60/70/80	124.49	86.225	64.898
C-1.8-60/70/80	127.55	99.490	82.857
C-1.6-45/50/60	174.90	169.18	131.94

3. Conclusion

An experiment for the fluidity of cement solidification was conducted to analyse the characteristics of cement solidification for residual radioactive waste. As the quantity of water increases, the fluidity of cement solidification shows an increasing trend. The fluidity of cement solidification is different from the ratio of cement to waste. As the quantity of water increases, the fluidity of cement solidification for residual radioactive waste shows an increasing trend. The workability of cement solidification shows about 175~190%. The compressive strength of all cement solidifications (C-1.6, C-1.8, C-2.0) was acceptable for the receiving criterion of compressive strength of KORAD. As the quantity of water for each cement solidification increases, the compressive strength of its cement solidification showed a decreasing trend.

REFERENCES

[1] G.N. Kim, H.J. Won, C.H. Jung, J.H. Yoo, W.Z Oh, “Effect of pH on Soil Remediation by Eletrokinetic”, Journal Korean Solid Wastes Engineering Society, 17, 781-788 (2000).

[2] G.N. Kim, S.S. Kim, H.M. Park, W.S. Kim, J.K. Moon, J.H Hyeon, (2012) “Development of Complex Electrokinetic Decontamination Method for Soil Contaminated with Uranium”, Electrochimica Acta, 86, 49-56 (2012).

[3] K.H. Kim, J.W. Lee, Y.G. Ryue, (1998) “Evaluation on the Long-Term Durability and Leachability of Cemented Waste Form”, KAERI/TR-1118/98.

[4] G.H. Jeong, K.J. Jung, S.T. Baik, U.S. Chung, K.W. Lee, S.K. Park, D.G. Lee, H.R. Kim, (2001) “Solidification of Slurry Waste with Ordinary Portland Cement”, KAERI/RR-2194/2001.

[5] Y.J. Lee, K.W. Lee, B.Y. Min, D.S. Hwang, J.K. Moon, (2015) “The Characterization of Cement Waste Form for Final Disposal of Decommissioning Concrete Wastes”, Annals of Nuclear Energy. 77, 294-299 (2015).

Feasibility Study on the Laser Cutting of Stainless Steel Pipes for Dismantling of Nuclear Power Plants

Sangwoo Seon*, Jae Sung Shin, Seong Yong Oh, Hyunmin Park, Taek-Soo Kim, Lim Lee, Chin-Man Chung, and Jonghwan Lee

Korea Atomic Energy Research Institute, 111, Daedeok-daero 989beon-gil, Yuseong-gu, Daejeon, Republic of Korea

*sangwoo7@kaeri.re.kr

1. Introduction

Dismantling of nuclear power plants requires the remote cutting because human access is limited to the work place having a high radiation. Laser cutting with optical fiber delivery is advantageous for remote control because not only a small laser head is placed in a work space, but also non-contact cutting does not generate reaction force [1]. In addition, laser cutting has been attractive as a cutting technique with various advantages because it generates less secondary wastes than other cutting techniques and provides reasonable maintenance with inexpensive cost. For this reason, studies on the laser cutting technology for dismantling of nuclear power plants have been actively proceeded [2-4].

Korea Atomic Energy Research Institute (KAERI) has developed the laser cutting technology aimed at the dismantling of nuclear reactors from 2015. Utilizing its own development of cutting head, the laser cutting capability of 100 mm stainless steel and carbon steel was ensured. However, the inside of the reactor contains complicated structures in the form of pipes in addition to the thick metal plate. For field application of laser cutting, it is important to cut these pipes in one direction. In this study, cutting experiment of stainless steel pipe using 10 kW fiber laser was applied to evaluate the laser cutting technology to metal pipe structure.

2. Laser cutting experiment

2.1 Experimental setup

A 10 kW fiber laser was used in the cutting experiment. The laser beam was delivered by an optical fiber and focused on the specimen through a laser cutting head attached to the X-Y-Z axis stage device. At this time, the cutting head moved along the cutting direction, and the moving speed of cutting head determined the laser cutting speed. Fig. 1 shows the view of laser cutting experiment of the stainless steel pipe. The cutting head was moved from the bottom to the top. In order to remove the melt from the cut specimen, a high pressure assist gas was injected through the 2 mm diameter nozzle at a high flow rate to the cut specimen. The compressed air of 1 MPa gauge pressure was used as an assist gas.

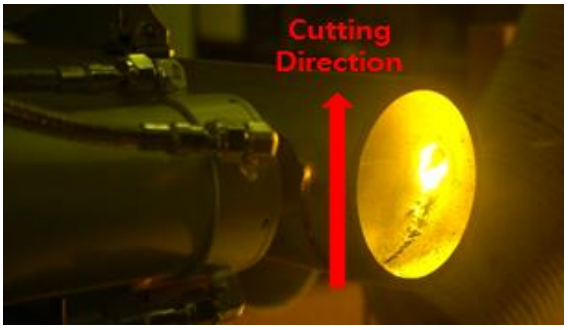


Fig. 1. View of the laser cutting experiment of stainless steel pipe.

2.2 Results and discussions

The first cutting experiment was carried out at a speed of 30, 50 and 100 mm/min for a stainless steel (SUS304L) pipe with a diameter of 90 mm and a thickness of 5.4 mm. The cutting interval for each cut line was 30 mm. The pipe was completely cut with one scan of the laser beam for all cutting speeds. Fig. 2 shows the cut pieces of the stainless steel pipe with a diameter of 90 mm and a thickness of 5.4 mm.



Fig. 2. Cut pieces of the stainless steel pipe with 90 mm diameter after laser cutting at speeds of (a) 30 mm/min, (b) 50mm/ min, (c) 100 mm/min.

The next cutting experiment was carried out at a speed of 50, 70, 100 mm/min for a stainless steel (SUS304L) pipe with a diameter of 165 mm and a thickness of 7 mm. The cutting interval for each cut line was also 30 mm. When cutting at a speed of 50 mm/min, the pipe was completely cut at one time. As shown in Fig. 3, when cutting at a speed of 70 or 100 mm/min, the pipe was incompletely separated or parts of the pipe was not cut due to the effect of the dross. Therefore, the cutting was carried out again in the opposite direction after the first cutting, and in this case, it was completely cut. Fig. 4 shows the cut pieces of the stainless steel pipe with a diameter of 165 mm and a thickness of 7 mm.



Fig. 3. View of the stainless steel pipe of 165 mm diameter after first cutting.



Fig. 4. Cut pieces of the stainless steel pipe with 165 mm diameter after laser cutting at speeds of (a) 50 mm/min, (b) 100 mm/min, (c) 70 mm/min.

3. Conclusion

In this study, the applicability of high power laser cutting technology to internal metal structures of the pipe type was evaluated with the aim of dismantling of nuclear power plants. One direction cutting of the stainless steel pipe with a 10 kW fiber laser resulted in successful cutting to a maximum diameter of 165 mm. The applicability of laser cutting technology was partially confirmed in order to dismantle internal structures of nuclear power plants. In the future, the laser cutting technology will be further evaluated through cutting experiments on various types of structures.

ACKNOWLEDGEMENT

This paper was supported by the nuclear research and development program through the national research foundation of Korea funded by the Ministry of Science, ICT & Future Planning.

REFERENCES

[1] J. S. Shin, S. Y. Oh, H. Park, S. Seon, C.-M. Chung, T.-S. Kim, L. Lee, B.-S. Choi, and J.-K. Moon, “Study on thick stainless steel cutting using a high power fiber laser for dismantling of nuclear power plants,” Abstracts of Proceedings of the Korean Radioactive Waste Society Autumn, 461-462 (2016).

[2] C. Chagnot, G. de Dinechin, and G. Canneau, “Cutting performances with new industrial continuous wave ND:YAG high power lasers: For dismantling of former nuclear workshops, the performances of recently introduced high power continuous wave ND:YAG lasers are assessed,” Nucl. Eng. Des. 240, 2604-2613 (2010).

[3] K. Tamura, R. Ishigami, and R. Yamagishi, “Laser cutting of thick steel plates and simulated steel components using a 30 kW fiber laser,” J. Nucl. Sci. Technol. 51, 916-920 (2016).

[4] K. Tamura, and R. Ishigami, “Laser cutting conditions for steel plates having a thickness of more than 100 mm using a 30 kW fiber laser for nuclear decommissioning,” Mechanical Engineering Journal 3, 15-00590 (2016).

Dismantling Process Development of the General Equipment/System of Nuclear Power Plant

Myungduck Yang*, Wanil Jung, Jaihoon Jung, and Yongbeom Kwon
KEPCO E&C, 269 Hyeoksin-ro, Gimcheon-si, Gyeongsangbuk-do, Republic of Korea
*yangm@kepco-enc.com

1. Introduction

Dismantling work can be roughly classified into dismantling of main equipment, dismantling of other remaining equipment/system and demolishing of buildings/structures. Among them, the dismantling of other remaining equipment/system is relatively easy in terms of difficulty of work, worker's risk and radiation protection compared to main equipment dismantling work. However, it is necessary to analyze the work order of each floor/area in consideration of the overall work quantity, type and work environment, and to establish a more efficient work schedule by applying a standard dismantling process that can be formalized.

Therefore, this paper proposes a standard dismantling process for these works and a work order for each floor/area of the main buildings in order to establish a detailed schedule for dismantling work of all other remaining equipment/system of Kori Unit 1.

2. Scope of Service

The scope of general equipment/system dismantling is to demolish large/small bore piping, electric cable, tray, conduit, measurement equipment and all the other equipment (pumps, HVAC, motors, transformers, pipes, etc.) except main equipment (reactor, steam generator, turbine, etc.). The processes such as preparing/submitting/obtaining of licensing documents related to dismantling of general equipment/system, removing the spent nuclear fuel, demolishing the structure and restoring the site will be managed by a separate schedule module.

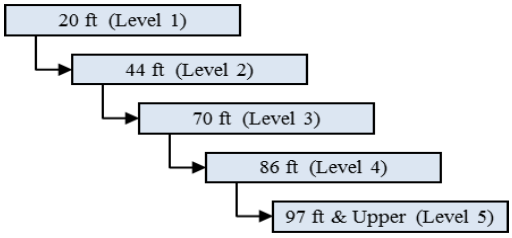
3. Work order by floor and area

The order of dismantling of general equipment/system by working area should be designed to maximize the efficiency of dismantling work and to minimize interference to work by area. Basically, the work for the floor starts at the power plant ground level (20ft) and proceeds upward and downward concurrently to facilitate carrying in and out of the dismantling equipment and waste. The work order for each area starts from the area where it is easy to get in and out of each floor, and the work progresses gradually toward the area far from the entrance.

The order of work for each floor/area of the main building is as follows, and the order of work for other buildings follows the general process of dismantling work from the lower floor to the upper floor.

3.1 Reactor Containment Building (RCB)

❍ Work order by floor



❍ Work order by area

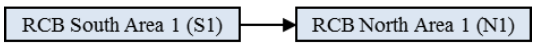
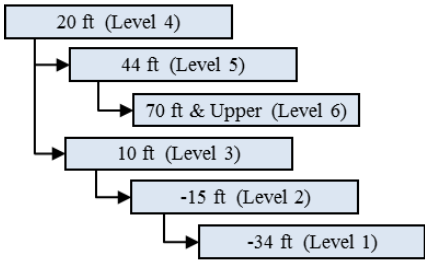


Fig. 1. Reactor Containment Building (RCB).

3.2 Primary Auxiliary Building (PAB)

❍ Work order by floor



❍ Work order by area

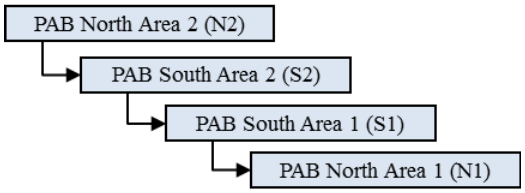


Fig. 2. Primary Auxiliary Building (PAB).

3.3 Turbine Generator Building (TGB)

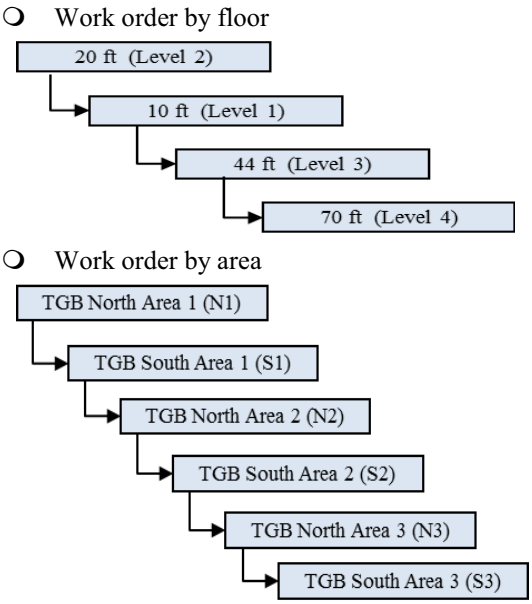


Fig. 3. Turbine Generator Building (TGB).

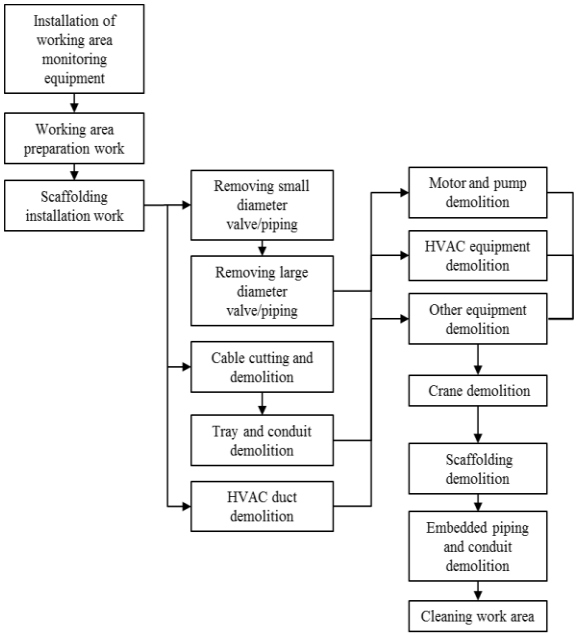


Fig. 4. Standard Logic Diagram.

4. . Standard logic for dismantling of general equipment/system

The order of dismantling of general equipment/system in each floor and each area of the buildings is forecasted to vary widely depending on the site conditions such as equipment complexity, density, accessibility, free space availability and radiation risk of each work area. And the standard logic diagram of dismantling work was created as shown below. It is expected that this standard logic can be modified in various ways such as change between predecessor and successor activity, concurrent execution of each detailed work considering site conditions, and it should be complemented by continuous review.

In particular, hazardous materials such as asbestos, which are included in some equipment and systems, are the main factors causing delays in the dismantling process, so they should be closely examined during the preparation of dismantling work areas and reflected in the work schedule.

In addition, the duration for each activity is calculated as follows considering the Work Difficulty Factor (WDF) that reflects the work environment conditions.

Duration for each activity = Quantity x WDF [1]

5. Conclusion

This paper describes the process for dismantling general equipment/system based on the limited Kori Unit 1 data. Therefore, it is necessary to revise the order of dismantling works by each floors/areas in this paper by obtaining information on the current status of the Kori Unit 1, such as actual dismantling quantity, contamination degree, the location of the waste treatment plant, the minimum space for work, securing of temporary passage, and so on.

Also, in order to calculate the required duration for each unit work, the detailed basis of Unit Cost Factor on which it is based should be reviewed, and the work group composition, work speed, work efficiency and work detail order should be reviewed.

In conclusion, this paper will be useful in understanding the dismantling sequence of general equipment/system of nuclear power plant and using as basic scheduling standard.

REFERENCES

[1] AIF/NESP-036, “Guidelines for Producing Commercial Nuclear Power Plant Decommissioning Cost Estimates” (1986).

[2] EPRI, “Maine Yankee Decommissioning Experience Report” (2005).

Thermal Decomposition of Chabazite-Cs and Chabazite-PCFC-Cs Zeolite

Eil-Hee Lee*, Ji-Min Kim, Maeng-Kyo Oh, Min-Jeong Kim, Keun-Young Lee, Kwang-Wook Kim,
Hyung-Ju Kim, Ik-Soo Kim, Dong-Yong Chung, Jei-Kwon Moon, and Jong-Won Choi
Korea Atomic Energy Research Institute, 111, Daedeok-daero 989beon-gil, Yuseong-gu, Daejeon, Republic of Korea
*nehlee@kaeri.re.kr

1. Introduction

The high-radioactive seawater waste (HSW) was generated the large amounts in a short time by feeding the large amounts of seawater as reactor cooling water due to the failure of reactor coolant system during nuclear severe accident such as Japan's Fukushima. Cs, Sr and I are contained in HSW as high-radioactive nuclides. Radioactivity of high-radioactive nuclides contained in HSW was very high, but its chemical concentration was very low. Removal of high-radioactive nuclides from HSW, therefore, is mainly performed by the adsorption with various zeolites. Our research team was also carried out the Cs adsorption by Chabazite-PCFC (potassium cobalt ferrocyanide) impregnated PCFC in chabazite zeolite. The removal efficiency of Cs was excellent. Zeolite system adsorbed high-radioactive nuclides, however, should be insoluble and ultimately solidified because the high-radioactive nuclides adsorbed into zeolite were slowly leached into water. In order to stabilize them, it should be solidified to block the route of zeolite cavity and pore by calcination at high temperature. This is to prevent the leaching of high-radioactive nuclides into the other solution systems from a zeolite system. So, it is important to understand the change of zeolite structure with thermal decomposition. This study, therefore, was investigated the formation of a recrystallization phase and a fixed phase to solidify Cs through the phase transformation analysis by X-ray diffraction (XRD).

2. Experiment

2.1 Thermal decomposition zeolites

Chabazite zeolite of K type ($KAlSi_2O_6 3H_2O$) prepared in this study, Chabazite-PCFC zeolite impregnated PCFC into Chabazite, Chabazite-Cs and Chabazite-PCFC-Cs zeolite adsorbed Cs by Chabazite and Chabazite-PCFC zeolite were selected as the thermal decomposition zeolites, respectively.

2.2 Experimental procedure

Chabazite prepared in this study was used after drying at 90℃ and cooling at 25℃. But Chabazite-Cs and Chabazite-PCFC-Cs adsorbed Cs were prepared by agitating of CsCl solution (1000 ppm, 1 ppm) for 2～3 hours, and these zeolites were used after drying at 90℃ and cooling at 25℃. Each of these zeolites was heated up to experimental temperature by increase of 8℃/min. When the experimental temperature was reached, it was calcined for 2 hours and XRD was measured after cooling at 25℃ for 12 hours.

3. Result and discussion

Fig. 1 was XRD patterns of Chabazite-Cs with calcined temperature. The structure of Chabazite-Cs was maintained up to 900℃, and recrystallized to pollucite ($CsAlSi_2O_6$) at 1,100℃. From this, Chabazite-Cs seems to have been recrystallized after the amorphous phase in 900～1,000℃ and it can be shown that Cs in Chabazite-Cs is converted to stable mineral phase (pollucite) by calcination of 1,100℃. Although volatility of Cs in Chabazite-Cs must be confirmed.

Fig. 2 was XRD patterns of Chabazite, PCFC, Chabazite-PCFC and Chabazite-PCFC-Cs at room temperature. Concentration of PCFC impregnated in Chabazite was about 11.8wt% and XRD pattern of Chabazite-PCFC was shown in form of Chabazite added that of PCFC. On the other hand, XRD pattern of Chabazite-PCFC-Cs was almost the same that of Chabazite-PCFC. This was attributed to the fact that XRD peak of Cs was not developed due to the low adsorption of Cs into Chabazite- PCFC.

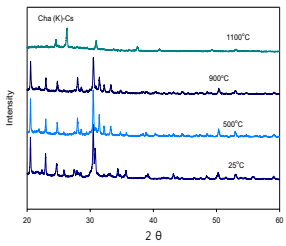


Fig. 1. XRD of Chabazite-Cs.

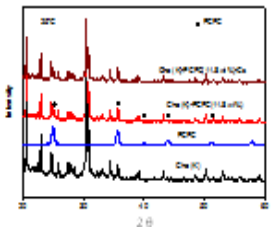


Fig. 2. XRD of each zeolite.

Fig. 3 was XRD patterns of Chabazite-PCFC-Cs with concentrations of PCFC impregnated into Chabazite-PCFC and calcined temperature. Regardless of impregnated PCFC concentration, Chabazite-PCFC-Cs structure was maintained up to 700℃ and recrystallized as pollucite ($CsAlSi_2O_6$) at above 900℃. From this, it was predicted that Chabazite-PCFC-Cs was broken in 700～900℃ and its structure has been converted to amorphous phase. Chabazite-PCFC-Cs can be also shown that Cs in Chabazite-PCFC is converted to stable mineral phase (pollucite) by calcination of 900℃ unlike the case of Chabazite-Cs.

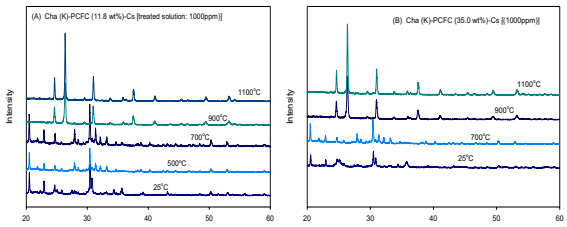


Fig. 3. XRD of Chabazite-x wt% PCFC-Cs.

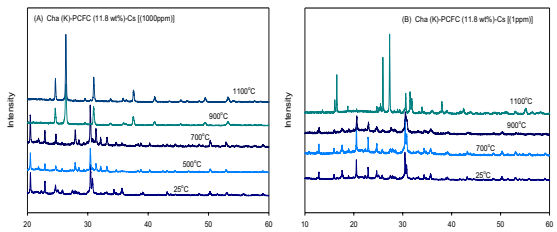


Fig. 4. XRD of Chabazite-PCFC-x ppm Cs.

Fig. 4 was XRD patterns of Chabazite-PCFC -Cs with adsorption concentration of Cs (1,000 ppm and 1 ppm) and calcined temperature. The PCFC concentration impregnated in Chabazite-PCFC was 11.8wt%. When the adsorption concentration of Cs was 1,000 ppm, it was shown that Chabazite-PCFC-Cs structure was maintained up to 700℃ and converted to amorphous in 700～900℃ and recrystallized as pollucite ($CsAlSi_2O_6$) above 900℃. But, when adsorption concentration of Cs was 1 ppm, XRD intensity peak of Chabazite-PCFC-Cs was reduced with increasing calcined temperature and its structure was maintained to 900℃ and recrystallized as leucite ($KAlSi_2O_6$) at 1,100℃ unlike the case of 1,000 ppm. This is due to the very small adsorption amount of Cs. In this case, amorphous seems to be converted in 900～1,100℃.

4. Conclusion

Both Chabazite-Cs and Chabazite-PCFC-Cs can be shown that Cs contained into these zeolites is converted to stable mineral phase (pollucite) by thermal decomposition at the calcined temperature of 1,100℃ and 900℃, respectively. However, it is necessary to check the volatility of Cs from above zeolites during the high temperature calcination

Acknowledgements

This work was supported by the national Research Foundation of Korea (NRF) grant funded by the Korea government (MSIP) (No. NRF-2017M2A8A5015147)

REFERENCES

[1] "H. Mimura and K. Akiba, "Adsorption behavior of Cs and Sr on synthetic zeolite P", J. Nucl. Sci. and Tech., 30(5), 436-443 (1993).

[2] P. Cappelletti, G. Rapisardo, B. de Gennaro, et.al., "Immobilization of Cs and Sr in aluminosilicate matrices derived from natural zeolites", J. Nucl. Mater., 414, 451-457 (2011).

Spent Fuel Pool Island System Configuration Concept – Comparison of German and the US Regulatory Standards

Kwangsoon Choi*, Dongjin Lee, and Jaihoon Jung

KEPCO E&C, 269 Hyeoksin-ro, Gimcheon-si, Gyeongsangbuk-do, Republic of Korea

*kschoi@kepco-enc.com

1. Introduction

The spent fuel management after nuclear power plant (NPP) permanent shutdown is one of the key factors to determine the NPP decommissioning strategy and related system design. But there are many uncertainties regarding the spent fuel management in Korea. In addition, the decommissioning regulatory standards for spent fuel pool island (SFPI) in case of Germany and the US should be reviewed in more detail, which are the representative international regulatory standards [1][2]. In this paper, the SFPI system configuration concept is reviewed with comparison of the regulatory standards of Germany and the US, and more efficient and regulatory adaptable design concept is derived.

2. Regulatory Standards of Germany and the US

2.1 German Regulatory Standards for SFPI

In Germany, the operating license is valid until decommissioning license permission after the NPP permanent shutdown. Accordingly any system modification/installation/removal/operation during "Decommissioning Transition Period" (permanent shutdown ~ decommissioning license permission) should be complied with the regulatory framework applied during the normal operational phase.

2.2 The US Regulatory Standards for SFPI

In case of commercial NPP in the US, the submission only of DSAR (Defueled Safety Analysis Report) and PSDAR (Post Shutdown Decommissioning Activities Report) after the permanent shutdown is necessary to start NPP decommissioning works. Therefore it is possible to perform system modification/installation/removal/ operation with just system function review during decommissioning phase, regardless of operating license compliance [2].

3. SFPI System Configuration Concept

3.1 Spent Fuel Pool Cooling System(SFPCS) Concept

During the operational phase, SFPCS shall consist of two(2) safety-related class trains to comply with operating license. Therefore, in Germany, SFPCS shall consist of two(2) safety-related class trains likewise.

However, in the US, SFPCS may consist of one(1) non-safety-related train if SFPCS with only one(1) train can achieve spent fuel pool cooling. This design concept has been already applied to several NPP decommissioning projects in the US. But it should perform more detailed analysis whether SFPCS can ensure spent fuel pool safety even if SFPCS loses its cooling function because of a certain accident.

3.2 Spent Fuel Pool Cleanup System Concept

The spent fuel pool cleanup system is designed to keep the dose rate at water surface below 0.025 mSv/hr by purifying spent fuel pool water. This allows the workers to access the spent fuel pool during fuel handling works.

At the operational phase, spent fuel pool cleanup system shall consist of two(2) non-safety-related trains. But only in the early stages of refueling phase, both two(2) trains are operated at the same time to quickly purify a lot of refueling pool water. Spent fuel pool cleanup system can consist of one(1) non-safety-related class train because after NPP permanent shutdown spent fuel refueling work isn't necessary any more. In addition, SRP (Standard Review Plan), which is used as a design guideline for

spent fuel pool, doesn't require two(2) trains composition.[3]

In other words, spent fuel pool cleanup system can consist of one(1) non-safety-related class train even under operating license. Thus, in both German and the US, it is possible to design only one(1) non-safety-related class train if system can achieve the own system goal.

3.3 Make-up Water System (Seismic Category I)

Under operating license, seismic category I make-up water shall be provided to the spent fuel pool as specified in SRP 9.1.3[3]. The goal of make-up water is to make up spent fuel pool water evaporated by the heat load of spent fuel when loss of SFPCS function happens. Therefore make-up volume for make-up water system (seismic category I) should be calculated considering spent fuel pool volume, accident recovery time, heating time and evaporating time of spent fuel pool water.

As the heat load of spent fuel decreases after NPP permanent shutdown, evaporation of spent fuel pool water can be prevented without specific seismic category I make-up source. However, in Germany, a specific seismic category I make-up water source shall be provided as well as NPP operational phase.

In contrast, in the US, if cooling requirement can be achieved without a specific seismic category I make-up source, make-up water system (seismic category I) is not required.

3.4 Make-up Water System (Other)

At the operational phase, make-up water system (other) consists of de-mineralized water, boric acid water, and emergency external makeup water. These three(3) water sources are essential for the operation of spent fuel pool. Therefore make-up water system (other) is provided in both Germany and the US.

3.5 Heat Exchanger Cooling Water System (HECWS)

HECWS supplies cooling water to the spent fuel pool heat exchanger. In both Germany and the US, HECWS is essential to cool spent fuel pool water.

In Germany, since SFPCS has two(2) safety-related class trains, HECWS shall have two(2) safety-related class trains as well. In the US, however, if SFPCS consists of only one(1) non-safety-related class train of non-safety-related class, HECWS can be composed of one(1) non-safety-related class train as well.

3.6 Emergency Diesel Generator System (EDGS)

EDGS supplies alternative power to SFPI systems, such as pumps, in loss of on-site power. EDGS is composed of two(2) Class 1E emergency diesel generators at the NPP operational phase.

In Germany, because EGDS shall supply emergency power to two(2) trains of SFPCS, EGDS shall consist of two(2) Class 1E emergency diesel generators, like the existing EDGS

In the US, Class 1E emergency diesel generator is not necessary if cooling requirements of spent fuel pool can be met, even if both on-site power and off-site power are lost. However, in the case of SONGS (San Onofre Nuclear Generating Station) and Zorita NPP, with small capacity Non-Class 1E emergency diesel generator was installed for decommissioning phase and an emergency plan was prepared for off-site power loss accidents. So these examples of SONGS and Zorita can be considered for KORI unit 1 decommissioning project.

4. Conclusions

This paper compares and reviews SFPI system configuration concept according to Germany and the US regulatory standards. If SFPI concept is adopted as spent fuel management plan after NPP permanent shutdown in the future, the practical design concept can be derived based on the assumptions described in this paper.

REFERENCES

[1] "High Level Radioactive Waste Management Plan", MOTIE, May 2016.

[2] DOE G 430.1-5, "Transition Implementation Guide", U.S. Department of Energy, 2011.

[3] SRP 9.1.3 "Spent Fuel Pool Cooling and Cleanup System", U.S. Nuclear Regulatory Commission.

Development of Decontamination Guidelines for the Management of Contaminated Areas as an Emergency Preparedness

Jin O Lee, Tae Gwan Do, Ji Young Song, and Kwang Pyo Kim*

Kyung Hee University: 1732 Deokyoungdaero, Giheung-gu, Yongin, Gyeonggi-do, Republic of Korea

*kpkim@khu.ac.kr

1. Introduction

In 2011, a nuclear power plant in Fukushima was damaged due to the occurrence of the East Japan Great Earthquake, and a large amount of radioactive material was discharged into the environment. As a result, decontamination works were carried out on large area in Japan.

Lessons learned from the responses to emergencies over the past years were led to similar conclusions. One of the lessons was that impossibility to establish standards consistent with radiological protection principles after an emergency. To reduce radiological and non-radiological (e.g. economic, social, and psychological) risks for emergency situation, it is necessary to pre-establish guidelines for emergency preparedness [1].

Korea government established a risk management standard manual for radiological emergency in 2016. However, there is no specific guideline on decontamination technology. In this study, we developed decontamination guidelines on the management of contaminated areas as a emergency preparedness.

2. Materials and Methods

The guidance for decontamination is a tool to support decision-makers in developing a recovery strategy following a radiological emergency. To facilitate decision-making, it is important to obtain abundant data. We reviewed decontamination methods and techniques in literature, including European Approach to Nuclear and Radiological Emergency Management and Rehabilitation Strategies (EURANOS) project [2], decontamination guidelines [3] used in actual decontamination planning in Japan, and the US Protective Action Guides (PAG) data.

In the EURANOS guidelines, decontamination techniques were proposed by dividing into buildings, roads areas, soils, grass and plants considering the surface. The EURANOS project has created a data sheet for all management measures and made it available for decision making.

Japanese decontamination guidelines reflected the accumulated technology based on the experience of decontamination pilot project. Similar to the EURANOS project, the decontamination technique data were presented as buildings and other structures, roads, soils, and vegetation depending on the surface of the object. In this study, as in the case of Europe and Japan, the subject of decontamination was largely divided into buildings, soil, roads, and vegetation depending on the material of the surface. Additionally, decontamination techniques in the guidelines were summarized.

In PAG, it detailed community support for recovery, public acceptability, and intergenerational equity. Therefore, in this study, decontamination guidelines were developed considering the participation of stakeholders.

3. Results and Discussion

In this study, the decontamination methods were divided into buildings, soils, roads, and vegetation. Each decontamination method was applied with reference to the decontamination technique data sheet.

The common decontamination procedure was presented in the guidelines shown in Fig. 1. The decontamination procedure can be divided into three parts. First, site characterization is performed for the area that is expected to be contaminated based on the monitoring data. Characterization work should be designed to define, in detail, the nature and extent of the contamination and to provide information necessary to develop and evaluate decontamination alternatives.

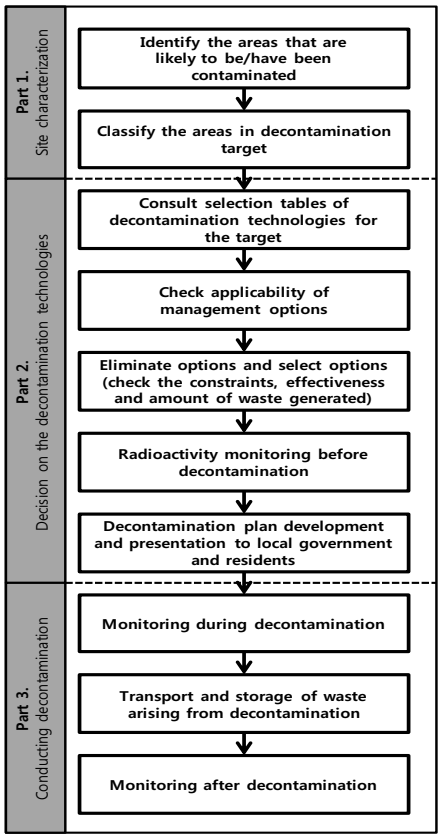


Fig. 1. Overview of the general decontamination planning process.

In the second part, government determines the decontamination technique, check the decontamination data sheet for the decontamination target, and verify the applicability. Afterward, the government establishes a decontamination plan based on the evaluation results (e.g. restrictions, work velocity, volume of wastes) and monitoring results. During the decontamination planning process, a seminar should be held to increase the credibility of the affected citizens in the area.

The third part is to conduct decontamination. To confirm the effectiveness during decontamination, monitoring is conducted before and after the decontamination. Generated wastes during decontamination are transported according to waste management plan.

Table 1 shows the main classification of the decontamination technique data sheet in this study. The decontamination techniques were made into a data sheet so that the decontamination technique can be quickly applied to the decontamination targets. Each decontamination technique was summarized in terms of decontamination procedure, construction speed, waste generation, and cost based on the precedent research.

Table 1. Classification of the Data Sheet

Major category	Contents
Land use type	Buildings, soils, roads, vegetation
Decontamination method	High-pressure washing, thin-layer topsoil stripping, brushing, trimming, mowing, reversal tillage, sand blasting, vacuum removal of debris, etc.
Application and implementation	Application conditions, implementation restrictions
Evaluation	Work velocity, volume of generated wastes, waste type, decontamination factor, gamma dose rate reduction, cost

4. Conclusion

In this study, decontamination guidelines for the management of contaminated areas were developed as an emergency preparedness. The decontamination methods were divided into buildings, soils, roads, and vegetation. Each decontamination method was applied with reference to the decontamination technique data sheet. The results of this study are expected to be used for development of decontamination standards.

ACKNOWLEDGMENTS

This research was supported by Grant (20141510101630) from the Energy Technology Development Project of Korea.

REFERENCES

[1] ICRP, “Application of the Commission's Recommendations for the Protection of People in Emergency Exposure Situations”, ICRP Publication 109, 23-24 (2009).

[2] EURANOS, “Generic Handbook for Assisting in the Management of Contaminated Inhabited Areas in Europe Following a Radiological Emergency version 2” (2010).

[3] MOE, “Decontamination Guidelines 2nd Ed.” (2013).

[4] EPA, “PAG Manual: Protective Action Guides and Planning Guidance for Radiological Incidents” (2017).

Decommissioning Strategy and Method for Preparation of Preliminary Decommissioning Plan for Research Nuclear Facilities

Seung-Kook Park[1*], Kook-Nam Park[1], Yun-Dong Choi[1], Young-San Choe[1], and Jin-Ho Park[2]

[1]Korea Atomic Energy Research Institute, 111, Daedeok-daero 989beon-gil, Yuseong-gu, Daejeon, Republic of Korea

[2]New Decom, Daejeon, Republic of Korea

[*]skpark2@kaeri.re.kr

1. Introduction

The decommissioning of a nuclear facility should be preceded by a decommissioning strategy before the operation is permanently stopped. The major decommissioning strategies may vary depending on many factors such as the characteristics of the facility, the occurrence or nonoccurrence of accidents during facility operation, national policies, and the surrounding environment. At present, we have chosen strategic considerations such as the scope of the decommissioning, the decommissioning method, the final condition of the site, radioactive waste, stakeholder participation, and the cost of decommissioning [1].

2. Decommissioning Principles and Methods

2.1 Decommissioning Basic Principles

The purpose of a decommissioning project is to safely dismantle a nuclear facility, completely remove radioactive materials in the facility, and decontaminate the remaining structures and soils to an unlimited level of use. Through such a decommissioning plan, a method for safe, practical, and economical decontamination and decommissioning is proposed.

The dismantling work will be carried out in accordance with domestic regulations and international regulatory requirements and will be carried out within the scope of ensuring safety. The proposed dismantling method minimizes the exposure dose of workers and residents and the release of gaseous radioactive material according to the ALARA principle. Therefore, it is designed to ensure the safety of workers and residents, and to ensure safety for protecting the environments. In the decommissioning project, a radiation safety management strategy will be established to minimize the exposure of workers participating in the decontamination and decommissioning activities. Radiological protection plans and health physics activities were carried out according to the evaluation of the radioactive inventory evaluation, and to establish a strategy to ensure safety first [2].

For the dismantling method and work procedure of the research reactor, the structural and radiological conditions of the reactor and the overall dismantling safety should be reviewed, and the best method adopted. Spent fuel is safely stored temporarily in the spent fuel pool of the reactor room until it is discharged/ transported according to the planned spent fuel treatment and disposal standards. Once the spent fuel is discharged from the facility, it does not enter the dismantling work despite the principle of instant dismantling.

2.2 Decommissioning Method

2.2.1 Decommissioning Schedule

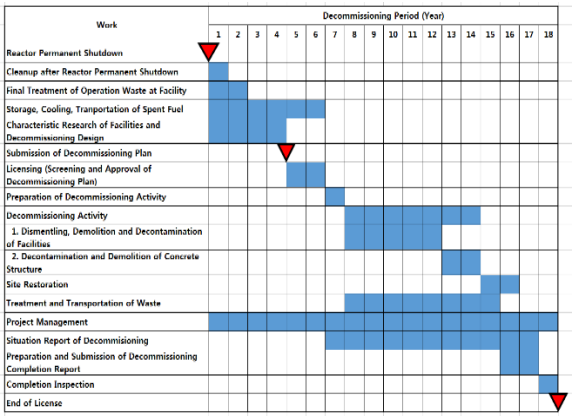


Fig. 1. Schedule for the Research Reactor and Related Facilities Decommissioning.

The decommissioning schedule of the research reactor is shown in Fig. 1. The cutting, dismantling and decontamination of the facilities including the buildings are subject to a preliminary decommissioning plan, chapter 8, and decontamination and decommissioning activities. All dismantling activities shall be carried out after submission of the decommissioning plan in accordance with domestic decommissioning laws, and after the examination and approval of the licensing authority have been completed.

2.2.2 Decommissioning Process. Dismantling preparation works are decontaminated solid waste, are equipped with temporary storage facilities, entrance and control facilities, changing rooms, ventilation facilities, and utilities for dismantling. In addition these are unnecessary interrupted utilities, are isolated from compartments and ventilation facilities, and so on. A research reactor consists of a reactor building, isotope production facility, irradiation material examination facility, cold neutron research facility, and accessory facilities [3]. The dismantling of Hanaro was planned in order of the accessory facility, cold neutron research facility, isotope production facility, irradiation material examination facility, and reactor building, and excludes the utilities required for dismantling, as shown in fig. 2. In the dismantling process of the research reactor, the order of dismantling from the facilities with a low radioactive level to the facilities with a high radioactive level was selected.



Fig. 2. Decommissioning Sequence for the Research Reactor and Related Facilities.

2.2.3 Method of decommissioning. In the case of reactor building, low pollution equipment will first be dismantled, such as the non-polluting secondary cooling system, and will be dismantled in order of high pollution, such as the primary cooling system and reactor. In the case of the nuclear fuel assemblies, they are cooled down in the spent nuclear fuel storage pool or in the reactor pool for a certain period of time and then completely discharged before the decommissioning of the reactor and related facilities is started [4]. The reactor assemblies are expected to have a high radiation level, and thus they are cut and packed in the field and managed as radioactive waste. For this cutting, a platform that can be shielded for remote cutting is installed in the upper part of the reactor pool, and will be cut and packed remotely there.

3. Conclusion

While preparing a preliminary decommissioning plan for a research reactor, the decommissioning strategies for the scope of dismantling, the dismantling method, the final condition of the site, the radioactive waste, stakeholder participation, and the cost of dismantling were considered. In this paper, the basic principles of the dismantling and dismantling methods were described. As the basic principles, these will be installed in temporary storage facilities, and utilities, such as ventilation systems for dismantling. For the decommissioning method the schedule, decommissioning process, dismantling of the main reactor body with high radioactivity, and so on are described. The order of dismantling is facilities with a low radiation level to facilities with a high radiation level, and the dismantling schedule was estimated to be 18 years after the permanent shutdown of the reactor.

REFERENCES

[1] Park Seung-Kook, Park Kook-Nam, Park Hee-Sung etc., “Decommissioning Strategy for HANARO”, Technical Report KAERI/TR-6518/2016, 61-91 (2016).

[2] Nuclear Safety and Security Commission, “Enforcement Decree of Nuclear Safety Act, Article 42 (2016).

[3] HANARO Center, Korea Atomic Energy Research Institute, “HANARO Construction Report” KAERI/PR-001/97, 287-297 (1997).

[4] Park Seung-Kook, Park Kook-Nam, Ha Jae-Hyun etc., “Study for Establishment the Initial Decommissioning Plan for Research Reactor and Related Facilities”, Technical Report KAERI/TR-6780/2017, 27-72 (2017).

Pressure Water Jet Cleaning of Residue Inside Tank in Foam Decontamination

Han Beom Yang*, In Ho Yoon, Seung Eun Kim, Chong Hun Jung, Wang Kyu Choi, and Seon Byeong Kim
Korea Atomic Energy Research Institute, 111, Daedeok-daero 989beon-gil, Yuseong-gu, Daejeon, Republic of Korea
*nhbyang@kaeri.re.kr

1. Introduction

Foam decontamination process well developed and widely used, especially for large components with complex shapes or large volumes. It can be applied to surfaces in any orientation and produces low volumes of secondary waste. The equipment is cheap, simple and suitable for either manual or remote deployment [1]. This study was conducted to evaluate the cleanup of residue on the inside surface area of a tank using a pressure water jet technique with foam decontamination. Pressure water jet equipment for the tank was designed and manufactured, and some performance tests were conducted. Foam can be used to assist with the application of chemical decontamination agents onto various materials. In the finished foam decontamination of a large tank, residual materials, such as the chemical materials, SiO_2 nanoparticles, radionuclides, and many other materials will remain on the surface of the inside tank.

2. Cleaning system

2.1 Manufacture of cleaning system

A cleaning system of high pressure water spray method was manufactured to remove radioactive materials, nanoparticles, and foam decontamination chemicals remaining on the inner surface of a large tank after foam decontamination.

This is a demonstration cleaning system having a function of performing a cleaning process of four stages. In the first step, the washing solution is sprayed at 360° with four linear nozzles (injection angle: 90°/one nozzle) capable of automatically moving up and down. The residual material remaining on the inner surface of the tank is removed by spraying. The second step, the washing waste solution used in the first stage washing process is recycled and the washing process is repeatedly washed until the remaining material on the inner surface of the tank is completely removed. The third step is a rinsing step, which uses a fresh washing solution to clean and remove material remaining on the inner surface of the tank. The fourth step is the drainage of the solution from the bottom of the tank.

Table 1. Main specification of cleaning system

Part name	Quantity
Decontamination tank	1 set
Cleaning solution tank	1 set
Cleaning waste solution tank	1 set
Nozzle up and down moving device	1 set
Control panel	1 set
Structure frame	1 set

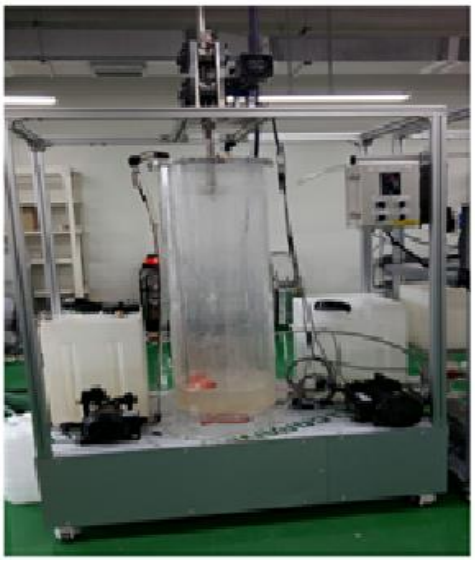


Fig. 1. Picture of cleaning system.

3. Results & discussion

It is important to consider the minimum production of secondary waste in foam decontamination technology. For the basic concept design and selection of suitable technology, we considered the safety, efficiency, cost effectiveness, waste management and feasibility of application. We selected the pressure water jet as a suitable technique among the chemical, physical, mechanical, and electrochemical methods. Recycling of a washing waste solution is crucial to avoid large secondary waste volume production. The flushing of water was operated at a low pressure of ~30 bars and a recycling system of a waste flushing solution was operated semi-automatically. This facility is operated with 4 steps. The first moving part is operated upward and downward vertically, and can be controlled by automatic or manual operation. The second part is the upper position, and the lower position was set up using limit sensors and controlled. Recycled washing solution was collected in a waste tank, and recycling then started using a pump. The final waste solution was transferred to the solid/liquid separation filter system.

The evaluation of this washing-cleaning facility was decided as based on the results of 5 cycles of washing with only a fresh washing solution, and the first and fifth cycles of washing with a fresh washing solution, and second through fourth cycle washings through a waste washing solution recycling operation. The removal percentage of SiO_2 nanoparticles is 96.4% in first cycle, 99.0% in the third cycle, and 99.2% in the fifth cycle. In the Recycling experiment of the washing solution, the removal percentage of SiO_2 nanoparticles is 96.4% in the first cycle and 99.1% in the fifth cycle. It was possible to reduce the considerable amount of secondary waste production in the recycling of the washing waste solution system.

4. Conclusions

Cleaning of the inside of a tank with a pressure water jet was proven with assured productivity, safety, environmental responsibility, cost, and versatility under our feasibility test conditions. We can find the possibility of a reduction of secondary waste production in the recycling of a washing waste solution system. In future studies, the cleaning of a larger scale tank contaminated with radionuclides will be conducted using a pressure water jet washing to remove the residue on the metal surface of inside the tank.

REFERENCES

[1] International Atomic Energy Agency, State of the art technology for decontamination and dismantling of nuclear facilities, Technical Report Series No. 395, IAEA, Vienna (1999).

Specification Requirements and Considerations Based on Operation Experiences of Spent Fuel Pool Island

Dongjin Lee* and Jaihoon Jung

KEPCO E&C, 269 Hyeoksin-ro, Gimcheon-si, Gyeongsangbuk-do, Republic of Korea

*djlee@kepco-enc.com

1. Introduction

The concept of spent fuel pool island (SFPI) is defined as a design change for the isolation of spent fuel pool cooling and cleanup system for efficient and easy decommissioning of structures, systems, and components during decommissioning and decontamination (D&D) period of nuclear power plant. The SFPI is one of the most important preparation activities for D&D during transition period in order to ensure safe and efficient spent fuel management. It is necessary for discussion of SFPI because Korea currently has uncertainty of spent fuel management strategy. In addition, the SFPI is one of the best alternatives to solve the problem due to the absence of intermediate spent fuel storage facility in Korea. In this paper, the specification requirement and considerations is reviewed based on operation experiences of SFPI in other D&D cases, and the applicable specification requirement of SFPI in Korea is derived through the review.

2. Specification Requirement and Considerations

2.1 Predominant Radionuclide Constituents

The predominant radionuclide constituents are the values of radionuclides created according to long term storage of spent fuel in the spent fuel pool. In other words, the values provided are representative of a pool configured for long-term fuel storage. Significant disturbances in the pool, such as movement of fuel elements or pool cleanup operations, would be expected to elevate the activity. While there is a consistency from plant-to-plant with regard to the types of soluble radionuclides, there may be more variation in radionuclide concentrations found in crud layers or particulates on the fuel pool floor. Notable would be the appearance of transuranics correlated to damaged fuel.

Most plants do not have an explicit specification regarding pool water radionuclide concentration. Whereas Homboldt, Trojan, LaCrosse nuclear power plant have the specification requirement, the value is reported about 2.5E3μCi/ml. The allowable activity is often defined by personnel radiological protection practices and system purification capability. Plant response indicated that plant criteria for pool water radionuclide removal after permanent shutdown did not change from those applied during plant operation. As a potentially unique practice, the Yankee Rowe plant evaluates Cs-137 generation rate twice yearly as a method of identifying cladding degradation.

2.2 Non-radiological Constituents

Most plant have technical specifications regarding non-radiological constituents in the fuel pool water. Interestingly, many of these specifications were added only after final shutdown (e.g., Rancho Seco). Control of fluorides and chlorides are most common. Boron requirements have been removed or reduced in several plants after demonstration that it is not needed for criticality control (e.g., through use of boral racks). Purification systems generally do not actively remove the boron, but its concentration may gradually decrease (e.g., through system leakage).

On case of Connecticut Yankee nuclear power plant, the requirement is to inject boron in the pool when the anion increases more than 10 times or silicon dioxide increases more than 30 times. SiO_2 factor need to be monitored periodically as indicate of the boral racks degradation

2.3 Resin Change-out Frequency and Basis

Most plants that modified the original system or installed a new cleanup system for post shutdown activities are using an ion-exchange vessel of about

30 ft^3 volume. Mixed-bed demineralizers are common. Criteria for vessel change-out include change in differential pressure(dp), change in flow(df), ALARA, and control of waste form classification. Change-out frequency is dependent on fuel pool operational activities. In a quiet pool, resin change-out frequencies of well over a year were often reported. Conversely, Trojan reported the need to change resin every few days after the use of a cesium selective removal resin (in preparation for cask loading) resulted in a higher proportion of soluble cobalt in the pool. As a result reviewing resin change-out frequency based on the SFPI operation experiences, the resin is needed to change out once per every 18 or 24 month in order to satisfy the ALARA requirement, and the reduction of flow rate in demineralizer determine replacement intervals of resin.

2.4 Spent Fuel Pool Area Dose Rates

In comparison to plant operation, most plants reported that spent fuel pool general area dose rates are unchanged and reduced. Dose rates in the area of new components (e.g, demineralizer) may require additional shielding for the radiological dose rate management. Over time, pool cleanup activities and radionuclide decay tend to decrease the importance of the pool water as a source of dose during fuel storage periods. Accordingly, it is not necessary to establish the limitation value of a radiological dose rate as a requirement. Therefore the setting of radiological dose rate in general area is less than 1mR/hr as the administration limit which is not mandatory.

3. Applicable Specification Requirement

This chapter derives applicable requirement of SFPI in Korea based on specification requirement and considerations reviewed above. The derived specification requirement for SFPI is conservative value and contents based on other cases. This value and contents are meaningful specification requirement as a reference. In addition, these are changeable according to the inherent characteristic of nuclear power plant, public acceptance, etc. The specification requirements in details are shown in Table 1.

Table 1. Specification requirement for SFPI

Specification	Contents
Radionuclide Constituents	H-3(4E-4 μCi/ml), Co-60(3E-5 μCi/ml), Cs-134(1E-7 μCi/ml) Cs-137(1E-5 μCi/ml) Cs-137 generation rate measured 2x per year to monitor cladding integrity
Non-radionuclide Constituents	Boron>2000 ppm, Fluoride<150 ppb Chloride<150 ppb, Sodium<1000 ppb Suspended Solids<1000 ppb SiO2 monitored as indicator of The boral racks degradation
Resin Change-out Frequency and Basis	Demineralizer flow reduction governs the change-out frequency; ALARA practices previously caused change-out on 18-24 month interval.
SFP Area Dose Rates	No significant change from operation (< 1 mR/hr in general area)

4. Conclusions

This paper reviewed the specification requirements through operation experiences of SFPI in other cases and derived applicable reference requirements for SFPI in Korea. The SFPI is an option that can be considered in order to manage spent fuel during transition period and reduce decommissioning cost in the implementation of D&D project in near future. If SFPI concept is adopted as spent fuel management plan after NPP permanent shutdown in the future, the practical requirements for SFPI can be derived based on specification requirement and considerations described in this paper.

REFERENCES

[1] DOE G 430.1-5, “Transition Implementation Guide”, U.S. Department of Energy, 2011.

[2] EPRI Technical Report, “Spent Fuel Pool Cooling and Cleanup System – Experience at Decommissioning Plants”, 2002.

Simulation-Based Evaluation for the Dismantling Scenario of the Reactor Vessel at Kori Unit 1

Dongjun Hyun*, Ikjune Kim, Jonghwan Lee, Kwan-Seong Jeong, Byung-Seon Choi, and Shin Young Kang
Korea Atomic Energy Research Institute, 111, Daedeok-daero 989beon-gil, Yuseong-gu, Daejeon, Republic of Korea
*dongjunn@kaeri.re.kr

1. Introduction

Dismantling of nuclear facilities takes considerable time and costs, so predicting how much time and budget is needed is an important concern in the preparing phase. After the government announced the shutdown of Kori Unit 1, existing methodologies based on prior data were attempted to estimate costs for dismantling of Kori Unit 1. These methodologies using prior data are very useful for obtaining approximate values but is not sufficient for planning the dismantling scenario that requires delicate analysis.

This paper proposes a simulation-based evaluation for the dismantling scenario of the reactor vessel at Kori Unit 1. This evaluation results time and costs for the dismantling scenario presented in this paper, and is useful for planning the dismantling scenario because the evaluation result is coordinated with the dismantling scenario.

2. Assessment system

The assessment system used in this paper consists of a process simulation module and a process evaluation module, and was originally developed by Decontamination and Decommissioning Research Division of Korea Atomic Energy Research Institute.

2.1 Process simulation module

The process simulation module basically simulates a dismantling scenario based on a commercial digital manufacturing platform, and simulates cutting processes included in the dismantling scenario using the function developed by Hyun et al., 2017 [1].

2.2 Process evaluation module

The process evaluation module evaluates the dismantling scenario based on Process Product Resource (PPR) tree structure, which is a data structure of the previously mentioned commercial digital manufacturing platform. The evaluated time consists of process cycle times and maintenance time, and the evaluated cost consists of initial costs, process costs, and maintenance costs.

3. Dismantling scenario

The target of the dismantling scenario is a reactor vessel of Kori Unit 1. The representative variables determining the dismantling scenario are the radioactive waste container, the remote dismantling system, and the segmentation plan.

3.1 Radioactive waste container

The radioactive waste container is selected as a Half Height ISO (HHISO), which is proposed by Lee et al., 2016 [2]. HHISO is a radioactive waste container capable of land transportation with a 20 ton truck, allowing efficient transport and storage of Low Level Waste (LLW) and Very Low Level Waste (VLLW). According to a recent conference paper published by KHNP [3], the reactor vessel is expected to be a low level, so segmented pieces of the reactor vessel can be stored in HHISO. In addition, low level radioactive waste can be accommodated in the shallow land disposal of the radioactive waste management facility operated by KORAD, so segmented pieces of the reactor vessel can be stored in HHISO for both transport and storage.

3.2 Remote dismantling system

The remote dismantling system is selected as a seamless remote dismantling system, which proposed by Hyun et al., 2014 [4]. The originality of the

dismantling system is in its ability to handle all the processes involved in the dismantling of major components of a nuclear power plant. The seamless remote dismantling system consists of a circular saw, gantry manipulator, waste container, band saw, and turn table.

3.3 Segmentation plan

The reactor vessel will be segmented into 37 pieces, and the segmented pieces will be stored in five HHISO containers as shown on Fig. 1. Since final states of HHISO containers is over 20 tons, segmented pieces should be stored in the HHISO container so that the weight of the container does not exceed 20 tons at transportation. Thereafter, HHISO containers are rearranged to final states.



Fig. 1. Segmentation Plan.

4. Process simulation and evaluation

The dismantling scenario is simulated as shown on Fig. 2 using the developed process simulation module, and the evaluation result is shown on Table 1.



Fig. 2. Dismantling process simulation.

Table 1. Evaluation result for dismantling scenario

Items		Values
Total Time [Hour]	Process	149.3
	Maintenance	10
Total Cost [Million Won]	Initial Cost	1,693
	Process Cost	10.14
	Maintenance Cost	3
	Waste Disposal	6,100

5. Conclusion

The presented result can be regarded as the first attempt of the simulation-based evaluation in the field of the nuclear facility dismantling, although the values themselves vary according to input constants. These attempts are expected to contribute significantly to improved dismantling scenarios

Acknowledgements

The research was supported by the Nuclear R&D Program through the Ministry of Science, ICT & Future Planning.

REFERENCES

[1] Hyun, D., Kim, I., Lee J., Kim G., Jeong K., Choi B., Moon J., “A methodology to simulate the cutting process for a nuclear dismantling simulation based on a digital manufacturing platform”, Annals of Nuclear Energy, 103, 369-383 (2017).

[2] Lee J., Park J. Sung N., Yang G., “Development of Multi-Purpose Containers for Managing LLW/VLLW from D&D”, J. of Fuel Cycle and Waste Tech., 14(2), 157-168 (2016).

[3] Kim H., “Preparation Program at the Pre-Decommissioning Phase for the D&D of the Kori-1 Nuclear Power Plant”, Tech. Meeting on Plant Life Management during the Transition from Operation to Decommissioning of Nuclear Power Plants, Session 1(1), 30 Aug. – 2 Sep., 2016, Kyungju.

[4] Hyun, D., Lee S., Seo Y., Kim G., Lee J., Jeong K., Choi B., Moon J., “Seamless remote dismantling system for heavy and highly radioactive components of Korean nuclear power plants”, Annals of Nuclear Energy, 73, 39-45 (2014).

Solid Liquid Separation for the Foam Decontamination Waste Treatment Using Candle Filter

Seung-Eun Kim, In-Ho Yoon, Wang-Kyu Choi, Seon-Byeong Kim, and Chong-Hun Jung*

Korea Atomic Energy Research Institute, 111, Daedeok-daero 989beon-gil, Yuseong-gu, Daejeon, Republic of Korea

*nchjung@kaeri.re.kr

1. Introduction

Foam decontamination technologies, in general, are advantageous to the reduction of secondary waste due to the minimized use of liquids and the delivering of decontamination agents due to the increased viscosity of foaming agents [1, 2]. The foaming agents developed in KAERI contain the silica nanoparticles to boost up the decontamination efficiency by increasing the stability of generated foams. After foam decontamination process, the treatment methods are needed to treat the waste solution of decontamination foam which is composed of radionuclides, surfactant, chemical reagent, and stabilizer (i.e. silica nanoparticles). Therefore the removal of the particulates in the waste solution is necessary to reduce the secondary waste thru the separation of solid–liquid. In this study, we investigated a candle filtration method [3] as a solid-liquid separation of silica nanoparticles from the waste solution.

2. Main subject

2.1 Selection of separation system of waste solution generated foam decontamination process containing silica nanoparticles

To choose a proper filtration system, we have considered five different systems – hydro-cyclone, tubular centrifuge, membrane, cross flow filtration, and candle filtration. In general cyclone is suitable for the particle separation in the range between 5 – 100 μm [4] and centrifugal systems could be disturbed by the foaming effect. Membrane filtration is capable to separate the particles below 100 nm, but its process is too complex and fouling in many cases can be a problem. Unlike such those direct filtration techniques, cross-flow filtration and candle filtration are known more suitable for the separation of nano-size particulates with high efficiency and capacity, but cross-flow filtration is typically used for the separation of liquid from concentrated slurry waste. The comparison of solid-liquid separation method is summarized in Table 1.

From the reasons described above, we have chosen the candle filtration system as the solid-liquid separation for the waste solution containing silica nanoparticles. It has been proven to be a cost-effective and reliable method for the removal of the contaminants with recovering of scrubbing liquid. Easy-removal as well as effective drying of cake formed on surface of the filter media is also advantageous for the post-treatment of wastes.

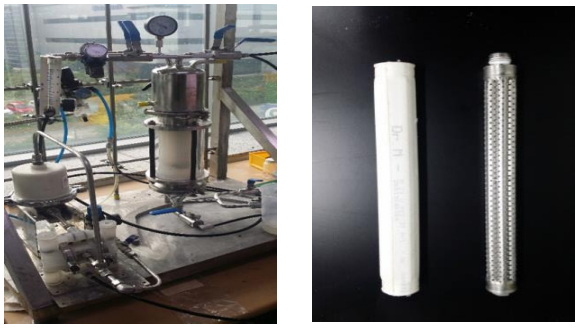
Table 1. Solid-liquid separation technology

division	Solid·liquid separation technology				
	Hydro Cyclone	Tubular Centrifuge	Membrane Filter	Cross Flow Filter	Candle Filter
Solids removal	△	△	○	○	○
Treated water recycling		△	○	○	○
Processing rate		60%	90~95%	90~95%	99%
Solid processing		△	Multiple processing	Multiple processing	Single processing

2.2 Experiment contents and results

The waste of decontamination foam solution containing silica nanoparticles were prepared using 1% (v/v) Elotant™ Milcoside 100 (EM 100, LG H & H) and 1wt.% silica nanoparticles (M-5, Cabosil). The candle filtration system (M21U002 model, Dr. M cooperation) and the filter module located inside the reactor are shown in Fig. 1 (a).

A turbidimeter (DRT-15CE, HF Scientific) was used to measure the separation and recovery efficiency of silica nanoparticles from the waste solution. The turbidity of the treated solution was measured every 30 minutes, and the test was conducted by circulating the treated solution until the particulates are removed over 99% in the turbidity value. After the filtration process is over, the air-blowing is operated to dry the cake and discharged by air-shock force from the candle filter media.



(a) (b)

Fig. 1. (a) Candle filtration experiment equipment (b) filter module.

The separation treatment for the waste solution of decontamination foam was shown in Fig. 2. As shown in the figure, about 99.4% of separation efficiency of nanoparticles was observed from 0.5 to 5 hours. It was found that the pore size of the filter was important factor for separating the silica nanoparticles.

The effect of surfactant on throughput of waste solution of decontamination foam was investigated. From the tests, the throughputs of waste solution of decontamination foam with and without surfactant were maintained at 11 and 14 L/m^2·hour for 5 hours, respectively as shown in Fig. 3.

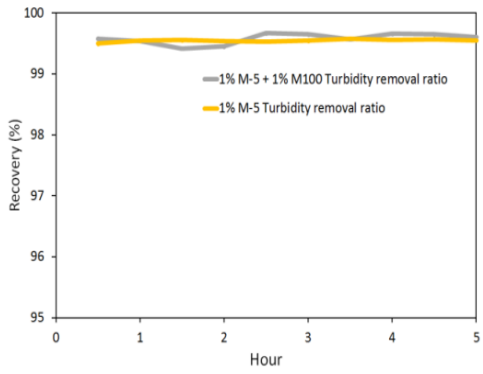


Fig. 2. Effect of Surfactants on Nanoparticle Recovery.

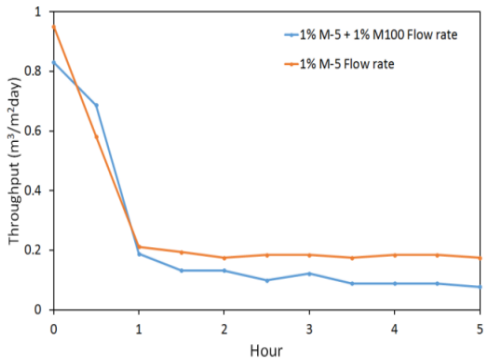


Fig. 3. Effect of surfactants on waste throughput.

In other words, the throughput of waste solution of decontamination foam in the presence of surfactants is reduced by 20% compared to the case without surfactants. It indicates that the silica nanoparticles bound to the surfactants might block the pore of candle filter. However the throughput was maintained constantly for 5 hour, which is still enough to treat the foam waste solution.

In the dry process of the cake formed on the candle filter media, the low pressure air drying about 1 bar resulted in 37% water content in the dried cake due to the suppression of crack formation. However, the water content by high pressure drying above 3 bar was 74% due to the early discharge of the cake from the filter media before it was not fully dried. From these results, the solids treatment method for candle filter by low pressure drying was suitable for the separation of silica nanoparticles.

3. Conclusion

In this study, we investigated the solid-liquid separation performance of silica nanoparticles in the waste solution generated foam decontamination process using a candle filter. The pore size of the filter was important factor to recover a various types of silica nanoparticles. The cake layer acts as a filter media, and the recovery rate increased after treated time. It is considered that the throughput of waste solution was reduced by surfactant due to the blocking of the pores in the candle filter, but the throughput of waste solution was maintained constantly for 5 hours.

Therefore, it is confirmed that the candle filtration can be an effective method for recovering silica nanoparticles in decontamination foam solution due to the formation of a cake layer in filter media.

REFERENCES

[1] B, Fournel.; S, Angot and P, joyer. (2002) Decontamination of Phebus experimental target chamber using sprayed foam. ICONE 10. Arlington. USA.

[2] Faury, M.; B, Fournel.; G, Boissonnet.; H, Provens. (1998) Foams for nuclear decontamination purposes: Achievements and prospects. Tucson. Waste Mangement .

[3] Towler, G.; Sinnott, R.K. (2013) Chemical Engineering Design - Principles, Practice and Economics of Plant and Process Design (2nd Edition). Elsevier.

[4] Gonzenbach, U.T.; Studart, A.R.; Tervoort, E.; Gauchkler, L.J. (2006) Stabilization of Foams with Inorganic Colloidal Particles Langmuir, 22: 10983.

Cesium Removal From Aqueous Solution by Bioaccumulation of Microalgae

Ilgook Kim[1*], Byung-Gon Ryu[2], Bum-Kyoung Seo[1], and Jong-Won Choi[1]
[1]Korea Atomic Energy Research Institute, 111, Daedeok-daero 989beon-gil, Yuseong-gu, Daejeon, Republic of Korea
[2]Nakdonggang National Institute of Biological Resources, 137, Donam 2-gil, Sangju-si, Gyeongsangbuk-do, Republic of Korea
[*]ilgook@kaeri.re.kr

1. Introduction

Radioactive cesium (Cs^+) in the environment has been a matter of serious concern because of its long half-life (30 yrs) and high water solubility. Thus, hazardous quantities of Cs^+ will remain in the environment for centuries and living organisms easily absorb Cs^+ mistaking it for harmless potassium [1]. Recently, increased attention has been directed on the use of biological technologies for the removal of radionuclides as the cheap and eco-friendly alternative to the non-biological methods. Metal including radioactive compounds uptake by microorganisms can be occurred by metabolism – independent and/or -dependent processes. One involves biosorption based on the ability of microbial cells to bind dissolved metals; on the other involves bioaccumulation, which depends on the metabolic ability of cells to transport metals into the cytoplasm [2, 3]. The purpose of this work is to investigate the feasibility of microalgae in bioaccumulation system to remove cesium from solution. The effect of different environmental parameters on cesium removal was also examined. Finally, the Cs-containing microalgae can be easily separated from a treated solution using positively charged surfactant coated magnetic nanoparticles.

2. Materials and methods

2.1 Microalgae

All experiments were carried out with *Desmodesmus armatus* SCK, which was isolated from wastewater treatment plant as cesium-accumulating microalgae (Fig. 1). Cells used for the bioaccumulation system were cultured in TAP medium and incubated at 25℃ (Fig. 2).



Fig. 1. New algal strain, Desmodesmus armatus SCK.

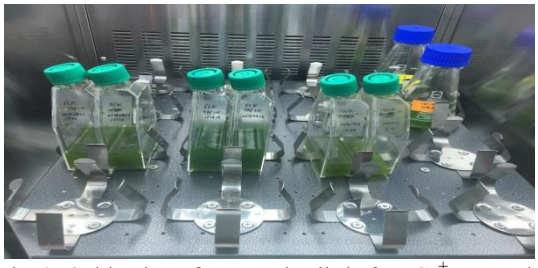


Fig. 2. Cultivation of prepared cells before Cs^+ removal tests.

2.2 Cs^+ removal experiments

For Cs^+ uptake tests, cells in the early stationary growth phase were collected by centrifugation and then suspended in 20 mM Tris buffer solution containing CsCl with 1 g/L biomass loading. All cell suspensions were incubated at 25℃ with rotary shaking (120 rpm). In order to measure the Cs^+ concentration, the medium was filtered through 0.2 micron filter and analyzed by inductively coupled plasma-mass spectrometry (ICP-MS). The Cs^+ removal efficiency was calculated as the difference in the Cs^+ concentration in the medium at initial and final condition.

2.3 Separation of Cs-containing microalgae

Cationic surfactant coated magnetic nanoparticles (MNP) were synthesized according to previously reported co-precipitation method using iron salts ($FeCl_3 \cdot 6H_2O$ and $FeCl_2 \cdot 4H_2O$), and polyethyleneimine (PEI) [4]. The microalgae-PEI coated MNP flocs were separated from the solution using an external magnet.

3. Results and discussion

3.1 Assessment of Cs^+ removal by D. armatus SCK

First of all, *D. armatus* SCK, cultivated in nutrient broth media amended with Cs^+, were able to survive Cs^+ concentration as high as 1 mM.

As shown in Fig. 2, Cs^+ uptake of the *D. armatus* SCK increased with increasing the initial Cs^+ concentration and reached a saturated value at 500 μM.

Maximum equilibrium uptake of Cs^+ ions was determined as 280 μM showing 70% removal efficiency at 400 μM.

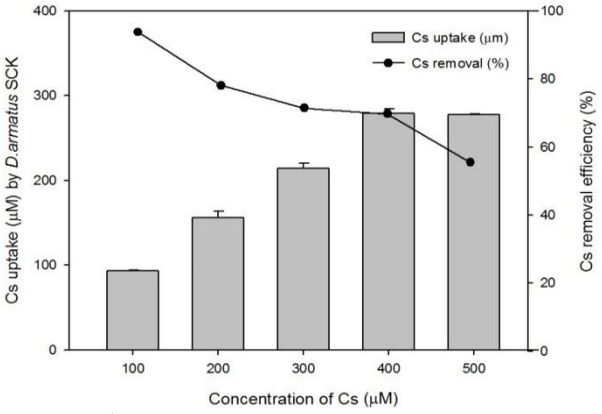


Fig. 3. Cs^+ uptake by *D. armatus* SCK with different Cs concentrations.

The chemical similarity of Cs^+ and other alkali monovalent cations, in particular K, is the key factor that governs the high mobility of Cs^+ in biological systems [5]. Cs^+ accumulation by *D. armatus* SCK was decreased at high K^+ concentrations as shown in Fig. 3, which can be explained by the inhibitory effects of K on microalgal Cs^+ uptake. In fresh water, however, K^+ concentrations are generally below 3 mg/L, and thus the inhibition of Cs^+ uptake by K^+ could be neglected.

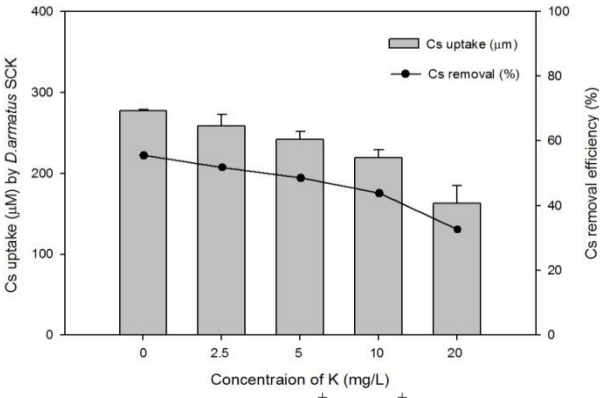


Fig. 4. Effect of potassium (K^+) on Cs^+ uptake by *D. armatus* SCK.

3.2. Separation of Cs-containing microalgae using PEI-MNP

Fig. 5 shows images of the flocculation of microalgae by PEI-MNP and the subsequent magnetic separation. The separation by the external magnetic field was completed within 3 min, as confirmed by the clear supernatant.

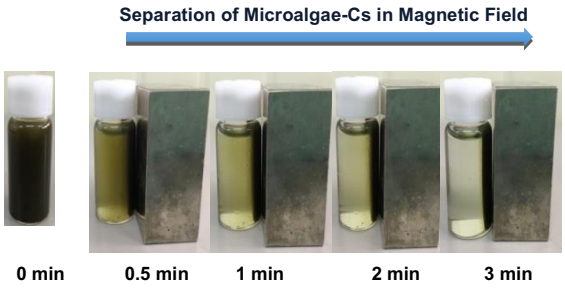


Fig. 5. Separation of Cs-containing microalgae using PEI-MNP.

4. Conclusion

The aim of this work is to confirm the possibility of selected one of microalgae in the uptake of Cs^+. The obtained results showed the maximum Cs^+ removal by *D. armatus* SCK was 280 μM indicating 70% removal efficiency. Also, *D. armatus* SCK could uptake Cs^+ in the presence of K^+, is particularly known to be transported into cells as an analog of Cs^+ in freshwater condition. Furthermore, the cationic surfactant coated magnetic nanoparticles were easily applied to separate Cs-containing microalgae from aqueous solution.

REFERENCES

[1] N. Tomioka, K. Tanaka, H. Uchiyama, O. Yagi, and E. Kokufuta, "Recovery of ^{137}Cs by a bioaccumulation system using *Rhodococcus erythropolis* CS98", Journal of Fermentation and Bioengineering, 85, 604-608, 1998.

[2] R. Jalali-Rad, H. Ghafourian, Y. Asef, S.T. Dalir, M.H. Sahafipour, and B.M. Gharanjik, "Biosorption of cesium by native and chemically modified biomass of marine algae: introduce the new biosorbents for biotechnology applications", Journal of Hazardous Materials, 116, 125-134, 2004.

[3] A. Kapoor and T. Viraraghavan, "Fungal biosorption- An alternative treatment option for heavy metal bearing wastewaters: A review", Bioresource Technology, 53, 198-206, 1995.

[4] S.C. Jang, S.B. Hong, H.M. Yang, K.W. Lee, J.K. Moon, B.K. Seo, Y.S. Huh and C. Roh, "Removal of Radioactive Cesium Using Prussian Blue Magnetic Nanoparticles", Nanomaterials, 4, 894-901, 2014.

[5] S.V. Avery, Caesium accumulation by microorganisms: uptake mechanisms, cation competition, compartmentalication and toxicity, Journal of Industrial Microbiology, 14, 76-84, 1995.

Electrochemical Behavior of Uranium(VI) in Ionic Liquid

Iksoo Kim*, Sumin Kwon, Dongyong Chung, Keunyoung Lee, and Jongwon Choi

Korea Atomic Energy Research Institute, 111, Daedeok-daero 989beon-gil, Yuseong-gu, Daejeon, Republic of Korea

*niskim@kaeri.re.kr

1. Introduction

Ionic liquids have attracted attention in the field of nuclear fuel cycle because they have several attractive properties such as an amazing ability to dissolve organic and inorganic compounds and a wide electrochemical window suitable for aqueous and non-aqueous reprocessing applications. Ionic liquids are being evaluated as an alternative to the conventional diluent, n-dodecane, in aqueous reprocessing, and as a substitute to the traditional high-temperature molten salts in the non-aqueous reprocessing of spent nuclear fuels [1, 2]. In this work, as a part of the research to recover uranium from spent nuclear fuel using ionic liquid, the electrolytic reduction of uranyl nitrate in ionic liquid, 1-butyl-3-methylimidazolium chloride (bmimCl), was studied. The electrochemical behavior of uranium(VI) in bmimCl was investigated within the temperature range of 343-373 K through cyclic voltammetry (CV).

2. Experimental

2.1 Chemicals and equipment

All the chemicals used in this study were of analytical grade and used without further purification. Ionic liquid, bmimCl, was procured from C-TRI, Korea. To remove the water and volatile impurities, bmimCl was kept for more than 3 hours under a reduced pressure at 373 K, and the residual water concentrations measured using a Karl Fisher moisture content meter (Metrohm 831 KF Coulometer) were below 100 ppm. The uranyl nitrate was procured from Merck.

2.2 Experimental method

All electrochemical experiments were carried out in a three-electrode cell. For cyclic voltammetric measurements, a glassy carbon (cylindrical, SA = 0.07 cm^2) and a platinum wire were used as a working electrode and a counter electrode, respectively. As a quasi-reference electrode, a platinum wire was used. Cyclic voltammograms of the ionic liquid solutions were recorded using ZIVE SP2 (WonATech) equipped with Smart Manager program.

3. Results and discussion

The cyclic voltammogram for the reduction of U(VI) in bmimCl on a glassy carbon working electrode at the potential sweep range of 50 ~ 500 mV/s is shown in Fig. 1. It is seen that the cathodic peak potential E_p^c is virtually constant with increase of scan rate and the anodic-to-cathodic peak current ratio, i_p^c/i_p^a, is unity. However, the difference in the value of $|E_p^c - E_{p/2}^c|$ is twice larger than the value required for the reversible process (32.5 mV at 343 K) indicating that the reduction of U(VI) in bmimCl at glassy carbon electrode is not only controlled by diffusion but also charge transfer kinetics.

The ionic liquid, bmimCl, exhibits an electrochemical window of 2.7 V with a cathodic stability of up to -1.4 V (vs. Pt), which is sufficient for enabling the reduction of uranyl ions. The cyclic

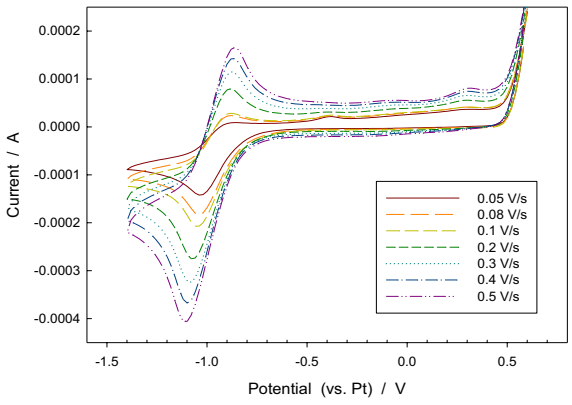


Fig. 1. Cyclic voltammogram of uranyl nitrate in bmimCl at various sweep rates.

voltammogram of $UO_2(NO_3)_2$ in bmimCl consists of a reduction wave occurring at the peak potential of −1.05 V owing to the reduction of U(VI) and an oxidation wave occurring at the peak potential of -0.90 V. The result from the CV experiments at various scan rates and temperatures indicates that a reduction of uranyl ions takes place through a quasi-reversible single-step two-electron transfer reaction.

The relation between the cathodic peak current and the scan rate for an irreversible reduction reaction is given by Eq. (1).

$$i_p^c = 0.496nFCAD^{1/2}\left(\frac{(\alpha n_\alpha F v}{RT}\right)^{1/2} \quad (1)$$

The linear dependence of cathodic peak current (i_p^c) on square root of scan rate ($v^{1/2}$) was shown in Fig. 2, which confirms that the reduction of U(VI) in bmimCl is diffusion controlled and the diffusion coefficient can be determined from the slope by Eq. (1) and the value αn_α can be obtained from Eq.(2).

$$|E_p^c - E_{p/2}^c| = \frac{1.857RT}{\alpha n_\alpha F} \quad (2)$$

The diffusion coefficient of U(VI) in bmimCl was calculated to be 0.69×10^{-7} cm^2/s at 343 K and at the scan rate of 0.10 V/s. Besides, the diffusion coefficient at other temperatures (353-373 K) were also determined, and the resultant values increase with temperature increment.

The diffusion coefficient is related to temperature by Arrhenius equation shown in Eq.(3).

$$D = A\, e^{-E_a/RT} \quad (3)$$

where E_a is the activation energy which can be obtained from the plot of ln D against 1/T. Effect of temperature on the cyclic voltammogram of U(VI) in bmimCl is shown in Fig. 3. It is seen that i_p^c increases and the peak potential E_p^c shifted towards

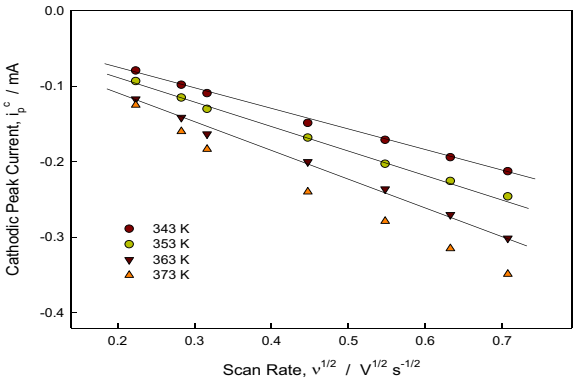


Fig. 2. Plot of cathodic peak currents against square root of scan rate at different temperatures for the reduction of U(VI) in bmimCl.

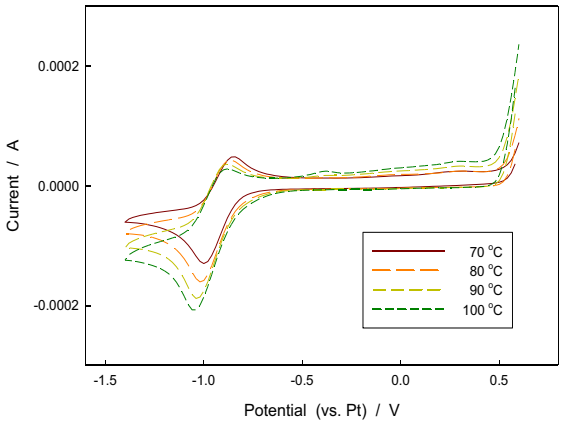


Fig. 3. Cyclic voltammogram of uranyl nitrate in bmimCl at various temperatures.

positive potential with increase of temperature. From the slope of the straight line of Arrhenius plot of Eq.(3), the energy of activation for the diffusion of U(VI) in bmimCl was found to be 43 kJ/mol.

4. Conclusion

The cyclic voltammogram of $UO_2(NO_3)_2$ in bmimCl consists of a reduction wave occurring at the peak potential of −1.05 V owing to the reduction of U(VI) and an oxidation wave occurring at the peak potential of -0.90 V. The result from the CV experiments at various scan rates and temperatures indicates that a reduction of uranyl ions takes place through a quasi-reversible single-step two-electron transfer reaction. The diffusion coefficient and the activation energy of U(VI) in bmimCl was found to be on the order of 10^{-8} cm^2/s and 43 kJ/mol, respectively.

REFERENCES

[1] P. N. Pathak, “N,N-Dialkyl amides as extractants for spent fuel reprocessing - an overview”, Journal of Radioanalytical and Nuclear Chemistry, 300, 7–15 (2014).

[2] M. Jayakumar, K.A. Venkatesan, T.G. Srinivasan, P.R. Vasudeva Rao, “Electrochemical behavior of ruthenium (III), rhodium (III) and palladium (II) in 1-butyl-3-methylimidazolium chloride ionic liquid”, Electrochimica Acta 54, 6747–6755 (2009).

The Study of Radiation Safety Treatment for Dismantling Contaminated Piping in NPP

Cheol-Young Jeong*, Min-Soo Kim, Dong-Kyu Jang, Duck- Chul Hwang, and Hee- Kyoung Kim

ACT-RMT 11-3, Techno 1-ro, Yuseong-gu, Daejeon, Republic of Korea

*jcy6535@naver.com

1. Introduction

The Kori Unit 1, which started commercial operation in 1978, will be decommissioned after a cooling process of about 5 years. There are several steps to be taken before the decommissioning the NPP. The most important thing is maintaining and managing System in the 'Alive state' even during the decommissioning process. For example, HVAC (Heating, Ventilation, Air Conditioning) of the building, the power supply system, the air supply system, the water utilization for fire protection, the water for living system and Area & Effluent Radiation Monitoring System should be maintained during the decommissioning process.

NPP's systems are originally designed for the purpose of transporting fluid (coolant or gas such as hydrogen, pneumatic gas). For example, the coolant is moved from a tank through pump, pipe line, valve, Hxs and other tanks or devices. These are built into the building with supports and various types of the gantries. Table 1 is information of piping in the major system of the NPP.

Table 1. Design information of major piping of PWR for referencing of dismantling (examples)

Related System (s/s)	Place	Type (NPS)	about Weight (lb/ft)	*Activation □Expected Contamination (Note)	Decontamination	
					*In&Out	Operator (line up)
RCS	cv	27~32	typ.	◉	◉	□
	cv to aux	3~14	14.3~40.6 (sch.160)	◉	◉	□
Residualheatremoval	cv to aux	8~14	19.3~63.2 (sch.80)	□	◉	□
CVCS	cv to aux	3~6	1.68 (sch.80)	◉	◉	□
Dipose of waste	cv thr aux to rad	4~8	5.5~21.7 (sch.10)	□	◉	□
Rx	yd thr aux to cv or aux to cv	8~14	21.7~68.7 (sch.40)	□	◉	□
Cable holding	cv, aux etc.	2~3/4 or3/8	1.28(0 (sch.0)	□	◉	□

Ref: Typical P&ID of NPP (PWR), Piping Hand Book
note: In Socket Welding Gap may contaminated foreign materials even after decontamination.

NPP is contaminated by radioactive materials during the operation, so it is required to accumulate 'know-how' through research and development of radiation safety management for dismantling

This paper describes the technical factors for the safe treatment of contaminated piping during dismantling

2. Main Subject

2.1 Overview

The basic purpose for the dismantling contaminated NPP is to reduce the amount of radioactive waste and secondary radioactive waste. In addition to prevent spreading from contaminated radioactive materials and reducing radiation exposure to NPP workers. The dismantling should be treated in the order from high-dose, high-pollution equipment, structures and systems, but in some countries high-dose reactor is left for later disposal of it. Dismantling is especially necessary to ensure suitability of disposal and public acceptance (PA). The key factor for safe handling of dismantling is shown in Tab.1 below.

Table 2. Factors of the objective for issue

	Education training	management and supervision	Procedure observance	Analysis of measurement	Reduction of exposure	protection of environment	related laws	international Cooperation
Prevention of safety-accident	○	○	○		○	○	○	
Radiation protection	○	○	○	○	○	○	○	
Reduction of RWT	○	○	○	○	○	○	○	○
Conform of disposal suitability	○	○	○	○	○	○	○	○
National consensus		○	○	○	○	○	○	
Work Performance	○	○	○		○	○	○	○

2.2 Strategy of safe treatment of dismantling

The basic strategy of safe treatment of contaminated components in NPP is to meet regulations of NSSC

(Nuclear Safety and Security Commission) and manage it in an economical way without any social confliction. Those components should be classified according to configuration and size, radioactivity concentration and maintaining structural integrity, satisfying key information markings in the dismantling process. It also needs to safely dispose of low, intermediate-level radioactive waste even after chemical treatment in dismantling process.

It is necessary to have place with facilities and equipments to perform the dismantling process in according to procedure. It also needs to find out and apply detailed techniques. For instance, standardization of cutting equipments considering unit weight and sizing, ease of packing by shape, handling of transportation, analysis of radionuclide to evaluate radiation characteristics, management of work and environment, identification of waste, transportation and transfer to regulatory agency for safe treatment of dismantling

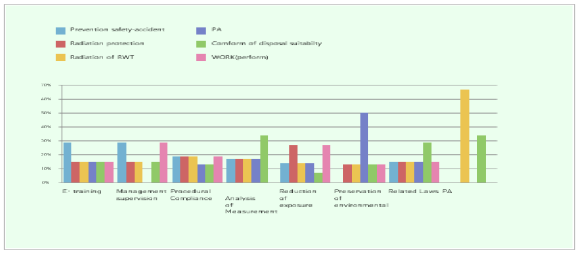


Fig. 1. The Importance of Key Factors.

2.3 Analysis of technical factors for a typically safe treatment of dismantling

For example, There are several detailed elements are derived from 7 subjects in the analysis results of technical factors for safe treatment of dismantling by using Fish Bone Diagram (FBD).

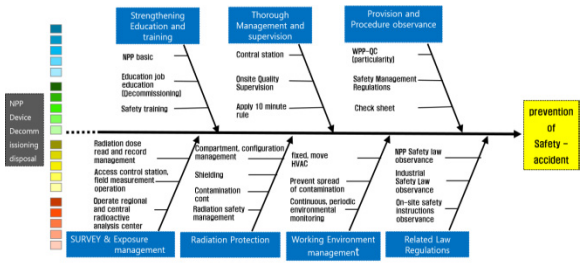


Fig. 2. Prevention of Safety Accident by using FBD.

2.4 Detailed factors for safe treatment (Excluding Administrative matters such as plans)

It is necessary to accumulate the academic and experiential knowledge of organization in order to accomplish the achievement corresponding to the derived detailed factors. Based on this, it should be written in the work procedures and the test report reflecting the data of dismantling techniques and regulations.

Table 3. The Detailed Elements for Piping's dismantling

	Prevention of safety-accident	Radiation protection	Reduction of RWT	Conform of disposal suitability	National consensus	Work Performance
Education training	basic education job education safety training safety culture	·basic education job education ·safety training ·Protection education	Basic education Procedure education transporting educaiton	Related law Procedure Transfer regulation Sign, Packing	Public hearing of dismantlement plan	Job Training Fire safety Protection Education
Management and supervision	Control Supervision Applying 10m's rule	Zone cont. Access cont. Exportion cont.	Equipment and waste management Work cont.	measurement Analysis Packing Record		Quality Transition Procedural Compliance Protection Safety
Procedure observance (WPP-QCI)	wpp-QCI Safety regulation Check sheet	Survey Access cont. Exportion cont. Contamination cont. Radiation safety	Procedures for entry and exit of wastes	Related Laws procedure Transfer regulations Cover record		Understanding Content sequence of the work Approved equipment Check the result
Analysis of measurement	Contral station site lane of transportation Package	mesurement skills Record amnagement Feedback Equipment management Contamination management	Analysis of radiological characterization Chearacteristic evaluation	Dose measurement Nuclide analysis Packing integrity Scale factor contamination inspection		Measurement accuracy, Data management Record results
Reduction of exposure	Compartment management Sheilding and decontamination Identification	Work management Prevention of contamination Work environment manage Procedural compliance	Prevention of contamination work environment manage Procedural compliance			Procedural Compliance Time reduction
Protection of environment	HVAC Prevention of scontamination Supervision	Compartment management Workplace vetilation Prevention of contamination Access cont.	Zone cont. Prevention of scontamination Supervision		Feedback from residents	
Related laws	Safety law Protection law fire law	Radiation safety law Procedure	Safety law Industrial Safety Law Procedure	Transfer regulation Nuclear safety law	Safety law	

3. Conclusion

Dismantling is a sophisticated work that can be described as art in terms of technology. Because all legal procedures and detailed requirements should be meet and the dismantling may be proceeded in the reverse order of construction and in addition to control of radiation. Particularly, in order to improve the efficiency, between the organization dealing with cutting components and organization of disposal waste must be established mutual cooperation and close relationships. Through this, it is expected that the achievement of the safe treatment of the NPP′s piping dismantling. The end

Removal of Sodium Dodecyl Benzene Sulfonate (SDBS) From Radioactive Liquid Wastes by Adsorption of Porous Polymer Resins

Jongho KIM[1], Young-Jin GWON[1], Hyunchul Kim[1], Kune-Woo Lee,[2] and Taek Seung LEE[1*]

[1] Chungnam National University, 99 Daehak-ro, Yuseong-gu, Daejeon, Republic of Korea

[2]Korea Atomic Energy Research Institute,111, Daedeok-daero 989 beon-gil, Yuseong-gu, Daejeon, Republic of Korea

[*]tslee@cnu.ac.kr

Massive amount of surfactants for separating the radioactive isotopes are included in radioactive liquid wastes (RLWs) which are generated during decontamination or decommissioning. Especially, sodium dodecyl benzene sulfonate (SDBS) is one of the surfactants which are generally used for decontamination or decommissioning as anionic surfactants of late. Discharging such radioactive liquid wastes including many surfactants has a great problem such as high toxicity to humans and animals. For that reason, RLWs contaminated with surfactants should be purified for discharging clean water into ocean and rivers.

The complete elimination of high concentration of SDBS from the RLWs is still undergoing serious hardships, though SDBS with low concentration (1-3 mg/L) from domestic waste water is completely removed by liquid waste treatment plants. SDBS can be efficiently eliminated from wastewaters by adsorption on adsorbents such as activated carbons or polymer resins with high porosity. So we proved that highly porous polymer resins could remove the SDBS effectively with batch system. We used two kinds of porous polymer resins composed with polystyrene or polymethacrylate, respectively, which can be easily synthesized by dispersion polymerization. In the present study, the removal of SDBS was studied by the time, concentration of SDBS or adsorbents. Finally, removal percentage of SDBS is reached to more than 90% after 100 min by 20 mg/ml of adsorbents.

Stoichiometry of Palladium Extraction in Ionic Liquid

Sumin Kwon*, Ik-Soo Kim, and Dong-Yong Chung

Korea Atomic Energy Research Institute, 111, Daedeok-daero 989beon-gil, Yuseong-gu, Daejeon, Republic of Korea

*sumin@kaeri.re.kr

1. Introduction

Ionic liquids (ILs) are organic salts that are benign and are normally liquid at ambient temperature. ILs have been studied as green solvent to substitute conventional organic solvents in various research areas such as separation, synthesis and electro-chemistry [1]. Recently, in this laboratory, ILs were studied to determine their efficiency for the extraction and electrochemical recovery of actinides and fission products. In this study, we used dibutyl sulfoxide (DBSO) as the extractant and 1-buty-3-methylimidazolium bis(trifluoromethanesulfonyl) imide (C_4mimTf_2N) as an IL extraction solvent, and we showed that IL obtained higher distribution ratios for palladium than conventional organic solvents, and observed a decline in distribution ratios of palladium acidity increased [2]. In our present study, the number of DBSO molecules involved in the metal complex was calculated. The stoichiometry was found to be 1:2.33 and 1:1.05 (M:L) in C_4mimTf_2N from 0.05 M and 5 M of nitric acid solution, respectively.

2. Experimental

2.1 Materials and method

DBSO and C_4mimTf_2N were obtained from Sigma-Aldrich. The extraction experiment was carried out by equilibrating the organic phase (0.003~1 M DBSO in C_4mimTf_2N) and the aqueous phase (1000 ppm of palladium in the desired HNO_3 concentration), with a phase ratio of 1:1 at 25℃. After equilibration, the solution was allowed to settle, and aqueous phase was separated from organic phase. The aqueous phase was used to determine the concentration of palladium by ICP-OES (Model No. PQ 9000 Elite). The distribution ratio of palladium (D_{Pd}) was calculated from the aqueous phase concentration and D_{Pd} value is defined in Eq. (1):

$$D_{Pd} = \frac{[Pd]_{IL}}{[Pd]_{aq}} = \frac{[Pd]_{aq,init} - [Pd]_{aq,fin}}{[Pd]_{aq,fin}} \quad (1)$$

The species with the subscripts ‘aq’ and ‘IL’ refer to those in the aqueous and ionic liquid phase, and ‘init’ and ‘fin’ refer to those of before and after equilibration, respectively.

2.2 Results and discussion

The extraction of palladium with varying concentration of DBSO, from 0.003 to 1 M, from 0.05 M or 5 M nitric acid feed was investigated in C_4mimTf_2N and the results are presented in Fig. 1. An increment in palladium extraction with increasing DBSO concentration in C_4mimTf_2N was observed, which indicates that DBSO is participating in the extraction process.

Results show the extraction mechanism of palladium into C_4mimTf_2N can be best represented by a cation exchange reaction and its reaction is as follows:

$$Pd^{2+}_{aq} + nDBSO_{IL} + 2C_4mim^{+}_{IL} \leftrightarrow \mathrm{Pd}(DBSO)^{2+}_{n\ IL} + 2C_4mim^{+}_{aq} \quad (2)$$

The species with the subscripts ‘aq’ and ‘IL’ refer to those in the aqueous and ionic liquid phase

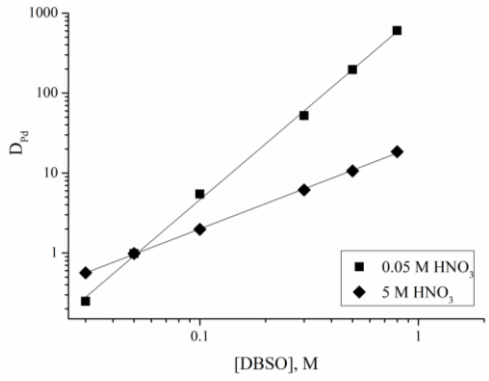


Fig. 1. Distribution ratio of palladium at varying DBSO concentrations extracted from 0.05 and 5 M HNO_3 feed into C_4mimTf_2N.

From eq. (2), the equilibrium constant for the extraction of palladium (K_{Pd}) can derived to Eq. (3):

$$K_{Pd} = \frac{[Pd(DBSO)_n^{2+}]_{IL}[C_4mim^+]_{aq}^2}{[Pd]_{aq}^{2+}[DBSO]_{IL}^n[C_4mim^+]_{IL}^2} \quad (3)$$

Substituting D_{Pd} for $[Pd(DBSO)_n{}^{2+}]_{IL}/[Pd]_{aq}$ and P_{Cnmim+} for $[C_4mim^+]_{aq}{}^2/[C_4mim^+]_{IL}{}^2$, and taking the logarithm and rearrange, one obtains

$$\log D_{Pd} = logK_{Pd} - logP_{C_nmim+} + nlog[DBSO] \quad (4)$$

A plot of $logD_{Pd}$ vs. the concentration of DBSO should result in straight lines with a slope 'n' and the intercept represents $logK_{Pd}$ - $logP_{Cnmim+}$ on the basis on Eq. (4). The slope 'n' represents the number of DBSO molecules associated with the metal complex during extraction. The slope 'n' for palladium extraction from 0.05 M and 5 M nitric acid feed was obtained from a slope analysis of the plot in Fig. 1. In case of DBSO in C_4mimTf_2N, the slope is 2.33±0.04 from 0.05 M nitric acid feed and 1.05±0.01 from 5 M nitric acid feed. In lower acidity (0.05 M HNO_3), extraction of mixed species of 1:2 as well as 1:3 M:L composition but 1:2 M:L composition is predominant, while in higher acidity (5 M HNO_3), 1:1 M:L composition is predominant. Extraction of mixed species has been reported previously in case of molecular diluents using TODGA [3]. Finally, the value of 'n' was obtained for the extraction of palladium from 0.05 M and 5 M nitric acid feeds Eq. (5) and Eq. (6), respectively.

$$Pd_{aq}^{2+} + 2DBSO_{IL} + 2C_4mim_{IL}^+ \leftrightarrow Pd(DBSO)_2^{2+}{}_{IL} + 2C_4mim_{aq}^+ \quad (5)$$

$$Pd_{aq}^{2+} + DBSO_{IL} + 2C_4mim_{IL}^+ \leftrightarrow Pd(DBSO)^{2+} + 2C_4mim_{aq}^+ \quad (6)$$

The number of DBSO molecules associated with the metal complex decreases as the feed acidity increases. This shows that the acid interferes with the metal-ligand complex formation. It is presumed that DBSO is protonated in the presence of the high nitric acid feed concentration, therefore, hydrogen ion competes with palladium ion, resulting in less DBSO molecules associated with the metal complex at higher acidity. The formation reaction of adducts of DBSO with nitric acid can be written such that

$$H_{aq}^+ + nDBSO_{IL} + C_4mim_{IL}^+ \leftrightarrow H(DBSO)_{n\,IL}^+ + C_4mim_{aq}^+ \quad (7)$$

In the previous study [1], we extracted palladium from varying concentration of nitric acid (0.05~8 M HNO_3) into C_4mimTf_2N containing 0.1 M DBSO, and a sharp drop of D_{Pd} values was observed as the feed acidity increases. We can explain the extraction tendency of palladium obtained from the previous study as well by using the competing reaction between Palladium and hydrogen ions (shown in Eq. (7)) in this present paper.

3. Conclusions

Extraction of palladium using DBSO was carried out in varying DBSO concentration (0.003~8 M) in C_4mimTf_2N from 0.05 M and 5 M nitric acid feeds. The stoichiometry of palladium extraction in C_4mimTf_2N was obtained from a slope analysis of a plot ($logD_{Pd}$ vs. the concentration of DBSO). The results indicated that, in high acidity, palladium is coordinated with 1.05 DBSO molecules, compared to 2.33 molecules in low acidity, due to competition between palladium and hydrogen ions, and the results gave a clue to understand the extraction behavior of palladium in the previous study.

REFERENCES

[1] R. D. Rogers and K. R. Seddon, "Ionic Liquids—Solvents of the Future?", Science, 302(5646), 793-793 (2003).

[2] S. Kwon, I. Kim and D. Chung, "Extraction Behavior of Palladium Using Imidazolium Based Ionic Liquid", Proc. of the KRS 2016 Spring Conference, 14 (1), May 25-27th, 2016, Mokpo.

[3] S. A. Ansari, P. N. Pathak, M. Hussain, A. K. Prasad, V. S. Parmar and V. K. Manchanda, "N,N,N',N'-Tetraoctyl Diglycolamide (TODGA): A promising Extractant for Actinide-Partitioning from High-Level Waste (HLW)", Solvent Extraction and Ion Exchange, 23(4), 463-479 (2005).

Effect of the Addition of Oxalic Acid to the Phosphoric Acid Electrolyte on the Electro-decontamination Behavior of the SUS Metal Surface

Kim Dong-Yeon*, Hyun-Kyu Lee, Won-Zin Oh, and Sang-June Choi
Kyungpook National University, 80 Daehakro, Bukgu, Daegu, Republic of Korea
*east.kite@knu.ac.kr

1. Introduction

As Kori Unit 1 is going to shut down permanently in June 2017, the securing of decontamination technology related to waste reduction occurring in the decommissioning process of nuclear power plants is being discussed as an important issue.

Electro-decontamination has a high decontamination factor and excellent decontamination effect on metals, which can be effectively used to primary system of nuclear power plants. Recently, there is a tendency to use an electrolytic decontamination process with phosphoric acid which is excellent in electrical conductivity and stability. This phosphoric acid electrolytic decontamination can be reused as a decontamination agent through the regeneration process as well as reducing waste.

Oxalic acid dissociates into electrolytes and regulates the pH by supplying hydrogen ions. In addition, oxalic acid precipitates from divalent metal ions such as Fe^{2+}, Ni^{2+} and radioactive species $^{60}Co^{2+}$, $^{59}Fe^{2+}$ metal oxalate, reducing the concentration of metal ions in solution.

This study was carried out to investigate the effect of oxalic acid on the decomposition reaction of metal when the dissociation of oxalic acid in the electrolysis reaction of SUS304 causes the precipitation reaction.

2. Experiments

2.1 Experimental method

For the electro-decontamination test of SUS metal, SUS304 pipe (I.D 9.7 cm, H 13 cm) was used for cathode and anode was used as a sus304 having a surface area of 10 cm for the experiment. 1 L beaker was used as a reactor for electro-decontamination reaction. TEX-300 product of Toyotech was used as a power supply. As the electrolyte, phosphoric acid of 2 M, 5 M and 8 M concentrations were used as the base solution, Experiments with and without 0.5 M oxalic acid injection per concentration of phosphoric acid were carried out and compared.

The solution information for each experiment is shown in Table 1.

Table 1. Solution information of each experiment

No	H_3PO_4	$H_2C_2O_4$
1-1	2 M	/
1-2	2 M	0.5
2-1	5 M	/
2-2	5 M	0.5
3-1	8 M	/
3-2	8 M	0.5

The voltage was constantly applied at 4 V for each experiment and the voltage application time was 1 hour. As the experimental data, the weight of the anode before and after the electro-decontamination was measured three times, and the average was recorded. At this time, the decomposition efficiency of SUS metal was evaluated through weight loss.

In addition, SUS metal decomposition efficiency was calculated by recording the electric power used for electrolytic decontamination of water and metal through the current measured during electrolytic decontamination.

2.2 Experimental result

As a result of electro-decontamination of SUS metal, it was confirmed that metal oxalate was formed in the experiment in which oxalic acid was injected.

Tables 2 and 3 show data on the weight loss of the anode and the electro-decontamination efficiency through the current in each experiment.

Table 2. Weight loss of SUS304

No	Initial weight [g]	Post weight [g]	Weight loss [g]
1-1	15.8596	15.5915	0.2681
1-2	15.7282	15.2581	0.4701
2-1	16.3194	15.6975	0.6219
2-2	16.3228	15.6258	0.6970
3-1	16.3148	15.5853	0.7295
3-2	16.3225	15.4944	0.8281

Table 3. Current density of Metal and Water

No	J_{Metal} [A/cm^2]	J_{Water} [A/cm^2]
1-1	0.03416	0.2681
1-2	0.05989	0.4701
2-1	0.07924	0.6219
2-2	0.08881	0.6970
3-1	0.09295	0.7295
3-2	0.10552	0.8281



Fig. 1. Metal oxalate.

The weight loss of SUS304 anode before and after the experiment was measured. In the oxalate infusion experiment, the weight loss was increased compared to the not-injected experiment. The results of the average current density measurement also show that the addition of oxalic acid increases the current for electro-decontamination of metals and water.

3. Conclusion

The effect of oxalic acid on the electro-decontamination behavior of the SUS metal surface was investigated in the phosphoric acid electrolyte system .

Addition of oxalic acid to the electrolyte is considered to increase the oxidative dissolution rate of the SUS metal. It is also thought that the addition of oxalic acid improves the current density.

ACKNOWLEDGEMENTS

This work was supported by the Korea Institute of Energy Technology Evaluation and Planning (KETEP) and the Ministry of Trade, Industry & Energy (MOTIE) of the Republic of Korea (No. 20141510300310)

REFERENCES

[1] Lee Seung Won et al, “Pyrolysis characteristics of metal oxalate dihydrate formed by precipitation reaction of phosphoric acid electrolytic solution”, Korean Radioactive Waste Society AUTUMN, 14(2), 449-450 (2016).

[2] Andre Angermann et al., “Synthesis of magnetite nanoparticles by thermal decomposition of ferrous oxalate dihydrate”, Journal of Materials Science, pp 5123–5130 (2008).

Effect of the Temperature and UV Reflector on the AOP Decomposition Behavior of the Oxalates From the Chemical Decontamination Waste

Jin-Hee Kim*, Hyun-kyu Lee, Won-Zin Oh, and Sang-June Choi

Kyung pook National University, Dae-Hak ro 80, Dae-Gu, Republic of Korea

*Kimjinhee33@knu.ac.kr

1. Introduction

Oxalic acid ($H_2C_2O_4$) is one of organic solvents used in nuclear industry. It is used as decontamination reagent for removing oxidation deposit that is formed at NPP system surface [1]. Especially, oxalic acid has feature that it is decomposed into CO_2 and H_2O. It is needed to remove remained oxalic acid which chelates with oxidation deposit [2].

In water treatment industry, advanced oxidation processes (AOPs), which decompose organics by forming OH radical from combination of UV, O_3 and H_2O_2, is studied.

In previous study, UV/H_2O_2 showed higher efficiency than other AOPs and it was applied easily [3]. In this study, therefore, UV/H_2O_2 process was applied for decomposing remained oxalic acid and effect of temperature and UV reflector, which were selected as influence factors in UV/H_2O_2 process, was estimated.

2. Experiments

2.1 Preparation of waste water and estimation of decomposition extent

The volume of waste water which was subject of decomposition in this study was set to 800 mL to maximize contact area of UV lamp. As the remained oxalate after removing oxidation deposit chelate with iron and chrome, 2 mM ferric chloride ($FeCl_3$), 1mM chromium nitrate ($Cr(NO_3)_3$) and 30 mM oxalic acid were mixed to prepare waste water. The extent of oxalic acid decomposition is estimated by total organic carbon (TOC) analysis.

2.2 Estimation of effect of temperature

50 mM hydrogen peroxide was used in UV/H_2O_2 process for removing remained oxalate in waste water. The temperature in UV/H_2O_2 process was set to room temperature, 50℃, 60℃ and 70℃ respectively and the decomposition of oxalate was conducted for 5 hours

2.3 Estimation of effect of UV reflector

In this study, quartz reactor was used for UV/H2O2 process as shown in Fig. 1. In order to confirm effect of UV reflector, the outside of quartz reactor was covered by aluminium foil to reflect UV light. 30 mM hydrogen peroxide was used in UV/H_2O_2 process and the decomposition was conducted for 2 hours.

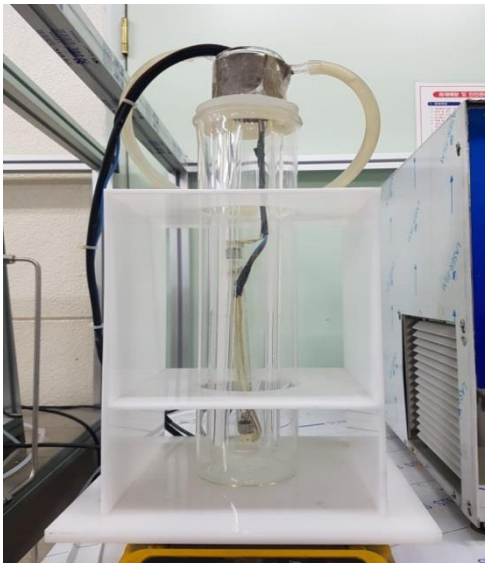


Fig. 1. Quartz reactor.

3. Results

3.1 Estimation result of effect of temperature

The decrease of oxalic acid concentration was represented in Fig. 2 to compare results of decomposing oxalic acid according to temperature in

UV/H_2O_2 process. At higher temperature, the rate of decomposing oxalic acid decreased slightly and more oxalic acid, finally, was remained.

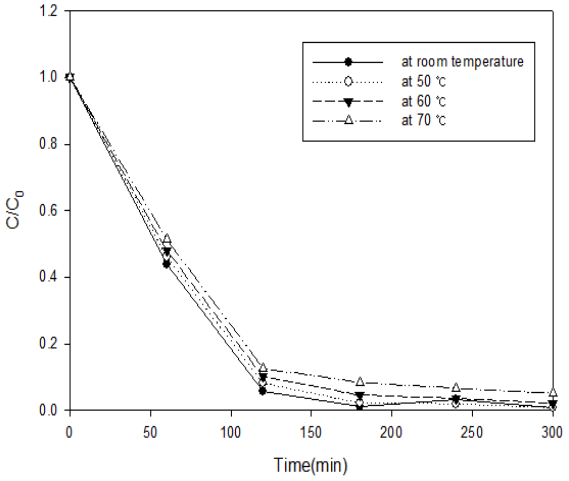


Fig. 2. Decomposition extent of oxalic acid according to temperature.

3.2 Estimation result of effect of UV reflector

The decrease of oxalic acid concentration by UV/H_2O_2 process was represented in Fig. 3 according to existence of UV reflector. It was confirmed that the rate of decomposing oxalic acid was increased slightly when UV reflector was used in UV/H_2O_2 process.

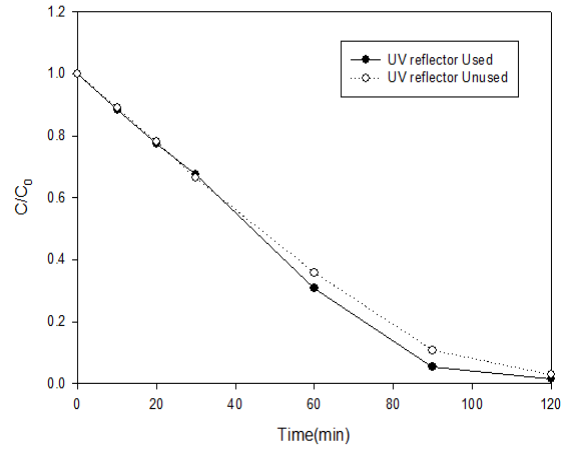


Fig. 3. Decomposition extent of oxalic acid according to existence of UV reflector.

4. Conclusion

The influence of temperature and UV reflector on the AOP kinetics of the oxalates from the chemical decontamination wastes containing the metallic ions was studied experimentally. We obtained the following conclusion in the experimental ranges:

1. The influence of temperature is considered to be limited, even though increasing temperature results in slight decrease in decomposition rate.
2. The role of the UV reflector is considered as unimportant factor, even though it slightly increases the decomposition rate.

Acknowledgement

This work was supported by the Korea Institute of Energy Technology Evaluation and Planning (KETEP) and the Ministry of Trade, Industry & Energy (MOTIE) of the Republic of Korea (No. 20141510300310).

REFERENCES

[1] Eung-Ho Kim et al., “Decomposition of oxalic acid by UV irradiation in nitric acid”, Journal of the Korean Industrial and Engineering Chemistry, 8(1), 108-113 (1997).

[2] Dong-Yun Ha et al., “Study of decomposition characteristic of oxalic acid and citric acid by UV/H_2O_2”, Journal of Korean Society of Environmental Engineers, 22(7), 1307-1318 (2000).

[3] Jin-Hee Kim et al., “Estimation of decomposition of decontamination waste liquid by Advanced Oxidation Processe(AOP)”, Korean Radioactive Waste Society AUTUMN, 14(2), 437-438 (2016).

Innovative Biological Method to Remove Cesium-137

Seung Yeop Lee*, Jae Kwang Lee, Min Hoon Baik, and Bum Kyoung Seo
Korea Atomic Energy Research Institute, 111, Daedeok-daero 989beon-gil, Yuseong-gu, Daejeon, Republic of Korea
*seungylee@kaeri.re.kr

1. Introduction

Nuclear accidents such as Chernobyl and Fukushima reactors' breakdown can cause an enormous emission of various radioactive nuclides into the environments. The main nuclides that were released from the reactor were radioactive I and Cs. The Cesium-137, one of them, could give an impact on ecosystem and human beings in the long-term period due to its long half-lives of 30 y.

Thus, we need to have an effective method to remove radioactive Cs-137. Recently, various exchanger and getter materials have been developed to uptake radioactive cesium from wastewaters. The adsorbent materials that have been developed usually showed a nice performance under fresh water conditions. However, the adsorption amounts were not large in seawater conditions. Furthermore, the cost to synthesize the adsorbents was high and their final waste volumes were not small.

Our new method that is proposed here offer great cost cutting by using bacteria, which are isolated from underground. This method is to crystallize soluble cesium into a solid matter through biochemical reactions. The biological selectivity of cesium in cation-rich seawater is relatively high and thus radioactive waste volume is very small. We think that it is an innovative and environment-friendly method that removes Cs-137 by both effective and low-cost way.

2. Methods & results

2.1 Methods

The SRB (sulfate reducing bacteria) isolated from natural bentonite or groundwater [1] were used in our experiment. To study the selective cesium removal and biomineralization from some cation-rich fresh or seawaters, we anaerobically prepared various solutions in serum bottles. From the cesium stock solution, 0.01-10 ppm of cesium were aseptically injected into the serum bottles containing other components, such as SO_4^{2-}, which was used as a basic chemical to biologically form "pautovite ($CsFe_2S_3$)", a cesium-mineral.

To perform a practical test using cesium radioisotope, a stock solution of radioactive cesium-137 (half-life of 30 years) was prepared and injected into serum bottles to be initially 133 Bq/ml radioactivity. Finally, cells were injected into the serum bottles providing ca. 0.75 mg/l cell protein, to determine the microbial effect on the removal of cesium. The prepared serum bottles were put into a shaker with 120 rpm at 30℃ in the dark for 5 days.

2.2 Removal of Aqueous Cesium

Among the additives, some organic matters were used as electron donors to reduce sulfate to sulfide by the activity of bacteria. When sulfide (S^{2-}) is produced by the reduction of sulfate (SO_4^{2-}) [2], it combined with metals to form 'sulfide minerals'.

In our experiment in a freshwater, about 95% of cesium was removed from the solution in a condition of Cs 0.1 ppm (Fig. 1). In 0.01 ppm concentration, most of cesium (nearly 100%) was removed from the solution after 1 day of the reaction. This result shows that our method is very effective to remove cesium compared with other previous technologies. This way has an additional advantage to produce a very small waste volume that is less than 0.1 g/l.

The traditional method to remove cesium was based on the adsorption of cesium onto the adsorbents. Thus, the selectivity of cesium is limited in the cation-rich wastewater such as seawater due to the competitive effect of various cations. However, our method is to make soluble cesium precipitated as a solid matter, "pautovite". In the process, the cesium removal is very selective and its byproduct is a solid sulfide mineral, which is stable at natural field (e.g., undergournd).

In seawater condition, our method was compared to the traditional way of using an adsorbent (IONSIV R9160-G), which is currently used as the practical adsorbent for removing radioactive cesium in Fukushima, Japan. The test was performed by injecting Cs-137 into seawater for 5 days under the same condition. As a result, it showed that the way that used bacteria was very powerful to effectively remove radioactive Cs-137.

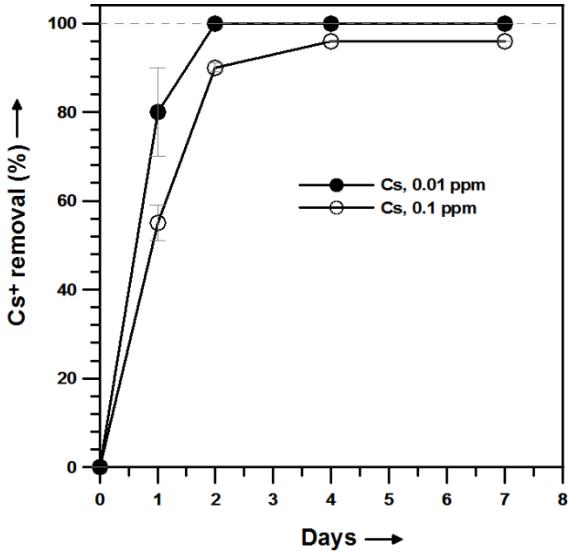


Fig. 1. Characteristic cesium removal patterns for Cs-containing freshwaters by microbial cesium biomineralization.

3. Conclusion

After the Fukushima reactor accident, many studies for the removal of Cs were carried out to make and develop very effective adsorbents. However, they have ignored the practical environment that highly costs to purify the wastewater and dispose a large volume of wastes, only focusing on the rapid removal of cesium. With our innovative biotechnology, we overcame such problems by using natural bacteria, by which soluble cesium can be easily transformed into a stable and solid matter with a compact volume even in seawater conditions.

REFERENCES

[1] J.M. Oh, S.Y. Lee, M.H. Baik, and Y. Roh, “Characterization of uranium removal and mineralization by bacteria in deep underground, Korea Atomic Energy Research Institute (KAERI)”, Journal of Mineralogical Society of Korea, 23(2), 107-115 (2010).

[2] S.Y. Lee, M.H. Baik, H.R. Cho, E.C. Jung, J.T. Jeong, J.W. Choi, Y.B. Lee, Y.J. Lee, “Abiotic reduction of uranium by mackinawite (FeS) biogenerated under sulfate-reducing codition”, Journal of Radioanalytical and Nuclear Chemisty, 296, 1311-1319 (2013).

Temperature Sensitive Strippable Coating for the Removal of Radioactive Cesium From Contaminated Surface

Hee-Man Yang*, Kyu Sun Hwang, Chan Woo Park, Kune-Woo Lee, Ilgook Kim, and In-Ho Yoon

Korea Atomic Energy Research Institute, 111, Daedeok-daero 989beon-gil, Yuseong-gu, Daejeon, Republic of Korea

*hmyang@kaeri.re.kr

1. Introduction

The nuclear accident at the Fukushima Daiichi nuclear power station in 2011 released a huge quantity of radioactive contaminants into atmosphere. They were deposited by wind and rain on the various surfaces of objects such as soil, road, and building in terrestrial and city areas [1]. Various surface decontamination methods using tools such as scabbling and milling have been tested for the removal of ^{137}Cs from contaminated surfaces. A strippable coating that can be easily peeled off from the surface upon drying is a widely used method to avoid the destruction of the original surface [2]. Although strippable coating showed good effectiveness, it becomes radioactive waste itself after use, requiring costly waste disposal. Therefore, new surface decontaminants that produce a low amount of radioactive waste after use are still desired.

In the present study, we developed a new strippable coating consisting of magnetic adsorbents having Cs adsorption ability [3] and an polyvinyl alcohol-borate based hydrogel for the removal of ^{137}Cs from contaminated surfaces and the volume reduction of radioactive waste after use.

2. Experiment

2.1 Fabrication of adsorbent/PVA-borate-based surface decontaminant

Magnetic adsorbents were synthesized by following the procedure previously reported by our group (Yang et al. 2016b). Briefly, 2.7 g of FeCl3•6H2O and 7.2 g of sodium acetate were dissolved in 100 mL of ethylene glycol. Then, the mixture solution was transferred to a Teflon-lined stainless-steel autoclave. The autoclave was sealed and heated to 200 °C for 8 h. After washing with excess ethanol and deionized water several times, the aqueous solution of magnetic nanoparticles (0.5 mg/mL) at pH 2 was reacted with a 2.5 mM $K_4[Fe(CN)_6]$ solution. After stirring for 1 h, the black particles were washed with deionized water several times. Finally, the product was dried in vacuum at 60 °C overnight.

For the fabrication of the surface decontaminant, the desired amount of sodium borate decahydrate was first dissolved in water or 0.1 M NH_4Cl solution. Then, the PVA(avg Mw 13000 – 24000) was dissolved by stirring and heating at 80 °C in sealed vials to prevent water from evaporating. The wt% of PVA ranged from 4 to 6 wt%, and the wt% of borax was fixed at half that of PVA. Finally, the magnetic adsorbents were added to the PVA-borate hydrogel solution.

2.2 Surface decontamination procedure .

Cement was deposited on the surface of a planchet (diameter = 4 cm) and then coated with paint (Ilshin Co. Ltd., South Korea) to serve as a model surface. The painted cement was contaminated with ^{137}Cs by dropping and evaporating a known amount of ^{137}Cs solution on the surface. While the temperature of decontamination solution was maintained at 50°C, the contaminated surface was treated with decontamination solution. Within a few minutes, an adsorbent/PVA-borate hydrogel film was generated and then peeled off the surface 3 h later. The radioactivity of the painted cement before and after treatment was measured using an automatic low-background Alpha/Beta counting system. Then, the adsorbent/PVA-borate hydrogel film was added to 20 g of water, and the adsorbent was magnetically collected using an external magnet.

3. Result and Discussions

It has been recently discovered that PVA-borate

hydrogel have temperature sensitive phase transition behavior [4], which allows them to be peeled from a surface after surface decontamination. For the surface decontamination, the aqueous polymeric solution containing adsorbent, PVA and borate at 50°C was applied to the contaminated surface by brushing to solubilize the ^{137}Cs. Then, the strippable PVA-borate hydrogel/adsorbent composite film was formed through reversible the cross-linking of the PVA with borate at room temperature for easy removal. After surface decontamination, the adsorbent capturing the ^{137}Cs was magnetically separated for the volume reduction of radioactive waste.

Fig. 1(a)) show that magnetic nanocluster was successfully coated with gray cubic shapes of PB (XRD data in fig. 1(b)). It exhibited superparamagnetic behavior, and the saturation magnetization of the magnetic nanoadsorbent at 1.5 T was 27.8 emu/g, which is sufficiently high to collect the adsorbent in water by using an external magnet. (fig 1(c)).

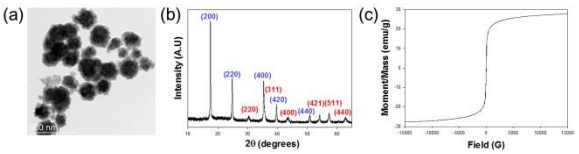


Fig. 1. (a) TEM image and (b) XRD pattern of the magnetic adsorbent (red: Fe_3O_4, blue: Prussian blue), and (c) Magnetization curve of magnetic adsorbent, as measured using a vibrating sample magnetometer.

To evaluate the decontamination ability of the adsorbent/PVA-borate complex, 137Cs-contaminated painted cement was used as a model surface. After generation of adsorbent/PVA-borate hydrogel film at room temperature, the films were easily removed from the surface (Fig. 2(a)). Fig. 2(b) and (c) show that the adsorbent/PVA-borate hydrogel film was completely removed from the surface in one piece and did not leave any residue.

The strippable coating displayed a good removal efficiency of 83.46% and a DF of 6.05 from the ^{137}Cs-contaminated surface due to the presence of the adsorbent, which had a large distribution coefficient for Cs (3.34×10^4 mL/g). Moreover, the PVA-borate complex can be reused following a simple addition of water via the magnetic separation of the adsorbent, which can capture 99.071% of the ^{137}Cs in the used hydrogel film.

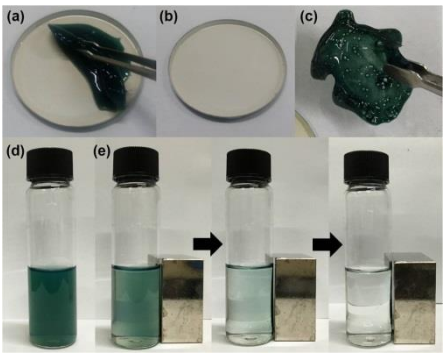


Fig. 2. Digital images showing (a) the stripping coating on a ^{137}Cs-contaminated surface, (b) lack of film residue of the adsorbent/hydrogel film on the surface after treatment, (c) the stripped adsorbent/hydrogel film, (d) aqueous solution of stripped coating (e) magnetic separation of adsorbent from solution using an magnet.

4. Conclusion

In this study, temperature sensitive hydrogel based strippable coating was successfully fabricated for the surface decontamination. The films displayed a good removal efficiency of 83.46% from the ^{137}Cs-contaminated surface. Thus, our strippable coating has good potential as a new surface decontaminant.

Acknowledgement

This research was supported by the Korea Ministry of Education, Science, technology Grant (No.2017M2A8A5015148)

REFERENCES

[1] H. M. Yang, K.-W. Lee, B.-K. Seo, and J.-K. Moonm, J. Nanosci. Nanotechnol. 15, 1695 (2015).

[2] H. N. Gray, B. Jorgensen, D. L. McClaugherty, and A. Kippenberger, Ind. Eng. Chem. Res. 40,3540 (2001).

[3] H.-M. Yang, S.-C. Jang, S. B. Hong, K.-W. Lee, C. Roh, Y. S. Huh, B.-K. Seo, J. Alloy. Compd. 657, 387 (2016).

[4] E. Carretti, S. Grassi, M. Cossalter, I. Natali, G. Caminati, R. G. Weiss, P. Baglioni, and L. Dei, Langmuir, 25(15), 8656, (2009).

Experimental Results of Oxidation / Reduction Process Based on Permanganic-Oxalic Acid

Chorong Kim* and Hak-Soo Kim

KHNP Central Research Institute, 70, 1312-gil, Yuseong-daero, Yuseong-gu, Daejeon, Republic of Korea

*chorong.kim@khnp.co.kr

1. Introduction

The primary goal of the Chemical Decontamination is to achieve a dose rate reduction for the decommissioning worker. The oxide film layer formed on the surface of the structural material of the Light-Water-Reactor is composed of metal oxides of iron, nickel and chromium[1]. The chromium oxide is dissolved by the oxidation reaction, and iron and nickel in metal oxides are dissolved by the reduction reaction.

In this study, the oxidation/reduction process experiments were conducted using System Decontamination Process Development Equipment of Lab scale. The removal rate of the oxides film in the specimen was evaluated and the decontamination process time was confirmed.

2. Methods

In this experiment, oxidation / reduction process experiments were conducted using a System Decontamination Process Development Equipment of Lab scale (Fig. 1). The experiment was carried out under the following conditions.

- Specimen Type: SUS304, SUS316, SUS410, Alloy600, SA508
- Oxidation / reduction process conditions

	Agent	Concentration	Time	Temperature
Oxidation	$HMnO_4$	300 ppm	48hr	95℃
Reduction	$C_2H_2O_4$	2000 ppm	24hr	

The oxide film thickness of each pre-decontamination specimen was analyzed using Glow Discharge Spectrometer (GDS) and the surface of the specimens was carried out using Videoscope.

The weight of the specimens before and after decontamination was measured to evaluate the oxide removal rate. The concentration of Fe, Cr and Ni ions was analyzed using inductively coupled plasma-optical emission spectrometry (ICP-OES).



Fig. 1. System Decontamination Process Development Equipment.

3. Results and Discussion

3.1 Characterization of the oxide film

As a result of the Glow Discharge Spectrometer (GDS) analysis of the pre-decontamination specimen, the thickness of the oxide film was found to be 15 μm for SUS304, 1.6 μm for SUS316, 7.11 μm for SUS410, 2.52 μm for SA508, 6.2 μm for Alloy 600.

For analyzing the surface of the specimen before and after decontamination, the specimen surface was observed using Videoscope. The pre-decontamination specimens were confirmed that black oxide layer was formed. Videoscope analysis of the specimens after decontamination showed that all of the oxide films were removed in SUS304 and SUS316. In particular, a large amount of pitting was occurred in the surface of SUS304. In the case of SUS410 and SA508, iron oxide was formed on the surface and serious localized corrosion was observed. In the case of Alloy 600, all of the oxide film was not removed and chromium oxide of green color was observed[2,3].

3.2 Experimental results of oxidation / reduction process

The removal rate of the oxide film was evaluated through an oxidation / reduction process experiment based on permanganic-oxalic acid. The weight of the specimens was shown in Table 1. As a result, in the case of SUS 304 and Alloy 600, the oxide film was removed by 75%.

Table 1. The weight of the specimens before and after decontamination

Type	Decontamination Process		Removed Weight(g)
	Before(g)	After(g)	
SUS304	10.12081	10.05679	0.06402
SUS316	10.18898	10.12936	0.05962
SUS410	9.86923	9.76737	0.10186
Alloy600	10.74154	10.71774	0.02380
SA508	9.97664	9.72351	0.25313

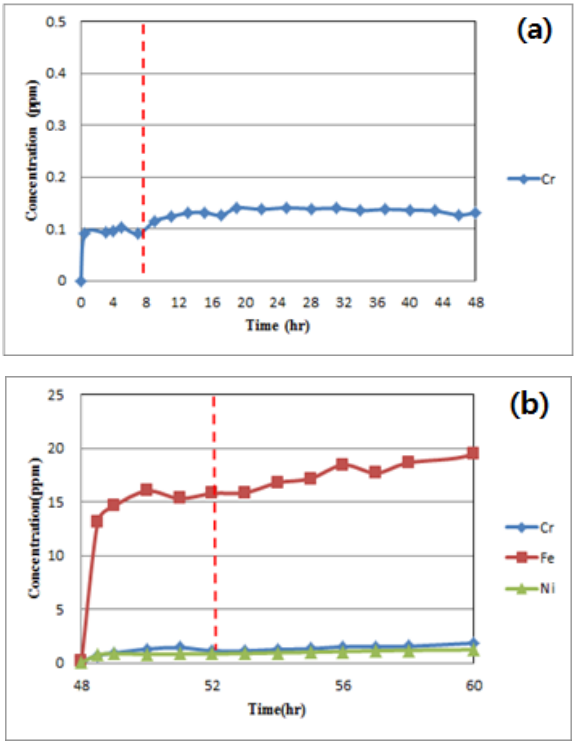


Fig. 2. The concentration of dissolved metal ions in the decontamination agent ((a) oxidation process, (b) reduction process).

The concentration of metal ions dissolved in decontamination agent was shown in Fig. 2. During oxidation, Cr ions were dissolved in 0.1132 ppm and Fe and Ni ions were not dissolved. It is considered that the Cr^{3+} in the oxide film is oxidized to Cr^{6+} by the permanganic acid. After the reduction process, Cr ions were dissolved at 2.057 ppm, Fe ions were dissolved at 22 ppm, and Ni ions were dissolved at 1.5 ppm. Through the analysis of the dissolved metal ions concentration with time, it can be confirmed that the oxidation and reduction processes are completed within 5 hours.

4. Conclusions

In this study, the removal rate of oxide film in the simulated specimen was evaluated and decontamination process time was determined through oxidation ($HMnO_4$) / reduction ($C_2H_2O_4$) process experiment.

SUS304 and Alloy 600 showed that the oxide film was removed by 75%. The decontamination process time was 5 hours for the oxidation process and 4 hours for the reduction process.

Based on these experimental results, an oxidation / reduction continuous process (more than 2 cycles) will be carried and determine the number of consecutive cycles of systematic decontamination.

Acknowledgments

This work was supported by the Korea Institute of Energy Technology Evaluation and Planning (KETEP), granted financial resources from the Ministry of Trade, Industry & Energy, Republic of Korea (Number 20141510300310)

REFERENCES

[1] Rolf Riess et al., Decontamination and steam generator chemical cleaning, Advanced Nuclear Technology International Krongjuntarvagen 2C, ANT international (2009).

[2] J.H. Carter et al., Corrosion and passivation studies on PWR primary materials to reduce corrosion product activity, Nucl. Energy, 24(1), 45-52 (1985).

[3] Wenjun Kuang et al., The mechanism of oxide film formation on Alloy 690 in oxygenated high temperature water, Corrosion Science, 53, 3853-3860(2011).

Estimation of Mixed Nuclide Inventory Using MicroShield Computer Program

Jonghoa Kim*, Homin Jeon, Yongsik Kim, Kyeongho Han, and Jangsoo Seo
Sae-An Engineering Co.. Ltd, 65 Techno 3-ro,Yuseong-gu, Daejeon, Republic of Korea
*jhkim4198@sae-an.co.kr

1. Introduction

The methods for evaluating the gamma nuclide inventory present on the inner surface of component subject to decommissioning Nuclear Power Plant are LABSOCS (Laboratory SOurceless Calibration Software) that indirectly measures a sample that can demonstrate the representativeness of component subject to decommissioning, ISOCS (In Situ Object Counting System) that measures directly from the surface of a component subject to decommissioning, and MicroShield® computer program that estimates the nuclide inventory on the inner surface of component using the dose rate of component subject to decommissioning and the radioactivity of the sample. In this study, we estimated the nuclide inventory on the inner surface of the pipe using the dose rate of the pipe subject to decommissioning and the radioactivity concentration of the sample by MicroShield® ver. 10.03 computer program.

2. Materials and Methods

2.1 Point Kernel 16 fixed geometry

The MicroShield® computer program uses 16 fixed geometry models for radiation shielding evaluation of point sources, line sources, and volume sources using the Point Kernel method. The basic concept of the Point Kernel method is to divide the volume source into a large number of small point sources and regard each as a point source, and add up the respective contributions. The fixed geometry model approach reduces the effort required to express the geometry numerically for shielding evaluation, and can be applied to most problems, except when an accurate evaluation of complex geometry is required [1,2,3].

2.2 Gamma-ray fluence-to-dose factors

MicroShield® is now includes the reference gamma dose conversion factors from ANSI/ANI-6.6.1-1977: Neutron and Gamma-Ray Fluence-To-Dose Factors to support calculations for NUREG-1617, "Standard Review Plan for Transportation Packages for Spent Nuclear Fuel".

MicroShield® calculates photon fluence rate at the dose point. This must be converted to more meaningful values for practical use. The fluence rate is converted to exposure in air, absorption in air, and effective dose equivalent to humans[3].

The general form of the analytic function is

$$\ln Dfg(E_p) = A + Bx + Cx^2 + Dx^3 \qquad (1)$$

where, $Dfg(E_p)$ = gamma flux to dose rate conversion factor (rem h^{-1})/(photon $cm^{-2}s^{-1}$)

E_p = gamma energy (MeV)

$x = \ln E$

The coefficient of the polynomial expression are given in ANSI/ANS6.6.1 Table A7.1-3[4].

2.3 Assumptions

Table 1 shows the radioactivity concentration of the system water samples to estimate the nuclide inventory on the inner surface of the pipe. It is assumed that the system water is 100% drained, the dose rate of the pipe is 120 mR/h, the inside is filled with air, and the parameters of the pipe are shown in Table 2.

Table 1. The radioactivity concentration in sample

Nuclide	Half life	Radioactivity concentration ($\mu Ci/cm^3$)
Ag-110m	249.8 days	8.32E-03
Co-58	70.88 days	6.84E-04
Co-60	5.271 years	4.05E-04
Mn-54	312.1 days	1.33E-03
Nb-95	34.97 days	1.25E-03
Sb-124	60.20 days	2.24E-04

Table 2. Geometry model parameter

Source dimension		Dose points	
Height	200.0 cm	X	49.16 cm
Inner Diameter	78.0 cm	Y	100.0 cm
Radius	39.0 cm	Z	0.0 cm
Shield			
Shield No.	Dimension	Material	Density (g/cm^3)
Cyl. radius	39.0 cm	Air	0.00122
Shield 1	7.62 cm	Iron	7.86
Transition		Air	0.00122
Air gap		Air	0.00122

3. Results and Discussions

The dose rate-radioactivity conversion factor calculated by using MicroShield® ver. 10.03 computer program was estimated as follows:

- Conversion factor without build-up factor: 6.52E+01 mCi/mR h^{-1}
- Conversion factor with build-up factor: 7.69E+00 mCi/ mR h^{-1}

The nuclide inventory on the inner surface of the pipe considering Build-up factor was estimated as follows:

- Ag-110m: 6.29E-01 Ci or 1.28E+01 μCi/cm^2
- Co-58: 5.17E-01 Ci or 1.05E+00 μCi/cm^2
- Co-60: 3.06E-02 Ci or 6.25E-01 μCi/cm^2
- Mn-54: 1.00E-01 Ci or 2.05E+00 μCi/cm^2
- Nb-95: 9.44E-02 Ci or 1.93E+00 μCi /cm^2
- Sb-124: 1.70E-02 Ci or 3.46E-01 μCi/cm^2

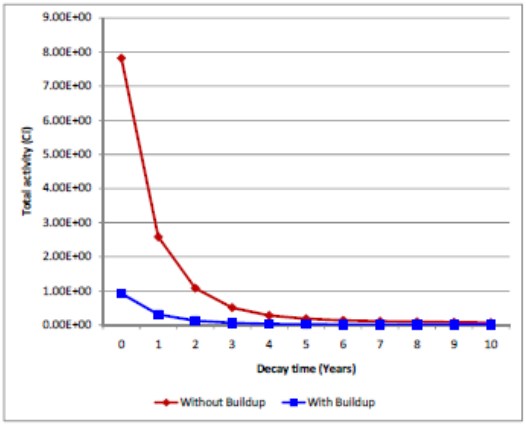


Fig. 1. Total activity vs. Decay time.

4. Conclusion

In this study, we estimated the nuclide inventory in the pipe according to the dose rate of pipe and the radioactivity concentration of the sample by using MicroShield® ver. 10.03 computer program. On the other hand, since the components subject to decommissioning have complicated shape and various materials, optimal modeling for this is important. In addition, for accurate error range and applicability, it is necessary to verify the validity of ISOCS and LABSOCS by performing radioactivity measurement and mutual comparison and analysis.

Acknowledgments

This study was conducted as part of the "Development of Decontamination Technology of Reactor Coolant System and Dismantled Equipment foe NPP Decommissioning" project supported by the MOTIE (Ministry of Trade, Industry and Energy) and the KETEP (Korea Institute of Energy Technology Evaluation and Planning (Project Number: 20141510300310).

REFERENCES

[1] Sang-Ho Kang, etc, "Development of Point Kernel Radiation Shielding Analysis Computer Program Implementing Recent Nuclear Date and Graphic User Interfaces", The Korean Association for Radiation Protection, Vol.26 No.3, pp 215-224, 2001.

[2] Grove Software, "MicroShield® ver. 10.03", 2015.

[3] Grove Software, "MicroShield® User's Manual", 2015.

[4] American National Standards Institute Inc., “American National Standard Neutron and Gamma-Ray Flux-To-Dose-Rate Factors", ANSI/ANS-6/1/1-1977 (N666). 1977.

Derivation of Surface Soil $DCGL_w$ for Kori-1 NPP Reuse Scenario

Ji Hyang Byon*, Sang June Park, and Seokyoung Ahn

Pusan National University, 2, Busandaehak-ro 63beon-gil, Geumjeong-gu, Busan, Republic of Korea

*quswlgid922@gmail.com

1. Introduction

Kori Nuclear Power Plant Unit 1, the first NPP in S. Korea, will be permanently suspended in June, 2017. The decommissioning procedure and related preparations are ongoing. By selecting less conservative but a realistic Industrial worker scenario for surface and subsurface exposure, the scope of the strategies according to the scenario type is condensed intensively. A derived, radionuclide-specific activity concentration within a survey unit corresponding to the release criterion, DCGL is based on the spatial distribution of the contaminant and hence is derived differently for the nonparametric statistical test ($DCGL_w$) and the Elevated measurement comparison ($DCGL_{EMC}$) [1]. For $DCGL_w$, which is a DCGL with a mean concentration over a wide area used with statistical tests, suite of radionuclide and peak of the mean dose have to be found using DandD ver.2.4.0 and RESRAD-ONSITE ver.7.2.

2. DCGLw Calculation

2.1 Classification of Radionuclides

Potential radionuclides suite selection is based on methodology which was used on the US NPPs decommissioning. For unified assumptions of radionuclides, Table 5.13 and 5.15 of NUREG-3474, Attatchment 8.2 of DTBD-04-001 were used. Discounted radionuclides were classified as nuclides which concentration contribute less than 0.1 percent of the total activity, with half-life less than 2 years [2,3]. Final selection and classification of radionuclides is shown in Table 1.

2.2 Potential dose from discounted radionuclides

Total discounted dose from discounted radionuclides is calculated by DandD Code ver.2.4.0. Radionuclides and inert gases not supported by DandD were excluded. Because of insufficiency of site-specific radionuclide concentrations of KORI Unit 1, initial concentrations assumption was based on total activity fraction. By running the DandD code with Industrial worker scenario, potential dose from discounted radionuclides was derived as 1.82E-04 mSv/yr.

Table 1. Classification of potential radionuclides

Concerned		Discounted		
H-3	Co-60	Cl-36	Eu-154	Tc-99
C-14	Ni-63	Ar-39	Eu-155	Sn121m
Co-60	Eu-152	Ca-41	Tb-158	I-129
Ni-63	Pu-239	Mn-53	Ho-166m	Ba-133
Fe-55	Ni-59	Se-79	Hf-178m	Cs-134
		Kr-81	Pb-205	Cs-135
		Kr-85	U-233	Cs-137
		Sr-90	Sm-151	Pm-145
		Zr-93	Mo-93	Sm-146

2.3 Peak of the mean dose consideration

Probabilistic dose modeling should use the “peak of the mean” dose distribution for demonstrating compliance with 10 CFR Part 20, Subpart E. The “peak of the mean” analysis is based on the time at which the average dose is maximum. [1] To calculate “peak of the mean” dose using RESRAD-ONSITE ver 7.2, the site condition for KORI Unit 1 with variable site-specific parameter values are needed. [4] 1 pCi/g of each concerned radionuclide and parameter distributions are entered for probabilistic run. More accurate values of “peak of the mean” dose can be obtained by entering assigned values through sensitivity test. The result is shown in Table 2.

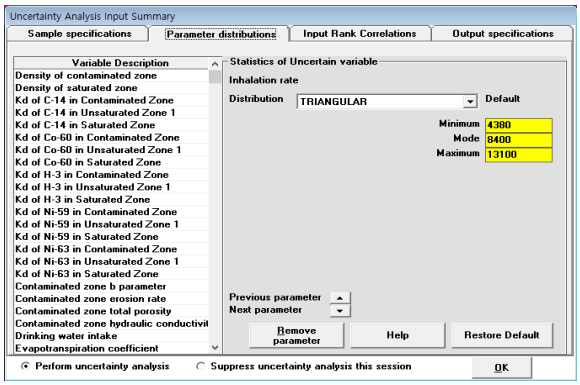


Fig. 1. RESRAD-ONSITE for probabilistic run.

2.4 DCGLw

Now, DCGLw of the site-specific radionuclides can be derived by [3]:

$$DCGL_w = \frac{Regulatory\ dose\ limit - Potential\ dose}{Peak\ of\ the\ mean\ dose} \quad (1)$$

The current proposed site release criteria for either restricted or unrestricted reuse is 0.1 mSv/yr [4]. By substituting dose limit, potential dose from discounted radionuclides and "peak of the mean" dose, the result is shown in Table 3.

3. Results & discussion

Table 2. Peak of the mean dose for selected radionuclides

Radionuclide	Peak of the mean dose (mSv/y per pCi/g)
H-3	1.836E-04
C-14	1.176E-03
Fe-55	1.367E-07
Ni-59	3.383E-06
Ni-63	8.079E-06
Co-60	2.032E-02
Nb-94	2.330E-02
Ag-108m	3.594E-02
Eu-152	9.198E-03
Pu-239	7.199E-05

Table 3. Surface soil DCGLw

Radionuclide	DCGLw (pCi/g)
H-3	5.43E+02
C-14	8.48E+01
Fe-55	7.30E+05
Ni-59	2.95E+04
Ni-63	1.23E+04
Co-60	4.91E+00
Nb-94	4.28E+00
Ag-108m	2.77E+00
Eu-152	1.08E+01
Pu-239	1.38E+03

In order to apply DCGLw to the underground soil, it is necessary to determine the mixture concentration using 'unity rule' by measuring accurate site-specific concentration, then considered through assessment of contamination layer thickness changes and depth contamination [3].

4. Conclusion

The derived DCGLw can be a criterion of survey unit, and also essential for deriving area factor classifying classes of impacted areas. For exact value of DCGLw, the concentration of each radionuclide in KORI Unit 1 and more site-specific parameter values are needed. Then, the applicability of surface soil DCGLw to sub-surface soil can be considered.

ACKNOWLEDGEMENT

This research was supported by a Korea Foundation of Nuclear Safety (KoFONS) grant funded by the Nuclear Safety and Security Commission (NSSC) (No. 1305009-0416-CG100).

REFERENCES

[1] NUREG/CR-1757,Vol.2, Rev.1,Consolidated Decommissioning Guidance Characterization, Survey, and Determination of Radiological Criteria, NRC, September 2006.

[2] NUREG/CR-3474, Long-Lived Activation Products in Reactor Materials, NRC, August 1984.

[3] DTBD-04-001 Rev.2, Radionuclides for Characterization During Rancho Seco Nuclear Generation Station Characterization or Final Status Surveys, U.S Nuclear Regulatory Commission, April 2005.

[4] KINS/HR-1169, Development of Safety Verification Technology for Reuse of Decommissioning Waste and Site in Nuclear Power Plant, KINS, February 2012.

Requirement of Conceptual Design for Decommissioning Information Integration Management System

Yunjeong Hong*, Seungkook Park, and Heeseong Park

Korea Atomic Energy Research Institute, 111, Daedeok-daero 989beon-gil, Yuseong-gu, Daejeon, Republic of Korea

*hong814@kaeri.re.kr

1. Introduction

Korea Atomic Energy Research Institute is the sole expert group that has nuclear decommissioning experiences. KAERI is developing a computer code to converge all data collected from KRR-1 & 2 and UCP (Uranium Conversion Plant) decommissioning. To date, many applications related to decommissioning of nuclear facilities are developed, but they do not provide integrated disassembly information management and regeneration environment as they are developed in forms of independent database and application. In addition, various development languages and database are used, which cause problems in system improvement and maintenance.

Therefore, in order to develop "Decommissioning Information Integration management System (DIIMS) of nuclear facilities", a conceptual design is performed with aim of increasing the efficiency of work.

2. Outline of System

Basic design results of system are documented to develop the IIMS for nuclear facilities.

2.1 Development Environment

Table 1. Development environment and specification

Classification		Contents
OS	Server	Windows Server 2012 R2
	Client	Higher than Microsoft Windows 7
Platform	DBMS	RDBMS
	Development Language	C#, WPF

2.2 System Requirement Management

2.2.1 Waste Management Procedures. The data obtained from decommissioning is mostly about waste management. This is an important clue to determine the data input system. All the solid waste generated from decommissioning is regarded as radioactive waste. And the data can be input according to the procedure.

2.2.2 Data Input. Data which is generated from decommissioning site should be input as much and as quickly. The most important thing is to minimize the input errors. In order to solve this problem, it made the input method a code.

2.2.3 Facilities Characterization. It is important to investigate and survey the facilities to decommissioned for establishment of decommissioning plan. The result of the characterization survey of the nuclear facilities is utilized to predict the amount of waste and estimate the cost of decommissioning project.

2.2.4 Decommissioning Work Unit Productivity Yield. The decommissioning work unit productivity yield derives the items which has the lowest level generated from the decommissioning activity and the productivity yield values which the items have. These values are used as data in the decommissioning plan establishment.

2.2.5 Code Management System. It can polysynthetically manage code used in the decommissioning information management system for nuclear facilities.

2.2.6 Decommissioning Process Management. This task consists of 11 steps.

2.2.7 Decommissioning Information Interface.

- Design, equipment/material supplier, decommissioning

work, evaluation process and post-decommissioning operation organization must be able to operate the system applicable to standard identification system.
- The data submitted from the facility design/operator should be able to be identified by all project participants such as the decommissioning company, supplier and worker

2.2.8 Requirement Management. Flexible requirement management system should be constructed through standard requirement management model.

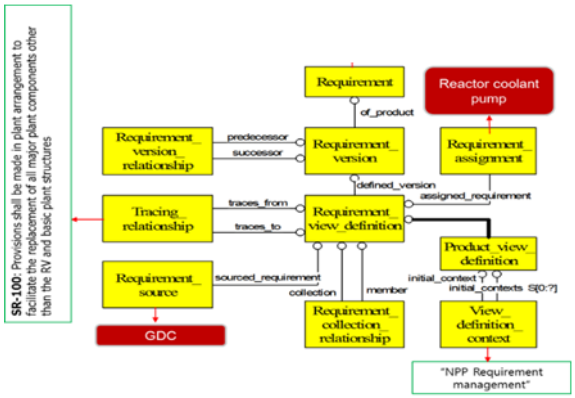


Fig. 1. Requirement management model.

2.2.9 Configuration Management System. Configuration Management system should be constructed for standard management about configuration decommissioning information in DIIMS.

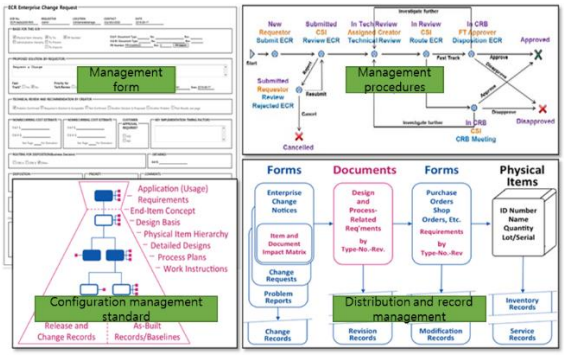


Fig. 2. Example of configuration management system.

2.2.10 System Structure.
- Server/Client and dispersion database environment should be supported.
- Big data should be managed.
- Integrated system functions should be provided by API(Application Programming Interface).
- Multiple databases (correspondence DB, technical document DB, SSAR reference DB, etc.) should be reduced in complexity by eliminating redundancy with existing processes.

2.2.11 User Interface.
- Interfaces regarding various users should realize.
- Report should be able to produce by extracting data required for the work.
- Decommissioning information should be able to search through simple/advanced search.

3. Conclusion

Many application programs related to decommissioning for nuclear facilities are developed so far. However, it is difficult to offer integrated decommissioning information management and inquiry environment as current programs have independent database and is form of application program system. In addition, there are problems in management and improvement of system due to the various development language and database.

This study develops a conceptual design of DIIMS for nuclear facilities. DIIMS provides a standardized information management environment and engineering software to support the decommissioning engineering work.

In the future, DIIMS would be developed based on the results of this study and it will provide the foundation for standard database management, decommissioning information management environment, and construct continuously expandable decommissioning engineering solution.

Characterization of Clay Minerals in Soil Near Nuclear Facilities in Korea

Chan Woo Park[1*], Bo Hyun Kim[1,2], Hee-Man Yang[1], Kune-Woo Lee[1], and In-Ho Yoon[1]
[1]Korea Atomic Energy Research Institute, 111, Daedeok-daero 989beon-gil, Yuseong-gu, Daejeon, Republic of Korea
[2]Chungnam National University, Youseong-gu, Daejeon, Republic of Korea
[*]chanwoo@kaeri.re.kr

1. Introduction

Unintended leakages of radioactive substances from nuclear facilities induce contamination of the environment. Among various radionuclides, cesium can be strongly bound to clay minerals in soil, and thus cesium is generally fixed in the top soil layer.

Clay minerals are classified into kaolinite, smectite, vermiculite, illite, mica and many others, and each clay mineral provides different Cs adsorption sites with different Cs selectivity. Highly expandable smectite and slightly expandable vermiculite generally adsorb much greater amount of Cs than do non-expandable clay minerals. Adsorption of Cs on expandable clay mineral mainly takes place through outer-sphere complexation of hydrated Cs^+ ions with negatively charged clay interlayers. Though non-expandable clay minerals such as illites and micas can adsorb smaller amount of Cs than expandable clay minerals, the clay minerals provide highly Cs selective adsorption sites, which is kwon as Frayed Edge Site (FES) that adsorb cesium through the formation of stable inner-sphere complexes. Because compositions of soil and clay minerals widely vary by region, characterization of clay minerals in domestic nuclear facility sites and their Cs adsorption behaviors are regarded as important subject to investigate.

2. Experimental

Soils were sampled from near nuclear facilities in Seoul, Wolseong, and Gori, and clay and silt components were separated from sand and gravel by wet-classification. Clay minerals in clay/silt samples were characterized by the classical clay identification method based on ethylene glycol and heat treatment. Cationic exchange capacity (CEC) of clay/silt sample was measured by quantifying desorbed Na^+ after NH_4^+ treatment to the Na^+ saturated clay/silt samples.

3. Result & discussion

Analysis of clay minerals in the soil samples from Seoul, Wolseong, and Gori revealed that a large amount of kaolinite and trace amounts of illite were found in all soil samples. In particular, Wolseong and Seoul soil contained vermiculite, and some hydrobiotite was also found. In the case of the Gori soil, chlorite component was identified (Fig. 1).

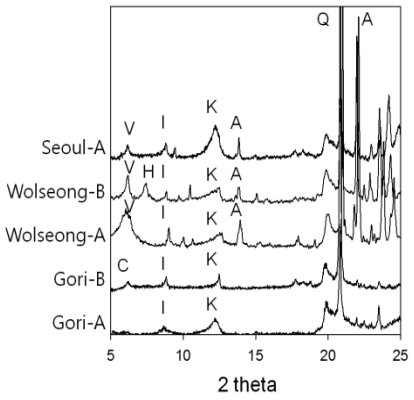


Fig. 1. XRD patterns of clays in Seoul, Wolseong, and Gori soils (C: chlorite, V: vermivulite, H: hydrobiotite, I: illite, K: kaolinite, A: albite, Q: quartz).

Analysis of CEC of clay/silt samples revealed that the Gori sample has a low CEC value because Gori sample is mainly composed of kaolinite and illite. However, Wolseong sample showed the highest CEC values due to vermiculite and hydrobiotite components.

4. CONCLUSIONS

We identified clay minerals in soils from domestic

nuclear facility sites. A large amount of kaolinite and trace amounts of Cs selective illite were found in all soil samples. In particular, Wolsong and Seoul soil contained vermiculite, which generally provides Cs selective FES as well as highly Cs adsorbable expandable interlayers.

REFERENCES

[1] Morino Y, Ohara T, Nishizawa M. Atmospheric behavior, deposition, and budget of radioactive materials from the Fukushima Daiichi nuclear power plant in March 2011. *Geophys Res Lett*. 2011;38(7).

[2] Fuller AJ, Shaw S, Ward MB, et al. Caesium incorporation and retention in illite interlayers. *Appl Clay Sci*. 2015;108:128-134.

Efficiency of Decontamination Foam With Silica Nanoparticles and Chemical Reagent for Radionuclide Contaminated Surface

In-Ho Yoon*, Chong-Hun Jung, Seung Eun Kim, So Hyeon Lee, Seon Byeong Kim, and Wang-Kyu Choi
Korea Atomic Energy Research Institute, 111, Daedeok-daero 989beon-gil, Yuseong-gu, Daejeon, Republic of Korea
*ihyoon@kaeri.re.kr

1. Introduction

A large amount of liquid waste is generated from the decontamination that occurs when dismantling nuclear facilities. A process is needed to decrease the amounts of chemical reagents and secondary waste produced during the decontamination process. Decontamination foam is a non-stable, two-phase fluid with aqueous and gas phases representing not more than 10% and 90% of the total volume, respectively. This formulation can significantly decrease the amounts of chemical reagents and secondary waste [1].

The advantage of decontamination foam is its potentially wide application for metallic walls, overhead surfaces, and the elements of complex components and facilities. In addition, foam is a good material for in situ decontamination because it generates low final waste volumes owing to its volume expansion. The application of foam allows for remote decontamination processing using only an injection nozzle and the equipment to generate the decontamination foam, which reduces operator exposure to high radioactivity [2,3].

The decontamination efficiency can be enhanced by improving the contact time between chemical reagents and a contaminated surface through the addition of surfactants and silica nanoparticles into the decontamination foam. In this study, various chemical reagent such as nitric acid and cerium(IV) were added in decontamination foam to decontaminate the corroded specimens contaminated with the radionuclide, Co-60 and Cs-137. We intend to discuss the effect of chemical reagent for the foam stability and decontamination efficiency to develop a new formulation of decontamination foam.

2. Materials and Methods

2.1 Stability test for the decontamination foam

Elotant™ Milcoside 100 (EM 100) is a decyl glucoside (non-ionic surfactant) supplied by LG Household & Health Care in Korea and Zonyl TBS is an anionic sulfonate fluorinated surfactant, purchased from DuPont Company and used without any further purification. Silica nanoparticles (M-5, Cabosil) were selected for testing as stabilizer.

In all tests on the foam stability and structure, the foam height and liquid volume in the foam were measured using a Dynamic Foam Analyzer (DFA-100, KRŰSS, Germany). During foaming, compressed air was passed through a sintered glass frit at the bottom of a cylindrical glass vessel (40 mm inner diameter) containing the solutions and the decontamination foam. The initial liquid volume was 60 ml; the gas flow was 0.2 l/min, and was stopped after 60 s of foaming.

2.2 Dissolution test using decontamination foam

Decontamination foams were prepared using 70 ml of 2 M HNO_3 or cerium(IV) in a 1.0% v/v EM100 surfactant solution containing 1 g silica NPs. Approximately 350 ml of each decontamination foam formulation was generated from a 70 ml solution by injecting nitrogen gas in a 350 ml glass column, with a gas to liquid ratio of 4:1. Various chemical reagent such as nitric acid and cerium(IV) were added with surfactant and silica nanoparticles to decontaminate the corroded specimens contaminated with the radionuclide, Co-60 and Cs-137. The corroded samples were placed in the middle of the glass column and left to react with the decontamination foam for 3 h at room temperature. The radioactive specimens were analyzed both before and after the decontamination tests using a multi-channel-analysis (MCA) device, and a high-purity Ge detector was used to evaluate the radioactivity of the radionuclides.

Table. 1. Composition of decontamination foam and chemical reagents.

	Foam formulation	Chemical reagent
1	1%(v/v) TBS + 1wt.% M-5	2M HNO_3 + 0.5M Ce(IV)
2	1%(v/v) EM100 + 1wt.% M-5	2M HNO_3 + 0.5M Ce(IV)

3. Results and Discussion

3.1 Stability test for the decontamination foam

Figure 1 shows the foam performance index (FPI) as the foam stability had a higher value with TBS surfactant than that with EM100 surfactant, indicating that a TBS surfactant is more suitable for cerium(IV) chemical reagents. Foam stability had a higher value with silica nanoparticles and surfactant (TBS or EM100) in the absence of cerium(IV) than that with silica nanoparticles and surfactant in the presence of cerium(IV), indicating that a cerium(IV) is to reduce the foam stability due to the oxidant reagent for the surfactant.

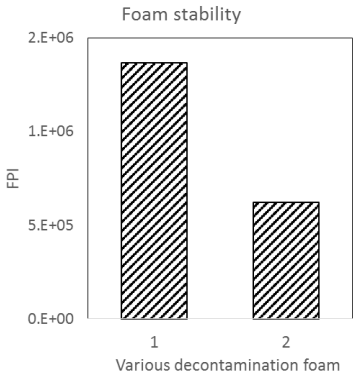


Fig. 1. Foam performances index (FPI) of decontamination foam with 1 wt.% silica nanoparticles and chemical reagent [2 M HNO_3 and 0.5 M Ce(IV)] in 1%(v/v) EM100 or TBS surfactant for 3 hrs.

3.2 Dissolution test using decontamination foam

The decontamination performances of the foams synthesized for this study were investigated in corroded specimens contaminated with the radionuclide, Co-60 and Cs-137. The radioactivity of Co-60 in the specimens was measured both before and after the decontamination test. These results indicated that the decontamination foam of TBS surfactant had a much greater decontamination efficiency for Co-60 than that with EM 100 surfactant. These results indicate that TBS surfactant with silica nanoparticles have a significant effect on the decontamination efficiency when combined with a chemical reagent and silica nanoparticles due to the foam stability and drainage prevention of drainage. Faure's study [4,5] indicates that the rate of oxide dissolution is directly proportional to the foam stability.

4. Conclusions

TBS surfactant with silica nanoparticles are an effective decontamination foam for chemical reagents such as HNO_3 and cerium(IV), resulting in a foam stable against collapse.

REFERENCES

[1] C. Dame, C. Fritz, O. Pitois, S. Faure, "Relations between physicochemical properties and instability of decontamination foams" Colloids and Surfaces A: Physicochemical and Engineering Aspects, 263 210-218 (2005).

[2] L. Nunez, M. Kaminski, "Foam and gel methods for the decontamination of metallic surfaces" US Patent 7,166,758 B2 (2007).

[3] J. Causse, J.-F. Valery, C. Roussignol, "Principles of a fission product storage tank decontamination using a foam process" Proceedings of Global, Paris, France (2009).

[4] US Pat., 7,662,754 B2, 2010.

[5] I. H. Yoon, C. H. Jung, S. B. Yoon, C. Kim, S. Kim, H. B. Yang, J. K. Moon and W. K. Choi, Ann. Nucl. Energy, 2016, 95, 102–108.

Parameters and Procedures of Electro-kinetic Decontamination Experiments for Radioactive Concrete

Chanyoung Kim, Sungyeol Choi, and Myoungsu Shin*

Ulsan National Institute of Science and Technology, 50 UNIST-gil, Ulju-gun, Ulsan, Republic of Korea

*msshin@unist.ac.kr

1. Introduction

The electro-kinetic method is a technology to transport ions and colloids by applying an electric field to a porous medium such as soil and concrete. This technology can allow to extract metallic nuclides deep inside of concrete without mechanical destruction of the structure. To maximize its advantages, the factors that affect the efficiency of decontamination should be properly taken into account. This study aims at developing optimized decontamination procedures through the investigation of test data from previous studies.

2. Normalization for Comparison of Decontamination Efficiency

2.1 Variable Selection for Normalization of Efficiency

Previous studies about the decontamination of radioactive concrete focused on variables such as variety of solution and zeta-potential at double-layer as the key factors that affect to efficiency [1]. Several researchers [2] pointed out the effects of pH on the extraction of cobalt from concrete, but quantitative analysis about the decontamination efficiency by pH values were not have been performed. Also, none of them discussed the effects of the contamination procedure in detail. In this paper, the separation factor that affects to decontamination are investigated for each pH values. Finally, the sample contamination procedures of each study were evaluated.

2.2 Separation Factor Description

The results of concrete leaching tests for different pH values conducted by Achternbosch et al. [3] were used to estimate the effect of pH on the mobilization of cobalt in concrete. The investigation conducted by Achternbosch et al. [3] are given in Table 1. Also, the test data from Faiz et al., 2016 [4] are used to estimate the mobilization of cesium. The pH effect factors are described in Table 2. Referring to Achternbosh et al. [3], metallic elements existing in concrete may have three bonding forms: sorption, incorporation, and encapsulation. The contamination procedure of each studies could affect to bonding forms of nuclides, which finally affect to proportion of contaminants released from concrete.

Table 1. Leaching Test Results by pH of Solution [3]

Element	Cement (unit: ppm)	
	DEV-S4 (water)	Availability (pH 4)
Ba	1.7	135
Co	< 0.1	1

Table 2. Separation Factor of Nuclides with different pH values of Solution

Author	pH	Nuclides	Separation factor
[2]-Series A[1)]	7	Cs Co	1 1
[2]-Series A[2)]	7	Cs Co	1 1
[2]-Series B[3)]	7	Cs Cs (non-voltage)	1
[1]-0.1 M acetic acid[4)]	2.87	Cs Co	1.15 5
[1]-0.01 M Acetic acid[4)]	3.37	Cs Co	1.15 5

1) samples contaminated during casting, non-carbonated
2) samples contaminated during casting, carbonated
3) samples contaminated after curing
4) samples contaminated after curing with solution has high concentration, In case of 0.01 M acetic acid, it is washed chemically before performing electro-kinetic experiment

Finally, numbers of moles of extracted contaminants were normalized by the separation factor and the volume of the specimen.

$$C_{i_eff} = \frac{m_i}{V_{sam} D_{pH}} \qquad (1)$$

Here, C_{i_eff} is the effective concentration of nuclides i, m_i is the numbers of moles of nuclides i in the concrete sample, V_{sam} is the volume of the concrete sample, and D_{pH} is the separation factor of nuclides i by the pH value of the solution. Equation 1 is used to normalize the efficiency of decontamination in this study. After the normalization, it was discussed by compared the value of each setup.

3. Results of Normalization & Discussion

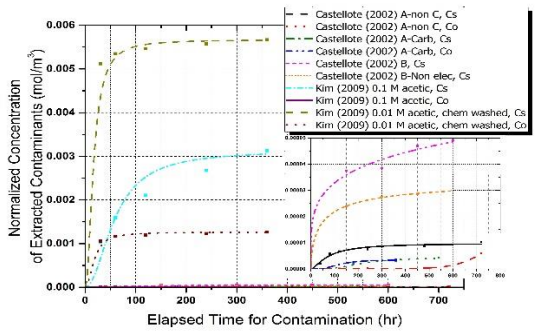


Fig. 3. Time vs Concentration of Extracted Contaminants.

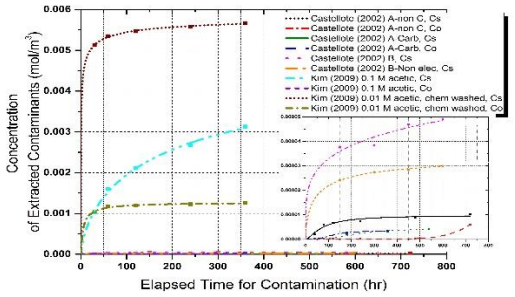


Fig. 4. Time vs Proportion of Extracted Contaminants.

Fig. 1. and Fig. 2. describe the normalized molar concentration and original molar concentration of the extracted contaminants with time-domain. For more correct evaluation, bonding forms of contaminants at each setup were discussed. In case of Series B of Castellote et al. [2], 60% of contaminants were extracted when the electric field was not applied to cell. As previously noted, it was contaminated after curing, so that the bond strength of contaminants with cement matrix would be weak. Kim et al. [1] also contaminated the samples after curing, but extraction of nuclides was not observed when proper solution and electric field were not applied. Considering this, contaminants in samples of Kim et al. [1] has stronger bonding form, and it is proper to compare with the results of samples contaminated during casting. From the result of series A of Castellote et al. [2], increase of extraction of cobalt and decrease of extraction of cesium were observed when samples were carbonated. In contrast, Kim et al. [1]'s setup using 0.01 M acetic acid with chemical washing shows high efficiency both for cesium and cobalt.

4. Conclusions

In this paper, result of normalization by separation factor for each pH value and effects of contamination method were studied.

- Trend of normalized data were similar with original data because of the trend of separation factor by each pH values.
- Using 0.01 M acetic acid with chemical washing shows highest efficiency from normalized concentration of extracted contaminants.
- Because the samples contaminated after curing shows weak bonding strength, it should be considered for correct comparison.

REFERENCES

[1] Kim, G.N.; Yang, B.I.; Choi, W.K.; Lee, K.W.; Hyeon, J.H. (2009) Washing-electrokinetic decontamination for concrete contaminated with Cobalt and Cesium, Nuclear Engineering and Technology, 41; 1079-1086.

[2] Castellote, M.; Andrade, C.; Alonso, C. (2002) Nondestructive Decontamination of Mortar and Concrete by Electro-Kinetic Methods Application to the Extraction of Radioactive Heavy Metals, Environmental science & Technology, 36; 2256-2261.

[3] Achternbosch, M.; Bräutigam, K.; Hartlieb, N.; Kupsch, C.; Richers, U.; Stemmermann, P.; Gleis, M.; (2003) Heavy metals in cement and concrete resulting from the co-incineration of wastes in cement kilns with regard to the legitimacy of waste utilisation, Forschung-szentrum Karlsruhe GmbH.

[4] Faiz, Z.; Fakhi, S.; Bouih, A.; Outayad, R.; Benkdad, A.; Hannache, H. (2016) Leaching study of cesium from spent ion-exchange resins and Portland cement package, International Journal of Environmental Science and Technology, 1-8.

Application Review of Clearance for Metallic Waste After Decommissioning

Sang-Ho Lee, Hyung-Woo Seo, and Chang-Lak Kim*

KEPCO International Nuclear Graduate School, 658-91 Haemaji-ro, Seosaeng-myeon, Ulju-gun, Ulsan, Republic of Korea

*clkim@kings.ac.kr

1. Introduction

It is estimated that the amount of metal waste generated by decommissioning nuclear facilities in the next 50 years will be about 30 million tons. Currently, Low Level Waste (LLW) repositories are insufficient to accommodate metal waste that will be generated when decommissioning worldwide. In addition, the amount of metal waste accounts for about 90% of total waste. Much of the radioactive waste generated during decommissioning of nuclear power plants is not highly polluted and can be recycled or reused. And separation according to radioactive waste levels can effectively solve the decommissioning cost according to waste management. Among the radioactive wastes, the radionuclides concentration is below the clearance permissible concentration.

If it is confirmed that the concentration of radionuclides in wastes is less than the allowable concentration, it is excluded from the application of Nuclear Safety Act and called self-disposal to manage by incineration, landfill, recycling, etc. as waste rather than radioactive waste.

2. Main Subject

2.1 Overseas Regulation for Clearance

The best treatment is through unrestricted recycling of metal waste by disposal, domestic acceptable concentration standards are lower than overseas standards. So recycling targets are low and processing takes a long time. Also, there is no domestic standard for limited recycling of Very Low Level Waste (VLLW) metal waste. Table 1 shows the documents for overseas Clearance, and Table 2 shows the release criteria proposed by the European Commission (EC) and the International Atomic Energy Agency (IAEA).

Table 1. Overseas Regulation for Clearance

Document	Content
NUREG-1640	Clearance Level
Radiation Protection 89	Metal Clearance Level
Radiation Protection 122	General Clearance Level
IAEA RS-G-1.7	Clearance Level

Table 2. Radionuclides Release Criteria of EC and IAEA

	EC RP89 (Metal Recycling)	EC RP122 (Clearance)	IAEA (RS-G-1.7)
Co-60	1	0.1	0.1
Cs-137	1	1	0.1

Comparing the EC and IAEA standards for clearance, the RS-G-1.7 is more conservative. Because IAEA standard has set the release standard in consideration of both artificial and natural radioactivity.

In domestic case, IAEA RS-G-1.7 is applied.

2.2 Current Status

The EC and IAEA provides a concentration standard for sum of limited reuse and metal recycling. But in Germany, different concentrations standards are provided for each scenario. Table 3 shows the clearance level standard in the world.

Table 3. Clearance Level Standard in the World

	EC RP-89	IAEA (RS-G-1.7)	German RPO	
			Unconditional	Recycling Metal
Co-60	1	0.1	0.1	0.6
Cs-137	1	0.1	0.5	0.6

Germany's clearance regulation is stipulated in the Atomic Energy Act and Radiation Protection Ordinance (RPO). And certain substances may be excluded from conditional regulation depending on

the scenarios. Even if the general regulatory clearance level of a specific nuclide is 0.1Bq/g, a different reference value may be applied for each scenario such as the clearance level for landfill or incineration is 4Bq/g, the clearance level for metal melting for recycling is 0.6Bq/g.

3. Overseas Metal Waste Melting Case

3.1 Germany

Since 1989, Siempelkamp has been using CARLA melting facilities to melt a total of 25,000 tons of carbon steel, stainless steel, aluminum, copper and lead. And then released 9,000 tons, 14,500 tons to produce shielding blocks or KONRAD containers for reuse in the nuclear industry.

Siempelkamp's radiological limitations are Max 200Bq/g (for β, ɣ), Max 100Bq/g (for α) separate limits for uranium.

3.2 Sweden

Over the past decade, 3,600 tons of WURGASSEN's decommissioning metal waste and

740 tons were unrestricted release among 143 tons of aluminum, 644 tons of carbon steel which were generated when the Siemens nuclear fuel plants was decommissioning. In 2009, Sweden built the Metal Recycling Facility (MRF) in Cumbria and has experience handling metal waste in 12 regions of England and Scotland. Currently, they are continuing to melt and decontaminate radioactive waste such as contaminated iron, aluminum, copper including large metal waste.

STUDSVIK's radiological limitations are varies with type of material and preparation to be done.

3.3 France

From 1999 to 2005, France were melted and reused 12,000 tons of carbon steel and stainless steel in the nuclear field.

Currently, radioactive metal wastes such as structures, valves, pumps, non-ferrous metals, ferrous metals (stainless steel, carbon steel) generated during operation of nuclear facilities, process maintenance, dismantling and dismantling of facilities are disposal using facilities with an average capacity of up to 20 tons/day.

In particular, France has no exemption regulatory. France is introducing the concept of Zoning (Nuclear zone, Non-Nuclear zone). Zoning is a way of classifying between regulated wastes and wastes that are excluded from regulation.

CENTRACO's radiological limitations are Max 20,000Bq/g (for β, ɣ), Max 370Bq/g (for α).

3.4 Russia

In 1996, 1,659Mg of metal waste composed of stainless steel and nonferrous metal was melted, and approximately 95% of the melted metal waste was reused and sent to industry.

ECOMET-S's radiological limitations are Max 100Bq/g.

4. Conclusion

When the radioactive waste concentration is slightly above the clearance level, it is necessary to reduce the radioactive concentration by decaying the radioactivity through a long-term storage depending on the type of radionuclide.

Many countries have now established their own standards for metal waste and operating. Therefore, it is necessary to analyze the criteria and characteristics of the IAEA and the countries who already implementing recycling, and establish a safe guideline for Korea situation.

Acknowledgement

This research was supported by the Nuclear Safety Research Program through the Korea Foundation of Nuclear Safety (KOFONS), granted financial resource from the Nuclear Safety and Security Commission (NSSC), Republic of Korea (No. 1305009).

REFERENCES

[1] Byeong-Yeon Min, Ki-Won Lee, Gyoung-Su Yun, Jei Kwon Moon, "Current Status and Future Issues for Melt Decontamination of Decommissioning Metal Wastes Generated from Nuclear Facilities", Journal of Korea Society of Waste Management, Vol.29, No.7, pp.603-515, 2012.

[2] KINS/GR-542, "Research on the improvement of the safety regulation system for the radioactive waste", 2013.

Assessment of Radiation Dose by Applying Cover Depth for the Site Reuse After NPP Decommissioning

Hyung-Woo Seo, Sang-Ho Lee, and Chang-Lak Kim*

KEPCO International Nuclear Graduate School, 658-91 Haemaji-ro, Seosaeng-myeon, Ulju-gun, Ulsan, Republic of Korea

*clkim@kings.ac.kr

1. Introduction

The oldest Nuclear Power Plant (NPP) in South Korea, Kori-1, will be decommissioned starting in 2017. When all facilities are removed and the site is opened, the soil within the site will be contaminated. To determine doses from the contaminated soil, RESRAD-ONSITE code has been used. There are many parameters to calculate dose from the various pathways, and it is necessary to identify what parameter influences significantly the results, and if it is adjustable, it can be applied for dose reduction. Therefore, in this study, we perform a sensitivity analysis by adjusting the parameters and observe the effect on dose results.

2. Methods

2.1 Exposure Pathways

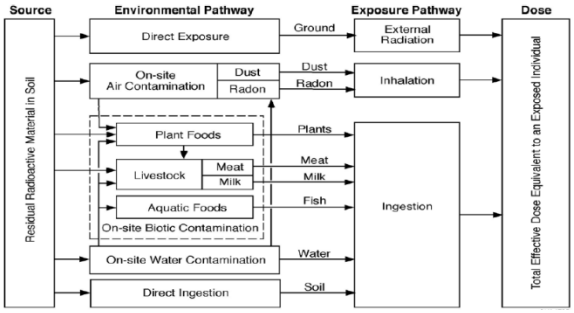


Fig. 1. Schematic Diagram of RESRAD Pathways [1].

Major pathways used to derive on-site dose in RESRAD-ONSITE are illustrated in Fig. . The exposure pathway consists largely of external, inhalation, and ingestion, which are received through routes such as ground, dust, radon, plants, meat, milk, fish, water, and soil. The food pathways can be classified as water-independent or water-dependent.

2.2 Exposure scenarios

Exposure scenarios are the human life patterns that can be affected by the release of radioactivity from the contaminated area. Since the residential farmer scenario is expected to result in the highest dose, we assume the land use as the resident farmer.

2.3 Key parameters

As the major radionuclides at the site, we assumed the representative radionuclides (^{137}Cs and ^{90}Sr) and set the radioactivity as shown in Table 1. The input radioactivity value are referenced to the Derived Concentration Guideline Levels (DCGLs) reflecting the decommissioning experience of Connecticut Yankee [2]. Since the DCGLs are derived from 0.25 mSv/y, which is the land reuse limit in the United States, it needs to be converted to the corresponding value considering 0.1 mSv/y in Korea [3]. In determining RESRAD-ONSITE parameter values, the site specific data such as the geological and hydrological data of Kori unit 1 was obtained from the research report [4] and other values are used by default.

Table 1. Input Radionuclides

Radionuclide	Concentration (Bq/g)
^{137}Cs	1.16×10^{-1}
^{90}Sr	2.40×10^{-2}

2.4 Sensitivity Analysis

Sensitivity analysis has been performed by multiplying or dividing the parameters by 2 and the results were compared against each other. Dose difference was observed over a period of 1,000 years, and the maximum of the differences was selected for comparison.

3. Results & discussion

As a result of sensitivity analysis, the cover depth found to be the most important for exposure dose and

can be modified during NPP decommissioning. By default, the resident farmer scenario use a value of cover depth as 0. As can be seen in Fig. 2, the dose rates of ^{137}Cs and ^{90}Sr were found to be lower than the limit of 0.1 mSv/y.

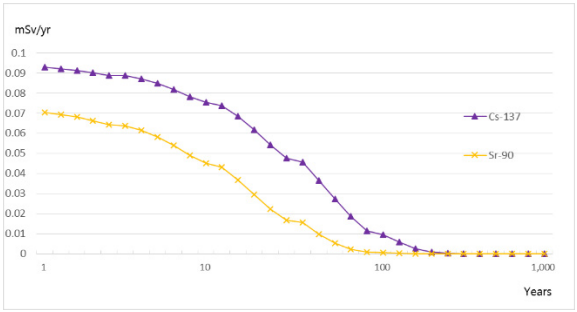


Fig. 2. Dose of Resident Farmer.

The graph of the component effect by the pathways is shown in Fig. 3 to Fig. 4. This indicates that the external and plants pathways are the dominant sources of ^{137}Cs and ^{90}Sr, respectively.

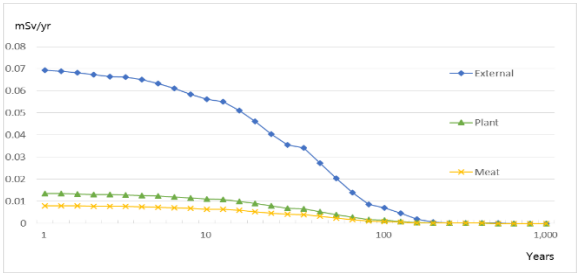


Fig. 3. Component Pathways Dose of ^{137}Cs.

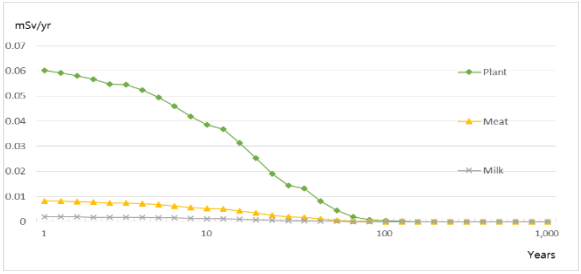


Fig. 4. Component Pathways Dose of ^{90}Sr.

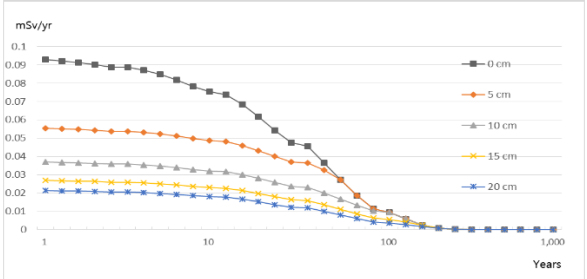


Fig. 5. Dose of ^{137}Cs by Cover Depth.

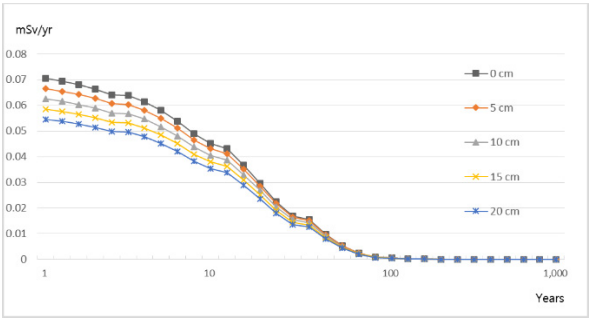


Fig. 6. Dose of ^{90}Sr by Cover Depth.

In the case of applying soil as a cover, the dose was found to be considerably reduced by increasing the depth as shown Fig. 5 to Fig. 6.

4. Conclusion

In this paper, dose assessment has been carried out for the site release after NPP decommissioning. Exposure doses were calculated assuming radionuclides and concentrations in resident farmer scenarios. Also, through the sensitivity analysis, it was found that the cover depth was the most significant parameter affecting the dose. Based on this information, applying cover depth will contribute to dose reduction when the site is opened to the public or reused for other purposes.

Acknowledgements

This research was supported by the Nuclear Safety Research Program through the Korea Foundation of Nuclear Safety (KOFONS), granted financial resource from the Nuclear Safety and Security Commission (NSSC), Republic of Korea (No. 1305009).

REFERENCES

[1] Environmental Assessment Division Argone National Laboratory, U.S. Department of Energy, User's Manual for RESRAD Version 6, July 2001.
[2] EPRI, Connecticut Yankee Decommissioning Experience Report, 2006.
[3] Nuclear Safety and Security Commission, Criteria for Reuse of Site and Remaining Buildings after Completion of Decommissioning of Nuclear Facilities, No. 2016-33, 2016.
[4] KINS, Development of Technology in Radiation Safety Regulations, KINS/GR-297, 2005.

Analysis on Disassembling Methods of Nozzle for PWR Spent Fuel

Younghwan Kim*, Yungzon Cho, and Youngsoon Lee

Korea Atomic Energy Research Institute, 111, Daedeok-daero 989beon-gil, Yuseong-gu, Daejeon, Republic of Korea

*Yhkim3@kaeri.re.kr

1. Introduction

Mechanical head-end processing of disassembly, extraction of the rods, and the shearing of the extracted rods shall be performed in advance as the head-end process of the pyro-process that can recycle the PWR. And efficient analysis of SF disassembling methods in connection with the pyro head-end shall be performed in advance. Therefore, this study compared and analyzed the characteristics of the SF disassembling methods for the design of a high efficiency head-end process. For this, radial blade cutting, axial single cutting, radial multi cutting, and slant multi cutting methods were analyzed. As a result of the comparison and the analysis, we selected the slant multi cutting method, which can handle the nuclear fuel rods of all shapes, can prevent fire from the dust generation, and generates less wastes with high disassembling efficiency. The above analysis results can be utilized for the design of the head-end process for SF dry process through the comparison and analysis of the PWR SF disassembling methods.

2. Disassembling analysis

2.1 Radial blade cutting

For the removal of the top/bottom nozzle of the assembly, radial blade cutting method, that is the saw rotation method, has an advantage of easy maintenance. This method is used for the cutting of the zircaloy rod in WSMP (Westinghouse Specialty Metals Plant). 2 saw devices are mounted in the cutting device part, and the process speed can be improved by about 5 minutes for each nuclear fuel assembly. This method may have the cases of the guiding tube (grid) spring becoming loose or rods being extended. But, for PWR SF assembly, when the end of the rod is closer to the top nozzle than the blade thickness, the rods cutting is not carried out. If rod top nozzle is cut in such condition, it will damage the seal welding of the rod pressure port and causes radiation of gas product from the rod, so the rod shall be verified whether it touches the top nozzle through the visual inspection in the hot cell in advance (Fig. 1).

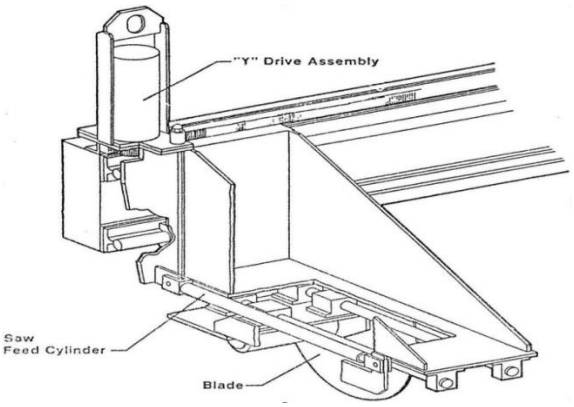


Fig. 1. Radial blade cutting methods on axis.

2.2 Axial single cutting

The removing method of PWR bottom nozzle is as follows.

Table is placed at the position to remove the nozzle, it is fixed to the bottom nozzle part with a short pin (②), the bottom nozzle fixture (④) and tube cutter (⑰) rotate to be in the position, touching the first fuel assembly, the fixture is placed on the bottom nozzle, and the clamp (⑧) starts.

As in Fig. 2, single-revolution tube cutter cuts each guiding tube from right above the selected welded part to the top grid space part. The tube cutter is moved to the position that can cut each guiding tube by the tool plate motion system. The positions of the guiding tubes are pre-programmed for all types of rods assembly types that will carry out the rods extraction. After the cutter cutting the last guiding tube of the assembly, the bottom nozzle is placed on the nozzle container plate. As such, PWR fuel assembly finishes the preparation to remove the rods.

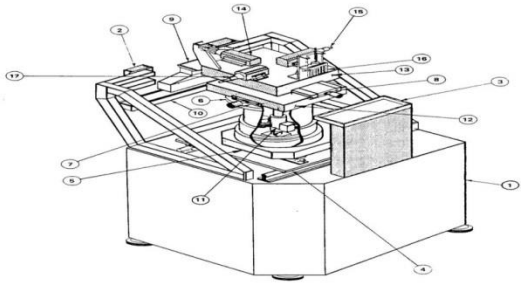


Fig. 2. Axial single cutting methods on axis.

2.3 Radial multi cutting

This method can place the fuel assembly on the transportation table by moving the tilting device to horizontal position, and when the tilting device returns to the initial vertical position, the transportation table moves to horizontal direction and moves to the bottom nozzle removing part. The top and bottom nozzles are separately removed, and the bottom nozzle is removed first (Fig. 3). After securing enough space between the nut and the bottom nozzle by pushing the bottom nozzle, 8 guiding tubes are removed at the same time with radial cutting at the point where the top and the bottom nozzle meet each other. During the cutting process, the spring is maintained to prevent falling off. For the bottom nozzle, to prevent the rods deformation during the cutting, comb is inserted between the rods, and 8 guiding tubes are cut and removed at the same time at the inner side of the bottom nozzle.

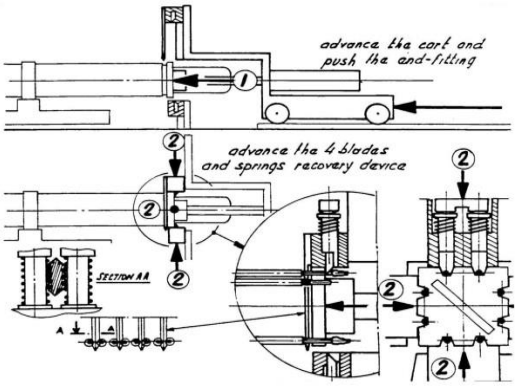


Fig. 3. Radial multi cutting methods on axis.

2.4 Slant multi cutting

For PWR SF assembly, the top guiding tube and instrument tube are cut from inside to outside using multi blade cutting head (Fig. 4). By drilling the instrument tube at the point where top and bottom nozzle meet the base plate, make a hole for multi blade cutter insertion. Insert the multi blade cutter far enough from each other and cut all guiding tubes and the instrument tube at the same time. At this time, the grid is removed along with the bottom nozzle while it is attached to the top and bottom nozzle along with some cut tubes. Through such a process, gripper can access to the rods more easily. During the cutting work, nitrogen is continuously supplied.

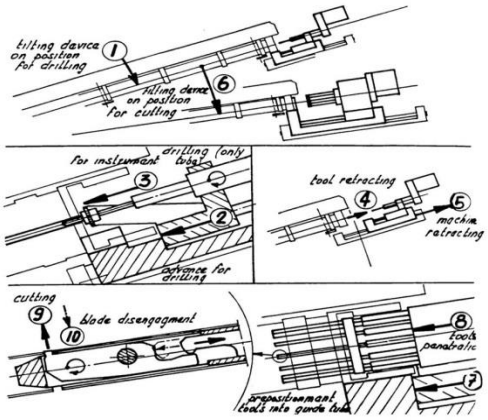


Fig. 4. Slant multi cutting methods on axis.

3. Conclusion

To select reasonable and high efficient target for PWR SF disassembling methods, major targets were selected and comparison and analysis were carried out. For this, radial blade cutting, axial single cutting, radial multi cutting, and slant multi cutting methods were analyzed. As a result of the comparison and the analysis, we selected the slant multi cutting method, which can handle the PWR SF assembly of all shapes, can prevent fire from the dust generation, and generates less wastes with high disassembling efficiency. Also, this method has the general usage that can be applied not just to dry process but also to wet process. The above analysis results can be utilized for the design of the head-end process for SF dry process through the comparison and analysis of the PWR SF disassembling methods.

ACKNOWLEDGEMENTS

This paper is the study carried out with the 2013 funding of the Ministry of Education, Science and Technology and the support from National Research Foundation of Korea (Nuclear Energy Technology Development Project, No. 2012M2A8A5025 696).

REFERENCES

[1] B. D. Cul, R. H. Hunt, "Advanced head-end processing of spent fuel," 2004 ANS Winter Meeting, Washington DC, Nov. 16, 2004.

Discussion on Non-fuel Waste Treatment in Connection With Dismantlement of Kori Unit 1

Ju-Young Yoon* and Cheon-Woo Kim

KHNP CRI, 70, 1312-gil, Yuseong-daero, Yuseong-gu, Daejeon, Republic of Korea

*august63@khnp.co.kr

1. Introduction

The decommissioning of Kori unit 1 is approaching. In order to dismantle, not only the spent fuel stored in the spent fuel pool but also the non-fuel wastes should be managed. The non-fuel wastes refer to non-spent fuel, and waste control rods, thimble plug, in-core instruments, neutron sources, burnable poison rod assembly and other foreign materials are typically used in nuclear reactors.

Most non-fuel wastes are wastes that have been inserted into reactor internal structures and fuel assemblies during operation and replaced due to mechanical lifetimes and defects.

It is anticipated that some activation will occur during reactor output, and unlike other radioactive waste treatment before waste treatment, it is necessary to prepare the treatment method in advance.

This paper describes the characteristics of non - fuel wastes and discusses the treatment methods associated with the dismantlement of Kori unit 1

2. Non-fuel wastes

Types of the non-fuel wastes include components inserted into nuclear fuel assemblies, such as control rods, thimble plug, neutron sources, in-core instruments, burnable poison rod assembly, dummy fuels and other foreign materials.

2.1 Control rod

It is inserted into the nuclear fuel assembly to control core reactivity or to stop the reactor, and its lifetime is 10-15 EFPY (Effective Full Power Year) depending on the row type / production year.

Table 1. Control Rod's Characteristic

Division	Material	Absorber
WH type	STS304	Ag-In-Cd

2.2 Thimble plug (TP)

It serves to reduce the bypass flow of the core by blocking the control rod guide of the nuclear fuel assembly without the control rod inserted. Its lifetime is 12EFPY, and material is STS304.

2.3 Neutron Source

The neutron flux is injected into the fuel to observe the core state during low periods, and the design life is 10 years and includes Cf-252 in the source.

2.4 In-core Instrument (ICI)

The neutron flux distribution of the core is measured by moving the inside of the core or loading in into the core if necessary. It's covered with stainless steel.

2.5 Burnable Poison Rod Assembly (BPRA)

The BPRA suppresses excess reactivity and limits the excessive boron concentration. Also, the radial power distribution is flattened. B-10 is used as the neutron absorber in the BPRA.

2.6 Dummy fuel

Used for pretesting of the crane handling nuclear fuel assemblies, not a radioactive device that is not inserted into the actual core.

2.7 Other foreign material

Foreign materials are found in the primary system or in the spent fuel pool.

3. Non-fuel waste treatment

3.1 Overseas case of the Non-Fuel Waste Treatment

Abroad does not have a special disposal method. Like the rest of the country, most of the waste control rods are stored in the spent pool.

In the case of the in-core instruments, it is also stored in the spent fuel pool, or it may be partially cut and dried and stored and managed in a shielded container.

This can be considered as the availability of the storage space due to the uncertain state of the spent fuel disposal facility or the intermediate storage of spent fuel in the site.

3.2 Non-Fuel Waste Treatment Plan

Most of the non-fuel wastes are kept in the storage tank because there is no suitable radiation storage container suitable for irradiated radioactive waste. But to remove it

First, an assessment of the radioactive emissions of non-fuel wastes should be undertaken. The maximum output at the time they were inserted into the core for combustion evaluation, the fuel burn rate of the zone, and the output should be investigated. Hysterical investigation of a reliable insert will be the most basic procedure of the activation analysis.

Based on this, it is necessary to perform radioactivity and dose assessment using MCNP or McCARD computer codes.

Second, based on the evaluation results, the non-fuel wastes should be classified according to dose and nuclide.

1) Waste that is below the standard value in intermediate and low level waste disposal facilities

2) Low to intermediate level waste disposal facility waste above standard level

Third, the sorted waste is cut and packed. Packaging containers should be developed to package the remainder, except for the wastes that can be brought into the intermediate and low level waste disposal facility.

There is also a method to develop in connection with research projects related to the treatment of radioactive waste generated in the reactor vessel and reactor internal structure of Kori unit 1.

In addition, a space for intermediate storage of radioactive waste in the site should be prepared separately.

4. Conclusion

This paper briefly describes the types of the non-fuel wastes in the spent fuel pool and the treatment methods associated with the dismantlement of Kori unit 1.

Considering the dismantlement of Kori unit 1 and the point of saturation of the spent fuel pool, treatment techniques for the non-fuel wastes should be developed and studied.

We will be able to develop a safe treatment method by making good use of the dismantlement technology currently being studied.

If the developed non-fuel wastes treatment method is applied and used in the reactor, it will be possible to treat / dispose of the continuous control rod and in-core instrument, and it will become easier to manage the spent fuel pool.

REFERENCES

[1] Utilization of lecture materials in KHNP Human Resource Development Institute.[Course : Core Management General].

Desorption of Cesium From Montmorillonite and Hydrobiotite by Cationic Detergent

Bo Hyun Kim[1,2], Chan Woo Park[1], Hee-Man Yang[1], Kune-Woo Lee[1*], and So Jin Park[2*]
[1]Korea Atomic Energy Research Institute, 111, Daedeok-daero 989beon-gil,Yuseong-gu, Daejeon, Republic of Korea
[2]Chungnam National University, Youseong-gu, Daejeon, Republic of Korea
kimbh@kaeri.re.kr

1. Introduction

Cesium desorption on soil have been of important issue after the severe environmental contamination of Fukushima area in Japan with radionuclides. Soils are composed of sand, silt and clay, and radionuclides are selectively adsorbed to clay in soil. Upon release of radioactive cesium from the nuclear facility, the dissolved cesium ions in waster can be transferred to the clay component in soil. Cesium is generally adsorbed in the interlayer of clay minerals, and irreversible adsorption takes places at the frayed edge site (FES), which is highly stable and hardly removable by conventional soil treatment methods.

Among the clay minerals, montmorillonite, which is a 2: 1 phyllosilicate clay mineral, is well known to adsorb cesium with the highest adsorption capacity, and cesium ions are generally adsorbed on clay interlayer. Hydrobiotite is an interstrified clay of vermiculite and biotite. Vermiculitic clay contains more cesium-specific adsorption sites than illitic clay and the amount of FES can increase as weathering of micaceous minerals.

In this study, we investigated the behavior of Cs desorption from montmorillonite and hydrobiotite by a cationic surfactant and a cationic polyelectrolyte. In order to remove cesium contaminated with montmorillonite, tetramethylammonium bromide (TMAB), Octyltrimethylammonium bromide (OTAB), Dodecyltrimetylammonium bromide (DTAB), Cetyltrimethylammonium bromide (CTAB) was selected as the cationic surfactant. In hydrobiotite, DTAB and polyethyleneimine (PEI) was selected as a cationic polyelectrolyte. To compare the Cs desorption efficiency, the adsorption and Cs desorption from montmorillonite and hydrobioite were analyzed.

2. Experimental

Montmorillonite and hydrobiotite were dispersed in an aqueous CsCl solution, and the mixtures were subjected to a horizontal shaker for one week at 20 °C. The Cs-adsorbed clay was collected by centrifugation at 7000 rpm followed by drying at 40 °C. The concentration of Cs in the solution was measured with inductively coupled plasma mass spectrometry.

Cs-MMT was mixed with TMAB, OTAB, DTAB and CTAB solution, and Cs-HBT was mixed with DTAB and PEI solution in deionized water. The clay was separated and washed twice with deionized water by centrifugation and was dried at 40 °C. The desorbed amount of Cs was analyzed by measuring the Cs concentration in the aqueous phase by inductively coupled plasma mass spectrometry.

3. Result & discussion

The Cs adsorption behaviors of MMT and HBT in CsCl solutions were observed at 20 °C. Both montmorillonite and hydrobiotite showed that Cs adsorption isotherm data fit well to the Langmuir Model ($R^2 = 0.999$), and the maximum Cs adsorption capacity was 0.684 mmol/g and 0.184 mmol/g based on the fitting analysis, respectively (Fig. 1).

Both montmorillonite and hydrobiotite showed increased Cs desorption as the concentration of desorption agent increased. The cationic surfactant showed efficient desorption of cesium ion by ion-exchange with trimethyl ammonium head group of surfactant on montmorillonite. PEI showed the highest Cs desorption efficiency by ion exchangers with high cationic charge of the polyelectrolyte originating from its large number of ionizable units on hydrobiotite (Fig. 2).

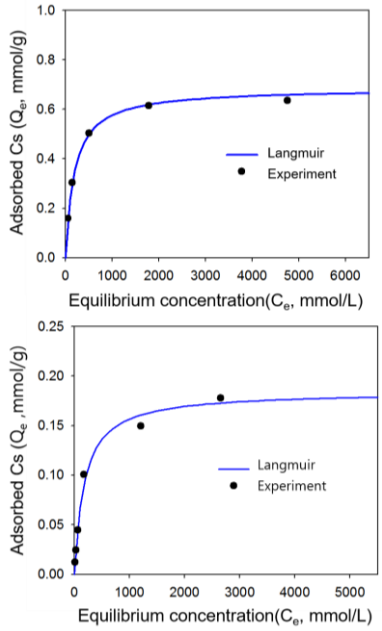


Fig. 1. Cs adsorption isotherm of montmorillonite and hydrobiotite at 20°C. The line indicates the result of fitting with the Langmuir adsorption model.

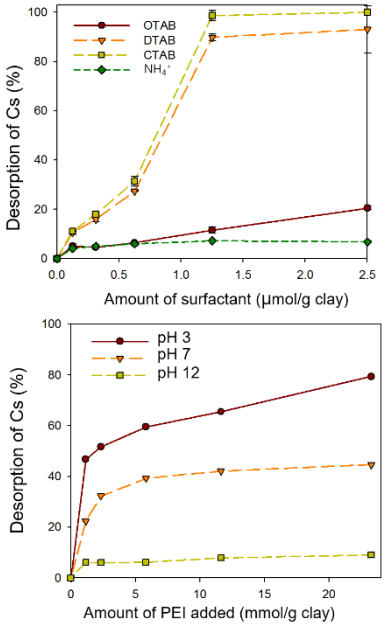


Fig. 2. Cs desorption after reaction of Cs-MMT and Cs-HBT with various amounts of desorption agent at 20°C.

4. CONCLUSIONS

We investigated adsorption of Cs ions on montmorillonite and hydrobiotite, and Cs desorption by ion exchange with cationic molecules including a cationic surfactant, cationic polyelectrolyte and ammonium ion. The maximum Cs desorption efficiency achieved was 99% on montmorillonite and 79% on hydrobiotite, respectively. This is because cesium ions in the interlayers were replaced by desorption agent by ion-exchange. This comparative Cs desorption study proved that polyelectrolyte-based desorption methods will have great potential for remediation of Cs-contaminated soil.

REFERENCES

[1] Morino Y, Ohara T, Nishizawa M. Atmospheric behavior, deposition, and budget of radioactive materials from the Fukushima Daiichi nuclear power plant in March 2011. *Geophys Res Lett*. 2011;38(7).

[2] Fuller AJ, Shaw S, Ward MB, et al. Caesium incorporation and retention in illite interlayers. *Appl Clay Sci*. 2015;108:128-134.

Study on Adsorption of Sodium Dodecylbenzenesulfonate by Using Amino Group-substituted Mesoporous Silica Nanoparticles

Daewon KIM, Jongho KIM, and Taek Seung LEE*

Organic and Optoelectronic Materials Laboratory, Department of Organic Materials Engineering, Chungnam National University, Daejeon, Republic of Korea

*tslee@cnu.ac.kr

Since radioactive waste is very harmful to human health and the environment, much attention has been paid to the removal of radioactive materials. Surfactants have been used for removal of radioactive atoms. Many liquid radioactive wastes, which generally contain such surfactants, are generated through this decontamination. The liquid radioactive waste treatment process can be a more efficient process through the removal of surfactants such as sodium dodecylbenzenesulfonate (SDBS). Mesoporous silica nanoparticle (MSN) has attracted a great deal of interest from researchers as biomedicine, biosensing, drug delivery materials. MSN has a particularly large surface area and high pore volume, uniform pore size distribution, ease of surface modification to internal pores or external particle surfaces. Due to these characteristics, MSN has the advantage of adsorbing a large amount of materials inside. In this study, we experimented to adsorb the surfactant SDBS using MSN. MSN was prepared through a modified sol-gel process and then functionalized with amino groups on the surface and inside of MSN using (3-aminopropyl)triethoxysilane (MSN-NH_2). The SDBS adsorption concentration of MSN-NH_2 was calculated by SDBS concentration of the filtrate after MSN-NH_2 and SDBS agitation. The SDBS adsorption concentration of MSN-NH_2 was measured by using different initial SDBS concentration, MSN-NH_2 concentration and reaction time as variables. Also, the concentration of SDBS adsorption of MSN-NH_2 was measured using a mixture of SDBS and Cs^+ ions.

A Scheme to Develop a Decommissioning Safety Case

Byung-Sik Lee

Dankook University, 119, Dandae-ro, Dongnam-gu, Cheonan, Chungnam, Republic of Korea

bslee@dankook.ac.kr

1. Introduction

The safety case is a collection of arguments and evidences to demonstrate the safety of a facility or activity. A safety case reflects the actual work performed at the facility, so that the safety case normally includes a safety assessment as well as information and assumptions (including support evidences and reasoning) on the robustness and reliability of the safety assessment.

In the decommissioning phase there are various issues, or at least in comparison with operation issues. So, it is needed to identify some remarkable points for the decommissioning safety. This paper is to review some major issues of the safety case on decommissioning of the nuclear facilities for various stakeholders. Information is provided that may be used by nuclear facility operators and managers for planning and developing strategies for the shutdown and decommissioning of a facility as it approaches the end of its operational phase.

2. Issues of the Decommissioning Safety Case

2.1 Potential Hazards during Decommissioning Phase

It is needed to protect workers by eliminating or reducing the radiological and conventional hazards that may happen during the decommissioning activities. The hazards with decontamination and dismantling of structures, systems and components are important not only because they may be a direct cause of harm to workers, but also because their occurrence may, indirectly, result in increased radiological hazard. In the radiological hazards, the established dose limits must be met and applicable dose constraints should restrict the projected individual doses based on ALARA principle. The conventional industrial hazards are critically considered during the decommissioning process because that may be greater than those experienced during the operation of the facility. Any hazards to the public and to the environment will be decreased progressively during the decommissioning phase.

Controlled releases of liquid and gaseous effluents into the environment and clearance of solid materials for reuse or disposal as conventional waste needs another control regime related to protection of the public and the environment.

2.2 Characterization of the Facility

Prior to developing a decommissioning plan, the radiological status of a facility must be determined. Characterization is not limited to simply collect data, facts and information necessary to identify situations, which may affect workers and the public or the environment. Characterization should be considered as a starting point of any decommissioning project and the results be maintained and updated as necessary throughout the whole decommissioning project.

- Prepare radiological and chemical inventories that might be hazardous to workers, the public or the environment.
- Analyze structural stability conditions of the facility that may affect the safety or protection of workers.
- Determine the nature and quantity of radioactive materials and conventional chemical contaminants

It may likely be important to check and review the various types of records and resources in the facility for characterization.

- Official documents associated with licensing of facility operation
- Safety and inspection reports describing actual and potential hazards and the measures taken to control them during the operation.
- Design records such as “as built” design drawings and documentation

- Construction records such as descriptions and photographs of the various construction stages
- Operating records with any modifications carried out on the facility during the operating phase
- Personal Account from facility operating staff

In addition to the characterization work described above it is also important to contact former employees of the facility to collect unidentified operational records.

2.3 Decommissioning Safety Assessment

The safety assessment is performed to demonstrate that exposures of workers and of the public are as low as reasonably achievable (ALARA) and do not exceed the relevant limits or constraints during the decommissioning phase.

The safety assessment for decommissioning is consistent with the decommissioning plan and with other relevant national and site specific strategies and requirements, for example, with requirements for radioactive waste management and for the release of material and sites from regulatory control.

Therefore, the safety assessment is developed in a systematic manner using a graded approach, commensurate with the hazards associated with the facility and with the possible consequences of the decommissioning activities under evaluation. The safety assessment for decommissioning may be based on the framework as defined in IAEA [3]. The results of safety assessments can serve to demonstrate compliance with regulatory requirements and criteria expressed in terms of effective dose

2.4 Management Procedures

Practical implementation of decommissioning depends on the technical, managerial and administrative tasks necessary for achieving the goals of the safety case for decommissioning. Management tasks must ensure that all decommissioning activities will be conducted in accordance with approved procedures and that the licensee has a methodology for managing the development, review and maintenance of the procedures.

- Selection of decommissioning technology
- In-process survey
- Containment of contamination
- Provision of radiological protection
- Management of radioactive waste
- Planning for emergencies and physical protection
- Quality assurance
- Project management
- Task management
- Personnel management
- Stakeholder involvement

These management tasks have to be prepared to meet the safety requirements with reflection to the safety assessment.

3. Conclusion

The key issue in the decommissioning of nuclear facilities is the progressive removal of hazards, by stepwise decontamination and dismantling activities that have to be carried out safely and within the boundaries of an approved plan. In addition, it is important to address conventional aspects in the decommissioning safety assessment, as they may outweigh some radiological aspects.

The decommissioning safety case is a strategic document specifically designed for analyzing these hazards, and the separate stages required for hazard reduction. So the safety case will be consistent with the decommissioning plan and address the changing hazards from the facility which may occur as a result of modifications to the facility which take place during the stages of decommissioning.

Therefore, to prepare the decommissioning safety case there needs its own facility characterization, safety assessment and, in most cases, management procedures.

REFERENCES

[1] Achieving the Goals of the Decommissioning Safety Case, NEA No. 5417, 2005.
[2] Decommissioning of Facilities Using Radioactive Material, IAEA Safety Standards Series No. WS-R-5, 2006.
[3] Safety assessment for the decommissioning of facilities using radioactive material, IAEA Safety Standards Series No. WS-G-5.2, 2008.

6분과

방사선환경 및 안전 (Oral)

Environmental Gamma Distribution of Ulsan City with the Highest Nuclear Power Plant Density in Korea

Ukjae Lee*, Jun Woo Bae, and Hee Reyoung Kim

Ulsan National Institute of Science and Technology, 50 UNIST-gil, Ulju-gun, Ulsan 44919, Republic of Korea

*dldnrwp@unist.ac.kr

1. Introduction

A system that can quickly check the distribution of radiation based on a mobile instrument was developed. The developed system was applied to the Ulsan area, which has the highest density of nuclear power plants. The nearby site of Ulsan's major non-destructive testing facility and radioactive material treating industry are scanned and the radiation dose rate distribution was measured. In addition, hospitals, transportation points such as airports, bus terminals and train stations, residential areas and three commercial areas were measured and compared. In this validation, the system was able to detect unexpected hot spots quickly in the affected environments.

2. Methods

2.1 Concept of system

The proposed system is consisted of the hardware of a detector for gamma spectrometry and the radiation dose measurement leading to radiation level distribution display at the laptop/desktop along with the software of the radiation information mapping program. The contour mapping program, which enables radiation level distribution displayed in 2D and 3D by one click of mouse right after the scanning of the corresponding area by the portable gamma radiation detector was finished and was composed by using the commercial software of MATLAB. The simultaneous display at both laptops of the on-site measurement and desktop at the main office is implemented by data transmission using CDMA method.

2.2 Monitoring sites

The major non-destructive testing industries and radioisotope treatment industries in Ulsan city were selected for validation of the rapid radiation distribution display system. In addition, three hospitals, three transportation hubs including an airport, bus terminal and train station, three apartment complexes, and three commercial areas were also measured for comparison. Scanning around each industrial site was performed in a vehicle with the installed system. The information on latitude, longitude, and radiation dose rate were obtained through actual measurements and used as data sets for the radiation contour mapping.

3. Results and Discussion

The system was tested and its performance was evaluated by applying it to environmental radiation monitoring in Ulsan city.

3.1 Quick contour mapping program for radiation distribution

Fig. 1 shows the result of contour mapping program for radiation distributions. The figures verify that the radiation distributions were shown in the 2D and 3D contour maps with geographical information.

The laptop used for this validation had an Intel® core i7-3537U CPU, 2.00 GHz processor, and 8 GB of memory; the time required by the proposed system's code using the "Profiler" function in MATLAB. The time required to generate the radiation distribution contours immediately after the measurement was approximately 11 s to process 10,000 data items whereas existing techniques for radiation distribution monitoring require more than 1h.

The designed monitoring system finds contamination by comparing detected radiation data with those of neighboring points; hence, this system can be used to find radiation hotspots. Therefore, the

developed monitoring system could be efficiently used when such hotspots need to be detected quickly, such as during a radiation emergency or at a large site, including D&D sites.

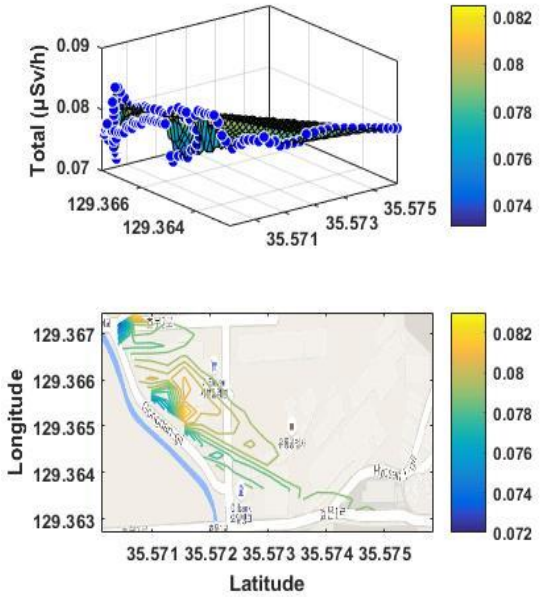


Fig. 1. The result of contour mapping program for radiation distributions.

3.2 Application to environmental radiation monitoring of Ulsan city

The radiation distribution measured for specified areas, including industrial facilities, hospitals, transportation hubs, and residential regions in Ulsan city can be checked in Table 1. It shows the maximum, minimum, and mean values of radiation dose distributions for each type of location.

The scanning of 17 sites around Ulsan city showed radiation levels ranging between 0.065–0.163 μSv/h, which are within the normal environmental level in Korea, demonstrating that Ulsan city is safe in terms of its radiation environment. The proposed Nuclide Recognizing Rapid Environmental Radiation Distribution Monitoring System could be directly applied to in-situ hotspot detection in the vast areas subject to D&D of NPPs. The system could also be effectively used in conjunction with drone technology to scan radioactive contamination in both rural and urban environments after a nuclear disaster.

4. Conclusion

Real measurement-based quick radiation distribution monitoring system with radionuclide recognition was established by employing the fundamental concept of combining detector-based hardware and MATLAB. The scanning of 17 sites of Ulsan city showed the radiation level had a range of 0.065 ~ 0.163 μSv/h falling on normal environmental level of Korea. It was demonstrated the Ulsan city were kept safe in terms of radiation environment from the measurement by using Nuclide Recognizing Rapid Environmental Radiation Distribution Monitoring System.

Table 1. Minimum, maximum and mean value of detected data at each monitoring point

Monitoring Site		Maximum (μSv/h)	Minimum (μSv/h)	Mean (μSv/h)
Industry	A	0.0830	0.0720	0.0779
	B	0.0930	0.0720	0.0821
	C	0.1220	0.0820	0.0963
	D	0.0833	0.0720	0.0776
	E	0.0980	0.0710	0.0803
Hospital	A	0.096	0.079	0.088
	B	0.110	0.077	0.086
	C	0.163	0.072	0.088
Market	A	0.092	0.065	0.079
	B	0.103	0.07	0.082
	C	0.100	0.086	0.094
Bus terminal		0.093	0.07	0.079
Airport		0.079	0.067	0.072
Train station		0.078	0.062	0.07
Apartment	A	0.087	0.074	0.078
	B	0.091	0.072	0.079
	C	0.099	0.081	0.093

REFERENCES

[1] Kim, H. R., et al. (2008). "The Establishment of an In-Situ Real Time Radiation Contour Mapping Technique." Journal of Nuclear Science and Technology 45(sup5): 662-665.

[2] Kim, H. R., et al. (2007). "The development of an on-line ERM system for the research reactors in Korea." Nuclear Instruments and Methods in Physics Research Section A: Accelerators, Spectrometers, Detectors and Associated Equipment 579(1): 518-521.

Dose Assessment of the Public in Ulsan Under Normal Operation of Nuclear Power Plants Using FLEXPART

Jaeseong Min* , Ukjae Lee, and Heereyoung Kim

Ulsan National Institute of Science and Technology, 50 UNIST-gil, Ulju-gun, Ulsan, Republic of Korea

*jsmin92@unist.ac.kr

1. Introduction

The radionuclides are released to the environment during normal operation though the air and the water. So, the evaluation of environmental impact due to dispersion of radionuclides is needed by the Nuclear Safety Act of Korea. Gaussian atmospheric dispersion models have been used to evaluate the dispersion. However, Gaussian atmospheric models are hard to simulate the complex meteorological conditions as the distance of dispersion is increasing. The long-range atmospheric transport model needed be used to simulate the transport of radionuclides more elaborately.

The Ulsan city is the place of the highest nuclear power plant density in Korea. This city is located between the Kori and Wolsong nuclear sites. As this location, the radiological impact due to atmospheric dispersion of radionuclides from normal operation of Kori and Wolsong nuclear power plants (NPP) could be overlapped. In this research, the radiological impact of Ulsan from the both nuclear sites were simulated using the FLEXPART long-range atmospheric transport model.

2. Methods and Materials

2.1 Simulation of atmospheric dispersion

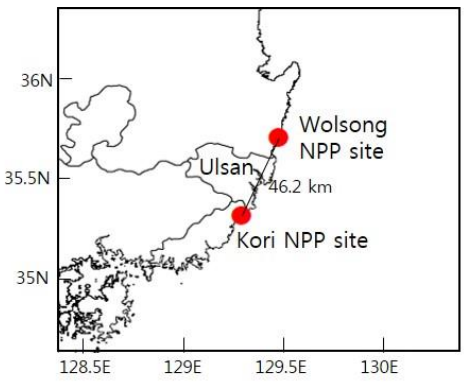


Fig. 1. The location of Ulsan city, Wolsong and Kori NPP.

Fig. 1 shows the location of Ulsan city, Wolsong and Kori NPP sites. The direction of Ulsan is N, NNE and NNW from Kori NPP site. The radionuclides were dispersed in the NPP sites. The simulation was performed using FLEXPART Lagrangian particle dispersion model [1]. The source terms of atmospheric dispersion from the report of Korea Hydro & Nuclear Power (KHNP) are shown in Table 1 [2]. The 0.5°×0.5° Global Forecast System (GFS) data from National Centers for Environmental Prediction (NCEP) in 2015 was used as meteorological data.

Table 1. The amounts of emitted radionuclides to the air [2]

	Kori	Wolsong
^{3}H	1.76E+01	1.41E+02
^{14}C	7.79E-01	9.50E-01
^{41}Ar	3.23E-02	5.19E+00
^{58}Co	8.63E-09	-
^{82}Br	9.66E-07	-
^{85}Kr	1.50E+00	5.45E-02
^{95}Nb	-	4.95E-08
^{131m}Xe	1.36E-02	4.94E-04
^{133}Xe	3.31E+00	1.63E+01
^{135}Xe	2.24E-05	3.26E-01
^{131}I	7.27E-08	2.44E-05
^{132}I	1.37E-05	-
^{133}I	2.36E-07	-

2.2 Dose calculation

The cloud shine and inhalation pathways are considered for dose calculation. The effective dose from cloud shine pathway through external exposure of radiation in the air was calculated as the equation (1):

$$E^{clo} = \sum C \cdot DC_{clo} \cdot (1 - F_{ind} + F_{ind} \cdot F_{loc}) \quad (1)$$

where E^{clo} is the effective dose, C is the air

concentration of radionuclide, DC^{clo} is the effective dose coefficient of cloud shine [3], F_{ind} is the indoor time fraction of 0.66, and F_{loc} is the dose reduction factor of 0.4 for indoors.

The effective dose of inhalation of radionuclides in the air was calculated as:

$$E^{inh} = \sum C \cdot V \cdot DC_{inh} \quad (2)$$

where E^{inh} is effective dose through inhalation, C is the air concentration of radionuclide, V is the breathing rate, DC_{inh} is the dose conversion coefficients [4].

3. Results & discussion

The total effective dose from cloud shine and inhalation pathways were shown in Table 2. The direction of N, NNE and NNW from the Kori nuclear site are the location of Ulsan. The effective dose of individual was the highest in 5 km and N direction from Kori as 3.8E-5 mSv.

Table 2. Effective doses as the direction and distance from the dispersion of Kori nuclear site (mSv)

Distance(km)	Direction		
	N	NNE	NNW
5	3.8E-05	3.5E-05	2.9E-05
10	1.8E-05	2.4E-05	1.7E-05
15	1.1E-05	1.3E-05	1.0E-05
20	6.0E-06	5.0E-06	5.0E-06
30	3.0E-06	4.0E-06	4.0E-06
40	3.0E-06	4.0E-06	3.0E-06

Table 3. Effective doses as the direction and distance from the dispersion of Kori and Wolsong nuclear sites

Distance(km)	Direction		
	N	NNE	NNW
5	4.7E-05	4.5E-05	3.8E-05
10	4.5E-05	5.5E-05	3.7E-05
15	3.0E-05	3.6E-05	2.8E-05
20	4.8E-05	8.1E-05	4.3E-05
30	6.9E-05	1.2E-04	4.6E-05
40	6.2E-06	2.7E-04	3.3E-05

Table 3 shows the effective doses as the direction and distance from the Kori nuclear site through the dispersion of Kori and Wolsong NPP. The effective doses were increased as the dispersion of Wolsong was considered. The location of NNE direction with 40 km was the highest because that location was 5 km far from the Wolsong NPP.

Although both dispersions from normal operation of Kori and Wolsong were considered, the effective doses were not exceed the 1 mSv which is the public dose limit.

4. Conclusion

The radiological impact in Ulsan due to the normal operation of both Kori and Wolsong was considered in this research because of the close distance from the nuclear sites using the atmospheric simulation. The highest effective dose was 2.7E-4 mSv which satisfied the legal limit.

The exposure from ground shine and ingestion pathways were not considered in this study. To calculate the effective doses of public more accurately, all the exposure pathways needed to be considered in the future research.

ACKNOWLEDGMENTS

This work was supported by the Korea Institute of Energy Technology Evaluation and Planning(KETEP) and the Ministry of Trade, Industry & Energy(MOTIE) of the Republic of Korea (No. 20151520302120).

REFERENCES

[1] Stohl, A.; Sodemann, H.; Eckhardt, S.; Frank, A.; Seibert, P.; Wotawa, G., "The Lagrangian particle dispersion model FLEXPART version 8.2", FLEXPART user guide, 2011.

[2] KHNP, "The investigation and evaluation report of environmetal radioactivity near the Nuclear power plant" (Korean), 2015.

[3] The International Commission on Radiological Protection. “The International Commission on Radiological Protection. Compendium of Dose Coefficients based on ICRP Publication 60”, ICRP Publication 119, Annals of the ICRP, 2012, Vol. 41(Suppl.).

[4] Eckerman, K. F.; Ryman, J. C. “External exposure to radionuclides in air, water, and soil”, FEDERAL GUIDANCE REPORT NO. 12, EPA-402-R-93-081, 1993.

Analysis of Inhalation Dose Rate to Workers in NORM Industries : Packing Area

Seung Woo Ji[1], Jung Hwan Jang[1], Il Park[1], Jae Kook Lee[2], and Kwang Pyo Kim[1*]

[1]Kyung Hee University, 1732 Deokyoungdaero, Giheung-gu, Yongin, Gyeonggi-do, Republic of Korea

[2]Korea Institute of Nuclear Safety, Gusongro, Yuseong, Deajeon, Republic of Korea

[*]kpkim@khu.ac.kr

1. Introduction

Internal exposure to workers can occur in industries handling naturally occurring radioactive materials (NORM) due to inhalation of airborne particulates containing radioactive materials. International Atomic Energy Agency (IAEA) suggested industry sectors as being the most likely to require some form of regulation consideration [1].

Inhalation dose to workers varies with particulate properties including airborne particulate concentration and radioactive concentration. It means that necessity of safety management may vary with exposure situation. Analysis of inhalation dose to the workers according to industry sector and working type is necessary to implement safety management to NORM industry.

The objective of this study was to analyze inhalation dose rate to the workers in NORM industries. We focused on packing area because workers at the area are highly exposed to airborne particulates. Analysis of inhalation dose rate was implemented for monazite, zircon, and bauxite industries in Korea.

2. Materials and Methods

The major processing area expected to generate airborne particulates was selected as packing area based on previous studies. In this study, we selected six facilities to analyze inhalation dose rate to the workers at packing area (Table 1).

Table 1. Six industries for inhalation dose assessment

Facility	Materials treated in the packing area
A, B	Product containing monazite
C, D	Product containing zircon
E, F	Product contacting bauxite

Airborne particulates concentration was measured by using cascade impactor. Airborne particulate was collected at a flow rate of 28.3 L/min.

The measurement of the radioactive concentration of materials taken from the packing area was performed using HPGe detector. Radioactive equilibrium of uranium and thorium decay series for the materials treated at packing area was assumed. Fig. 1 shows cascade impactor and HPGe detector that used in this study.



Fig. 1. Cascade impactor (left) and HPGe detector (right).

Inhalation dose rate to workers was calculated based on actual measurement data. Breathing rate was used as 1.2 m^3/h suggested by International Commission on Radiological Protection (ICRP).

3. Results and Discussion

Fig. 2 shows airborne particulate concentrations collected from six NORM facilities. Airborne particulates concentration ranged 0.067-0.511 μg/L. Airborne particulate concentration was the highest for facility B. It was the reason that ventilation system was not operated at the packing area for facility B.

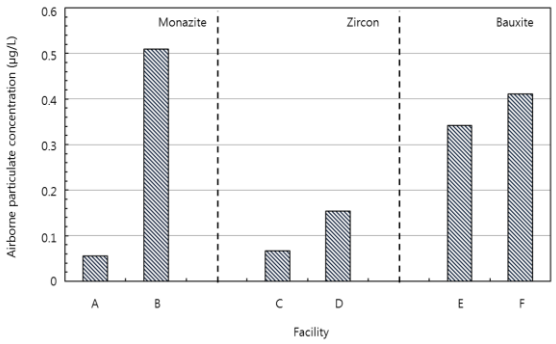


Fig. 2. Airborne particulate concentration in packing area for six NORM facilities.

Fig. 3 shows the radioactive concentrations. Radioactive concentration of material treated at packing area was 53.9-2,883 Bq/kg for uranium series and 145-11,900 Bq/kg for thorium series. Radioactive concentration of uranium decay series was the highest for zircon industry. In the case of thorium decay series, monazite treated in facility A was the highest.

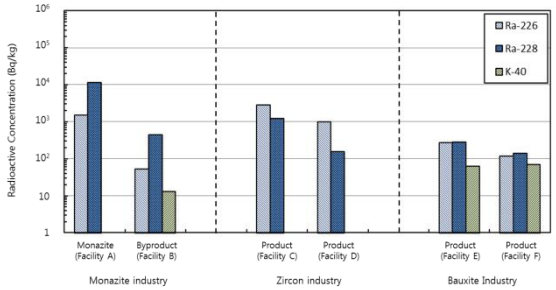


Fig. 3. Airborne particulate concentration in packing area for six NORM facilities.

Inhalation dose rate was calculated based on the particulates properties and exposure situation. Inhalation dose rate ranged 4.95×10^{-6} - 5.10×10^{-5} mSv/h. Inhalation dose rate was the highest at facility A as 5.15×10^{-5} mSv/h. It was reason that radioactive concentration of thorium decay series was up to 40 times higher than the other materials. The most difference of inhalation dose rate according to facilities was caused by airborne particulates concentration and radioactive concentration.

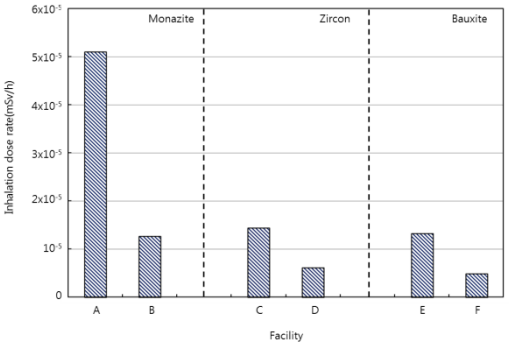


Fig. 4. Inhalation dose rate in packing area for six NORM facilities.

4. Conclusion

We analyzed the internal dose rate to the workers at packing area in NORM industries. Internal dose rate varied with airborne particulate properties. The results of this study can be used for characterizing radiation exposure at Korean NORM industries.

ACKNOWLEDGMENTS

This work was supported by a grant from “Establishment of Technical Basis for Implementation on Safety Management for Radiation in the Natural Environment” carried out by Korea Institute of Nuclear Safety.

REFERENCES

[1] IAEA, Assessing the Need for Radiation Protection Measures in Work Involving Minerals and Raw Materials, SRS 49 (2006).

[2] ICRP, Recommendations of the International Commission on Radiological Protection, ICRP 66 (1994).

Asia-Pacific ALMERA Group Proficiency Test and Intercomparison Exercise on the Determination of Gross-Alpha and –Beta and Gamma Radionuclides

C. S. Kim*, J. Y. Yun, and M. H. Song

Korea Institute of Nuclear Safety (KINS) Center for Environmental Radiation and Radioactivity Assessment (CERA), 62 Gwahak-ro, Yuseong-gu, Daejeon 34142, Republic of Korea

*cskim@kins.re.kr

1. Introduction

The KINS, as an ALMERA regional coordinator in the Asia-Pacific area since 2011, has been actively involved in the IAEA ALMERA activities [1]. In the regional group meeting, many Asia-Pacific members expressed their interest in the regional proficiency test (PT) or inter-comparison exercise like as IAEA PT campaign. The KINS organized from sample preparation except for soil to evaluation report.

The main task of the participating laboratories was to quantify the activity levels of ^{40}K, ^{134}Cs and ^{137}Cs in the soil and gross-alpha in the Styrofoam and gross-beta in the glass fiber filter. 14 laboratories from 11 countries participated in this campaign and reported to the KINS their results.

2. Sample Preparation

2.1 Gross-alpha (GA) sample (Styrofoam)

About Styrofoam was selected as bedding material for the alpha radiation source. ^{241}Am standard solution (NIST4332C) used as spiking solution on the surface of Styrofoam. The spiked solution was dried in the desiccator for 1 day, and then it was dried again under the IR ramp at a mild temperature. The homogeneity was tested and gave a satisfactory result.

Additional blank labelled GA-blank Styrofoam was prepared and delivered for background and efficiency.

2.2 Gross-beta (GB) sample (GF filter)

A diluted ^{90}Sr standard solution was spiked on the 47 mm diameter glass fiber (GF) filter which was fixed on a stainless steel planchette used for alpha beta counting. The ^{90}Sr solution was spiked on the surface of GF filter with a similar method used in the preparation of GA sample. Additional blank filter can be used for background and efficiency measurement.

2.3 Preparation of the natural soil

The raw material was collected and pretreated by the JCAC, and then it was transferred to the KINS. The homogeneity was tested by the KINS using the ANOVA method. The packing unit contains about 125 g of dried soil.

2.4 Homogeneity testing

A total of 8 sample bottles at 30 g sample intake for homogeneity test were selected randomly of the 25 bottles. In the ANOVA evaluation, the observed F values are less than the critical F values in both table, so we accept the null hypothesis and homogeneity in the soil sample [2].

3. Performance Criteria

The PT and inter-comparison testing scoring system applied were based on the IAEA evaluation method used in the ALMERA-PT-2015, which takes into consideration the trueness and the precision of the reported data, and it includes in the evaluation both the total combined uncertainty associated with the target value of PT testing samples and the total uncertainty reported by the participating laboratories.

4. Results and Discussion

4.1 Overall Evaluation

58 measurement results were reported to the KINS in this PT from 14 laboratories. The overall evaluation (Table 1) showed that 81% of all reported results were “Accepted” and 17 were “Not acceptable”.

Table 1. Data evaluation of Gross-alpha in spiked Styrofoam

	Gross-alpha	Gross-beta	K-40	Cs-134	Cs-137
Number of reported results	9	10	13	13	13
Acceptable (%)	67	50	92	85	100
Warning (%)	0	0	8	0	0
Not Acceptable (%)	33	50	0	15	0

4.2 Proficiency test

Tables 2 and 3 show that the distribution of results scored for Gross-alpha and Gross-beta. In the case of Gross-alpha, 3 reported results are deviated to the higher value from the target. For Gross-beta measurement, many laboratories showed a poor performance worse than gross-alpha measurement. 68% of the participant laboratories gave a "Not Acceptable" results. The main reason for these "Not Acceptable" results could be attributed to the underestimation of detector efficiency or unclarified problem in the calibration of the detector.

Table 2. Data evaluation of Gross-alpha in spiked Styrofoam

Lab. Code	Rep. Value	Rep. Unc.	Rel. Bias(%)	Accuracy	P	Precision	Final Score
12	5.68	0.29	1.61	A	7.94	A	A
14	5.45	0.06	2.50	A	6.18	A	A
15	6.8	0.4	21.65	NA	8.46	A	NA
16	4.77	0.16	14.67	A	6.95	A	A
18	5.2	0.14	6.98	A	6.65	A	A
20	6.9	0.02	23.43	NA	6.09	NA	NA
22	5.42	0.63	3.04	A	13.12	A	A
23	5.01	0.1	10.38	A	6.40	A	A
24	6.77	0.1	21.11	NA	6.26	NA	NA

* Target value: 5.59 ± 0.34, MARB: 15%

Table 3. Data evaluation of Gross-beta in spiked glass filter

Lab. Code	Rep. Value	Rep. Unc.	Rel. Bias(%)	Accuracy	P	Precision	Final Score
12	2.21	0.11	-3.07	A	7.90	A	A
14	2.19	0.04	-3.95	A	6.41	A	A
15	1.7	0.1	-25.44	NA	8.50	A	NA
16	2.36	0.08	3.51	A	7.01	A	A
18	1.15	0.05	-49.56	NA	7.52	A	NA
20	2.3	0.015	0.88	A	6.17	A	A
21	1.113	0.023	-51.18	NA	6.48	A	NA
22	1.02	0.18	-55.26	NA	18.68	NA	NA
23	2.3	0.08	0.88	A	7.06	A	A
24	1.49	0.03	-34.65	NA	6.46	A	NA

* Target value: 2.28 ± 0.14, MARB: 15%

4.3 Inter-Comparison exercise (Gamma radionuclides)

Fig. 1 shows the z-score evaluation results sorted by the laboratories code. Comparing to the PT test, these three gamma radionuclides results are mostly | z- Score | < 2. The ^{40}K results' evaluation demonstrated that just one laboratory is "Warning" and others are "Acceptable". While the evaluation of ^{134}Cs is a little worse than ^{40}K with one extremely low value, a mistake in the calculation procedure is suspected. The result for ^{137}Cs are all located within 2 in z-score without failure in performance.

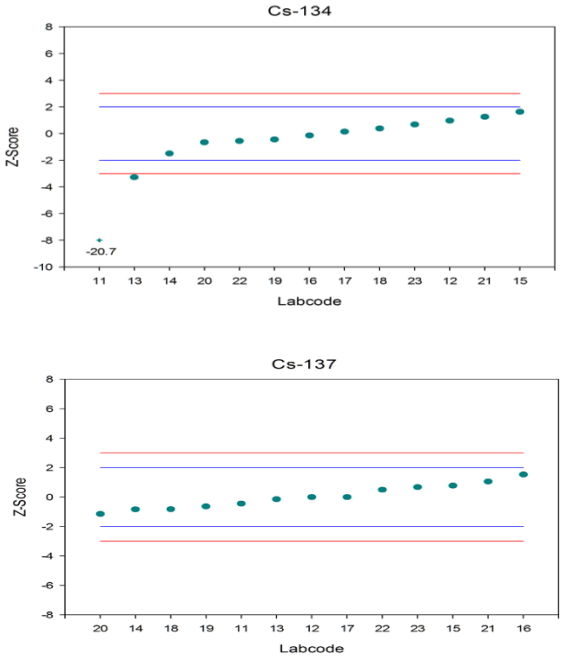


Fig. 1. z-scores in ^{134}Cs and ^{137}Cs in soil.

5. Conclusion

Overall, this exercise provided that the level of analytical performance of the Asia-Pacific ALMERA network members is good enough in the determination of three above gamma emitting radionuclides (for ^{40}K, ^{134}Cs and ^{137}Cs) in environmental soil. It is recommended, however, that a repeat of this exercise for the Gross-alpha and Gross-beta analysis be conducted at some time in the near future to provide an opportunity for laboratories to introduce proper corrective actions in the filter type of samples.

REFERENCES

[1] A. Shakhashiro, Z. Radecki, A. Trinkl, U. Sansone and T. Benesch, "Final Report on the Proficiency Test of the Analytical Laboratories for the Measurement of Environmental Radioactivity (ALMERA) Network", IAEA/AL/152, p.242, August 2005.

[2] Pagano, R. R. (2004). Understanding Statistics in the Behavioral Sciences (7th ed.) Belmont, CA: Thomson/Wadsworth.

Preliminary Studies on Reuse of Particle Accelerator Rooms After Decommissioning

Jae Min Lee, Na Yoon Choi, and Jae Hak Cheong*
Department of Nuclear Engineering, Kyung Hee University, Gyeonggi-do 17104, Republic of Korea
*jhcheong@khu.ac.kr

1. Introduction

Unlike diagnostic radiation generators using photons, the particle accelerator for radiation therapy and isotope production emits high-energy particle radiation. The structures and equipment in the accelerator room are to be activated by energetic particles, and the residents in the room will be exposed by the residual radioactivity present in the activated structures even after dismantling or relocation of the accelerator. As the number of particle accelerators reaching closer to the design-lifetime increases, verification of the acceptable residual radioactivity of the former accelerator rooms is becoming an important issue. Case studies on actual dismantling of particle accelerators have been reported in USA and a preliminary study on decommissioning planning criteria for a cyclotron was reported in Korea [1-3].

The site release criteria for major nuclear facilities after decommissioning are set forth in the NSSC Notice No. 2016-33, however particle generators are excluded from the scope of the Notice. Furthermore, no specific studies on the methodology to calculate the Derived Concentration Guideline Levels (DCGLs) for structures activated by particle accelerators have been reported.

In this study, we proposed three methodologies to derive DCGLs for the rooms to be remained after decommissioning of particle accelerators based upon residual radioactivity in terms of surface and volumetric contamination (i.e. Bq/m^2 or Bq/m^3).

2. Method & Calculation

2.1 Method I : DCGLs in Surface Radioactivity

In NUREG-1757 (Consolidated Decommissioning Guidance), derived site release criteria for buildings and soils are given in terms of surface activity and volumetric activity, respectively. Since the particle accelerator rooms belong to a building, a method to derive DCGLs in terms of residual surface activity can be assumed for a first.

In this study, RESRAD-BUILD code was used to calculate expected dose from remaining room surfaces (i.e. four walls, one ceiling, and one floor) and to derive DCGLs. However, simply assuming the volumetrically activated indoor structures as surface-contaminated surfaces may induce limitations of not taking into consideration of the exposure to be caused by the activated volume sources.

2.2 Method II : DCGLs in Volumetric Radioactivity

DCGLs in terms of volumetric activity may represent the radiological conditions of the remaining actual room structures activated by energetic particles very well. Method II is based on the assumption that the room structures of a certain depth are three-dimensionally activated. In this study, DCGLs were derived assuming homogeneous residual radioactivity in all surrounding indoor concrete structures by use of RESRAD-BUILD code.

It is expected that the surface region of structure is much highly activated than the innermost part of the structure. Therefore, DCGLs derived by Method II may be too much conservative if all structures are assumed to be activated at the same level of activity concentration. Due to the potential presence of various activation products in concrete, however, determination of DCGLs may be more complex than simple direct application of the available pre-set Default Screening Values (DSVs) in NUREG-1757.

2.3 Method III : Balanced DCGLs

Another approach to calculate dual DCGLs for external and internal exposures separately was reported in USA [1-2]. The rationale for this approach relies on the fact that volumetrically activated inner concrete layers mainly contribute to the external exposure pathway because the activation products are not available for intake. However, removable contamination layers on the surface of concrete structures may dominate the internal exposure pathway. Accordingly, they proposed the DCGL for external exposure (i.e. from activated concrete volume) in dose rate (μSv/h) and the DCGL for internal exposure (i.e. from removable surface contamination) in surface activity concentration (Bq/m^2) as shown in Table 1 and as below [1-2]:

$$\mathrm{DCGL_{external}} = 0.24\ \mathrm{mSv/y} \div 2360\ \mathrm{h/y} = 0.1\ \mu\mathrm{Sv/h}$$

In this study, the concept of "Balanced DCGLs" were proposed for which the site release dose constraint is proportionated to the separate DCGLs for external and internal exposure pathways, respectively, as appropriate in consideration of the actual conditions of the residual rooms as:

$$\mathrm{DC_{total}} = \mathrm{DC_{external}} + \mathrm{DC_{internal}}$$

$DC_{external} = \alpha DC_{total}$
$DC_{internal} = (1-\alpha) DC_{total}$
where, DC_{total} is the overall dose constraint,
$DC_{external}$ is the DC for external pathway,
$DC_{internal}$ is the DC for internal pathway, and α is the fraction appropriately balanced ($\alpha \leq 1$).

Table 1. Removable activity contribution to total dose

Nuclide	Annual internal dose			Removable activity equivalent to 1 mrem/y
	mrem per 0.1 Bq/m^2			
	inhalation	ingestion	total	Bq/m^2
^{60}Co	2.92E-03	1.75E-04	3.08E-04	3.24E+02
^{134}Cs	5.59E-04	4.32E-04	9.94E-04	1.01E+03
^{152}Eu	3.07E-03	4.38E-05	3.11E-03	3.22E+02
^{154}Eu	3.92E-03	6.35E-05	3.98E-03	2.50E+02

2.4 Assumptions to derive DCGLs

Based on the above three methods, RESRAD-BUILD code is used to calculate DCGLs for a hypothetical room geometry shown in Fig. 1. All surrounding structures are assumed to be ordinary concrete. The radionuclides formed from activation are assumed as ^{60}Co, ^{134}Cs, ^{152}Eu, and ^{154}Eu [1-2]. The location of the receptor is in the center of the room. The criteria for reuse of the site is assumed to be 0.1 mSv/y. Additionally, other input data such as ingestion rate, breathing rate, deposition velocity etc. are determined by referring to industrial practices and/or proper values for the situation.

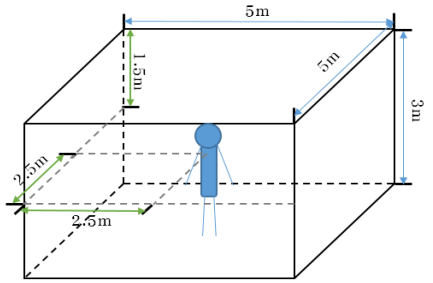


Fig. 1. Geometry in RESRAD-BUILD code.

In case of unit surface/volumetric activity, surface contamination is assumed to be 1 Bq/m^2 and volumetric activity concentration is assumed to be 1 Bq/g. The wall thickness was assumed to be 150 cm when estimating the DCGLs for volumetric activation situation. Occupancy factor is derived from the working time of 2000 hours per year.

3. Results

DCGLs derived by use of the three methods are shown in Table 2. In proportionating the contributions from internal and external pathways, α is set to 96%. That is 4% of the total dose constraint was assumed to be from internal exposure and 96% from external exposure. The value of α can be determined as appropriate taking into account the field conditions.

Table 2. Calculated DCGLs per each methodology proposed

		DCGLs			
		^{60}Co	^{134}Cs	^{152}Eu	^{154}Eu
Method I : Surface, Total (Bq/m^2)		1.52 E+04	2.47 E+04	2.80 E+04	2.59 E+04
Method II : Volumetric, Total (Bq/g)		5.98 E-02	1.09 E-01	1.30 E-01	1.21 E-01
Method III: Volumetric, Total	Surface, Internal (Bq/m^2)	6.82 E+02	6.27 E+02	5.11 E+02	4.17 E+02
	Dose rate, External (mSv/y)	0.096			

4. Conclusion

Three approaches to calculate DCGLs for the particle accelerator rooms remained after decommissioning were proposed. The Method 1 is best applicable for the non-activated surface contamination areas. Therefore, it is not suitable for the application to activated structures and devices. Method II, solely based on the volumetric contamination DCGLs, is most direct forward to derive values in using RESRAD-BUILD code. This method can be applied assuming that all the concrete structures are evenly activated to the depth. However, this method cannot reflect the fact that the extent of actually activated regions are not uniform in practice. Method III is very flexible because total dose constrain is to be proportionated into dual DCGLs for external and internal exposures. However, this method is practically applicable only when the derived are dose rate from proportionated external dose constraint can be discernable from the background radiation level of the remaining room areas. If the official site release criteria for the radiation facilities including particle accelerators are promulgated, applicable DCGLs for the dominantly activated room structures can be derived by use of either of Method II or Method III. The relative feasibilities of the two methods may vary depending on the actual conditions of the remained rooms such as the characteristics of the extent of activation, radioactivity measurement and survey techniques to apply, and the level of site release criteria, and so forth.

REFERENCE

[1] U.S. NRC, Pfizer Inc., Eclipse Cyclotron Facility Decommissioning Final Status Report, pp. 4-6A.
[2] U.S. NRC, PETNET Inc., RDS-112 Cyclotron Facility Decommissioning Plan (41-32720-04MD), May 25.
[3] Rina Woo, et al., Studies on the Introduction of Decommission Planning Criteria through Case Analyses of Relocation of Domestic Cyclotron and Overseas Decommissioning, Journal of Radiation Protection, 38(2), 2013.

Synthesis of Graphene Oxide Based Material for Removing Radioactive Iodine

Sangsoo Han*, Won-Seok Kim, and Wooyong Um

Division of Advanced Nuclear Engineering (DANE), Pohang University of Science and Technology (POSTECH), Pohang, Republic of Korea

*sshan1214@postech.ac.kr

1. Introduction

Radioactive iodines (125/129/131I) are released into environments during nuclear fuel processing, nuclear power plant operation and severe accidents such as Chernobyl and Fukushima. Environmental concern is mostly for ^{129}I due to its high toxicity and long half-life, $t^{1/2} = 1.6 \times 10^7$ years [1]. Usually, to remove the radioactive iodine, activated carbon based organic materials and silver exchanged zeolite were used as sorbents in aqueous phase. However, these materials have the limits in removal efficiency, cost, and high selectivity [2]. Therefore, this study investigated the bismuth functionalized graphene oxide (Bi-GO) to test high removal efficiency and selectivity of iodide and iodate species under the various Cl^- background solution conditions.

2. Methods

2.1 Synthesis of graphene based sorbent

To functionalize the sorbent, the graphene oxide (GO) has been synthesized from natural graphite powder (99.95%) by the modified Hummers method [3], and then graphene oxide was functionalized with $Bi_2O_3 \cdot 2H_2O$ in deionized water.

2.2 Characterizations

After synthesis, sorbent was characterized using X-ray diffraction (XRD) to identify the crystalline minerals, Scanning Electron Microscope (SEM) / Energy Dispersive Spectrometer (EDS) for microstructure and elemental chemistry of samples, and Fourier transformed-infrared (FT-IR) for the functionalized group identification.

2.3 Iodine removal experiments

Iodine batch adsorption experiments were conducted using a 10 mL glass amber vial with non-radioactive iodine solutions such as iodide (I^-) and iodate (IO_3^-). The Bi-GO (0.05 g) was mixed with 10 mL of Cl^- (1, 10, and 100 ppm) background solutions with different iodide or iodate concentrations (0.1, 1, and 4 ppm). Using Bi-GO, iodine adsorption experiments were carried out for different reaction times (15 min, 30 min, 1 h, 1 day, 3 days, and 7days) to check the adsorption kinetics. After each reaction, the supernatants were separated by syringe filter (0.45 μm). The final concentration of iodine in batch solution was analyzed by Inductively Coupled Plasma Mass Spectrometry (ICP-MS). The removal efficiency of iodine and the results were compared with 35% silver exchanged zeolite from Sigma Aldrich.

3. Results & Discussion

3.1 Characterizations

Graphene oxide is a layered material consisting of hydrophilic oxygen functional groups on their basal planes and edges. The bismuth-functionalized graphene oxide used in this study was a major sorbent material from the synthesis of bismuth and graphene oxide; photographic images of the graphene oxide and bismuth-functionalized graphene oxide samples are shown in Fig. 1.

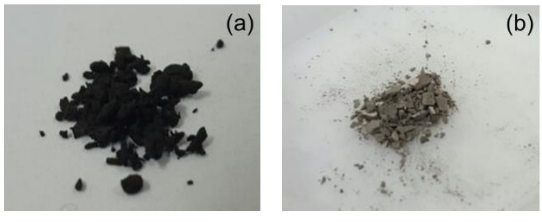


Fig. 1. (a)Graphene oxide and (b) Bismuth-functionalized graphene oxide.

After functionalization, graphene oxide color has been changed from deep black to light grey.

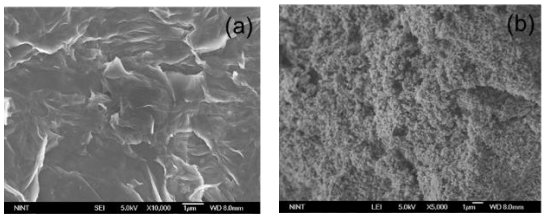


Fig. 2. SEM images of (a) graphene oxide and (b) bismuth-functionalized graphene oxide.

In Fig. 2, SEM images showed the morphology of the graphene oxide and the presence of functionalized bismuth on graphene oxide surfaces. The bismuth in these images appears to adhere to the surface of the graphene oxide, forming discrete Bi particles.

3.2 Iodine removal efficiency

The results of iodine removal experiments under the Cl^- background solution condition and iodine initial concentration (4 ppm) are presented in Fig. 3. These experiments were performed to compare the removal efficiency between the developed material and commercial Ag-zeolite sorbents. The grapheme oxide based material with Bi presented high removal efficiencies (≥95%) for iodide and iodate regardless of background solution concentrations. In contrast, the Ag-zeolite showed similar tendencies for iodide without effect of background solutions. However, removal efficiencies for iodate was decreased to less than 25% with increasing Cl^- concentrations in Ag-zeolite.

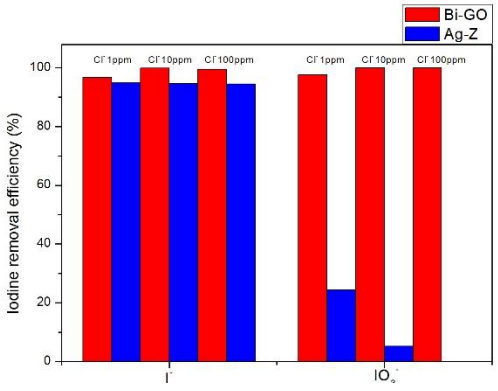


Fig. 3. Selective adsorption for iodide and iodate under the Cl^- background solution condition.

These results suggest that the bismuth-functionalized graphene oxide demonstrate higher iodine removal performance (especially for iodate) than the Ag-zeolite and the possibility of selective iodine removal from wastewater containing various radionuclides generated from severe accident or operation of nuclear power plant.

4. Conclusion

In summary, we report bismuth-functionalized graphene oxide synthesis as novel absorbent for iodine removal and compare the results with the commercial Ag-zeolite under different ionic strength conditions. The bismuth based materials show higher iodine removal efficiencies (≥95%) than Ag-zeolite for iodide and iodate. In contrast, the Ag-zeolite has a limitation for removal capacity for iodate. Our study provides potential role of the grapheme based material on selective removal of both radioactive iodide and iodate in wastewaters.

REFERENCES

[1] K.A.Schwehr, P.H.Santschi, D.I.Kaplan, C.M.Yeager and R.Brinkmeyer “Organo-iodine formation in soils and aquifer sediments at ambient concentrations”, Environ, Sci. Technol., 43, 7258–7264 (2009).

[2] Haefner DR and Tranter TJ. “Methods of gas phase capture of iodine from fuel reprocessing off-gas: a literature survey”, Idaho National Laboratory, INL/EXT-07-12299 (2007).

[3] Hummers WS and Offeman RE J Am “Preparation of Graphitic Oxide”, J. Am. Chem. Soc., 80(6), 1339-1339 (1958).

Leak Path Factor Calculation of RIPF Hot-cell During an Accident

Goanyup Lee*, Bongseok Kim, Hyunki Kim, Haecho Lee, Jongsoo Kim, and Munja Kang
Korea Atomic Energy Research Institute, 111, Daedeok-daero 989beon-gil, Yuseong-gu, Daejeon, Republic of Korea
*gylee@kaeri.re.kr

1. Introduction

Korea Atomic Energy Research Institute (KAERI) produce various radioisotopes at hot-cell facility in Radioisotope Production Facility (RIPF). The RIPF building has 4 hot-cell banks to produce each radioisotope [1]. Emergency Preparedness Act in Korea demands emergency plan for the licensee who operates the facility producing radioisotope more than 18.5PBq. The RIPF at KAERI produce radioisotope more than 18.5PBq in a year, but the 18.5PBq of radioisotope are distributed in 1 year period at each hot-cell banks during the production. It means that there is no chance having 18.5PBq radioisotope in a same time at RIPF building. RIPF SAR only considers a stack release during an accident. RIPF stack has a 68m height, so the radioactive materials released through the stack will be diffused in air. In case of stack release, there is no needs to respond in a point of view of emergency protective action. U.S. DOE requests to calculate source-term by a building leakage of the facility handling radioactive materials, and suggest methodology to get Leak Path Factor (LPF) by building leakage using MELCOR computer code [2]. The LPF of RIPF hot-cell during an accident was calculated by using MELCOR code and the characteristics was analyzed.

2. Method description

2.1 Major factors to get the source-term

Source-term in a nuclear facility can be calculated by using under equation.

$$ST=MAR \times DR \times ARF \times RF \times LPF$$

Where,
ST = Source-term
MAR = Material at Risk
DR = Damage Ratio
ARF = Airborne Release Fraction
RF = Respirable Fraction
LPF = Leak Path Factor

RIPF can handles and produces about 100 radionuclides in hot-cells based on the license. Each radionuclide is handled in a batch process, and the each batch has maximum amount to treat, so an accident considers the maximum amount of a radionuclide processed at a hot-cell bank. In a point of view of emergency preparedness, only enough amount which can cause a harm of a human outside is interested. RIPF SAR chose 8 nuclides, the maximum batch amount (MAR) of each nuclides, and the accident type possible. So the accident condition in SAR was applied here also. But the RIPF SAR didn't consider DR, ARF and RF, sot these values reviewed through the technical documents from IAEA, U.S.DOE, and determined as Table 1.

Table 1. Major values to calculate the RIPF source-term

Bank No.	Nuclide	Accident Type	MAR (Ci)	DR	ARF	RF
1	Co-60	Fire	50,000	1	0.001	1
	Ir-192		100,000	1	0.001	1
	Yb-169		100	1	0.01	1
	Se-75		1,000	1	0.01	1
3	I-125	Spill	10	1	0.01	1
	I-131		60	1	0.01	1
4	Mo-99 Tc-99m	Spill &Fire	700	1	0.01	1

2.2 MELCOR input design to get LPF

LPF of a building can be calculated by MELCOR simulation. To get the LPF by MELCOR simulation, the building structure should be designed as a numerical data, to accomplish this, the RIPF building structure was investigated and measured on the design drawing. After this procedure, all rooms and doors of RIPF building were designed and defined for the generation of the MELCOR input file. For

example, the definition drawing of the first floor of RIPF building as a result is described as Fig. 1.

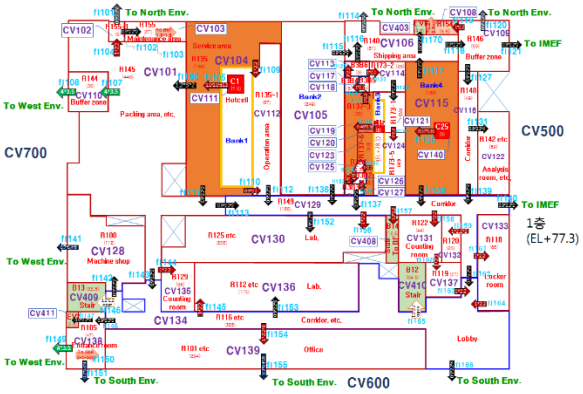


Fig. 1. Definition drawing of RIPF 1st floor for MELCOR input.

2.3 Scenario input for simulation

To simulate the effect of winds outside of the RIPF, 5 m/sec which was the maximum wind speed measured for recent 4 years at 10m height was considered as scenario input file. Normally the heat generated by a fire can reach to 1200℃, so the energy generated by a fire at hot-cell bank was also considered to simulate the effect of 1200℃.

3. Results and discussion

The diffusion of 1 kg radioactive element at each hot-cell bank for 10 sec in a fire condition was simulated as it was 5 m/sec wind from each direction outside RIPF building.

3.1 Effect of fire and wind during release

LPF of Co-60 from hot-cell bank 1 for 10hr at each wind direction and a fire was described as Fig. 2.

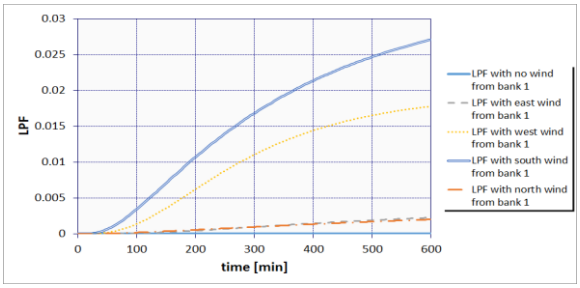


Fig. 2. LPF form hot-cell bank 1.

In the result, the maximum LPF was found when the wind from south and a fire were applied, but the effect of fire was negligible.

At a fire and 5m/sec wind from south, the LPF of each element from bank 1 was described as Fig. 3.

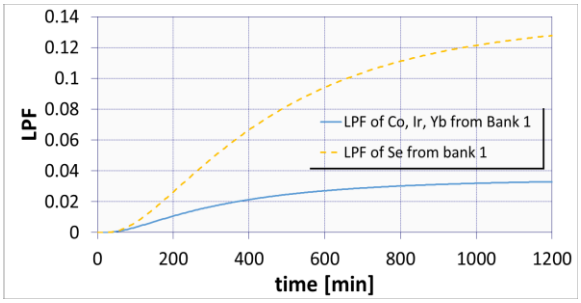


Fig. 3. LPF of each element from bank 1.

All LPF values calculated from each hot-cell bank were described as Table 2.

Table 2. LPF of all nuclide considered at each bank

Bank No.	Nuclide	LPF
1	Co-60, Ir-192, Yb-169	0.033
	Se-75	0.13
3	I-125, I-131	0.28
4	Mo-99/Tc-99m	0.042

As a result, the bank 3 shows the maximum LPF value, but the maximum source-term appears from Ir-192 at bank 1 because of the biggest MAR.

4. Conclusion

The LPF of RIPF hot-cell at KAERI was calculated by using MELCOR code. The maximum source-term was found from bank 1, but the maximum LPF was found from bank 3. These results will be used for dose assessment for the optimization of the emergency preparedness of RIPF hot-cell accident at KAERI.

REFERENCES

[1] "HANARO Safety Analysis Report", Chapter 11, Korea Atomic Energy Research Institute, 2016.

[2] "MELCOR Computer Code Application Guidance for Leak Path Factor in Documented Safety Analysis", Final Report, U.S. Department of Energy, 2004.

A Study on the Correlation Between Earthquakes and Nuclear Power Plants Analyzed Using SNS Big Data

Seungkook Roh[1*], Ik Jeong[1], Yongjun Kim[2], Kibo Sim[2], and Jaesung Lee[3]

[1]Korea Atomic Energy Research Institute,lll,Daedeok-daero 989beon-gil, Yuseong-gu, Daejeon, Republic of Korea

[2]KNEA, 1418 Nambusunhwanno, Geumcheon-gu, Seoul, Republic of Korea

[3]GoGreat, 551-24, Yangcheon-ro, Gangseo-gu, Seoul, Republic of Korea

[*]skroh@kaeri.re.kr

1. Introduction

Several earthquakes occurred in Korea in 2016. These earthquakes were large enough to instill a fear of nuclear power plant accidents in Koreans owing to the influence of Fukushima in Japan [1]. Several media outlets have reported a great deal about earthquakes and nuclear power plants, but it was not enough to specifically tell how the public opinion has changed in real time. A big data analysis is a very useful methodology to solve these problems and to explain these situations. This study analyzed the reactions of the Korean people to earthquakes and nuclear power plants using an SNS Big Data Analysis Method.

2. Methodology and Data

2.1 Methodology

The method of analyzing atypical big data has a great advantage in the collection and analysis of people's unfiltered thoughts in real time [2]. While many analytical methodologies have focused on revealing causal relationships in the past, big data analytic methods find their meaning through correlations. First, the SNS analysis method is used to collect and analyze contents related to an online SNS and newspaper articles such as Twitter and Facebook. Second, the analysis method mainly consists of a statistical correlation analysis or visualization analysis [3].

2.2 Data

For a big data analysis, this study collected data from various online SNSs and media such as Twitter, Naver blog, and Facebook (the data were collected by GoGreat). The data collection period was from January 1, 2016 to December 14, 2016.

The amount of data related to nuclear power and earthquakes during this period were 4,735,492 for Twitter, 1,552,638 for Naver, and 43,430 for other media. After removing the meaningless data, 367,743 Twitter, 31,281 Naver, and 3,833 media data were analyzed.

3. Results and Discussion

Fig. 1 shows that the occurrence of earthquakes is highly correlated with nuclear power plants. Normally, the average data generation of nuclear power plants is between 600 and 800. However, when an earthquake occurred in Kumamoto in April 2016, 47,000 earthquake-related data occurred, and at the same time, 8,000 nuclear power plant data were generated. In July 2016, when an earthquake occurred in Ulsan, 47,000 earthquake-related data occurred, and 12,000 nuclear power plant data were generated. When an earthquake occurred in Gyeongju in September 2016, 280,000 earthquake-related data occurred, and 42,000 nuclear power plant data were generated, simultaneously.

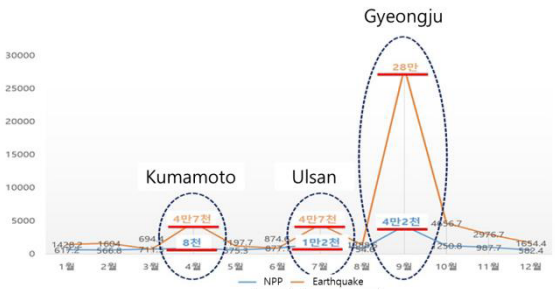


Fig. 1. Data trends for earthquakes and nuclear power plants in 2016.

As shown in Fig. 2, 2,188 data were generated 95 times within 2 hours from 20:33 at the time of the earthquake in Ulsan. The amount of data decreased sharply, and after 4 hours, the data amount reached a normal level.

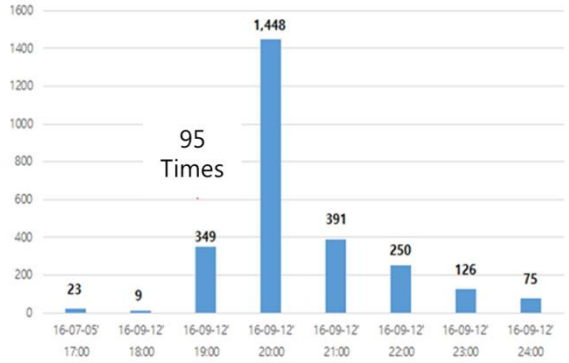


Fig. 2. Data trends for earthquake in Ulsan.

As shown in Fig. 3, 5,291 data were generated 264 times within 2 hours from 20:32 at the time of the earthquake in Gyeongju. The amount of data decreased gradually after 3 hours.

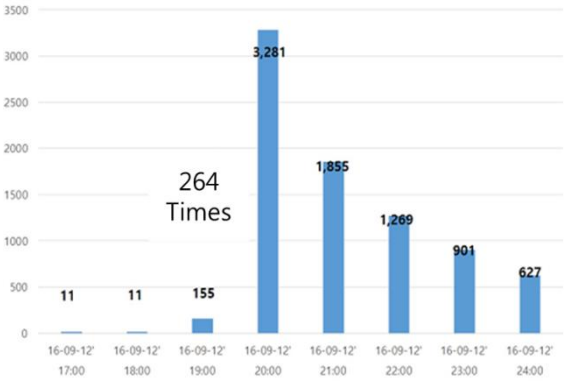


Fig. 3. Data trends for earthquake in Gyeongju.

4. Conclusions

The above results show that many people simultaneously express their opinions about nuclear power plants when an earthquake occurs. In particular, it can be seen that when an earthquake occurs in Korea, it results in more opinions about nuclear power plants. In addition, this study found that the date of the earthquake and nuclear power plant mostly occurred within 2 hours after the earthquake. Based on these results, this study suggests the following policy implications.

First, nuclear power plants will have to provide sufficient safeguards to ensure that the public can be assured after an earthquake.

Second, the government should disclose the safety of nuclear power plants through an online SNS and the media within two hours after an earthquake.

This study analyzed the correlation between earthquakes and nuclear power plants using atypical big data and suggested policies for it. In addition, this study did not conduct an emotional analysis of people regarding earthquakes and nuclear power plants. The limitations of this study are not comparing the data generated by each region. These limitations will be dealt with in future studies.

REFERENCES

[1] Simons, M., et al., The 2011 magnitude 9.0 Tohoku-Oki earthquake: Mosaicking the megathrust from seconds to centuries. science, 2011. 332(6036): p. 1421-1425.

[2] Roh, S., Big Data Analysis of Public Acceptance of Nuclear Power in Korea. Nuclear Engineering and Technology, 2017.

[3] Chen, M., et al., Big data analysis, in Big Data. 2014, Springer. p. 51-58.

6분과

방사선환경 및 안전 (Poster)

Development of Radiation Emergency Movable Access Control System

Cheol Hyun Kang[1*], Jung Bok Lee[2], Jang-Lyul Kim[1], and Jong Il Lee[1]

[1]Korea Atomic Energy Research Institute, 111, Daedeok-daero 989beon-gil, Yuseong-gu, Daejeon, Republic of Korea

[2]University of Science and Technology, 217 Gajeong-ro, Yuseong-gu, Daejeon, Korea

[*]chkang1@kaeri.re.kr

1. Introduction

When radiation workers work in radiation emergency situation, it is essential to set radiation controlled area, and control the access [1].

There are several risks, like missing record sheet, write down mistakes when workers misunderstand the record sheet forms, if workers use already printed record sheet. Therefore, it is necessary that access control system has to be taken into account, especially for the emergency time.

Particularly, when radiation emergency happens, it is difficult to use static access control systems due to the changeable condition. In addition, it is more useful that battery backups are equipped for the power dissipation accident.

Furthermore, the access control system in radiation emergency has to be user friendly system used for workers who are not used to handle the system.

The ICRP 103 Recommendation suggests people who work during the radiation emergency, are restricted the radiation exposure [2]. For this occasion, radiation workers use personal dosimeters to be alerted with alarms they set. Sometimes, it is difficult because there are variety of personal dosimeters which have numerous methods of setting alarms and inexperienced workers. Therefore, it is more valuable for workers put alarm setting function in the access control system.

In this study, Radiation Emergency Movable Access Control System (REMACS) has been developed for replacing the record sheet of radiation emergency with Remtech Co.

2. Main title

2.1 The physical composition of REMACS

The REMACS is consist of a tablet computer which has a program for access control and manipulating EPD (Electronic Personal Dosimeter, Thermo Fisher Scientific), four adaptors for accessing EPDs, a rechargeable battery backup module, keyboard to input access data, and two USB ports to connect printers and an USB sticks (Table 1).

Table 1. Specification of REMACS

Item	Specification
Tablet	· CPU : Intel dual core · RAM : 4G · HDD : 60GB SSD · Display : 10.4“ Touch LCD
Interface	· RJ45 Ethernet · USB Port 2EA
IR Reader	· For EPD 4 EA
Power Source	· AC 220 · DC 12V(Chargeable)

There are under four people can be taken access process with four ports that REMACS has. Furthermore, the rechargeable batteries can be replaced with the other ones if the performance of machine is deteriorated. A TFT LCD touch screen provides simple GUI as long as keyboard it has cannot provide. The Fig. 1 below shows the 3D Design of REMACS

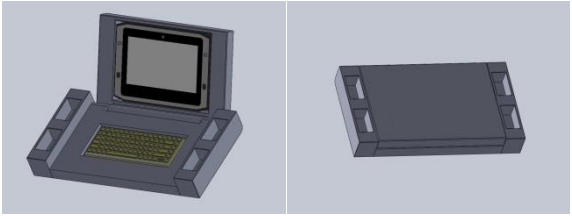


Fig. 1. The 3D Design of REMACS.

2.2 Developing REMACS Program

Four personal dosimeter slots can be managed by the REMACS program individually or simultaneously. As a result, under the four people can easily manipulate the personal dosimeters and rapidly check in or check out the active area.

In addition, when radiation workers check out the radiation zone, they can check radiation exposure with graphs which REMACS Program has been made. It can help the workers figure out when or where they have highly got the radiation exposure.

Lastly, after the events, managers can confirm the record of check-in and check-out of workers. Besides, they can save the record, and print it out. Therefore, it is not necessary for mangers to prepare the extra forms for recording the access and radiation exposures of workers.

Fig. 2 shows the main screen of REMACS Program. It displays the capacity of a battery, selecting the slots of personal dosimeters, selecting the menu related with the access and the radiation exposure of workers.

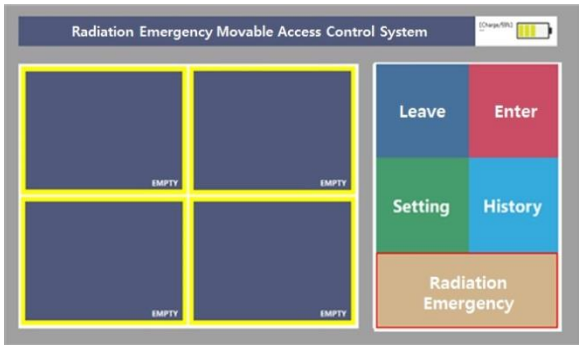


Fig. 2. The Main Screen of REMACS.

2.3 The Process of REMACS

2.3.1 Personal Dosimeter Alarm Setting. Before workers go into the radiation zone, they set personal dosimeter with REMACS. This function simplified the Electronic Personal Dosimeter (EPD, Mk 2.5, Thermo Fisher Scientific) management system, "Easy EPD" to make user friendly environment.

2.3.2 Check in and Check out Process. The record of check-in starts with putting personal dosimeters into the slots, and then workers put personal information on the program. After finishing their works, put personal dosimeters into the slots again and touch the check-out button so that they exit.

2.3.3 Confirmation of Access records. Total work hours, maximum and minimum radiation rates which personal dosimeters recorded, total radiation exposure workers got can be founded in access records. Graphs and *.txt files have been made depending on radiation exposure and work hours. Furthermore, *.txt files shows exact radiation doses and radiation rates depending on time.

3. Conclusion

In this study, Radiation Emergency Movable Access Control System (REMACS) has been developed, and it is assessed whether REMACS can be adoptable in the radiation emergency field.

REMACS can manage entrance and exit in radiation emergency site without continuous electrical power supply. With battery backups, it can be operated for certain period.

In addition, user friendly screen has been made to make utilization handy even when workers are not experienced and the urgent situation.

This equipment is not only managing check-in, check-out process, but also managing radiation dose of workers and personal dosimeters.

Without copying forms, bringing the handy REMACS can produce various documents related with access of workers.

REFERENCES

[1] IAEA, "Preparedness and Response for a Nuclear or Radiological Emergency", pp. 25-27 (2002).

[2] ICRP, "The 2007 Recommendations of the international Commission on Radiological Protection" (2007).

Gap Analysis Between the National Arrangements on Emergency Preparedness and Response and IAEA GSR Part7

Youngmin Lee*, Seung-Young Jung, and Namyoung Kim

Korea Institute of Nuclear Safety, 62, Gwahak-ro, Yuseong-gu, Daejeon, Republic of Korea

*k722lym@kins.re.kr

1. Introduction

In 2015, IAEA published the revised safety requirements in emergency preparedness and response (EPR), IAEA Safety Standards Series No. GSR Part 7. It includes the update developments on the nuclear or radiological emergency preparedness and response, the experience and lessons learned from the Fukushima accident, and the 2007 recommendations of the International Commission on Radiological Protection (ICRP). Korea EPR arrangements have been taken into account the GS-R-2 and the related IAEA safety guidelines. In this paper, gap analysis between GSR Part 7 and Korean EPR arrangements on the EPR strategy was conducted to take into account the revised requirements in emergency preparedness and response system.

2. Structure and contents of GSR Part 7

2.1 Major updates from GS-R-2 to GSR Part 7

The requirements of GSR Part 7 [1] are comprised of 3 categories of requirements, which are general requirements (5), functional requirements (14) and requirements for infrastructure (7), guidance values for restricting exposure of emergency workers and generic criteria for use in emergency preparedness and response.

Major updates from GS-R-2 [2] to GSR Part 7 are as follows.

2.2 New or strengthened concepts in GSR Part 7

The new or strengthened concepts in GSR Part 7 are Interface with nuclear security in EPR; Protection strategy and the role of different dosimetric concepts (generic criteria, operational criteria and reference level); Protection of emergency workers and helpers in an emergency; Termination of a nuclear or radiological emergency; Waste management following a nuclear or radiological emergency; International assistance in EPR; Emergency management system; Graded approach in EPR with focus on the hazard assessment and emergency

Table 1. Updates from GS-R-2 to GSR Part 7

GS-R-2	GSR Part 7
General Requirements	
Basic Responsibility	***Emergency management system***
	Roles and responsibility
Threat assessment	Hazard assessment
	Protection strategy
Functional Requirements	
Carrying out urgent protective actions	Taking urgent protective actions and ***other response actions***
Protecting emergency workers	Protecting emergency workers and ***helpers in an emergency***
Carrying out countermeasures (agriculture, ingestion, longer term protective actions)	Taking early protective actions and ***other response actions***
	Managing radioactive waste in an emergency
Conducting recovery operations	***Terminating an emergency***
-	***(NEW) Requesting, Providing and receiving international assistance for EPR***
-	***(NEW) Analysing the emergency and the emergency response***
Requirements for Infrastructure	
Organization	Organizations and ***staffing*** for EPR

planning zones and distances; and System for placing radiological health hazards in perspective.

IAEA has the plan to provide technical documents to support the revised requirements implementation and has been developing Safety Standards and EPR Series publications such as Termination of emergency, communication with the public and so on. Through adoption of the revised safety requirements, IAEA intends to establish the EPR arrangements for adequate level of preparedness and response for a nuclear or radiological emergency.

2.3 Identified gaps in protection strategy

GSR Part 7 requires to develop the protection strategy justified and optimized in the preparedness stage. Protection strategies are developed by considering two dosimetric concepts: first is reference level in terms of residual dose and second is generic criteria in terms of projected dose and received dose. Generic criteria in terms of projected dose is impossible to be measure directly. Therefore, generic criteria is needed the operational criteria; operational intervention levels (OILs), Emergency action levels (EALs) and Observable indicators.

Reference level isn't applied yet. Korea has been studying the adoption of 2007 recommendations of ICRP and according to these result, reference level of emergency situation also would be set.

Current protection strategies of EPR system in Korea are based on intervention level to be regarded as projected dose. Standards for determining urgent public protective actions such as evacuation, sheltering, administration of thyroid blocking agent are determined according to the Act on Physical Protection and Radiological Emergency (APPRE). The values of standards for determining urgent public protective actions are estimated by using simulation code and they are not directly measured values. Therefore, after radioactive release, according to the characteristics of emergency stage, OILs should be set to allow for effective emergency response, derived from generic criteria and agreed upon in the preparedness stage. Current OILs are based on Generic procedures for monitoring in a nuclear or radiological emergency (TECDOC-1092) and have some problems for example plum survey. So it should be revised by applying the new documents which are Use in Preparedness and Response for a Nuclear or Radiological Emergency (GSG-2) and Operational Intervention Levels for Reactor Emergencies (EPR-NPP-OILs).

3. Conclusion

In this paper, we identified the gaps of the revised requirements in protection strategy. Identifying the gaps between GSR Part 7 and Korean EPR arrangements and reflecting the results in the legislation and manuals can strengthen the EPR system and contribute to make practical and efficient national EPR framework.

REFERENCES

[1] INTERNATIONAL ATOMIC ENERGY AGENCY, Preparedness and Response for a Nuclear or Radiological Emergency, IAEA Safety Standards Series No. GSR Part 7, IAEA, Vienna, 2015.

[2] INTERNATIONAL ATOMIC ENERGY AGENCY, Preparedness and Response for a Nuclear or Radiological Emergency, IAEA Safety Standards Series No. GS-R-2, IAEA, Vienna, 2002.

The Evaluation of Radiation to Zinc Injection of Pressurized Water Reactor(PWR)

Hee-Gyeong Kim*, Min-Soo Kim, Dong-Kyu Jang, and Cheol-Young Jeong
ACT-RMT 11-3, Techno 1-ro, Yuseong-gu, Daejeon, Republic of Korea
*kimhphp@ssu.co.kr

1. Introduction

Recently, due to the increase in the number of years of operation and the extension of the life span of NPPs in Korea, accumulation of radioactive corrosion products in the primary system has caused the increase of radiation exposure of workers during the O/H (Overhaul).

In the case of overseas, it has started in the mid-1990s with US Farley 2, as of October 2011 a slight amount of zinc (5 to 40 ppb) was injected into RCS from 76 PWRs (PWR 29%)[Fig. 1]. Consequently, the radioactive corrosion products (Ni, Fe, Co, etc.) existing in the corroded oxide film of the primary system were stabilized by displacement reaction, so the corrosion was delayed and radiation exposure was reduced.

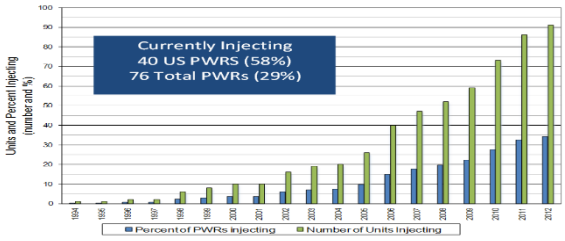


Fig. 1. Foreign PWR reactor coolant zinc injection status.

In the initial stage after the zinc injection, the increase in the amount of corrosion products affects the loads of treating waste water in RCS.

However, the results of applying continuous zinc injection and dense mesh filter, we could see the reduction of radiation dose more than 30% before & after injection at the points of loop piping and channel heads of SG (steam generator) in Hanul unit #1.

In this paper, we study the effects of zinc injection on the management of radiation safety and what should be considered for better management of radiation safety.

2. Main Subject

2.1 The formation process of radioactive products

The main cause of the formation of the radioactive product is that corrosion oxide on the internal surface is moved to the core in the primary coolant. So, it is activated and the radioactive corrosion oxide is left from the core and re-deposited on the pipe surface in the system.

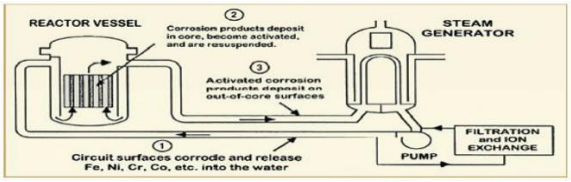


Fig. 2. Formation process of radioactive product.

In addition, the oxide film formed in the RCS is divided into inner and outer part. Firstly, the inner oxide film exists as a general spinel compound in the form of chromite. It is relatively stable in the coolant water. Secondly, the external oxide film is formed to outward. It is located at the outermost part of the oxide film of the system and directly contact with the reactor coolant.

Table 1. Composition of Corrosion oxide

	deposited oxide			grown on oxide			
Oxide / Cation	Fe_3O_4 (Magnetite)	Fe_2NiO_4 (Nikel Ferrite)	NiO (Nikel Oxide)	$Fe_{3-x-y}Ni_xCr_yO_4$ (Mixed Ferrite Chromite)	$FeCr_2O_4$ (Iron Chromite)	$NiCr_2O_4$ (Nickel Chromite)	Cr_2O_3 (Chromia)
Fe^{2+}	33.6	0	0	(1-x)/3×100	33.3	0	0
Fe^{3+}	66.6	66.6	0	(1-y)/3×100	0	0	0
Ni^{2+}	0	33.3	100	x/3×100	0	33.3	0
Cr^{3+}	0		0	y/3×100	66.6	66.6	100

2.2 Analysis of change of dose rate before & after zinc Injection

Zinc was continuously injected in the form of zinc acetate aqueous solution in RCS (concentration: 5 ppb, average : 14 g/day) and the location of injection is at the pipe between the charging pump and VCT of the CVCS system.

Table 2. Zinc (Zn) injection amount per cycle

operating cycle	Zinc injection cycle	Period of operation	Period of Zinc injection	Average concentration of Zinc injection	Total amount of Zinc
17cycle	1cycle	'09.03 ~ '10.08	'10.04~'10.08 (129days)	5.6 ppb	1.8 kg

Standardized and stable dose measurement is required to evaluate dose rate of the system before & after zinc injection. So, in order to reduce the measurement error and obtain a stable dose rate, standardized method should be considered for the location of measuring dose rate, the time of measurement and equipment of measurement. For method of standardized dose measurement, SRMP (Standard Radiation Monitoring Program, TR-1015119_ Nov.2007) was applied. The SRMP proposed by EPRI is standardized method to measure dose rate for each type of NPPs.

In order to obtain the dose rate of the same condition for each cycle, firstly, the time of measuring the dose rate at the loop piping was immediately after the end of the oxidation ditch (OD) process during OH (Overhaul) satisfying the drainage condition. Secondly, the time of measuring the dose rate at the channel head of the SG (steam generator) was immediately after opening the SG 'Man-way' (just before nozzle dam installation) within three weeks after plant shutdown. In addition, measuring points of dose rate were located in loop Piping (15 measuring points) and channel heads of SG (36 measuring points) in RCS.

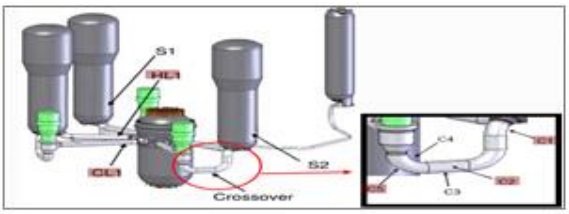


Fig. 3. The points of dose rate measurement at reactor coolant Loop Piping.

In conclusion, points of dose rate were reduced by 31.7% after one cycle zinc injection and the phenomenon of dose reduction occurred overall in the system. This effect was confirmed by the fact that zinc injection can reduce the dose rate without being restricted by the size, shape and physical accessibility of the system respectively.

Table 3. Comparison of dose rate before and after zinc injection

Cycle	Total dose of RCS Loop piping	Total dose of SG water box	Average reduction rate
OH 116 (before Zinc injection)	9.40 mSv/hr	1101.00 mSv/hr	31.7%
OH 117 (after Zinc injection)	6.41 mSv/hr	752.20 mSv/hr	
Reduction amount(%)	2.99(31.8%)	348.8(31.6%)	

2.3 Effect and consideration on radiation safety management by injecting Zinc

As can be seen from the above results, the major consideration on management of radiation safety in reduction of dose rate after zinc injection is to reevaluate the dose rate of the workplace in RCS and to reduce the number of workers considering the reduction of the shielding volume during OH (Overhaul)

3. Conclusion

The zinc injection of the first NPP in Korea was carried out in Hanul unit #1 at the 17th cycle starting from april 2010. It was found that the effects of dose reduction through displacement reaction of Zinc injection in the corrosion products of RCS. It is considered to be highly applicable to future technologies of dose reduction and expected to contribute to management of dose exposure to workers and improvement in management of radiation safety.

REFERENCES

[1] Pressurized Water Reactor Primary Water Zinc Application Guidelines, EPRI, Palo Alto, 2006, 1013420.

[2] Pressurized Water Reactor Primary Water Chemistry Guidelines: Volume 1, Revision 6, EPRI, Palo Alto, CA: 2007. 1014986.

[3] PWR Operating Experience with Zinc Injection and the Impact on Plant Radiation Fields, EPRI, 2003, 1003389.

[4] Overview Report on Zinc Addition in PWRs, EPRI, Feb. 2001, 1001020.

[5] Experience with Zinc Injection in European PWRs, 1003378, EPRI Topical Report.

[6] KHNP, The radiation dose rate measurement way of Zinc injection power generation shutdown (2009).

[7] KHNP, Dose rate reduction report after 1-cycle zinc injection (2010).

[8] EPRI, Application of the EPRI Standard Radiation Monitoring Program for PWR Radiation Field Reduction (TR-1015119) (2007).

A Study on Applicability of Evaluation Code for Calculation of Exposure Dose of Workers for NPPs Decommissioning

Seungsu Shin and Jongsoon Song*

Chosun University, Pilmun-Daero 309, Gwangju, Republic of Korea

tmdsoo@naver.com

1. Introduction

Along with deterioration of domestic NPPs, various technologies for NPPs decommissioning are currently being studied. Accessing NPPs for decommissioning is difficult due to high level of radiation. Therefore, in order to ensure efficient performance of work, decontamination and forecasting of highly radioactive area must be made in order to minimize the exposure dose received by the workers.

This study introduces various Monte Carlo assessment codes for calculating workers exposure dose and makes analysis to present applicability of such codes for calculating workers exposure dose upon NPPs decommissioning.

2. Main title

2.1 Considerations for NPPs decommissioning

According to SCK·CEN considerations for workers upon NPPs decommissioning are as follows[1]

- Safety : Not increased radiological or classical hazards
- Efficiency : Sufficient DF to reach the objectives
- Cost Effectiveness : Should not exceed the cost for waste treatment and disposal
- Waste Minimisation : Should not rise large quantities of waste resulting in added costs, work power and exposure
- Feasibility of Industrialisation : Should not be laboure intensive, difficult to handle or difficult to automate

When working in a highly radioactive area in preparation of decommissioning, workers are highly likely to be exposed to radiation within a relatively short period of time. For such reasons, workers working times are sometimes controlled based on effective dose and equivalent dose.

2.2 Introduction of Monte Carlo assessment code

Monte Carlo method is a method for solving statistical problems using random sample extraction that uses random number, and is useful for solving complex problems where measurement is not possible.

2.2.1 EGS. EGS computer simulation code is a universal Monte Carlo code that can simulate the behavior of electrons and photons in multiple KeV ~ TeV area of energy within various forms of substance that have been configured by the user. This code has a very high scope of application, is well-documented, and has been verified by many people in numerous areas of study. When using the code, programming using a high quantity of MORTRAN language is required.

2.2.2 ITS. ITS code that simulates behavior of electrons and photos in consideration of time within various forms and substances, and is is a set of various programs that share source code library for solving highly complex radiation transport equation. ITS code consists of TIGER code, CYLTRAN code, ACCEPT code, Standard code, P code, and M code. User can select and sue the appropriate code from the library. When using the code, programming using a high quantity of FORTRAN language is required.

2.2.3 MCNP. MCNP code is simulates the behavior of neutrons, photons, and electrons, in a various 3 dimensional structure of substances. For photons, simulations such as incoherent scattering, coherent scattering, photoelectric effect, annihilation radiation, braking radiation, and positron annihilation are available. The reason that MCNP code can be

applied for various purposes is that it has good applicability by including various data, such as high number of general sources, critical sources, area sources, geometrical structures, and floaters of output tally.

2.2.4 GEANT4. GEANT4 code was originally developed to simulate physical experiment with high energy, but is now being applied and used in areas such as medicine, biology, and radiation protection, Major area of application for GEANT4 code is experiment setting for detector response simulation and calculation of particle behavior through visualization of particle orbit [2].

2.3 Analysis of Monte Carlo codes

This introduces Monte Carlo codes of EGS, ITS, MCNP, and GEANT4 that have been discussed above. Table 1 below shows the comparisons and characteristics of the codes [3].

Table 1. Classification of Monte Carlo Code with Respect to Key Features

Parameters		General Purpose Code			
		EGS4	MCNP	ITS	GEANT4
Accuracy Interactions	Photoelectric	Y	Y	Y	Y
	Compton Scatter	Y	Y	Y	Y
	Coherent Scatter	Y	Y	Y	Y
	Non-Colinearity	Y	Y	Y	Y
	Positron Range	Y	Y	Y	Y
Components	Crystal	Y	Y	Y	Y
	Collimator	Y	Y	Y	Y
	Septa	Y	Y	Y	Y
	Debugging	Y	Y	Y	Y
	Geometry Based	Y	Y	Y	Y
	Voxel Based	N	Y	N	N
	Plane	Y	Y	Y	Y
	Ring	Y	Y	Y	Y
	Single Unit	Y	Y	Y	Y
	Block Unit	N	Y	Y	N
Data	Energy Spectra	Y	Y	Y	Y
	Unscattered	Y	Y	Y	Y
	Scattered	Y	Y	Y	Y
	Randoms	N	Y	Y	N
	Singles	Y	Y	Y	Y
Easy of Use	Familiar Language	Fortran	Fortran 77+C	Fortran	C, C++
	Public Domain	Y	Y	Y	Y
	Docum / Support	Y	Y	Partially	Y

2.4 Application of Monte Carlo code

To study the applicability of assessment code, GEANT4 code that was introduced above, was selected. RCP sealing device of Kori unit 1 was modeled into the form of cylinder, and gamma-ray energy value Cobalt-60 was used.

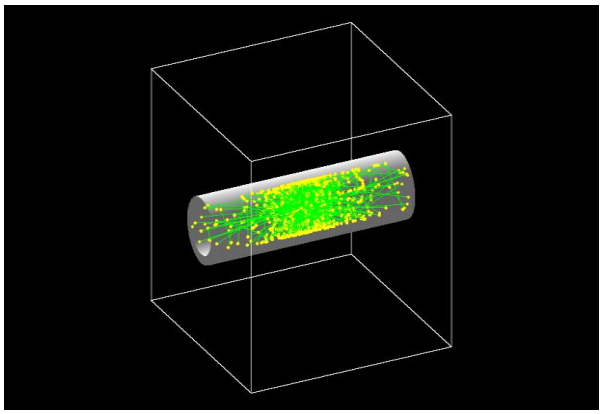


Fig. 1. Modeling of RCP Seal Using GEANT4 Code.

3. Conclusion

This study introduced assessment codes for calculating worker's exposure dose when decommissioning NPPs compared and analyzed the characteristics on applicability of assessment codes. Optimal assessment method out of the assessment codes that have been presented above may be considered to be used on exposure management for workers.

REFERENCES

[1] Massaut Vincent.; Decontamination for Decommissioning Decontamination of Building and Nuclear Research Centre, (SCK·CEN).

[2] Choi, K.J. (2014) Study of the Simulation of GEM by Geant4.

[3] Chung, Y.H.; Beak, C.H.; Lee, S.J. (2008) Monte Carlo Simulation Codes for Nuclear Medicine Imaging. N.Med Soc.Vol.42, No.2: 127-136.

The Improvement Method of Oxidation Furnace of Chemical Cleaning Liquid Waste Treatment System

Kyung-Wook Shin, Gyung-Sun Chae, Byeong-Mok Park, Jae-Young Hong, Yun-Soon Jeong, and Hee-Kon Jang

SAE-AN ENGINEERING CO., 481-10 Gasan-dong, Geumcheon-gu, Seoul, Republic of Korea

and9211@sae-an.co.kr

1. Introduction

The corrosion products flowing into the steam generator in the nuclear power plant might be deposited on secondary side of the steam generator and fixed in the form of sludge. These products could causes some kind of defect to effect the tube integrity and reduces the heat transfer efficiency of the steam generator tube. In order to remove the sludge adhered to the steam generator tube, the chemical cleaning with ethylenediaminetetraacetic acid (EDTA) is carried out. After the chemical cleaning, the chemical cleaning liquid waste containing EDTA is treated by the pyrolysis. The pyrolysis process generates air pollution matter such as NOx and SOx when the pyrolysis is firstiy performed at 850℃ in the electric furnace. In order to remove air pollution matter, it have burned around 500 to 900℃ once again in the oxidation furnace in the downstream of the electric furnace. In the oxidation furnace, zigzag type partition walls are settled in order to completely remove harmful gases such as NOx. However, due to the high temperature inside the oxidation furnace, the settled partition walls might be damaged such as decrease in thickness.

In this study, we have reviewed a method to prevent damage of the partition wall inside the oxidation furnace due to the high temperature in the chemical cleaning liquid waste pyrolysis treatment process.

2. Methodology

2.1 Pyrolysis process procedure

The chemical cleaning liquid waste treatment process pyrolyzes the liquid waste to about 850℃ while supplying a certain amount of liquid waste from the temporary tank storing the liquid waste to the electric furnace. At this time, due to the high temperature of the liquid waste, the sludge is accumulated on the bottom of the electric furnace, and the generated harmful gases are introduced into the oxidation furnace in the downstream of the electric furnace. The injected harmful gases are burned once again in the oxidation furnace, then removed through the catalytic device, condensed in a heat exchanger, and discharged into the environment with water and gas. Table 1 shows the permissible emission level.

Table 1. Permissible emission level of air Pollution Matter

Air Pollution Matter	Emission Facility	Permissible emission level (ppm)
NOx	Facility less than 2 tons per hour	90(12) or less
SOx	Facility less than 200 kilogram per hour	40(12) or less
CO	Facility less than 2 tons per hour	200(12) or less

※ ( ) is standard oxygen concentration (O_2 percentage)

2.2 Main function of pyrolysis plant

1) Pyrolysis furnace: An electric furnace with a heater at the top and bottom and pyrolyzing the liquid waste containing EDTA and ammonia at operating temperatures of 800 to 1000℃.

- Top heater (Bobbin): 380V, 4.5kW/unit(4unit).
- Bottom heater: 380V, 36kW/unit(4unit).
- Heating rate: 20℃/min.

2) Oxidation furnace: Air pollution matter such as NOx after pyrolysis in an electric furnace is oxidized at 500 to 900℃ using LPG burner.

3) Catalytic device: Conversion of air pollution matter such as CO and NOx from oxidation furnace to gas below permissible emission level through catalyst.

- SCR (Selective Catalytic Reduction) Catalyst: Reduce NOx to N_2 by injecting ammonia as a selective reduction catalyst.
- VOC (Volatile Organic Compounds) Catalyst: Remove CO and THC (Total Hydrocarbon) as

catalyst for removal of volatile organic compounds.

- NH_3 Catalyst: Ammonia removal catalyst.

4) Heat exchanger: An oxidation furnace, a catalytic device, and a device installed downstream of the HEPA filter to lower the temperature of the exhaust gas as required.

5) HEPA filter: Removal of particulate matter contained in the exhaust gas.

- Collection efficiency: 99.986%

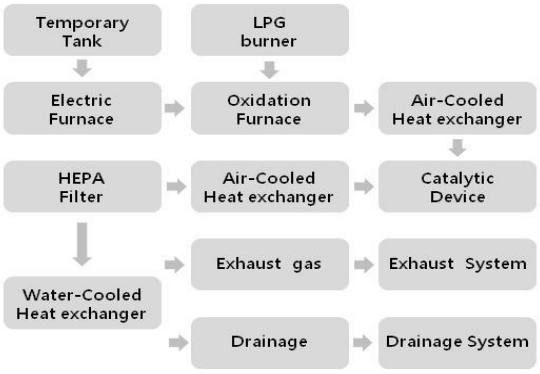


Fig. 1. Pyrolysis process flow diagram.

2.3 Secondary combustion in oxidation furnace

The secondary combustion of the oxidation furnace is intended to reduce the harmful gas by completely burning the harmful gas generated due to the incomplete combustion at the time of pyrolysis in the electric furnace. The harmful gases such as NOx are oxidized in the combustion process of high temperature when pyrolysis of waste liquid is regulated as air pollution matter. Therefore, in order to discharge the harmful gas generated during pyrolysis to the environment, it should be reduced according to the effluent quality standard, and the following points should be considered when burning.

- Maximum temperature reduction
- Reduced residence time of gas
- Reduced oxygen concentration

In an oxidation furnace using an LPG gas burner, it is very difficult to maintain a constant temperature and residence time while the secondary combustion is maintained at a constant temperature and the residence time of the gas is an important factor for reducing harmful gas. If the high temperature which is much higher than the proper temperature for removing the harmful gas is continuously maintained, there may be a problem that the partition walls are damaged inside the oxidation furnace. In order to solve such problems, it is desired to change the structure of the partition walls inside the oxidation furnace which is fixedly installed in advance so that the residence time of the gas can be adjusted, thereby securing the integrity of the oxidation furnace by secondary combustion.

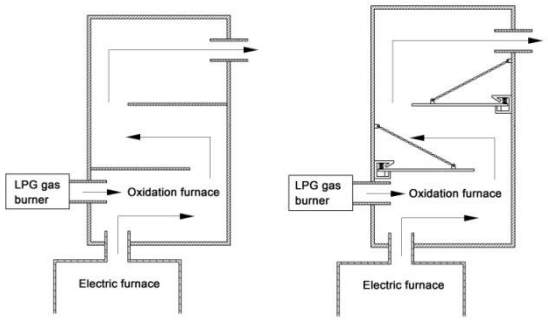


Fig. 2. Oxidation furnace design concept.

3. Conclusion

A function of the secondary combustion at the liquid waste treatment system is a method for reducing harmful gases such as NOx generated by pyrolysis during chemical cleaning liquid waste treatment containing EDTA. To maintain the constant temperature of the secondary combustion and to reduce the harmful gases such as NOx, the design of the partition walls were changed to secure the integrity of the oxidation furnace. Further studies such as gas flow according to the moving angle of the partition wall in the future should more effectively reduce the harmful gas and ensure the integrity of the oxidation furnace.

REFERENCES

[1] A. name, B. name, and C. name, “Article Title”, Journal of Nuclear Fuel Cycle and Waste Technology, 1(1), 1-10 (2003).

[2] Kyun-Ha Jin “A Study on the Incineration of Sewage Sludge by NOx Reduction Technology in Fluidized Bed Combustor” (2009).

[3] “Enforcement Rule Of The Clean Air Conservat -ion Act”.

Impact Analysis on the Uranium Evaluation Related to the Collecting Location of the Environmental Sample

Ju Young JEON*, Ji-Yeon SONG, Sung-Hwan KIM, Jong-Ho YOON, Seungho JEONG, and Hana SEO

Korea Institute of Nuclear Nonproliferation And Control, 1534 Yuseong-daero, Yuseong-gu, Daejeon, Republic of Korea

*jeonjy@kinac.re.kr

1. Introduction

International Atomic Energy Agency (IAEA) have been operating Environmental Sampling program (ES) based on the conclusion that nuclear material from the declared facilities or undeclared location could provide the basis to compare with the declaration. ES program process is as shown as Fig. 1. The step of planning and sampling could be easily underestimated rather than laboratory analysis



Fig. 1. Environmental sampling process.

There was a special case where the tons of Depleted Uranium (DU) sludge were deposited in the several tanks, out of compliance, in 2016. KINAC inspectors collected and analyzed it to determine whether the safeguards implementation is required [1].

This article shows the importance of the location of sample collection, based on the analysis results with the Monochromatic Micro X-ray Fluorescence (MMXRF), Alpha spectrometry (Alpha), and Thermal Ionization Mass Spectrometry (TIMS).

2. Method

Fig. 2 shows the specific tank (D: 12 m, H: 20 m) which was chosen for the analysis. This tank had included the many catalyst elements, such as Sb, SiO_2, Mo, etc. with the DU below 2.3 m height over 20 years [1]. The potable HM-5 device showed the DU seemed to exist only below 1.5 m. The inspectors assumed there was difference of uranium distribution caused by aggregation and remobilization, based on this result [2].

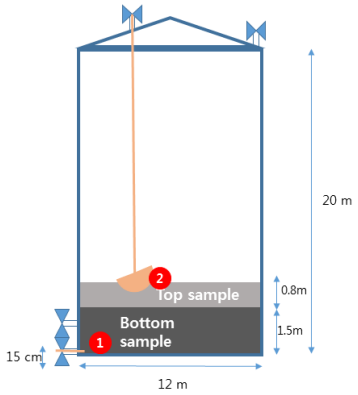


Fig. 2. Tank and sample location description.

Therefore, the inspectors collected the sample from top and bottom for expecting each sediment's representative. The samples were swiped and collected from (i) the drain nozzle which is located 15 cm off the bottom ground, (ii) the top hatch of the tank with the bucket. The type top and bottom sample was sludge with different density 1.01 and 1.06, respectively.

3. Result

The results with the TIMS (Isotopx), Alpha (Canberra) and MMXRF (ISP) are shown in Table 1. It shows that the uranium concentration of the bottom sample is about 221 to 414 times higher than top. TIMS and Alpha provided the result, 1996.6 ppm and 1366 ppm in the bottom parts. MMXRF, which is the equipment for mapping the uranium in the swipe sample, could not analyze the whole uranium concentration of each sample. But it could provide the comparison result and showed the difference between 221 to 414. It showed the top and bottom part has difference of uranium concentration.

Table 1. Analysis result of sample

Analysis Methods	Concentration [ppm]		Comparison
	Top	Bottom	
TIMS	5.69	1996.6	351
Alpha	3.34	1366 1036	310~408
MMXRF	-		221~414

Total uranium mass is calculated with the top and bottom mass assuming the values represent each sediments of the tank. Uranium mass of each part are calculated as below;

$$U = \frac{\pi D^2}{4} \mathrm{H}\ \rho\ C_U \qquad (1)$$

Where,

U = Uranium mass [kg]

D = Tank diameter [m]

H = Tank height [m]

ρ = Density [g/ml]

C_U = Uranium concentration [ppm]

TIMS results were adapted for uranium concentration as the most reliable result. Approximately 360 kg of the uranium is estimated to exist in the tank.

Only one sample would be collected from the tank, if the inspectors ignored the uranium remobilization effect of the tank. In that case, the analyzers have one sample from the top, because of the mixing concern and the easy approach to open the tank without overflow. Approximately 1.49 kg of uranium is estimated to exist in the tank, if the analyzers have one sample from the top. It showed that there is huge underestimation of the total uranium mass in the tank if the sampling procedure is ignored in the field.

4. Conclusion

The samples collected from tank without the information related to its homogeneity, axial and radial distribution of uranium in the tank. It leads to the misjudgment of the total uranium mass calculated with the concentration of the specific spot. It means the location of the sample could impact the quantity analysis. Therefore, the planning with pre-information and sampling is important as the analyze.

KINAC expected the further study, the way uranium with the flocculant remobilize in the closed system, could increase the accuracy of the quantity analysis of uranium.

REFERENCES

[1] Seungho Jeong, Heejun Chung, et al. “Management and Evaluation of Environmental Sampling 2016 Annual Report”, KINAC/RR-006/2017 (2016).

[2] International Atomic Energy Agency, “Uranium Extraction Technology”, Technical reports series No.359 (1993).

A Comparison Between Alpha-emitting Calibration Source and Electro-deposited Plate of KINAC

Jong-Ho Yoon*, Ju Young Jeon, JiYeon Song, and Hana Seo

Korea Institute of Nuclear Nonproliferation And Control, 1534 Yuseong-daero, Yuseong-gu, Daejeon, Republic of Korea

*2bwiths@kinac.re.kr

1. Introduction

Alpha Spectrometry is used for isotopic composition measurement of radioactive elements that decay by the emission of an alpha particle [1]. The detector energy, efficiency and resolution has to be calibrated by a calibration source (CS) in prior to analysis by alpha spectrometry [2]. After calibration, the element of interest is chemically separated from the sample matrix (pure uranium samples may not be required any additional purification prior to mounting) and then deposited on a metal plate (typically stainless steel) by electro-deposition [3]. Consequentially, the shape of the electrodeposited sample depends on the pretreatment process (ex. dilution, valence control, deposition condition and so on).

The CS was manufactured to the highest standards and fully complied with applicable international standards. therefore, it is necessary to analyze the surface of CS with the actual sample KINAC made. By comparing the surface condition of two samples, our pretreatment process is needed to constantly evolve.

In this paper, alpha-emitting calibration source was morphologically analyzed using optical microscope and scanning electron microscope (SEM) - Energy Dispersed Spectrometry (EDS) in comparison with electro-deposited plate of KINAC.

2. Experimental

2.1 CS sample

The alpha-emitting CS used in this study was standard radionuclide source (24.1 mm Diameter x 0.65 mm Thick Stainless Steel Disk) by Eckert & Ziegler. The source is shown in Fig. 1.



Fig. 1. Alpha-emitting calibration source (SRS 94370).

2.2 Electro-deposited plate of KINAC

^{232}U tracer solution taken from NIST standard solution (SRM 4324B) was used for raw material of KINAC's sample. The pH was adjusted to 1.7 and controlled with NH_4OH (base) and (1:9) H_2SO_4 (acid) using the litmus paper. For preparation of stainless steel plate for alpha spectrometry, the solution was put in the electro-deposition cell which was made of Teflon, as shown in Fig. 2. The anode was a platinum wire. After electro-deposition process, the plate was heated by fire torch [4].

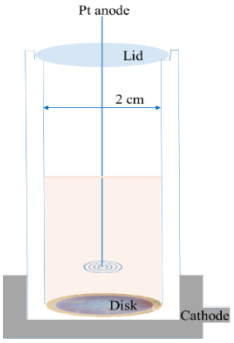


Fig. 2. Electro-deposition module.

3. Results

3.1 Microscope analysis

The two samples were analyzed using optical microscope (OLYMPUS, BX53TRF) and the image of samples was as shown Fig. 3, respectively. According to the images, the particles in CS were

remarkably observed as shown Fig. 3-b in comparison with electro-deposited plate of KINAC (Fig. 3-d).

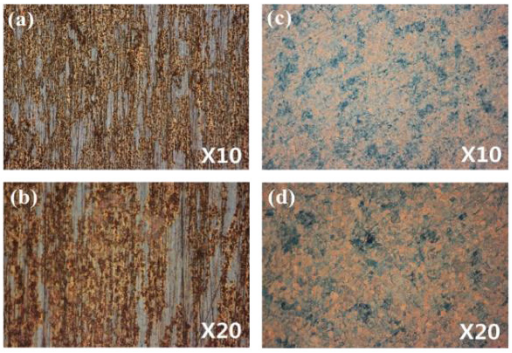


Fig. 3. Microscope image of the CS (a) X10, (b) X20 and electrodeposited plate of KINAC (c) X10, (d) X20.

In CS sample, the suspicious depositions were observed patterns like a scratch not similar to electro-deposited plate of KINAC.

3.2 SEM analysis

In order to analyze particle size in detail, the samples were analyzed using a SEM(JEOL JSM-6610LV) coupled with an EDS microanalysis.

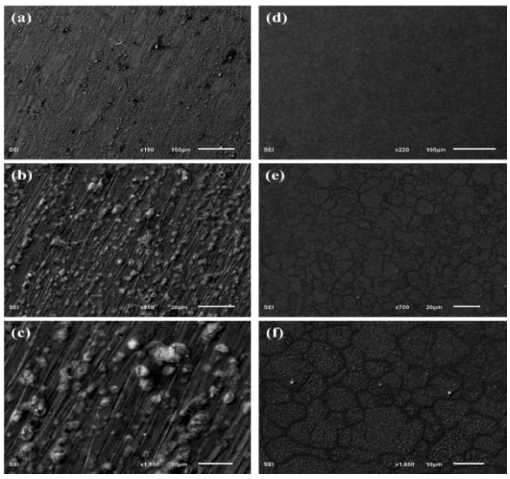


Fig. 4. SEM image of the surface of CS (a) 100 ㎛, (b) 20 ㎛, (c) 10 ㎛ and electro-deposited plate of KINAC (d) 100 ㎛, (e) 20 ㎛, (f) 10 ㎛.

In the case of the CS, the particle size ranges from 3 to 10 ㎛ approximately (Fig. 3-c) and electro-deposited plate of KINAC was less than 1 ㎛ (Fig. 3-f).

3.3 EDS analysis

As shown Fig. 4-a, the uranium particles were found several spot in the CS by EDS results. The particles were usually verified as U, Mn, Fe and Cr. However, the particles size of sample that KINAC made was too small to detect the EDS equipment and most of the particles was usually verified as Cr, Zr and Fe in shown Fig. 4-b.

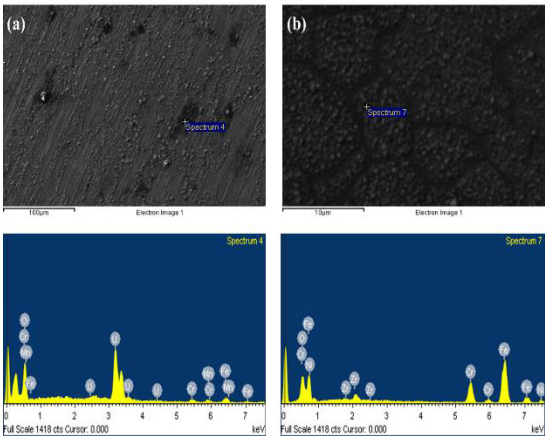


Fig. 5. EDS element results of the particle in CS (a) 100 ㎛ and electrodeposited plate of KINAC (b) 1 ㎛.

4. Conclusion

Through the surface analysis of the two samples, the difference of pretreatment process between the CS and the sample that KINAC made were verified morphologically. The particles in CS was easily observed using SEM and the elements were confirmed by EDS unlike electro-deposited plate of KINAC. Further work is necessary to research particle size changes depending on the pre-treatment condition in electro-deposition plate.

REFERENCES

[1] Donna Beals, “INFL GUIDELINE FOR ALPHA SPECTROMETRY”, ITWG-INFL-ALPH, ver. 1, (2012).

[2] Nora Vajda, Paul Martin, Chang-Kyu Kim, “Handbook of Radioactivity Analysis”, chapter 6, 363-422 (2012).

[3] Talvitie, N.A., “Electro-deposition of Actinides for Alpha Spectrometry Determination,” Analytical Chemistry, 44, 280-283 (1972).

[4] Jong-Ho Yoon, “The Capability of isotopic uranium analysis in nuclear material at KINAC”, Transactions of the Korean Nuclear Society Spring Meeting, Jeju, Korea, May 7-8, 2015.

Research of Self-disposal Evaluation for Domestic Hard-to-treat Radioactive Waste

Yongho Hong*, Hyoungmin Park, Eunsuk Choi, and Wonjin Jeong

ACT Co., Ltd., 406, IT Venture Town, 3, Techno 9 Ro, Yuseong-gu, Daejeon, Republic of Korea

*hyh@actbest.com

1. Introduction

The volume of domestic radioactive waste which is difficult to treat can be reduced by applying the patented technology of Korea Atomic Energy Research Institute. The support structure which occupies most of the waste volume is separated and subjected to self-disposal. We would like to bury the waste in the landfill by proving that the waste form satisfies regulatory requirement [1,2,3]. We will evaluate the dose of industrial worker and resident farmer scenarios and prove that they satisfy the disposal limit of domestic nuclear safety law (maximum individual dose: 10μSv/y, collective dose: 1man·Sv/y). Therefore, in this study, radiological effect of landfill disposal of support structure from the volume reduction process of domestic industrial radioactive waste will be evaluated using RESRAD 7.2.

2. Evaluation method

RESRAD was developed by Argonne National Laboratory with the support from DOE for the purpose of assessing the radiation dose and risk of residents due to radioactive contaminants. It was approved by DOE for evaluation of radioactive contaminated sites. Also, US NRC approves dose evaluation through RESRAD for nuclear decommissioning licenses [4].

3. Selection of input data

For the purpose of selecting input variable to evaluate landfill scenario using RESRAD, we obtained characteristic data of the landfill and surrounding area. When the local data was not available, domestic survey data and values from literature were selected and applied in a conservative manner. In case appropriate data is unavailable, the default values of RESRAD was used. In this study, we evaluated the industrial workers at the landfill and the general public residence in the upper part of the landfill after closure.

3.1 Disposal capacity and radionuclide concentration

If the volume of the domestic industrial radioactive waste is reduced by 50% using the patented technology of KAERI, the volume of the resultant waste is 710 m^3 and the fraction of mass of each nuclide is shown in Table 1.

Table 1. Landfill capacity & Mass fraction

Classification		Value	Unit
Landfill capacity		710	m^3
Mass Fraction[1)]	U-234	0.001	wt%
	U-235	0.194	wt%
	U-238	99.805	wt%

[1)] Nuclide Concentration ratio: www.wise-uranium.org site, Composition of uranium isotopes in depleted uranium from enrichment of natural uranium

3.2 Evaluation target and period

In case of industrial workers who bury waste for self-disposal, external exposure, inhalation of dust, and inadvertent soil ingestion are considered. For resident farmer scenario, additional pathways are surface water, groundwater, plant food, and fish. Also, evaluation period is chosen as 1000 years which is the default value of RESRAD.

3.3 Other input data

Significant factors among the input variables of the hydrological data of cover, contaminated zone, aquifer and vadose zone, residential and environmental data, inhalation and ingestion, and external exposure are shown in Table 2.

Table 2. Input factors of landfill worker and resident after closure

Parameter		Value	Unit
Nuclide Concentration	U-234	142	mBq/g
	U-235	11	mBq/g
	U-238	847	mBq/g
Area of contaminated zone		355	m^2
Thickness of contaminated zone		2	m
Cover depth[1)]	Worker	0.15	m
	Resident	0.6	
Density of contaminated zone		1.5	g/cc
Wind speed[2)]		2.2	m/s
Precipitation[2)]		1.28	m/yr
Water transport model		MB	-
Well pump rate[3)]		8,288	m^3/yr
Inhalation rate[4)]	Worker	10,519	m^3/yr
	Resident	8,400	m^3/yr
Indoor time fraction	Worker	0.057	m^3/yr
	Resident	0.5	-
Outdoor time fraction	Worker	0.171	-
	Resident	0.25	-
Plant food ingestion[5)] (Resident)		290	kg/yr
Drinking water intake[5)] (Resident)		196.3	liter/yr

[1)] Enforcement Rule of Wastes Control Act asterisk 11 Data
[2)] KMA(Korea Meteorological Administration) Data
[3)] MOLIT(Ministry of Land, Infrastructure, and Transport) Data
[4)] EPA(United States Environmental Protection Agency) Data
[5)] KINS(Korea Institute of Nuclear Safety) Report(KINS/RR-808)

4. Evaluation result

Based on the input data, RESRAD was executed to calculate the dose for industrial worker and resident farmer. The deregulated waste of concentration 1 Bq/g is of volume 710 m^3 and satisfies the annual radiation dose limit of 10 μSv/y according to Nuclear Safety Act Article 70 and Enforcement Rule 94 (Table 3).

Table 3. Targeted Individual dose

Classification	Radioactive nuclide			Total (μSv/yr)
	U-234 (μSv/yr)	U-235 (μSv/yr)	U-238 (μSv/yr)	
Worker	2.438E-4	1.691E-2	7.758E-1	0.793
Resident	0.3876	0.02472	2.05	2.463

In order to evaluate the collective dose, it is assumed that the total number of people in waste treatment is 10. For the number of residents after closure of landfill, Statistics Bureau data is used. City of Ulsan has population density of 1099.6 man/km^2 (2015) and the area of landfill is 0.355 km^2. For population of the contaminated area, 390 people are assumed by multiplying population density and the area of landfill. As a result of the evaluation, it was confirmed that it satisfies the domestic standard of collective dose for self-disposal which is 1 man·Sv/y (Table 4).

Table 4. Targeted Individual dose

Classfication	Individual dose (μSv/yr)	Persons	Collective dose (man·Sv/yr)
Worker	0.793	10	7.93E-06
Resident	2.463	390	9.61E-04

5. Conclusion

The volume of domestic industrial radioactive waste which is difficult to treat is planned to be reduced by applying the patented technology of KAERI. In this study, regulatory compliance of self-disposal of the resulting deregulated waste was evaluated using RESRAD 7.2. As a result, it was confirmed that the disposal limit proposed by the Nuclear Safety Act was satisfied for both the industrial worker scenario and resident farmer scenario. Therefore, it is expected that this paper would be used as evidence that the landfill disposal of deregulated waste resulting from the volume reduction process is safe.

Acknowledgment

This study was carried out as a project of nuclear science research and development project of Ministry of Science, ICT and Future Planning.

REFERENCES

[1] KAERI. Patent Publication, 2013.
[2] ACT, Co., Ltd. Nuclear Technology Development Project Annual Report, 2016.
[3] Hong et al, Development of Optimum Treatment Process for Volume Reduction of Domestic Industrial Radioactive Waste, Korean Radioactive Waste Society, 2016.
[4] KAERI, Environmental Impact Assessment Study for Self-Disposal of Deregulated Radioactive Contaminated Soil and Concrete Waste, 2007.

The Performance Test of Induction Type Furnace for the Design of Tritium Desorption System

Eunkyung Jung*, Kyu Min Song, Byunwook Ko, Kahee Jeong, and Seungchul Park

KHNP Central Research Institute, 70, 1312-gil, Yusong-daero, Yusong-gu, Daejeon, Republic of Korea

*jungek1554@khnp.co.kr

1. Introduction

Since 2007, Wolsong TRF (Tritium Removal Facility) is operated and tritium removed from moderator and primary coolant system is safely stored in stainless steel vessels with titanium sponge (titanium bed). Tritium as high value material and product can be used in war industry, fusion research and medical care. In order to extract tritium from the titanium beds, new furnace system is developed. In this study, adsorption and desorption experimental apparatus with induction type furnace is introduced and tested. Hydrogen recovery rate as a performance index of the furnace is investigated as function of operating temperature.

2. Hydrogen adsorption and desorption experimental apparatus

2.1 Feature of hydrogen adsorption and desorption experimental apparatus

Main systems of this apparatus are the hydrogen adsorption and desorption system, and the vacuum exhaust system. The hydrogen adsorption and desorption system consists of a metering tank, induction type furnace, a RF controller and feed pumps (TMP, MBP). The amount of adsorption and the amount of desorption can be calculated by measuring the pressure change over time. The evacuation system removes impurity gases before filling the system with hydrogen, or removes remaining hydrogen in the next experimental step. The compressed air (CDA, Compressed Dry Air) module, the cooling water (PCW) supplied to the RF coil, and the cooling water supply part from the water bath for cooling the drawing heater were designed for the operation of the tritium extractor. In addition, a controller for all control and data acquisition was constructed. The scale of the device was made about 4m in width, and about 2.3m in height (Fig. 1).

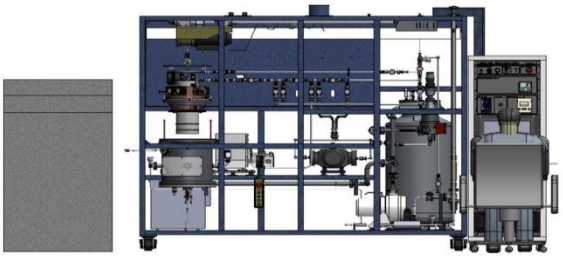


Fig. 1. Hydrogen adsorption and desorption experimental apparatus (front side).

2.2 Heat transfer analysis

During the hydrogen desorption, the thermodynamic limit on the PTC (pressure-concentration-temperature) curve) exists. For the sufficient desorption of hydrogen, the temperature should be raised to 650°C or more. When heating at that temperature, the most vulnerable part of the vessel is the tritium storage vessel's main valve. So, a heat exchanger is installed to remove the heat transfer generated by the vessel heating. Heat transfer analysis is performed to confirm the integrity of the valve portion [2].

3. Operation procedure

The hydrogen desorption is performed in four steps. As a first step, the vacuum evacuation was performed by using a rotary pump and TMP. The second step is the activation of the tritium storage vessel. The titanium bed is evacuated and the temperature of the titanium bed is heated by 525°C for 2 hours. When the activation is complete, close the valve and keep it in vacuum. The third step is the adsorption process. It is to fill the metering tank (MT) with hydrogen. The volume of the tank is 191.45L, so the pressure is 0.9768 atm. At this time, the pressure of the tank and the storage vessel temperature are recorded with time. The last step is to heat the storage vessel to perform desorption. First,

the metering tank and piping are evacuated in advance. Measure the pressure of the titanium bed while heating at set temperatures. When the temperature reaches the set temperature, the MBP (or TMP) is operated to transfer the hydrogen from the titanium bed to the metering tank. Measure the temperature and pressure of the metering tank over time.

4. Result & discussion

Five titanium beds are manufactured and tested. Experiments are performed at 500, 600, 650, 670°C to determine recovery rate with each different titanium bed for the independent experiment.

4.1 Activation and Adsorption

Before adsorption test, the titanium bed is activated. It is heated up to 525°C and evacuation for 2 hours to remove impurities in the vessel. This procedure is the same with that of manual in WTRF TGHSS. During the adsorption, the temperature of titanium bed can be increased very high so the hydrogen adsorption is performed separately by 10 times in 10 kPa units which is one tenth of the total hydrogen storage capacity.

4.2 Desorption

The pressure of the metering tank is measured according to the operation time. The pressure in the metering tank refers to the amount of hydrogen in the tritium storage vessel. The operating time is 24 hours and the initial pressure is 97.68 kPa. There are many differences in the recovery rate of desorption depending on the operating temperature. Fig. 2 is the result of the recovery rate depending on the operating temperature. At 550°C, the recovery rate is over 48% for 24 hours. At 600°C, the recovery rate is over 60. The recovery rate is over 80% at 650 and 670°C. It is expected that it takes about 48 hours or more to obtain a recovery rate of 90% or more.

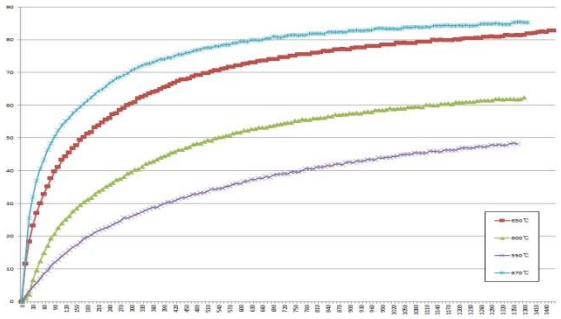


Fig. 2. The recovery rate in desorption process depending on the operating temperature.

5. Conclusion

The performance test of the hydrogen adsorption-desorption apparatus is performed. The amount of hydrogen desorption is determined by the temperature on the PCT curve of the titanium vs. tritium. It takes more than 48 hours to extract more than 90% of tritium at design temperature (650°C). To increase the yield of tritium, it is necessary to increase the operating temperature near 800 ~ 900°C. In this case, safety design should be considered to reduce the damage of the storage vessel. Induction type furnace is one of solutions to increase the safety and performance.

REFERENCES

[1] K. Song, “Introduction to Tritium Application Program in KHNP” KO-JA Tritium Workshop July 5-6, 2016, Seoul.

[2] E. Jung, et al., “Development of the Adsorption and Desorption Experimental Apparatus for Tritium Extraction from Titanium Bed”, Proc. of the KRS 2016 Autumn Conference, Oct. 10-14, 2016, Jeju.

Introduction of the Environmental Sampling Network for the Safeguards in KINAC

Ju Young Jeon*, Jong-Ho Yoon, and Hana Seo

Korea Institute of Nuclear Nonproliferation And Control, 1534 Yuseong-daero, Yuseong-gu, Daejeon, Republic of Korea

*jeonjy@kinac.re.kr

1. Introduction

The Environmental sampling (ES) program is known as the one of the most powerful verification technique for the detection of undeclared nuclear activities. It has grown to be a main investigative tool in the last 15 years since it was approved as a safeguards verification measures [1]. The application of ES usually involves two stages [2] ; (i) baseline sampling and (ii) routine sampling

(i) Baseline sampling is performed to establish a reference 'environmental signature'

(ii) Routine sampling is subsequently performed to obtain data that can be compared for consistency with the established baseline environmental signature and the declared operations.

The KINAC has established the ES program to build 'the baseline of environmental signature' for domestic nuclear facility with the KBSI (Korea) and ITU (Germany).

This paper will describe the current status of ES system of swipe sample at KINAC for the purpose of the safeguards.

2. Methods and Results

2.1 Sample preparation

The particles in cotton swipe sample taken from domestic nuclear facility were attached onto carbon planchet using the pump and vacuum impactor in the clean room (ISO class 5 cleanliness level). All of work is done in a glove bag to minimize the risk of cross-contamination. After deposition step, the planchet was heated to 250 ℃ using a hot plate.

2.2 Screening (SEM-EDS method)

The morphology and elemental composition of particles could be identified by Scanning Electron Microscope (SEM, JEOL JSM-6610LV) and Energy Dispersed Spectrometry (EDS) respectively. Therefore, the deposited planchet was screened to select uranium particles by SEM-EDX. Fig. 1 shows the uranium particles in the planchet by SEM.



Fig. 1. Environmental sampling procedures in ROK.

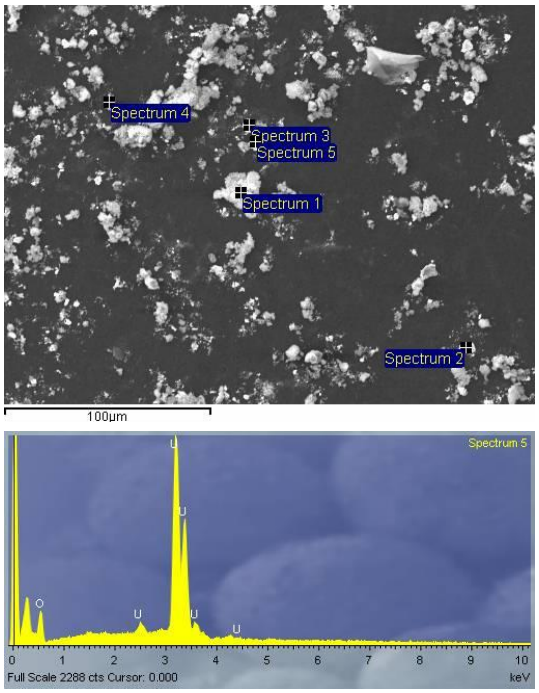
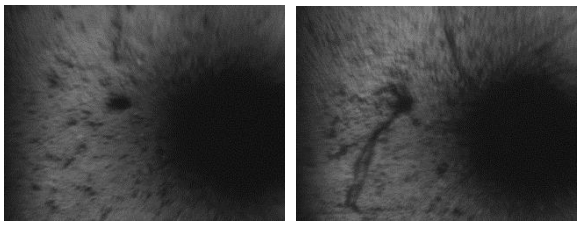


Fig. 2. SEM image of uranium particles.

2.3 Particle analysis (SIMS method)

The SIMS analyze the isotope composition ratio by separating the accelerated particles according to the mass difference. First, UO standard sample measurements were preceded for equipment calibration. And then, the analysis are performed in the order of selected sample (#1) and (#2). Each sample is collected from the pellet manufacturing process point and the conversion process point. And the Beam current was set as weak energy (3μA) in order to prevent the sample from damaging caused by the strong energy beam. The SIMS optical images of samples were shown in Fig. 3.



(a) Sample (#1) (b) Sample (#2)

Fig. 3. Optical image of samples using SIMS.

2.4 Inter-comparison

The accuracy is the mainly required for the particle analysis. As this reason, (#1), (#2) samples were sent to the ITU for cross-analysis. Lastly, the results of KINAC-KBSI joint research and the ITU commissioning analysis are compared in Table 1.

Sample #1 could be interpreted as a scattered material in the process of producing pellets which as nuclear fuel into a heavy water reactor. The samples #2 obtained 4.5wt% enrichment that is the level of concentration of common nuclear fuel materials used in light water reactors.

Table 1. Uranium Enrichment Results

Sample ID	KINAC-KBSI	EC-JRC-ITU
#1	0.7 ~ 0.8wt%	0.7wt%
#2	3.0 ~ 4.5wt%	2.0 ~ 4.5wt%

3. Conclusion

KINAC have been developing the ES program for safeguards since 2010. KINAC keeps discussing on the research initiatives and equipment operating plan with the KBSI, for further improvement. From the above environmental sample analysis network, KINAC will develop analytical capabilities.

REFERENCES

[1] D. M. Fischer 'The Evolution of Environmental Sampling for Safeguards', IAEA-CN-184/138, SGIM-IDS, Vienna, Austria.

[2] IAEA SAFEGUARD GLOSSARY, INTERNATIONAL VERIFICATION SERIES No. 3, 2001 IAEA (VIENNA), 2002.

Development of Emergency Plan for Permanently Defueled Condition of Kori Unit 1

Jeongmi Kim
Central Research Institute of KHNP, 70, 1312-gil, Yuseong-daero, Yuseong-gu, Daejeon, Republic of Korea
Jeongmi00@khnp.co.kr

1. Introduction

Kori Unit 1, the first PWR (Pressurized Water Reactor) plant in Korea, will permanently shut down in June, 2017 for decommissioning. Along with the other operating license document, Emergency Plan also should be revised for the permanently defueled condition. After ceasing the plant operation, various systems are isolated and the spent fuels are stored in SFP (Spent Fuel Pool). Therefore, Radiation Emergency Plan for permanently defueled condition (PDEP) should reflect those changed plant conditions and be revised for effective radiation preparedness. This paper will describe the development concept and draft result of PDEP for Kori Unit 1.

2. Main Discussion

2.1 Overview

Plant operation licensee of Kori Unit 1 will be revised for permanently defueled condition, and the plant's Final Safety Analysis Report (FSAR) needs to be updated as DSAR(Defueled Safety Analysis Report).

DSAR involves revision of SSC (System, Structure, Component), source terms, and accident analyses as is reflects the lowered radiological source term and risks associated with spent fuel pool storage relative to reactor at-power operation.

Basically, Kori Unit 1 PDEP development is focused on the consistency with DSAR. Additionally, associated guidance and cases of U.S. were reviewed for further considerations.

2.2 Consideration of consistency with DSAR

The plant structures, components, and systems have been reclassified in DSAR according to their functions and the degree of integrity required to protect the public and to maintain the plant safety. This includes elimination of the need for various ECCS systems to mitigate reactor or containment accidents. After a reactor is permanently defueled, the accidents that dominate plant risk during power operation are no longer applicable.

To reflect those changes effectively, EALs (Emergency Action Levels) for operating power plant were reviewed based on the reclassification of SSC and other revisions in DSAR, which shown in Table 1.

Table 1. EAL Related DSAR Analysis

DSAR Section	EAL Related Terms in DSAR
3.2	Reclassification of SSC and Quality Assurance Categories for Permanently Defueled Condition
6.2, 6.4	Fire Impact Analysis : Containment Systems, Habitability Systems
8	Electric Power Effectiveness(On/Off-Site Power System)
11.4	Process and Effluent Radiological Monitoring Systems
12.1	Area Radiation Monitoring System
15	Accident Analysis

As a result of considering the reclassification of SSCs and Accident Analysis in DSAR, EALs that are not applicable for plant defueled condition were removed and others were reasonably revised for consistency with DSAR.

2.3 Study of NEI guidance

NEI 99-01 "Methodology for Development of Emergency Action Levels" (Rev.6) was officially approved by NRC and it provides guidance for an emergency classification scheme applicable to a permanently defueled (PD) station.

According to this guidance, the owner of a permanently defueled station must demonstrate that

no credible event can result in a significant radiological release beyond the site boundary. Therefore, EALs applicable to a permanently defueled station may limited to only either a Notification of Unusual Event (NOUE) or an Alert classification. It means that PDEP may not need to cover Site Area Emergency (SAE) and General Emergency. Applicable Alert EALs for PD station are shown in Table 2.

Table 2. Applicable Alert EALs of NEI 99-01(rev.06) for Permanently Defueled Condition

EAL	Description
PD-AA1	PD-AA1 Release of gaseous or liquid radioactivity resulting in offsite dose greater than 0.1 mSv Effective Dose or 0.5 mSv thyroid Equivalent Dose.
PD-AA2	UNPLANNED rise in plant radiation levels that impedes plant access required to maintain spent fuel integrity.
PD-HA1	HOSTILE ACTION within the OWNER CONTROLLED AREA or airborne attack threat within 30 minutes.
PD-HA2	Other conditions exist which in the judgment of the Emergency Director warrant declaration of an Alert.

2.4 Case Study of U.S. Plants

Kewaunee Plant Station (KPS) is the first plant under decommissioning with the renewed NEI 99-01 Rev.06 (‘12) and its EP exemptions had approved based upon the reduction of risk to the health and safety of the public. For those exemptions, site specific spent fuel pool accidents analyses was performed (including beyond design basis accident) and their result should meet the conditions 1) the projected dose to the public is within the limit or 2) there is sufficient time to take mitigation actions and implement offsite protective measures if needed. After the exemptions were approved the PDEP was implemented. KPS was able to reduce the EALs, EP facilities, equipment, and ERO (Emergency Response Organization) which allowed reduction of plant staffing.

Zion Station also developed its EP plan for Defueled Station. The analysis of the potential radiological impact of accidents for Zion Station in a permanently defueled condition indicated that any releases beyond the Restricted Area Boundary (RAB) are limited to small fractions of regulatory guidance. For this reason, radiological emergency plan was focused onsite and reduced cases of EALs down to 6 Unusual Events and 4 Alerts without any Site Area Emergency and General Emergency (same as the NEI 99-01 guidance).

3. Conclusion

KHNP CRI developed the Emergency Plan for permanently defueled condition to meet the DSAR which involves revised SSCs, source terms, and accident analysis. The reduced EALs shown in Table 3 were derived as 11 Alerts, 7 Site Area Emergency, 4 General Emergency, by eliminating and revising the EALs for normal operation conditions. Just after defueled, the SFP source term condition is not very different from normal operating. But after a certain period of the time, exemption of EALs especially for Site Area Emergency and General Emergency would be possible. For this exemption, additional accident analysis (for design basis and beyond design basis) and discussion with regulatory body are required referring to guidance and cases of overseas.

Table 3. Reduced EALs for Permanently Defueled Condition of Kori Unit 1

EAL category	Number of Cases	
	Operation Condition	Permanently Defueled
Alert	20 Cases	11 Cases
Site Area Emergency (SAE)	17 Cases	7 Cases
General Emergency	13 Cases	4 Cases

REFERENCES

[1] NEI 99-01, “Emergency Action Levels for Non-Passive Reactors”, Rev.6 (2012).

[2] Zion Station, “Defueled Station Emergency Plan(DSEP)”, Rev.13 (2010).

Thousand-fold Sensitivity Enhancement of Lanthanide by Capillary Electrophoresis

Jihye Kim[1*], Kihwan Choi[2], and Tae-Hong Park[1]

[1]Korea Atomic Energy Research Institute, 111, Daedeok-daero 989beon-gil, Yuseong-gu, Daejeon, Republic of Korea

[2] Korea Research Institute of Standards Science, 124, Gwahak-ro, Yuseong-gu, Daejeon, Republic of Korea

[*]jihyekim21@kaeri.re.kr

1. Introduction

Capillary electrophoresis (CE) is a highly suitable tool to analyze inorganic ions with fast separation and high separation efficiency. Here, we applied stacking method called as electrokinetic supercharging (EKS) in CE for detection of lanthanide. Thousand-fold sensitivity enhancement was achieved without any modification of commercial capillary electrophoresis system.

2. Materials and methods

2.1 Electrophoretic conditions

CE was performed on a CESI 8000 system from Beckman (Fullerton, CA, USA) (Fig. 1) with preprogrammed Karat software. Analytes were monitored using a UV detector at 214 nm. The run buffer was 10 mM 4-methylbenzylamine (4-MB), 4 mM 2-hydroxyisobutyric acid (HIBA), 0.4 mM malonic acid, and 0.1% hydroxypropyl cellulose (HPC), adjusted to pH 4.8 with 2-ethylbutyric acid. Electrophoresis was carried out with a voltage of 25 kV. The capillary cartridge temperature was set to 25 °C (Fig. 2). A new fused silica capillary of 50 μm ID and 360 μm OD and effective/total length of 50/60 cm (Polymicro Technologies, Phoenix, AZ, USA) was washed with 0.1 M NaOH for 5 min, water for 5 min, and a run buffer for 5 min, each at 50 psi. Between runs, the capillary was treated by rinsing it with 0.1M NaOH for 2 min, water for 2 min, and the run buffer for 3 min at 50 psi.

4-MB was used as a UV absorbing probe for indirect UV detection. HPC was employed as EOF modifier. HIBA and malonic acid acted as a complexing agents for sufficient selectivity of lanthanide.

2.2 Instrument



Fig. 1. CESI 8000 system from Beckman.

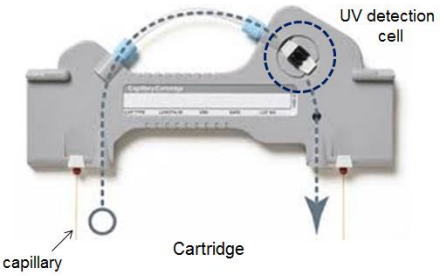


Fig. 2. Cartridge for CESI 8000 system.

2.3 Principle of capillary electrophoresis

Capillary electrophoresis is an analytical technique that separates ions based on their electrophoretic mobility with the use of an applied voltage in Fig. 3. The electrophoretic mobility of analyte is dependent upon the charge of the molecule, the viscosity, and the atom's radius.

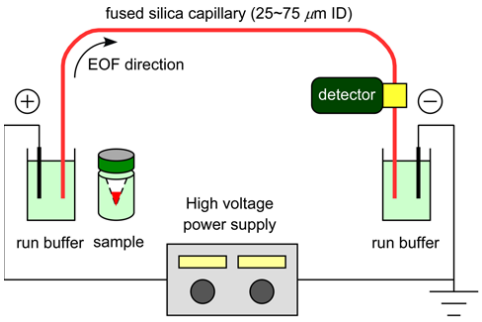


Fig. 3. Schematic diagram of capillary electrophoresis.

2.4 Advantages of capillary electrophoresis

- *Fast analysis time: 10 ~ 30 min*
- *High efficiency: N > 10^5 ~ 10^6*
- *Small sample volume required: 1 ~ 50 nL*
- *Numerous modes to vary selectivity and wide applications*
- *Simple and automated instrumentation*

2.5 Purpose of this study

The physical and chemical characteristics of lanthanide are so similar that for many years it was very difficult to separate them from each other. Here, we applied electrophoretic method using HIBA and malonic acid as complexing agents for enhancing high selectivity. Additionally, EKS method was used for thousand-fold enrichment of sensitivity.

3. Results and discussion

3.1 Comparison of EKS stacking and conventional method (capillary zone electrophoresis, CZE)

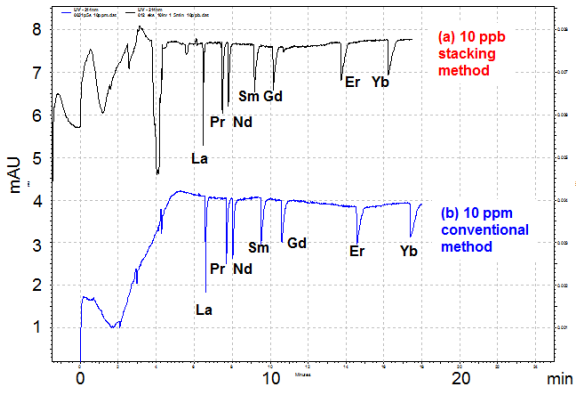


Fig. 4. Electropherogram of (a) a sample enriched by EKS using 10 ppb lanthanide and (b) 10 ppm lanthanide by CZE.

Fig. 4 described the EKS system was performed to concentrate and fully separate some lanthanides. In Fig. 4a, the electropherogram was obtained using CZE as a conventional method in CE. In this case, 10 ppm of some lanthanides was injected hydrodynamically at 0.5 psi for 5 s. However, for EKS method, the electropherogram in Fig. 4b showed same peak heights with the conventional method. In EKS method, 10 ppb of some lanthanides was injected electrokinetically for 90 s under a voltage of 10 kV.

Furthermore, seven lanthanides were sufficiently separated in CE using these conditions.

4. Conclusions

Thousand-fold sensitivity enhancements of lathanides were obtained by using EKS stacking method using indirect UV detection without any modification commercial CE system. This result is very compared to ICP-OES in terms of detection limit at the level of parts- per-billion (ppb).

REFERENCES

[1] Z. Xu, K. Kawahito, X. Ye, A. R. Timerbaev, T. Hirokawa “Electrokinetic supercharging with a system-induced terminator and an optimized capillary versus electrode configuration for parts-per-trillion detection of rare-earth elements in CZE” Electrophoresis, 32, 1195-1200 (2011).

[2] F. Foret, S. Fanali, A. Nardi, P. Boček, “Capillary zone electrophoresis of rare earth metals with indirect UV absorbance detection” Electrophoresis 11, 780-783 (1990).

Mock-up Training Effects for Steam Generator Lancing & FOSAR

Byeong-Mok Park*, Kyung-Wook Shin, Cheol-Wan Park, Ah-Ran Cha, Dong-Hyun Yoo, Min-Gyu Kim, and Do-Yeong Jung
SAE-AN ENGNIEERING.CO., 481-10 Gasan-dong, Geumcheon-gu, Seoul, Republic of Korea
*pbm@sae-an.co.kr

1. Introduction

The sludge lancing and foreign object search and retrieval (FOSAR) work on the secondary side of steam generator in nuclear power plant aims to improve the thermal efficiency and to preserve the tube integrity of the steam generator.
It is generally performed during planned outage overhaul.

Nuclear power plants (NPP's) are subject to the constraints of the working environment, unlike the general industry. Typical examples are radiation working environment involving radiation exposure, working environment contaminated by radioactive materials, low illumination environment and different types of steam generator structures for NPP's.

As a means to overcome the limitation of such a working environment, The Mock-up system can provide the useful utility. Before the sludge lancing & FOSAR work of the steam generator, mock-up is exercised before actual work is put in order to overcome the working environment of the nuclear power plant and to perform the work smoothly.

In this study, we analyze the work environment of sludge lancing & FOSAR and establish the mock-up system to reduce the work time.

2. Mock-up training

2.1 Mock-up training definition

The police dictionary defines the definition of mock-up training as follows;

Mock-up training is training for trainees to achieve the set objectives or to perform a specific plan in a given situation. In other words, it is a training method that assumes the situation that the trainee will encounter during the work and allows the trainee to cope in that situation. Especially, the advantage of mock-up training is to reduce the gap between theory and reality, and emphasizing the teamwork and communication, and to improve the applicability and analysis to the real situation.

2.2 Work environment around steam generator

The steam generator sludge lancing & FOSAR work in the reactor building is performed by a regular radiation work permit (RRWP) or a specific radiation work permit (SRWP). Especially lancing & FOSAR work, It is performed SRWP due to the large amount of radiation exposure.

According to the recent collective dose case, it can be seen that set up and dissolve of the lancing & FOSAR equipment of the It's occupied 22.3% of total exposure dose. The collective dose for each work is specified in Table. 1.

Table 1. Collective Dose Case

Work		Collective dose (Man-mSv)	Percentage
Lancing	Equipment Set up	10.78	16.7%
	Equipment Dissolve	3.59	5.6%
	Lancing	21.70	33.7%
	Sum	36.07	56.1%
FOSAR		28.23	43.9%

The radiation controlled area of NPP's have various levels of radioactive contamination. In the case of lancing & FOSAR, it is grouped work the secondary side of the steam generator, but the work site may be contaminated with the high contamination level to the reactor building steam generator hand hole area. Because of the presence of body and equipment contamination, decontamination of the body and equipment can cause problems such as radioactive waste generation, internal exposure, and inhibit the integrity of equipment. Be careful of contamination when equipment transporting, set up and dissolve.

NPP's have high ceilings and are divided into

many compartments compared to other general industries, so installation and replacement of lighting equipment may not be smooth. Therefore, if necessary, a separate lighting fixture is installed to improve the low illumination working environment. However, the lighting of the overall working environment is in the dark, and the ability to perform work at low illumination is required.

The lancing & FOSAR equipment according to NPP's type may be the same or may be different. The power plant planned for lancing & FOSAR notify the purchase bid. As a qualified supplier make a successful bid, and the probability of the same company continuing to perform the same power plant is low. Therefore, It is necessary to check the equipment of the power plant where the work is to be performed, need to mastery, and to check that the equipment is in normal operation because there is an unused time for equipment that has been checked after use.

2.3 Mock-up training

The mock-up training system in the general work environment will reduce the time and safety accidents through mastery of work considering the following points.

- Theory of equipment training
- Actual equipment operation training
- Repeat training of equipment operation
- Carry out the actual work

The radiation working environment is a poor working environment such as contamination by radioactive material and relatively low illumination compared to general working environment. Mock-up training in the radiation working environment should have the following effects in addition to the general working environment to reduce radiation exposure and prevent the diffusion of contamination by radioactive material.

- Theory of equipment for prevent of foreign object inflow and occurrence of equipment contamination
- Actual equipment operation and inspection training
- Repeat training of equipment operation
- Repetitive training in consideration of radiation exposure reduction and time reduction in the radiation working environment

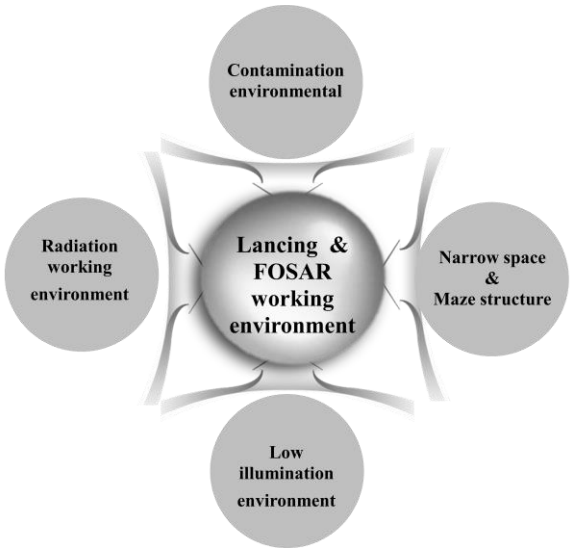


Fig.1. Lancing & FOSAR Work Environment.

3. Conclusion

Unlike general mock-up training, there are several constraints of working environment for mock-up training of steam generator lancing & FOSAR in NPP. In order to obtain optimal operation efficiency, Mock-up training suitable to the working environment in NPP should be established and implemented. In terms of the number of mock-up exercise, the mock-up training cannot be performed many times because of the time limitation before the field work. Also, a fewer times of the mock-up exercise can be problem. The number of times of mock-up exercise could contribute to the reduction of radiation exposure by shortening the time of lancing & FOSAR work.

Therefore, it is necessary to study the optimal number of times of mock-up by analyzing the characteristics of equipment and work environment in the steam generator lancing & FOSAR.

REFERENCES

[1] Developed a cartridge filter cutting device after removing sludge on secondary side of steam generator of nuclear power plant, 2013. 10. 17 Korea radioactive waste society fall conference.
[2] Police Dictionary.
[3] Regulation about the industry safety and health Standard, Ministry of employment and labor No 160. 2016. 7. 11.

Quality Management for Steam Generator Lancing & FOSAR

Byeong-Mok Park*, Jae-Hyun Han, Kwan-Seok Choi, Young-Kug Kim, Sam-Hyun Kim,
Chang-Yul Lee, and Hee-Kon Jang
SAE-AN ENGNIEERING.CO., 481-10 Gasan-dong, Geumcheon-gu, Seoul, Republic of Korea
*pbm@sae-an.co.kr

1. Introduction

Sludge Lancing and FOSAR(Foreign object Search and Ratrieval) such as removal of deposit inside the secondary side of the steam generator are being performed to improve the thermal efficiency and to prevent the thermal stress of the steam generator tube in NPP. Sludge Lancing & FOSAR process creates a "Quality Plan (QP)" based on the work performance plan and maintenance procedure during the plant outage. In the QP, systematic Quality Management (QM) is performed by determining the Witness Point (WP) and Hold Point (HP). QM activities can achieve the effects such as quality improvement, cost reduction, improvement of production (yield), atmosphere of workplace, improvement of corporate credit, enhancement of organizational competitiveness and improvement of organizational structure.

In this study, we would analyze the contents of quality management in Lancing & FOSAR process, and suggest a more efficient and systematic work execution plan.

2. QM for S/G Lancing & FOSAR

2.1 Concept and definition of QM

According to Armand Vallin Feigenbaum, quality is a holistic feature of production, technology and marketing that meets the diverse needs and expectations of customers for a product or service. QM has the meaning of establishing management and quality policies and plans, creating and implementing the organization, and taking necessary control over the process. QM always refers to the control of certain behaviors while setting standards and limitations. In the past, the main activity area was to reduce manufacturing quality defects, so it was close to quality control. However, recent quality concept is called "Quality Management" rather than "Quality Control" because of the importance of the design.

2.2 Principles of QM

When applying the principle of QM to be Lancing & FOSAR, it can be classified into 5 kinds in total. The main contents are as follows;

- Principles of prevention
  When performing the Lancing & FOSAR, it means preventing the cause before the problem occurs. QM focuses on prevention activities.
- Principles of staff advice
  In order to effectively manage QM, the staff department with the expertise in management technology and the performance department appropriately share the necessary work for good quality and utilize the advantages of the organization.
- Principles of all the workers
  All workers should cooperate with each other in terms of quality, execution cost and performance time.
- Principles of scientific management
  The QM activities are based on scientific basis, it consists of five steps as follows;
  - Problem recognition
  - Materialize facts about the problem
  - Plan for problem solving
  - Execution according to plan
  - Investigate plan and performance
- Principle of Comprehensive adjustment
  In QM, emphasizing part of the quality of the consultation and ignoring the cost and performance time, the process required by the client cannot be performed at economically appropriate time. Therefore, it is possible to realize satisfaction of the client by coordinating the three elements of quality,

execution cost, and execution time in a well-balanced and should cooperate with relevant department.

2.3 QP of Lancing & FOSAR

By executing and reviewing the QP of Lancing & FOSAR systematically, the reliability of Lancing & FOSAR performance will be further improved. The main contents of the Lancing & FOSAR maintenance / plan checklist are as follows;

- Determine the adequacy of qualification for worker.
- Identification of equipment and apparatus.
- Mock-up training
- Check site preparation and procedural compliance
- Confirmation of maintenance / inspection checklist

2.4 WP of Lancing & FOSAR

The setting of WP is the checkpoint designated by the quality inspector for testing during Lancing& FOSAR process. WP is a checkpoint which can proceed to the next step without the prior consent of the quality inspector if the quality inspector does not join the inspection point. The WP at Lancing & FOSAR process includes “Check mock-up training”, “Check work procedures in on-site and check procedures”, “Check equipment before and after inspection” and “preventing foreign object inflow management”. The work that the quality inspector has set up for WP is an important task. Most of them are carried out continuously or the quality inspectors are made to participate.

2.5 HP of Lancing & FOSAR

The HP setting in QM is a checkpoint that the quality inspector cannot proceed to the next step without inspection or prior written approval of the quality inspector unlike the WP. HP is “Lancing & FOSAR qualification certificate confirmation”, “S/G ECT result of foreign object evaluation signal” and so on. HP is QM that is critical to ensuring safety and reliability.

2.6 Lancing & FOSAR maintenance / inspection checklist

The Lancing & FOSAR maintenance inspection checklist is a format that records the contents of the QP in detail and records smooth measure to be taken and problem to be solved when problems are found. The main contents are divided into “initial conditions of execution”, “precaution to perform”, “equipment installation and removal” and “equipment operation”, and the details of the Lancing & FOSAR procedure and reflect the content.

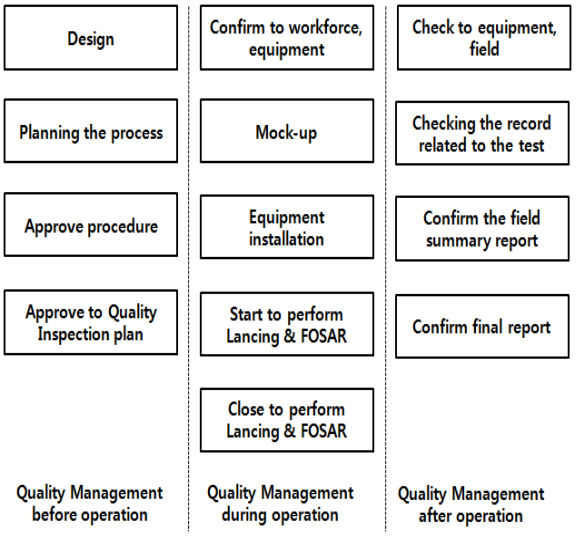


Fig. 1. Schematic diagram of QM.

3. Conclusion

During the Lancing & FOSAR process of steam generator, checking and managing the main provision according to the principle of QM before, during and after the operation. The systematic management of the planned process, the quality improvement of the process performance, and the measure to be taken at the time of finding the problem, would enable efficient operation of the steam generator Lancing & FOSAR in NPP.

REFERENCES

[1] Quality assurance procedure, Quality inspection (SAE-AN ENGINEERING CO. 2017.03.03).
[2] Service & Maintenance procedure (maintenance procedure for secondary side of the steam generator).
[3] Academic name encyclopedia (Engineering).

Compression Behavior Studies on Ammonium Molybdophosphate (AMP)

Junhyuck Im and Yongjae Lee*

Yonsei University, Yonsei-ro 50, Seodaemun-gu, Seoul, Republic of Korea

*yongjaelee@yonsei.ac.kr

1. Introduction

The recent event at the Fukushima Daiichi nuclear power plant (NPP), Japan, has emphasized the criticality of radiological monitoring and decontamination and confinement actions for radionuclides released into the atmosphere, land and water surfaces. Because of their long half-life, activities of ^{135}Cs and ^{137}Cs in various environmental compartments would either be monitored to evaluate mobility, or isolated if Cs sequestration occurs above national or international guidelines [1].

Evaporation, precipitation, extraction, adsorption, ion-exchange methods have been considered as the remediation for radiocesium in aqueous radioactive wastes. Among them, the ion-exchange technique has outstanding efficiency for removal cesium and ion-exchange properties of ammonium molybdophosphate (AMP) have been known for a long time [2]. AMP has shown its noticeable qualities in selectivity of Cs and stability in acid solutions [3].

Though many meaningful results are reported in AMP every year, its pressure behavior is not well known yet. In this study, compression behavior of AMP was observed by using diamond anvil cell (DAC) and synchrotron high-energy and -flux X-ray beam.

2. Materials and Experimental Methods

2.1 Sample powder preparation

AMP sample showing yellow color was purchased from ACS reagent grade from Sigma-Aldrich (ideally, its chemical formula is $H_{12}Mo_{12}N_3O_{40}P\cdot xH_2O$, Fig. 1). Structural characterization of AMP was performed at the beamline 10-2 at the SSRL (Stanford Synchrotron Radiation Lightsource) and its structure model is shown in Fig. 1.

2.2 High-pressure experiments

A cylindrical type diamond anvil cell (DAC) with two opposed diamonds supported by tungsten-carbide plates was used for the high pressure experiments. The powdered sample was loaded into a 400 μm diameter and less than 150 μm thick sample chamber. A few ruby spheres of ~20 μm diameter were added as a pressure gauge. Subsequently, methanol and ethanol 4:1 mixture solution (labeled ME41), and silicone oil were added as hydrostatic pressure-transmitting medium (PTM). The pressure at the sample in the DAC was measured by detecting the shift of R1 emission line of included ruby spheres (precision: ±0.05 GPa). The pressure was calculated using the equation below (1):

$$P = A/B\,[1 + (\Delta\lambda / \lambda_0)]\,B \qquad (1)$$

Changes in the unit cell lengths and volume were derived from a series of whole profile fitting procedures using the GSAS suite of programs.

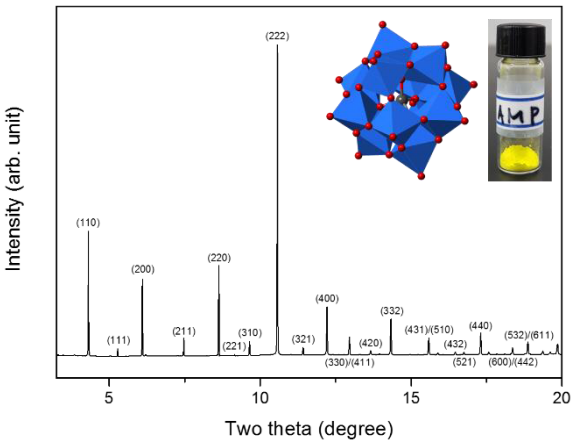


Fig. 1. Structure model and X-ray powder diffraction pattern of AMP.

3. Results and Discussion

3.1 Under methanol-ethanol pressure medium

The XRD patterns and unit-cell volume changes of AMP upon increase pressure up to 6.0(1) GPa have been exhibited in Fig. 2. At around 1.0(1) GPa, the peak splitting of most hkl peaks are observed ((211) peak is emphasized in grey bar in Fig. 1) with

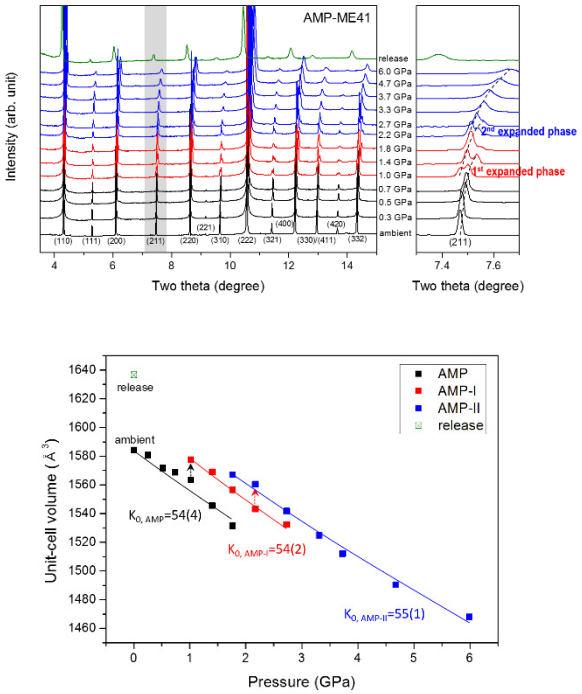


Fig. 2. X-ray powder diffraction pattern of AMP up to 6.0 GPa under ME41 PTM condition (up) and the unit-cell volume contraction as function of pressure (down).

volume expansion by ca. 0.9%. Subsequently, the X-ray powder diffraction pattern of AMP reveals a slight 1.1% volume expansion at 2.2(1) GPa again. According to the bulk modulus calculation, ambient phase, the 1st and the 2nd expanded phases of AMP have the similar values which is around 54, interestingly. These expanded phases are taken place due to the insertion of PTM molecules into the interlayered space of AMP. The unit-cell volume of the AMP after pressure release is ca. 3.3% larger than that of ambient AMP.

3.1.1 Under silicone-oil pressure medium. In the presence of non-penetrating silicone oil, the diffraction peak shifts indicated by the dashed line in Fig. 2 reveal a contraction of the unit-cell volume up to 10.1(1) GPa. The bulk modulus of AMP under silicone oil PTM is 24(3) until 2.1(1) GPa. In the post region of pressure, the unit-cell volume contraction hardly occur up to 10.1(1) GPa with 276(27) bulk modulus which is the largest measured in our experiments. Above 6.0(1) GPa, the diffraction peaks gradually disappear indicating pressure induced amorphization, but slightly re-crystallization to the original phase was found after pressure. Compared to AMP under ME41 PTM, there was no evidence of any unit-cell volume expansion in the presence of non-penetrating silicone oil PTM.

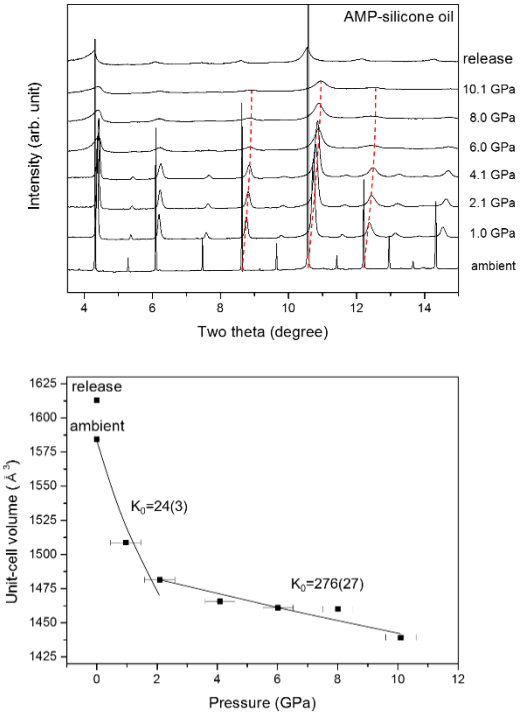


Fig. 3. X-ray powder diffraction pattern of AMP up to 10.1 GPa under silicone oil PTM condition (up) and the unit-cell cell volume contraction as function of pressure (down).

4. Conclusions

In summary, we have demonstrated the compression behavior of AMP in the methanol-ethanol mixture and silicone oil medium. Upon pressure increase under mixture PTM, the unit-cell volume expansions occur, indicating pressure induced insertion of PTM molecules into the AMP interlayer.

REFERENCES

[1] S. Solange, C.G. Adriana, T. Mélodie, B. François, L. Dominic, and K. Freddy, "Nanoporous ammonium molybdophosphate–silica hybrids as regenerable ultra-selective extraction agents for radiocesium monitoring", New Journal of Chemistry, 37, 3877-3880 (2003).

[2] F. Šebesta, and V. Štefula, "Composite ion exchanger with ammonium molybdophosphate and its properties", Journal of Radioanalytical and Nuclear Chemistry, 140(1), 15-21 (1990).

[3] T. Zhaoyi, H. Zhaoya, Z. Dong, and W. Xiaolin, "Structural characterization of ammonium molybdophosphate with different amount of cesium adsorption", Journal of Radioanalytical and Nuclear Chemistry, 299(3), 1165-1169 (2014).

2017 춘계학술논문요약집

발행인 송기찬

발행처 한국방사성폐기물학회

주 소 대전광역시 유성구 대덕대로 989번길 111
한국원자력연구원 원자력성과확산관(E7) 202호

연락처 **Tel** +82-42-861-5851, +82-42-866-4205
Fax +82-42-861-5852 **E-mail** krs@krs.or.kr

인쇄처 신진기획인쇄사 **Tel** +82-42-638-7887

Abstracts of Proceedings of the
Korean Radioactive Waste Society Spring 2017

www.krs.or.kr

KOREAN RADIOACTIVE WASTE SOCIETY

사단 한국방사성폐기물학회
법인 Korean Radioactive Waste Society